THE TECTONO-SEDIMENTARY EVOLUTION OF THE SOUTHERN FREE STATE GOLDFIELD IN THE WITWATERSRAND BASIN, WITH IMPLICATIONS FOR THE GEODYNAMIC EVOLUTION OF THE KAAPVAAL CRATON, SOUTH AFRICA

Andreas Eberhard Walter Friese



APPENDICES

A thesis submitted to the Faculty of Science, University of the Witwatersrand, Johannesburg
in fulfilment of the requirements for the degree of

Doctor of Philosophy

Johannesburg
2020

LIST OF APPENDICES

APPENDIX 1 : Publication list of studies related to the geology of the Free State Goldfield.

APPENDIX 2 : Surface borehole location plan for intersections of (A) Harmony Formation, (B) Dagbreek Formation, (C) Kimberley Formation, (D) 'B' Reef, (E) Eldorado Formation, (F) VS5 Reef Zone and (G) Karoo Supergroup.

APPENDIX 3 : Computer-generated channel thickness plot for the Bedelia Placer at Harmony Gold Mine.

APPENDIX 4 : Diagrammatic representation of the concept of a slip linear diagram.

APPENDIX 5 : Diagrammatic representation of cleavage vergence and the method of determination.

APPENDIX 6 : Diagrammatic representation of a stress field analysis for fault groups A, B, C and D.

Group A (A1-A6): Cataclastic faults with normal dip-slip lineations.

Group B (B1-B9): Cataclastic faults with oblique-normal lineations.

Group C (C1-C10): Mylonitic faults with strike-slip lineations.

Group D (D1-D12): Mylonitic faults with oblique-reverse lineations.

APPENDIX 7 : Structural interpretation plans of the Free State Goldfield.

APPENDIX 8 : Reinterpreted sections (A-F) of seismic lines across the lease area of H.J. Joel Gold Mine.

APPENDIX 9 : Reinterpretation of (A) Bouguer gravity contour map, (B) aeromagnetic contour map and (C) magnetotelluric survey line "J" / southeastern FS Goldfield.

APPENDIX 10 : Fracture analysis logs (A-D) of surface boreholes JDR7, JDR17, JDR21 and JDR23 within the Doornrivier prospect area.

APPENDIX 11 : Plan and north-south section of 33-19E Haulage South / Harmony Gold Mine, illustrating the main structural elements of the Merriespruit Thrust Zone.

APPENDIX 12 : Restoration of Merriespruit Thrust Zone along geological section 33-19E Haulage South / Harmony Gold Mine.

APPENDIX 13 : X-ray diffraction analyses of selected fault rock specimens from H.J. Joel Gold Mine.

APPENDIX 14 : X-ray fluorescence analyses of selected fault rock specimens from H.J. Joel Gold Mine.

APPENDIX 15 : Dyke sample localities in the southern Free State Goldfield.

APPENDIX 16 : Geochemical analysis of intrusives from the southern Free State Goldfield.

APPENDIX 17 : Discriminant Function Analysis.

APPENDIX 18 : Previously proposed genetic models for the tectonic framework of the "Witwatersrand Triad".

APPENDIX 19 : Reconstruction of the geodynamic evolution of the southern African lithosphere.

APPENDIX 20 : Palaeogeographic reconstruction maps depicting the geodynamic evolution of the southern Africa lithosphere from Neoarchaean until the Mesoproterozoic (~3.1-1.0 Ga):

20-A : Geodynamic evolution of southern Africa during the period ~3.1-3.0 Ga.

20-B : Geodynamic evolution of southern Africa during the period ~3.0-2.97 Ga.

20-C : Geodynamic evolution of southern Africa during the period ~2.97-2.87 Ga.

20-D : Geodynamic evolution of southern Africa during the period ~2.87-2.81 Ga.

20-E1 : Geodynamic evolution of southern Africa during the period ~2.81-2.75 Ga.

20-E2: Conceptual model for escape tectonics in the area of the Gaborone Granite Complex.

20-F : Limpopo Orogenic Cycle-related magmatism within the Kaapvaal Craton during the period ~2.786-2.64 Ga.

20-G : Geodynamic evolution of southern Africa during the period ~2.75-2.64 Ga.

20-H : Geodynamic evolution of southern Africa during the period ~2.64-2.585 Ga.

20-I : Geodynamic evolution of southern Africa during the period ~2.585-2.43 Ga.

20-J : Geodynamic evolution of southern Africa during the period ~2.43-2.35 Ga.

20-K : Geodynamic evolution of southern Africa during the period ~2.35-2.22 Ga.

20-L : Geodynamic evolution of southern Africa during the period ~2.22-2.1 Ga.

20-M1: Geodynamic evolution of southern Africa during the period ~2.1-2.05 Ga.

20-M2: Tectono-structural setting of the Bushveld Complex.

20-N : Geodynamic evolution of southern Africa during the period ~2.05-1.93 Ga.

20-O : Ubendian (~2.1-1.86 Ga) and Kheis (~1.83-1.73 Ga) Orogenic Cycle-related magmatism within the Kaapvaal Craton.

20-P : Geodynamic evolution of southern Africa during the period ~1.93-1.83 Ga.

20-Q : Geodynamic evolution of southern Africa during the period ~1.83-1.73 Ga.

20-R : Geodynamic evolution of southern Africa during the period ~1.73-1.4 Ga.

20-S : Kibaran (~1.4-1.25 Ga) and Lomanian (~1.2-1.0 Ga) Orogenic Cycle-related magmatism within the Kaapvaal Craton.

20-T : Geodynamic evolution of the proto-Kaapvaal Craton during the period ~1.4-1.25 Ga.

20-U : Geodynamic evolution of the Kalahari Craton during period ~1.2-1.0 Ga.

20-V : Geodynamic evolution of the Kalahari Craton during the period ~900-650 Ma.

20-W : Geodynamic evolution of supercontinent Gondwana during the period~650-450 Ma.

20-X : Geodynamic evolution of supercontinent Gondwana during the period ~290 - 215 Ma.

20-Y : Geodynamic evolution of southern Africa during the period ~200-80 Ma.

20-Z : Geodynamic evolution of southern Africa during the period ~190-120 Ma.

APPENDIX 21 : Summary of selected geochronological data pertinent to southern Africa, Western Australia, India and East Antarctica.

21-A : Summary of selected geochronological data pertinent to the Kaapvaal Craton

21-B : Summary of selected geochronological data pertinent to the Zimbabwe Craton

21-C : Summary of selected geochronological data pertinent to the Limpopo Central Zone Terrane

APPENDIX 22 : Correlation of Palaeoproterozoic (~2.6-1.45 Ga) stratigraphic units and tectonic events within the Kaapvaal, Rehoboth, Zimbabwe, Pilbara and Yilgarn cratons and Limpopo Central Zone Terrane

APPENDIX 23 : Summary of Palaeoproterozoic (syn-Transvaal Supergroup; ~2.49-2.41 Ga) formation and resetting ages reported from the Kaapvaal and Zimbabwe cratons and Limpopo Central Zone Terrane

APPENDIX 24 : Summary of Palaeo- to Mesoproterozoic (post-Transvaal Supergroup; ~2.15-1.0 Ga) deformation events reported from the area of the Witwatersrand Basin and Bushveld Complex (*i.e.,* central Kaapvaal Craton) and their correlation with far field stress related to the Magondi and Okwa orogenies, Bushveld Complex emplacement, and Vredefort meteorite impact, as well as Kheis, Kibaran and Lomanian (Namaqua-Natal) orogenies.

APPENDIX 25 : Summary of Palaeo- to Mesoproterozoic (post-Transvaal Supergroup; ~2.1-1.0 Ga) (A) formation and (B) resetting ages reported from the Kaapvaal Craton.

APPENDIX 26 : Tectono-structural and terrane interpretation summary map for the Kaapvaal Craton, Limpopo Central Zone Terrane and Zimbabwe Craton, covering the countries of Botswana, Zimbabwe, South Africa and parts of Mozambique.

APPENDIX 1

PUBLICATION LIST OF STUDIES RELATED TO THE GEOLOGY OF THE FREE STATE GOLDFIELD

A summary of publications and their main findings regarding the geology of the Free State Goldfield is listed below according to subject and date of appearance.

STRATIGRAPHY AND SEDIMENTOLOGY

Borchers & White (1943) described the strata intersected in surface exploration boreholes in the area comprising today the Western Holdings, President Brand and President Steyn gold mines. They studied the lithology of the strata between the Ventersdorp lava and the Basal Reef, proposed a tentative correlation of the strata, and suggested the possible pre-Karoo structure. The value of the geophysical work, which preceded the drilling, is discussed and historical information given about the discovery of the auriferous conglomerate reefs in depth.

Frost *et al.* (1946), after reviewing the history of the pioneering prospecting operations, described the succession of pre-Karoo strata intersected in exploration surface boreholes from an area around the present St. Helena Mine. Tentative correlations were made of the intersected strata with possible equivalents in the Ventersdorp and Witwatersrand Supergroups, and structural/geological interpretations for the pre-Karoo strata were given, as well the importance of geophysical methods to the exploration for shallow auriferous beds stressed.

Baines (1949) correlated the Basal Reef and the Vaal Reef with the Main Reef group conglomerate beds from the Central Rand, and inferred an unconformity at the base of these reefs. Furthermore, the Leader Reef on St. Helena Mine was correlated with a conglomerate that in other parts of the area is named the "B-Reef".

Sharpe (1949) drew identical conclusions to Baines (1949) concerning the correlation of the Basal Reef, the Vaal Reef and the Main Reef group of conglomerate beds, and pointed out the position of most conglomerate reefs upon erosional unconformities. Sharpe and Baines also made suggestions concerning modifications to the terminology of the Witwatersrand System.

Borchers (1950) discussed the lithology and correlation of the strata intersected in boreholes, as well as the nature of intraformational unconformities and trends of mineralisation in the Leader and Basal Reefs.

Cousins (1950) studied the Karoo System in the Odendaalsrus-Virginia area, and demonstrated that the Ecca Series is represented by the Middle and Upper Ecca Stage, and that sediments of the Lower Beaufort Stage cover the southeastern part of the area.

Feringa (1954) described and correlated the stratigraphy of the Free State Goldfield with other areas in the Witwatersrand Basin and submitted a detailed subdivision of the Kimberley Reef group of conglomerate bands, which were compared with their correlatives on the East Rand.

Pienaar (1956) described the petrography and stratigraphy of the Ventersdorp lava and of the intercalated sediments. He concluded that the Lower Volcanic Stage was erupted along a series of fissures, and that the sediments and pyroclastics were deposited in depressions or troughs generated by faults. Four markers in the Lower Volcanic Stage, observed in both the Odendaalsrus and the Klerksdorp areas, are described.

Van der Vyver (1956) studied the Van den Heeversrust or Rainbow Reefs which occur in a narrow strip of ground to the northwest of Odendaalsrus. It was suggested that the Lower Volcanic Stage of the Ventersdorp System should be included in the Upper Division of the Witwatersrand System, or alternatively that the strata from Zone VS1C upwards should be correlated with the Ventersdorp System.

Antrobus (1956) demonstrated that the Basal Reef on President Steyn Mine consists in places of two distinct, both oligomictic reefs which are of different age and associated with unconformities. The younger Steyn Reef rests unconformably on the older Basal Reef, and was formed at the expense of the latter. It was further shown that the Basal and Leader Reefs, and the Elsburg Stage overlap onto progressively older footwall stratigraphy from President Steyn Mine in a southward direction.

Winter (1957) studied in detail the stratigraphy and structure of the Upper Witwatersrand Division at the Virginia and Merriespruit mines. The limits of the Basal, Leader, and some of the Kimberley Reefs are deduced from isopach maps, and an unconformity is proved at the base of the Zone EL1.

Coetzee (1960) presented for the first time a regional and comprehensive overview of the geology of the Free State Goldfield, covering aspects such as the exploration history, lithostratigraphy, sedimentology, correlation, structure, hydrogeology, and economic geology of the goldfield.

Winter (1964a) investigated the stratigraphy and structure of the mines in the northern portion of the Free State Goldfield and concluded a more complete and thicker stratigraphic succession in this area compared with the Welkom area to the south. He identified marginal unconformities associated with the Basal and "B"-Reefs, and the upper portion of the Elsburg Stage and describes the overlapping nature of the Upper Witwatersrand System stratigraphy along the basin margins.

Winter (1964b) analysed the structure and stratigraphy of the mines in the Virginia area where he identified several unconformities in the Upper Witwatersrand System and concluded that most reefs were formed in a neritic environment associated with marginal unconformities. He further viewed the unconformities as favourable surfaces for the concentration of heavy minerals like gold and uraninite and described the palaeoenvironmental evolution of the Upper Witwatersrand System.

McKinney *et al.* (1964) summarized the geology of the Anglo American Group mines in the central part of the Free State Goldfield in which they give, besides an overview of the structural and tectono-sedimentary evolution, a detailed sedimentological description of the Basal Reef and the sediments comprising the Upper Witwatersrand System.

Hodgson (1967) examined the relationship between the sedimentology and the gold distribution of the Basal Reef Zone at Harmony Gold Mine and concluded that gold values can be forecasted from sedimentary evidence.

Pienaar (1969) carried out similar investigations on the Basal Reef in the Free State Saaiplaas Mine area and demonstrated a close relationship between the sedimentology and gold distribution, as well as envisaged the topography of the folded pre-Basal Reef floor as the main controlling factor for the distribution of gold and sedimentological facies.

Sims (1969) studied the detailed sedimentology of the main auriferous conglomerates of the Upper Witwatersrand System at President Brand and President Steyn Mines, concluding that deposition occurred with a fluvial system entering a land-locked sea.

Knowles (1969) undertook a detailed sedimentological study of the Basal Reef based on borehole intersections in the southern part of the Free State Goldfield.

Minter (1978) conducted for the first time a regional study of the Basal/Steyn Reef in the central Free State Goldfield and defined the characteristics and regional extent of both placers, which he envisaged to be deposited by a fluvial braided stream system on an alluvial fan.

Kleynhans (1979) examined the Elsburg Formation on Western Holdings and Welkom mines and interpreted the coarse gravels as alluvial fan deposits.

Kennedy (1979) analysed borehole core from the central part of the Free State Goldfield, reconstructed the palaeoenvironment of the Upper Witwatersrand Supergroup and proposed a depositional model for the investigated area, encountering syn-depositional tectonism in Kimberley and Elsburg time.

Buck (1980) discussed the occurrences of stromatolite and ooid deposits within the fluvial and lacustrine sediments of the Klippan and Bothaville Formations of the Ventersdorp Supergroup within the Free State Goldfield, and interpreted the distinctly different palaeoenvironmental setting of both formations.

Smith & Minter (1980) studied the relation between sedimentology and gold/uranium mineralisation on the Leader Reef in the Free State Goldfield and concluded that deposition took place in a fluvial, braided stream setting with placer minerals preferentially concentrated on scour surfaces and as matrix in well-sorted, pebble-supported conglomerates.

Ellis (1981) analysed the depositional and palaeocurrent history of the Middle Reef Zone at Unisel Mine and stressed the point that gold was detritally introduced from the west and northwest into the reef zone by discrete, braided fluvial channel systems, the latter being responsible for its present distribution and concentration. Source materials are thought to represent a mixture of primary detrital materials and reworked Basal Reef deposits from western regions.

Frey (1980, 1981) conducted a sedimentological, geochemical and mineralogical study of the Intermediate Reef Zone in the central Free State Goldfield.

Visser & Kingsley (1982) identified an Upper Carboniferous sediment-filled glacial valley (Virginia Valley) in the Karoo Basin covering parts of the Free State Goldfield, recognized seven lithofacies in a glacial sequence, and constructed a glacial history for the area.

Minter (1982) conducted, on the basis of surface borehole core, a combined sedimentological and geostatistical analysis of the Basal Reef, and compared the evaluation predictions with mining results.

Buck (1983) studied channel-like bodies of quartz arenite in the Harmony Formation within the central Free State Goldfield, with particular interest in the gold- and uranium-bearing Saaiplaas Quartzite Member, which is thought to be a deposit of a northwards prograding, alluvial fan system. The precious minerals were seen to be derived locally from the reworking of the underlying Steyn Placer.

Kingsley (1984) proposed a detailed, fan-delta depositional model for the Dagbreek Formation, as well as for the Leader Reef consisting of two placers, namely the Alma and Bedelia placers, which both are interpreted as braided, eastwards prograding channel-fill deposits upon a fan-delta.

Minter *et al.et al.*. (1985) studied mineralogical changes of the uranium within various reef horizons in the Free State Goldfield and concluded Proterozoic weathering processes to be the cause.

Minter *et al.et al.*. (1986) presented a general and comprehensive overview regarding economical, sedimentological and structural aspects of the Free State Goldfield.

King (1986) analysed and developed a sedimentological model for the Spes Bona and Aandenk Formations in the central Free State Goldfield, identified four and five upwards-fining cycles composing the Spes Bona and Aandenk Formations respectively, as well as identified two distinct placers (Witpan and Uitsig Placers) within the "A"-Reef Zone, and recognized three sub-environments of gold deposition.

Kingsley (1987) proposed for the first time a detailed depositional model for the Eldorado Formation within the Free State Goldfield, postulating that the gravels and sands were deposited from west to east as alluvial fans and then redistributed longitudinally as gravel and sand bars on a broad plain down a southeastward palaeoslope. He contributed the cyclic alluvial fan sedimentation within the Eldorado Formation to syn-sedimentary tectonics.

Minter *et al.* (1988) carried out sedimentological and mineralogical investigations of the conglomerates at the base of the Eldorado Formation from the southern part of the Free State Goldfield and concluded that fluvial and debris flow sediments on the Eldorado palaeosurface contain placer concentrates derived by the repeated erosion of subcropping placers.

Meintjes (1988) and **Meintjes *et al.* (1989)** examined the volcano-sedimentary sequences of Platberg Group basins in the Free State Goldfield on the basis of borehole core data. They established a subdivision of the Platberg Group into five sedimentary units arranged in two major upward-fining sequences and reconstructed the palaeoenvironmental setting for each unit. The deposition of the Platberg Group was interpreted to be controlled by footwall topography, volcanic activity, subsidence/uplift, and growth faulting.

Genis (1990) conducted a detailed sedimentological study of the Eldorado Formation and in particular of the Beatrix Reef at Beatrix Mine, described their lithologic and sedimentary facies and erected depositional models and palaeoenvironmental settings for both. He envisaged the Beatrix Reef to be deposited within a fluvial, braided system on a coarse-grained braid-delta and demonstrated the close relationship between mineralisation and sedimentary facies.

Evans (1990) studied the sedimentology and mineralogy of the EA12-Reef of the Van der Heeversrust Member at Loraine Mine and established that gold mineralisation within the reef package is a primary function of fluvial processes within a fan-delta setting, with post-depositional modification and further gold concentration due to regional metamorphism.

Blamey (1990, 1991) studied the geology and undertook a geostatistical evaluation of the “A”-Reef at No.3 Shaft of Western Holdings Mine.

Bailey (1991) documented the stratigraphy and sedimentology of the Upper Johannesburg and Turffontein Subgroups at St. Helena Mine in the central Free State Goldfield, constructed a tectono-stratigraphic framework and determined the distribution of economic mineralisation.

Minter & Loen (1991) established in a palaeocurrent analysis of various reef horizons throughout the Witwatersrand Basin also the palaeocurrent dispersal pattern of the Basal, Steyn, Saaiplaas, Leader and ‘B’ placers in the Free State Goldfield.

Loen (1992b) estimated for various reef horizons throughout the Witwatersrand Basin, and in particular for the Steyn and Bedelia Reef Facies and VS5 Reef, the distance to the source area, based on rates of pebble-size decrease.

Swart (1992) performed a sedimentary and palaeoenvironmental analysis of the "A"-Reef Zone at Harmony Mine and showed a direct relation between sedimentology and economic gold/uranium mineralisation.

Repsold (1992) studied the stratigraphy, facies types, sedimentary environments and coal seam occurrences/distribution of the Vryheid Formation in the Hennenman area within the eastern FS Goldfield.

Peattie (1993) investigated the depositional setting of the Basal Reef Zone at No.4 Shaft, Saaiplaas Mine, identified two distinct Basal Reef facies and concluded a detrital origin of the gold within.

Mitchell (1993) undertook sedimentological studies on the EA13 Top-Reef of the Eldorado Formation at Loraine Mine, which he envisaged to be derived from a source area to the southwest and deposited within an alluvial fan setting during contemporaneous tectonics activity.

Minter *et al.* (1993) analysed the morphology of gold grains from the Basal Reef and believed to have found unequivocal evidence for their detrital origin.

Dwyer (1993) summarized the geology in particular of the 'A', 'B' and Beatrix reef zones in the Free State Goldfield and discussed the various techniques and other aspects of ore evaluation of Witwatersrand auriferous deposits.

Young & Viljoen (1994) described the stratigraphy, sedimentology and gold distribution of the VS5/Beatrix Composite Reef at H.J. Joel Gold Mine.

Rose (2004) studied the relationship between sedimentology and gold tenor of the Aandenk Reef at Beatrix 3 Shaft and developed a geological model to subdivide the Aandenk geozone and make grade predictions ahead of mining.

Van den Heever (2008) undertook a sedimentological investigation of the B-Reef at Masimong 5 Shaft to establish its depositional environments.

Buys (2014) carried out a stratigraphic and sedimentological study of the depositional environment of the A Reef in the Ventersburg-Hennenman District, thereby establishing its economic value as a low grade, shallow ore body (<1000m below surface) across the Ventersburg Project of Gold One International Ltd.

Shivambu (2016) studied the sedimentology of, and established a depositional model for the VS5 Reef at Beatrix Mine and surrounding areas.

Several extended abstracts from a Free State Goldfield symposium, held in Welkom on 20-21 July 1989 and organized by the Sedimentological Division of the Geological Society of South Africa, provide either reviews of early sedimentological studies or cover various new findings regarding sedimentology, geochemistry, and metamorphism, as well as economical aspects mainly within the Central Rand Group strata of the Free State Goldfield.

Further extended abstracts of contributions at various Geocongresses held in South Africa by the Geological Society represent an additional literature source, regarding stratigraphic and sedimentological aspects within the Free State Goldfield and can be found in the specific congress handouts.

An Aandenk-Spes Bona workshop held in Welkom in 1991 (unpublished) and organized by the Sedimentological Division (O.F.S. Branch) of the Geological Society of South Africa, attempted to solve correlation problems across the goldfield and provides valuable sedimentologic/stratigraphic information.

Three contributions by C. Kingsley, J. Genis and A. Cadle *et al.* to a "Short Course Reviewing Recent Developments In The Understanding Of The Witwatersrand Basin" held by the University of the Witwatersrand on 7-9 April 1992, provided a general overview of the sedimentology and stratigraphy of the Free State Goldfield, as well as a summary of the Beatrix Reef studies at Beatrix Gold Mine, and emphasized the influence of marine processes in the formation of economic Central Rand Group placers in the Free State Goldfield and elsewhere, respectively.

METAMORPHISM

Borrego (1986) and **Borrego & Phillips (1987)** examined mineralogically and geochemically three shale horizons in the Free State Goldfield and proved widespread greenschist facies metamorphism involving temperatures of 350 ± 50 °C throughout the Free State Goldfield. They drew comparison with metamorphic conditions in Archaean greenstone belts and the other Witwatersrand goldfields and invalidated an earlier suggestion that the Free State Goldfield lacks metamorphism.

Ramos (1987) conducted petrographic and geochemical studies on shales at Harmony Mine, and determined quantitatively the syn-metamorphic alteration process in the mineral assemblage of these lithologies.

Law (1990) examined the mineralogy, geochemistry and alteration of Witwatersrand meta-sediments in the Welkom area, evaluated their post-depositional evolution from diagenesis to regional greenschist facies metamorphism associated with hydrothermal alterations of the initial detrital mineral assemblages, and proposed a new classification scheme for Witwatersrand quartzites.

STRUCTURE

Borchers & White (1943) and **Frost *et al.* (1946)** presented initial interpretations of the pre-Karoo structure within of the Free State Goldfield, which were solely based on surface exploration borehole data.

Borchers (1950) provided a comprehensive structural interpretation of the Odendaalsrus-Virginia area and described the formation of a border fault, parallel to the western margin of the Free State Goldfield and Witwatersrand Basin, which was contemporaneous with deposition of the sediments to the east of the fault-scarp. He envisaged the structure to be responsible for the formation of the Elsburg reefs.

Antrobus (1952) identified similar groups of faults on President Steyn Mine and derived at similar conclusions as Schwellnus (1953) concerning age relationships. He regarded flat or bedding-plane faults as the youngest and made the significant observation, that the east-trending faults would cause structural complications due to their strike-slip component and their wide, water-bearing fracture zones.

Schwellnus (1953) classified the faults within the Free State Goldfield into eight groups and assumed that the main group of faults existing within goldfield would be normal, steeply dipping to the west. Notably none of the major north-trending, westward dipping faults had been intersected by underground development at that time, and were only interpreted on the basis of surface borehole data.

He further recognized younger, approximately east/west-trending strike-slip faults cutting these major north-striking normal faults.

Antrobus (1953) observed: "It is almost certain that there has been horizontal shift of the west-side north on the north-trending west-dipping faults...". The amount of lateral shift remained unsolved.

Ferringa (1954) interpreted the structure of the Free State Goldfield on the basis of surface borehole data and showed, contrary to the prevailing belief that the structure is determined by faulting only, that folding occurred prior to the faulting and has played an important part in the tectonics of the goldfield. He identified faults of different ages, recognized reactivation of the normal De Bron Fault in form of reverse movements, and emphasized the influence of faulting on the preservation of economic horizons in grabens.

Brock (1954) pointed out that in the Welkom Sector the auriferous reefs have been preserved in the Odendaalsrus Graben, bounded by the De Bron and the "Border" faults. Types of faults encountered on some of the mines are described and practical applications given to faulting induced mining problems.

Van der Vyver (1956) described the general structure of the Loraine Mine area as inferred from surface borehole information. He supported the border fault idea of Borchers (1950).

Pienaar (1956) studied the Ventersdorp System in the Free State Goldfield and analysed its syn-depositional tectonic evolution, with faulting commencing prior to the cessation of volcanity of Ventersdorp Lower Lava, followed by intensification of faulting during deposition of Ventersdorp Upper Sediments and cessation of faulting prior to extrusion of Ventersdorp Upper Lava.

Winter (1957) conducted, besides of the stratigraphy, a comprehensive study of the structure of the Upper Witwatersrand Division at the Virginia and Merriespruit mines.

Coetzee (1960) covered in his comprehensive overview of the geology of the Free State Goldfield, among various other aspects, in detail the general structural geology of the goldfield, by describing major faults and fault-bounded blocks, as well as types and ages of faults and folding, and supported the idea of a "Border Fault" to the west of the goldfield, which he named as such.

McKinney *et al.* (1964) described types and ages of faults and folds encountered in Anglo American mines within the central Free State Goldfield and summarized the tectono-sedimentary history of the area.

Winter (1964a/b) presented two studies concerning the geology of Loraine and Harmony mines, with particular emphasis of the structure of the western margin and the Merriespruit Thrust respectively. He postulated 2.7 km of dextral displacement on the De Bron Fault on the western side of Harmony Mine, by calculating the amount of displacement on the basis of the Leader Reef-subcrop. He further contributed much to the understanding of the syn-Witwatersrand depositional tectonics in the Loraine Mine area.

Olivier (1965) studied the structure of the Upper Witwatersrand System in the Loraine Mine area. He recognized a relationship between sedimentation and syn-depositional thrusting and folding during Elsburg time, and described three post-Witwatersrand tectonic periods of Klipriviersberg, Platberg and post-Ventersdorp age.

Collins (1967) investigated the structure of Freddies Consolidated Mine, described the age and origin of major structural features, and acknowledged structural control on sedimentation since Basal-Reef time.

Pienaar (1969) envisaged pre-Basal Reef folding to have controlled the deposition and gold distribution of the Basal Reef on Saaiplaas Mine.

Sims (1969) recognized syn-depositional tectonics in form of gentle folding of the basin and movements along the "Border Fault" in Upper Witwatersrand time, controlling sedimentation and gold distribution.

Ellis (1981) envisaged tectonic activity to have played an important part in the nature and cyclicity of the deposition of the Middle Reef Zone at Unisel Mine.

Dell (1982) studied the Dagbreek Fault at Western Holdings Mine and concluded the fault to be a complex system, which formed as a tear fault under a compressive stress regime in pre-Ventersdorp time, with later reactivation and vertical movement.

Tweedie (1986) described the discovery and exploration of Beisa and Beatrix mines and outlined the late-Central Rand syn-sedimentary tectonics, as well as the structure of the western margin of the southern Free State Goldfield.

Minter *et al.* (1986) covered in his comprehensive geological overview of the Free State Goldfield also aspects regarding the structural setting and evolution of the goldfield.

Meintjes (1988) and **Meintjes *et al.* (1989)** considered syn-depositional growth faulting to have controlled sedimentation during Platberg Group time and envisaged wrench tectonics to be of post-Ventersdorp age.

Bailey (1991) studied the stratigraphy and sedimentology of the Central Rand Group on St. Helena Mine, and identified syn-depositional tectonics as controlling factor of sedimentation during that time.

Swart (1992) recognized syn-sedimentary tectonics controlling the deposition of the "A"-Reef Zone at Harmony Mine.

Mitchell (1993) identified compressional, structural features like thrusts and folds along the western basin margin at Loraine Gold Mine, which controlled sedimentation of the EA13-Reefs (Eldorado Formation).

Rompel (1995) described the structural geology and tectonic history of the central Welkom Sector within the Free State Goldfield, and analysed mineralogically and geochemically dyke intrusives for calculating the strike-slip magnitude along major faults.

APPENDIX 2

SURFACE BOREHOLE LOCATION PLANS

The collar position and name of surface borehole intersections that were utilized for the construction of isopach and elevation contour maps for various stratigraphic intervals (see Chapter 2), are illustrated in surface borehole location plans (Appendices 2-A - 2-G) individually for the:

APPENDIX 2-A : Harmony Formation

APPENDIX 2-B : Dagbreek Formation

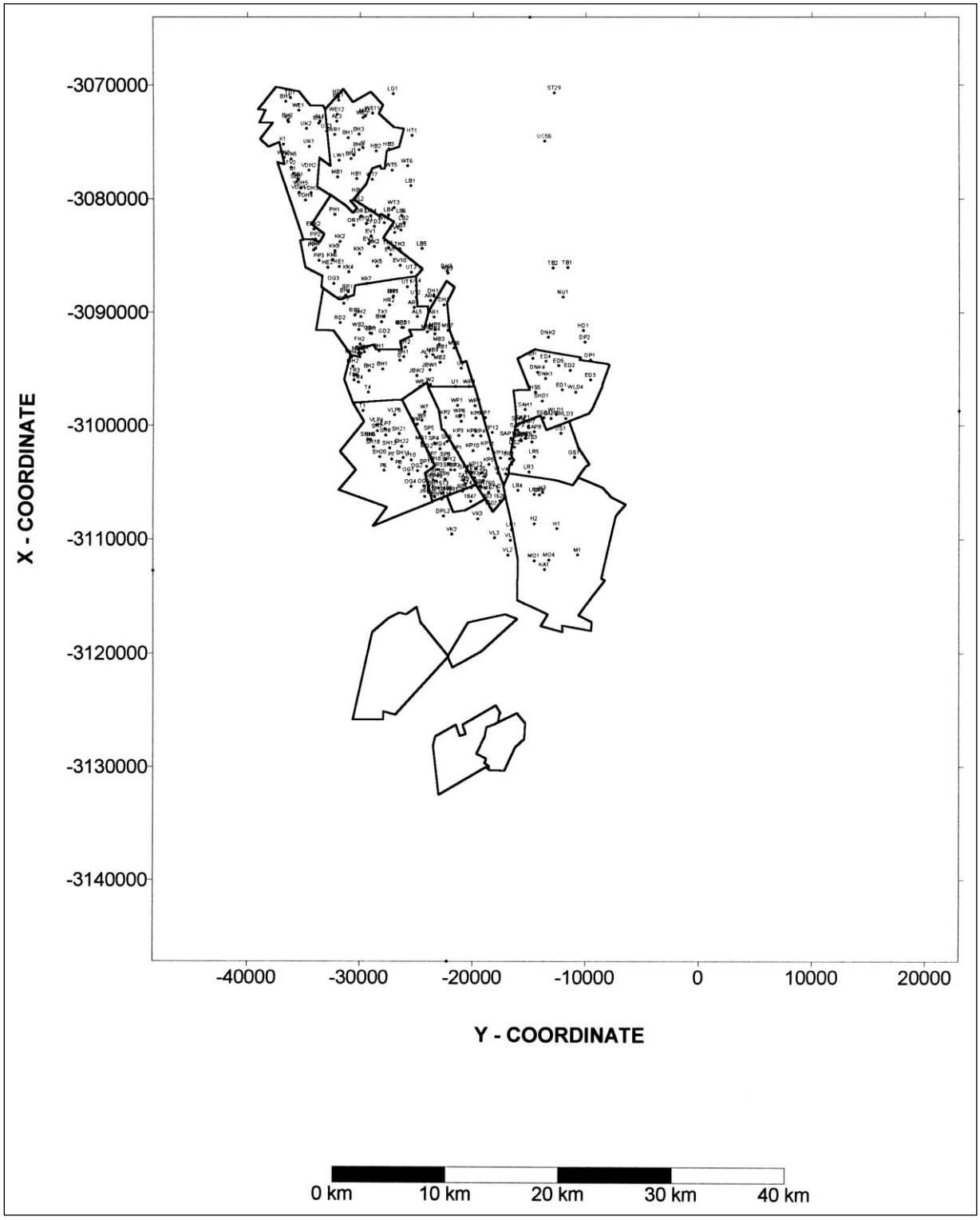
APPENDIX 2-C : Kimberley Formation

APPENDIX 2-D : 'B'-Reef

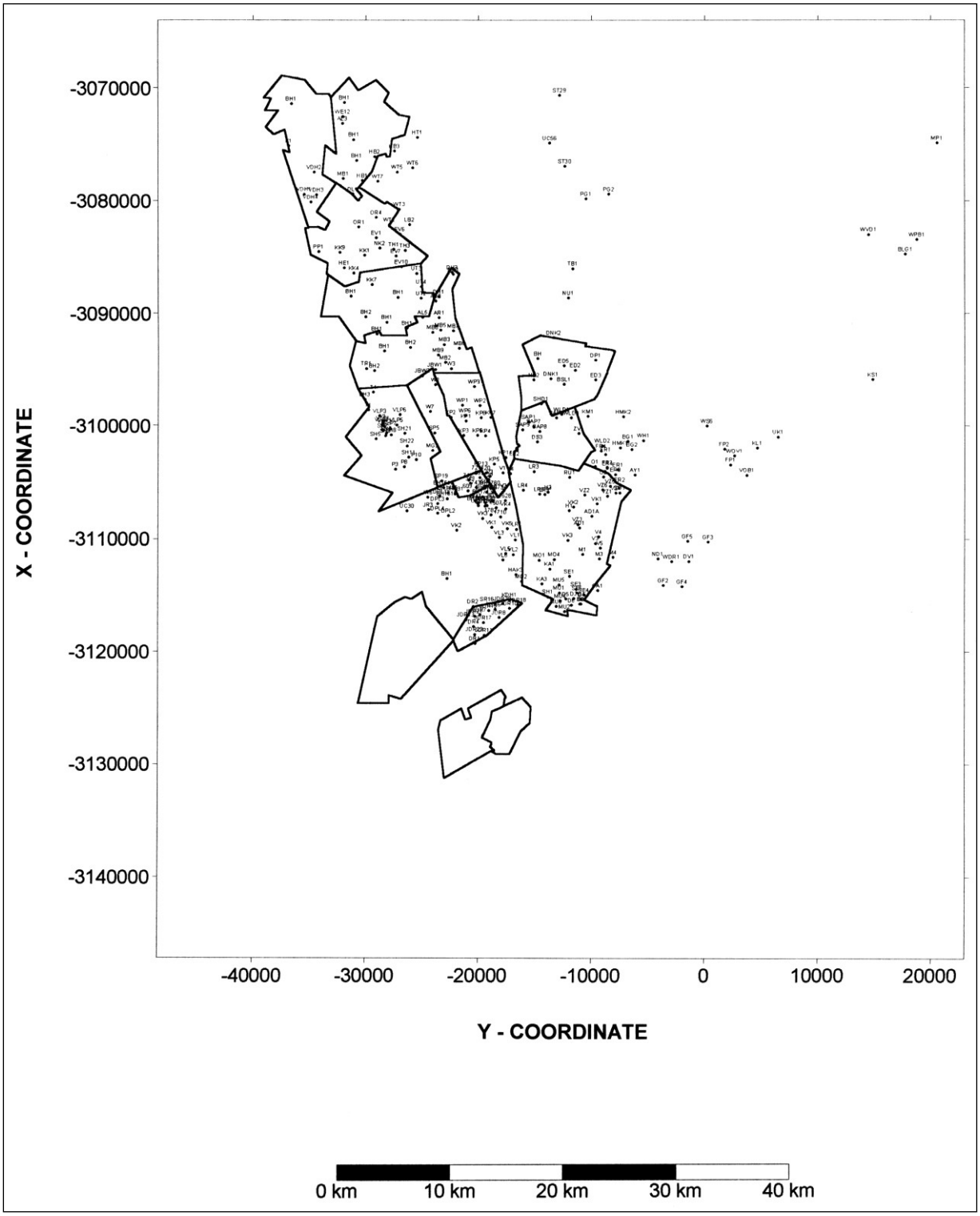
APPENIDX 2-E : Eldorado Formation

APPENDIX 2-F : VS5 Reef Zone

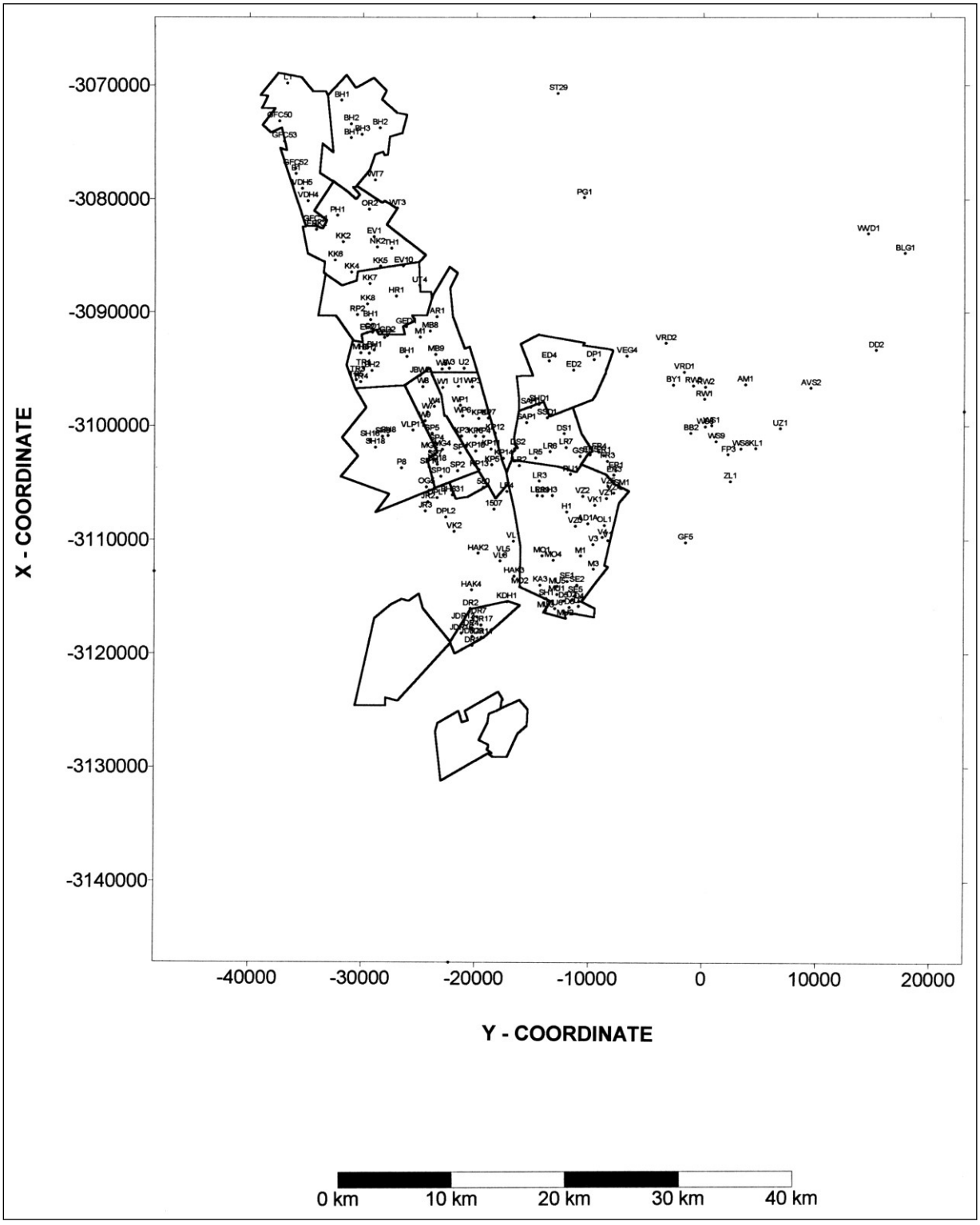
APPENDIX 2-G : Karoo Supergroup



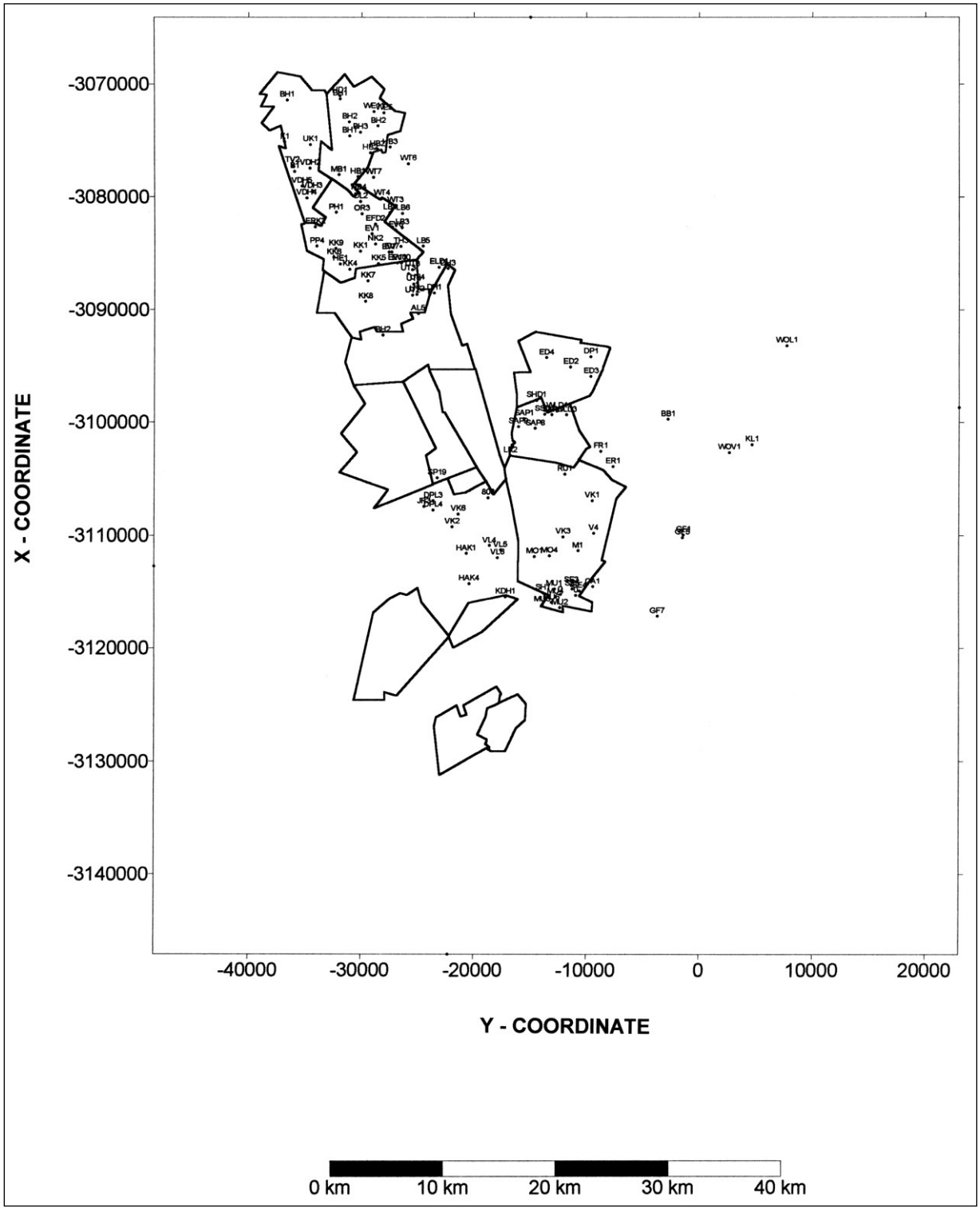
APPENDIX 2-A : Surface borehole location plan for intersections of the Harmony Formation in the Free State Goldfield.



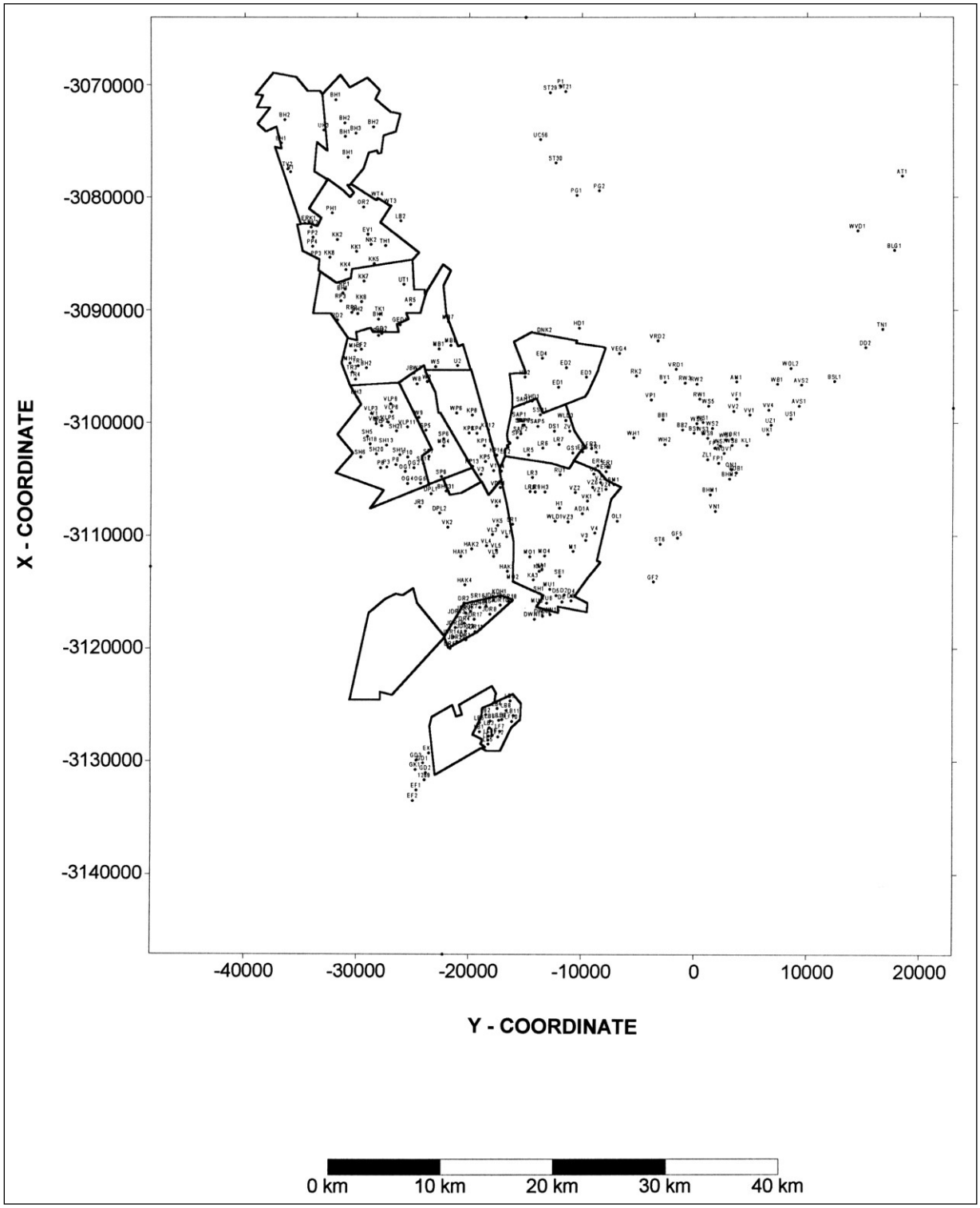
APPENDIX 2-B : Surface borehole location plan for intersections of the Dagbreek Formation in the Free State Goldfield.



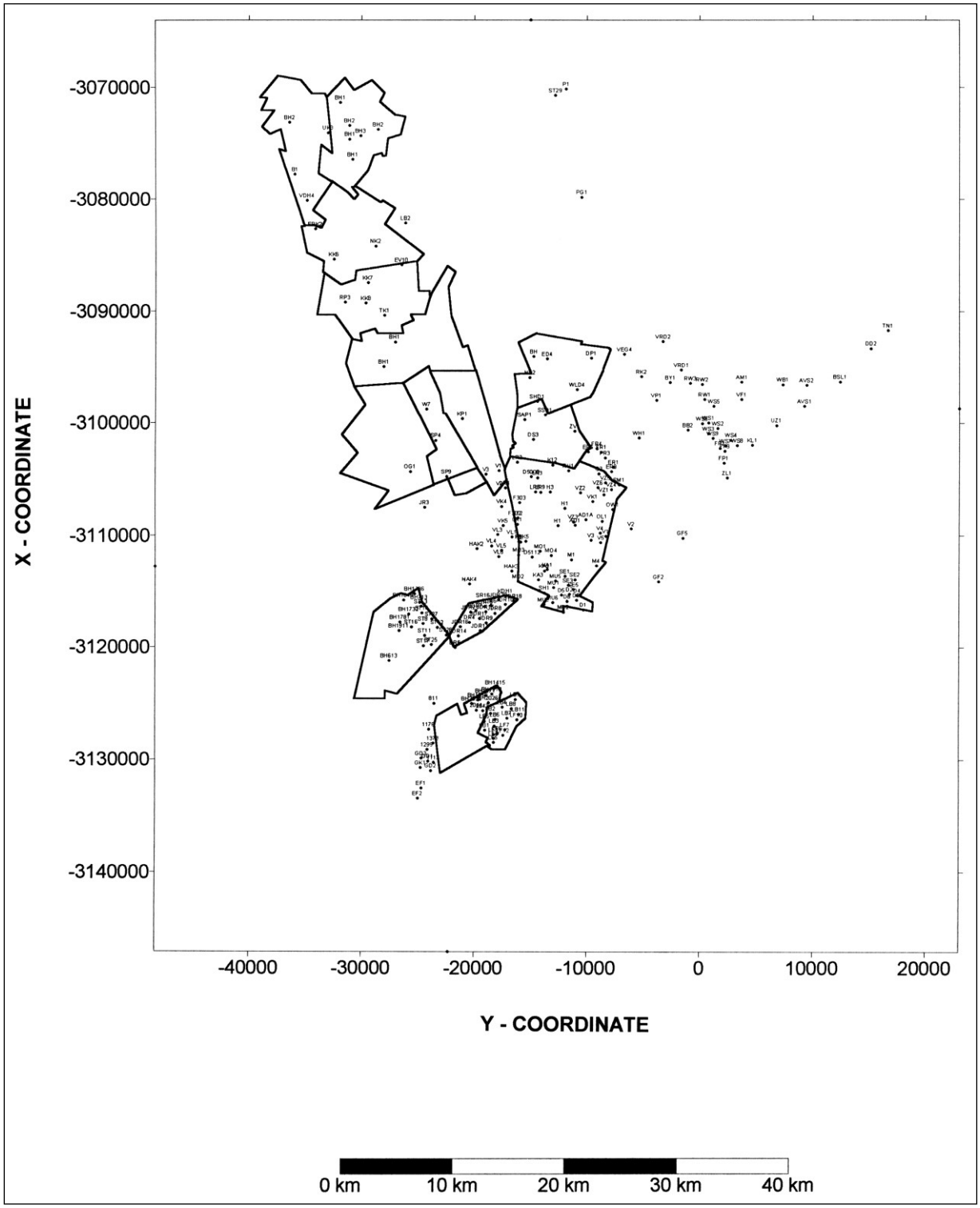
APPENDIX 2-C : Surface borehole location plan for intersections of the Kimberley Formation in the Free State Goldfield.



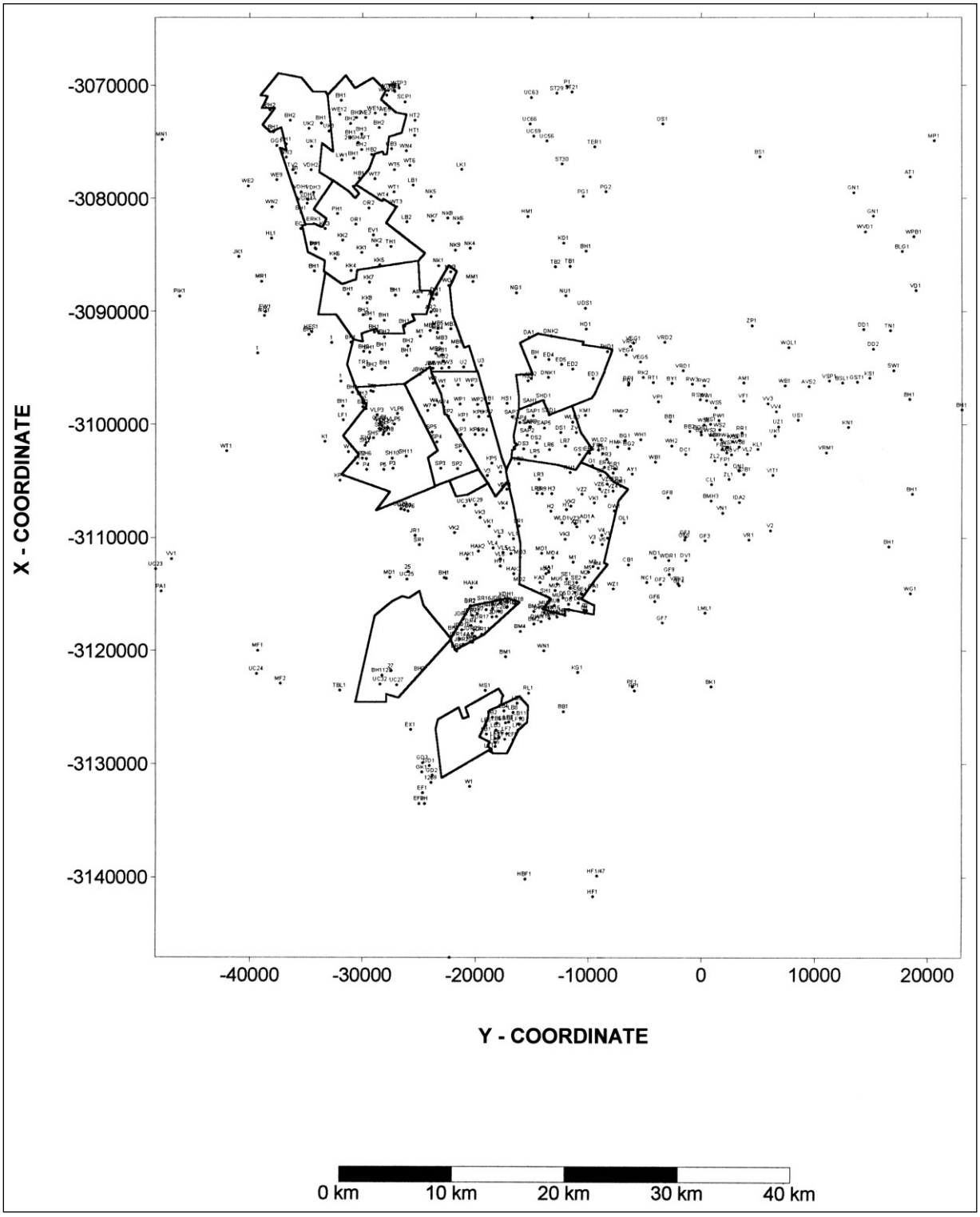
APPENDIX 2-D : Surface borehole location plan for intersections of the 'B' Reef in the Free State Goldfield.



APPENDIX 2-E : Surface borehole location plan for intersections of the Eldorado Formation in the Free State Goldfield.



APPENDIX 2-F : Surface borehole location plan for intersections of the VS5 Reef Zone in the Free State Goldfield.



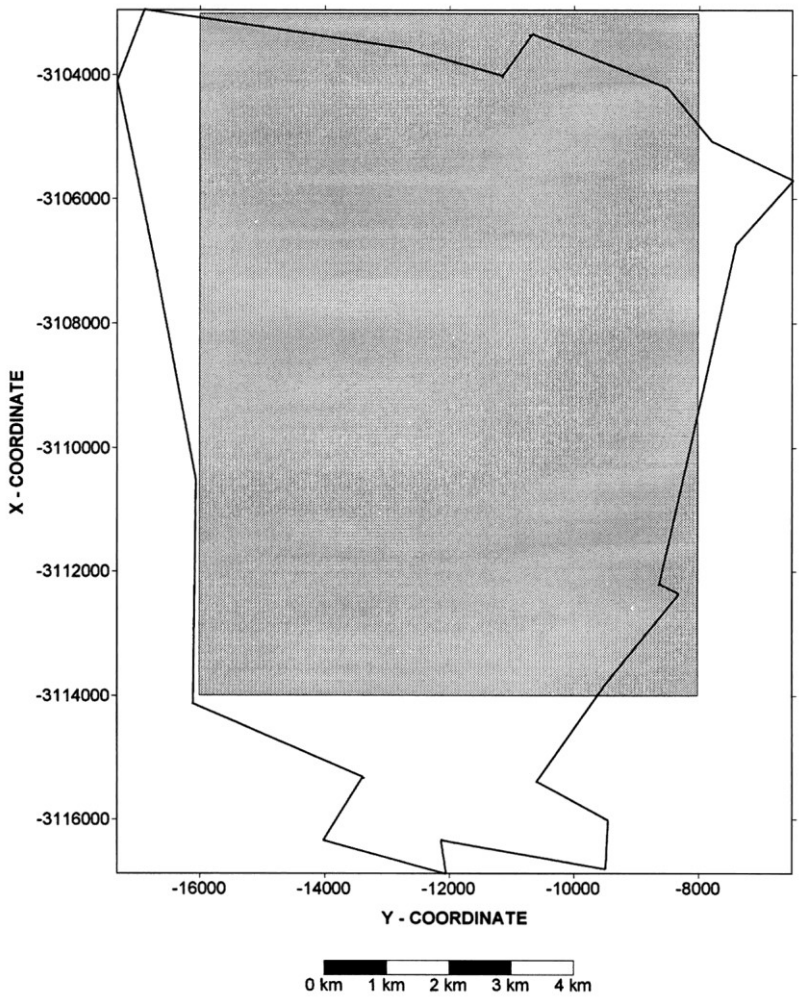
APPENDIX 2-G : Surface borehole location plan for intersections of the Karoo Supergroup in the Free State Goldfield.

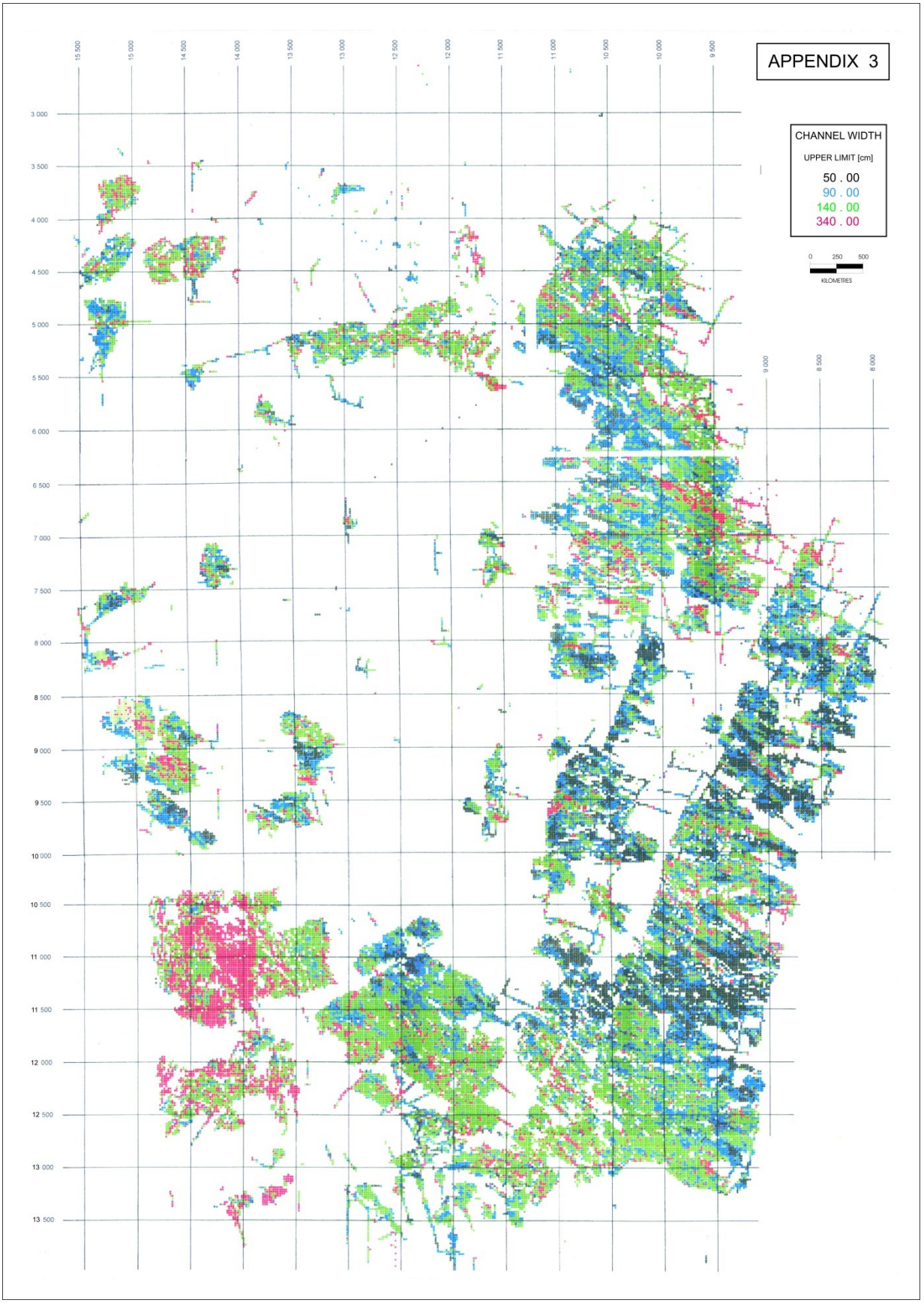
APPENDIX 3

COMPUTER-GENERATED CHANNEL THICKNESS-PLOT FOR THE BEDELIA PLACER AT HARMONY GOLD MINE

The channel thickness-plot of the Bedelia Placer (Leader Reef Zone) at Harmony Gold Mine represents individual values determined by averaging four thickness measurements taken at 5 m horizontal intervals in underground excavations; hence, these values represent averages over 20 m^2 blocks.

Diagram below illustrates the lease area of Harmony Gold Mine and the area covered by the channel thickness-plot.



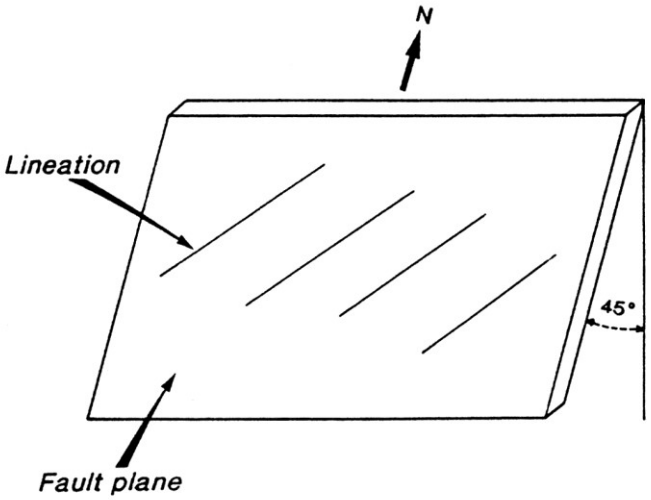


APPENDIX 3 : Channel thickness-plot of the Bedelia Placer (Leader Reef Zone) at Harmony Gold Mine (provided courtesy of Harmony Gold Mine, 1992). Note: The plot represents individual values determined by averaging four thickness measurements taken at 5 m horizontal intervals in underground excavations; hence, these values represent averages over 20 m^2 blocks.

APPENDIX 4

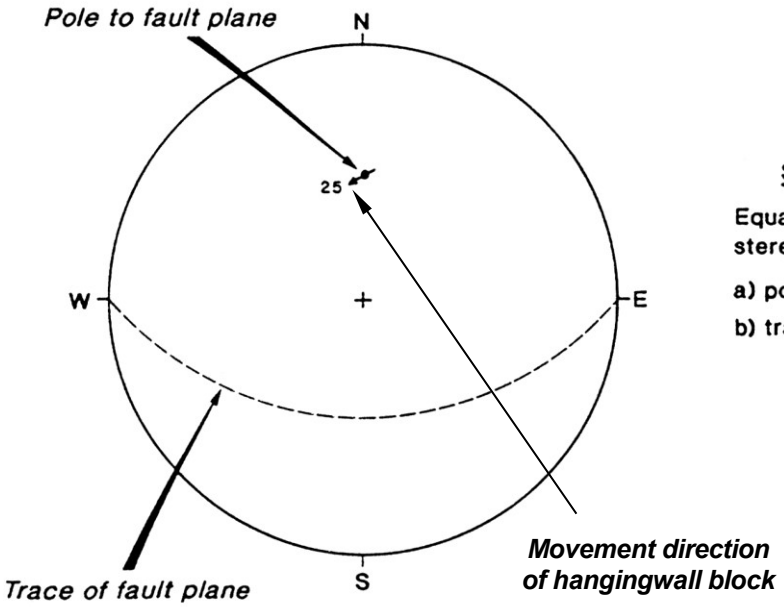
DIAGRAMMATIC REPRESENTATION OF THE CONCEPT OF A SLIP LINEAR DIAGRAM

The following diagrams illustrate the representation of movement orientation data (lineations) using a slip linear diagram (see also Aleksandrowski, 1985). A slip linear diagram represents the trend and plunge of lineations plotted at the position of the pole to the corresponding fault plane. The trace of the fault has been added to the diagram below only for the purpose of better understanding.



ORIENTATION READINGS

Fault plane : 180/45 (dip-direction/dip-angle)
Lineation : 240/25 (trend/plunge)
Sense of movement : oblique - normal



SLIP LINEAR DIAGRAM

Equal - area lower hemisphere stereographic projection of:-

a) pole to fault plane
b) trace of fault plane

APPENDIX 5

DIAGRAMMATIC REPRESENTATION OF CLEAVAGE VERGENCE AND THE METHOD OF DETERMINATION

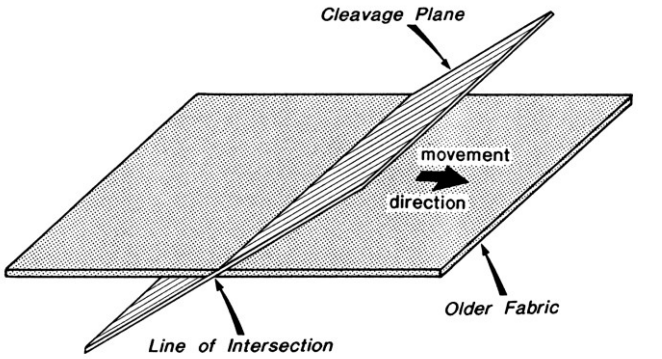
"Cleavage vergence is defined as the horizontal direction within the plane normal to the fabric intersection lineation, towards which a younger fabric needs to be rotated (through the acute angle) so that it becomes parallel to the older fabric" (Bell, 1981).

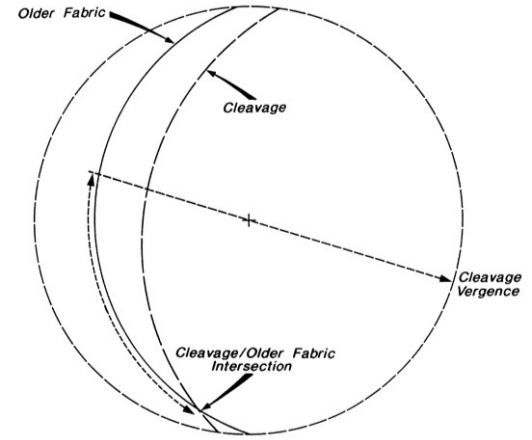
In thrust tectonics the cleavage vergence can be used to give a rough idea of the movement direction. The assumption is made in this study that the bedding or the fault plane are the planes in which movement takes place (Y shear) and correspond to the 'older fabric' in the definition. The direction of movement in this plane is assumed to be perpendicular to the intersection between the cleavage (P shear) and the 'older fabric'.

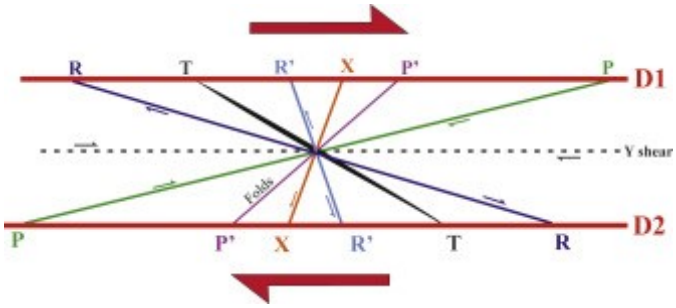
This concept is shown graphically in the attached diagram where the stereographic procedure for determining cleavage vergence is also outlined.

Analogous to the concept of cleavage vergence, the Riedel (R shear) vergence method (Wilcox *et al.*, 1973) has been applied to strike-slip and brittle normal-slip tectonics in this study.

A comparison between measured movement directions (*e.g.* slickenfibres, slickensides) and those calculated with the cleavage and Riedel vergence methods, has revealed good agreement between the measured and calculated movement vectors, thus confirming the reliability and accuracy of both methods, as well as the applicability of the Riedel vergence method for brittle deformation analogously to the cleavage vergence concept for ductile deformational processes.







APPENDIX 6

DIAGRAMMATIC REPRESENTATION OF A STRESS FIELD ANALYSIS

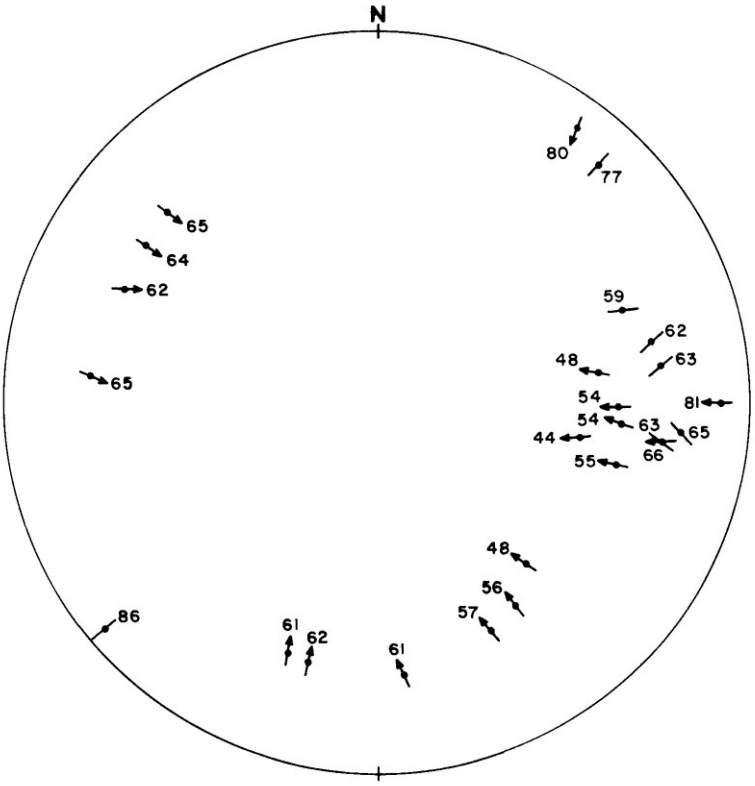
The procedure and results of a stress field analysis, which was carried out for different fault groups established within the present mining area of H.J. Joel Gold Mine (see Chapter 2.1), is graphically presented (Appendices 6-A1 - A6, 6-B1 - B9, 6-C1 - C10 & 6-D1 - D12) below for:

Group A (Cataclastic faults with normal dip-slip lineations)

Group B (Cataclastic faults with oblique-normal lineations)

Group C (Mylonitic faults with strike-slip lineations)

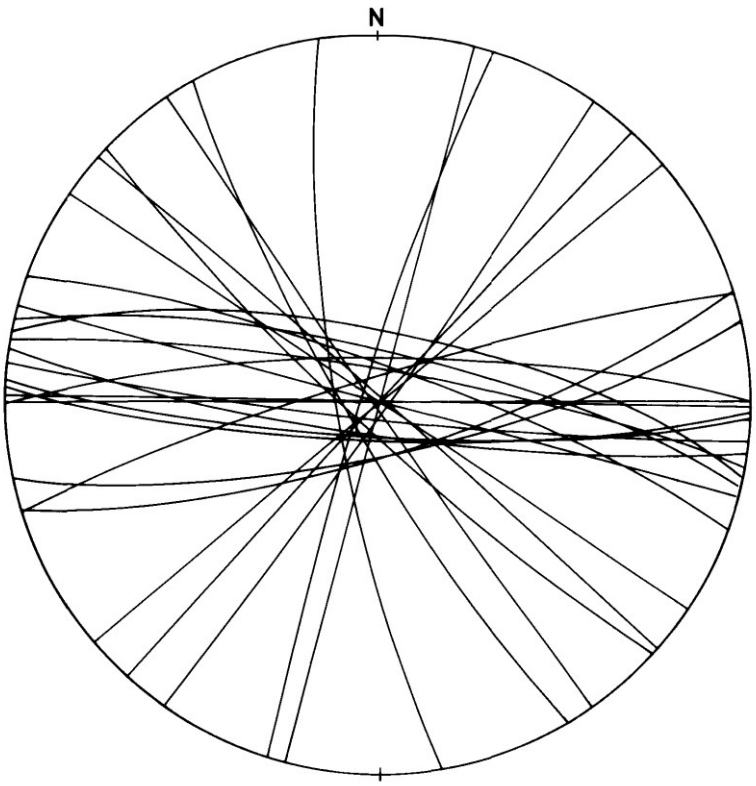
Group D (Mylonitic faults with oblique-reverse lineations)



A1

SLIP LINEAR DIAGRAM

No. of slip linears = 31

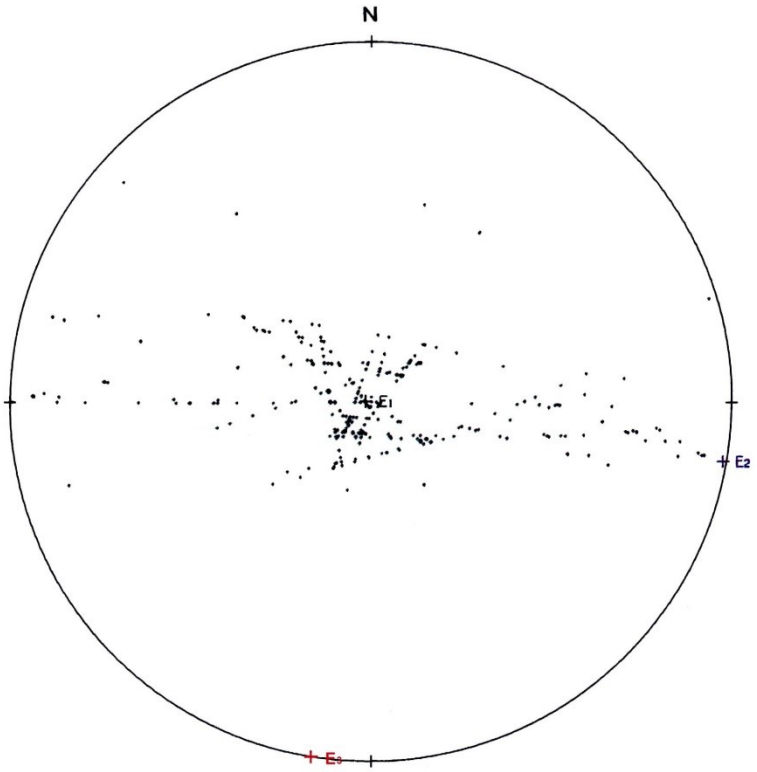


A2

M-PLANE DIAGRAM

No. of m-planes = 31

APPENDIX 6 : Diagrammatic representation of a stress field analysis for Fault Group A (A1-A2): Cataclastic faults with normal dip-slip lineations.



A3

M-PLANE INTERSECTION DIAGRAM

No. of intersections = 460

Equal-area scatter plot

TREND	PLUNGE	EVALS/460
282.1	88.9	0.8105
99.6	1.1	0.1679
189.6	0.0	0.0216

A4

PROBABILITY DENSITY DIAGRAM

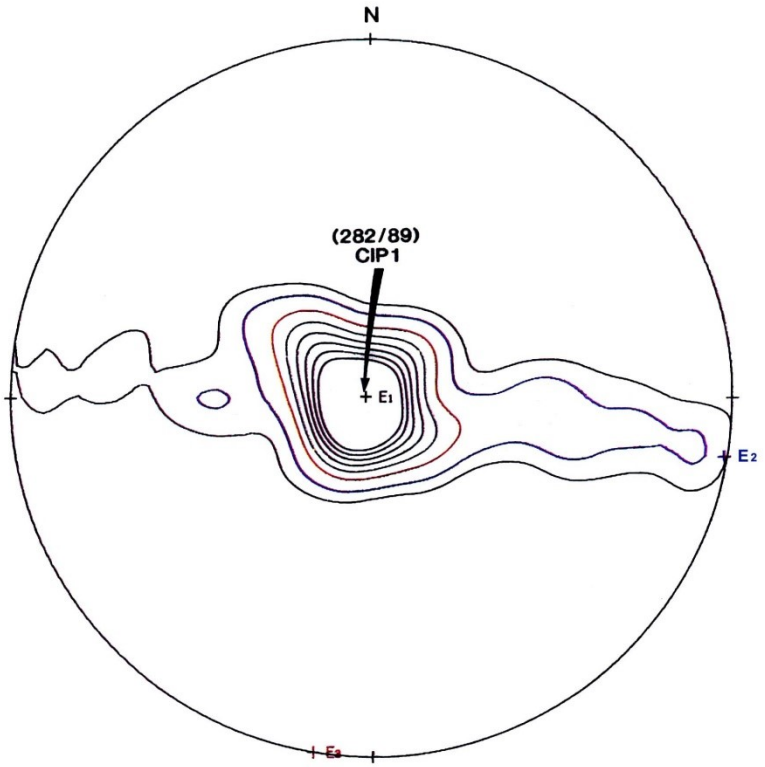
No. of intersections = 460

Concentration parameter = 100

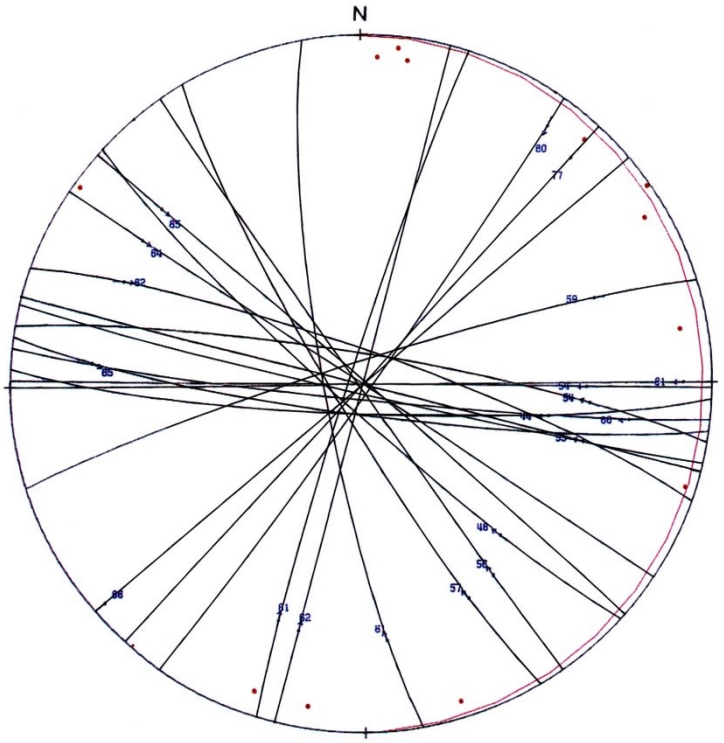
Contours are multiples of a uniform density

Contours at densities of:-

1 2 4 6 8 10 12 14



APPENDIX 6 : Diagrammatic representation of a stress field analysis for Fault Group A (A3-A4): Cataclastic faults with normal dip-slip lineations.



A5

SUBSET OF CATACLASITES FOR CIP1

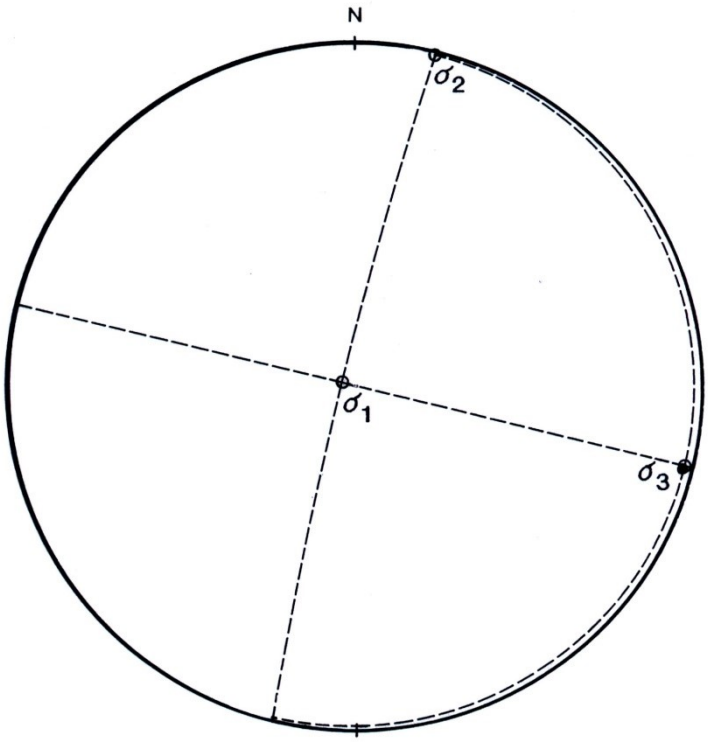
No. of faults = 25

M-PLANE

GCF

GCP

SIGMA 104 3



A6

SIGMA SYNOPTIC DIAGRAM

No. of stress axes = 1

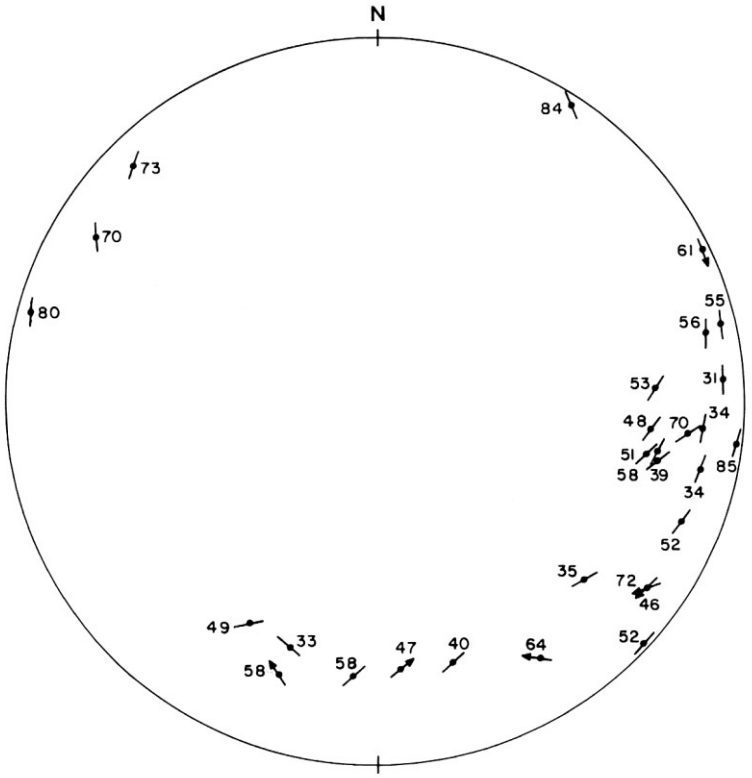
Principal stress axis positions:

σ_1 = 284/87

σ_2 = 14/0

σ_3 = 104/03

APPENDIX 6 : Diagrammatic representation of a stress field analysis for Fault Group A (A5-A6): Cataclastic faults with normal dip-slip lineations.



B1

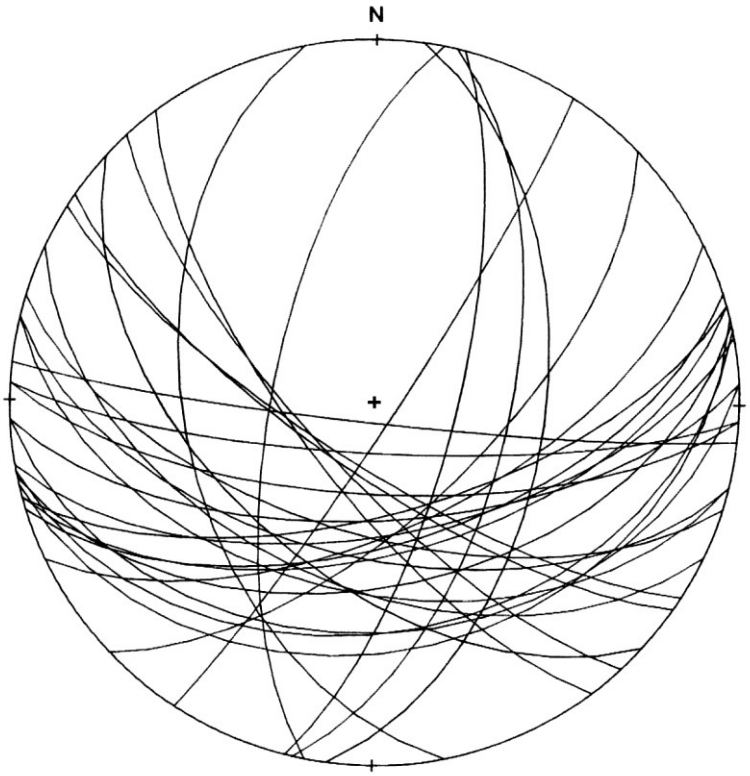
SLIP LINEAR DIAGRAM

No. of slip linears = 35

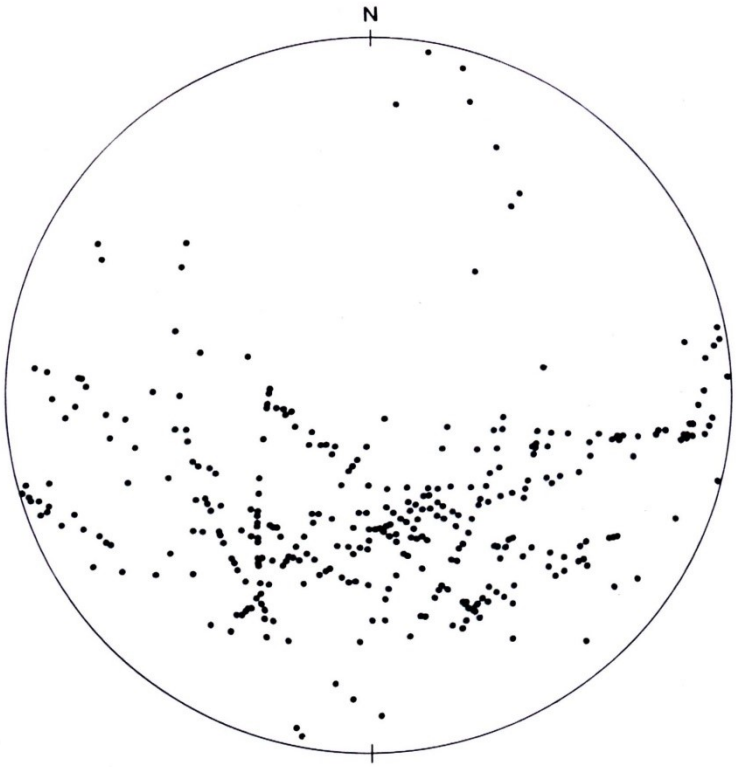
B2

M-PLANE DIAGRAM

No. of m-planes = 35



APPENDIX 6: Diagrammatic representation of a stress field analysis for Fault Group B (B1-B2): Cataclastic faults with oblique-normal lineations.

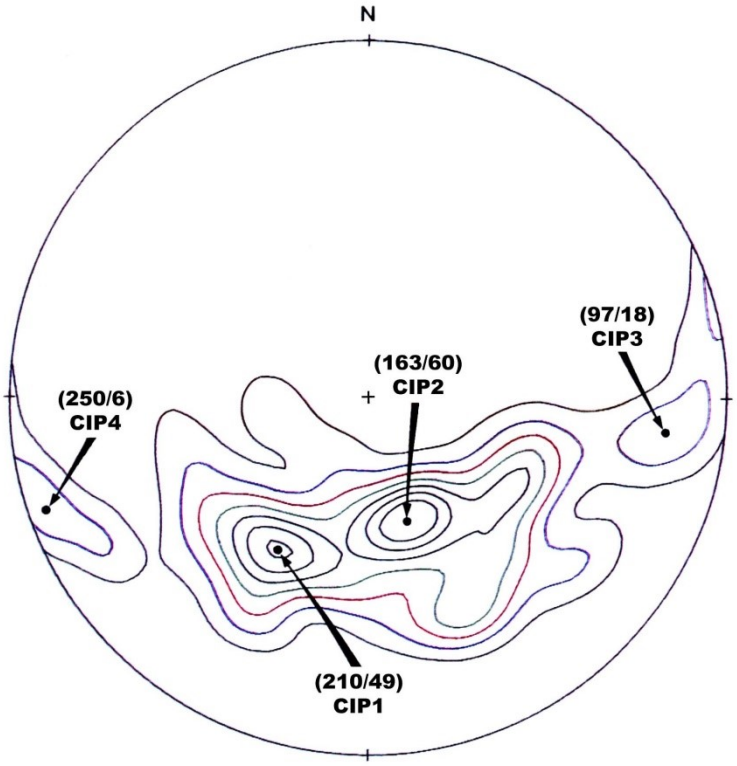


B3

M-PLANE INTERSECTION DIAGRAM

No. of intersections = 589

Equal-area scatter plot



B4

PROBABILITY DENSITY DIAGRAM

No. of intersections = 589

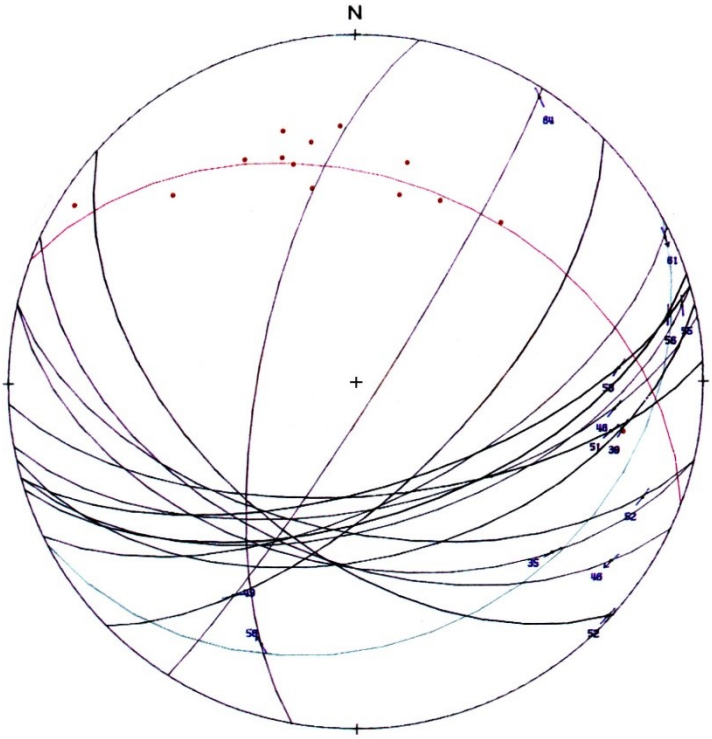
Concentration parameter = 100

Contours are multiples of a uniform density

Contours at densities of:-

1 2 3 4 5 6 7

APPENDIX 6: Diagrammatic representation of a stress field analysis for Fault Group B (B3-B4): Cataclastic faults with oblique-normal lineations.



B5

SUBSET OF CATACLASITES FOR CIP1

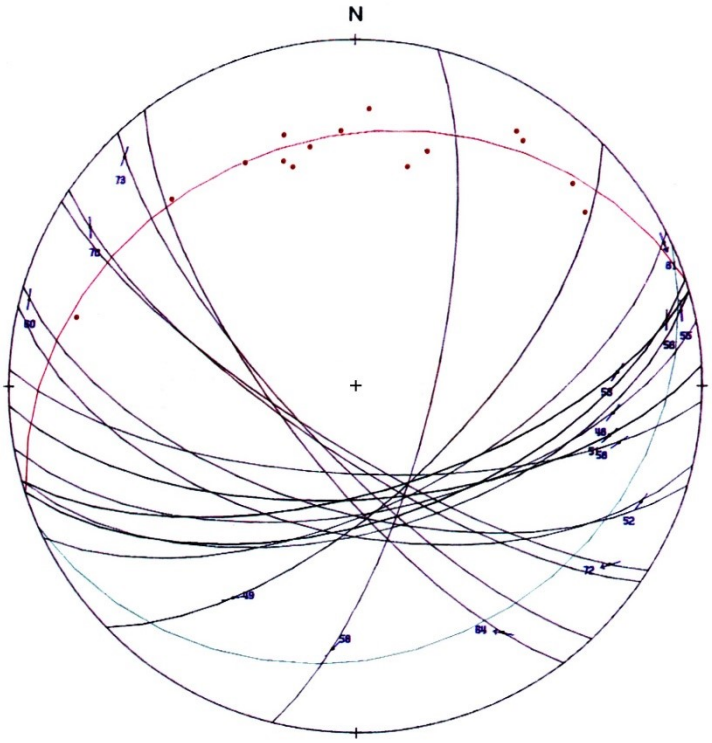
No. of faults = 19

M-PLANE

GCF

GCP

SIGMA 94 14



B6

SUBSET OF CATACLASITES FOR CIP2

No. of faults = 18

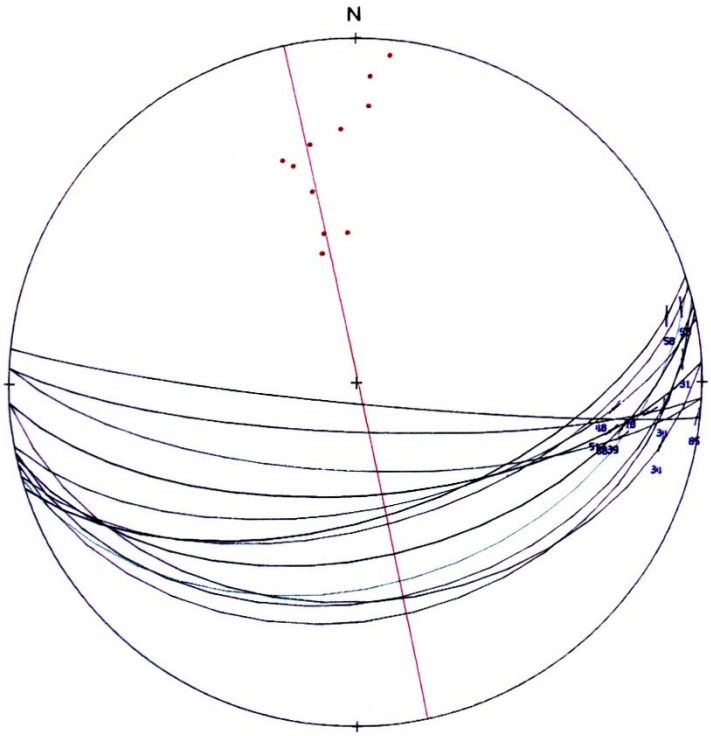
M-PLANE

GCF

GCP

SIGMA 70 2

APPENDIX 6 : Diagrammatic representation of a stress field analysis for Fault Group B (B5-B6): Cataclastic faults with oblique-normal lineations.



B7

SUBSET OF CATACLASITES FOR CIP3

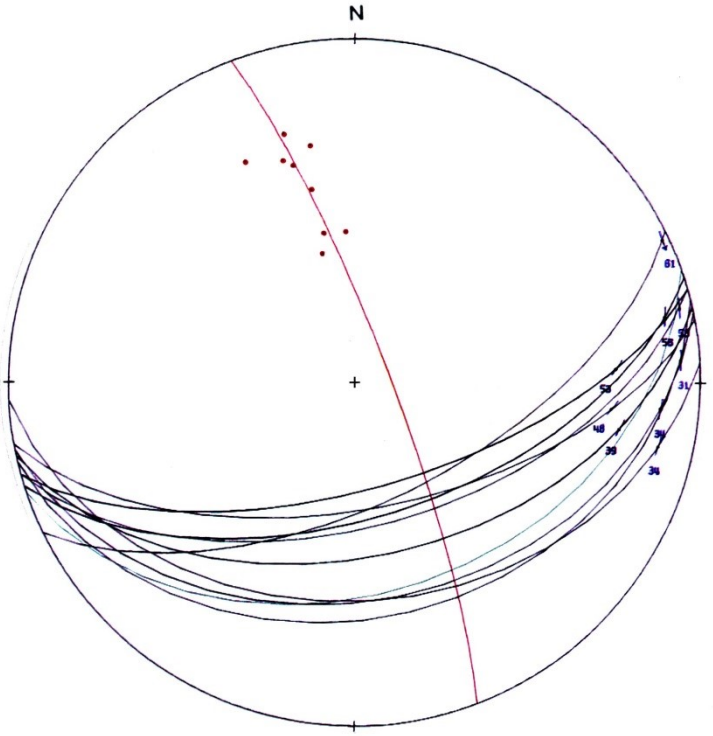
No. of faults = 14

M-PLANE

GCF

GCP

SIGMA 168 40



B8

SUBSET OF CATACLASITES FOR CIP4

No. of faults = 12

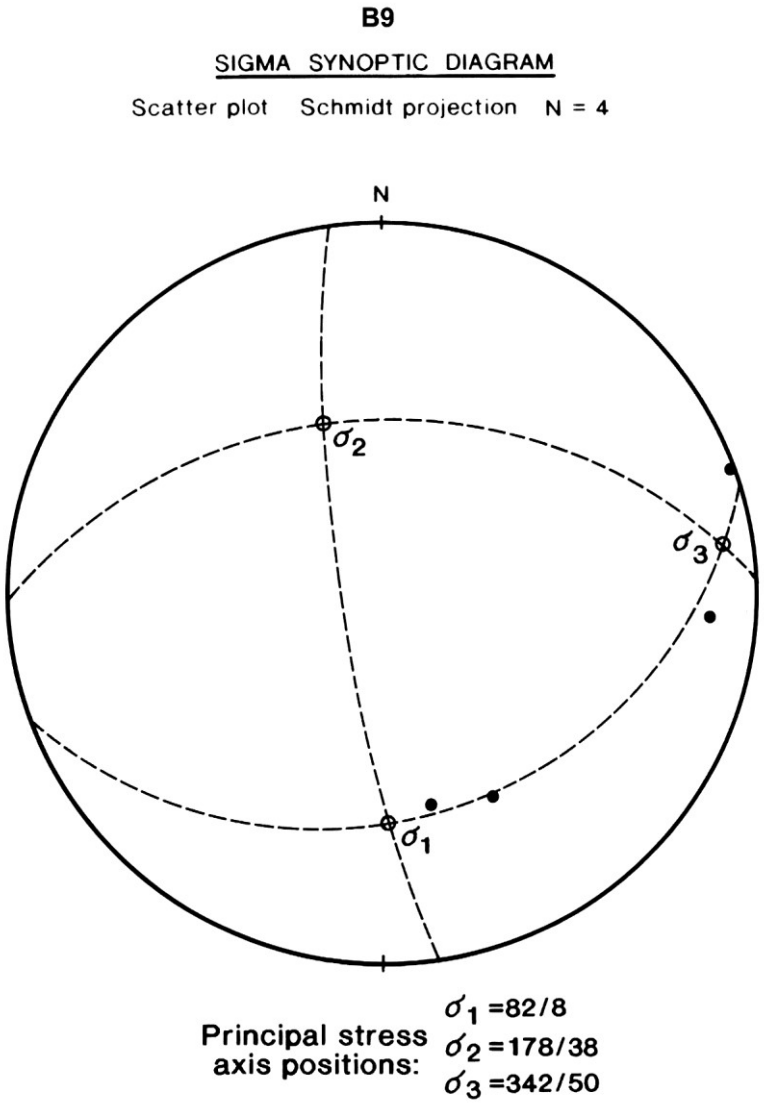
M-PLANE

GCF

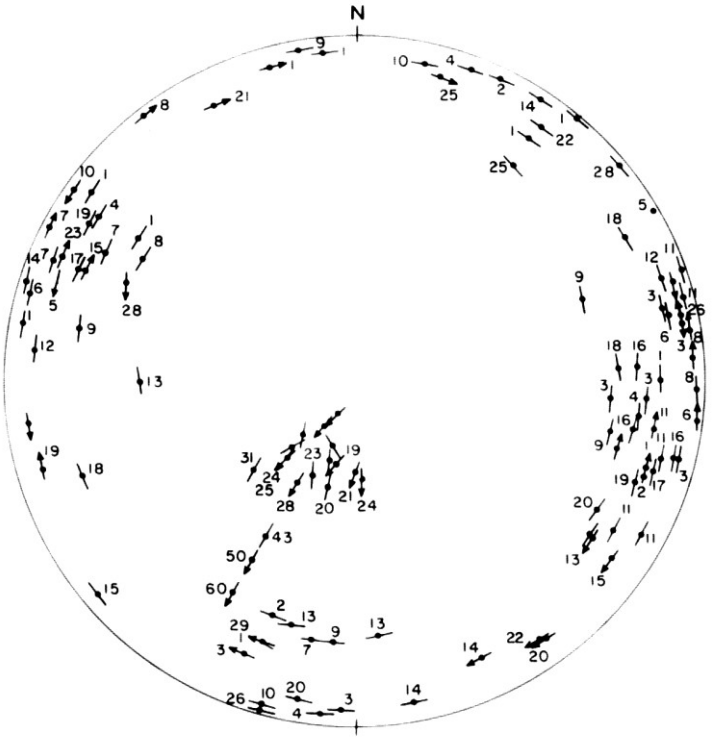
GCP

SIGMA 153 38

APPENDIX 6 : Diagrammatic representation of a stress field analysis for Fault Group B (B7-B8): Cataclastic faults with oblique-normal lineations.



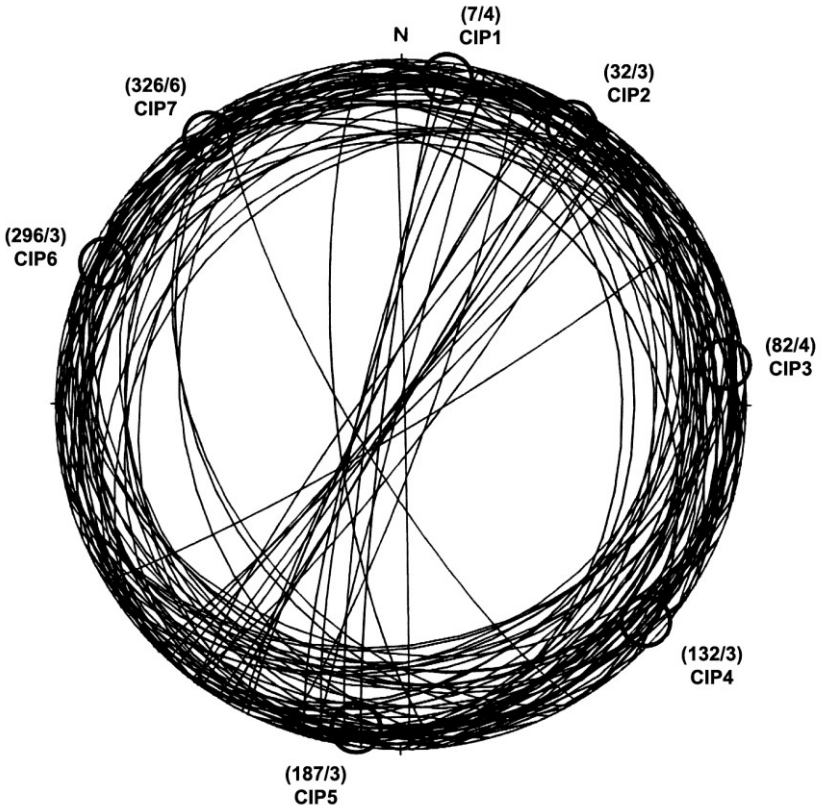
APPENDIX 6 : Diagrammatic representation of a stress field analysis for Fault Group B (B9): Cataclastic faults with oblique-normal lineations.



C1

SLIP LINEAR DIAGRAM

No. of slip linears = 137

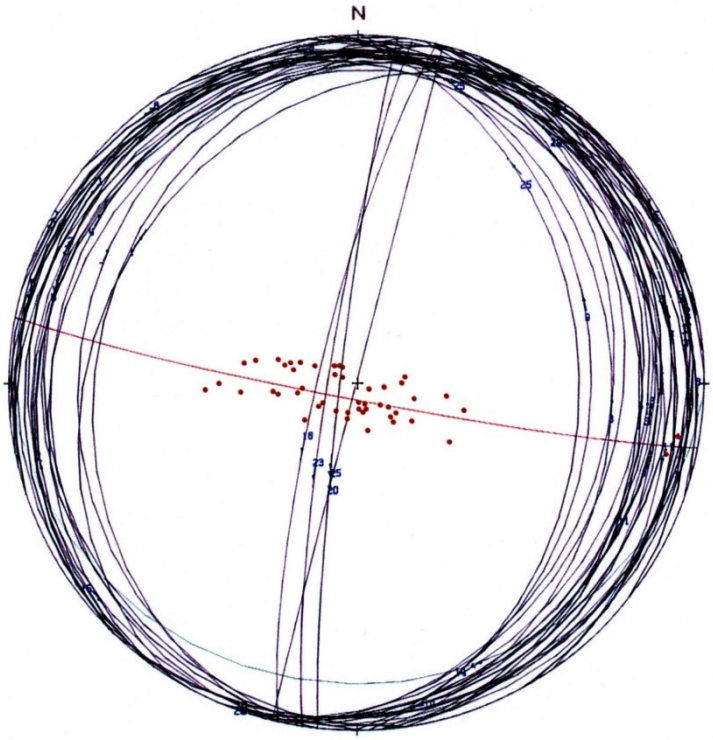


C2

M-PLANE DIAGRAM

No. of m-planes = 137

APPENDIX 6 : Diagrammatic representation of a stress field analysis for Fault Group C (C1-C2): Cataclastic faults with oblique-normal lineations.



C3

SUBSET OF MYLONITES FOR CIP1

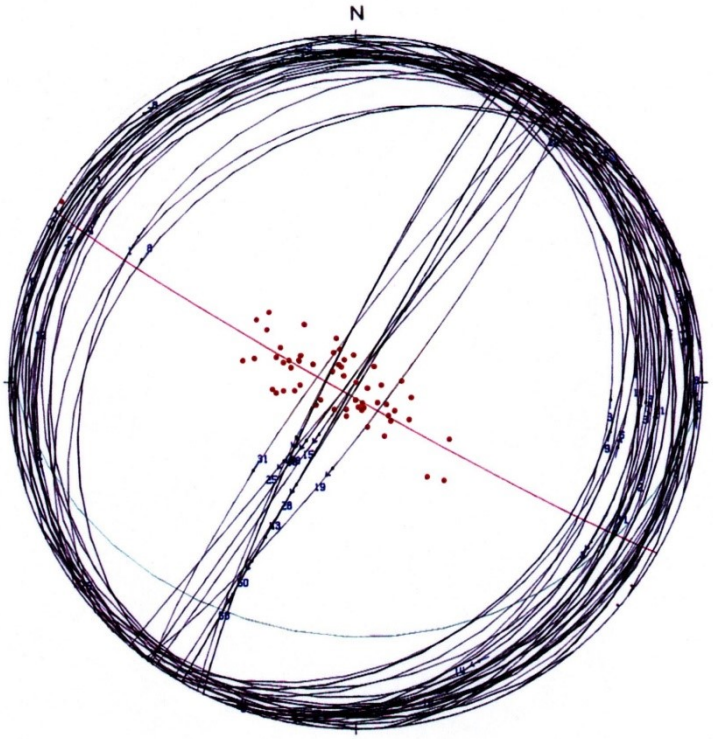
No. of faults = 56

M-PLANE

GCF

GCP

SIGMA 101 2



C4

SUBSET OF MYLONITES FOR CIP2

No. of faults = 74

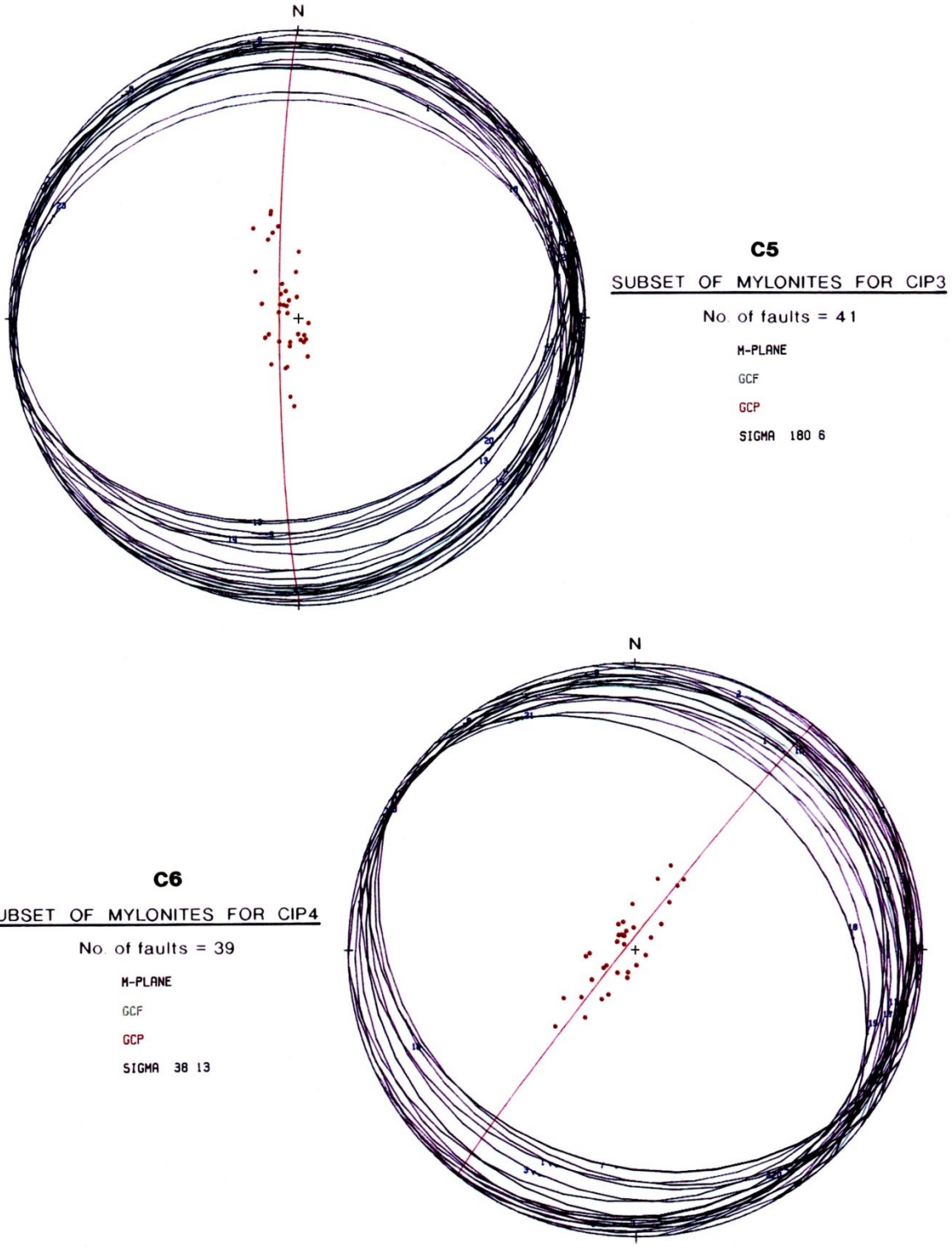
M-PLANE

GCF

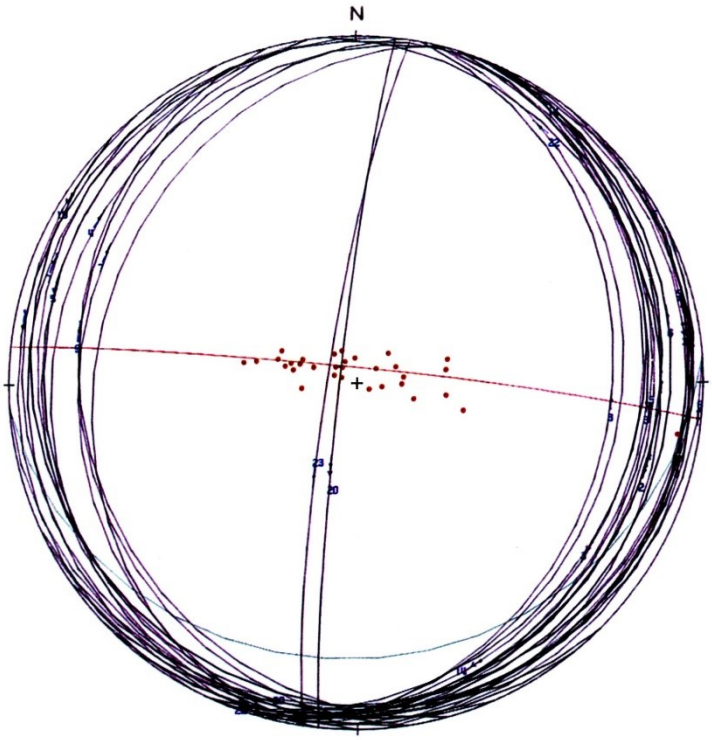
GCP

SIGMA 120 14

APPENDIX 6 : Diagrammatic representation of a stress field analysis for Fault Group C (C3-C4): Cataclastic faults with oblique-normal lineations.



APPENDIX 6 : Diagrammatic representation of a stress field analysis for Fault Group C (C5-C6): Cataclastic faults with oblique-normal lineations.



C7

SUBSET OF MYLONITES FOR CIP5

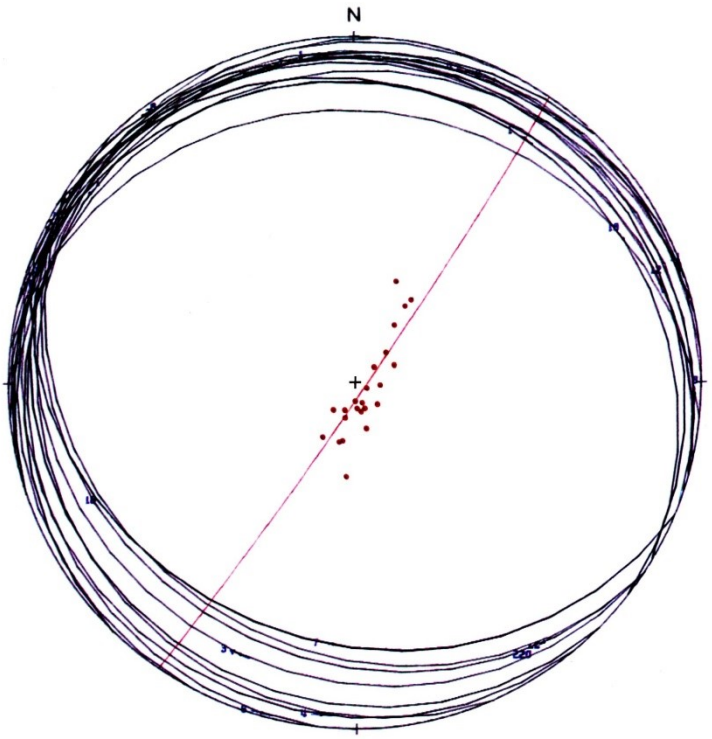
No. of faults = 39

M-PLANE

GCF

GCP

SIGMA 96 4



C8

SUBSET OF MYLONITES FOR CIP6

No. of faults = 28

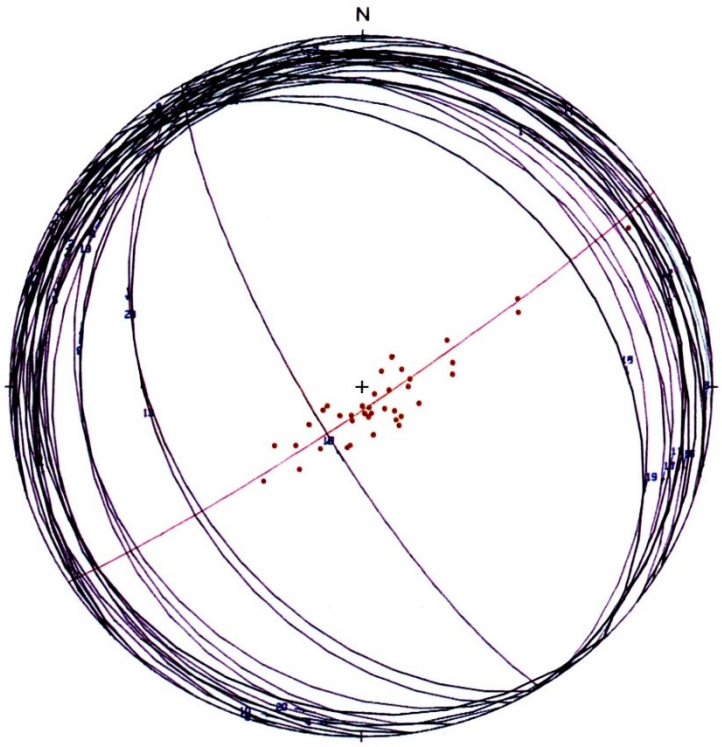
M-PLANE

GCF

GCP

SIGMA 35 7

APPENDIX 6 : Diagrammatic representation of a stress field analysis for Fault Group C (C7-C8): Cataclastic faults with oblique-normal lineations.



C9

SUBSET OF MYLONITES FOR CIP7

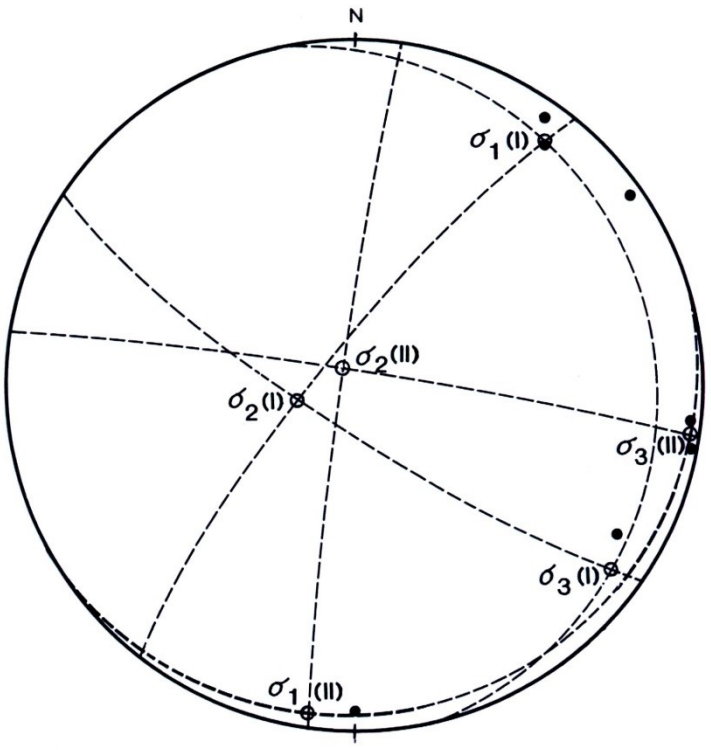
No. of faults = 45

M-PLANE

GCF

GCP

SIGMA 55/ 5



C10

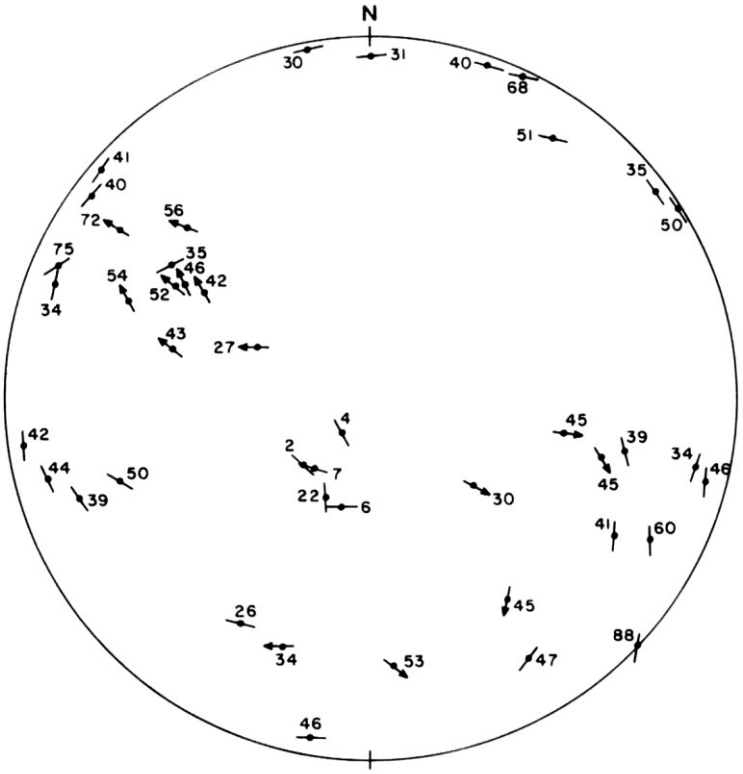
SIGMA SYNOPTIC DIAGRAM

No. of stress axes = 7

Principal stress axis positions:

Stress field (I)	Stress field (II)
σ_1 =36/10	σ_1 =188/04
σ_2 =255/78	σ_2 =98/03
σ_3 =126/10	σ_3 =356/86

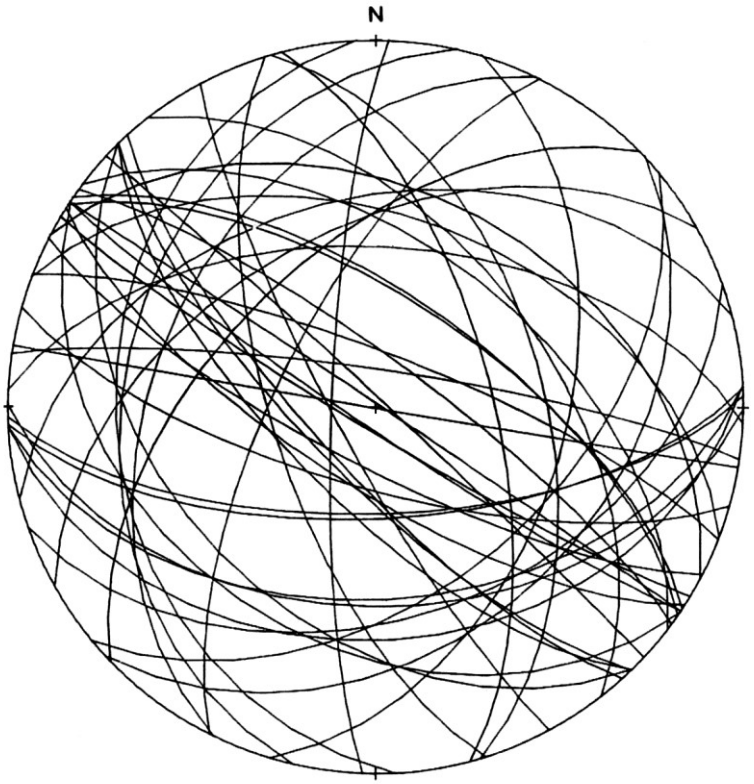
APPENDIX 6 : Diagrammatic representation of a stress field analysis for Fault Group C (C9-C10): Cataclastic faults with oblique-normal lineations.



D1

SLIP LINEAR DIAGRAM

No. of slip linears = 50

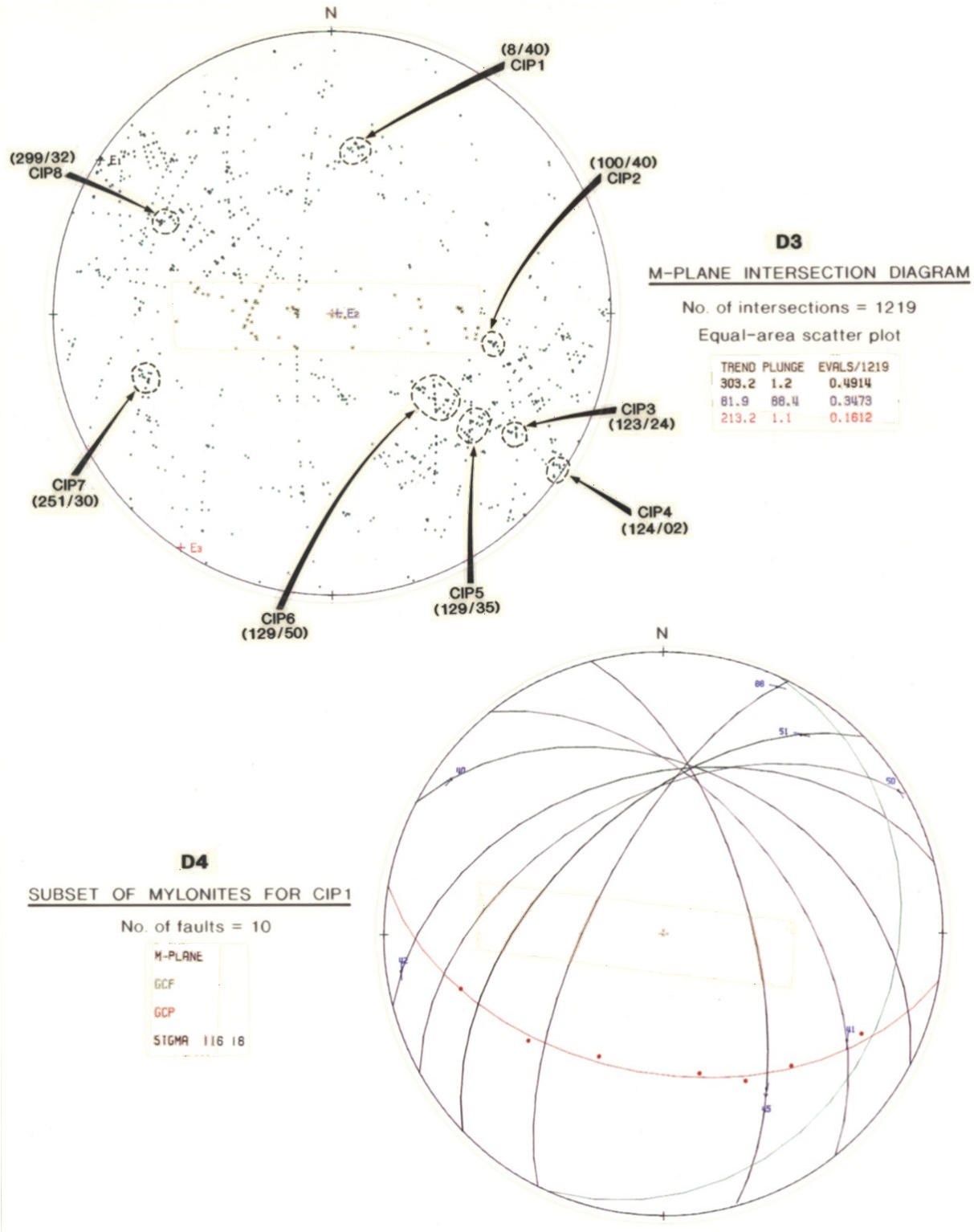


D2

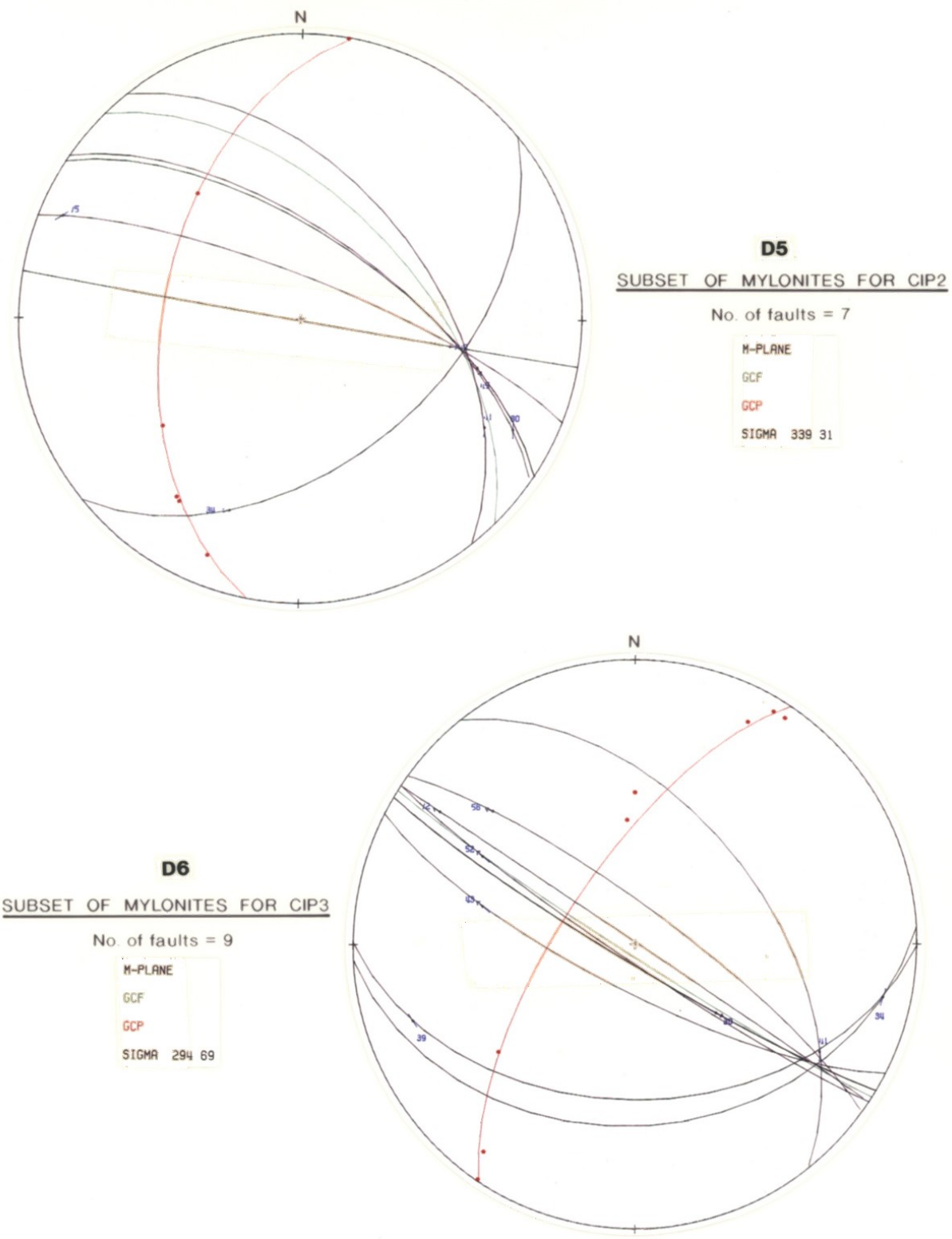
M-PLANE DIAGRAM

No. of m-planes = 50

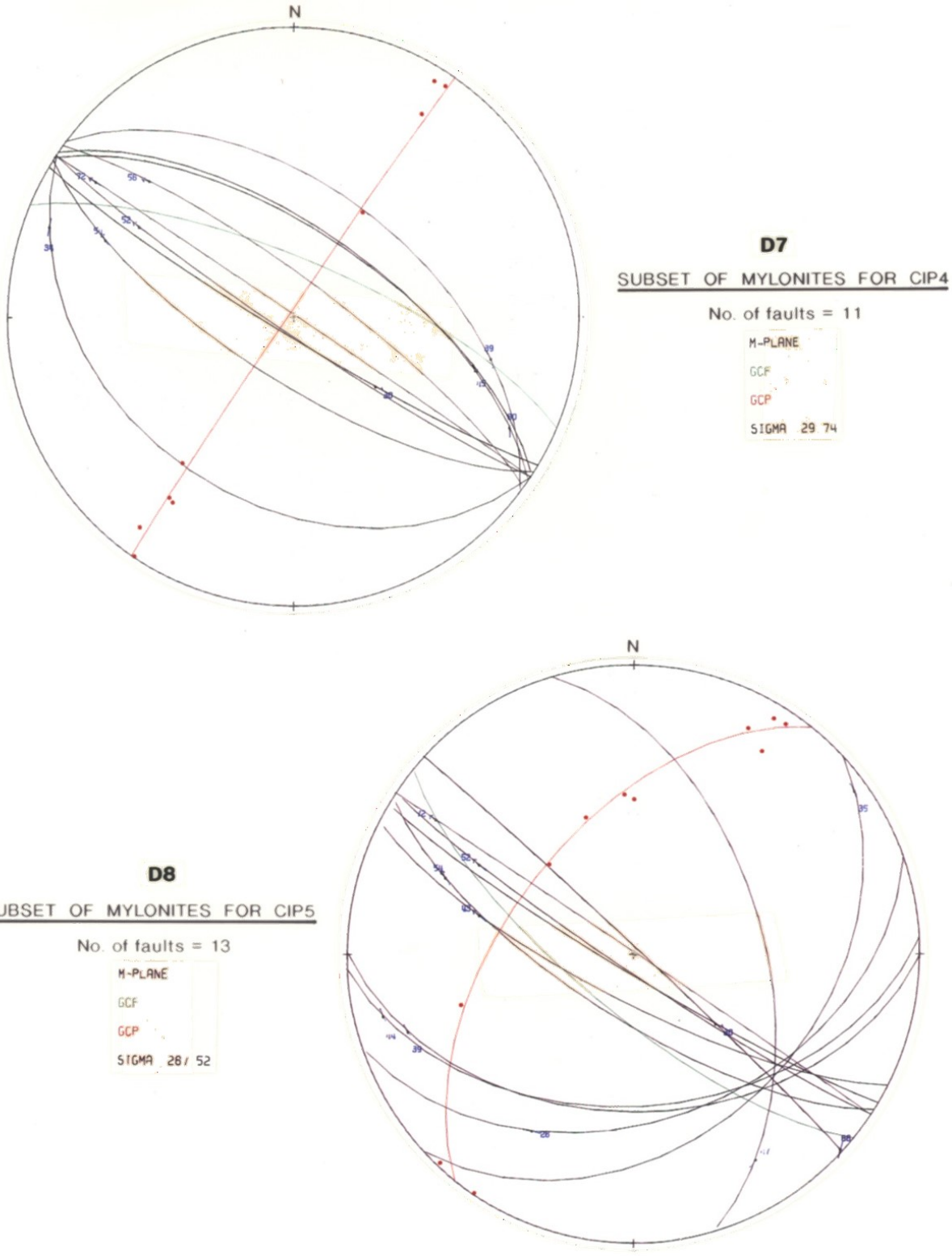
APPENDIX 6 : Diagrammatic representation of a stress field analysis for Fault Group D (D1-D2): Cataclastic faults with oblique-normal lineations.



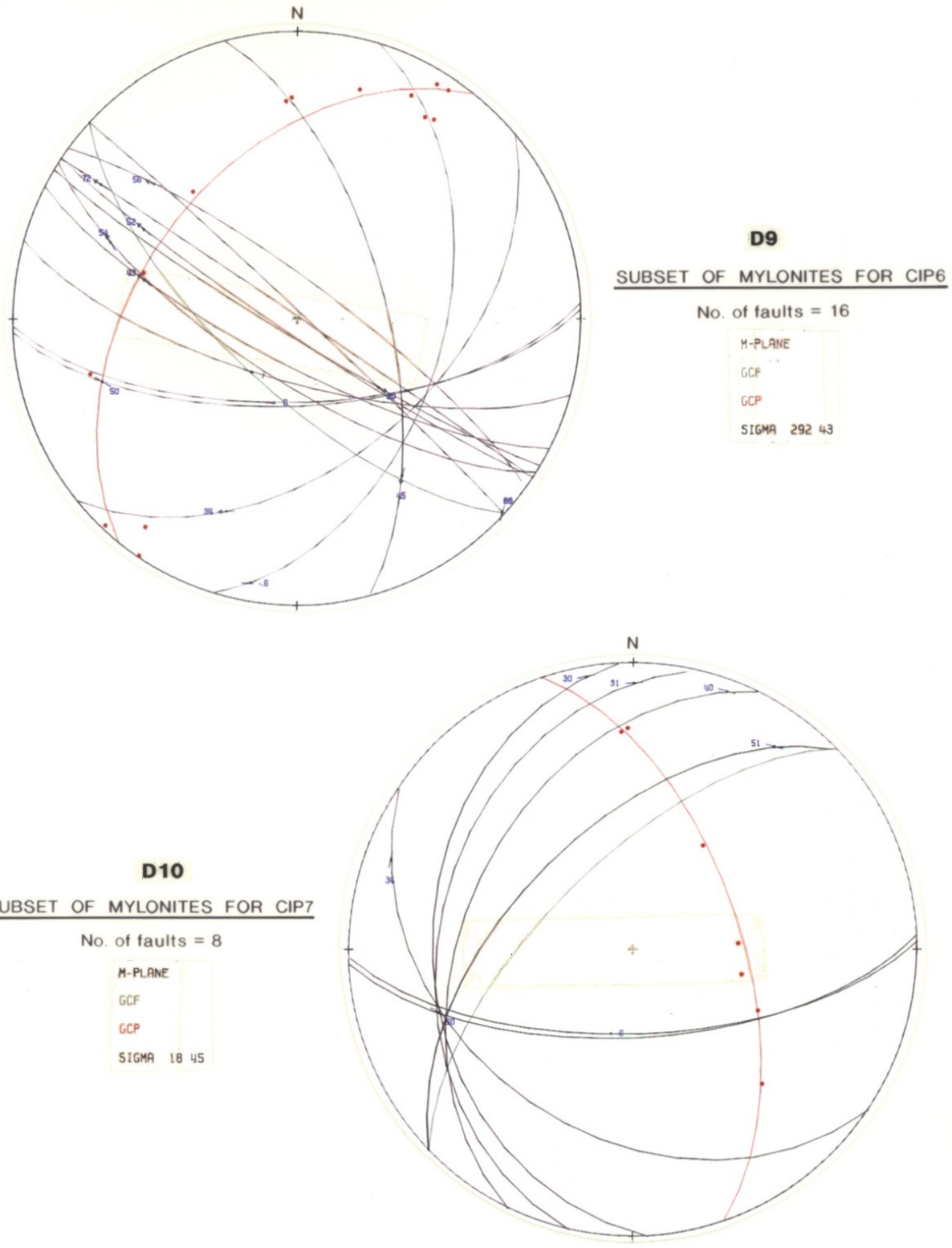
APPENDIX 6 : Diagrammatic representation of a stress field analysis for Fault Group D (D3-D4): Cataclastic faults with oblique-normal lineations.



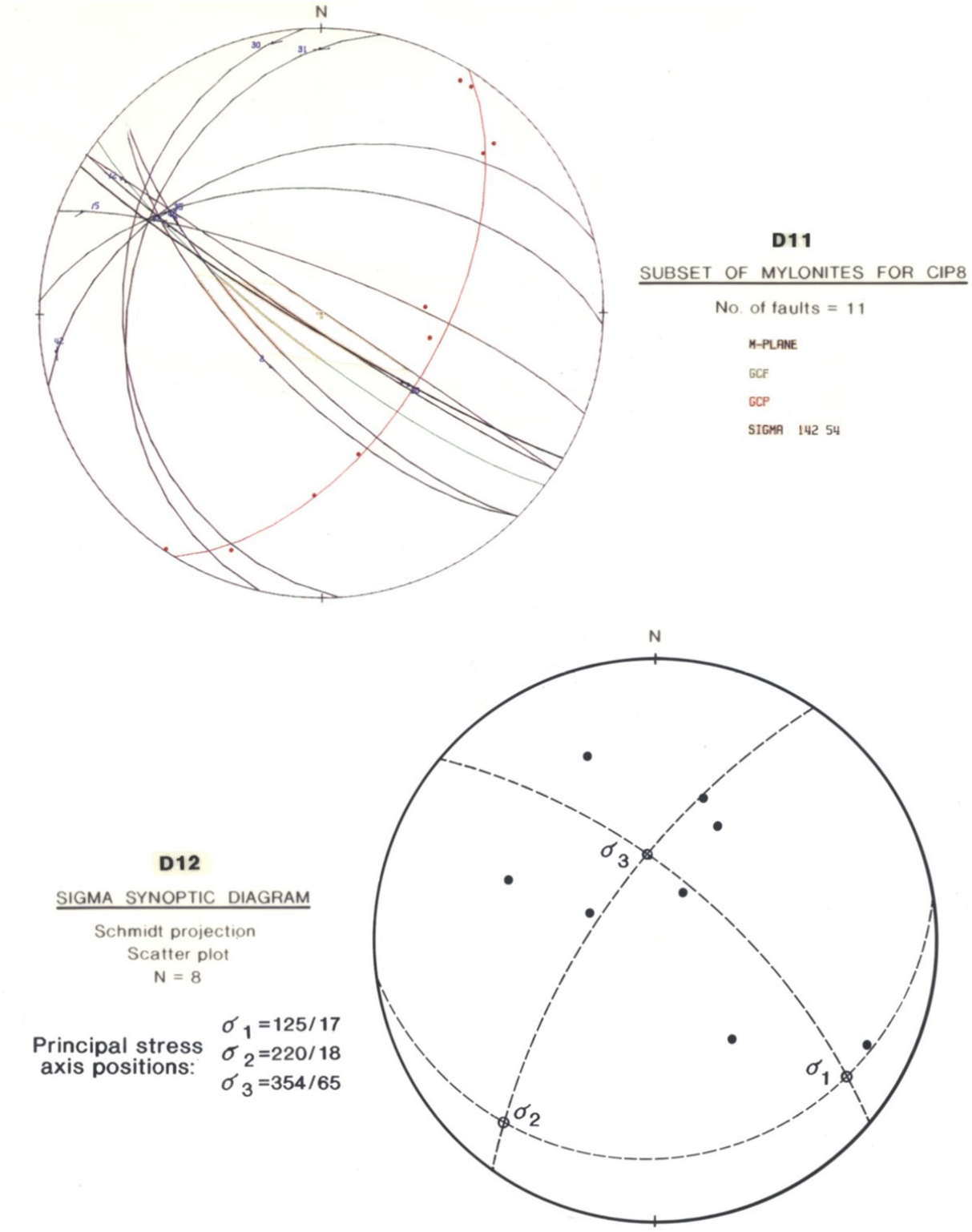
APPENDIX 6 : Diagrammatic representation of a stress field analysis for Fault Group D (D5-D6): Cataclastic faults with oblique-normal lineations.



APPENDIX 6 : Diagrammatic representation of a stress field analysis for Fault Group D (D7-D8): Cataclastic faults with oblique-normal lineations.



APPENDIX 6 : Diagrammatic representation of a stress field analysis for Fault Group D (D9-D10): Cataclastic faults with oblique-normal lineations.

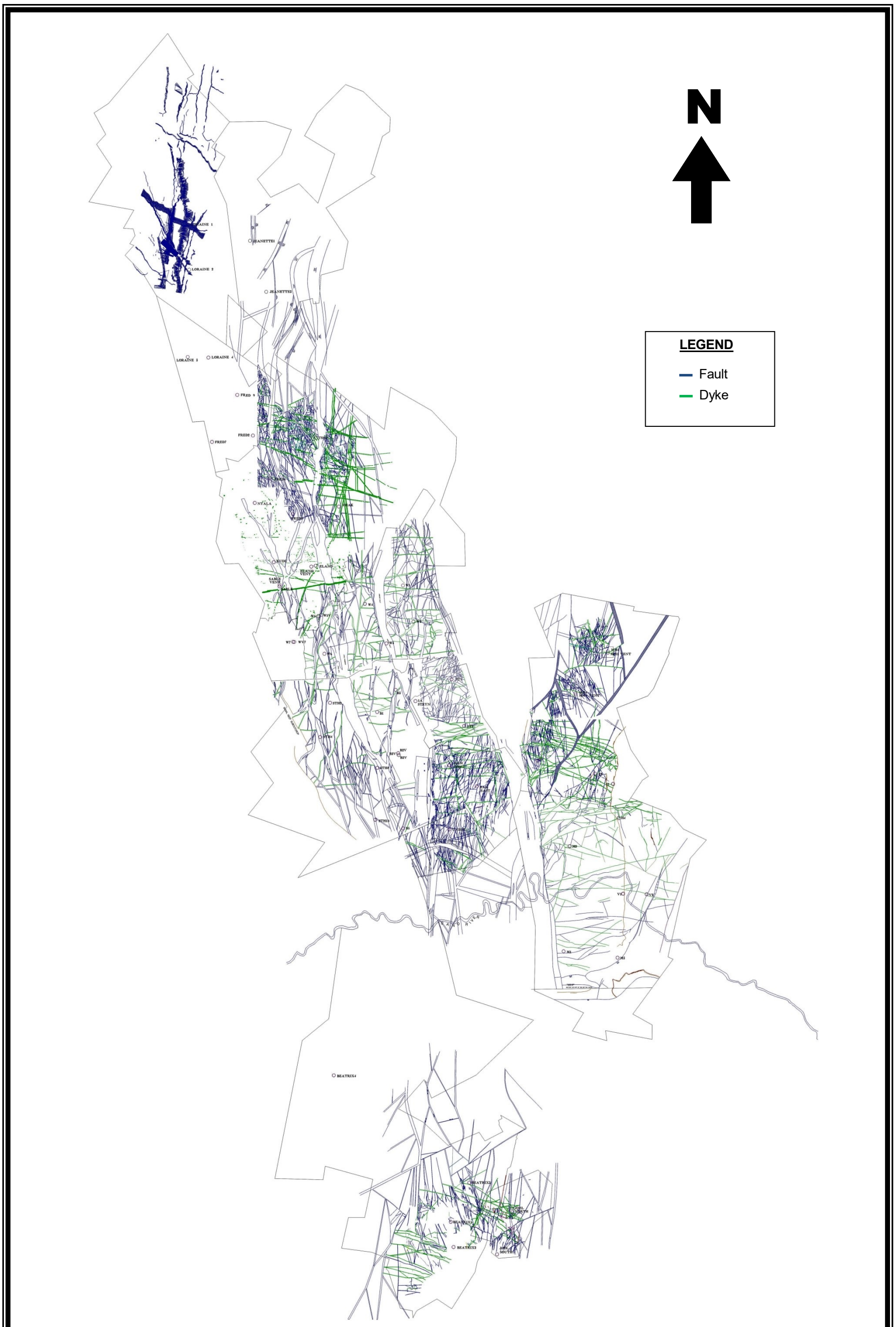


APPENDIX 6 : Diagrammatic representation of a stress field analysis for Fault Group D (D11-D12): Cataclastic faults with oblique-normal lineations.

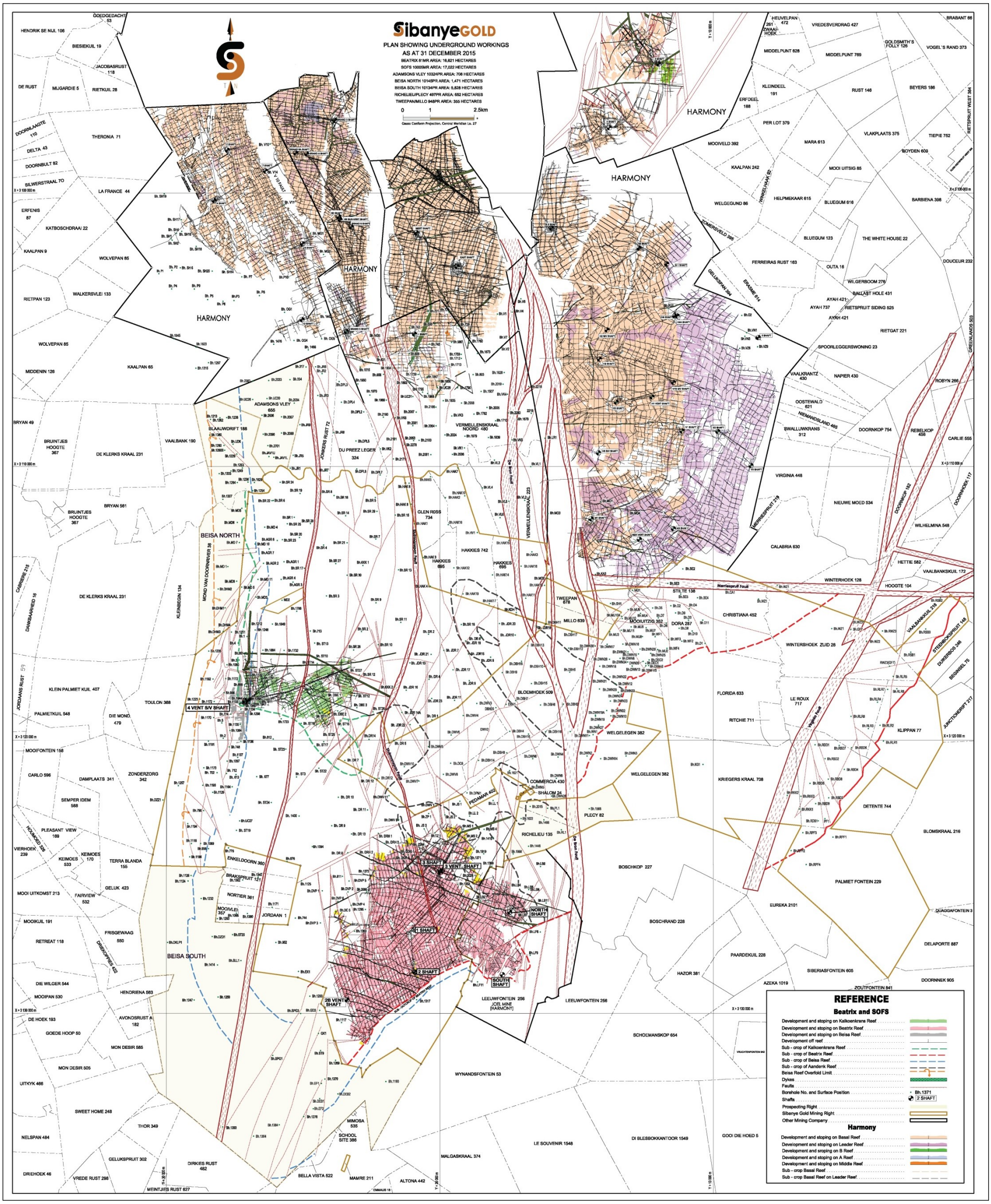
APPENDIX 7

STRUCTURAL INTERPRETATION PLANS FOR THE FREE STATE GOLDFIELD

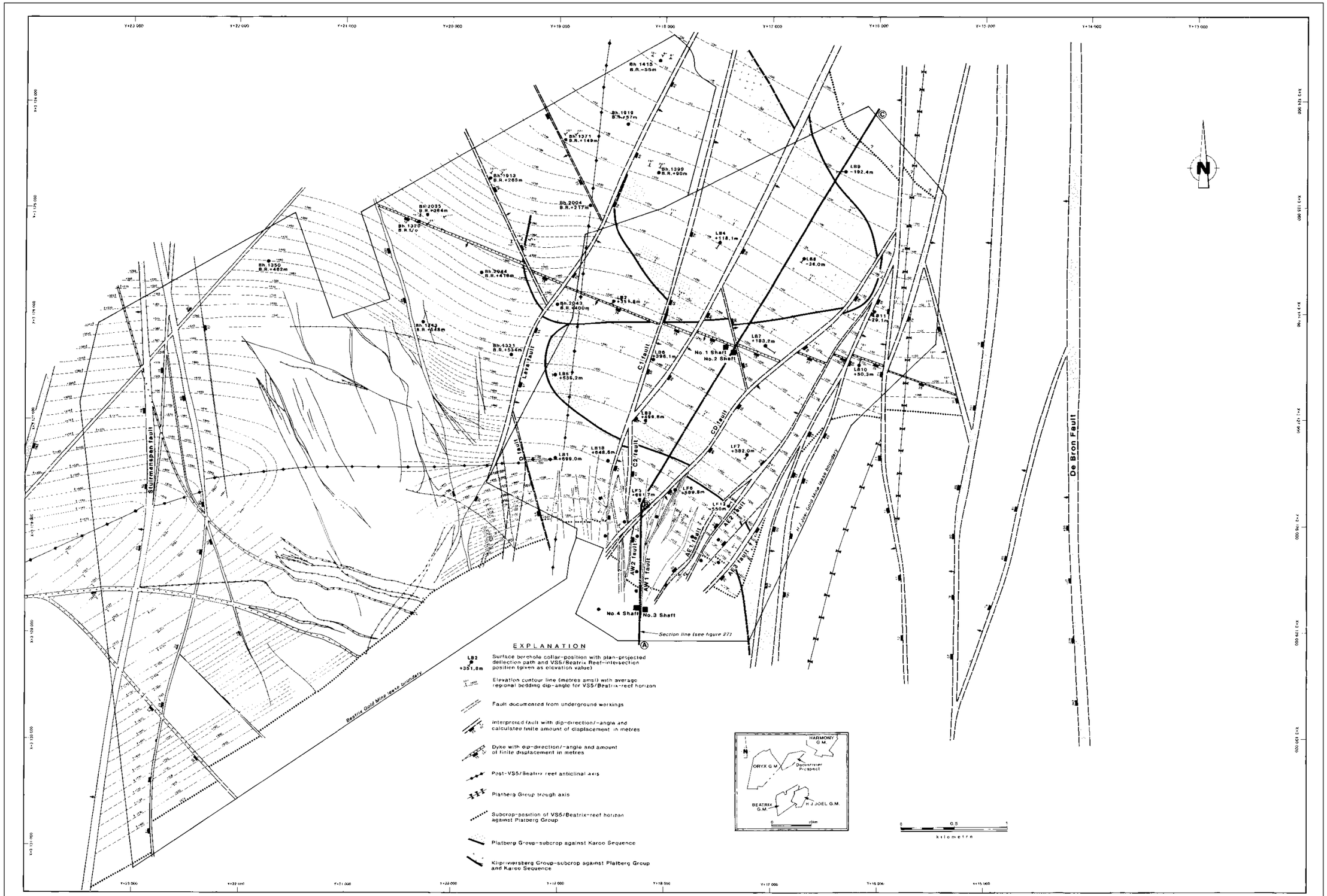
Structural compilation plan for (A) the Free State Goldfield (AngloGold Ashanti, 2004) and (B) the southern Free State Goldfield (Sibanye Gold, 2015), and (C) the lease areas of H.J. Joel and Beatrix gold mines in the southern Free State Goldfield (Geology Departments of H.J. Joel & Beatrix gold mines, 1992), based on an integrated interpretation of historical and recent exploration drilling, geophysical and underground mining information.



APPENDIX 7-A: Structural compilation plan for the Free State Goldfield (AngloGold Ashanti, 2004).



APPENDIX 7-B: Structural compilation plan for the southern Free State Goldfield (Sibanye Gold, 2015).



APPENDIX 7-C: Structural compilation plan for the lease areas of H.J. Joel and Beatrix gold mines in the southern Free State Goldfield (Geology Departments of H.J. Joel & Beatrix gold mines, 1992).

APPENDIX 8

REINTERPRETED SECTIONS OF SEISMIC LINES ACROSS H.J. JOEL GOLD MINE

The results of a reinterpretation of seismic lines across the lease area of H.J. Joel Gold Mine (for location see Figs. 3.35 & 3.36) are graphically illustrated (Appendices 8-A - 8-F) below for:

APPENDIX 8-A : Seismic line LBF-142

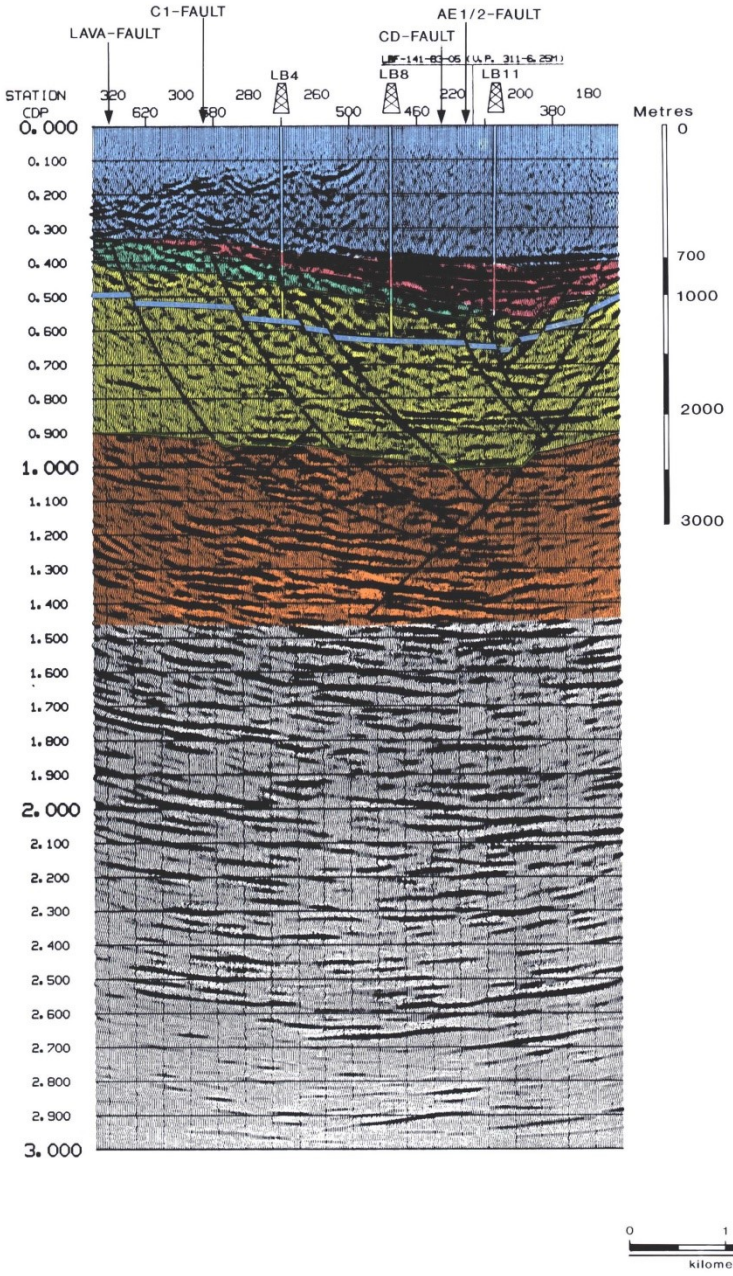
APPENDIX 8-B : Seismic line LBF-144

APPENDIX 8-C : Seismic line LBF-146

APPENDIX 8-D : Seismic line LBF-148

APPENDIX 8-E : Seismic line LBF-150

APPENDIX 8-F : Seismic line LBF-152



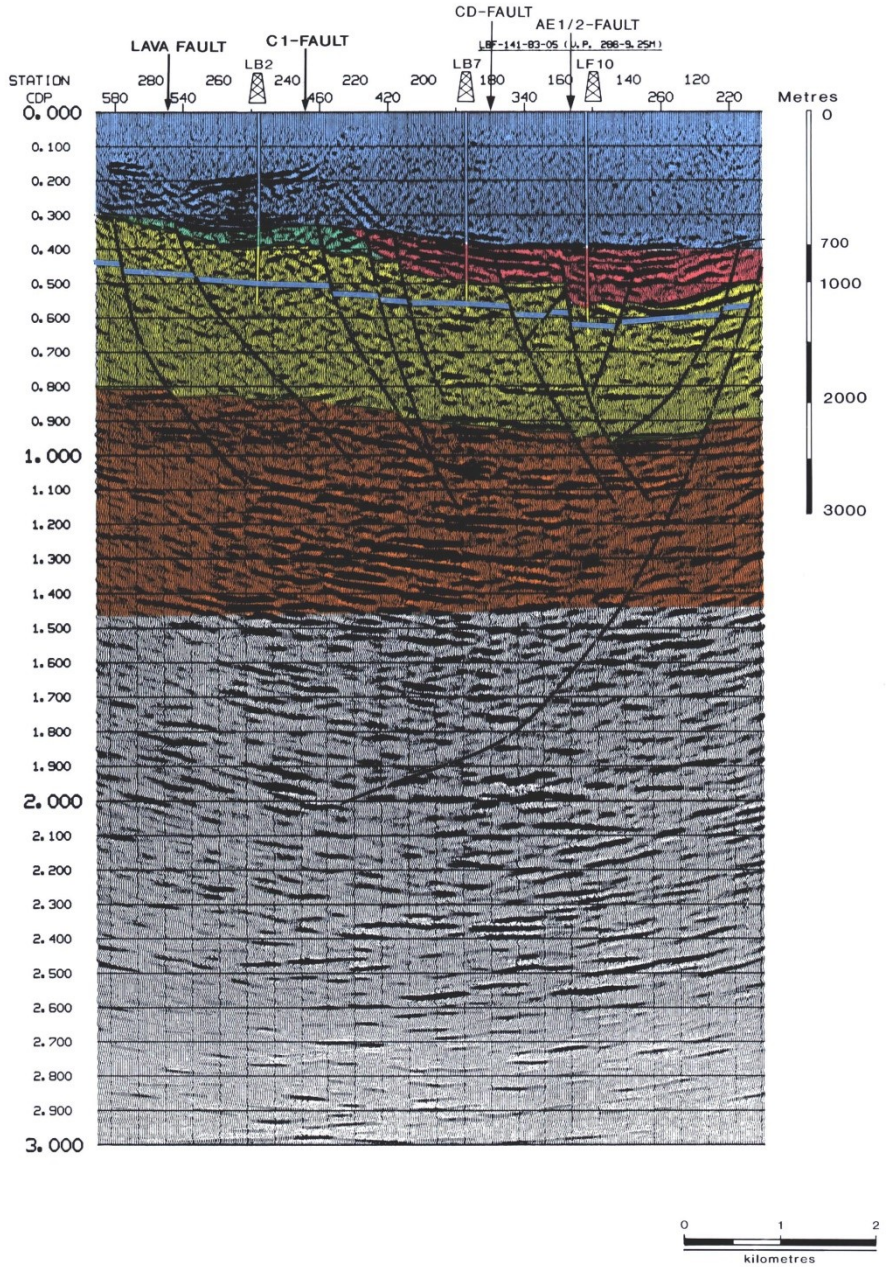
Fault interpreted from seismic section

Karoo Supergroup
Platberg Group
Klipriviersberg Group
Central Rand Group
VS5/Beatrix Reef
West Rand Group

LB4
Surface borehole

APPENDIX 8A

Reinterpreted section of seismic line LBF-142



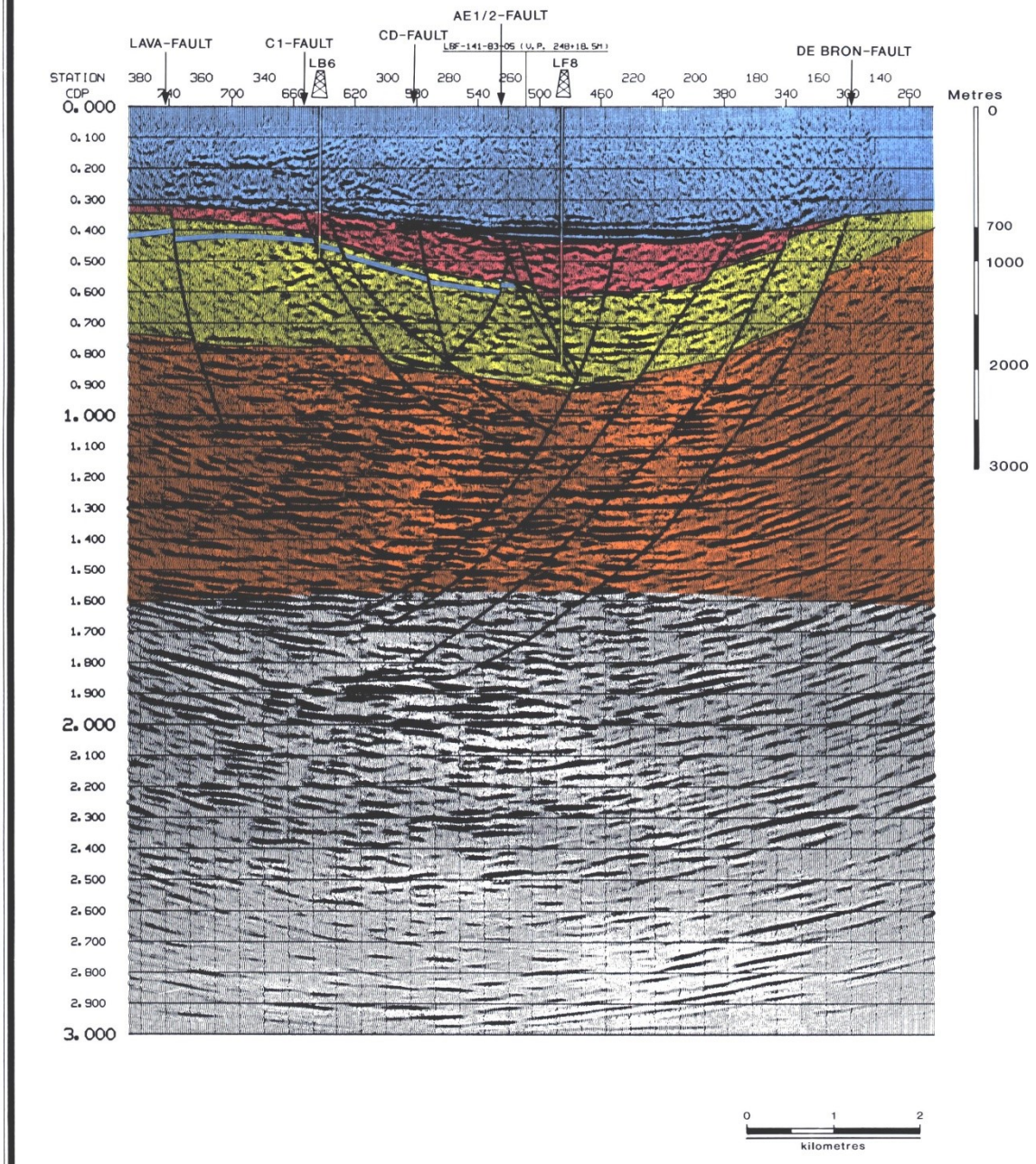
Fault interpreted from seismic section

- Karoo Supergroup
- Platberg Group
- Klipriviersberg Group
- Central Rand Group
- VS5/Beatrix Reef
- West Rand Group

LB2 Surface borehole

APPENDIX 8B

Reinterpreted section of seismic line LBF-144



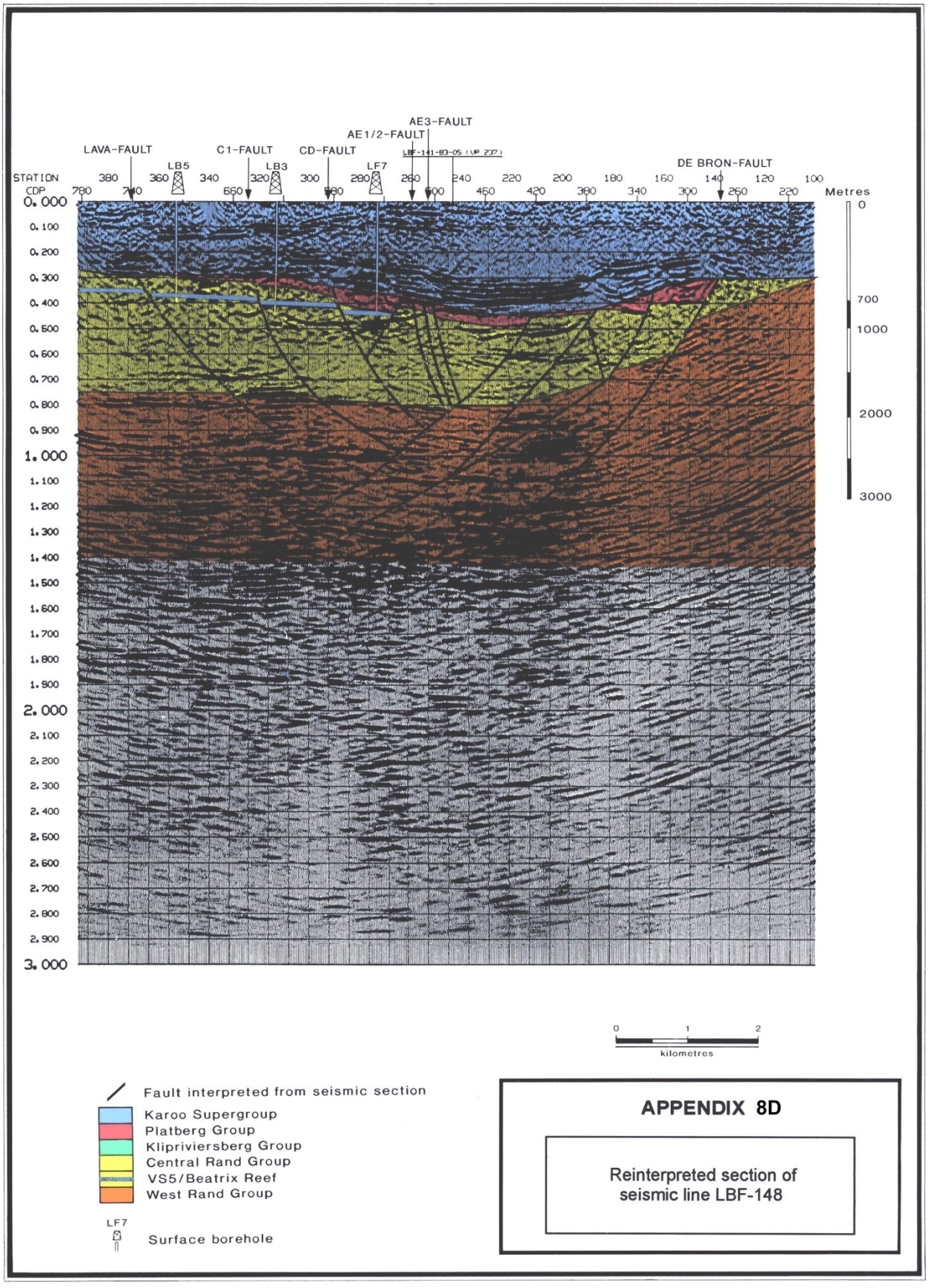
Fault interpreted from seismic section

- Karoo Supergroup
- Platberg Group
- Klipriviersberg Group
- Central Rand Group
- VS5/Beatrix Reef
- West Rand Group

LB6 Surface borehole

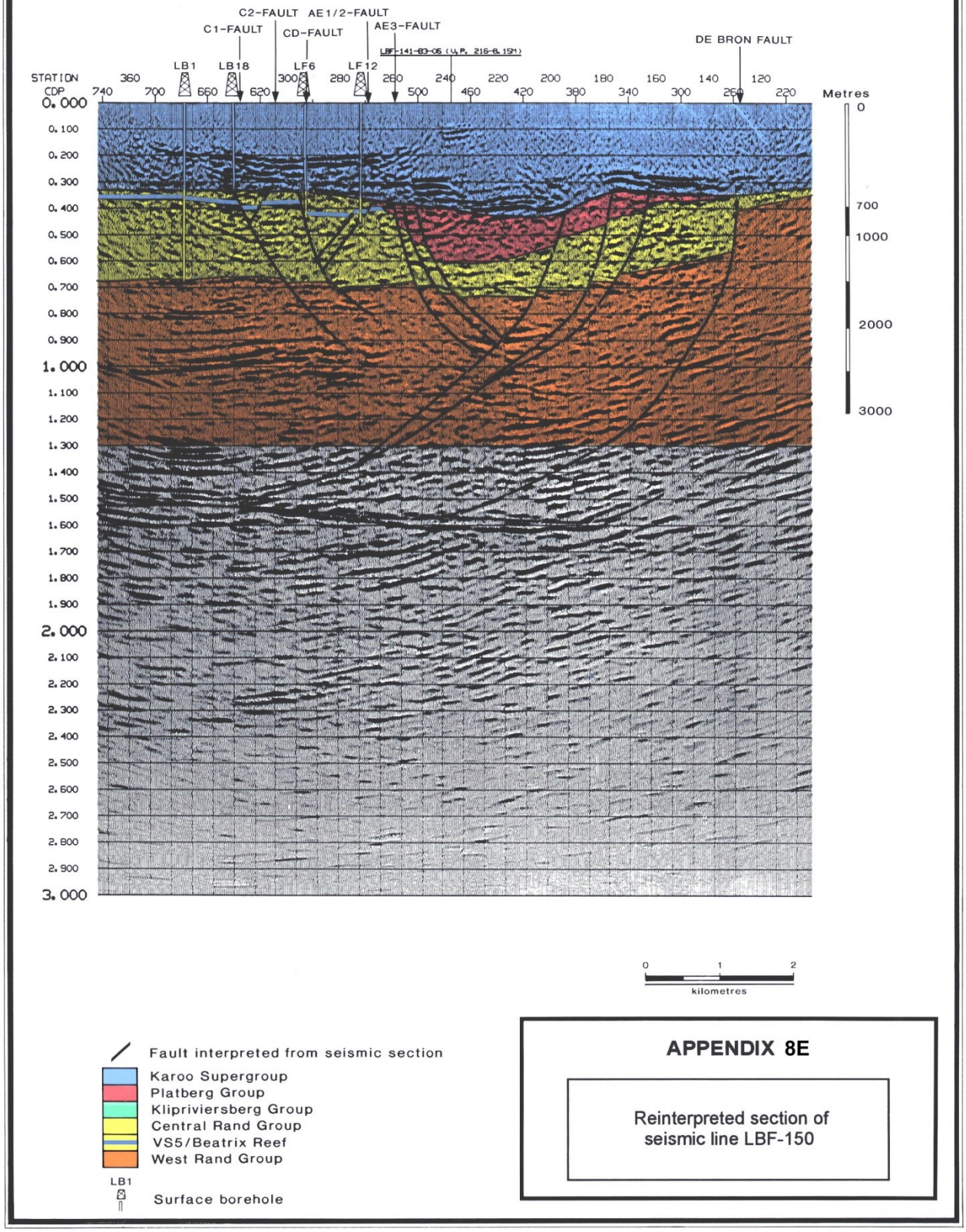
APPENDIX 8C

Reinterpreted section of seismic line LBF-146



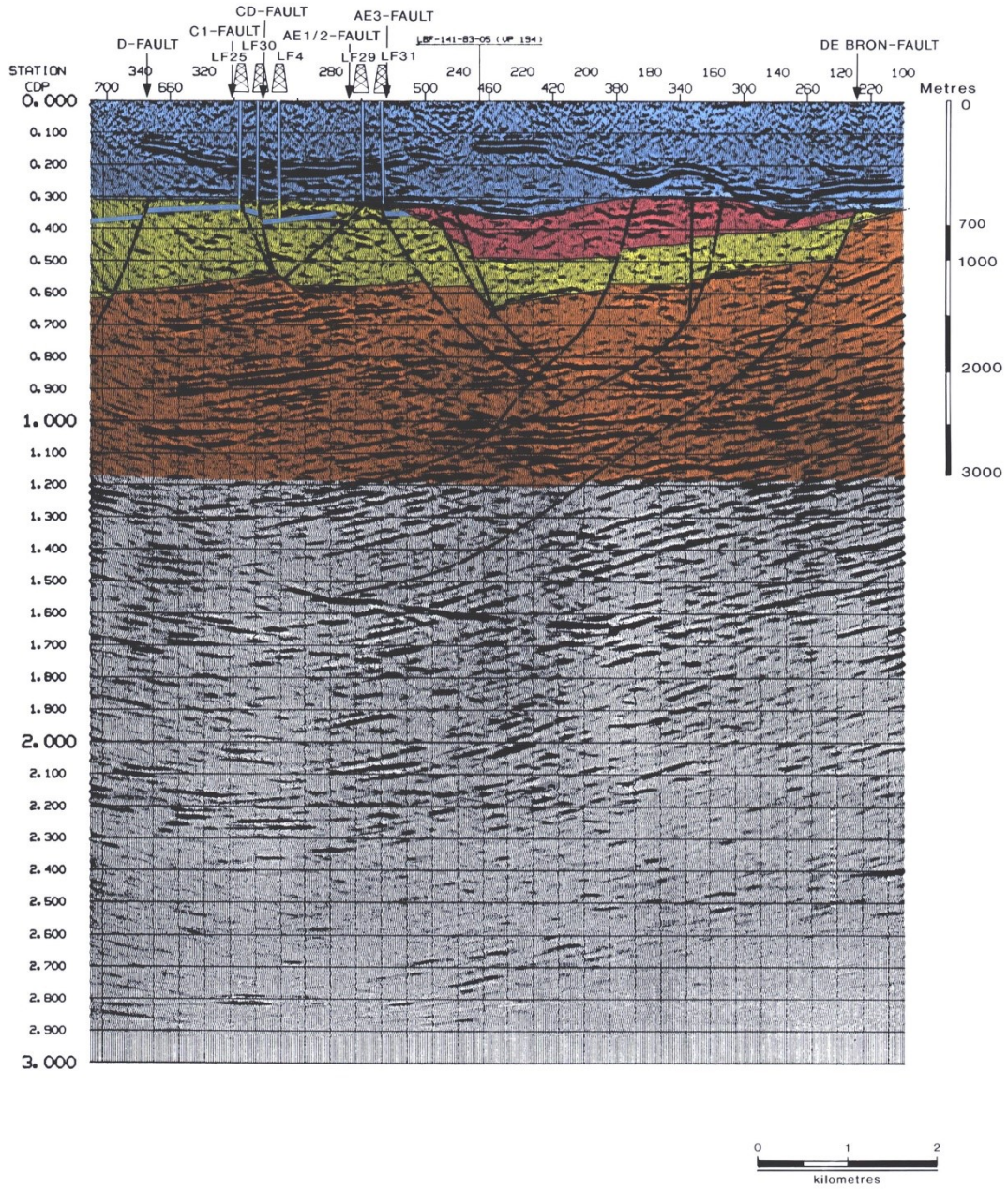
APPENDIX 8D

Reinterpreted section of seismic line LBF-148



APPENDIX 8E

Reinterpreted section of seismic line LBF-150



Fault interpreted from seismic section

- Karoo Supergroup
- Platberg Group
- Klipriviersberg Group
- Central Rand Group
- VS5/Beatrix Reef
- West Rand Group

LF4 Surface borehole

APPENDIX 8F

Reinterpreted section of seismic line LBF-152

APPENDIX 9

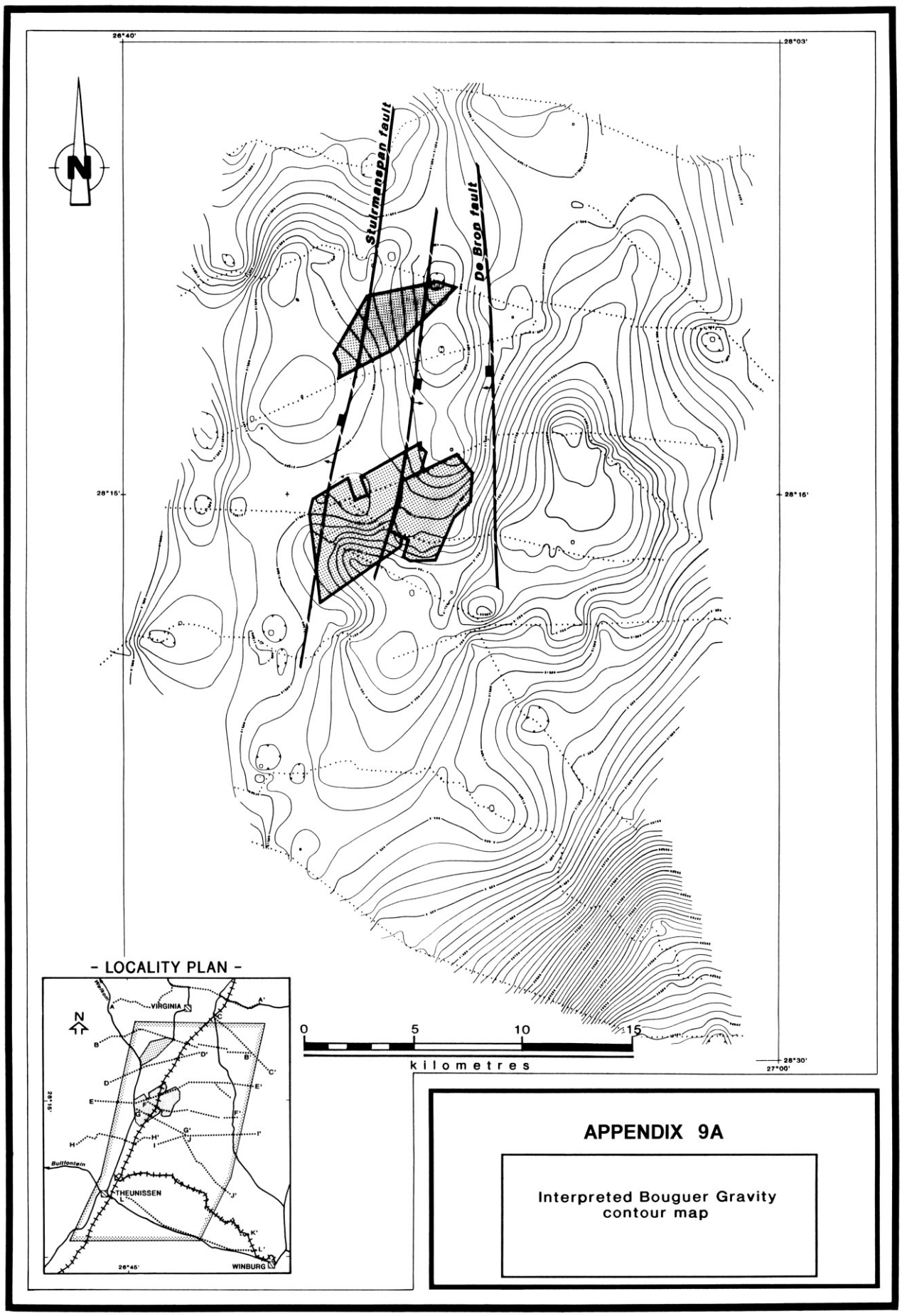
REINTERPRETATION OF GRAVIMETRIC, AEROMAGNETIC AND MAGNETOTELLURIC DATA

The results of a reinterpretation of geophysical data available for the southeastern part of the Welkom Sector within the FS Goldfield, is represented below in form of:

APPENDIX 9-A : Bouguer gravity contour map

APPENDIX 9-B : Aeromagnetic contour map

APPENDIX 9-C : Comparison between frequency pseudo (a1) / interpreted (a2) magneto-telluric line “J” (b) modelled section along gravity traverse “F” and (c) interpreted seismic line LBF-148.



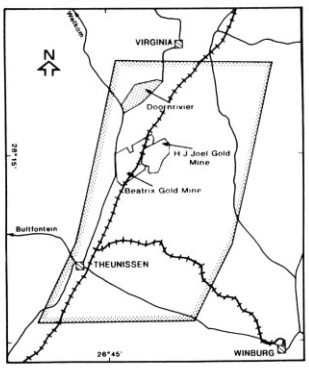
- LOCALITY PLAN -

APPENDIX 9A

Interpreted Bouguer Gravity contour map



- LOCALITY PLAN -

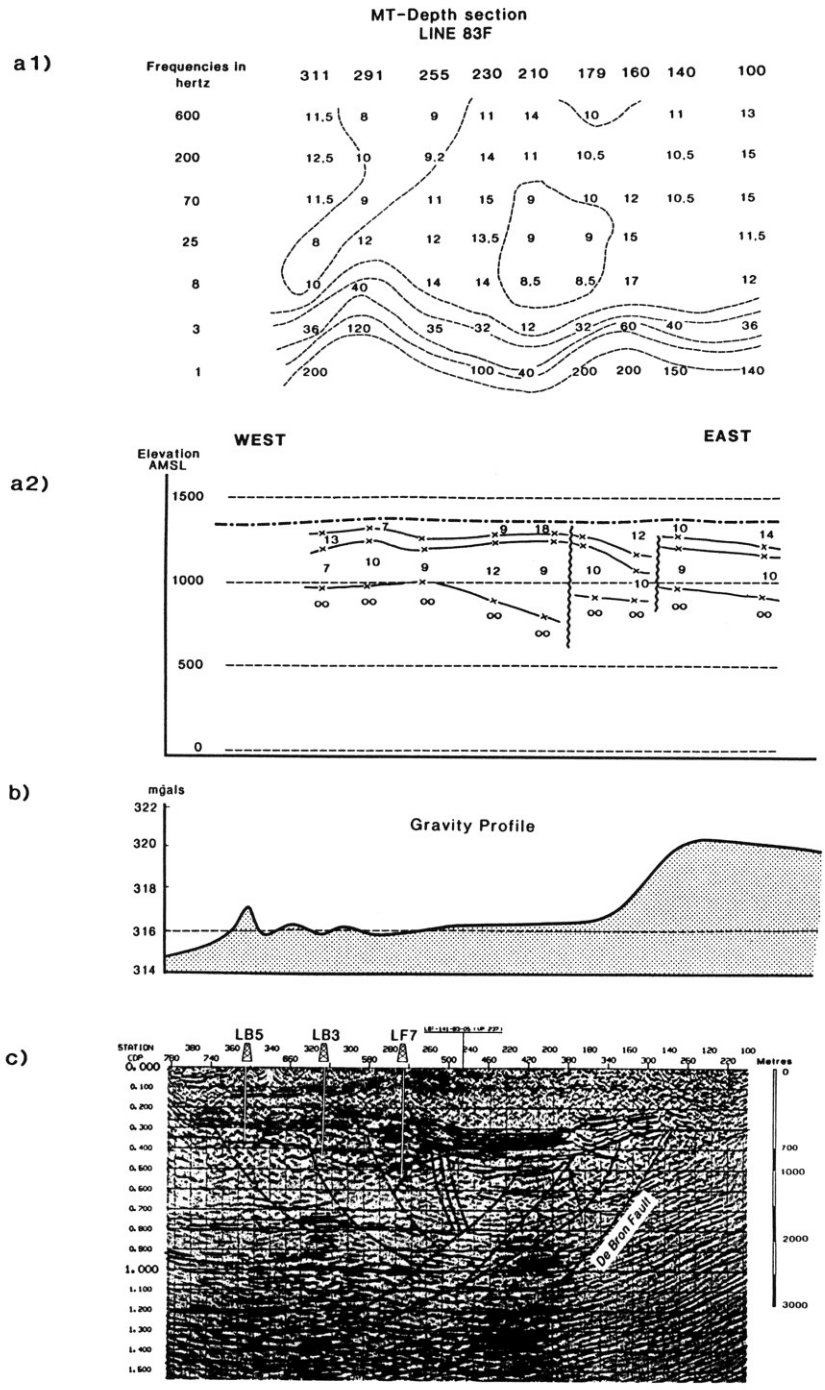


0 5 10 15

kilometres

APPENDIX 9B

Interpreted Aeromagnetic contour map



For location see Appendix 9A

APPENDIX 9C

Comparison between frequency pseudo (a1)/interpreted (a2) magneto-telluric line "J", b) modelled section along gravity traverse "F" and c) interpreted seismic line LBF-148

APPENDIX 10

FRACTURE ANALYSIS LOGS FOR SURFACE BOREHOLES WITHIN THE DOORNRIVIER PROSPECT AREA

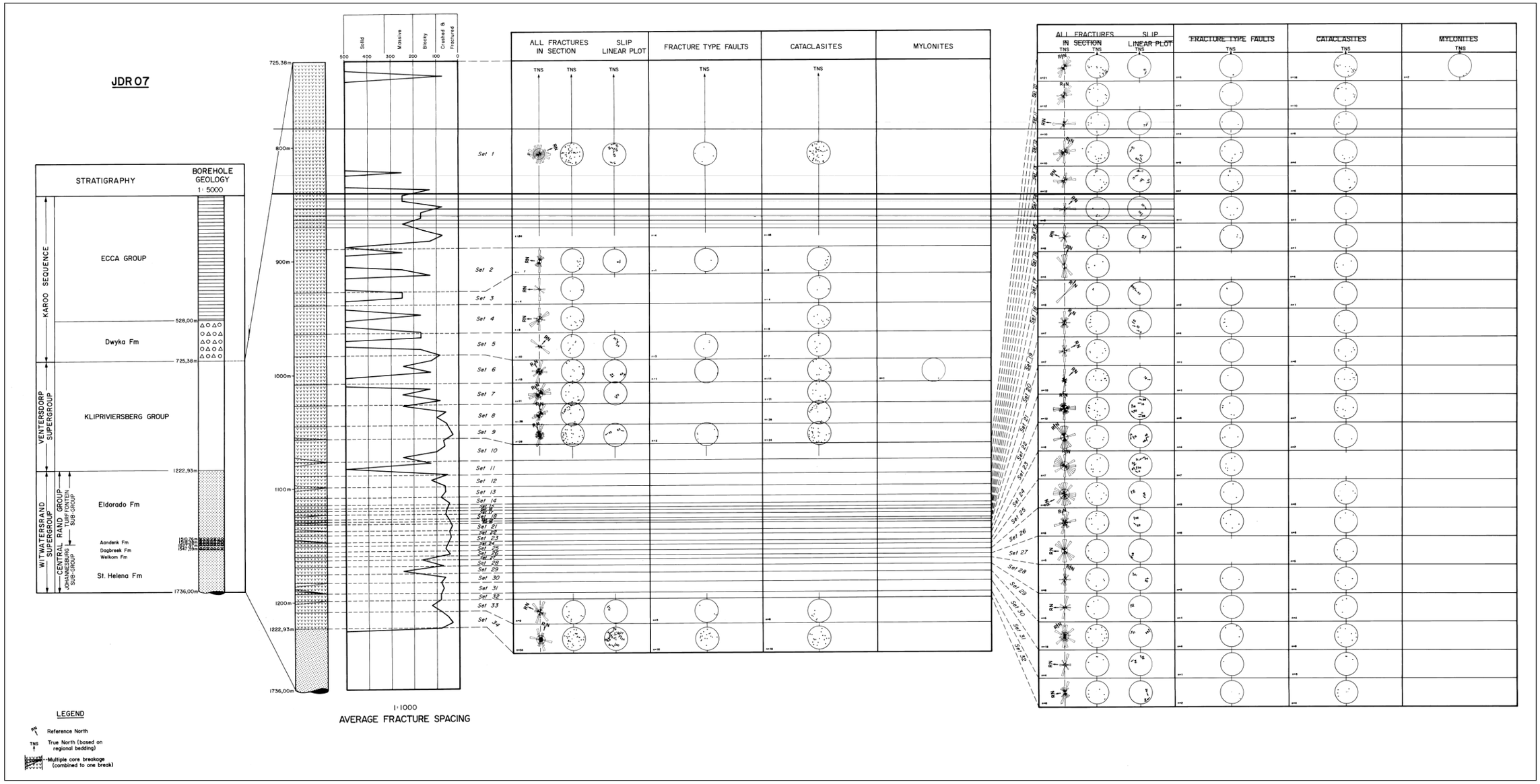
Fracture analysis logs for four selected surface boreholes from the Doornrivier Prospect Area are represented below as:

APPENDIX 10-A : Fracture analysis log for surface borehole JDR 7

APPENDIX 10-B : Fracture analysis log for surface borehole JDR 17

APPENDIX 10-C : Fracture analysis log for surface borehole JDR 21

APPENDIX 10-D : Fracture analysis logs (a & b) for surface borehole JDR 23



APPENDIX 10-A : Fracture analysis log for surface borehole JDR 7.

JDR 17

AVERAGE FRACTURE SPACING
1:1000

Solid | Massive | Blocky | Crushed & Fractured
500 400 300 200 100 0

STRATIGRAPHY | BOREHOLE GEOLOGY 1:5000

KAROO SEQUENCE
- ECCA GROUP
- 516,00m
- Dwyka Fm.
- 709,50m

VENTERSDORP SUPERGROUP
- KLIPRIVIERSBERG GROUP
- 1126,11m

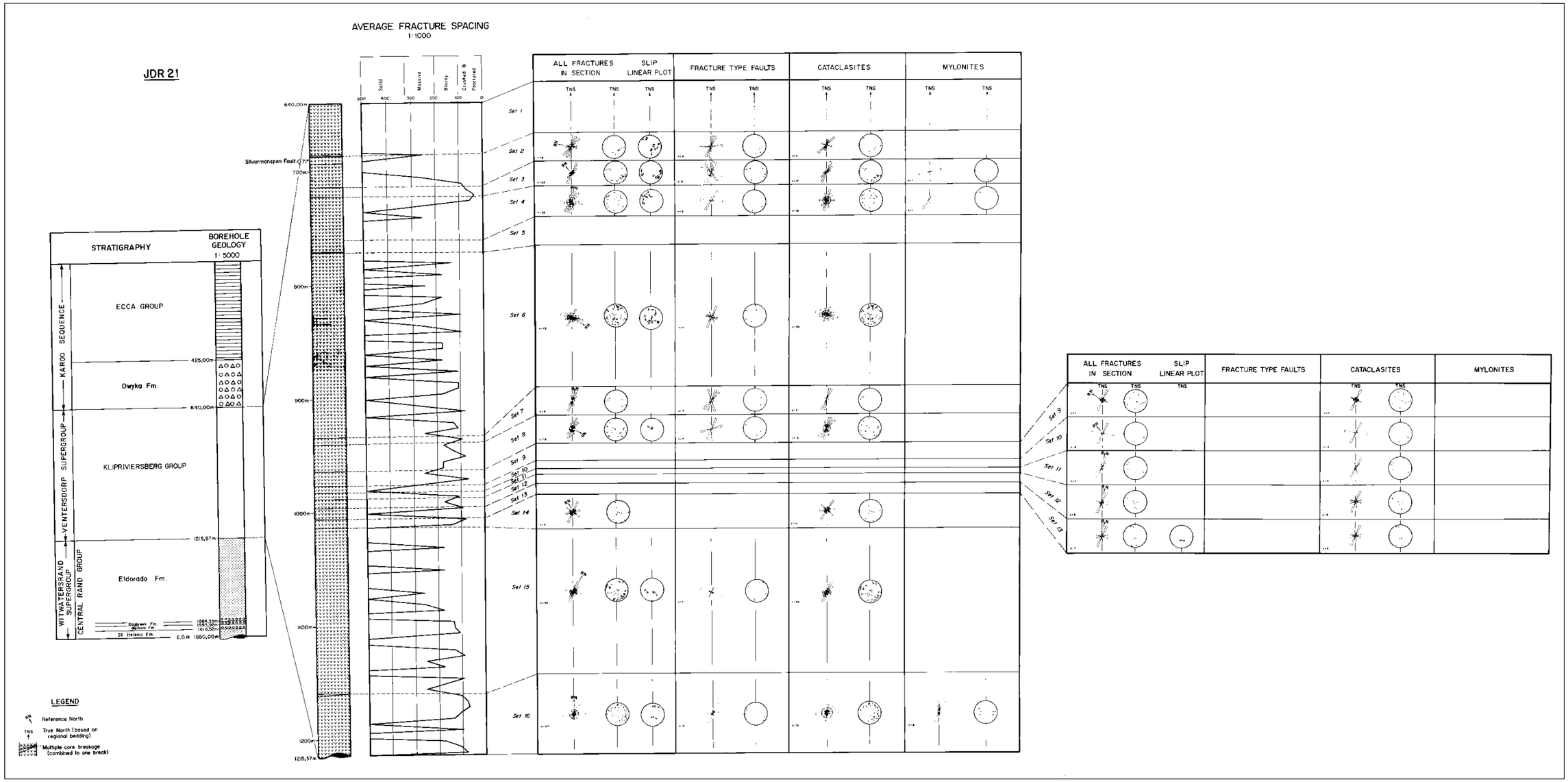
WITWATERSRAND SUPERGROUP — CENTRAL RAND GROUP
- Eldorado Fm.
- Aandenk Fm. 1481,90m
- Dagbreek Fm. 1484,11m
- Welkom Fm. 1513,85m
- St Helena Fm.
- 1686,38m

709,50m
800m
900m
1000m
1100m
1126,11m
1686,38m

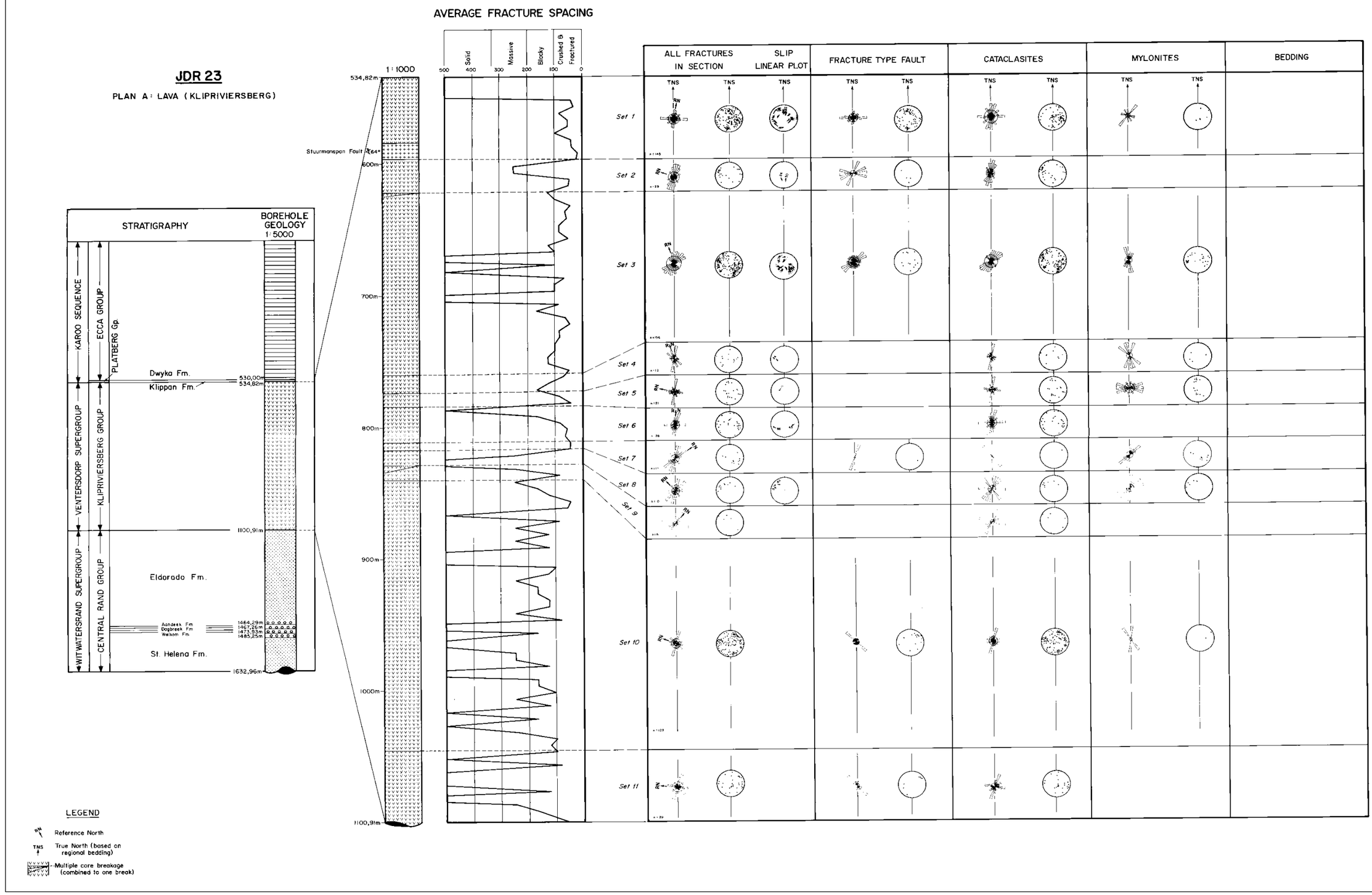
	ALL FRACTURES IN SECTION (TNS / TNS)	SLIP LINEAR PLOT (TNS)	FRACTURE TYPE FAULT (TNS / TNS)	CATACLASITES (TNS / TNS)	MYLONITES (TNS / TNS)	BEDDING (TNS / TNS)
Set 1						
Set 2						
Set 3						
Set 4						
Set 5						
Set 6						
Set 7						
Set 8						
Set 9						
Set 10						
Set 11						
Set 12						
Set 13						
Set 14						
Set 15						
Set 16						
Set 17						
Set 18						

LEGEND
- RN — Reference North
- TNS — True North (based on regional bedding)
- Multiple core breakage (combined to one break)

APPENDIX 10-B : Fracture analysis log for surface borehole JDR 17.



APPENDIX 10-C : Fracture analysis log for surface borehole JDR 21.



APPENDIX 10-D : Fracture analysis logs (a & b) for surface borehole JDR 23.

APPENDIX 11

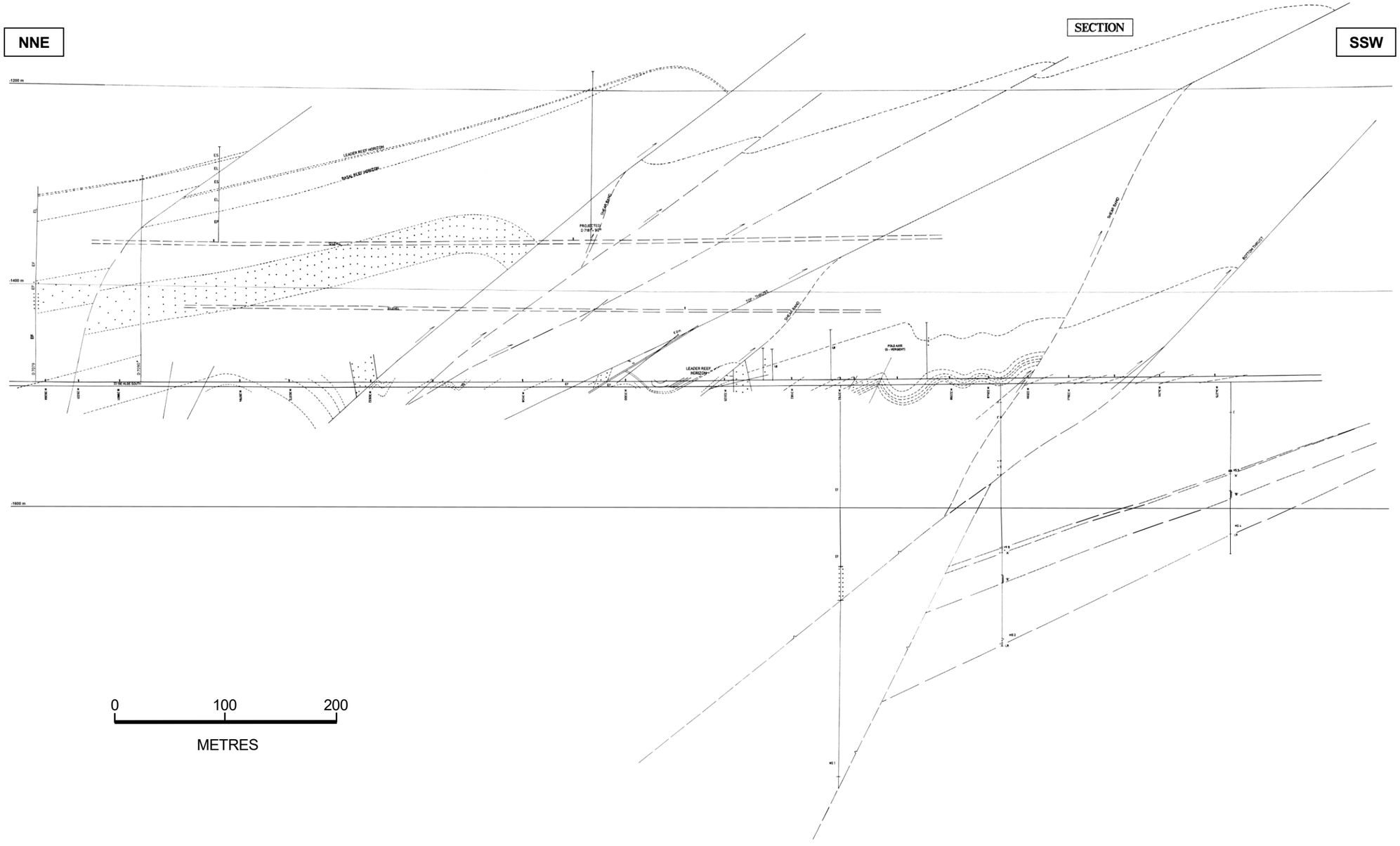
PLAN AND NORTH-SOUTH SECTION OF 33-19E HAULAGE SOUTH AT HARMONY GOLD MINE

A plan and north-south section of the underground excavation 33-19E Haulage South at Harmony Gold Mine is represented in a scale 1:1000, which illustrates the main structural elements of the Merriespruit Thrust Zone.

NNE

SECTION

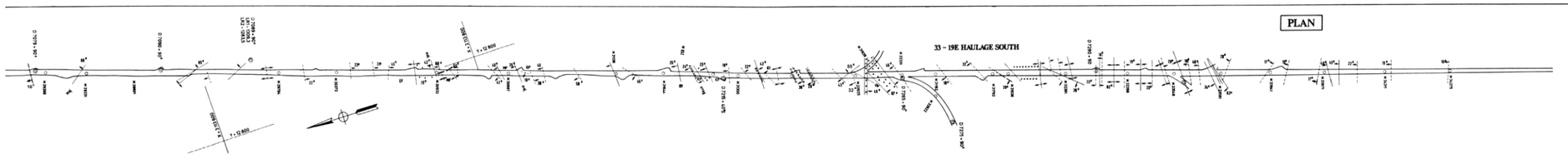
SSW



0 100 200

METRES

PLAN



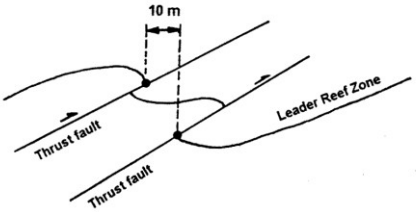
APPENDIX 12

RESTORATION OF THE MERRIESPRUIT THRUST ZONE ALONG GEOLOGICAL SECTION 33-19E HAULAGE SOUTH / HARMONY GOLD MINE

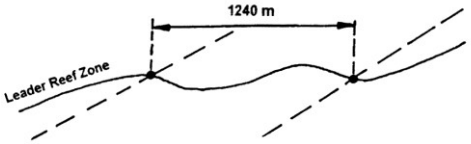
Methodology:

Being well constrained by underground exposures and boreholes, the section along 33-19E Haulage South was regarded as favourable for a restoration and estimation of the amount of shortening across the Merriespruit Thrust Zone. Furthermore, the near parallelism between the NNE/SSW (20°/200°)-trending plane of section 33-19E Haulage South, the south-directed (180°) movement vector of the east/west-striking (90°/270°) thrust zone, and the northerly (360°) regional dip-direction of the Central Rand Group strata, favours a restoration to be performed along this section. Due to the fact that the shortening across the Merriespruit Thrust Zone is composed of thrusting and folding, the restoration of the section along 33-19E Haulage South was performed in two separate steps, individually for (b) thrusting and (c) folding, and is schematically illustrated below. In this regard, the intersections of the Leader Reef Horizon with the Merriespruit Thrust Zone in the Top and Bottom blocks served as reference points for the hanging and footwall blocks respectively. After restoring the section step-wise to a (b) pre-thrusting and (c) pre-folding stage, the horizontal distance between the reference points was individually measured for step (b) and (c), and then added to obtain the total distance between both reference points before deformation. The subtraction of the present-day distance between both reference points from the obtained total pre-deformation distance provides the total minimum (apparent) amount of horizontal shortening across the Merriespruit Thrust Zone along 33-19E Haulage South. Finally, the true amount of horizontal shortening, that is parallel to the thrust direction (180°), was established by adjusting for the angle of 20° between the line of section of 33-19E Haulage South and the south-directed movement vector of the Merriespruit Thrust Zone.

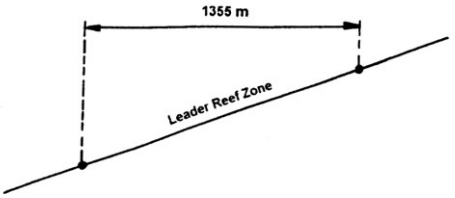
(a) Post-deformational stage
(Present-day situation)



(b) Pre-deformational (thrusting) stage



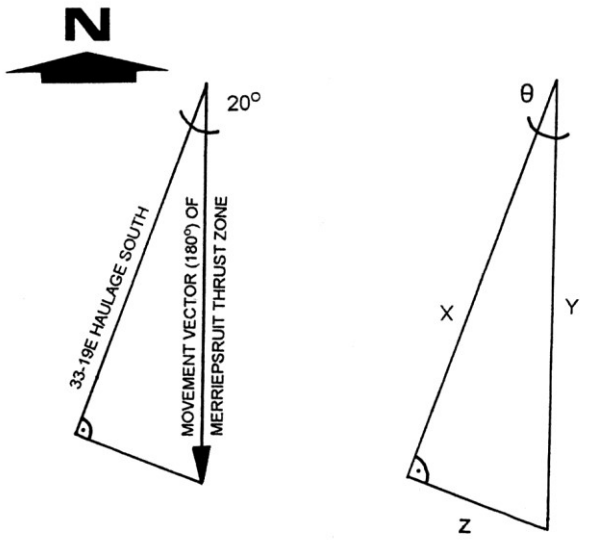
(c) Pre-deformational (folding) stage



Results:

The restoration of the section along 33-19E Haulage South to (a) pre-thrusting and (b) pre-folding stage, reveals **1230 m** (1240 m - 10 m) and **115 m** (1355 m – 1240 m) of apparent horizontal shortening due to thrusting and folding respectively. The overall minimum (apparent) value of horizontal shortening across the Merriespruit Thrust Zone amounts to **1345 m** (1230 m + 115 m or 1355 m - 10 m) along 33-19E Haulage South.

The true amount of (1) total horizontal shortening (folding and thrusting) and (2) horizontal shortening due to thrusting alone, that is in plane with the thrust direction (180°), was calculated to approximately **1431 m** and **1309 m** respectively, as illustrated below:



y = true amount of total horizontal shortening (?)

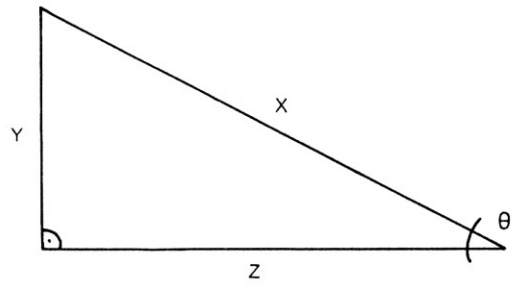
x = amount of (1) total (1345 m) and (2) thrust-related (1230 m) horizontal shortening along section 33-19E Haulage South

θ = angle between line of section 33-19E Haulage South and movement vector of Merriespruit Thrust Zone (20°)

(1) $y = x / \cos \theta$
$= 1345 \text{ m} / \cos 20^o$
$= 1431.31 \text{ m}$
$\approx$ **1431 m**

(2) $y = x / \cos \theta$
$= 1230 \text{ m} / \cos 20^o$
$= 1308.93 \text{ m}$
$\approx$ **1309 m**

Based on the established true amount of horizontal shortening due to thrusting (1309 m), the amount of south-directed reverse dip-slip movement along the fault planes of the Merriespruit Thrust Zone was calculated to approximately **1709 m**, as illustrated below:



x = reverse dip-slip movement across thrust zone (?)

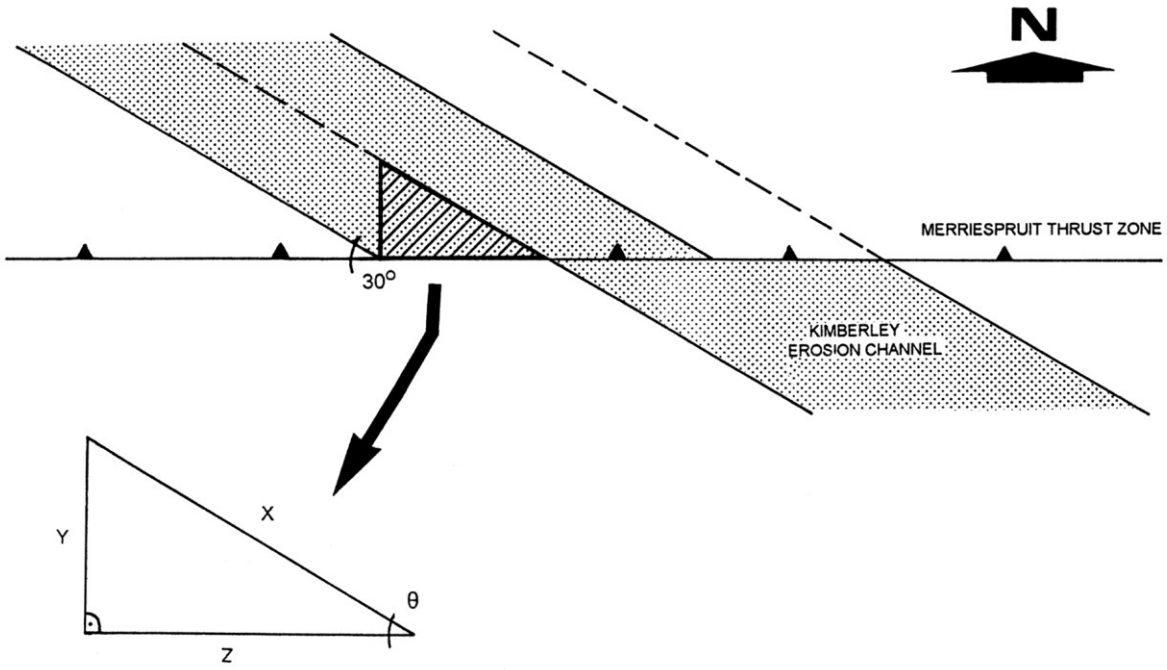
z = horizontal shortening due to thrusting (1309 m)

y = known net vertical upthrow across thrust zone (600 m)

θ = dip-angle of thrust zone (40°)

$x = z / \cos \theta$
$= 1309 \text{ m} / \cos 40^o$
$= 1708.77 \text{ m}$
$\approx$ **1709 m**

Detailed underground mapping did not reveal any evidence for strike-slip movements along the Merriespruit Thrust Zone. The approximately 2000 m apparent sinistral displacement of the Kimberley Erosion Channel (Geol. Dept. / Harmony G.M., pers. comm., 1994) is consequently envisaged to be the result of south-directed thrusting across the Merriespruit Thrust Zone alone, an interpretation that can be supported by the following calculation:



z = apparent left-lateral off-set across thrust zone (± 2000 m)
y = horizontal shortening due to thrusting (1309 m)
θ = angle between strike of erosion channel and thrust zone (30°)

$z = y / \tan \theta$
$= 1309 \text{ m} / \tan 30^{\circ}$
$= 2267.25 \text{ m}$
$\approx$ **2267 m**

APPENDIX 13

X-RAY DIFFRACTION ANALYSES OF SELECTED FAULT ROCK SPECIMENS FROM H.J. JOEL GOLD MINE

APPENDIX 13-A : List of analysed peaks of the X-ray diffraction angle [$^{o}2\theta$] and diffraction-value ($\alpha1$ and $\alpha2$ [Å]) and 2D-plot of diffraction-angle [$^{o}2\theta$] vs peak intensity [counts] for sample HJJ-60-1.

APPENDIX 13-B : List of analysed peaks of the X-ray diffraction angle [$^{o}2\theta$] and diffraction-value ($\alpha1$ and $\alpha2$ [Å]) and 2D-plot of diffraction-angle [$^{o}2\theta$] vs peak intensity [counts] for sample HJJ-70-18.

APPENDIX 13-C1 : List of analysed peaks of the X-ray diffraction angle [$^{o}2\theta$] and diffraction-value ($\alpha1$ and $\alpha2$ [Å]) and 2D-plot of diffraction-angle [$^{o}2\theta$] vs peak intensity [counts] for sample HJJ-70-19a (dark, chlorite-rich, pseudotachylitic layers).

APPENDIX 13-C2 : List of analysed peaks of the X-ray diffraction angle [$^{o}2\theta$] and diffraction-value ($\alpha1$ and $\alpha2$ [Å]) and 2D-plot of diffraction-angle [$^{o}2\theta$] vs peak intensity [counts] for sample HJJ-70-19b (light, sericite-pyrophyllite-rich, ultracataclastic layers).

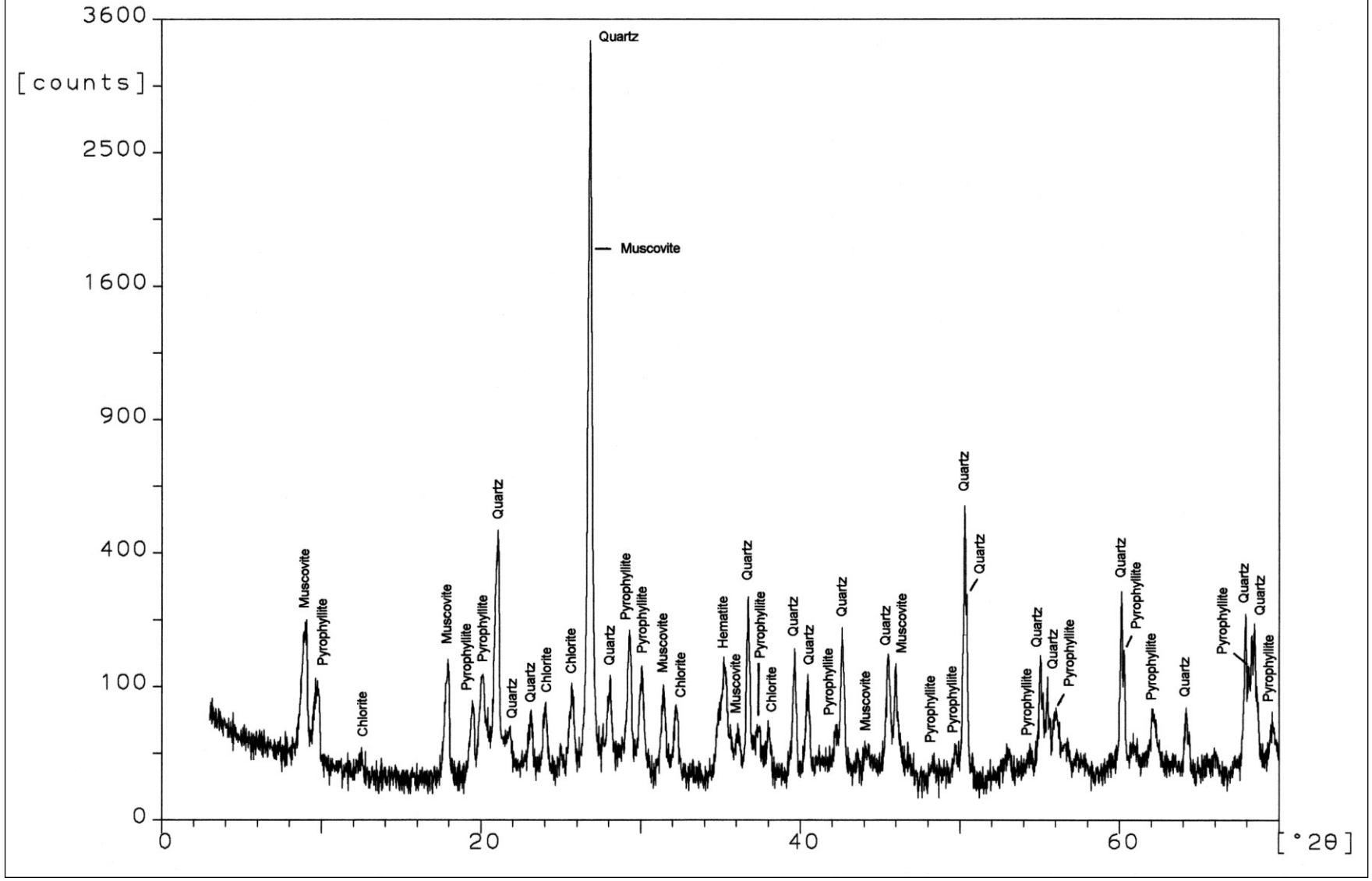
APPENDIX 13-A

Sample identification:	HJJ-60-1
Data measured at:	13-Sep-1996 11:19:00
Diffractometer type:	PW1710 BASED
Tube anode:	Cu
Generator tension [kV]:	40
Generator current [mA]:	20
Wavelength Alpha1 [Å]:	1.54056
Wavelength Alpha2 [Å]:	1.54439
Intensity ratio (alpha2/alpha1):	0.500
Divergence slit:	1°
Receiving slit:	0.1
Monochromator used:	YES
Start angle [°2θ]:	3.000
End angle [°2θ]:	70.000
Step size [°2θ]:	0.020
Maximum intensity:	3398.890
Time per step [s]:	0.800
Type of scan:	CONTINUOUS
Minimum peak tip width:	0.01
Maximum peak tip width:	1.00
Peak base width:	2.00
Minimum significance:	0.75
Number of peaks:	51

APPENDIX 13-A

Angle [°2θ]	d-value α1 [Å]	d-value α2 [Å]	Peak width [°2θ]	Peak int [counts]	Back. int [counts]	Rel. int [%]	Signif.
3.365	26.2349	26.3001	0.960	22	37	0.6	2.47
9.090	9.7206	9.7448	0.060	190	21	5.6	3.85
9.885	8.9405	8.9628	0.080	66	18	1.9	0.86
12.510	7.0698	7.0874	0.320	10	12	0.3	0.95
17.985	4.9281	4.9403	0.120	117	10	3.4	2.74
19.545	4.5381	4.5494	0.160	62	10	1.8	2.33
20.160	4.4010	4.4120	0.120	104	10	3.1	1.19
21.090	4.2090	4.2195	0.120	400	10	11.8	5.96
21.795	4.0744	4.0846	0.160	37	10	1.1	0.76
23.150	3.8389	3.8485	0.160	44	10	1.3	1.34
24.075	3.6935	3.7027	0.240	58	10	1.7	3.78
25.710	3.4622	3.4708	0.280	81	10	2.4	5.92
26.750	3.3299	3.3382	0.100	1849	10	54.4	0.81
26.855	3.3171	3.3253	0.120	3399	10	100.0	16.01
28.095	3.1735	3.1813	0.060	106	10	3.1	1.08
29.310	3.0446	3.0522	0.080	193	10	5.7	0.81
30.055	2.9708	2.9782	0.240	108	10	3.2	5.30
31.430	2.8439	2.8510	0.200	83	10	2.4	3.13
32.265	2.7722	2.7791	0.200	59	10	1.7	2.52
35.355	2.5367	2.5430	0.120	112	10	3.3	0.75
36.120	2.4847	2.4908	0.240	28	10	0.8	1.65
36.740	2.4442	2.4502	0.080	269	10	7.9	2.10
37.370	2.4044	2.4104	0.240	37	10	1.1	2.50
38.005	2.3657	2.3715	0.160	35	10	1.0	1.21
39.665	2.2704	2.2760	0.080	144	10	4.2	1.42
40.490	2.2260	2.2316	0.100	110	10	3.2	1.17
42.190	2.1402	2.1455	0.160	36	9	1.1	0.85
42.620	2.1196	2.1248	0.100	204	9	6.0	2.19
44.090	2.0523	2.0574	0.400	17	9	0.5	1.33
45.515	1.9913	1.9962	0.060	146	9	4.3	0.80
45.975	1.9724	1.9773	0.120	119	9	3.5	3.10
48.245	1.8848	1.8894	0.320	8	9	0.2	0.85
49.670	1.8340	1.8385	0.240	17	8	0.5	1.36
50.310	1.8121	1.8166	0.080	543	8	16.0	3.23
50.450	1.8074	1.8119	0.060	272	8	8.0	1.03
53.155	1.7217	1.7259	0.280	14	8	0.4	1.59
54.380	1.6857	1.6899	0.160	14	8	0.4	0.80
55.060	1.6665	1.6706	0.100	128	8	3.8	2.09
55.490	1.6546	1.6587	0.060	106	8	3.1	2.01
56.030	1.6399	1.6440	0.240	55	8	1.6	1.17
57.590	1.5992	1.6031	0.640	10	8	0.3	0.82
60.120	1.5378	1.5416	0.080	289	8	8.5	2.15
60.300	1.5336	1.5374	0.060	137	8	4.0	0.87
62.075	1.4940	1.4977	0.160	55	8	1.6	1.16
64.175	1.4500	1.4536	0.080	62	8	1.8	0.77
66.020	1.4139	1.4174	0.240	13	8	0.4	1.02
67.905	1.3792	1.3826	0.080	219	8	6.4	1.62
68.080	1.3761	1.3795	0.060	121	8	3.6	1.14
68.280	1.3725	1.3759	0.060	182	8	5.4	0.76
68.460	1.3693	1.3728	0.080	174	8	5.1	3.74
69.600	1.3497	1.3530	0.200	40	8	1.2	1.01

APPENDIX 13-A



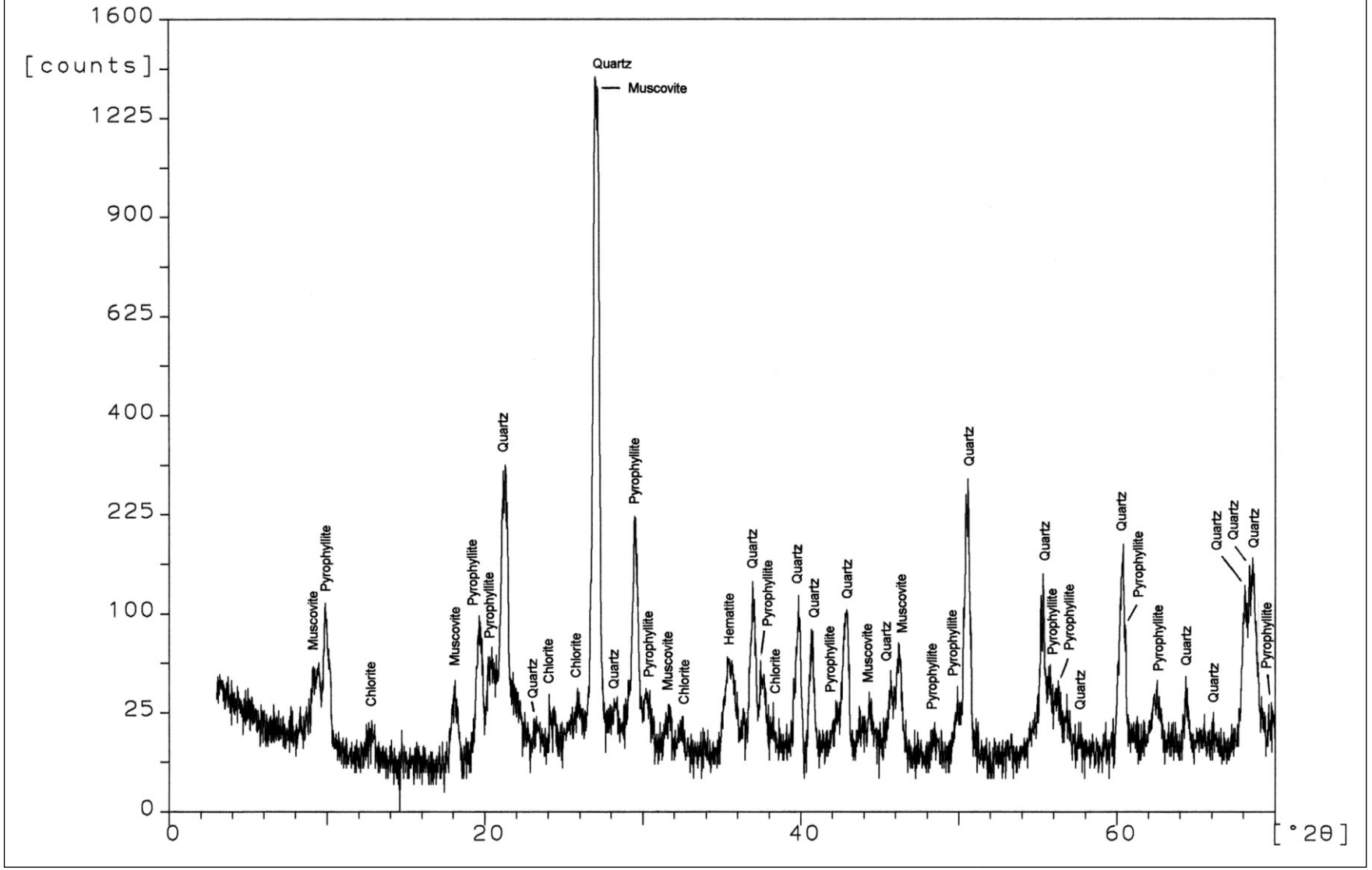
APPENDIX 13-B

Sample identification:	HJJ-70-18
Data measured at:	13-Sep-1996 14:02:00
Diffractometer type:	PW1710 BASED
Tube anode:	Cu
Generator tension [kV]:	40
Generator current [mA]:	20
Wavelength Alpha1 [Å]:	1.54056
Wavelength Alpha2 [Å]:	1.54439
Intensity ratio (alpha2/alpha1):	0.500
Divergence slit:	1°
Receiving slit:	0.1
Monochromator used:	YES
Start angle [°2θ]:	3.000
End angle [°2θ]:	70.000
Step size [°2θ]:	0.020
Maximum intensity:	1376.410
Time per step [s]:	0.800
Type of scan:	CONTINUOUS
Minimum peak tip width:	0.01
Maximum peak tip width:	1.00
Peak base width:	2.00
Minimum significance:	0.75
Number of peaks:	45

APPENDIX 13-B

Angle [°2θ]	d-value α1 [Å]	d-value α2 [Å]	Peak width [°2θ]	Peak int [counts]	Back. int [counts]	Rel. int [%]	Signif.
3.225	27.3734	27.4415	0.320	15	28	1.1	0.98
9.090	9.7206	9.7448	0.120	35	12	2.5	1.03
9.870	8.9541	8.9763	0.080	100	11	7.3	0.77
10.190	8.6736	8.6952	0.120	42	10	3.1	0.87
12.855	6.8808	6.8979	0.480	8	6	0.6	1.80
18.105	4.8957	4.9078	0.480	28	5	2.0	5.24
19.660	4.5118	4.5230	0.280	81	5	5.9	4.16
20.310	4.3689	4.3797	0.320	49	5	3.6	1.33
21.110	4.2051	4.2155	0.160	231	5	16.8	1.54
21.300	4.1680	4.1783	0.060	299	5	21.7	2.07
21.420	4.1449	4.1552	0.060	193	5	14.0	1.03
23.250	3.8226	3.8321	0.480	12	5	0.9	1.69
24.125	3.6859	3.6951	0.120	18	5	1.3	0.83
25.930	3.4333	3.4418	0.320	24	5	1.7	1.00
27.000	3.2996	3.3078	0.140	1376	5	100.0	6.33
27.160	3.2805	3.2887	0.120	1274	5	92.6	5.95
28.335	3.1471	3.1549	0.240	23	5	1.7	1.15
29.450	3.0305	3.0380	0.080	193	5	14.0	0.90
30.285	2.9488	2.9561	0.320	27	5	2.0	1.05
31.725	2.8181	2.8251	0.160	19	5	1.4	0.90
32.540	2.7494	2.7562	0.320	12	5	0.9	1.16
35.455	2.5297	2.5360	0.640	49	5	3.6	7.78
36.920	2.4327	2.4387	0.060	125	5	9.1	1.51
37.580	2.3914	2.3974	0.240	37	5	2.7	0.89
39.900	2.2576	2.2632	0.240	85	6	6.1	4.18
40.720	2.2140	2.2195	0.320	67	6	4.9	6.29
42.975	2.1029	2.1081	0.360	83	6	6.0	10.56
44.305	2.0428	2.0479	0.200	21	6	1.5	0.99
45.695	1.9838	1.9888	0.200	36	6	2.6	1.30
46.255	1.9611	1.9660	0.280	56	6	4.1	4.38
48.490	1.8758	1.8805	0.480	7	6	0.5	1.50
50.300	1.8125	1.8170	0.060	94	6	6.8	0.77
50.465	1.8069	1.8114	0.060	228	6	16.6	2.98
50.605	1.8023	1.8067	0.080	243	6	17.7	1.66
55.195	1.6627	1.6669	0.060	112	8	8.2	0.82
55.335	1.6589	1.6630	0.060	135	8	9.8	3.73
56.230	1.6346	1.6386	0.240	24	9	1.7	0.76
56.895	1.6170	1.6211	0.240	13	9	0.9	0.90
60.395	1.5314	1.5352	0.080	166	10	12.1	0.79
60.545	1.5280	1.5318	0.080	74	10	5.4	0.83
62.670	1.4812	1.4849	0.560	18	11	1.3	3.97
64.370	1.4461	1.4497	0.160	23	12	1.7	0.83
68.045	1.3767	1.3801	0.200	98	13	7.1	2.00
68.370	1.3709	1.3743	0.040	139	14	10.1	1.44
68.605	1.3668	1.3702	0.200	132	14	9.6	2.05

APPENDIX 13-B



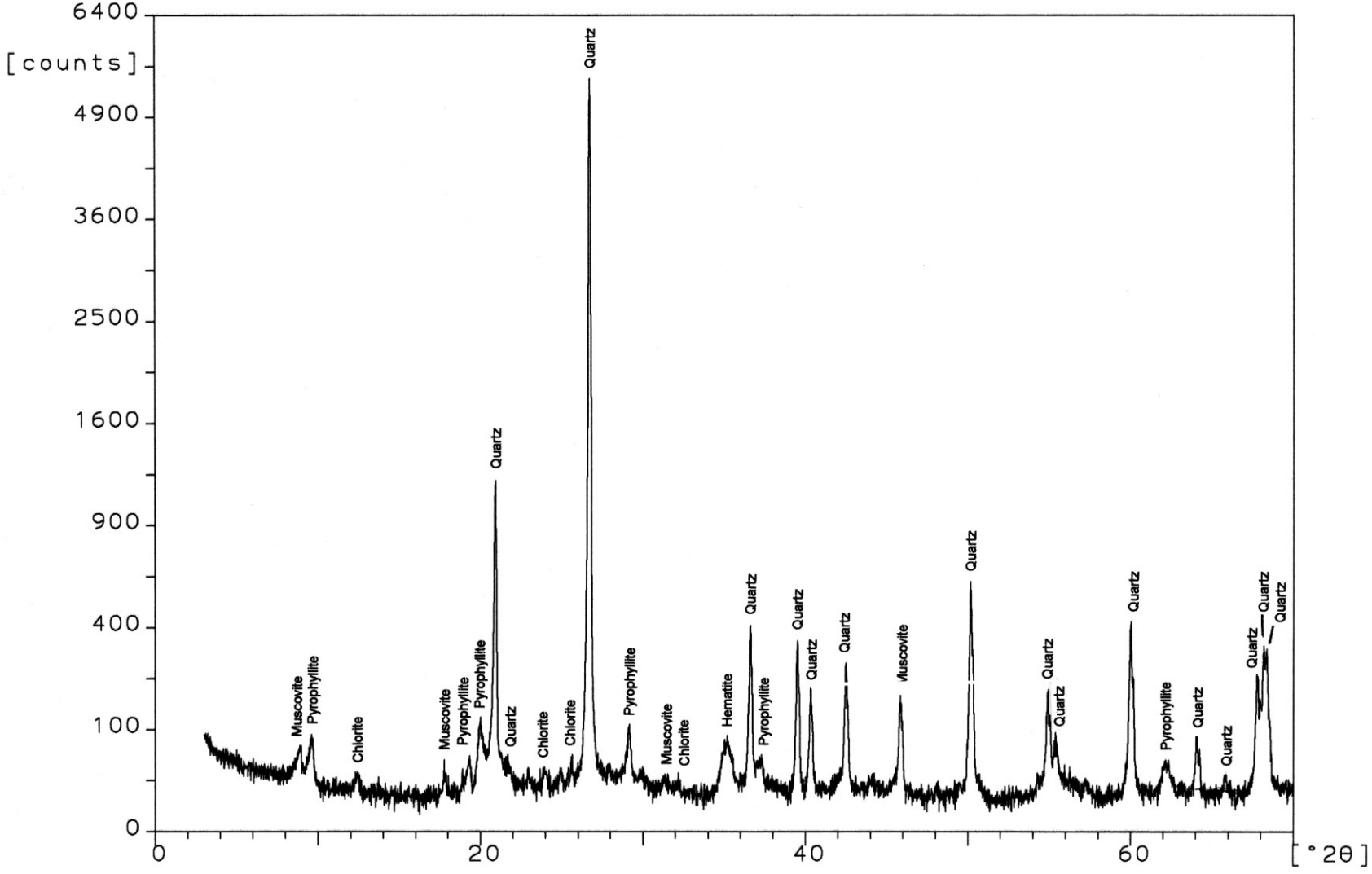
APPENDIX 13-C1

Sample identification:	HJJ-70-19a
Data measured at:	13-Sep-1996 13:06:00
Diffractometer type:	PW1710 BASED
Tube anode:	Cu
Generator tension [kV]:	40
Generator current [mA]:	20
Wavelength Alpha1 [Å]:	1.54056
Wavelength Alpha2 [Å]:	1.54439
Intensity ratio (alpha2/alpha1):	0.500
Divergence slit:	1°
Receiving slit:	0.1
Monochromator used:	YES
Start angle [°2θ]:	3.000
End angle [°2θ]:	70.000
Step size [°2θ]:	0.020
Maximum intensity:	5402.250
Time per step [s]:	0.800
Type of scan:	CONTINUOUS
Minimum peak tip width:	0.01
Maximum peak tip width:	1.00
Peak base width:	2.00
Minimum significance:	0.75
Number of peaks:	36

APPENDIX 13-C1

Angle [°2θ]	d-value α1 [Å]	d-value α2 [Å]	Peak width [°2θ]	Peak int [counts]	Back. int [counts]	Rel. int [%]	Signif.
8.905	9.9221	9.9468	0.200	42	25	0.8	1.34
9.640	9.1672	9.1900	0.200	59	22	1.1	2.51
12.425	7.1180	7.1357	0.240	16	15	0.3	2.46
17.810	4.9761	4.9884	0.120	17	11	0.3	1.25
19.310	4.5928	4.6042	0.200	38	11	0.7	1.81
19.950	4.4469	4.4579	0.280	96	12	1.8	4.83
20.925	4.2418	4.2524	0.140	1176	12	21.8	16.43
22.955	3.8711	3.8807	0.240	19	12	0.4	1.19
23.980	3.7079	3.7171	0.320	22	12	0.4	1.48
24.910	3.5715	3.5804	0.160	21	12	0.4	0.75
26.710	3.3348	3.3431	0.160	5402	13	100.0	48.44
27.940	3.1907	3.1986	0.240	26	13	0.5	0.78
29.190	3.0569	3.0644	0.120	92	14	1.7	1.43
31.655	2.8242	2.8312	0.640	6	14	0.1	1.33
35.155	2.5506	2.5570	0.640	64	12	1.2	8.99
36.580	2.4545	2.4606	0.100	380	12	7.0	3.86
37.255	2.4115	2.4175	0.240	36	12	0.7	2.40
39.515	2.2787	2.2843	0.100	342	12	6.3	3.48
40.330	2.2345	2.2400	0.100	185	12	3.4	2.66
42.505	2.1250	2.1303	0.080	253	12	4.7	1.77
44.035	2.0547	2.0598	0.320	14	12	0.3	0.77
45.865	1.9769	1.9818	0.100	142	11	2.6	1.81
50.180	1.8165	1.8210	0.080	600	11	11.1	2.87
50.320	1.8118	1.8163	0.080	296	11	5.5	1.34
52.550	1.7400	1.7444	0.080	7	10	0.1	0.81
54.910	1.6707	1.6749	0.100	159	10	2.9	2.06
55.390	1.6574	1.6615	0.160	72	10	1.3	1.06
57.260	1.6076	1.6116	0.320	12	11	0.2	0.85
59.995	1.5407	1.5445	0.080	392	12	7.3	2.40
60.175	1.5365	1.5403	0.080	202	12	3.7	1.65
62.135	1.4927	1.4964	0.240	34	12	0.6	0.75
64.050	1.4526	1.4562	0.100	61	12	1.1	1.21
65.810	1.4179	1.4214	0.200	15	12	0.3	1.29
67.780	1.3814	1.3849	0.120	210	14	3.9	3.22
68.165	1.3746	1.3780	0.100	313	14	5.8	2.03
68.370	1.3709	1.3743	0.080	292	15	5.4	1.13

APPENDIX 13-C1



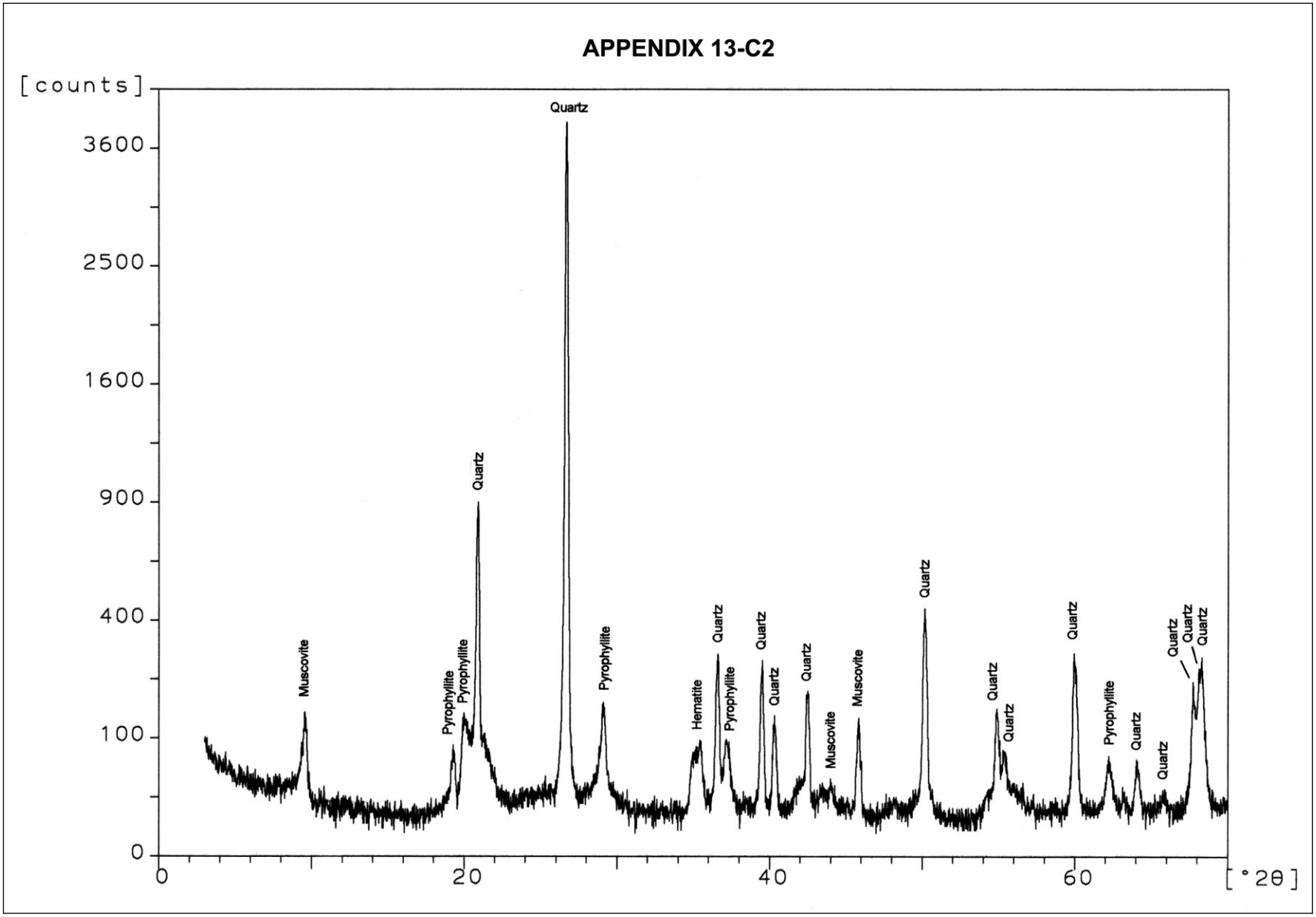
APPENDIX 13-C2

Sample identification:	HJJ-70-19b
Data measured at:	13-Sep-1996 12:13:00
Diffractometer type:	PW1710 BASED
Tube anode:	Cu
Generator tension [kV]:	40
Generator current [mA]:	20
Wavelength Alpha1 [Å]:	1.54056
Wavelength Alpha2 [Å]:	1.54439
Intensity ratio (alpha2/alpha1):	0.500
Divergence slit:	1°
Receiving slit:	0.1
Monochromator used:	YES
Start angle [°2θ]:	3.000
End angle [°2θ]:	70.000
Step size [°2θ]:	0.020
Maximum intensity:	3745.440
Time per step [s]:	0.800
Type of scan:	CONTINUOUS
Minimum peak tip width:	0.01
Maximum peak tip width:	1.00
Peak base width:	2.00
Minimum significance:	0.75
Number of peaks:	32

APPENDIX 13-C2

Angle [°2θ]	d-value α1 [Å]	d-value α2 [Å]	Peak width [°2θ]	Peak int [counts]	Back. int [counts]	Rel. int [%]	Signif.
9.630	9.1767	9.1995	0.200	104	25	2.8	3.35
13.035	6.7862	6.8031	0.480	3	14	0.1	1.00
19.320	4.5904	4.6018	0.280	58	18	1.5	4.47
19.925	4.4524	4.4635	0.200	102	19	2.7	1.79
20.920	4.2428	4.2534	0.200	858	22	22.9	21.47
26.705	3.3354	3.3437	0.220	3745	25	100.0	62.04
29.155	3.0604	3.0680	0.100	135	21	3.6	0.83
34.885	2.5698	2.5761	0.200	50	14	1.3	1.13
35.480	2.5280	2.5343	0.200	77	14	2.1	2.14
36.505	2.4593	2.4655	0.080	216	14	5.8	0.83
36.610	2.4525	2.4586	0.080	276	14	7.4	1.20
37.150	2.4181	2.4241	0.200	81	14	2.2	1.35
39.545	2.2770	2.2827	0.180	234	13	6.2	7.55
40.385	2.2316	2.2371	0.100	102	13	2.7	0.99
41.710	2.1637	2.1691	0.400	20	12	0.5	0.77
42.395	2.1303	2.1356	0.060	174	12	4.7	2.32
42.525	2.1241	2.1294	0.120	174	12	4.7	1.96
44.010	2.0558	2.0609	0.240	24	12	0.6	1.40
45.790	1.9799	1.9849	0.160	100	12	2.7	3.44
48.130	1.8890	1.8937	0.640	10	12	0.3	1.14
50.155	1.8174	1.8219	0.200	437	11	11.7	10.80
54.855	1.6722	1.6764	0.120	135	14	3.6	1.64
55.345	1.6586	1.6627	0.120	62	14	1.7	1.19
59.930	1.5422	1.5460	0.120	282	14	7.5	2.49
60.120	1.5378	1.5416	0.080	154	14	4.1	1.57
62.135	1.4927	1.4964	0.280	40	14	1.1	2.41
63.240	1.4692	1.4729	0.240	9	14	0.2	1.23
64.025	1.4531	1.4567	0.280	46	14	1.2	3.69
65.865	1.4169	1.4204	0.320	10	15	0.3	0.75
67.725	1.3824	1.3858	0.080	193	16	5.2	1.03
68.100	1.3757	1.3791	0.160	219	17	5.8	0.81
68.320	1.3718	1.3752	0.120	219	17	5.8	3.45

APPENDIX 13-C2



APPENDIX 14

X-RAY FLUORESCENCE ANALYSES OF SELECTED FAULT ROCK SPECIMENS FROM H.J. JOEL GOLD MINE

APPENDIX 14 : X-ray fluorescence analyses for major and trace elements of selected fault rock specimens from H.J. Joel Gold Mine.

Sample	HJJ-60-1	HJJ-70-18	HJJ-70-19a	HJJ-70-19b	HGM-31-4	HGM-31-8	HGM-33-4	HGM-33-7	HGM-33-10	HGM-35-1A
Major elements (wt%)										
SiO_2	75.68	82.76	86.43	86.54	82.34	79.08	66.23	62.77	63.91	46.87
TiO_2	0.33	0.26	0.21	0.25	0.37	0.51	0.77	0.34	0.63	0.96
Al_2O_3	16.46	12.56	10.38	8.91	13.04	12.27	20.51	16.45	26.25	20.61
Fe_2O_3	0.79	0.75	0.48	0.59	0.46	0.87	1.65	3.41	0.40	16.78
MnO	0.06	0.06	0.06	0.06	0.03	0.05	0.07	0.10	0.03	0.13
MgO	0.28	0.28	0.20	0.24	0.00	0.45	1.24	4.76	0.00	6.17
CaO	0.00	0.00	0.00	0.00	0.11	0.76	1.27	4.45	3.23	1.68
Na_2O	0.32	0.12	0.16	0.28	0.58	1.14	1.55	0.00	0.35	0.05
K_2O	3.46	1.40	0.25	0.93	0.44	0.64	0.94	0.05	1.03	0.24
P_2O_5	0.09	0.08	0.07	0.06	0.07	0.03	0.04	0.05	0.07	0.24
Total	99.96	100.36	100.31	99.76	100.00	98.65	100.46	98.56	100.49	100.35
Trace elements (ppm)										
Rb	92	35	5	23	17	20	43	36	11	29
Sr	57	33	17	24	34	76	109	65	8	71
Y	13	6	13	16	9	14	32	16	16	12
Zr	228	122	132	177	119	187	546	189	126	164
Nb	10	8	6	8	6	9	25	17	7	13
Co	8	6	4	5	9	17	30	<9	74	19
Ni	8	5	13	20	18	52	95	<9	257	22
Cu	Nd	nd	Nd	nd	20	102	24	3	111	9
Zn	10	11	11	9	10	19	48	10	177	14
V	63	45	28	31	42	49	76	82	410	52
Cr	228	134	111	143	192	275	423	314	120	231
Ba	189	72	19	61	127	179	258	385	<5	32
LOI	2.50	2.13	2.07	1.90	2.54	2.83	6.18	6.16	4.58	6.59

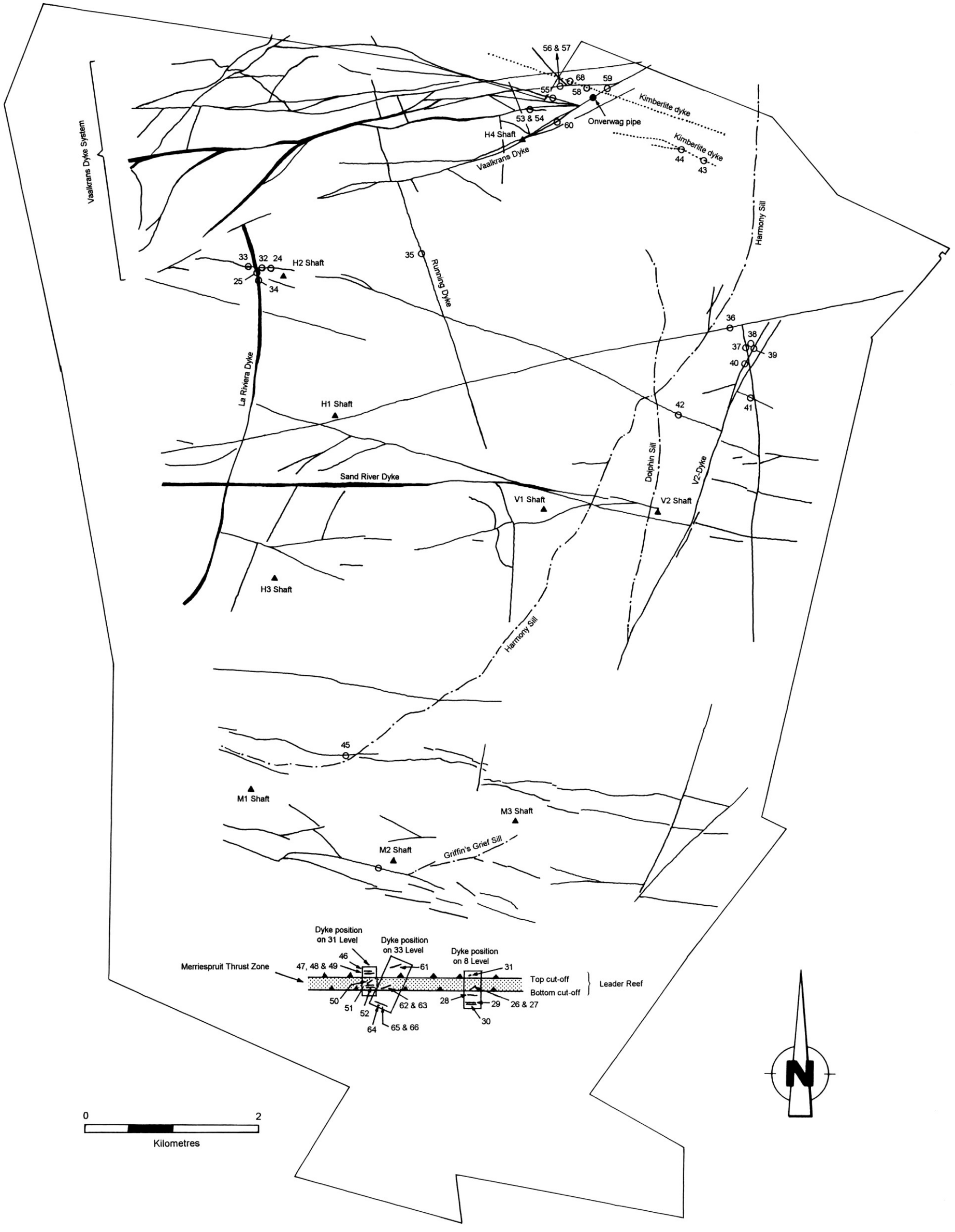
Note: HJJ-70-19a was taken from a cataclasite band, whereas HJJ-70-19b is from a pseudotachylitic zone.

APPENDIX 15

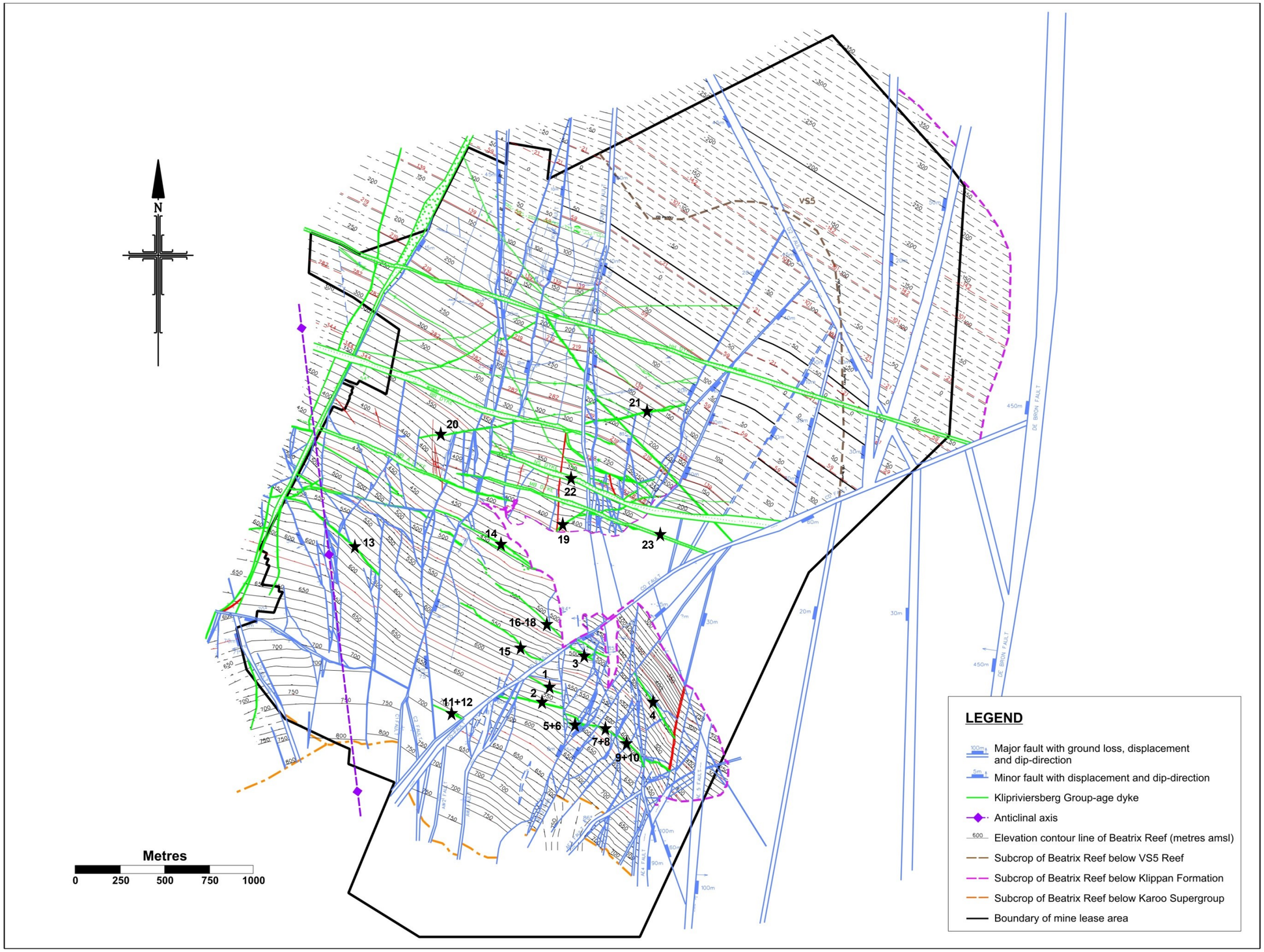
DYKE SAMPLE LOCALITIES IN THE SOUTHERN FREE STATE GOLDFIELD

APPENDIX 15-A : Lease area plan of Harmony Gold Mine, showing the occurrence of major dyke and sill intrusions, as well as sample localities of petrographically and geochemically studied specimens. Note: Sample numbers are laboratory sample numbers (Lab. No.) as indicated in Appendices 16-A & B.

APPENDIX 15-B : Lease area plan of H.J. Joel Gold Mine, showing the occurrence of major dyke and sill intrusions, as well as sample localities of petrographically and geochemically studied specimens. Note: Sample numbers are laboratory sample numbers (Lab. No.) as indicated in Appendices 16-A & B.



APPENDIX 15-A : Lease area plan of Harmony Gold Mine, showing the occurrence of major dyke and sill intrusions, as well as sample localities of petrographically and geochemically studied specimens. Note: Sample numbers are laboratory sample numbers (Lab. No.) as indicated in Appendices 16-A & B.



APPENDIX 15-B : Lease area plan of H.J. Joel Gold Mine, showing the occurrence of major dyke and sill intrusions, as well as sample localities of petrographically and geochemically studied specimens. Note: Sample numbers are laboratory sample numbers (Lab. No.) as indicated in Appendices 16-A & B.

APPENDIX 16

GEOCHEMICAL ANALYSIS OF INTRUSIONS FROM THE SOUTHERN FREE STATE GOLDFIELD

APPENDIX 16-A : Results of chemical analysis of major elements and stratigraphic classification of intrusions.

APPENDIX 16-B : Results of chemical analysis of trace elements and stratigraphic classification of intrusions.

Explanation

6 = Unit 6 (Orkney Formation)

7 = Unit 7 (Jeannette Formation)

8 = Unit 8 (Loraine Formation)

( ) = misclassification

APPENDIX 16-A : Results of chemical analysis of major elements and stratigraphic classification of intrusions.

Lab No.	Sample No.	SiO2	TiO2	Al2O3	Fe2O3	MnO	MgO	CaO	Na2O	K2O	P2O5	LOI	Total	Strat. Class.
1	HJJ-70-1	60,039	0,807	14,973	11,842	0,109	4,982	0,043	0,145	1,271	0,160	4,341	98,711	7
2	HJJ-70-2	46,015	0,647	16,340	13,142	0,216	6,379	5,502	0,131	1,063	0,154	9,187	98,775	7
3	HJJ-70-3A	53,451	0,571	13,933	10,345	0,169	5,645	5,549	0,106	0,859	0,140	8,444	99,211	7
4	HJJ-70-3B	45,477	1,273	34,520	0,994	0,061	0,934	0,655	0,806	8,168	0,114	5,869	98,870	7 (Allanridge)
5	HJJ-70-4	47,705	0,859	22,081	13,147	0,128	5,768	0,227	0,259	2,715	0,166	5,833	98,888	8
6	HJJ-70-5	41,243	0,805	22,678	17,447	0,136	7,601	0,186	0,190	1,824	0,194	6,472	98,775	8
7	HJJ-70-6	47,663	0,709	19,035	15,855	0,176	7,510	0,416	0,224	0,894	0,225	6,126	98,831	7
8	HJJ-70-7	52,914	0,782	20,535	11,513	0,123	4,752	0,236	0,290	2,755	0,190	5,000	99,091	7
9	HJJ-70-8	45,812	0,605	14,964	10,580	0,295	4,356	9,928	0,166	1,553	0,139	11,257	99,654	7
10	HJJ-70-9	32,188	0,724	22,624	25,870	0,189	9,415	0,169	0,066	0,101	0,190	7,569	99,106	7
11	HJJ-70-11A	65,755	0,743	19,727	5,001	0,066	1,802	0,062	0,270	2,348	0,127	3,909	99,812	7
12	HJJ-70-11B	54,691	0,643	18,745	12,989	0,117	4,405	0,095	0,212	1,772	0,163	4,785	98,617	8
13	HJJ-70-12	57,524	0,888	17,235	11,255	0,102	4,245	0,140	0,236	2,293	0,165	4,544	98,627	7
14	HJJ-70-13	40,439	0,926	23,583	17,994	0,148	6,492	0,233	0,264	2,288	0,203	6,358	98,929	7 (3)
15	HJJ-70-14	50,274	1,046	28,037	4,599	0,070	1,787	0,290	0,487	6,867	0,258	4,678	98,390	7 (3)
16	HJJ-70-15A	37,969	1,242	31,504	10,812	0,096	3,707	0,000	0,361	6,477	0,091	6,155	98,413	7 (Allanridge)
17	HJJ-70-15B	48,973	1,064	28,067	4,376	0,073	1,797	0,250	0,532	6,843	0,263	6,249	98,486	7 (3)
18	HJJ-70-15C	35,962	1,893	30,856	13,868	0,116	4,848	0,065	0,369	5,600	0,155	4,811	98,543	7 (4)
19	HJJ-90-1	20,191	0,318	4,141	1,894	0,077	2,085	49,501	0,422	0,052	0,091	22,229	101,001	8
20	HJJ-90-2	66,875	0,493	12,765	9,751	0,114	4,283	0,067	0,137	1,050	0,147	3,606	99,288	8
21	HJJ-90-3	60,456	0,597	16,541	10,510	0,122	4,531	0,112	0,175	2,101	0,178	4,155	99,476	8
22	HJJ-90-4	48,080	1,115	18,353	17,735	0,159	5,894	0,123	0,128	1,232	0,186	5,317	98,321	7 (5)
23	HJJ-90-5	54,147	0,720	18,506	12,104	0,147	4,917	0,689	0,237	2,264	0,158	5,081	98,968	7
24	HGM-8-1	47,064	0,356	9,246	8,787	0,115	13,230	6,127	0,045	0,000	0,104	13,715	98,790	8
25	HGM-8-2	44,230	0,434	11,727	10,645	0,137	12,540	5,705	0,018	0,000	0,117	13,218	98,771	8
26	HGM-8-1M	58,319	0,601	13,874	13,845	0,136	7,411	0,059	0,093	0,023	0,141	5,061	99,562	7
27	HGM-8-2M	52,432	0,646	15,674	15,959	0,137	8,259	0,074	0,095	0,043	0,148	5,717	99,185	7
28	HGM-8-4M	51,331	0,525	17,685	15,535	0,129	7,182	0,237	0,352	0,248	0,167	6,003	99,394	8
29	HGM-8-5M	71,257	1,530	11,734	7,841	0,077	1,904	0,313	0,369	1,396	0,268	2,739	99,427	7 (4)
30	HGM-8-6M	51,880	1,465	14,282	13,983	0,129	5,849	6,494	0,070	0,099	0,258	5,728	100,237	7 (4)
31	HGM-8-7M	50,532	0,432	11,580	9,720	0,126	12,572	8,229	0,064	0,016	0,116	5,714	99,099	8 - Sill
32	HGM-11-1	49,282	0,383	10,118	8,552	0,116	10,787	6,453	0,033	0,000	0,109	12,659	98,492	8
33	HGM-11-2	38,859	0,378	10,689	10,743	0,153	15,334	6,963	0,026	0,003	0,101	15,727	98,976	8
34	HGM-11-3	45,953	0,349	8,858	8,026	0,109	12,467	7,872	0,021	0,015	0,093	15,595	99,360	8
35	HGM-11-4	50,550	2,890	8,230	16,910	0,200	10,510	5,230	0,260	0,010	0,320	4,880	99,791	Karoo
36	HGM-12-1	54,878	0,723	13,924	10,398	0,116	5,067	7,351	2,400	0,311	0,167	3,860	99,195	8
37	HGM-12-2	47,219	1,448	8,293	14,389	0,119	10,783	7,982	1,834	0,188	0,295	6,416	98,966	Karoo
38	HGM-12-3	41,897	0,728	11,933	9,201	0,335	5,617	10,240	0,234	2,263	0,138	17,230	99,818	7 - Sill
39	HGM-12-4	14,331	0,331	9,542	12,349	0,201	13,983	18,771	0,038	0,046	0,081	30,907	100,581	8
40	HGM-12-5	50,522	0,547	18,971	12,756	0,115	6,990	0,804	0,187	1,561	0,119	6,637	99,208	8
41	HGM-12-6	40,663	0,407	12,066	13,463	0,235	10,747	7,403	0,009	0,001	0,117	15,227	100,338	8
42	HGM-16-1	43,274	0,356	9,768	9,782	0,134	15,294	6,751	0,000	0,000	0,093	14,761	100,211	8
43	HGM-21-1	32,875	4,006	4,251	14,857	0,128	23,357	11,152	0,480	2,238	0,708	5,438	99,490	Kimberlite
44	HGM-25-1	33,254	4,090	4,666	15,576	0,132	19,959	7,681	0,464	2,396	1,012	9,456	98,686	Kimberlite
45	HGM-28-1	48,680	1,320	14,000	15,720	0,230	6,050	10,960	0,880	0,020	0,140	2,000	99,638	7 (1)
46	HGM-31-1	47,189	0,450	11,474	12,894	0,139	11,392	5,406	0,024	0,111	0,111	9,459	98,648	8
47	HGM-31-2A	37,465	1,222	11,705	13,253	0,176	6,732	14,750	0,620	0,009	0,229	14,621	100,225	6 (1)
48	HGM-31-2B	48,941	1,386	13,320	13,529	0,123	6,249	10,377	0,069	0,020	0,261	5,168	99,442	6
49	HGM-31-2C	40,189	1,217	11,289	11,585	0,162	5,395	14,844	0,140	0,277	0,234	14,579	99,908	6 (5)
50	HGM-31-5	50,039	0,409	11,336	10,499	0,144	11,205	5,491	0,029	0,003	0,126	9,623	98,903	8
51	HGM-31-6	48,272	0,444	10,611	9,615	0,122	15,928	3,163	0,019	0,000	0,115	10,878	99,167	8
52	HGM-31-7	52,042	1,646	15,797	19,209	0,104	4,389	0,386	0,323	0,562	0,299	5,549	100,306	6 (2)
53	HGM-32-1	39,316	0,487	12,855	12,281	0,254	7,342	12,270	0,115	0,012	0,135	13,959	99,024	8
54	HGM-32-2	46,811	0,490	12,567	11,828	0,221	7,176	8,063	0,046	0,016	0,080	10,955	98,252	8
55	HGM-32-3	38,008	0,855	27,438	13,111	0,100	8,203	0,056	0,358	3,206	0,126	7,275	98,736	8 (1)
56	HGM-32-4	55,926	0,528	14,739	12,929	0,117	9,762	0,079	0,042	0,020	0,149	5,829	100,120	8
57	HGM-32-5	67,735	0,602	21,100	0,225	0,054	0,513	0,000	0,542	0,573	0,102	2,826	99,432	8
58	HGM-32-6	30,284	3,428	3,184	13,518	0,131	15,743	13,995	0,441	1,168	0,653	16,279	98,825	Kimberlite
59	HGM-32-7	55,257	0,458	13,154	11,036	0,099	8,752	2,797	0,049	0,025	0,097	7,329	99,052	8
60	HGM-32-9	49,250	0,420	12,446	10,115	0,171	7,044	7,341	0,078	0,192	0,117	11,176	98,349	8
61	HGM-33-2	40,992	0,656	17,918	19,864	0,147	12,123	0,057	0,034	0,007	0,149	7,264	99,211	7
62	HGM-33-5	63,512	0,404	11,133	9,286	0,107	9,749	0,067	0,036	0,000	0,123	5,122	99,539	8
63	HGM-33-6	48,022	0,457	11,657	10,033	0,118	12,905	5,964	0,007	0,007	0,126	10,298	99,595	8
64	HGM-33-8	55,696	0,338	9,154	7,113	0,150	7,903	7,792	0,039	0,005	0,104	10,028	98,323	8 - Sill
65	HGM-33-9A	42,892	1,413	13,540	12,922	0,138	5,756	13,130	0,061	0,000	0,262	8,871	98,985	7 (5)
66	HGM-33-9B	47,347	0,598	13,951	11,449	0,161	10,469	5,526	0,041	0,012	0,137	9,627	99,317	7
67	HGM-33-13	52,980	0,900	14,790	13,650	0,180	5,110	6,300	2,610	1,080	0,120	2,290	99,748	6
68	HGM-33-H4-1	33,248	3,591	3,599	13,757	0,135	16,721	11,839	0,448	1,682	0,717	13,050	98,788	Kimberlite
69	DRP-JDR 23-1	53,623	0,503	14,165	8,871	0,128	7,414	6,760	3,911	0,591	0,143	2,567	98,676	8 - Lava
70	DRP-JDR 23-2	36,399	0,404	14,268	23,433	0,168	13,130	3,451	0,370	0,247	0,135	7,630	99,634	8
71	DRP-JDR 23-3	52,211	0,741	14,958	10,588	0,125	6,416	10,543	2,217	0,774	0,217	0,767	99,555	Karoo
72	DRP-JDR 23-4	56,043	0,508	15,122	8,644	0,128	5,924	4,678	3,700	1,413	0,144	2,459	98,763	8 - Lava

APPENDIX 16-B : Results of chemical analysis of trace elements and stratigraphic classification of intrusions.

Lab No.	Sample No.	Rb	Sr	Y	Zr	Nb	Co	Ni	Cu	Zn	V	Cr	Ba	Strat. Class.
1	HJJ-70-1	43,320	25,190	15,980	93,810	7,700	71,290	417,630	63,710	187,570	366,650	1409,060	165,300	7
2	HJJ-70-2	40,080	48,910	13,370	93,710	7,150	36,710	183,850	27,960	147,080	233,270	216,930	162,430	7
3	HJJ-70-3A	33,820	41,840	8,070	85,420	7,730	34,310	140,970	24,120	131,190	198,020	168,730	173,210	7
4	HJJ-70-3B	231,830	268,830	28,800	190,500	11,550	11,490	39,670	0,000	21,310	419,670	383,740	863,500	7 (Allanridge)
5	HJJ-70-4	85,430	66,150	57,990	106,210	8,370	89,860	346,450	22,160	150,630	390,120	831,540	347,480	8
6	HJJ-70-5	63,000	43,100	66,850	102,250	8,160	71,420	506,040	55,050	264,600	384,310	826,650	212,330	8
7	HJJ-70-6	33,760	54,970	8,910	107,390	8,930	60,550	251,740	50,270	190,150	272,080	227,540	167,240	7
8	HJJ-70-7	84,780	71,090	13,060	116,410	7,510	30,020	180,580	124,010	134,930	315,580	257,270	377,370	7
9	HJJ-70-8	56,260	62,350	11,120	89,030	7,530	34,330	157,540	52,890	134,890	212,350	182,980	236,210	7
10	HJJ-70-9	19,120	23,320	12,560	106,550	7,250	109,810	396,740	486,310	288,600	325,090	228,170	47,260	7
11	HJJ-70-11A	64,660	45,870	29,110	110,160	7,810	24,020	103,320	49,940	63,710	265,180	224,280	369,900	7
12	HJJ-70-11B	56,260	41,620	64,400	92,990	7,280	99,650	191,720	12,830	147,690	247,770	302,920	255,500	8
13	HJJ-70-12	72,510	38,490	24,990	104,960	8,000	44,610	405,080	44,300	178,880	422,050	1573,200	251,080	7
14	HJJ-70-13	76,080	64,830	14,320	140,680	8,980	88,400	302,710	22,610	234,510	349,840	301,580	275,970	7 (3)
15	HJJ-70-14	196,590	93,820	22,770	159,000	10,030	38,710	124,100	87,840	67,780	378,580	373,840	551,870	7 (3)
16	HJJ-70-15A	180,000	72,000	30,000	194,000	13,000	99,000	532,000	25,000	147,000	598,000	2242,000	533,000	7 (Allanridge)
17	HJJ-70-15B	202,950	96,870	24,770	163,310	9,480	30,120	109,430	64,670	67,030	371,550	352,140	553,270	7 (3)
18	HJJ-70-15C	166,420	78,890	28,010	217,700	12,060	67,770	489,760	425,600	293,540	678,750	2808,650	425,550	7 (4)
19	HJJ-90-1	21,280	135,490	10,650	97,280	6,950	8,250	19,670	2,010	25,000	59,580	71,900	181,850	8
20	HJJ-90-2	34,680	25,990	18,930	64,500	6,710	97,820	424,170	41,350	194,820	242,490	2678,630	217,120	8
21	HJJ-90-3	62,500	30,840	14,200	77,260	6,700	71,820	408,370	32,810	207,960	299,610	2996,100	262,910	8
22	HJJ-90-4	48,000	24,000	15,980	130,430	9,070	115,410	776,150	17,770	272,660	479,000	1974,330	158,940	7 (5)
23	HJJ-90-5	72,690	46,100	20,900	108,790	7,050	47,950	164,690	27,180	141,010	276,070	237,080	360,780	7
24	HGM-8-1	7,710	34,330	6,360	42,920	5,580	49,610	389,130	5,030	97,150	152,810	2190,050	30,770	8
25	HGM-8-2	8,430	59,750	6,280	59,630	6,300	61,720	531,910	36,720	115,070	208,140	3247,630	56,240	8
26	HGM-8-1M	9,320	9,110	15,870	75,830	7,260	42,580	214,490	52,030	433,400	244,000	519,350	39,460	7
27	HGM-8-2M	10,580	11,950	9,180	83,420	7,350	73,610	254,160	20,860	245,510	275,820	582,710	37,320	7
28	HGM-8-4M	19,200	98,890	10,870	88,750	7,820	54,330	196,340	6,410	192,060	215,430	461,450	128,900	8
29	HGM-8-5M	46,910	48,760	23,470	169,710	12,350	29,170	148,080	262,680	134,290	180,620	219,660	290,780	7 (4)
30	HGM-8-6M	13,720	169,720	36,230	152,760	10,010	49,840	78,630	55,080	100,040	297,210	216,950	4873,520	7 (4)
31	HGM-8-7M	7,970	153,800	10,320	52,970	6,080	55,610	332,710	36,570	75,590	167,460	1873,420	49,780	8 - Sill
32	HGM-11-1	6,810	51,550	6,650	46,680	4,590	51,110	374,550	17,610	119,240	160,270	2157,580	32,010	8
33	HGM-11-2	8,110	51,620	6,450	46,230	6,190	46,180	424,470	43,090	125,190	165,860	2590,820	31,750	8
34	HGM-11-3	7,170	65,970	5,900	42,710	5,390	47,770	374,750	23,980	117,110	140,070	2063,600	32,280	8
35	HGM-11-4	1,000	95,000	24,000	256,000	25,000	71,340	615,240	227,680	106,810	318,000	1102,000	275,470	Karoo
36	HGM-12-1	19,000	275,000	22,000	139,000	12,000	45,000	86,000	91,000	98,000	245,000	54,000	204,000	8
37	HGM-12-2	12,000	632,000	18,000	251,000	29,000	75,000	429,000	214,000	112,000	210,000	807,000	366,000	Karoo
38	HGM-12-3	63,000	104,000	24,000	75,000	7,000	31,000	87,000	76,000	131,000	290,000	137,000	396,000	7 - Sill
39	HGM-12-4	10,000	213,000	11,000	44,000	6,000	28,000	411,000	0,000	166,000	163,000	2187,000	74,000	8
40	HGM-12-5	46,000	34,000	10,000	81,000	7,000	175,000	605,000	8,000	364,000	271,000	4104,000	250,000	8
41	HGM-12-6	6,000	37,000	11,000	55,000	6,000	64,000	409,000	11,000	212,000	198,000	2340,000	48,000	8
42	HGM-16-1	4,000	83,000	4,000	48,000	6,000	42,000	386,000	0,000	104,000	181,000	1980,000	29,000	8
43	HGM-21-1	100,230	896,520	26,780	314,320	194,250	97,540	894,800	110,990	112,250	188,560	686,830	1392,060	Kimberlite
44	HGM-25-1	100,790	708,170	33,190	543,190	224,840	111,280	971,040	163,370	129,610	236,020	633,140	1215,300	Kimberlite
45	HGM-28-1	1,000	210,000	26,000	77,000	2,000	57,000	193,000	41,320	138,590	338,000	194,000	343,000	7 (1)
46	HGM-31-1	8,390	28,510	10,060	55,780	6,260	57,160	340,570	10,230	101,560	178,110	1432,680	34,170	8
47	HGM-31-2A	12,690	49,360	36,880	131,710	9,880	39,180	73,670	50,090	226,590	256,510	178,230	26,310	6 (1)
48	HGM-31-2B	13,490	330,870	40,070	150,360	9,890	48,080	83,910	51,760	127,120	266,790	236,660	36,320	6
49	HGM-31-2C	21,330	51,630	28,260	125,120	9,400	35,980	64,720	31,610	130,220	246,450	163,100	194,160	6 (5)
50	HGM-31-5	6,590	19,500	11,450	52,150	4,910	61,180	408,340	129,890	536,970	197,760	1744,140	36,580	8
51	HGM-31-6	6,340	14,300	8,920	57,580	6,000	45,890	324,430	17,450	84,610	186,780	2001,140	31,120	8
52	HGM-31-7	27,970	60,710	48,850	177,190	11,970	47,010	101,620	43,850	197,030	378,760	247,060	186,960	6 (2)
53	HGM-32-1	11,920	59,580	7,170	58,880	5,590	59,470	554,590	123,260	308,550	218,380	3377,810	35,680	8
54	HGM-32-2	9,800	58,920	8,210	59,730	6,210	59,730	562,770	128,770	307,900	207,800	3180,270	29,910	8
55	HGM-32-3	104,160	71,020	12,250	117,780	7,400	80,600	589,020	0,000	275,480	418,800	3058,070	644,540	8 (1)
56	HGM-32-4	9,010	9,710	6,630	76,060	6,420	53,160	267,710	1,900	165,000	241,620	1364,210	35,530	8
57	HGM-32-5	178,210	106,210	13,720	88,900	7,340	5,380	6,790	0,000	14,020	270,670	1491,750	1776,460	8
58	HGM-32-6	70,610	1235,240	22,800	463,520	179,180	94,230	883,380	90,000	103,610	202,600	685,880	718,280	Kimberlite
59	HGM-32-7	7,640	25,700	6,780	61,430	6,390	56,780	244,270	14,470	90,070	197,500	1099,710	51,930	8
60	HGM-32-9	11,000	42,000	11,000	60,000	6,000	49,000	256,000	23,000	213,000	188,000	1004,000	86,000	8
61	HGM-33-2	12,620	9,240	8,250	82,630	7,100	138,330	723,400	0,000	260,900	323,450	4198,750	32,590	7
62	HGM-33-5	5,330	8,940	9,940	53,840	6,210	72,650	275,880	0,000	138,550	176,080	1358,630	30,970	8
63	HGM-33-6	7,420	23,200	7,650	59,180	5,790	46,530	322,030	21,640	95,540	198,410	1632,650	35,400	8
64	HGM-33-8	6,980	38,460	13,310	45,750	5,690	38,850	194,680	9,180	166,690	153,460	966,630	51,320	8 - Sill
65	HGM-33-9A	12,570	264,740	38,040	152,470	10,410	44,520	76,100	36,890	170,690	284,660	218,760	85,170	7 (5)
66	HGM-33-9B	8,090	20,630	14,680	76,270	6,630	37,200	222,400	21,110	210,070	232,280	539,530	32,540	7
67	HGM-33-13	25,000	510,000	18,000	106,000	3,500	60,000	131,720	49,580	156,840	211,000	14,000	31,860	6
68	HGM-33-H4-1	87,440	980,130	23,690	552,920	187,760	101,930	932,550	106,460	111,150	222,420	712,620	861,850	Kimberlite
69	DRP-JDR 23-1	20,000	497,000	14,000	82,000	7,000	45,000	172,000	45,000	88,000	189,000	275,000	1376,000	8 - Lava
70	DRP-JDR 23-2	20,000	91,000	8,000	55,000	6,000	134,000	526,000	20,000	191,000	253,000	2930,000	295,000	8
71	DRP-JDR 23-3	23,000	207,000	26,000	112,000	10,000	37,000	46,000	75,000	99,000	260,000	262,000	283,000	Karoo
72	DRP-JDR 23-4	37,000	336,000	13,000	87,000	7,000	40,000	138,000	44,000	77,000	167,000	158,000	2116,000	8 - Lava

APPENDIX 17

DISCRIMINANT FUNCTION ANALYSIS

APPENDIX 17-A : Calculation of Discriminant Function 1 (Fn1)

$$FN1 = 15.1483 \times TiO_2 - 0.12907 \times Y - 0.01643 \times Zr - 11.9865$$

(after Linton & McCarthy, 1993)

APPENDIX 17-B : Calculation of Discriminant Function 2 (Fn2)

$$FN2 = -9.60491 \times TiO_2 - 0.14676 \times Y + 0.14589 \times Zr - 4.43084$$

(after Linton & McCarthy, 1993)

APPENDIX 17-A : Calculation of Discriminant Function 1 (Fn1)

Lab No.	Sample No.	Constant	TiO2	Constant	Y	Constant	Zr	Constant		FN1
1	HJJ-70-1	11,9865	0,807	15,1483	15,980	0,12907	93,810	0,01643		-3,3656588
2	HJJ-70-2	11,9865	0,647	15,1483	13,370	0,12907	93,710	0,01643		-5,4508711
3	HJJ-70-3A	11,9865	0,571	15,1483	8,070	0,12907	85,420	0,01643		-5,7818662
4	HJJ-70-3B	11,9865	1,273	15,1483	28,800	0,12907	190,500	0,01643		0,4501549
5	HJJ-70-4	11,9865	0,859	15,1483	57,990	0,12907	106,210	0,01643		-8,2039099
6	HJJ-70-5	11,9865	0,805	15,1483	66,850	0,12907	102,250	0,01643		-10,1004155
7	HJJ-70-6	11,9865	0,709	15,1483	8,910	0,12907	107,390	0,01643		-4,1607867
8	HJJ-70-7	11,9865	0,782	15,1483	13,060	0,12907	116,410	0,01643		-3,7387999
9	HJJ-70-8	11,9865	0,605	15,1483	11,120	0,12907	89,030	0,01643		-5,7197998
10	HJJ-70-9	11,9865	0,724	15,1483	12,560	0,12907	106,550	0,01643		-4,3908665
11	HJJ-70-11A	11,9865	0,743	15,1483	29,110	0,12907	110,160	0,01643		-6,2984696
12	HJJ-70-11B	11,9865	0,643	15,1483	64,400	0,12907	92,990	0,01643		-12,0860768
13	HJJ-70-12	11,9865	0,888	15,1483	24,990	0,12907	104,960	0,01643		-3,4847617
14	HJJ-70-13	11,9865	0,926	15,1483	14,320	0,12907	140,680	0,01643		-2,118829
15	HJJ-70-14	11,9865	1,046	15,1483	22,770	0,12907	159,000	0,01643		-1,6926721
16	HJJ-70-15A	11,9865	1,242	15,1483	30,000	0,12907	194,000	0,01643		-0,2318314
17	HJJ-70-15B	11,9865	1,064	15,1483	24,770	0,12907	163,310	0,01643		-1,748956
18	HJJ-70-15C	11,9865	1,893	15,1483	28,010	0,12907	217,700	0,01643		9,4971702
19	HJJ-90-1	11,9865	0,318	15,1483	10,650	0,12907	97,280	0,01643		-10,1422465
20	HJJ-90-2	11,9865	0,493	15,1483	18,930	0,12907	64,500	0,01643		-8,0214182
21	HJJ-90-3	11,9865	0,597	15,1483	14,200	0,12907	77,260	0,01643		-6,0451407
22	HJJ-90-4	11,9865	1,115	15,1483	15,980	0,12907	130,430	0,01643		0,698351
23	HJJ-90-5	11,9865	0,72	15,1483	20,900	0,12907	108,790	0,01643		-5,5647067
24	HGM-8-1	11,9865	0,356	15,1483	6,360	0,12907	42,920	0,01643		-8,119766
25	HGM-8-2	11,9865	0,434	15,1483	6,280	0,12907	59,630	0,01643		-7,2024183
26	HGM-8-1M	11,9865	0,601	15,1483	15,870	0,12907	75,830	0,01643		-6,1765995
27	HGM-8-2M	11,9865	0,646	15,1483	9,180	0,12907	83,420	0,01643		-4,7561514
28	HGM-8-4M	11,9865	0,525	15,1483	10,870	0,12907	88,750	0,01643		-6,8947959
29	HGM-8-5M	11,9865	1,53	15,1483	23,470	0,12907	169,710	0,01643		5,3727908
30	HGM-8-6M	11,9865	1,465	15,1483	36,230	0,12907	152,760	0,01643		3,0197066
31	HGM-8-7M	11,9865	0,432	15,1483	10,320	0,12907	52,970	0,01643		-7,6447339
32	HGM-11-1	11,9865	0,383	15,1483	6,650	0,12907	46,680	0,01643		-7,809969
33	HGM-11-2	11,9865	0,378	15,1483	6,450	0,12907	46,230	0,01643		-7,852503
34	HGM-11-3	11,9865	0,349	15,1483	5,900	0,12907	42,710	0,01643		-8,1629816
35	HGM-11-4	11,9865	2,89	15,1483	24,000	0,12907	256,000	0,01643		24,488327
36	HGM-12-1	11,9865	0,723	15,1483	22,000	0,12907	139,000	0,01643		-6,1575891
37	HGM-12-2	11,9865	1,448	15,1483	18,000	0,12907	251,000	0,01643		3,5010484
38	HGM-12-3	11,9865	0,728	15,1483	24,000	0,12907	75,000	0,01643		-5,2884676
39	HGM-12-4	11,9865	0,331	15,1483	11,000	0,12907	44,000	0,01643		-9,1151027
40	HGM-12-5	11,9865	0,547	15,1483	10,000	0,12907	81,000	0,01643		-6,3219099
41	HGM-12-6	11,9865	0,407	15,1483	11,000	0,12907	55,000	0,01643		-8,1445619
42	HGM-16-1	11,9865	0,356	15,1483	4,000	0,12907	48,000	0,01643		-7,8986252
43	HGM-21-1	11,9865	4,006	15,1483	26,780	0,12907	314,320	0,01643		40,0768176
44	HGM-25-1	11,9865	4,09	15,1483	33,190	0,12907	543,190	0,01643		36,761602
45	HGM-28-1	11,9865	1,32	15,1483	26,000	0,12907	77,000	0,01643		3,388326
46	HGM-31-1	11,9865	0,45	15,1483	10,060	0,12907	55,780	0,01643		-7,3846746
47	HGM-31-2A	11,9865	1,222	15,1483	36,880	0,12907	131,710	0,01643		-0,3993743
48	HGM-31-2B	11,9865	1,386	15,1483	40,070	0,12907	150,360	0,01643		1,3667941
49	HGM-31-2C	11,9865	1,217	15,1483	28,260	0,12907	125,120	0,01643		0,7457413
50	HGM-31-5	11,9865	0,409	15,1483	11,450	0,12907	52,150	0,01643		-8,1255213
51	HGM-31-6	11,9865	0,444	15,1483	8,920	0,12907	57,580	0,01643		-7,3579986
52	HGM-31-7	11,9865	1,646	15,1483	48,850	0,12907	177,190	0,01643		3,7313006
53	HGM-32-1	11,9865	0,487	15,1483	7,170	0,12907	58,880	0,01643		-6,5021082
54	HGM-32-2	11,9865	0,49	15,1483	8,210	0,12907	59,730	0,01643		-6,6048616
55	HGM-32-3	11,9865	0,855	15,1483	12,250	0,12907	117,780	0,01643		-2,5509364
56	HGM-32-4	11,9865	0,528	15,1483	6,630	0,12907	76,060	0,01643		-6,0935975
57	HGM-32-5	11,9865	0,602	15,1483	13,720	0,12907	88,900	0,01643		-6,0986908
58	HGM-32-6	11,9865	3,428	15,1483	22,800	0,12907	463,520	0,01643		29,3834428
59	HGM-32-7	11,9865	0,458	15,1483	6,780	0,12907	61,430	0,01643		-6,9329681
60	HGM-32-9	11,9865	0,42	15,1483	11,00	0,12907	60,00	0,01643		-8,029784
61	HGM-33-2	11,9865	0,656	15,1483	8,250	0,12907	82,630	0,01643		-4,4716536
62	HGM-33-5	11,9865	0,404	15,1483	9,940	0,12907	53,840	0,01643		-8,0341338
63	HGM-33-6	11,9865	0,457	15,1483	7,650	0,12907	59,180	0,01643		-7,0234398
64	HGM-33-8	11,9865	0,338	15,1483	13,310	0,12907	45,750	0,01643		-9,3359688
65	HGM-33-9A	11,9865	1,413	15,1483	38,040	0,12907	152,470	0,01643		2,003143
66	HGM-33-9B	11,9865	0,598	15,1483	14,680	0,12907	76,270	0,01643		-6,0756803
67	HGM-33-13	11,9865	0,9	15,1483	18,000	0,12907	106,000	0,01643		-2,41787
68	HGM-33-H4-1	11,9865	3,591	15,1483	23,690	0,12907	552,920	0,01643		30,2689014
69	DRP-JDR 23-1	11,9865	0,503	15,1483	14,000	0,12907	82,000	0,01643		-7,5211451
70	DRP-JDR 23-2	11,9865	0,404	15,1483	8,000	0,12907	55,000	0,01643		-7,8027968
71	DRP-JDR 23-3	11,9865	0,741	15,1483	26,000	0,12907	112,000	0,01643		-5,9575897
72	DRP-JDR 23-4	11,9865	0,508	15,1483	13,000	0,12907	87,000	0,01643		-7,3984836

APPENDIX 17-B : Calculation of Discriminant Function 2 (Fn2)

Lab No.	Sample No.	Constant	TiO2	Constant	Y	Constant	Zr	Constant		FN2
1	HJJ-70-1	4,43048	0,807	-9,60491	15,980	0,14676	93,810	0,14589		-0,84092627
2	HJJ-70-2	4,43048	0,647	-9,60491	13,370	0,14676	93,710	0,14589		1,06431393
3	HJJ-70-3A	4,43048	0,571	-9,60491	8,070	0,14676	85,420	0,14589		1,36268699
4	HJJ-70-3B	4,43048	1,273	-9,60491	28,800	0,14676	190,500	0,14589		6,90782657
5	HJJ-70-4	4,43048	0,859	-9,60491	57,990	0,14676	106,210	0,14589		-5,69673319
6	HJJ-70-5	4,43048	0,805	-9,60491	66,850	0,14676	102,250	0,14589		-7,05608605
7	HJJ-70-6	4,43048	0,709	-9,60491	8,910	0,14676	107,390	0,14589		3,11913431
8	HJJ-70-7	4,43048	0,782	-9,60491	13,060	0,14676	116,410	0,14589		3,12484968
9	HJJ-70-8	4,43048	0,605	-9,60491	11,120	0,14676	89,030	0,14589		1,11516495
10	HJJ-70-9	4,43048	0,724	-9,60491	12,560	0,14676	106,550	0,14589		2,31683906
11	HJJ-70-11A	4,43048	0,743	-9,60491	29,110	0,14676	110,160	0,14589		0,23213067
12	HJJ-70-11B	4,43048	0,643	-9,60491	64,400	0,14676	92,990	0,14589		-6,49147003
13	HJJ-70-12	4,43048	0,888	-9,60491	24,990	0,14676	104,960	0,14589		-1,31455808
14	HJJ-70-13	4,43048	0,926	-9,60491	14,320	0,14676	140,680	0,14589		5,09757534
15	HJJ-70-14	4,43048	1,046	-9,60491	22,770	0,14676	159,000	0,14589		5,37756894
16	HJJ-70-15A	4,43048	1,242	-9,60491	30,000	0,14676	194,000	0,14589		7,54008178
17	HJJ-70-15B	4,43048	1,064	-9,60491	24,770	0,14676	163,310	0,14589		5,53994646
18	HJJ-70-15C	4,43048	1,893	-9,60491	28,010	0,14676	217,700	0,14589		5,03693077
19	HJJ-90-1	4,43048	0,318	-9,60491	10,650	0,14676	97,280	0,14589		5,14434382
20	HJJ-90-2	4,43048	0,493	-9,60491	18,930	0,14676	64,500	0,14589		-2,53396243
21	HJJ-90-3	4,43048	0,597	-9,60491	14,200	0,14676	77,260	0,14589		-0,97714187
22	HJJ-90-4	4,43048	1,115	-9,60491	15,980	0,14676	130,430	0,14589		1,54325325
23	HJJ-90-5	4,43048	0,72	-9,60491	20,900	0,14676	108,790	0,14589		1,4580739
24	HGM-8-1	4,43048	0,356	-9,60491	6,360	0,14676	42,920	0,14589		-2,52162276
25	HGM-8-2	4,43048	0,434	-9,60491	6,280	0,14676	59,630	0,14589		-0,82124304
26	HGM-8-1M	4,43048	0,601	-9,60491	15,870	0,14676	75,830	0,14589		-1,46927341
27	HGM-8-2M	4,43048	0,646	-9,60491	9,180	0,14676	83,420	0,14589		0,18763514
28	HGM-8-4M	4,43048	0,525	-9,60491	10,870	0,14676	88,750	0,14589		1,87939855
29	HGM-8-5M	4,43048	1,53	-9,60491	23,470	0,14676	169,710	0,14589		2,1885424
30	HGM-8-6M	4,43048	1,465	-9,60491	36,230	0,14676	152,760	0,14589		-1,53263155
31	HGM-8-7M	4,43048	0,432	-9,60491	10,320	0,14676	52,970	0,14589		-2,36657102
32	HGM-11-1	4,43048	0,383	-9,60491	6,650	0,14676	46,680	0,14589		-2,27496933
33	HGM-11-2	4,43048	0,378	-9,60491	6,450	0,14676	46,230	0,14589		-2,26324328
34	HGM-11-3	4,43048	0,349	-9,60491	5,900	0,14676	42,710	0,14589		-2,41751569
35	HGM-11-4	4,43048	2,89	-9,60491	24,000	0,14676	256,000	0,14589		1,63657001
36	HGM-12-1	4,43048	0,723	-9,60491	22,000	0,14676	139,000	0,14589		5,67516007
37	HGM-12-2	4,43048	1,448	-9,60491	18,000	0,14676	251,000	0,14589		15,63832032
38	HGM-12-3	4,43048	0,728	-9,60491	24,000	0,14676	75,000	0,14589		-4,00334448
39	HGM-12-4	4,43048	0,331	-9,60491	11,000	0,14676	44,000	0,14589		-2,80490521
40	HGM-12-5	4,43048	0,547	-9,60491	10,000	0,14676	81,000	0,14589		0,66512423
41	HGM-12-6	4,43048	0,407	-9,60491	11,000	0,14676	55,000	0,14589		-1,93008837
42	HGM-16-1	4,43048	0,356	-9,60491	4,000	0,14676	48,000	0,14589		-1,43414796
43	HGM-21-1	4,43048	4,006	-9,60491	26,780	0,14676	314,320	0,14589		-0,98183746
44	HGM-25-1	4,43048	4,09	-9,60491	33,190	0,14676	543,190	0,14589		30,6604628
45	HGM-28-1	4,43048	1,32	-9,60491	26,000	0,14676	77,000	0,14589		-9,691551
46	HGM-31-1	4,43048	0,45	-9,60491	10,060	0,14676	55,780	0,14589		-2,0913509
47	HGM-31-2A	4,43048	1,222	-9,60491	36,880	0,14676	131,710	0,14589		-2,36501692
48	HGM-31-2B	4,43048	1,386	-9,60491	40,070	0,14676	150,360	0,14589		-1,68753806
49	HGM-31-2C	4,43048	1,217	-9,60491	28,260	0,14676	125,120	0,14589		-2,01333627
50	HGM-31-5	4,43048	0,409	-9,60491	11,450	0,14676	52,150	0,14589		-2,43112669
51	HGM-31-6	4,43048	0,444	-9,60491	8,920	0,14676	57,580	0,14589		-1,60381304
52	HGM-31-7	4,43048	1,646	-9,60491	48,850	0,14676	177,190	0,14589		-1,55913876
53	HGM-32-1	4,43048	0,487	-9,60491	7,170	0,14676	58,880	0,14589		-1,57033717
54	HGM-32-2	4,43048	0,49	-9,60491	8,210	0,14676	59,730	0,14589		-1,6277758
55	HGM-32-3	4,43048	0,855	-9,60491	12,250	0,14676	117,780	0,14589		2,74243615
56	HGM-32-4	4,43048	0,528	-9,60491	6,630	0,14676	76,060	0,14589		0,62150212
57	HGM-32-5	4,43048	0,602	-9,60491	13,720	0,14676	88,900	0,14589		0,74343798
58	HGM-32-6	4,43048	3,428	-9,60491	22,800	0,14676	463,520	0,14589		26,92069332
59	HGM-32-7	4,43048	0,458	-9,60491	6,780	0,14676	61,430	0,14589		-0,86253888
60	HGM-32-9	4,43048	0,42	-9,60491	11,00	0,14676	60,00	0,14589		-1,3255022
61	HGM-33-2	4,43048	0,656	-9,60491	8,250	0,14676	82,630	0,14589		0,11281974
62	HGM-33-5	4,43048	0,404	-9,60491	9,940	0,14676	53,840	0,14589		-1,91494044
63	HGM-33-6	4,43048	0,457	-9,60491	7,650	0,14676	59,180	0,14589		-1,30886767
64	HGM-33-8	4,43048	0,338	-9,60491	13,310	0,14676	45,750	0,14589		-2,95584768
65	HGM-33-9A	4,43048	1,413	-9,60491	38,040	0,14676	152,470	0,14589		-1,34111993
66	HGM-33-9B	4,43048	0,598	-9,60491	14,680	0,14676	76,270	0,14589		-1,20162268
67	HGM-33-13	4,43048	0,9	-9,60491	18,000	0,14676	106,000	0,14589		-0,252599
68	HGM-33-H4-1	4,43048	3,591	-9,60491	23,690	0,14676	552,920	0,14589		38,26704259
69	DRP-JDR 23-1	4,43048	0,503	-9,60491	14,000	0,14676	82,000	0,14589		0,64659027
70	DRP-JDR 23-2	4,43048	0,404	-9,60491	8,000	0,14676	55,000	0,14589		-1,46099364
71	DRP-JDR 23-3	4,43048	0,741	-9,60491	26,000	0,14676	112,000	0,14589		0,97620169
72	DRP-JDR 23-4	4,43048	0,508	-9,60491	13,000	0,14676	87,000	0,14589		1,47477572

APPENDIX 18

PREVIOUSLY PROPOSED GENETIC MODELS FOR THE TECTONIC FRAMEWORK OF THE "WITWATERSRAND TRIAD"

APPENDIX 18-A : The interference-fold pattern of the Witwatersrand Basin (after Pretorius, 1986b).

APPENDIX 18-B : Basin-and-dome structures resulting from the superimposition of two sets of orthogonal folds (after Pretorius, 1984).

APPENDIX 18-C : Diagrammatic illustration of the Basin Edge Concept for the Witwatersrand Basin, showing classic depositional response to taphrogenic basin development (after Brock & Pretorius, 1964b).

APPENDIX 18-D : The relationship between goldfields, fluvial fans, palaeocurrent directions and major fold axes in the Witwatersrand Basin (after Pretorius, 1976b).

APPENDIX 18-E : The location of the major goldfields in synclinal downwarps between basement granite domes (after Pretorius, 1976b).

APPENDIX 18-F : The southeasterly-directed, regressive nature of the western basin margin and shift of the depositional axis in the Klerksdorp Goldfield (after Pretorius, 1976b).

APPENDIX 18-G : Schematic illustration of Witwatersrand Basin evolution; inward migration of the basin-margins occurred contemporaneously with marginal uplift and basin-subsidence (after Vos, 1975).

APPENDIX 18-H : The relative position of the depositional axes of progressively younger Proterozoic sedimentary basins on the Kaapvaal Craton (after Pretorius, 1976b).

APPENDIX 18-I : Reconstructed subsurface plan of the Central Rand Group, with adjacent granite domes and sites of major fluvial influx (after Hutchison, 1975; Minter, 1976, 1978 and Minter *et al.*, 1986).

APPENDIX 18-J : Compression and associated overthrusting along the boundaries of the Kaapvaal and Zimbabwe cratons, envisaged as cause for cross-folding in the Witwatersrand Basin (after Pretorius, 1984).

APPENDIX 18-K : Tectonic setting and schematic illustration of the evolution of the Witwatersrand Basin, according to the continent-continent collisional theory of Van Biljon (1980).

APPENDIX 18-L : Map and cross-sections illustrating the formation of the Witwatersrand Basin as a foreland basin within the Kaapvaal Craton in response to continental collision between the Kaapvaal and Zimbabwe cratons at approximately 2.7 Ga (after Burke *et al.*, 1986).

APPENDIX 18-M : Schematic NW-SE cross-sections of the central and northern Kaapvaal Craton, illustrating the evolution of the Witwatersrand Basin in a cratonic, back-arc, plate-tectonic setting from syn-Witwatersrand compression to mid-Ventersdorp extension. The rapid transition to Klipriviersberg volcanism is envisaged to be due to subduction of a mid-ocean ridge (after Winter, 1987).

APPENDIX 18-N : The strike-slip reactivation of major, pre-existing fault zones within the Kaapvaal Craton, as well as the development and movement of large fault-bounded basement blocks within the area of the Witwatersrand Basin during the Limpopo Orogeny, controlled sedimentation particularly in the last stages of the basin history (after Myers *et al.*, 1990 and Stanistreet & McCarthy, 1991).

APPENDIX 18-O : Evolution of the Witwatersrand Basin, including (A) the formation of the extensional Dominion Group basin with subsequent thermal subsidence sedimentation during lower West Rand Group, (B) the formation of a retro-arc basin due to subduction beneath the northeastern margin of the Kaapvaal Craton during upper West Rand Group and lowermost Central Rand Group deposition, (C) tectonic escape due to collision of the Kaapvaal and Zimbabwe cratons during Central Rand Group sedimentation, and (D) the development of the Ventersdorp impactogenic rift during Platberg Group sedimentation due to ultimate indentation (after Stanistreet & McCarthy, 1991).

APPENDIX 18-P : (A) Map of the Limpopo Belt and adjoining parts of the Zimbabwe and Kaapvaal cratons showing structural elements interpreted to have formed in response to the collision of both cratons during the Limpopo Orogeny, (B) schematic section from the Witwatersrand Basin to north of Harare showing the northward migration of deformation during the Limpopo Orogeny (for explanation see original), and (C) simplified tectonic map of the India-Asia collision zone showing the Himalayan S-verging thrusts, the major Tibetan strike-slip zones and the formation of the Central Asian hinterland basins (*e.g.,* Tarim basin) as proposed analogy to the formation of the Witwatersrand Basin (after Treloar *et al.*, 1992).

APPENDIX 18-Q : (A) Structural setting and evolution of the Witwatersrand and Ventersdorp basins in relation to the Limpopo Orogeny and (B) comparison of the Witwatersrand Basin with sub-Andean basins in South America (after Coward *et al.*, 1996).

APPENDIX 18-R : Map and cross-section of the Kaapvaal and Zimbabwe cratons, illustrating the formation of the Ventersdorp Rift System within the Kaapvaal Craton as impactogen, in response to continental collision between the Kaapvaal and Zimbabwe cratons at 2.64 Ga (after Burke *et al.*, 1985a).

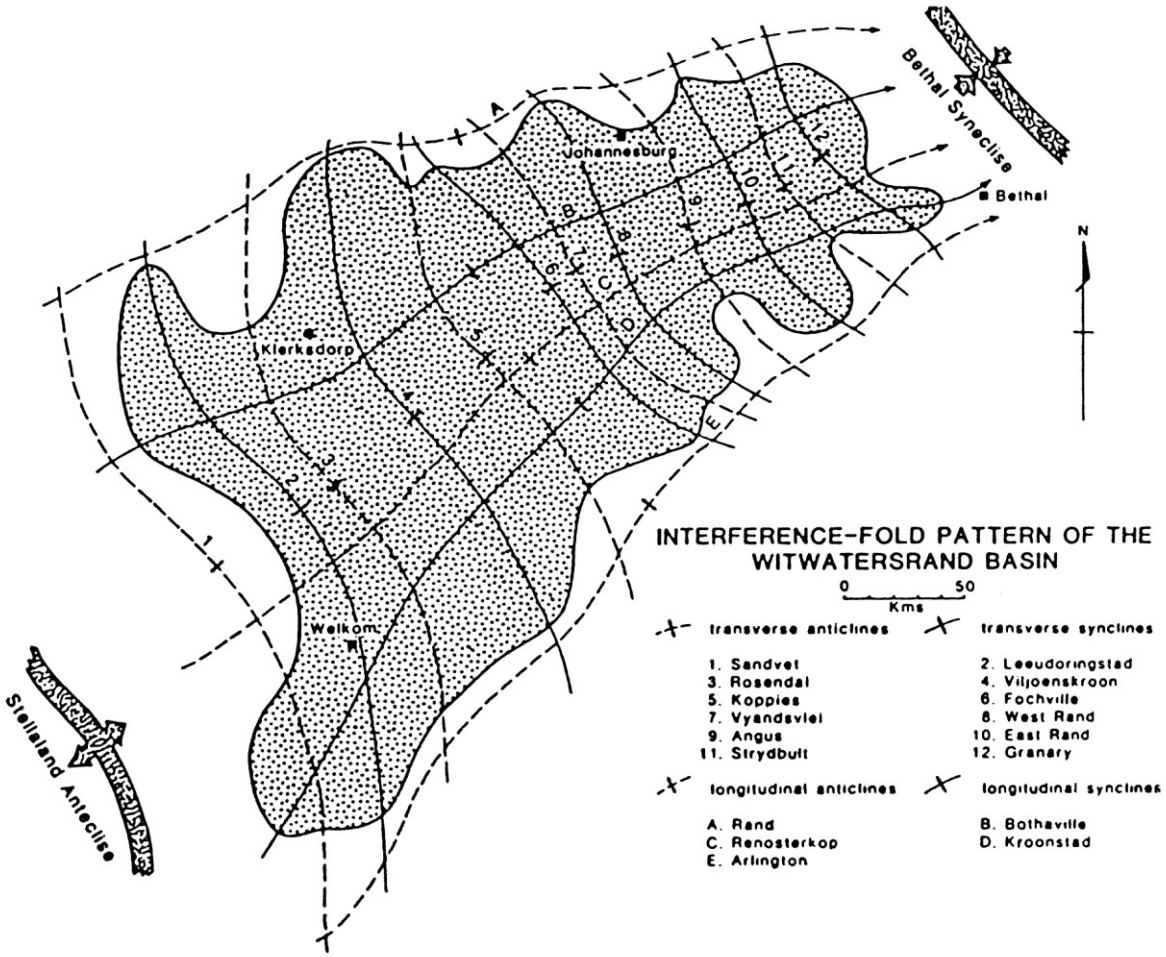
APPENDIX 18-S : Wernicke's normal simple shear hypothesis as applied to the development of the Ventersdorp Supergroup. Initial down-to-the-west, listric normal faulting during Klipriviersberg Group time, followed by overprinting of the detached terranes by large fault-block ranges due to the development of a second breakaway producing the Platberg Group grabens (after Clendenin *et al.*, 1988c).

APPENDIX 18-T : (A) & (B) palaeogeographical reconstructions of intraplate deformation and successor basin development within the Kaapvaal Craton prior to and following oblique collision of the Kaapvaal and Zimbabwe cratons from 3.0 to pre-2.2 Ga (after Clendenin *et al.* 1988a) and (C) proposal of a three-stage rift model for the evolution of the successor basin sequence (after Clendenin *et al.*, 1988b).

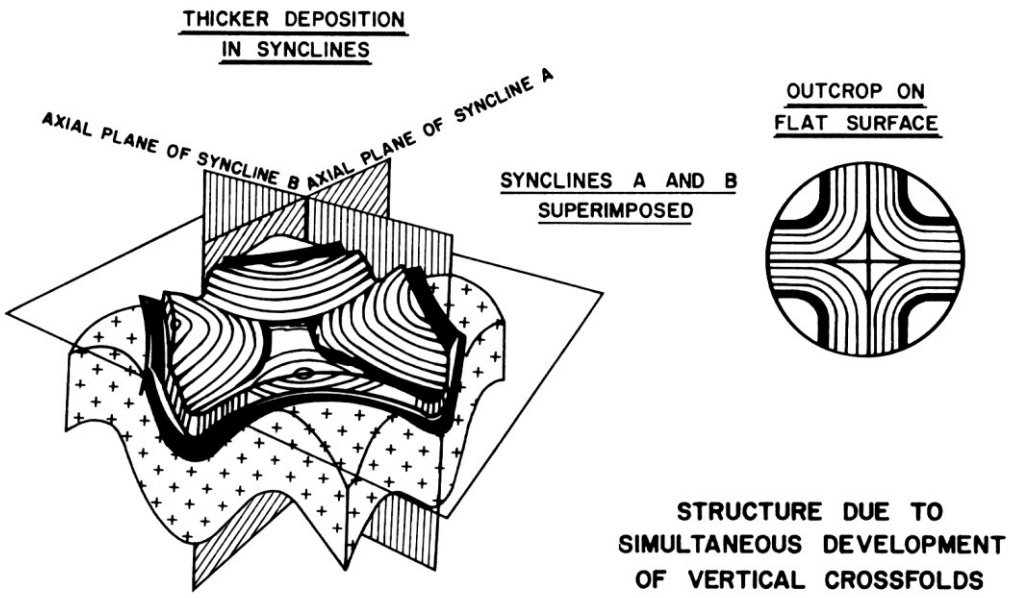
APPENDIX 18-U : (A) Schematic representation illustrating the stages of tectonic evolution in the formation of the "Witwatersrand Triad" (after Robb *et al.*, 1991) and (B) magmatic and sedimentary events pertaining to the evolution of the Witwatersrand Basin and environs (after Robb & Meyer, 1994).

APPENDIX 18-V : Schematic diagrams showing (A) the Archaean crustal subdomains/terranes of the Kaapvaal Craton, (B) the distribution of granite-greenstone terranes of the Kaapvaal Craton and (C) a composite N-S profile across the Limpopo Mobile Belt, indicating northwards-directed tectonic transport at 2.9-2.7 Ga, overprinted by the ~2.7 Ga southward-directed thrusting related to the climax of the Limpopo Orogeny (after De Wit *et al.*, 1992).

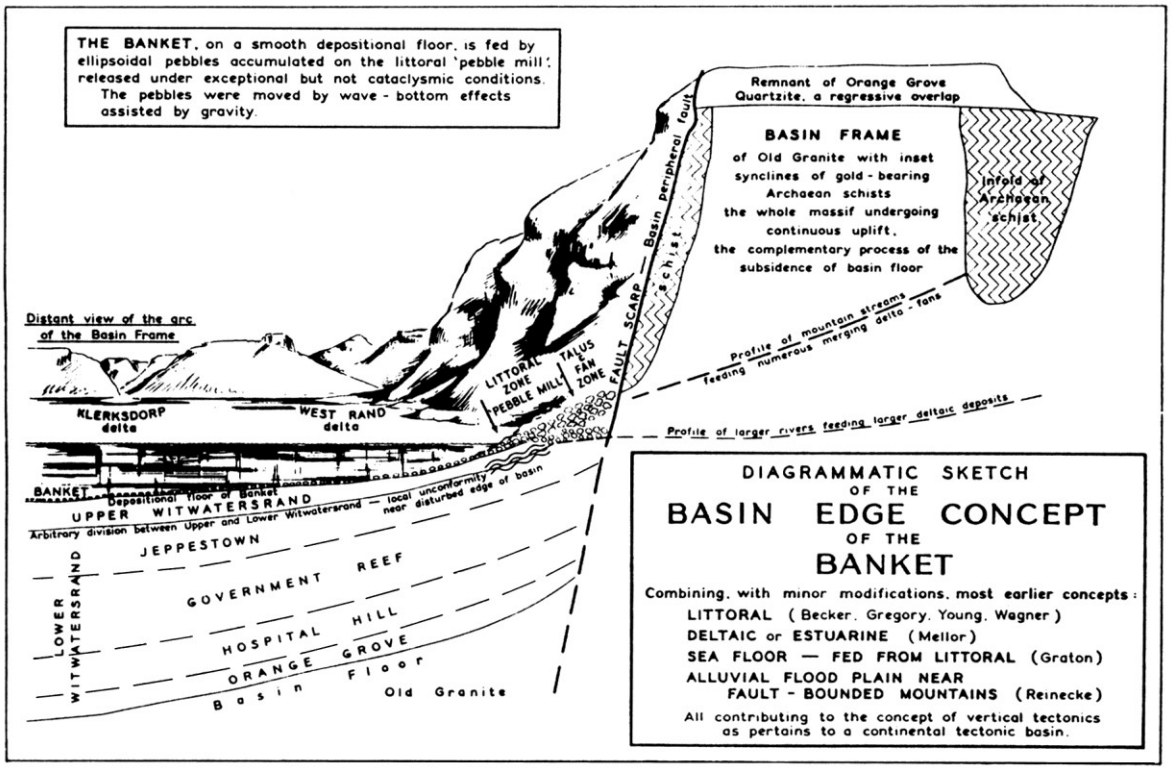
APPENDIX 18-W : (A) Archaean to early-Proterozoic tectonic features in Southern Africa and (B) proposed crustal evolution model for the western Kaapvaal Craton, showing: 1. convergence of Kraaipan and Swazi subprovinces with fore-arc basin deposition, granite intrusions and deposition of West Rand and Marydale groups, 2. collision of both subprovinces along Colesberg-Mafikeng gravity anomaly, with thrusting, granitic plutons and deposition of Central Rand Group in a foreland basin, 3. formation of a new subduction zone with reversed dip direction and deposition of Klipriviersberg and Platberg groups in an extensional retro-arc setting (after Hartnady & Stowe, 1991).



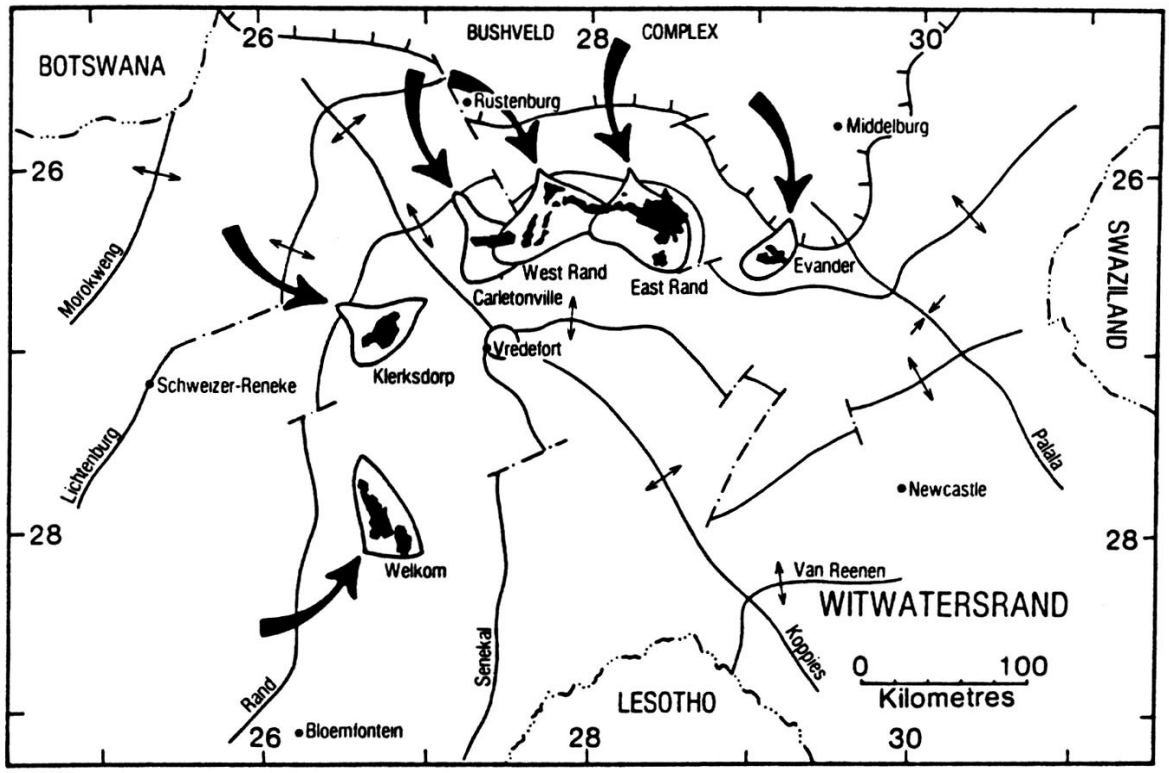
APPENDIX 18-A : The interference-fold pattern of the Witwatersrand Basin (after Pretorius, 1986b).



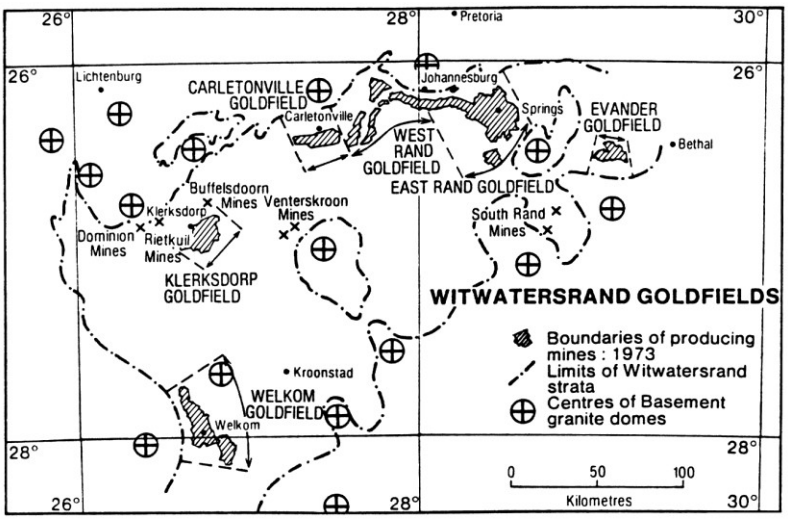
APPENDIX 18-B : Basin-and-dome structures resulting from the superimposition of two sets of orthogonal folds (after Pretorius, 1984).



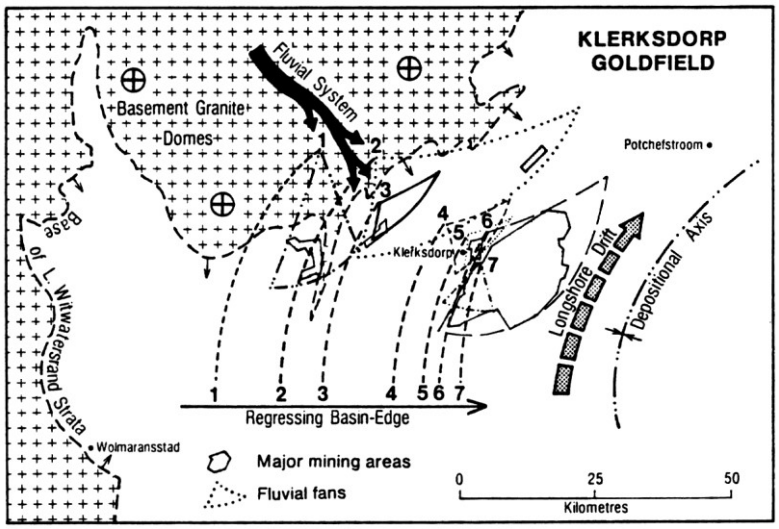
APPENDIX 18-C : Diagrammatic illustration of the Basin Edge Concept for the Witwatersrand Basin, showing classic depositional response to taphrogenic basin development (after Brock & Pretorius, 1964b).



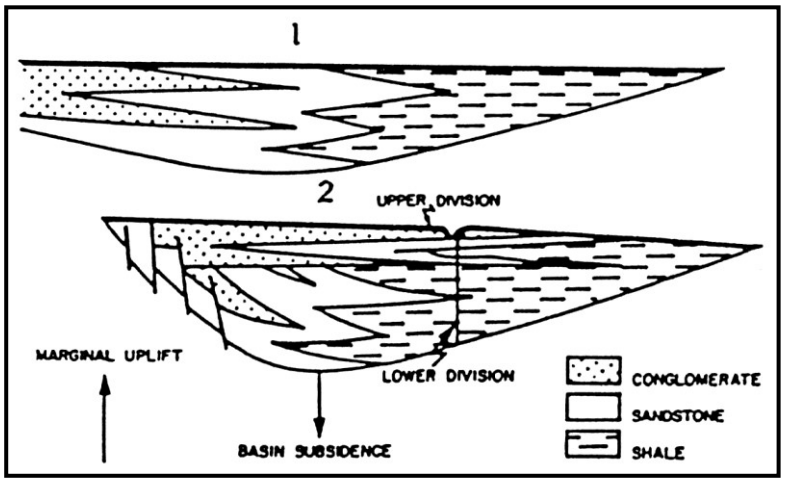
APPENDIX 18-D : The relationship between goldfields, fluvial fans, palaeocurrent directions and major fold axes in the Witwatersrand Basin (after Pretorius, 1976b).



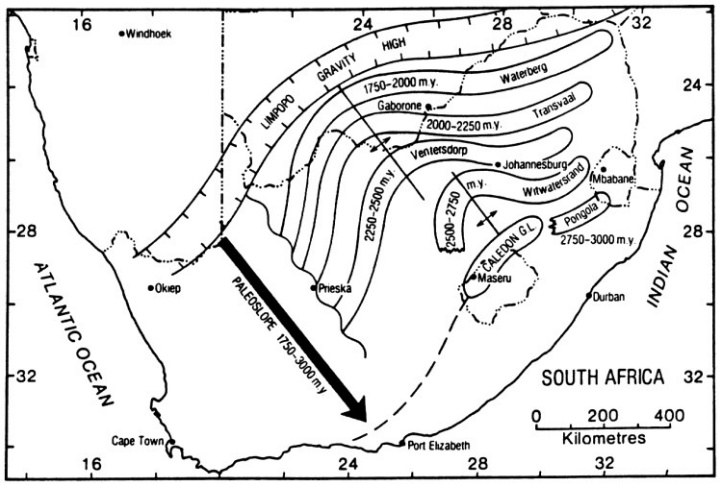
APPENDIX 18-E : The location of the major goldfields in synclinal downwarps between basement granite domes (after Pretorius, 1976b).



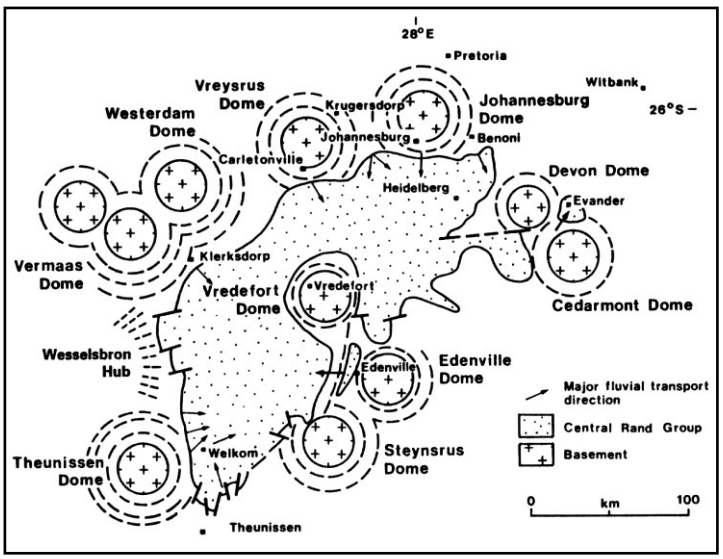
APPENDIX 18-F: The southeasterly-directed, regressive nature of the western basin margin and shift of the depositional axis in the Klerksdorp Goldfield (after Pretorius, 1976b).



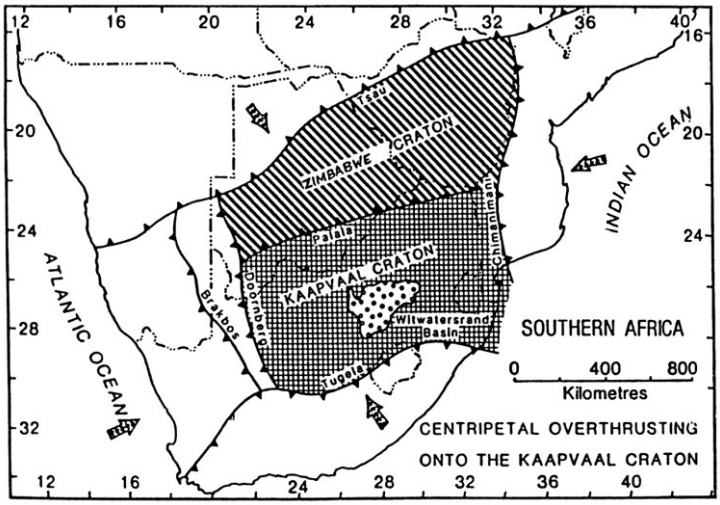
APPENDIX 18-G : Schematic illustration of Witwatersrand Basin evolution; inward migration of the basin-margins occurred contemporaneously with marginal uplift and basin-subsidence (after Vos, 1975).



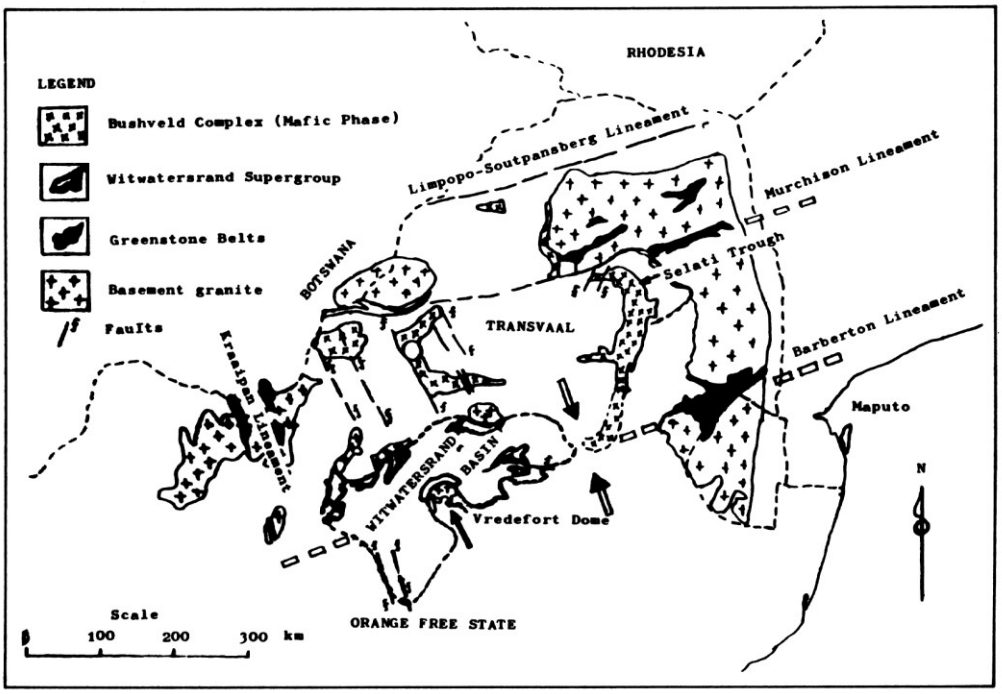
APPENDIX 18-H : The relative position of the depositional axes of progressively younger Proterozoic sedimentary basins on the Kaapvaal Craton (after Pretorius, 1976b).

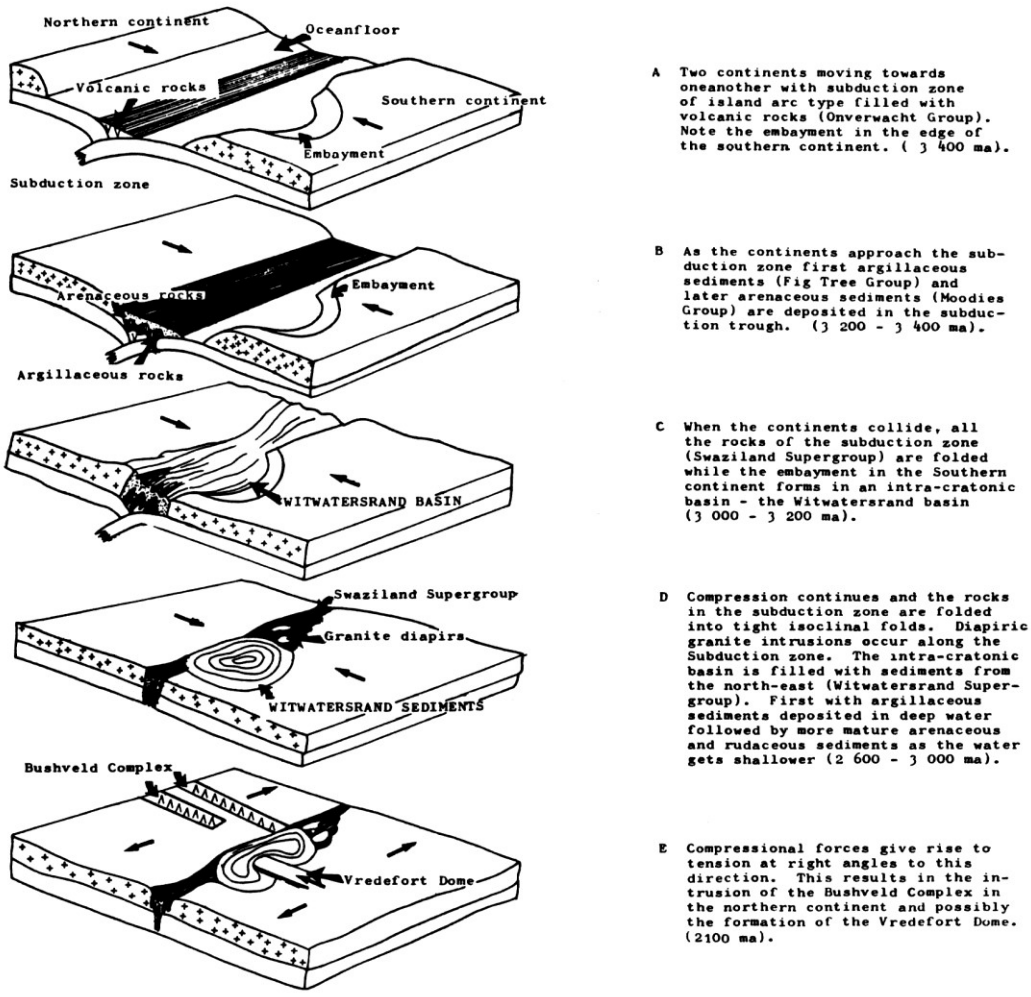


APPENDIX 18-I : Reconstructed subsurface plan of the Central Rand Group, with adjacent granite domes and sites of major fluvial influx (after Hutchison, 1975; Minter, 1976, 1978 and Minter *et al.*, 1986).



APPENDIX 18-J : Compression and associated overthrusting along the boundaries of the Kaapvaal and Zimbabwe cratons, envisaged as cause for cross-folding in the Witwatersrand Basin (after Pretorius, 1984).





A Two continents moving towards oneanother with subduction zone of island arc type filled with volcanic rocks (Onverwacht Group). Note the embayment in the edge of the southern continent. (3 400 ma).

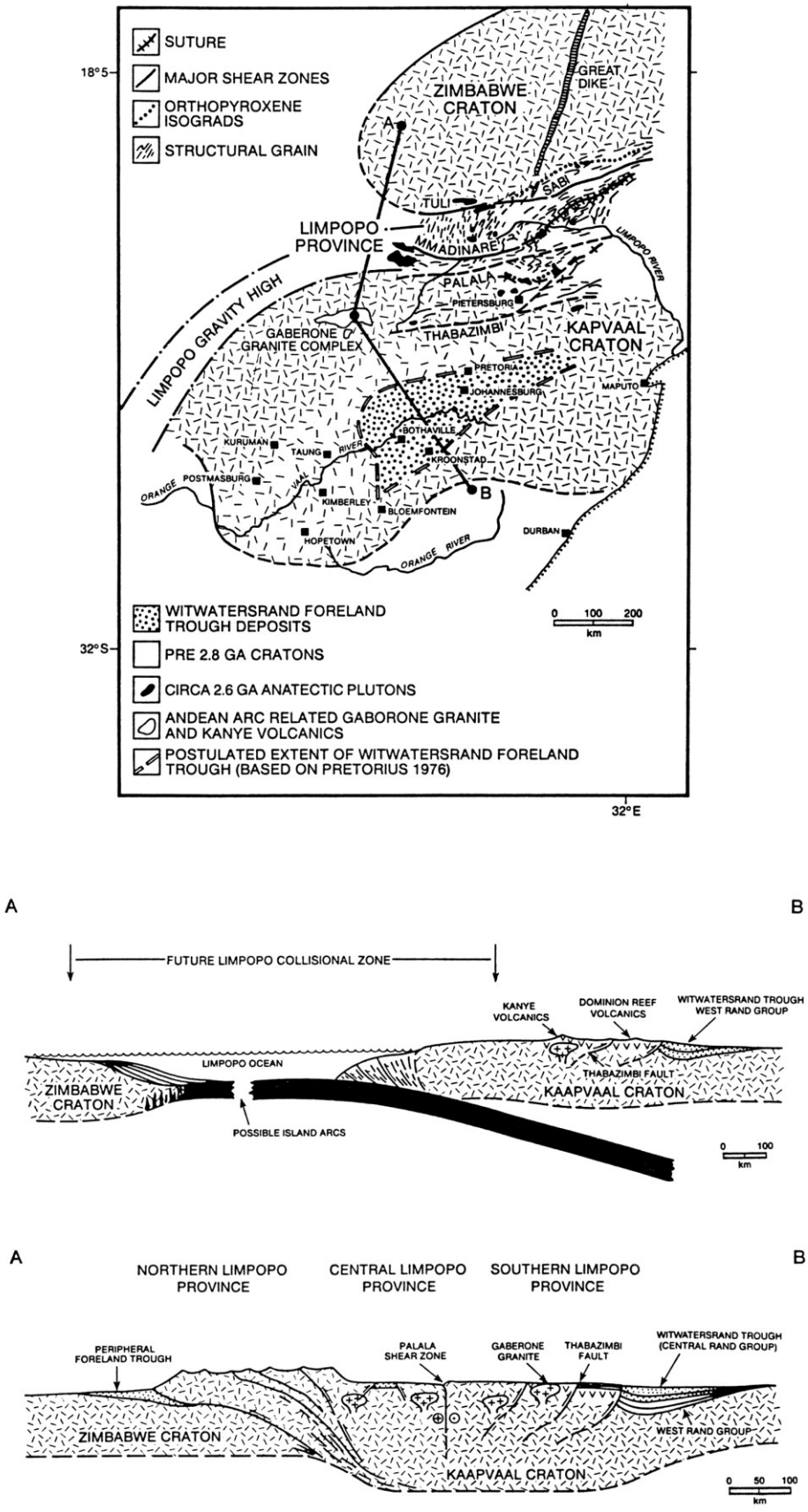
B As the continents approach the subduction zone first argillaceous sediments (Fig Tree Group) and later arenaceous sediments (Moodies Group) are deposited in the subduction trough. (3 200 - 3 400 ma).

C When the continents collide, all the rocks of the subduction zone (Swaziland Supergroup) are folded while the embayment in the Southern continent forms in an intra-cratonic basin - the Witwatersrand basin (3 000 - 3 200 ma).

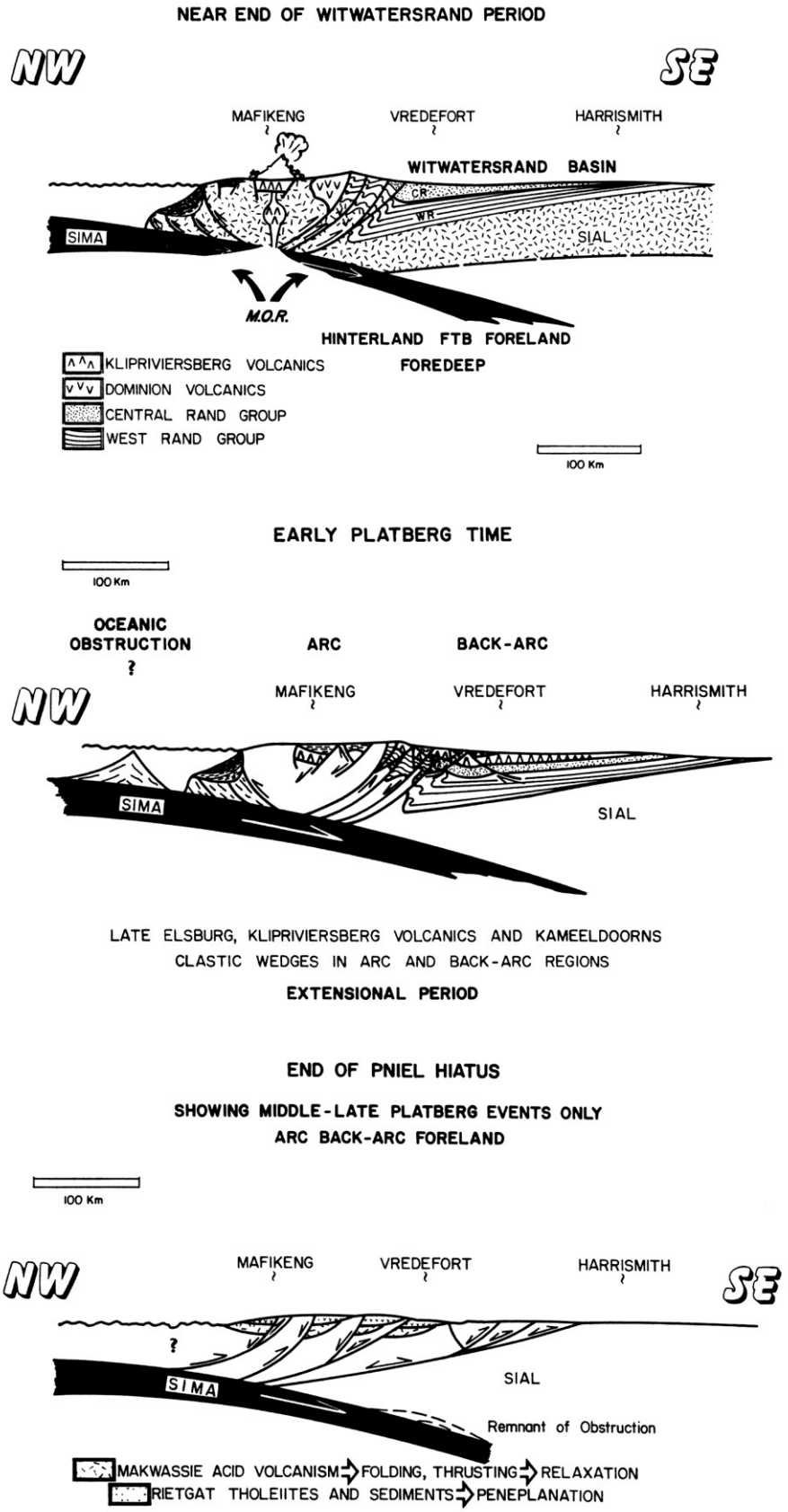
D Compression continues and the rocks in the subduction zone are folded into tight isoclinal folds. Diapiric granite intrusions occur along the Subduction zone. The intra-cratonic basin is filled with sediments from the north-east (Witwatersrand Supergroup). First with argillaceous sediments deposited in deep water followed by more mature arenaceous and rudaceous sediments as the water gets shallower (2 600 - 3 000 ma).

E Compressional forces give rise to tension at right angles to this direction. This results in the intrusion of the Bushveld Complex in the northern continent and possibly the formation of the Vredefort Dome. (2100 ma).

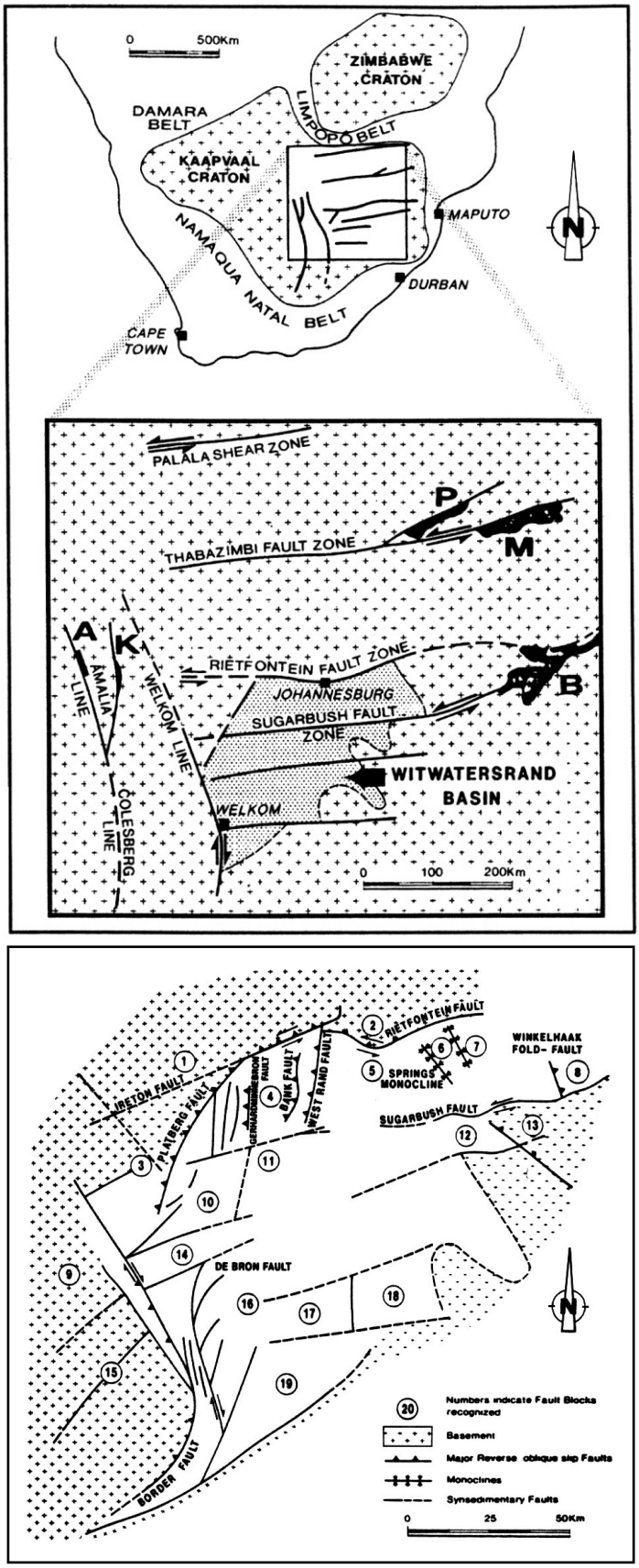
Appendix 18-K : Tectonic setting and schematic illustration of the evolution of the Witwatersrand Basin, according to the continent-continent collisional theory of Van Biljon (1980).



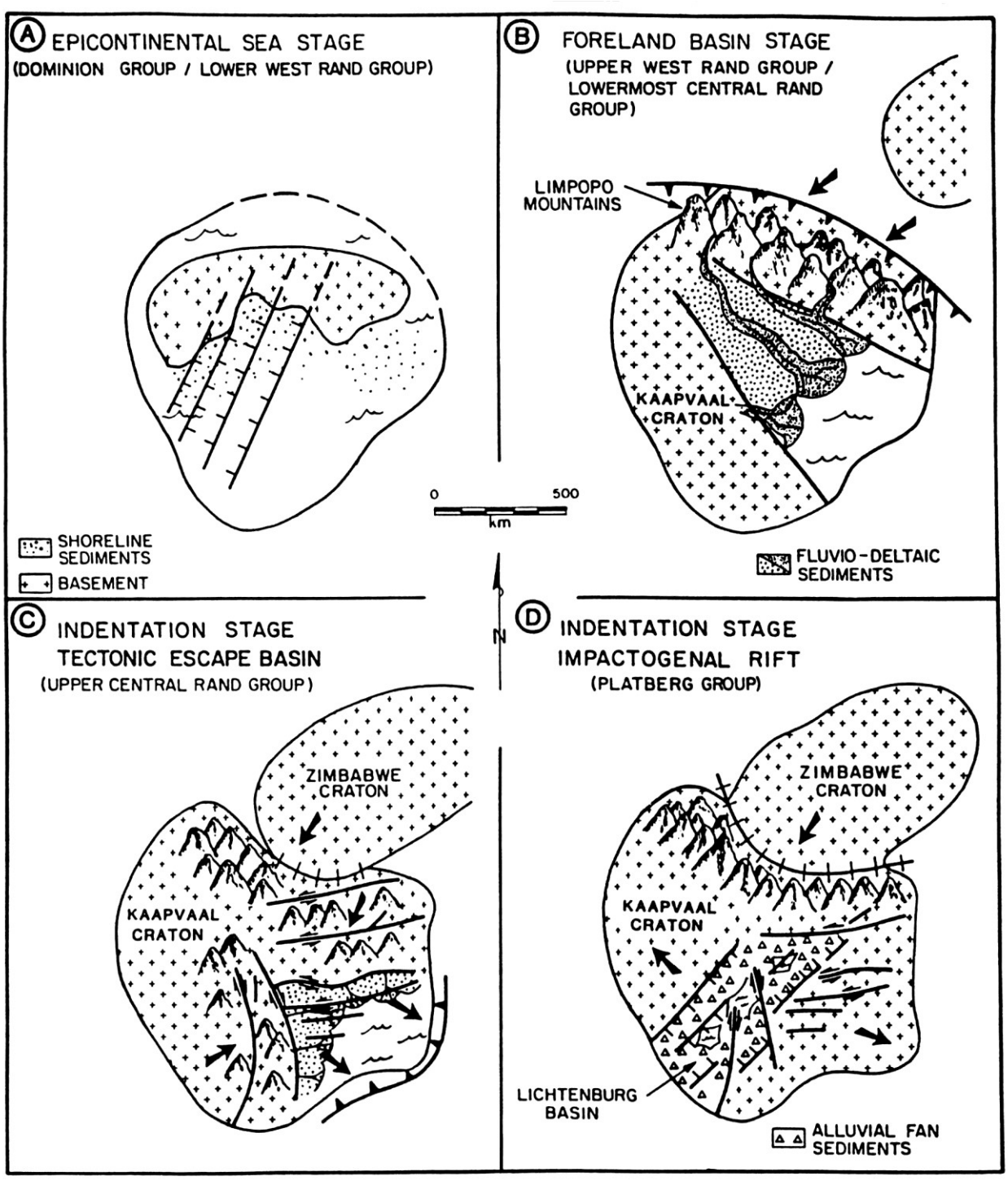
APPENDIX 18-L : Map and cross-sections illustrating the formation of the Witwatersrand Basin as a foreland basin within the Kaapvaal Craton in response to continental collision between the Kaapvaal and Zimbabwe cratons at approximately 2.7 Ga (after Burke *et al.*, 1986).



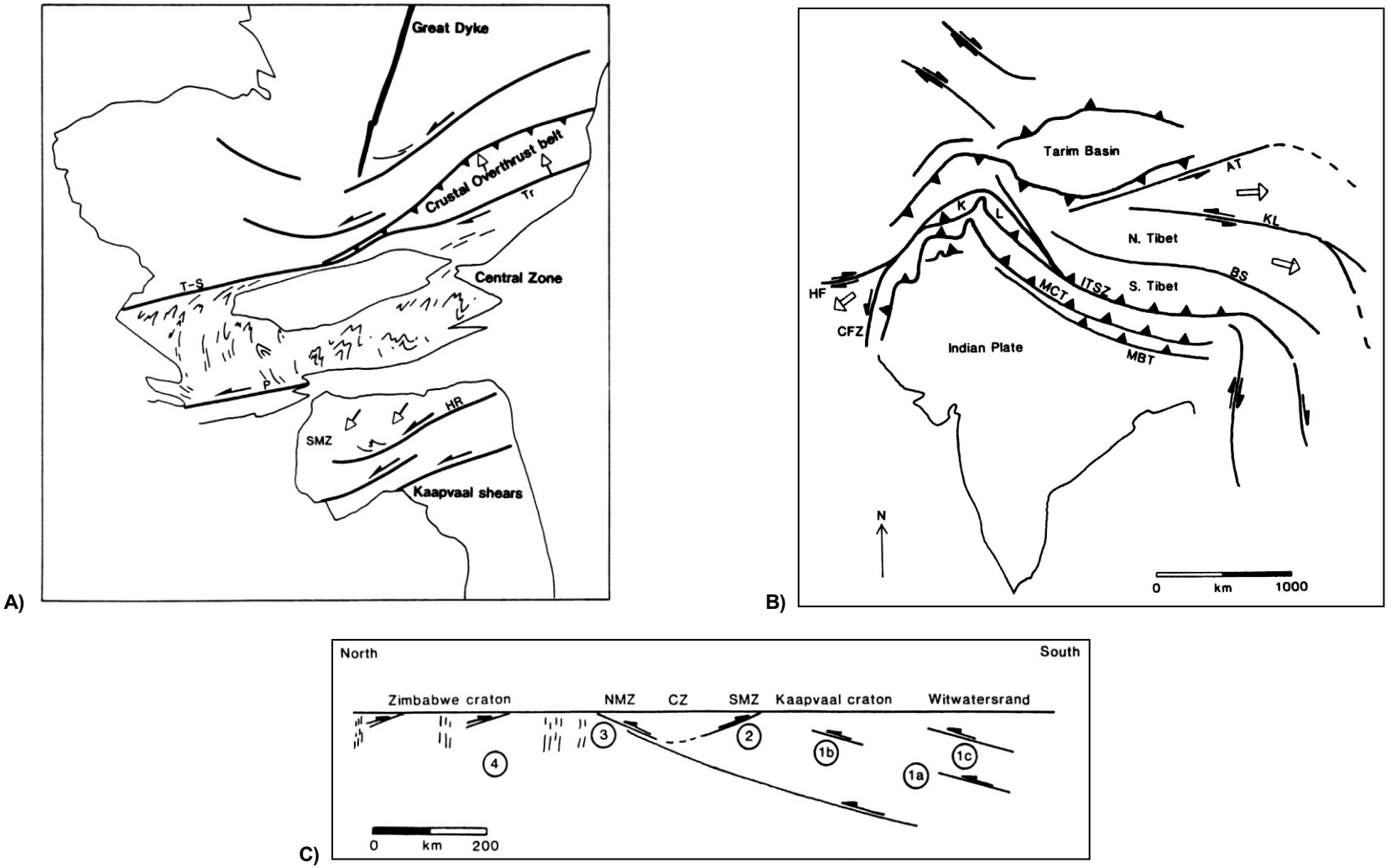
APPENDIX 18-M : Schematic NW-SE cross-sections of the central and northern Kaapvaal Craton, illustrating the evolution of the Witwatersrand Basin in a cratonic, back-arc, plate-tectonic setting from syn-Witwatersrand compression to mid-Ventersdorp extension. The rapid transition to Klipriviersberg volcanism is envisaged to be due to subduction of a mid-ocean ridge (after Winter, 1987).



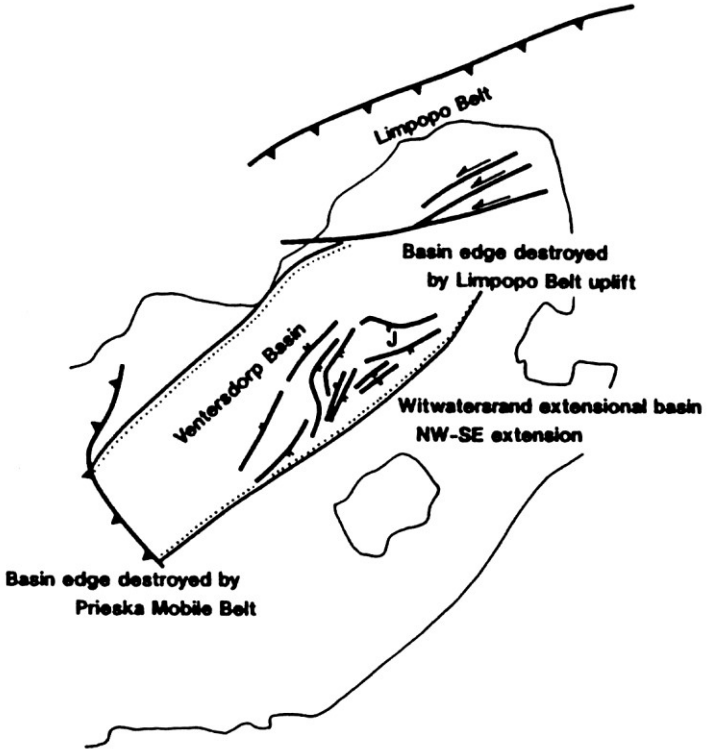
APPENDIX 18-N : The strike-slip reactivation of major, pre-existing fault zones within the Kaapvaal Craton, as well as the development and movement of large fault-bounded basement blocks within the area of the Witwatersrand Basin during the Limpopo Orogeny, controlled sedimentation particularly in the late stages of the basin history (after R.E. Myers *et al.*, 1990a; Stanistreet & McCarthy, 1991).



APPENDIX 18-O : Evolution of the Witwatersrand Basin, including (A) the formation of the extensional Dominion Group basin with subsequent thermal subsidence sedimentation during lower West Rand Group, (B) the formation of a retro-arc basin due to subduction beneath the northeastern margin of the Kaapvaal Craton during upper West Rand Group and lowermost Central Rand Group deposition, (C) tectonic escape due to collision of the Kaapvaal and Zimbabwe cratons during Central Rand Group sedimentation, and (D) the development of the Ventersdorp impactogenic rift during Platberg Group sedimentation due to ultimate indentation (after Stanistreet & McCarthy, 1991).



APPENDIX 18-P : (A) Map of the Limpopo Belt and adjoining parts of the Zimbabwe and Kaapvaal cratons showing structural elements interpreted to have formed in response to the collision of both cratons during the Limpopo Orogeny, (B) schematic section from the Witwatersrand Basin to north of Harare showing the northward migration of deformation during the Limpopo Orogeny (see original for explanation), and (C) simplified tectonic map of the India-Asia collision zone showing the Himalayan S-verging thrusts, the major Tibetan strike-slip zones and the formation of the Central Asian hinterland basins (*e.g.,* Tarim basin) as proposed analogy to the formation of the Witwatersrand Basin (after Treloar *et al.*, 1992) (see original for explanation of abbreviations).

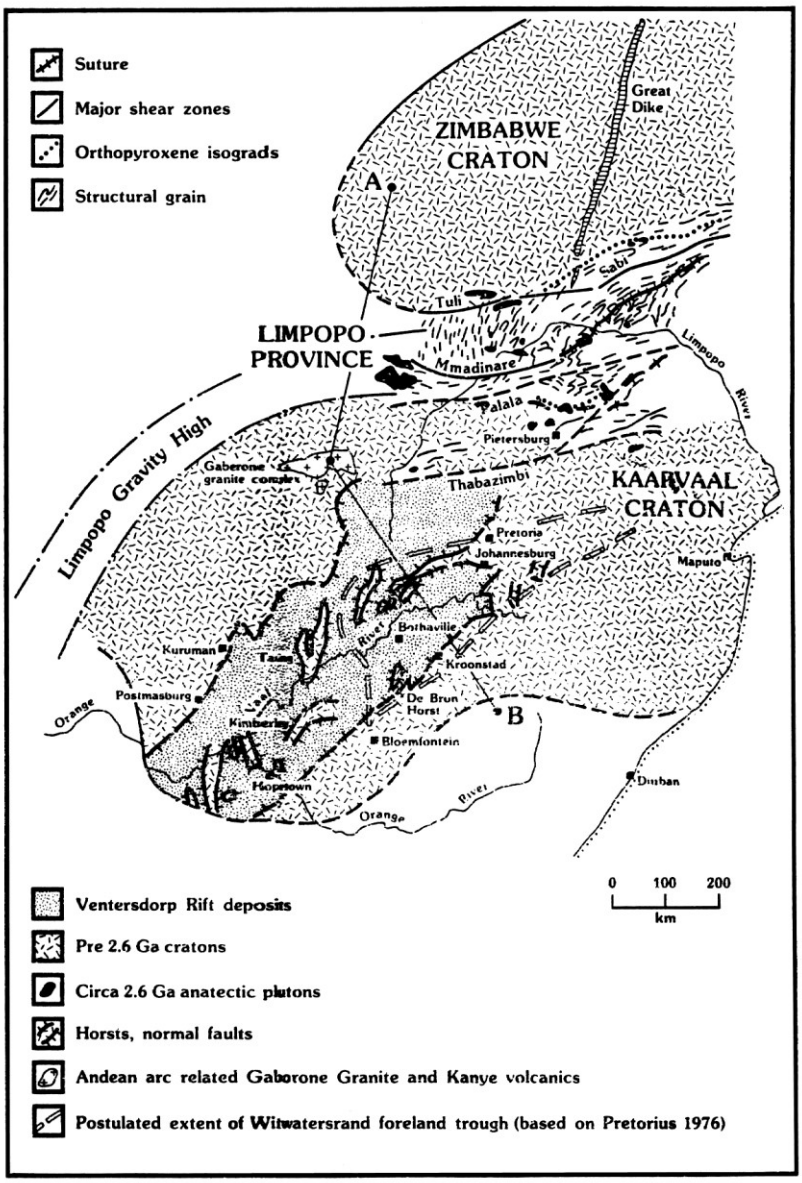


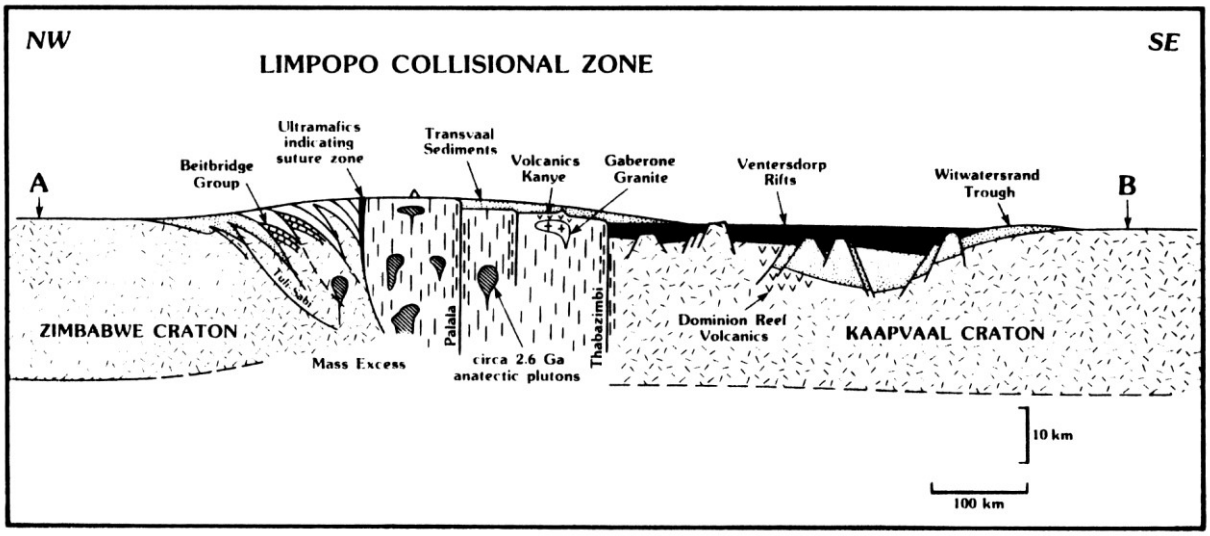
A)



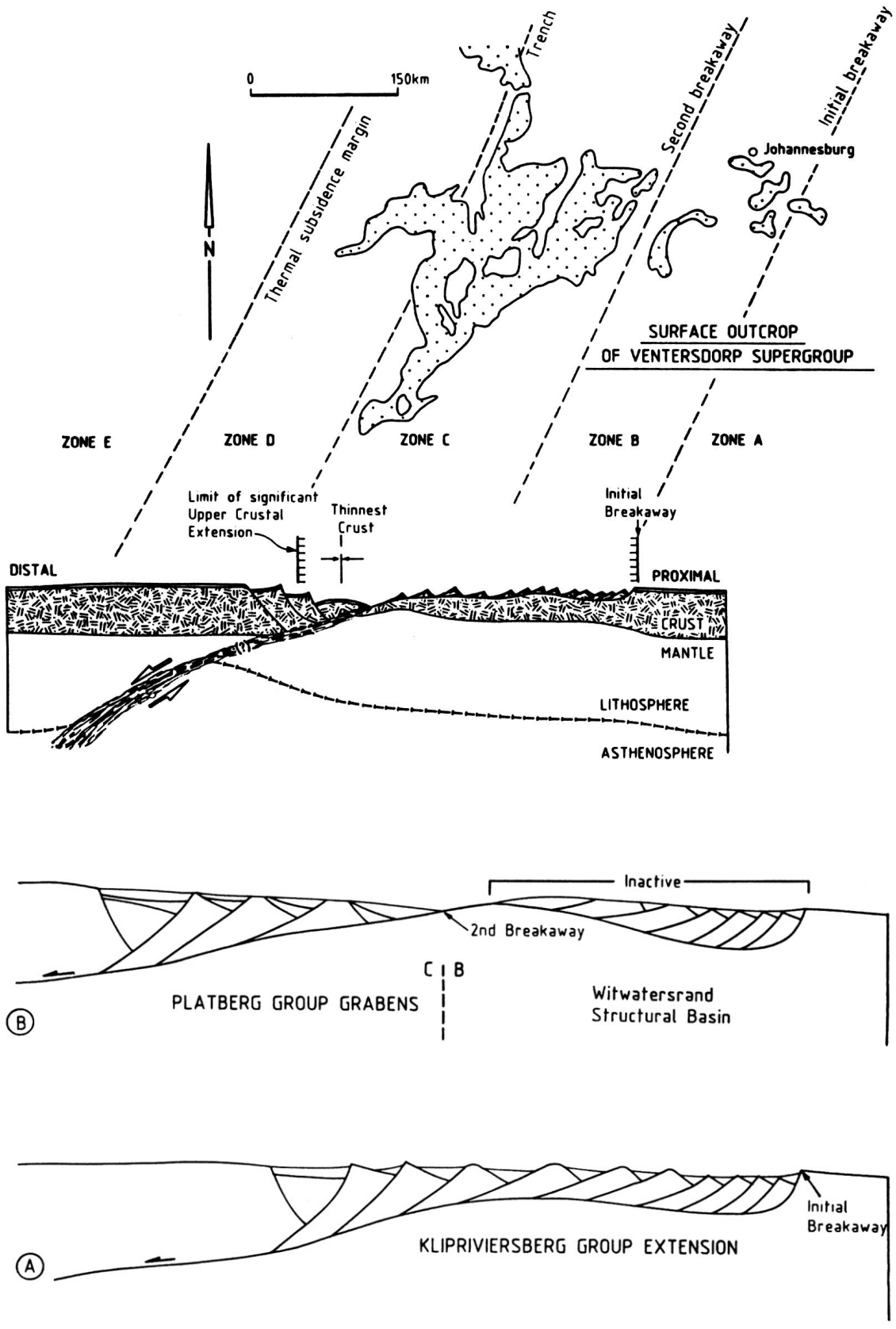
B)

APPENDIX 18-Q : (A) Structural setting and evolution of the Witwatersrand and Ventersdorp basins in relation to the Limpopo Orogeny and (B) comparison of the Witwatersrand Basin with sub-Andean basins in South America (after Coward *et al.*, 1995).



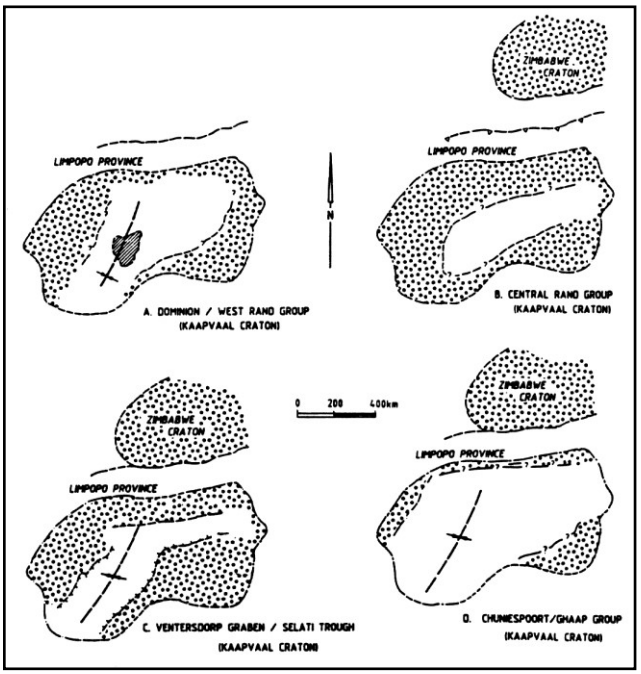


APPENDIX 18-R : Map and cross-section of the Kaapvaal and Zimbabwe cratons, illustrating the formation of the Ventersdorp Rift System within the Kaapvaal Craton as impactogen, in response to continental collision between the Kaapvaal and Zimbabwe cratons at 2.64 Ga (after Burke *et al.*, 1985a).

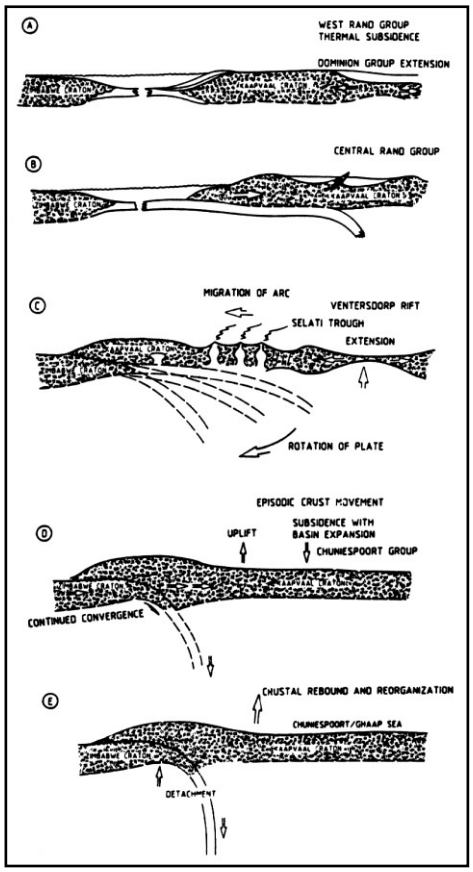


APPENDIX 18-S : Wernicke's normal simple shear hypothesis as applied to the development of the Ventersdorp Supergroup. Initial down-to-the-west, listric normal faulting during Klipriviersberg Group time, followed by overprinting of the detached terranes by large fault-block ranges due to the development of a second breakaway producing the Platberg Group grabens (after Clendenin *et al.*, 1988c).

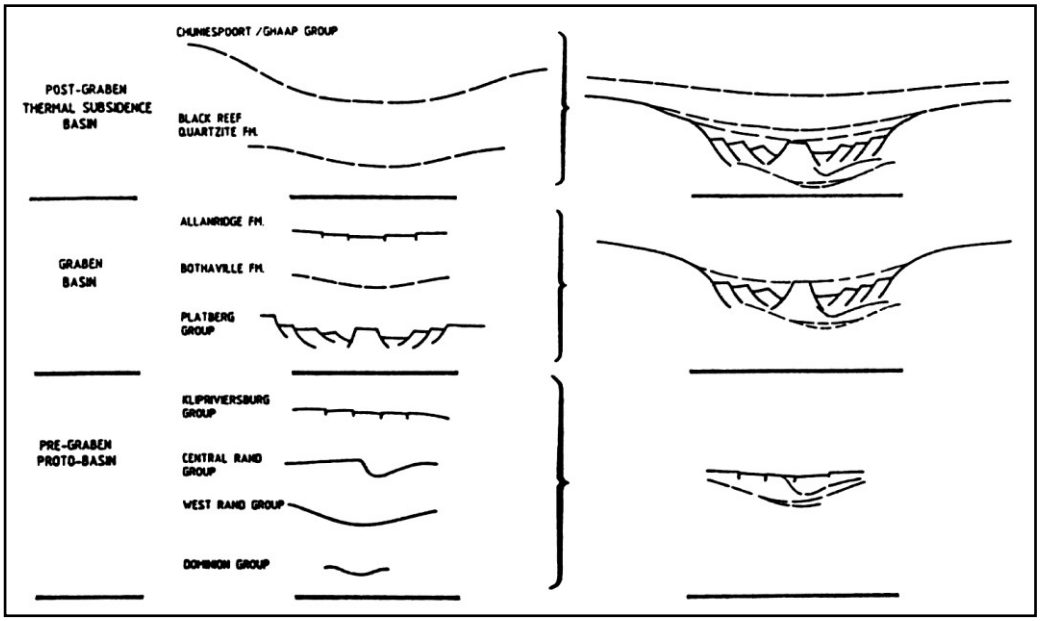
A)



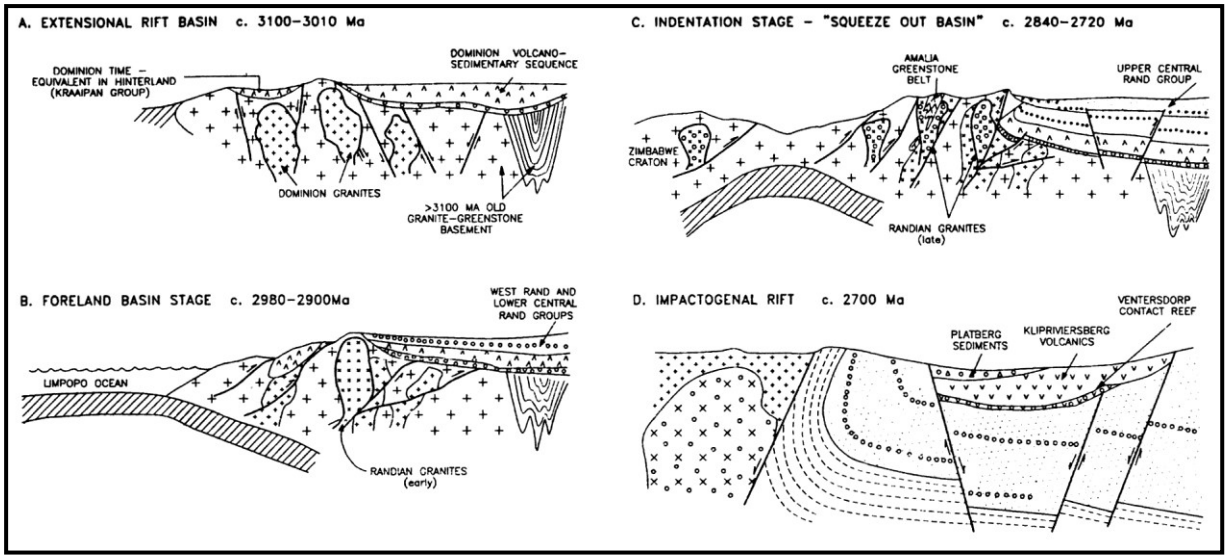
B)



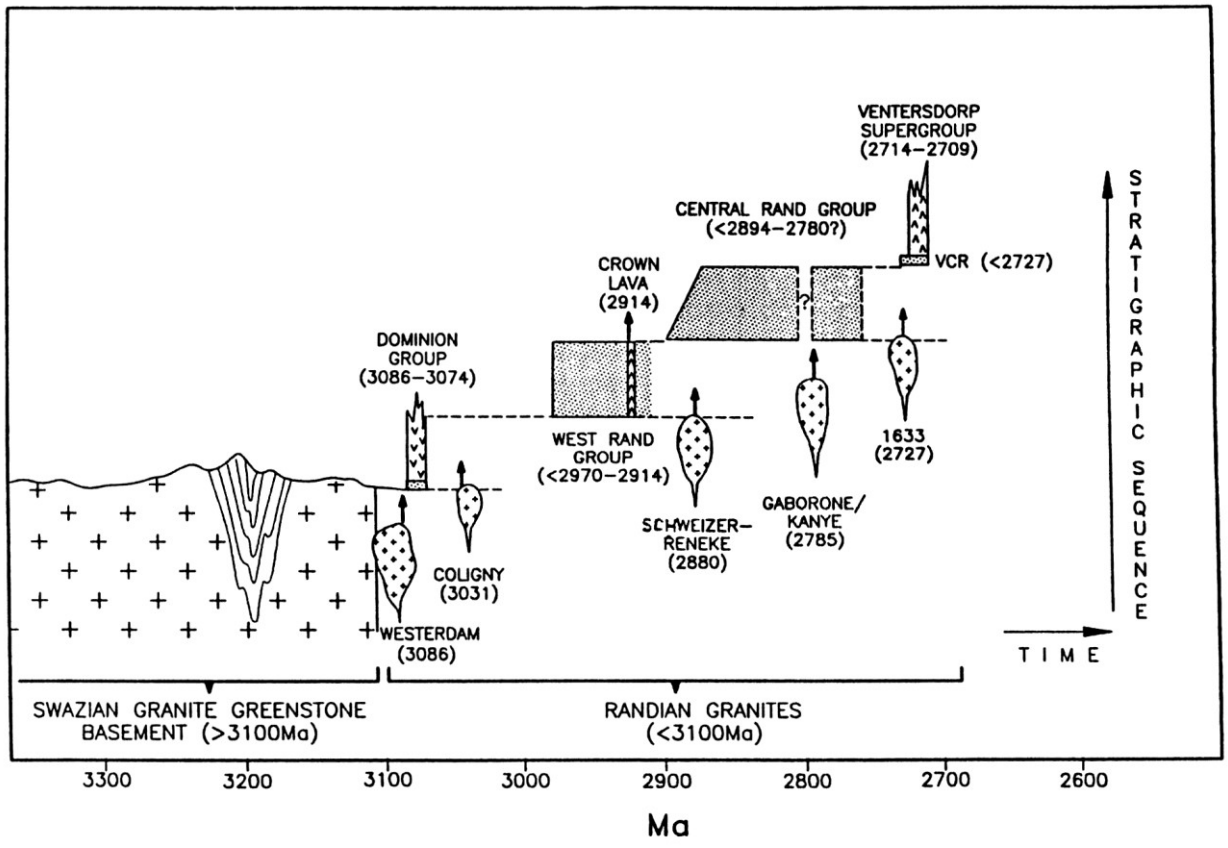
C)



APPENDIX 18-T : (A) & (B) Palaeogeographical reconstructions of intraplate deformation and successor basin development within the Kaapvaal Craton prior to and following oblique collision of the Kaapvaal and Zimbabwe cratons from 3.0 to pre-2.2 Ga (after Clendenin *et al.* 1988a) and (C) proposal of a three-stage rift model for the evolution of the successor basin sequence (after Clendenin *et al.*, 1988b).

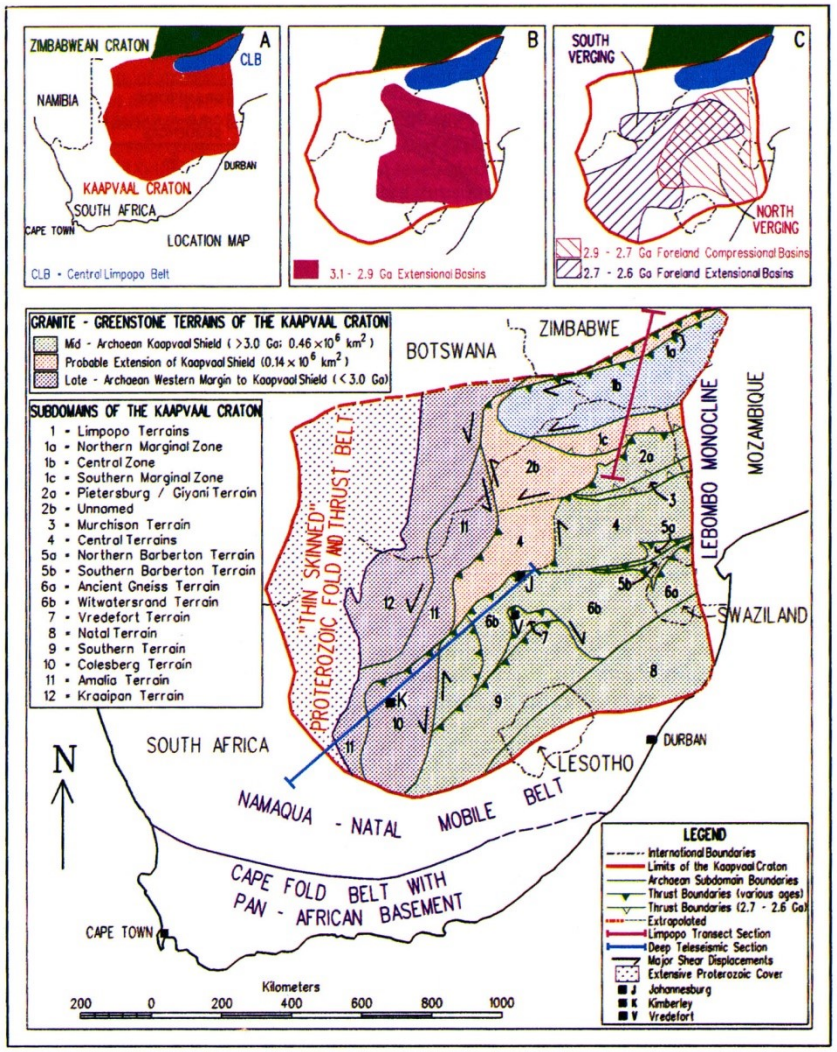


A)

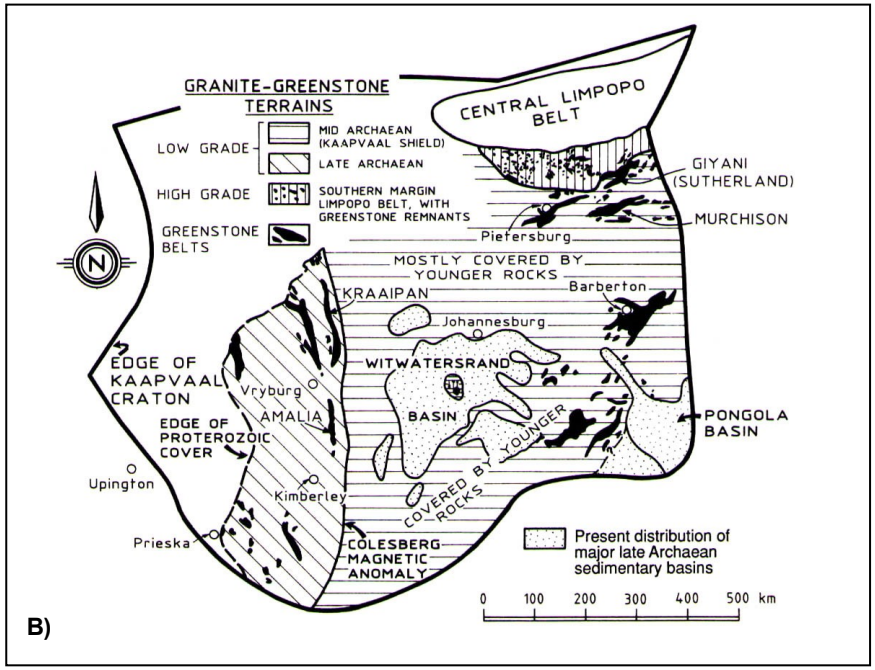


B)

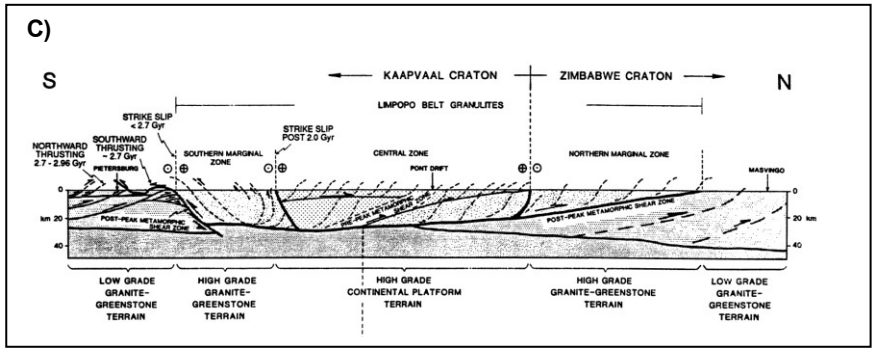
APPENDIX 18-U : (A) Schematic representation illustrating the stages of tectonic evolution in the formation of the "Witwatersrand Triad" (after Robb *et al.*, 1991) and (B) magmatic and sedimentary events pertaining to the evolution of the Witwatersrand Basin and environs (after Robb & Meyer, 1994).



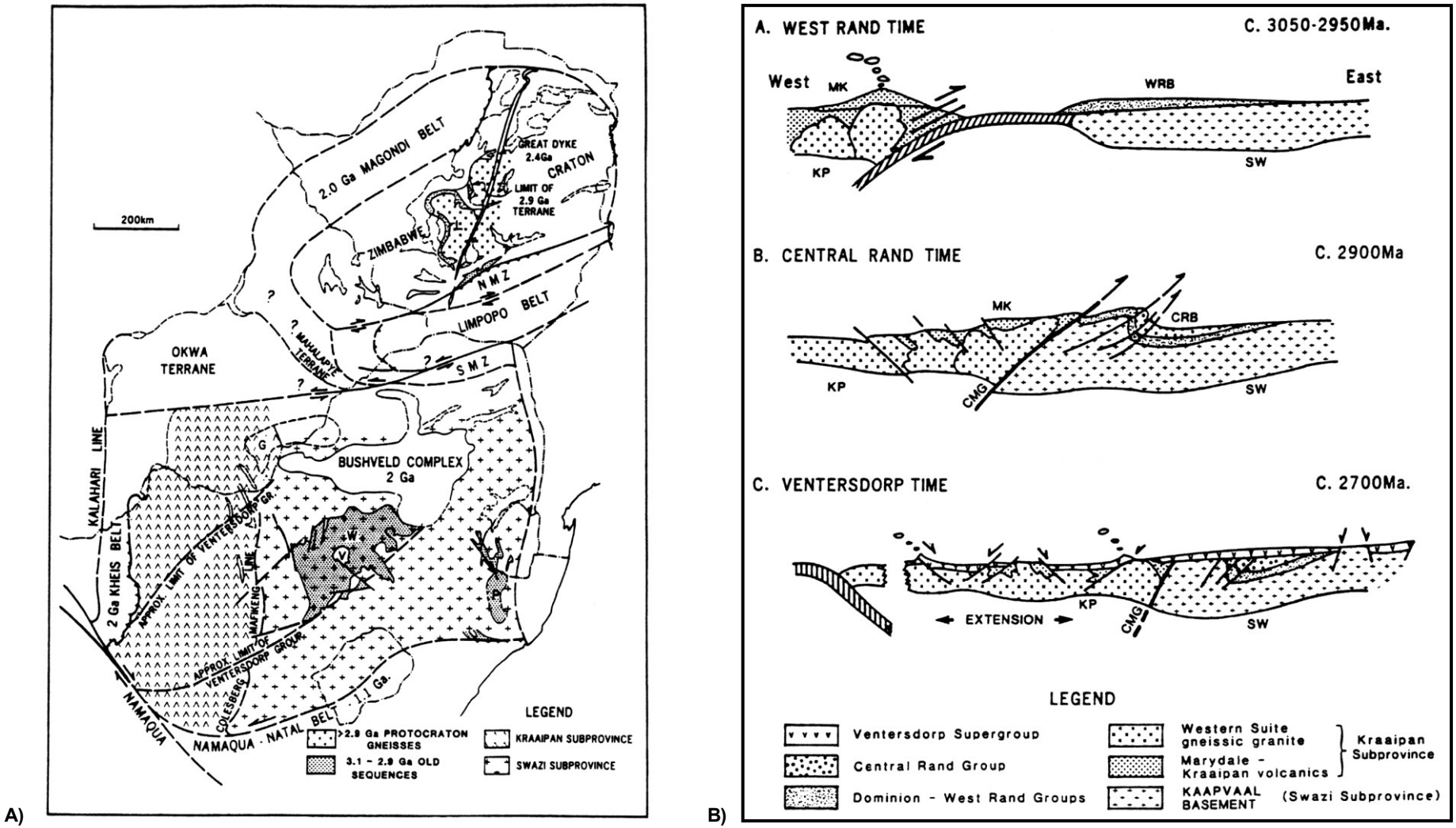
A)



B)



APPENDIX 18-V : Schematic diagrams showing (A) the Archaean crustal subdomains/terranes of the Kaapvaal Craton, (B) the distribution of granite-greenstone terranes of the Kaapvaal Craton and (C) a composite N-S profile across the Limpopo Mobile Belt, indicating northwards-directed tectonic transport at 2.9-2.7 Ga, overprinted by the ~2.7 Ga southward-directed thrusting related to the climax of the Limpopo Orogeny (after De Wit *et al.*, 1992).



APPENDIX 18-W : (A) Archaean to early-Proterozoic tectonic features in Southern Africa and (B) proposed crustal evolution model for the western Kaapvaal Craton, showing: 1. convergence of Kraaipan and Swazi subprovinces with fore-arc basin deposition, granite intrusions and deposition of West Rand and Marydale groups, 2. collision of both subprovinces along Colesberg-Mafikeng gravity anomaly, with thrusting, granitic plutons and deposition of Central Rand Group in a foreland basin, 3. formation of a new subduction zone with reversed dip direction and deposition of Klipriviersberg and Platberg groups in an extensional retro-arc setting (after Hartnady & Stowe, 1991).

APPENDIX 19

RECONSTRUCTION OF THE GEODYNAMIC EVOLUTION OF THE SOUTHERN AFRICAN LITHOSPHERE

1 INTRODUCTION 1

2 GLOBAL MANTLE DYNAMICS AND PLATE TECTONIC PROCESSESS 2

2.1 Concept of Bicellular Mantle Convection and Geotectonic Bipolarity 2

2.2 Tectonic Stress 8

2.3 Plate Tectonics 9

2.4 Supercontinental and Superoceanic Cycles 9

3 REGIONAL FRAMEWORK AND CRUSTAL ARCHITECTURE OF THE KAAPVAAL AND ZIMBABWE CRATONS AND LIMPOPO PROVINCE 11

3.1 Kaapvaal Craton 11

3.2 Zimbabwe Craton 27

3.3 Limpopo Province 29

4 GEODYNAMIC EVOLUTION OF THE KAAPVAAL AND ZIMBABWE CRATONS AND LIMPOPO CENTRAL ZONE TERRANE 38

4.1 PALAEOARCHAEAN-MESOARCHAEAN EVOLUTION (~3.8-3.1 Ga) 38

4.1.1 Kaapvaal Grunehogna Protocraton 38

4.1.2 Zimbabwe Protocraton 41

4.1.3 Limpopo Central Zone Terrane 42

4.2 MESOARCHAEAN-NEOARCHAEAN EVOLUTION (~3.1-2.53 Ga) 43

4.2.1 Kaapvaal-Grunehogna Craton 44

4.2.1.1 Murchison Orogenic Cycle (~3.1-2.97 Ga) 44

4.2.1.2 Limpopo Orogenic Cycle/Phase 1 (~2.97-2.81 Ga) 47

4.2.1.3 Bengal Orogenic Cycle (~2.97-2.87 Ga) 49

4.2.1.4 Kraaipan-Vaalbara Orogenic Cycle (~2.95-2.81 Ga) 51

4.2.1.5 Limpopo Orogenic Cycle/Phase 2 (~2.81-2.64 Ga) 53

4.2.1.6 Late- to Post-Limpopo Orogenic Phase (~2.64-2.585 Ga) 58

4.2.2 Zimbabwe Craton 59

4.2.2.1 Bulawayan Orogenic Cycle (~3.1-2.81 Ga) 59

4.2.2.2 Limpopo Orogenic Cycle (~2.81-2.64 Ga) 60
4.2.2.3 Hurungwe Orogenic Cycle (~2.72-2.64 Ga) 62
4.2.2.4 Nyassa Orogenic Cycle (~2.64-2.53 Ga) 63
4.2.3 Indian Cratons 67
4.2.3.1 Bundelkhand Orogenic Cycle (~2.775-2.5 Ga) 67
4.2.3.2 Dharwar Orogenic Cycle (~2.72-2.5 Ga) 68
4.3 LATE NEOARCHAEAN-PALAEOPROTEROZOIC EVOLUTION (~2.585-1.73 Ga) 69
4.3.1 Post-Limpopo and Late-to Post-Nyassa (~2.585-2.47 Ga) Orogenic Period 69
4.3.2 Mtshingwe-Kalahari-Gascoyne Orogenic Cycle (~2.47-2.22 Ga) 72
4.3.3 Ubendian Orogenic Cycle (~2.22-1.86 Ga) 74
4.3.4 Aravalli Orogenic Cycle (~2.2-1.73 Ga) 86
4.3.5 Kheis Orogenic Cycle (~2.05-1.73 Ga) 87
4.4 MESOPROTEROZOIC EVOLUTION (~1.73-0.82 Ga) 92
4.4.1 Post-Kheis Orogenic Crustal Extension (~1.73-1.4 Ga) 92
4.4.2 Kibaran and Lomanian Orogenic Cycles (~1.4-0.82 Ga) 93
4.4.2.1 Kibaran Orogenic Cycle (~1.4-1.25 Ga) 94
4.4.2.2 Lomanian Orogenic Cycle (~1.25-1.0 Ga) 95
4.5 NEOPROTEROZOIC-Late PALEOZOIC EVOLUTION (~1000-320 Ma) 97
4.5.1 Pan-African Orogenic Cycle (~1000-480 Ga) 97
4.5.2 Late- to Post-Pan-African Orogenic Relaxation and Collapse (~480-320 Ga) 99
4.6 LATE PALEOZOIC-RECENT EVOLUTION (~320-0 Ma) 100
4.6.1 Late-Gondwana (“Karoo”) Stage (~320-157 Ma) 100
4.6.1.1 Early Gondwana Rifting Phase/Gondwanide Orogenic Cycle (~320-205 Ma) 101
4.6.1.2 Late (~205-157 Ma) to Post (~157-0 Ma) Gondwana Rifting Phase 102
4.7 NEOTECTONIC EVOLUTION (~35-0 Ma) 106

LIST OF FIGURES

Page

FIGURE 2.1: (a-c) Three-dimensional illustrations of bicellular convection in the Earth's mantle depicting the existence of the African and Pacific superplumes; (d) Cross-section through the bicellular convection system in the mantle along the equatorial plane of the Earth, according to the geotectonic model (Pavoni, 1997). The convection system consists of two torus-like cells, the Pacific cell and the African cell. Ascending flow in the mantle underneath the central Pacific region and under Africa, descending flow beneath Indonesia and Central America. Note the horizontal flow underneath the active oceanic ridges. The different colours indicate a hypothetical distribution of relative temperatures. 4

FIGURE 2.2: (a) Geotectonic bipolarity as revealed by the simultaneous, concentric growth of the African and Pacific plates during the last ~180 Ma (after Pavoni, 1991, 1997, from Frisch & Loeschke, 1993). (b) Schematic representation of the bipolar pattern of sub-lithospheric flow produced by axisymmetric bicellular convection in the mantle (after Pavoni, 1969, 1997). Light areas = diverging lithosphere, Shaded areas = zone of converging lithosphere.. Note: Poles A and P mark the centres of the African and Pacific plumes. 5

FIGURE 2.3: Geophysical evidence for global geotectonic bipolarity: (a) Density anomaly at a depth of 2259km (top left), surface dynamic topography (centre left), surface uplift rate (bottom left), and density and viscosity cross sections along a great circle for a density model at a depth of 2439km (right) (after Gurnis *et al.*, 2002). (b) Vertical cross sections (B-D) through the seismic tomography model S20RTS (A) at the core-mantle boundary (2850km) and 2000km (after Gurnis *et al.*, 2000). (c) Heterogeneity of lower mantle P-wave velocity (degree 2; contour interval 2m/sec.) (top) and residual geoid (degree 2; contour interval 20 m) (bottom) (after Richards *et al.*, 1988). Note: Arrows indicate the bipolar, sub-lithospheric flow pattern according to the geotectonic bipolarity model proposed by Pavoni (1969, 1997) (see Fig. 2.2). 6

FIGURE 2.4: Stress map of the African plate (after Andreoli *et al.*, 1996; and references therein). Note: Thick bars = Hmax; stippled = regions with average elevation higher than 1000m; heavy stippled = East African Rift; light stippled = African Superswell; ----- f = major Mesozoic and Cenozoic faults; TIF = Trans-Indian Fabric; arrows = absolute velocity trajectories; light contours relate to long-wavelength undulations in the African geoid. 7

FIGURE 2.5: Summary diagram illustrating the sources of tectonic stress effecting oceanic and continental lithosphere (after Zoback *et al.*, 1989). Note: red= first-order tectonic stress ; blue = second-order tectonic stress. 8

FIGURE 3.1: Crustal architecture of southern Africa according to an interpretation by (a) Webb (in prep.) (Note: Bouguer gravity data provided by Council for Geoscience) and (b) Thomas *et al.*, 1993a (modified in this study). 13

FIGURE 3.2: (A) Palaeomagnetic reconstruction of continents between ~2.2-2.7 Ga after Piper (1982); (B) Palaeogeographical configuration of the Archaean-Palaeoproterozoic continent 'Ur' after Rogers (1996); (C) Proposed configuration of the 'Vaalbara' continent after Cheney (1996). 15

FIGURE 3.3: A) Approximate chronology of glaciations and atmospheric oxygen oscillations according to related redox indicators in the Huronian and Transvaal basins, as well as dated mafic and felsic magmatic events and δ13C ranges for carbonates and the extent of stratigraphic records in each basin denoting gaps in records at unconformities and disconformities (Gumsley *et al*., 2017). (B) Early Paleoproterozoic geography of the Superior, Kola–Karelia, Hearne, and Wyoming cratons as integral parts of the supercraton Superia (Ernst & Bleeker, 2010; Bleeker & Ernst, 2006) with the addition of the Kaapvaal and Pilbara cratons in the supercraton Vaalbara configuration (De Kock *et al*., 2009), both assembled within the supercontinent Supervaalbara (Gumsley *et al*., 2017). 16

FIGURE 3.4: (a) Reconstruction of the fundamental crustal architecture of the Kaapvaal Craton (this study); (b) Schematic seismic section from data projected onto a deep teleseismic line across the southwestern part of the Kaapvaal Craton (modified after de Wit & Hart, 1993). Lithospheric depths taken from Chichowick & Green (1992), Peberdy (1992) and Vinnik (unpublished) and S-wave velocities and all crustal data from Chichowick & Green (1992), Green & Durrheim (1990) and Vinnik (unpublished). Note: The depth to the top of a low-velocity zone within the lithosphere increases from ~160 km in the Witwatersrand Terrane of the Swazi Subprovince to ~210 km in the Kraaipan Subprovince across the Colesberg-Mafikeng suture. 18

FIGURE 3.5: (a) Maps of southern Africa, showing (a) the direction of polarization of the fast split wave (indicated by a straight line; the length of the line is proportional to lapse time δt of the slow wave (see scale bar)) at various stations across the Kaapvaal Craton, as well as the direction of the absolute plate motion of southern Africa since the end of the Jurassic (large arrow) (modified after Vinnik *et al*., 1996b); and (b) the orientation of shear wave splitting fast polarisation direction across the southern African mantle in relation to relevant geological crustal features (after Silver *et al*., 2001). 19

FIGURE 3.6: Three-dimensional image of the deep mantle structure beneath southern Africa, as derived from the present distribution of seismic velocity contrasts (O'Reilly, 2001). Note: Top: Topography and principal geological boundaries (black lines) in southern Africa. Vertical lines connect the surface outcrop of some kimberlite magmas to the deep features revealed by interpretation of the seismic data (blue lines = ~2.5 Gyr; green lines = ~2.5-2.0 Gyr; red lines = <2.0 Gyr.). Centre: Mohorovičić discontinuity (Moho) exhibiting varying depth extent. Bottom: Cratonic cores (blue) reveal themselves as regions of high seismic velocity lying beneath the Kaapvaal and Zimbabwe cratons and the Limpopo Belt. Regions of lower velocity (red) underlie the southern mobile belts and the huge magmatic intrusion of the Bushveld Igneous Complex. Yellow outline shows the surface geological boundaries. 20

FIGURE 3.7: Horizontal and vertical P- and S-wave velocity perturbation models determined by inversion of delay times after correction for elevation and colour thickness, illustrating (a & b) P-wave and (c & d) S-wave depth slices at 150km and 300km respectively, and vertical cross section views of (c) P-wave and (f) S-wave velocity perturbations (after Fouch *et al*., 2004). 21

FIGURE 3.8: (a & b) Colour-coded contour map of depth to Moho beneath southern Africa (Nguuri *et al*., 2001). Note: Crustal thickness colour scale is shown on right. Thin crust tends to be associated with undisturbed areas of craton, particularly in the southern and eastern parts of the Kaapvaal craton and in the Zimbabwe craton north of the Limpopo belt. Greater crustal thickness is associated with the Bushveld region and its westward extension into the Okwa and Magondi belts, and with the central zone of the Limpopo belt and the Proterozoic Namaqua–Natal mobile belt. 22

FIGURE 3.9: (a) Archaean stratigraphic units and different crustal blocks of the Kaapvaal Craton (Frimmel *et al*., 2014). Note: Bold line outlines the boundary of the Kaapvaal Craton as inferred from aeromagnetic data; (b) Palaeogeographical juxtaposition of the Kalahari Craton (with present-day Africa coordinates) (Marshall *et al*., 2010). Note: ZC, Zimbabwe Craton; LB, Limpopo Belt; KvC, Kaapvaal Craton (consisting of the following terranes: PB, Pietersburg Block; KB, Kimberley Block; WB, Witwatersrand Block; SB, Swaziland Block). 24

FIGURE 3.10: Deep teleseismic line and section across the southwestern part of the São Francisco Craton in Brazil (provided with courtesy of De Beers Brazil). Note: Clearly higher and lower P-wave velocities characterising the Archaean São Francisco and Rio de la Plata cratons and intervening Neoproterozoic Southern Brasilia Mobile Belt respectively. The cratons extend to depths in excess of 400 km and are characterised by subvertical margins. 25

FIGURE 3.11: (a) Reconstruction of the fundamental crustal architecture of the Kaapvaal and Zimbabwe cratons, showing major lithospheric lineaments, interpreted to represent the boundaries of Archaean-age accreted terranes/subdomains (this study). Interpretation is based on unpublished/published geological, geophysical and geochronological data; (b) Distribution of Archaean granite-greenstone terrains and sedimentary basins within the Kaapvaal and Zimbabwe cratons, as based on surface geological and geophysical data (this study). Note the change in regional tectonic anisotropy as delineated by the greenstone belts, from ENE-WSW and NE-SW in the eastern, to N-S in the western, parts of the Kaapvaal Craton. 27

FIGURE 3.12: Archaean terrane interpretation for the Zimbabwe craton, showing the distribution of various greenstone belts and gneissic terranes (after Kusky, 1998). Note: Greenstone belts: 1 = Mount Darwin; 2 = Chipuriro; 3 = Harare; 4 = Chegutu; 5 = Midlands; 6 = Gweru-Mvuma; 7 = Shurugwi; 8 = Bubi; 9 = Bulawayo; 10 = Filabusi; 11 = Gwanda; 12 = Antelope-Lower Gwanda; 13 = Matsitama; 14 = Tati; 15 = Vumba; 16 = Mweza; 17 = Buhwa; 18 = Belingwe; 19 = Masvingo; 20 = Mutare. 28

FIGURE 3.13: Schematic crustal cross-section of the Limpopo Belt (after Holzer *et al*., 1998). 30

FIGURE 3.14: Schematic summary of the metamorphic evolution in each of the Limpopo Province subzones (after Holzer *et al*., 1999) and interpretation of a N-S seismic profile across the Limpopo Province (after De Beer & Stettler, 1992). Note the lack of seismic reflectors within the LCZ, which might be attributed to the existing complex structural pattern produced during polymetamorphism and polyphase ductile folding. Note: SMZ = Southern Marginal

Zone; LCZ = Limpopo Central Zone; NMZ = Northern Marginal Zone; KC = Kaapvaal Craton; HRSZ = Hout River Shear Zone; TSZ = Triangle Shear Zone. 34

FIGURE 3.15: (a) Bouguer anomaly map of the Limpopo-Shashe Belt and adjacent cratons upward continued to 10km and (b) tectonic interpretation (also as overlay on (a)) based on surface geology and gravity data, showing the distribution of the three tectonic zones of the Archaean Limpopo-Shashe Belt and relations with the Zimbabwe and Kaapvaal cratons and the Palaeoproterozoic Magondi Belt and the Indian Ocean extensional province (after Ranganai *et al*., 2002). 36

FIGURE 3.16: Schematic model for the geodynamic evolution of the Limpopo Belt from~ 2.7 to 2.0 Ga (Brandt *et al*, 2018). Abbreviations: CZ: Central Zone; NMZ: Northern Marginal Zone; SMZ: Southern Marginal Zone; NLTZ: North Limpopo Thrust Zone; TSZ: Triangle Shear Zone; PSZ-TSZ: Palala Shear Zone-Tshipise Straightening Zone; HRSZ: Hout River Shear Zone. 38

FIGURE 4.1: Schematic model depicting the formation of the earliest continental lithosphere, through linked intra-oceanic processes of spreading and obduction-dominated tectonics. (a) Intra-oceanic obduction and stacking of oceanic lithosphere. (b) Continuous imbrication of oceanic lithosphere leads to tectonic loading and subsidence of hydrated thrust-stacks, which in turn causes in situ differentiation and density inversions during dehydration melting of the "wet" oceanic-like rocks to form vast amounts of tonalite-trondhjemites and associated calc-alkaline extrusives. (c) Schematic model for the evolution of oceanic plates with respect to sea level and related formation of the earliest continental crust (granite-greenstone terrains) and associated peridotite-eclogite keels of the continental tectosphere, following gradual 'drowning' of mid-oceanic ridges at ~4.1-3.6 Ga (after de Wit *et al*., 1992a and de Wit & Hart, 1993). 40

FIGURE 4.2: Proposed Bushveld Complex intrusion mechanism utilising the Thabazimbi-Murchison, Barberton-Magaliesberg and Palala suture zones as conduits for ascending magmas of Rustenburg Layered Suite (RLS) along these translithospheric shear zones. At a critical level in the crust, the magmatic pressure equals the lithostatic pressure, which allows the massive "sill-like" RLS intrusion of the Bushveld Complex to occur (modified after Good, 1999). Insert: Sketch models illustrating the emplacement of the RLS as initial SE-advancing finger system to final sill system (Clarke *et al*., 2000, 2009) and formation of diapirs/domes of metamorphosed Pretoria Group between coalescing intrusive fingers (Uken & Watkeys, 1997) proposed to be controlled by NW-SE striking, reactivated Pongola rift faults (this study). 79

1 INTRODUCTION

An attempt was made to place the proposed tectono-sedimentary evolution of the Free State Goldfield and the Witwatersrand Basin into the context of the geodynamic evolution of the Kaapvaal Craton, including the Zimbabwe Craton and Limpopo Central Zone Terrane, as all share a common and linked geodynamic evolution since the Neoarchaean. This was achieved through a comprehensive compilation and synthesis of a large published and unpublished geoscientific dataset. The outcome is a plate-tectonic reconstruction of the geodynamic evolution of the Kaapvaal and Zimbabwe cratons (and the southern African lithosphere in general) in time and relative space, since their stabilisation as protocratons in the Neoarchaean at ~3.1 Ga until present time, is summarised pictorially in a series of palaeogeographic and palaeogeologic reconstruction 'time-slice' maps to provide a perspective not previously available (Appendices 20-A – 20-Z). For each time period of the reconstructed sequential geodynamic evolution, these 'time-slice' maps show: (1) Archaean continental/cratonic crust, (2) the main structures that were active, (3) the lithostratigraphic units that were deposited, and (4) areas of juvenile crust formation within regions of magmatic-arc/back-arc basin development. Gaps indicate areas, of unknown extent, inferred to have been occupied by either oceanic crust or lost fragments of continental crust that separated the continental crust at the time.

Note: Given their illegibility, all time-slice maps presented in A3 format as Appendices 20-A – 20-Z are available digitally in PDF file format on the supplementary CD.

A summary of geochronological ages used for the plate-tectonic reconstruction is divided into various epochs and/or orogenic cycles (*i.e.* Archaean, Palaeoproterozoic, Kibaran, etc.) for the Kaapvaal and Zimbabwe cratons, and the Limpopo Central Zone Terrane separately, and is presented in tabular format in Appendices 21-A – 21-C respectively.

A proposed correlation of Palaeoproterozoic-Mesoproterozoic (~2.6-1.45 Ga) stratigraphic units and tectonic events within the Kaapvaal, Rehoboth, Zimbabwe, Pilbara, Yilgarn, Singhbhum, Bastar and Dharwar cratons, as well as the Limpopo Central Zone Terrane, is provided in Appendix 22.

Summaries of Palaeoproterozoic (syn-Transvaal Supergroup; ~2.49-2.41 Ga) formation and resetting ages reported from the Kaapvaal and Zimbabwe cratons and Limpopo Central Zone Terrane are presented in Appendices 23-A and 23-B, respectively.

A summary of Palaeo- to Mesoproterozoic (post-Transvaal Supergroup; ~2.1-1.0 Ga) deformation events reported from the area of the Witwatersrand Basin and Bushveld Complex (*i.e.*, central Kaapvaal Craton) and their correlation with far field stress related to the Magondi and Okwa orogenies, Bushveld Complex emplacement, and Vredefort meteorite impact, as well as Kheis, Kibaran and Lomanian (Namaqua-Natal) orogenies is presented in Appendix 24.

Summaries of Palaeo- to Mesoproterozoic (post-Transvaal Supergroup; ~2.1-1.0 Ga) formation and resetting ages reported from the Kaapvaal Craton are presented in Appendices 25-A and 25-B, respectively.

A tectono-structural and terrane interpretation summary map for the Kaapvaal Craton, Limpopo Central Zone Terrane and Zimbabwe Craton, covering the countries of Botswana, Zimbabwe, South Africa, and parts of Mozambique, is presented in Appendix 26.

2 GLOBAL MANTLE DYNAMICS AND PLATE TECTONIC PROCESSESS

A brief overview of the current understanding of global mantle dynamics and associated plate tectonic processes is presented in order to provide the reader with a framework in which to understand the reconstructed geodynamic evolution of southern Africa over the past ~3.1 Ga.

The proposal that plate motions are driven by some form of mantle convection is now almost universally accepted, and the pattern of mantle convection must be considered as the fundamental control on plate tectonic cycles (Runcorn, 1962; Sutton, 1963). Heat is distributed by mantle convection in two different ways, by plate-scale flow and by rising plumes (Loper, 1985; Bercovici *et al.*, 1989). Plumes are sometimes considered to be a secondary mode of mantle convection that operates almost independently of plate tectonics (Davies & Richards, 1992). However, in considering spherical models of mantle convection, Bercovici *et al.* (1989) concluded that plumes are probably the only form of active upwelling and play a primary role in mantle convection.

2.1 CONCEPT OF BICELLULAR MANTLE CONVECTION AND GEOTECTONIC BIPOLARITY

Up until the end of the 20th Century the general held believe was that numerous, randomly distributed plumes existed and were responsible for the breakup of supercontinents throughout geological time. However, global tomographic studies over the past 25 years (*e.g.*, Su *et al.*, 1994; Li & Romanowicz, 1996; Masters *et al.*, 1996; Gurnis *et al.*, 2000) support Pavoni's (1969, 1985, 1997) proposed model of bicellular, whole-mantle convection (Fig. 2.1) and associated global geotectonic and geophysical bipolarity (Figs. 2.2 & 2.3). According to this model, two torus-like convection cells, the Pacific cell and the African cell, with ascending flow in the mantle underneath the central Pacific and African plates respectively, and converging and descending flow beneath Indonesia and Central America, are responsible for the formation of two large-scale zones of both, lithospheric divergence (marked by growth of the Pacific and African plates from two spreading centres) and convergence (marked by the belt of young folded mountains) since the Mid-Jurassic (Figs. 2.1 & 2.2).

Mantle convection is driven both by heat (generated by the decay of K, Th and U present in the Earth's deep mantle and core) within the mantle and by escaping from the core. Heat from the deep mantle and core is transported by the two rapidly rising superplumes which originate from the core-mantle boundary (being characterised by a large thermal discontinuity/temperature contrast across it; Stacey & Loper, 1983; Ribe & DeValpine, 1994; Boehler, 1996) and are not randomly distributed, but located in antipodal position on the equator within an African and Pacific ring centred on 0º N 10º E and 0º N 190º E respectively (Pavoni, 1985, 1997; Hatton, 1997). The rising plumes continually introduce hot lower mantle into the upper mantle within the rings, and the resultant stresses cause preferential rifting along their margins. Mid-ocean ridges develop on rings of 60º radius about the centres of the superplumes and ocean floor grows away from the rings. Ocean floor grows from one ring and overrides ocean floor generated at the other ring, in a cycle of approximately 400-500 Ma duration, which is referred to as Wilson Cycle (Worsley *et al.*, 1984; Nance *et al.*, 1986; Murphy & Nance, 1992).

The cycle began within 100 Ma of the formation of the Earth's core, *i.e.* at ~4.4 Ga, hence the bicellular whole-mantle convection system is envisaged to be in operation since that time, with the two superplumes having remained fixed in their equatorial and antipodal positions (Hatton, 1997). Support for this proposal is provided by the mantle viscosity profile, which clearly shows that the deep mantle is about 30 times stiffer than the shallow mantle. Convection in the deep mantle will therefore be much less vigorous than in the upper mantle. This means that the plume source is far less likely to undergo lateral movements than the

shallow mantle and supports the argument that viscosity of the lower mantle is high enough to allow such fixity of the two superplumes (Richards, 1991; Hatton, 1997). Due to their geostationary nature the two superplumes might be used as a geotectonic reference system (Pavoni, 1997).

Evidence for the existence of the African and Pacific superplumes is provided by the following geophysical and geological phenomena:

- Two large-scale, NW-trending regions of seismic (S- and P-wave) velocities 3% lower than the average mantle exist beneath the central Pacific Ocean and southern Africa, making these anomalies the most significant low seismic velocity structures in the deep mantle (Masters *et al.*, 1982; Dziewonski, 1984; Dziewonski & Woodhouse, 1984, 1987, 1989; Giardini *et al.*, 1987; Richards *et al.*, 1988; Tanimoto, 1990; Su *et al.*, 1994; Li & Romanowicz, 1996; Grand *et al.*, 1997), which originate from the core-mantle boundary and exhibit rather sharp sides (Ritsema *et al.*, 1998) (Figs. 2.3a-c).
- The long-wavelength lower than average seismic velocities generally correlate with three long-wavelength mantle features of a similar northwesterly trend, namely a geoid high (*e.g.* Chase, 1979; Crough & Jurdy, 1981; Hager *et al.*, 1984, 1985; Doucouré & Antoine, 1994) (Fig. 2.3d), a thermal anomaly containing most of the world's hotspots (Chase, 1979), and the DupaI geochemical anomaly which can be interpreted as the mantle region of basalts enriched in radiogenic lead and strontium isotopes (Castillo, 1989) (Fig. 2.4b).
- The region of the African Superswell, extending from the south Atlantic mid-ocean ridge across the submarine Agulhas Plateau and southern Africa to the East African Plateau and East African Rift Valley (Fig. 2.4a), has a 500-700 m higher topography than expected (Nyblade & Robinson, 1994; Burke, 1996; Partridge, 1997) which is continuous with the anomalous bathymetry of the surrounding Atlantic and Indian Ocean basins (Nyblade & Robinson, 1994), as well as an unusual elevated physiography and distinctive hypsometry (*i.e.* true uplift to the geoid) indicative of uplift that may be dynamically supported by flow within the lower mantle (Harrison *et al.*, 1983; Cogley, 1985; Hagner *et al.*, 1985; Lithgow-Bertelloni & Silver, 1998). Another uplifted area of comparable dimensions is located in the central and western Pacific and has been described by Davies & Pribac (1993). This anomaly encompasses both the Darwin Rise and the South Pacific Superswell (Figs. 2.3a & d, 2.4a & b).
- Plate reconstructions demonstrate a simultaneous, concordant evolution of the lithosphere of the Pacific and African plates during the last ~200 Ma. Break-up of pre-Jurassic lithosphere was followed by large-scale diverging plate movements away from to spreading centres located in antipodal position on the equator, as well as growth of the Pacific and African plates to their present large size (Figs. 2.2a-c).

The African seismic anomaly has been interpreted already for a long time as a long-lived, hot mantle upwelling (Hagner *et al.*, 1985) and support for the connection between deep-seated seismic anomalies and thermal signatures associated with large-scale mantle convection has grown over the past two decades.

Most of the smaller size plumes lie within either the African or the Pacific ring (Matyska, 1989; Matyska *et al.*, 1994), thus the African and Pacific superplumes may perhaps act as a fertile incubator for diapir or cavity plumes of more conventional size (*e.g.* Afar, Hawaii and Iceland plumes). Both plumes exhibit a southeasterly to east-southeasterly tilt, indicating convecting flow within the mantle in this direction (Figs. 2.3a & b). The cause for the SE- to ESE-orientation of mantle convection within both plumes is not known, but it is worth to note that this orientation is approximately perpendicular and parallel to the rotational axis and counter-clockwise rotation of the Earth respectively.

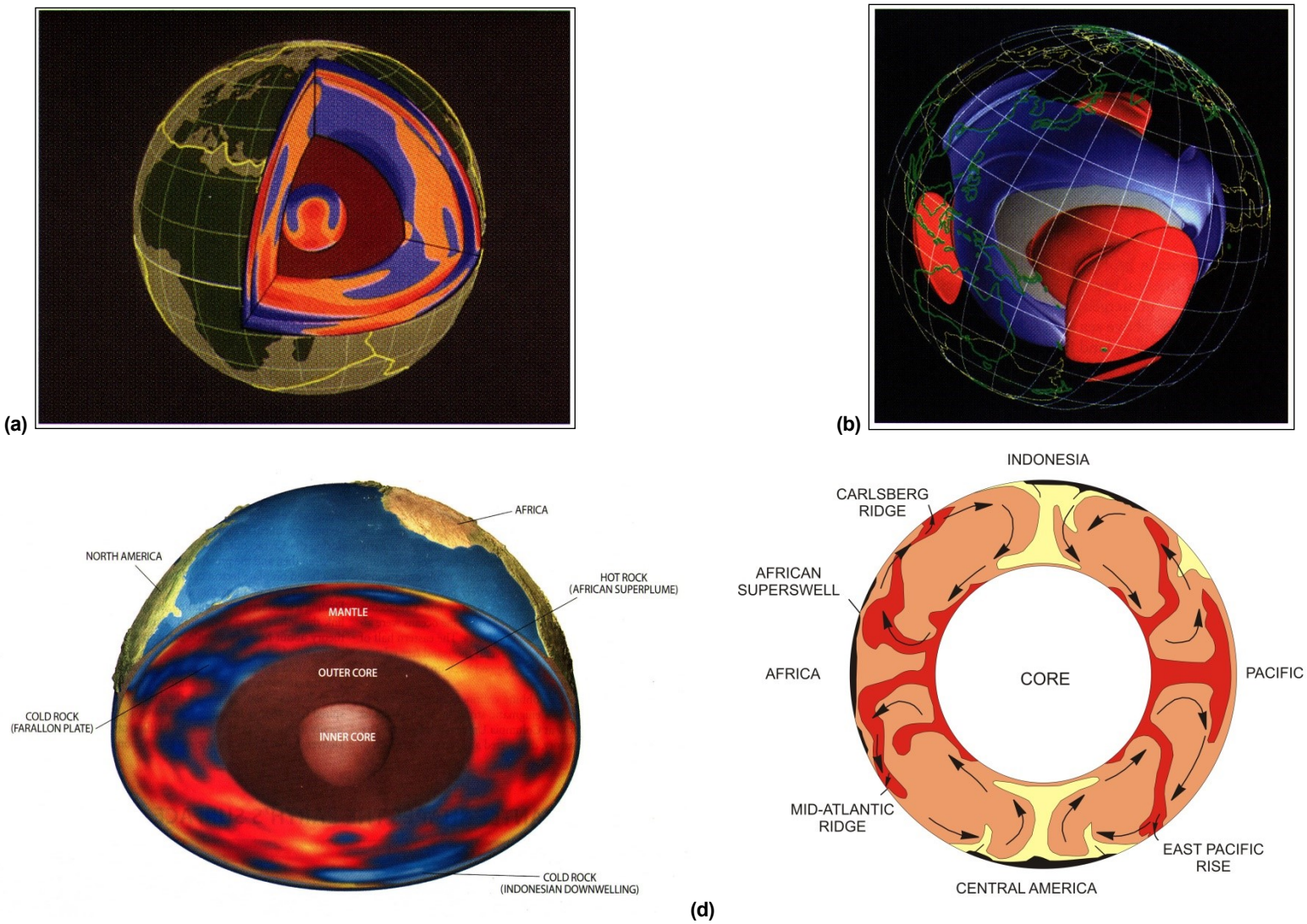
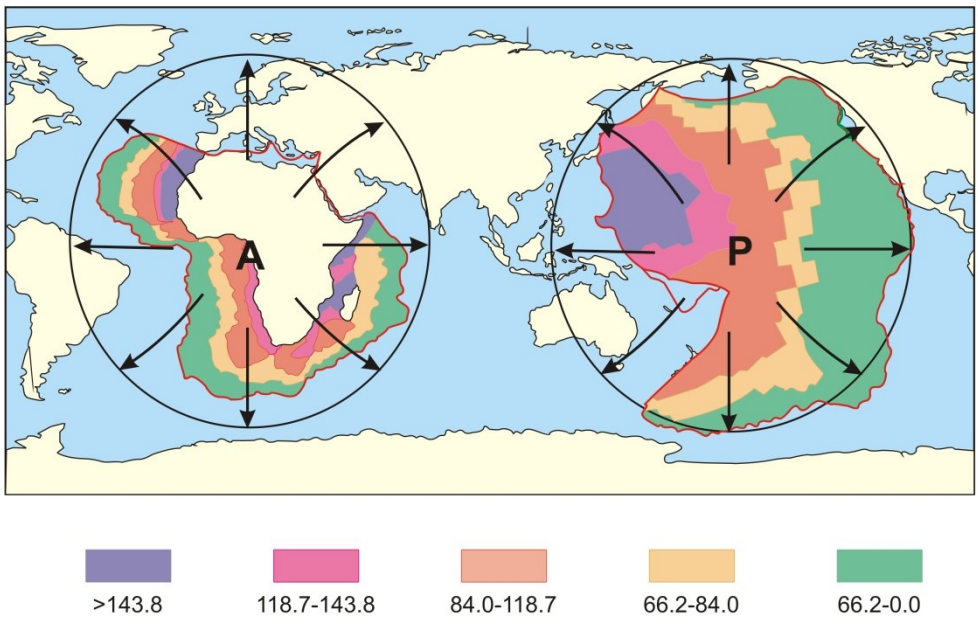
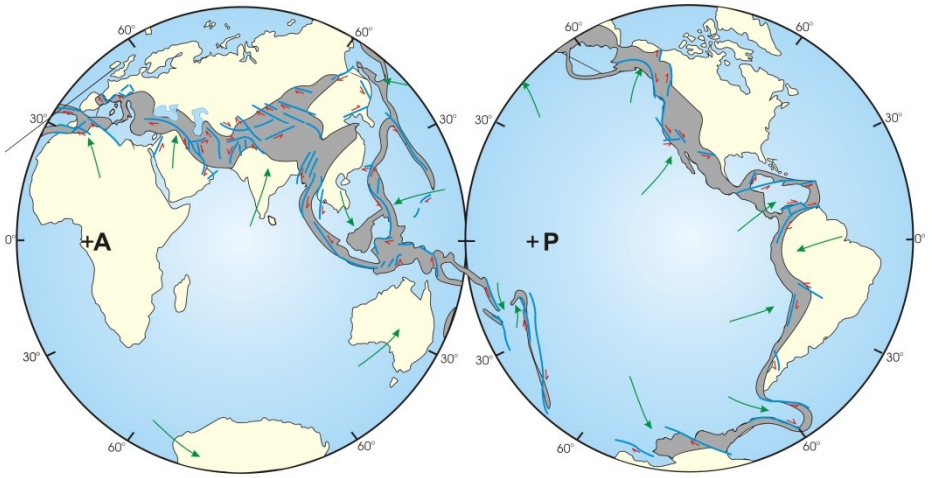


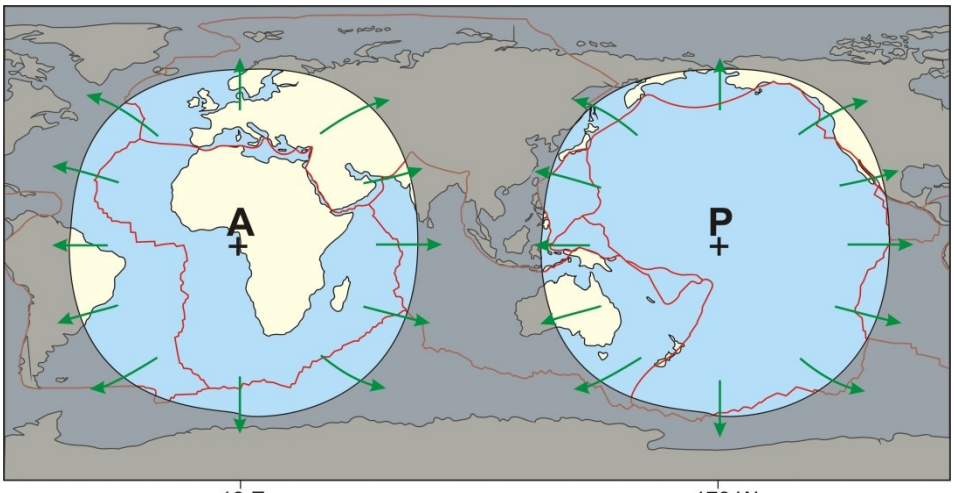
FIGURE 2.1 : (a-c) Three-dimensional illustrations of bicellular convection in the Earth's mantle depicting the existence of the African and Pacific superplumes; (d) Cross-section through the bicellular convection system in the mantle along the equatorial plane of the Earth, according to the geotectonic model (Pavoni, 1997). The convection system consists of two torus-like cells, the Pacific cell and the African cell. Ascending flow in the mantle underneath the central Pacific region and under Africa, descending flow beneath Indonesia and Central America. Note the horizontal flow underneath the active oceanic ridges. The different colours indicate a hypothetical distribution of relative temperatures.



(a)



(b)



(c)

FIGURE 2.2 : (a) Geotectonic bipolarity as revealed by the simultaneous, concentric growth of the African and Pacific plates during the last ~180 Ma (after Pavoni, 1991, 1997, from Frisch & Loeschke, 1993). (b) Schematic representation of the bipolar pattern of sub-lithospheric flow produced by axisymmetric bicellular convection in the mantle (after Pavoni, 1969, 1997). Light areas = diverging lithosphere, Shaded areas = zone of converging lithosphere.. Note: Poles A and P mark the centres of the African and Pacific plumes.

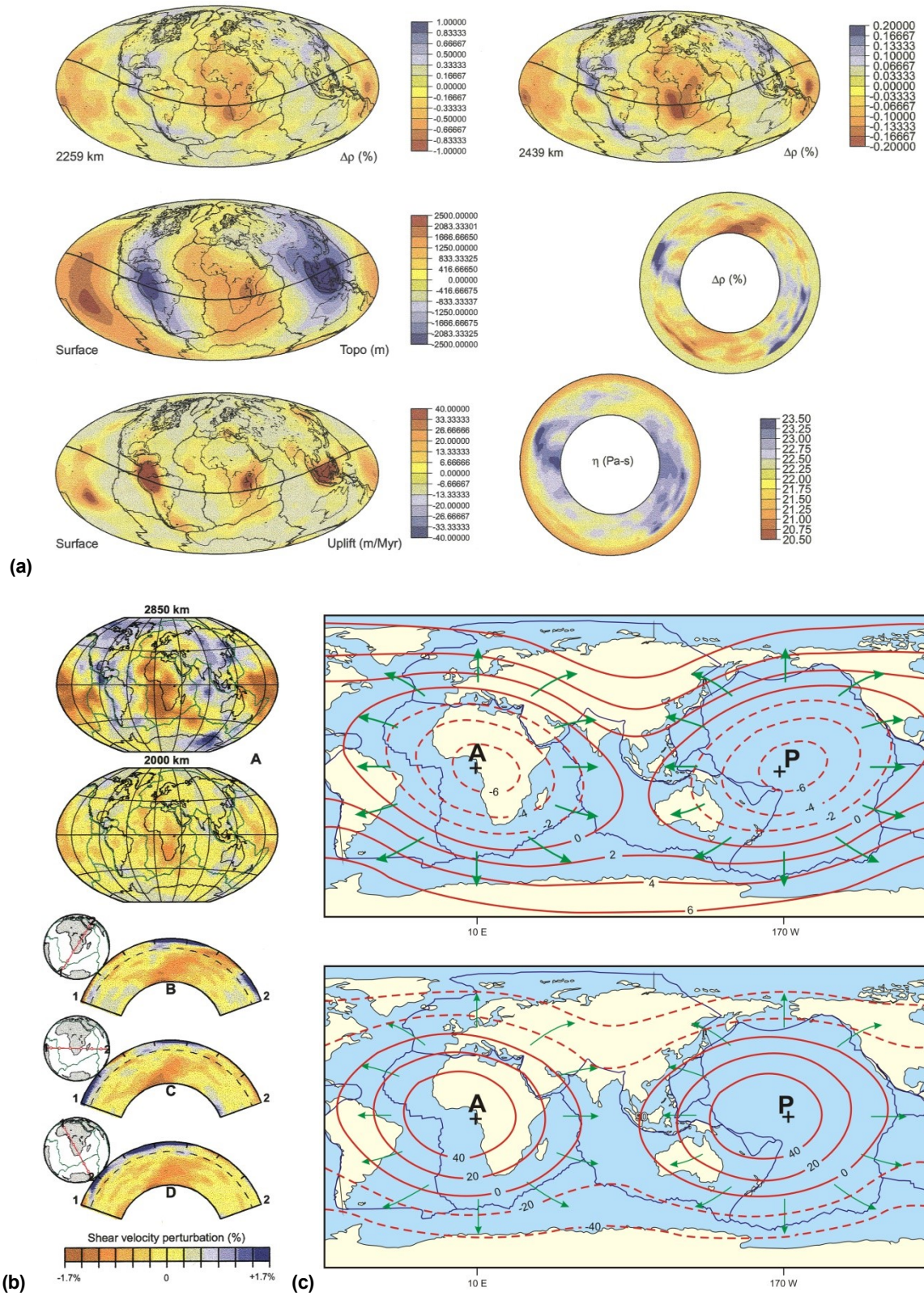


FIGURE 2.3 : Geophysical evidence for global geotectonic bipolarity: (a) Density anomaly at a depth of 2259km (top left), surface dynamic topography (centre left), surface uplift rate (bottom left), and density and viscosity cross sections along a great circle for a density model at a depth of 2439km (right) (after Gurnis *et al.*, 2002). (b) Vertical cross sections (B-D) through the seismic tomography model S20RTS (A) at the core-mantle boundary (2850km) and 2000km (after Gurnis *et al.*, 2000). (c) Heterogeneity of lower mantle P-wave velocity (degree 2; contour interval 2m/sec.) (top) and residual geoid (degree 2; contour interval 20 m) (bottom) (after Richards *et al.*, 1988). Note: Arrows indicate the bipolar, sub-lithospheric flow pattern according to the geotectonic bipolarity model proposed by Pavoni (1969, 1997) (see Fig. 2.2).

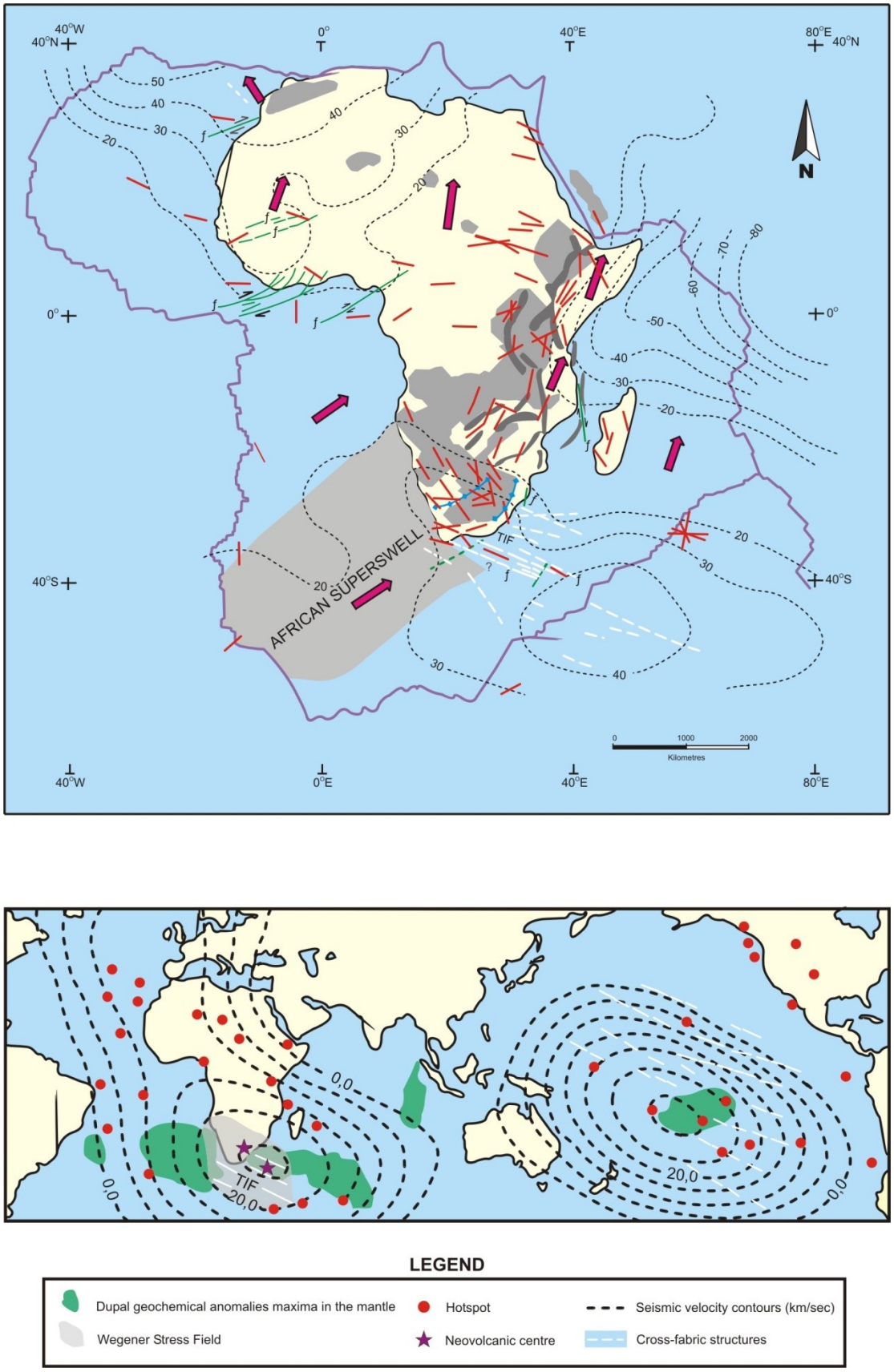


FIGURE 2.4 : Stress map of the African plate (after Andreoli *et al.*, 1996; and references therein). Note: Thick bars = $_{Hmax}$; stippled = regions with average elevation higher than 1000m; heavy stippled = East African Rift; light stippled = African Superswell; ----- f = major Mesozoic and Cenozoic faults; TIF = Trans-Indian Fabric; arrows = absolute velocity trajectories; light contours relate to long-wavelength undulations in the African geoid.

2.2 TECTONIC STRESS

Klemme (1975) recognised that changing tectonic styles, *e.g.* regional extensional to compressional stress regimes, can lead to the development of a succession of basin types along zones of pre-existing tectonic weakness, *i.e.* fault/shear zones. The type of basin produced is controlled primarily by reactivation of these zones of weakness. Such reactivation is termed inversion and will commonly be favoured over new fault generation (Etheridge, 1986). It results in a change in polarity of structural relief (Lake & Karner, 1987). A polyphase history of inversion produces multiple periods of fault reactivation and the superimposed fault arrays that commonly underlie successor basin sequences (Etheridge, 1986).

Since vertical crustal movements are recorded in the stratigraphy, the correlation of the regional stress field, *i.e.* extension or compression, with the stratigraphy can be used to time geological events and structural styles of faulting (inversion) developed by these events.

In comparison, the interpretation of changing palaeo-far field stress orientations can prove to be difficult. This is highlighted by the compilation of the World Stress Map. On a global scale, the World Stress Map collates the orientation of present-day stresses within the lithosphere that result from a variety of forces acting on and within the tectonic plates (Tapponier *et al.*, 1986; Zoback *et al.*, 1989; Zoback, 1992; Zoback & Burke, 1993). It is believed that these stresses primarily emanate from tectonic plate interactions at their boundaries and that these stresses control the intraplate stresses and, in turn, local stress fields (Figure 2.5).

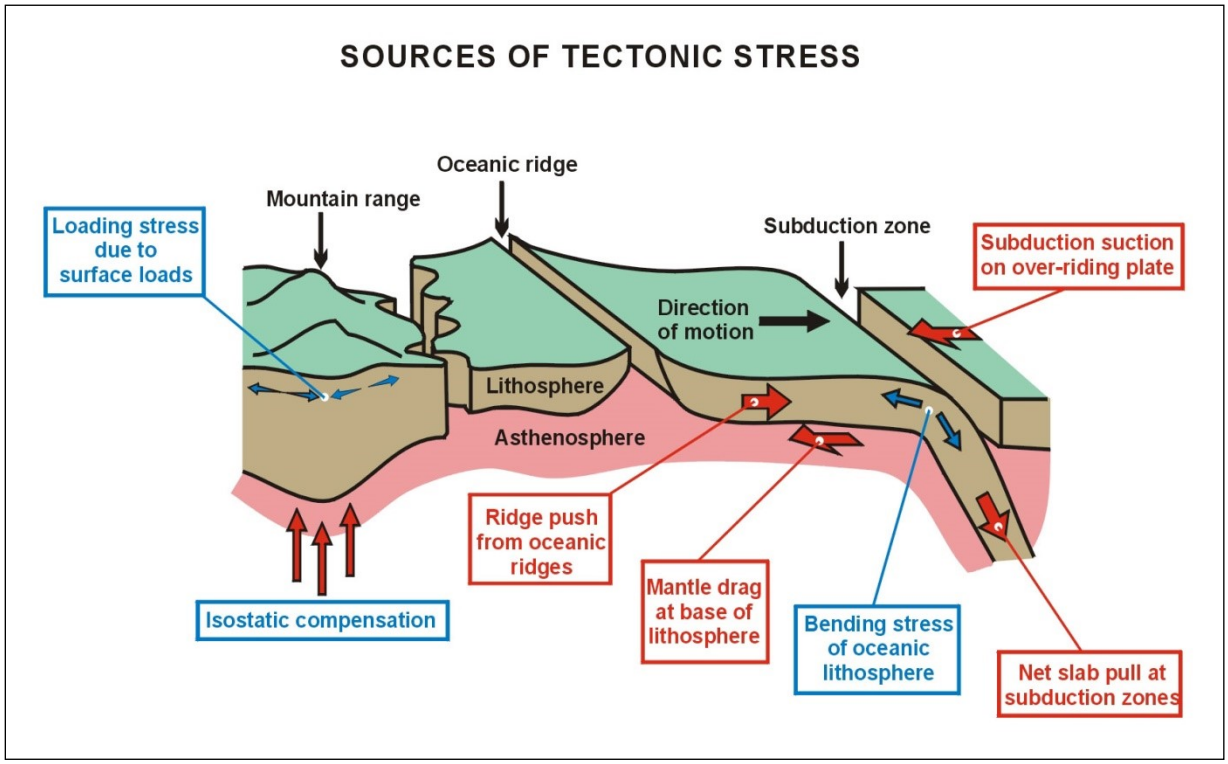


FIGURE 2.5 : Summary diagram illustrating the sources of tectonic stress effecting oceanic and continental lithosphere (after Zoback *et al.*, 1989). Note: red= first-order tectonic stress; blue = second-order tectonic stress.

Within individual tectonic plates, local mapping the present-day stress-field has demonstrated that "inboard" (within plate) effects of plate boundary deformation are experienced thousands of kilometres away from the originating stress at the plate boundary. Information of such far-field stresses is valuable in interpreting past geologic deformation and palaeo-stress fields (Zoback & Burke, 1993). This type of stress data may aid us

in understanding the apparent “weakness” of major continental transform faults. This kind of information is of particular value in unravelling the tectonism of areas along major intracratonic suture zones/terrane boundaries (particularly during their early evolution), of which faults like the San Andreas Fault may be used a present-day analogy.

In this regard, Duane & De Wit (1988) noted that heat and fluids expelled from the cores of continent-marginal orogenic belts can be tectonically driven into continental interiors over distances in excess of 1000 km. Similarly, Marshak & Pluijm (1997) recognised that continental interiors, previously thought to be rigid and undeformable, can act as sensitive recorders of tectonic activity at plate boundaries. Orogenic stresses of the order of megapascals, at plate margins within the North American plate have been found to transmit over distances up to 2,000 km. The implication of this, in light of intraplate fault reactivation is, that the orientation of the fault zone relative to the plate margin is the controlling factor in intraplate stress release, and not necessarily its orientation to the far-field stresses (Pluijm *et al.*, 1997).

With these gross influences in mind, it is not surprising that local stress field orientation of a specified area can be difficult to ascertain. However, possibly in a manner similar to a fractal, smaller structures often appear to mimic the larger ones, allowing one to apply a similar local stress-field to that of the intraplate stress. This is supported by the remarkable uniformity that midplate or intraplate stress field displays in the upper brittle part of the lithosphere (despite the complex vertical and horizontal tectonic structure and fabric of the earth’s crust), often over very broad regions, 20-200 times the approximately 10-25 km thickness of the upper brittle lithosphere (Zoback & Burke, 1997). Using the general knowledge, local stress orientations along smaller features might be predictable.

2.3 PLATE TECTONICS

Based on the assumption that the process of Earth-style plate tectonics require the presence of a surface layer of water (*e.g.* Mian & Tozer, 1990), the onset of plate tectonics would then be coincident with the time when this surface layer formed, which is inferred to have taken place after the core ceased to react with the mantle (Hatton, 1997). This is the time when Pb loss to the core ceased at ~4.46 ± 0.02 Ga, at approximately the same time that radiogenic Xe was retained in the atmosphere, which is ~100 Ma after formation of chondritic meteorites at 4.566 Ga (Allègre *et al.*, 1995). Degassing of water and different noble gases, although at different rates, of the Earth was initially very rapid and almost 90% complete by 4.4 Ga (Allègre *et al.*, 1987). As a layer of water in excess of 100 m deep is proposed to have covered the Earth by ~4.4 Ga, which was probably sufficient to allow plate tectonics to operate, this is the time that plate tectonics had probably begun (Zhang & Zindler, 1989; Allègre *et al.*, 1995). Latest research, however, indicates that plate tectonics are likely to have started approximately 1 billion years after Earth's birth at ~4.54 ± 0.05Ga (*e.g.*, Manhesa *et al*., 1980; Dalrymple, 2001; Braterman, 2013), *i.e.*, in the Mesoarchaean at ~3.5-3.2 Ga (*e.g.,* Tang *et al*., 2020; Brenner *et al*., 2020).

2.4 SUPERCONTINENTAL AND SUPEROCEANIC CYCLES

Although the existence of the supercontinent Pangea was first proposed a century ago (Wegener, 1912), the proposition that other supercontinents existed prior to Pangea (*e.g.*, Valentine and Moores, 1970; Piper, 1974, 1975; Piper *et al.*, 1976) has only become widely accepted over the past three decades (*e.g.*, Hoffman, 1989, 1991; Dalziel, 1991, 1992, 1997; Williams *et al.*, 1991; Stump, 1992; Powell *et al.*, 1993;

Powell, 1995). This has led, in recent years, to a rapidly widening recognition that much of Earth history has been punctuated by the episodic amalgamation and breakup of supercontinents (*e.g.*, Zhao *et al.*, 2002, 2004; Murphy & Nance, 2003, 2012, 2013; Rogers & Santosh, 2002, 2003, 2004; Santosh & Zhao, 2009; Condie, 2011; Yoshida & Santosh, 2011; Huston *et al.*, 2012; Mitchell *et al.*, 2012) with profound consequences to the Earth's geologic, climatic and biological evolution (*e.g.*, Hoffman *et al.*, 1998; Hoffman & Schrag, 2002; Lindsay and Brasier, 2002; Dewey, 2007; Condie *et al.*, 2009, 2011; Goldfarb *et al.*, 2010; Hawkesworth *et al.*, 2010; Santosh, 2010a,b & c; Bradley, 2011; Hannisdal & Peters, 2011; Strand, 2012; Young, 2012a,b, 2012a, 2013b; Melezhik *et al*., 2013). This history of episodic supercontinent assembly and breakup, which constitutes the supercontinent cycle, has influenced the rock record more profoundly than any other geologic phenomenon (*e.g.*, Condie, 2011). Its existence points to fundamental aspects of the Earth's interior dynamics (*e.g.*, Condie, 2003; Evans, 2003; Zhong *et al.*, 2007; Santosh *et al.*, 2009a; Zhang *et al.*, 2009) and its recent recognition is arguably the most important advance in Earth Science since the advent of plate tectonics over 50 years ago. Yet the idea of a supercontinent cycle was first advanced thirty years ago, and the notion of episodicity in tectonic processes predates plate tectonics by decades. So while the widespread recognition of the significance of supercontinents in Earth history is a relatively recent phenomenon, a long history has led to this fundamental realization (Nance & Murphy, 2007).

The distribution of continental and oceanic lithosphere has changed constantly through time, with large continental masses periodically fragmenting into smaller crustal blocks, and re-amalgamating in different configurations as new supercontinents (*e.g.*, Hoffman, 1991; Rogers, 1996).

The apparent random nature of this process hinders the reconstruction of ancient supercontinents. However, because granitoids often inherit geochemical characteristics from crustal sources, their isotopic compositions can “fingerprint” basement terranes and provide useful information for delineating crustal provinces/terrane mapping (*e.g.*, Kistler & Peterman, 1973; Aleinikoff *et al.*, 1987; Ayuso & Bevier, 1991) and for evaluating plate reconstructions (*e.g.*, Tosdal, 1996). Palaeogeographic reconstructions of supercontinents throughout geological time are generally based on litho-stratigraphic, geochronologic, tectono-structural, palaeomagnetic and geophysical data. Only in combination with each other can precise and reliable reconstructions of continental configurations at certain time intervals be achieved.

In particular, tectono-structural data are best suited for precise continental reconstructions because the intersection of subvertical shear zones with continental margins represents piercing points with which to test precrustal extension supercontinent fits, using the complementary piercing points of other continental fragments. In addition, the tectonic evolution of shear zones can help track the birth and break-up of a supercontinent because they record either the accretion/amalgamation of continental fragments during the formation of orogens, or the fragmentation and dispersal phase of a supercontinent during the development of rifts, respectively.

Based on the bicellular mantle convection system, supercontinents and superoceans formed episodically by oceans expanding away from one ring and driving the continents to the other. Expansion of the ocean floor will thus continue until all the earth’s surface, with the exception of non-subductible components, is covered by the expanding ocean floor. At this stage, subduction of expanding ocean floor is inevitable. This provides the opportunity for growth of ocean floor from within the non-subductible components crowded together by the expanding ocean floor. Now the previously expanding ocean floor is overridden. In the next cycle the newly expanding ocean floor will expand at the expense of the superocean created in the previous cycle. At present, ocean floor is spreading from the African ring and overriding, by subduction, ocean floor expanding from the Pacific ring.

3 REGIONAL FRAMEWORK AND CRUSTAL ARCHITECTURE OF THE KAAPVAAL AND ZIMBABWE CRATONS AND LIMPOPO PROVINCE

3.1 KAAPVAAL CRATON

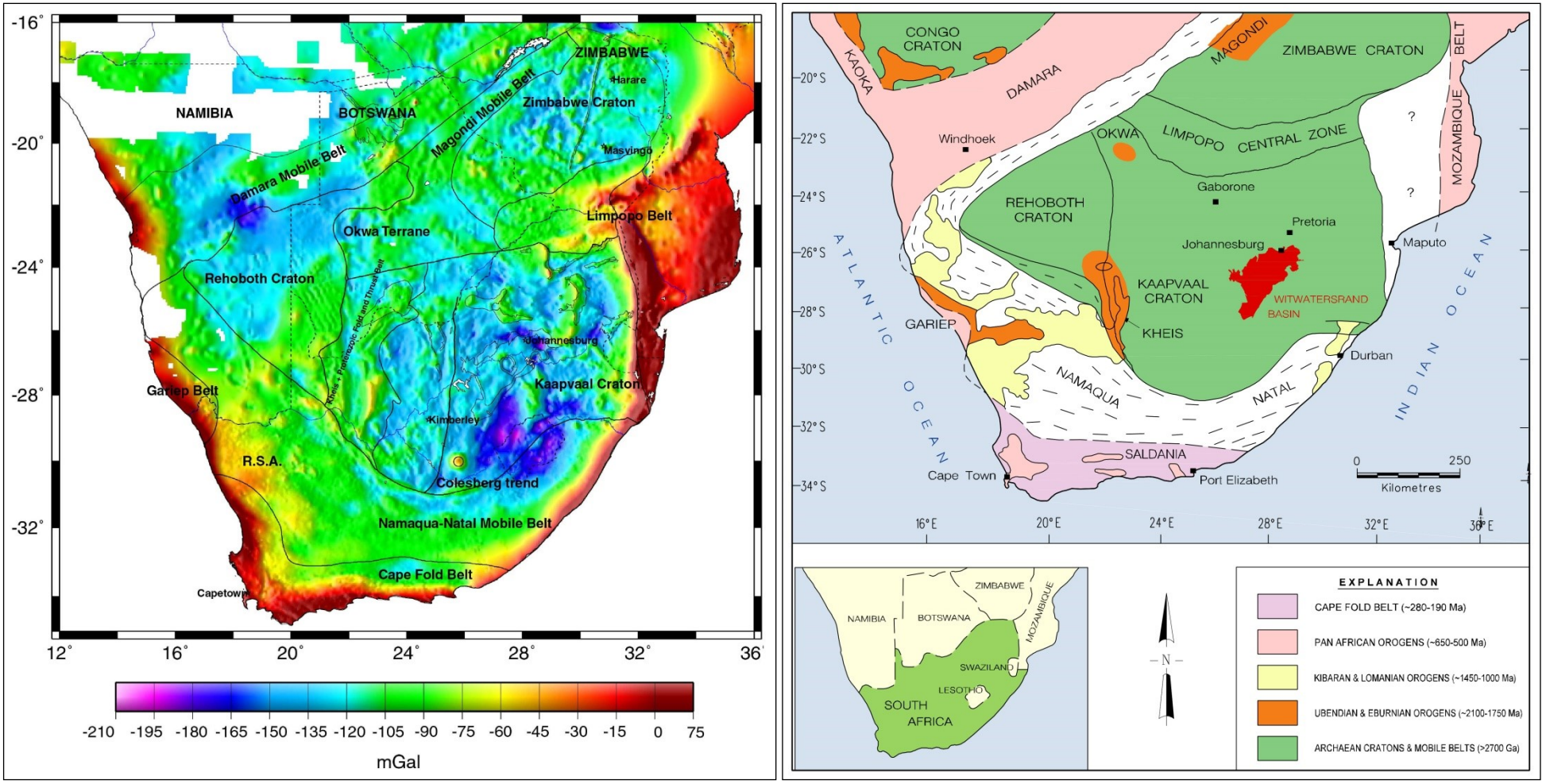
The Kaapvaal Craton represents one of the few regions on earth that has retained a substantial portion of relatively pristine Palaeo- to Mesoarchaean rocks. The craton covers an area of about 1.2 x 10^6 km^2 and its boundaries, although somewhat obscured by younger deposits, have been reasonably well defined by geological mapping, geochronology and geophysical data (*e.g.* De Wit *et al.*, 1992a; Corner *et al.*, 1990; Corner, 1991, 1993, 1994, 1995, 1997; Thomas *et al.*, 1993a, 1994; McCourt, 1995, Brandl & de Wit, 1997, Brett *et al.*, 2000; Ranganai *et al.*, 2002).

To the east, the Kaapvaal Craton is bounded by the Lebombo monocline that contains Jurassic igneous rocks associated with the break-up of Gondwana, and to the south and west, the craton is flanked by the Mesoproterozoic Namaqua-Natal mobile belt. Its western boundary is the Kalahari Suture Zone/Palaeoproterozoic Kheis belt, whilst the northern margin of the craton is defined by a major shear zone, the so-called Palala suture zone, which forms the boundary between the Central Zone Terrane of the Archaean Limpopo Province and the Kaapvaal Craton (Figs. 3.1a & b).

The Kaapvaal Craton comprises a mixture of minor Palaeoarchaean (~3.64-3.5 Ga) tonalitic gneisses and migmatites and predominantly Mesoarchaean (~3.5-3.2 Ga) TTG granitoids (from essentially sodium-rich tonalitic and trondhjemitic granitoids) with interspersed greenstone sequences and volcano-sedimentary basins, is intruded by a great variety of granitic (potassium-rich granodiorite, monzogranite and granite) plutons (~3.2-2.7 Ga) and is overlain by a succession of Neoarchaean (~3.1-2.5 Ga) and Palaeoproterozoic (~2.6-1.7 Ga) basins that are filled with thick cover sequences of both volcanic and sedimentary rocks (*e.g.* Anhaeusser & Wilson, 1981; Armstrong *et al.*, 1991; de Wit *et al.*, 1992a; Brandl & de Wit, 1997) (see Appendix 21-A for a summary of available geochronological ages). Hence, the Archaean evolution of the Kaapvaal Craton covers a time span of more than 1 Ga and can be subdivided into two main periods (de Wit *et al.*, 1992a; de Wit & Hart, 1993).

The first, Palaeo-/Mesoarchaean period (~3.64-3.1 Ga) records the initial separation of the continental lithosphere of the Kaapvaal Craton from the asthenosphere, resulting in the formation of small, deep-rooted continental nuclei, and terminates with a major pulse of accretionary tectonics between ~3.2 Ga and ~3.1Ga to form the Kaapvaal Shield (Kaapvaal proto-Craton). This period of continental growth can be equated with plate tectonic processes occurring in modern-day oceanic basins. However, the difference is that in the Palaeo- to Mesoarchaean, these oceanic processes appear to have occurred in shallower water depths than the modern ocean basins. Although the basic uniformitarian precepts of global plate tectonics can be applied to the Archaean crustal evolution, certain conditions (such as heat flow, magmatic production rates, extent of continental re-cycling, ocean water depth, etc.) must have been significantly different (De Wit *et al.*, 1992a; de Ronde & de Wit, 1994; de Wit & Hart, 1993; Brandl & de Wit, 1997).

Subsequently to the stabilization of the Kaapvaal Shield at approximately 3.1 Ga, the second and Neoarchaean period (~3.1-2.6 Ga) in the evolution of the craton was dominated by both intra-continental and continental-margin processes. Continental growth took place mainly along the northern and western margins of the stable shield through a combination of Cordillera-type tectonic aggregation of crustal fragments (terrain accretion) and subduction-related igneous processes that enlarged the Kaapvaal Shield to form the Kaapvaal Craton (De Wit *et al.*, 1992a; de Wit & Hart, 1993; Brandl & de Wit, 1997).



(a) (b)

FIGURE 3.1: Crustal architecture of southern Africa according to an interpretation by (a) Webb (in prep.) (Note: Bouguer gravity data provided by Council for Geoscience) and (b) Thomas *et al.*, 1993a (modified in this study).

The Kaapvaal Craton represents one of approximately 35 small Archaean (>2.5 Ga) continental fragments or cratons (Bleeker, 2003), of which some formed part of a hypothetical large Neoarchaean continent, possibly the first "supercontinent" of planet Earth and referred to as 'Ur' (Rogers, 1993, 1996) (Fig. 3.2a). This supercontinent formed at approximately 3.0 Ga by the amalgamation of "juvenile" cratons that had not been part of other continents (Rogers, 1993, 1996). Other continental fragments of Ur are found today embedded in the Antarctic continent (western Dronning Maud Land (*i.e.,* Grunehogna Craton), Napier and Vestfold Hills), in the Indian subcontinent (west and east Dharwar, Bastar (Bhandara), Singhbhum cratons) and in the Australian continent (Pilbara Craton) (De Wit *et al.*, 1988; Cheney *et al.*, 1988, 1990a; Hunter *et al.*, 1991; Groenewald *et al.*, 1991; Black *et al.*, 1991; Meen *et al.*, 1992; Sarkar, *et al.*, 1992; Thorpe *et al.*, 1992; Bickle *et al.*, 1993; Blake, 1993; Sharma *et al.*, 1994; Rogers, 1993, 1996; Cheney, 1996; Corner, 1998).

Note: *The Grunehogna Craton of East Antarctica formed an integral part of the proto-Kaapvaal Craton (e.g., Groenewald et al., 1991, 1995; Corner, 1991) at least during latest Mesoproterozoic times (e.g., Peters et al., 1991; Gose et al., 1997; Jones et al., 2003), or since ~3.1 Ga as proposed in this study, which was detached during Mesozoic break-up of Gondwana, and will be referred to in the following Sections as Kaapvaal-Grunehogna Craton, or simply Kaapvaal Craton.*

Uncertainty, however, exists with regard to the plate tectonic history of the Kaapvaal Craton and its palaeogeographic relation to the other cratonic nuclei in the early Precambrian. Piper (1982) suggested, based on palaeomagnetic data, the existence of a late Neoarchaean to Palaeoproterozoic supercontinent in which the Kaapvaal craton is placed next to South America, very distal to the Pilbara craton of Australia (Fig. 3.2a). In the Ur configuration of Rogers (1996), Antarctica is situated between the Kaapvaal and Pilbara cratons, with the Zimbabwe craton situated to the immediate north of the Kaapvaal craton (Fig. 3.2b). However, Rogers (1996) indicates that the Zimbabwe craton only became stable at ca. 2.5 Ga. Cheney (1996) suggested that the Kaapvaal and Pilbara cratons were located adjacent to each other forming the continent "Vaalbara", with the Pilbara craton to the south of the Kaapvaal craton based on the striking resemblance between late Neoarchaean to early Palaeoproterozoic sedimentary sequences on the two cratons (Fig. 3.2c). Based on palaeomagnetic evidence, Wingate (1998) proposed that the Kaapvaal and Pilbara craton were not even in close proximity to each other in the Neoarchaean and rejected the "Vaalbara" theory of Cheney (1996). Zegers *et al.* (1998) placed the Pilbara craton immediately to the east of the Kaapvaal craton based on structural, geochronological and palaeomagnetic data, but stated that it remains uncertain when the Limpopo Belt accreted to the Kaapvaal Craton. Based on palaeomagnetic, lithostratigraphic, palaeoenvironmental, geochronological, and structural data, De Kock *et al*. (2009) constrained the position of the Pilbara Craton in close immediate proximity towards the northwest of the Kaapvaal craton in a present-day Kaapvaal reference frame.

Gumsley *et al*. (2017) adopted the palaeoreconstruction of De Kock *et al*. (2009) but proposed that the Pilbara and Kaapvaal cratons were part of a much larger continent or supercontinent in the Neoarchean to Paleoproterozoic termed 'Supervaalbara'. This large crustal block likely included the Wyoming, Superior and Hearne cratons of North America, together with the Kola-Karelia Craton located between Russia and Finland, as well as possibly the Singhbhum Craton of India and the Samartia terrane of Russia and Ukraine. This continent or supercontinent allows for the Kaapvaal and Pilbara cratons to share many geological similarities without being nearest neighbours, along possibly the same passive margin. The geological evolution of all these cratons is very similar, particularly in the Paleoproterozoic, and which may have been driven by global processes. These global processes may include true polar wander, the submergence and subsequent re-emergence of continents with sea-level rise and fall, as well as atmospheric oxygenation and global glaciation. Palaeomagnetic studies provide further continuity supporting the existence of

Supervaalbara, which appears geologically distinct from the Rae family of cratons, suggesting perhaps two different continents in the early Paleoproterozoic before the assembly of the supercontinent Columbia (Nuna) in the late Paleoproterozoic (Gumsley *et al*., 2017) (Fig. 3.3).

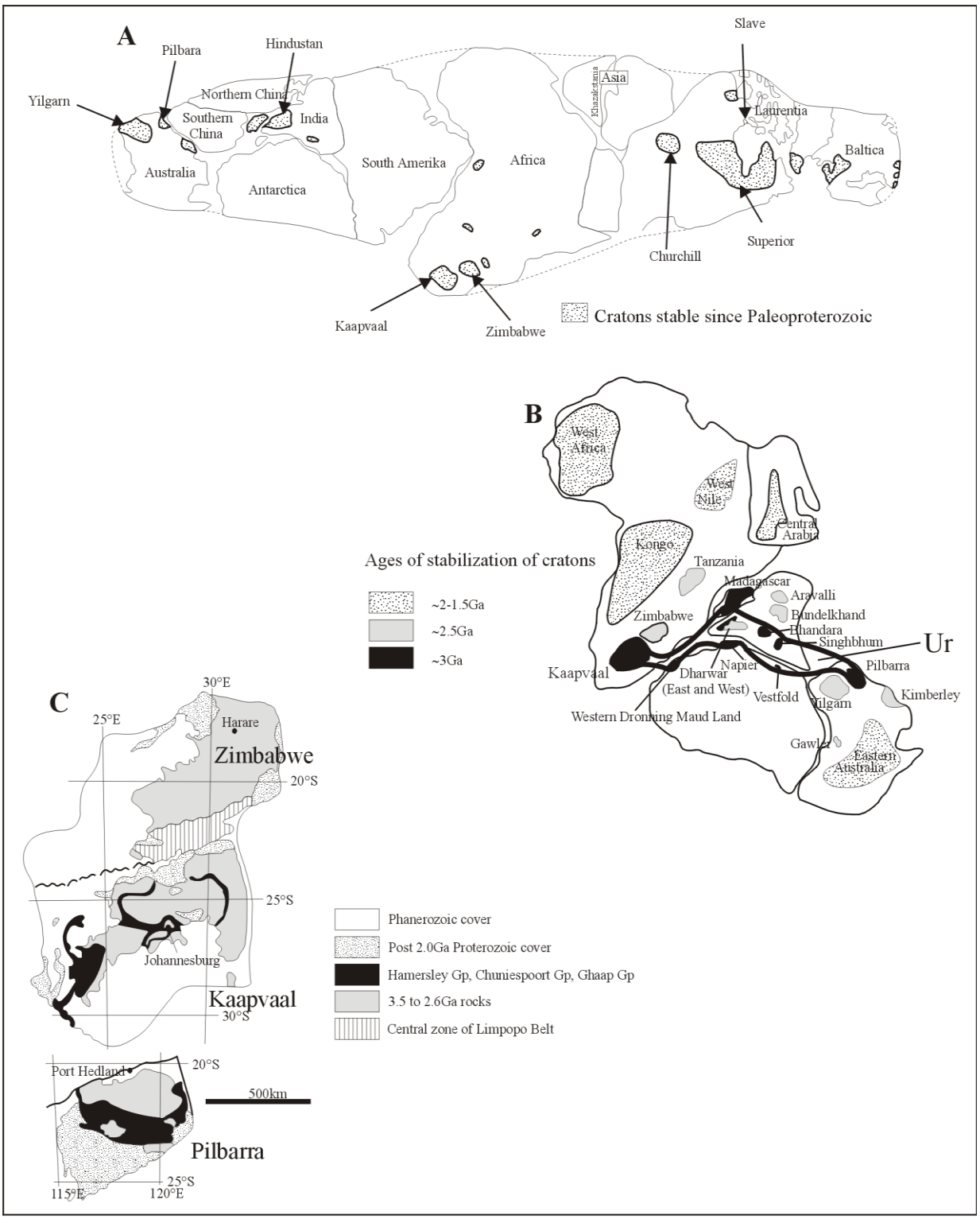


FIGURE 3.2: (a) Palaeomagnetic reconstruction of continents between ~2.7-2.2 Ga (Piper, 1982); (b) Palaeogeographical configuration of the Archaean-Palaeoproterozoic continent 'Ur' (Rogers, 1996); (c) Proposed configuration of the 'Vaalbara' continent (Cheney, 1996).

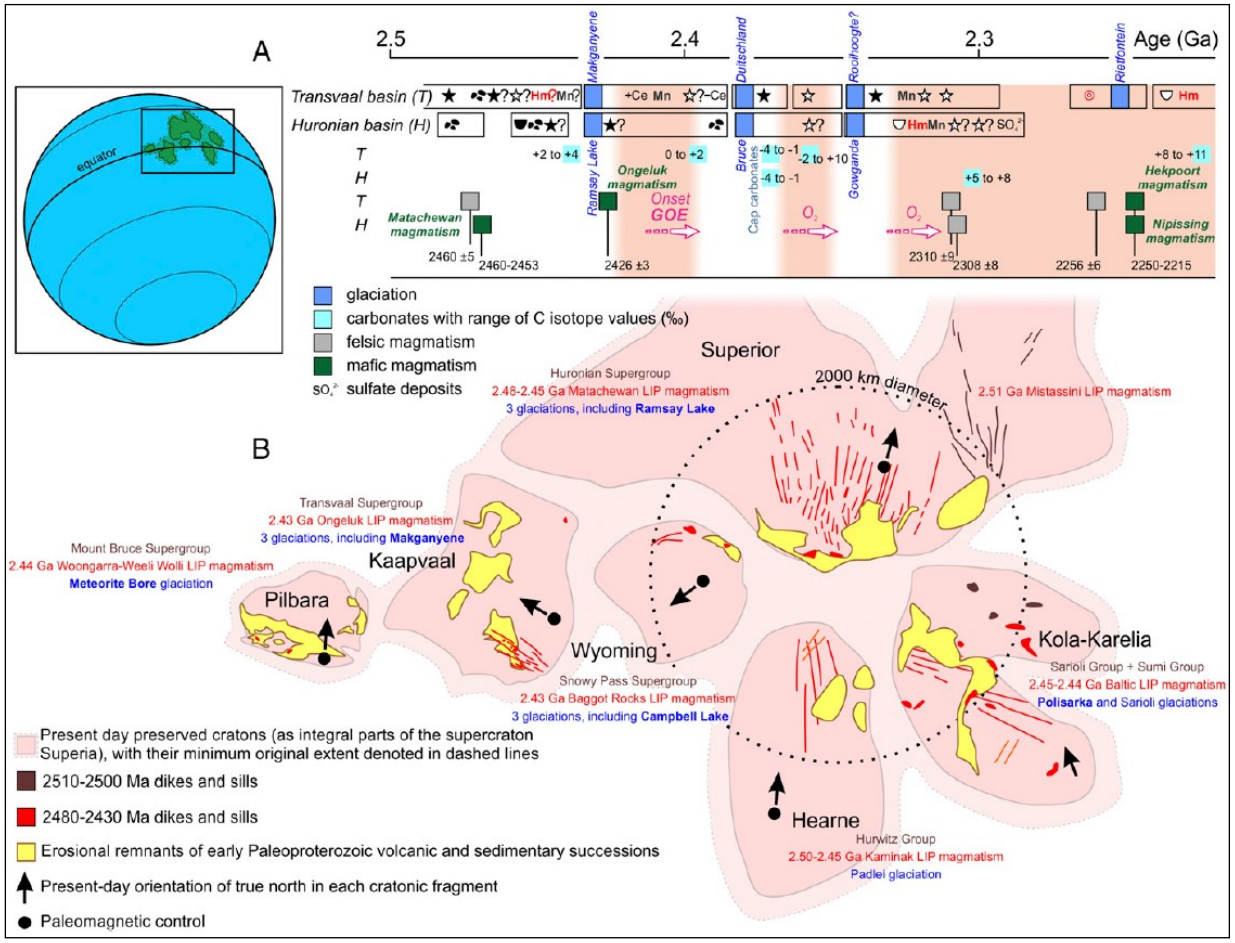


FIGURE 3.3: A) Approximate chronology of glaciations and atmospheric oxygen oscillations according to related redox indicators in the Huronian and Transvaal basins, as well as dated mafic and felsic magmatic events and $\delta^{13}C$ ranges for carbonates and the extent of stratigraphic records in each basin denoting gaps in records at unconformities and disconformities (Gumsley *et al.*, 2017). (B) Early Paleoproterozoic geography of the Superior, Kola–Karelia, Hearne, and Wyoming cratons as integral parts of the supercraton Superia (Ernst & Bleeker, 2010; Bleeker & Ernst, 2006) with the addition of the Kaapvaal and Pilbara cratons in the supercraton Vaalbara configuration (De Kock *et al.*, 2009), both assembled within the supercontinent Supervaalbara (Gumsley *et al.*, 2017).

It is important to note that in most reconstructions, the Zimbabwe and Kaapvaal cratons are placed next to each other since around 2.7 Ga, the time of granulite facies metamorphism in the Limpopo metamorphic belt (Barton & Van Reenen, 1992). However, this model was challenged since the identification of a ~2 Ga old metamorphic event in the Limpopo metamorphic belt (Watkeys, 1983; Barton *et al.*, 1994a; Kamber & Biino, 1995; Kamber *et al.*, 1995a & b; Berger *et al.*, 1995; Hisada & Miyano, 1996; Barton & Sergeev, 1997; Jaeckel *et al.*, 1997; Holzer *et al.*, 1996, 1997, 1998, 1999) (see Section 3.3 for details).

In depth, the Kaapvaal Craton has also been reasonably well defined by seismic and petrological, geochemical and geochronological investigations on kimberlite nodules from the mantle. Seismic refraction studies revealed that the intermediate-velocity rocks (6.6-6.9 kms^{1}) of the craton are represented by only 15 km of the lower crust, and that the depth to Moho is about 37-40 km. In contrast, the Mesoproterozoic Namaqua-Natal mobile belt along the southern margin of the craton has a substantial (30 km) component of intermediate-velocity rocks and a depth to Moho of approximately 42 km (Green & Durrheim, 1990, Durrheim & Mooney, 1991; Durrheim & Green, 1992 ; de Wit *et al.*, 1992a; de Wit *et al.*, 1993b; De Wit & Hart, 1993; Nguuri *et al.*, 2001; Niu & James, 2002; Stankiewicz *et al.*, 2002) (Fig. 3.4).

S-wave velocities with a mean of 4.3 km/s are apparent in the crust and upper mantle down to 80 km depth, followed by an upper mantle lid with a positive velocity gradient and a higher velocity of about 4.6 km/s

between 110 and 220 km depth (Chichowich & Green, 1992; Qui *et al.*, 1996; Priestley, 1999) (Fig. 3.4). S-, P- and converted P-S and PPPS-wave velocity data indicate a variable thickness of 220-330 km, with a maximum of ca. 380 km for the subcontinental mantle lithosphere (tectosphere) of the Kaapvaal Craton (Chichowich & Green, 1992; Peberdy, 1992; Vinnik *et al.*, 1996a; Stankiewicz *et al.*, 2002; Wright *et al.*, 2002). An extensive intra-cratonic, in average 50 km wide low-velocity zone has been detected between 160 and 260 km depth, using P-wave residual analysis (De Wit & Hart, 1993; Qui *et al.*, 1996; De Wit & Ashwal, 1997; Priestley, 1999) (Fig. 3.4). The 160-220 km thickness of the seismic lithosphere (crust plus upper mantle lid) is supported by petrological studies of garnet nodules and diamond inclusions from kimberlites (Boyd *et al.*, 1985; Boyd & Gurney, 1986; Boyd, 1989; Gurney, 1990).

Compared to relatively high heat flows (~80 m/Wm^2) and the presence of only barren kimberlites in the surrounding younger mobile belts, low-heat flow (45 m/Wm^2 on average) and the presence of diamondiferous kimberlites characterise the Kaapvaal Craton (Jones, 1988). This indicates that the craton has a deep keel of relatively cool, chemically reduced lithospheric root of dunite-harzburgite, which had already formed at ca. 3.5 Ga, with peridotitic diamonds developing around 3.2 Ga (Gurney, 1990).

Seismic anisotropy of the southern African mantle is evident from fast wave polarization directions determined from both shear-wave splitting and surface wave observations. This anisotropy (lattice-preferred orientation of olivine) in the lithospheric mantle keel of the Kaapvaal and Zimbabwe cratons and Limpopo Central Zone Terrane is dominated by at least two regional orientations (*i.e.*, NE-SW and E-W) (Vinnik *et al.*, 1995, 1996b; Silver *et al.*, 2001) (Figs. 3.5a & b), but the current debate centres around the question, if this anisotropy is inherited from Archaean-Proterozoic tectonism (Silver *et al.* 2004), or from recent thermo-tectonics (Vinnik *et al.*, 1995, 1996b).

Vinnik *et al.* (1996b) favoured northeast-directed absolute plate motion of southern Africa and associated deformation of the root of the Kaapvaal Craton, due to resistive drag at the base of the lithosphere, since the end of the Jurassic, to be the cause for the NE-SW trending seismic mantle anisotropy (Fig. 3.5a). Contrary to this interpretation, Silver *et al.* (2004) found that the mantle anisotropy beneath southern Africa is dominated by deformational events in Archaean times occurring within the lithosphere, rather than present-day processes in the sublithospheric mantle. Silver *et al.* (2004) presented evidence that the observed mantle fabric producing seismic anisotropy constitutes fossil structure in the mantle that is subsequently reactivated, much like the more commonly acknowledged reactivation of crustal structures. These workers argued that Neoarchaean collisional orogenies between ~2.9 Ga and 2.6 Ga, accreting the western Kimberley and northern Pietersburg blocks onto the eastern shield of the Kaapvaal Craton, imparted a continuous arc of mechanical anisotropy to the mantle that controlled the subsequent magmatic history of the cratonic southern Africa. Furthermore, four major magmatic events, *i.e.* the Great Dyke, Ventersdorp, Bushveld, and Soutpansberg, all represent extensional failure along planes oriented parallel to the local splitting fast polarisation direction (Fig. 3.5b). Each of these events is interpreted to be a collisional rift, where the stress field associated with collision produces extension and rifting for orientations at a small angle to the direction of the collision. Since the timing of these basaltic intrusions is controlled by temporal variations in lithospheric stress associated with orogenies, it implies either that the melting process is genetically related to the evolution of the far-field collision, or that there was a semi-permanent reservoir of basaltic magma residing in the sublithospheric mantle during the ~1 billion year time period spanned by these magmatic events. The existence of an extensive magma reservoir would argue for elevated temperatures just beneath the lithosphere during this time. The eastern Mesoarchaean Kaapvaal shield appears to be seismically isotropic and to have been relatively devoid of rifting and magmatism, suggesting it has not acquired the mechanical anisotropy and is mechanically stronger than surrounding areas (Silver *et al.*, 2004).

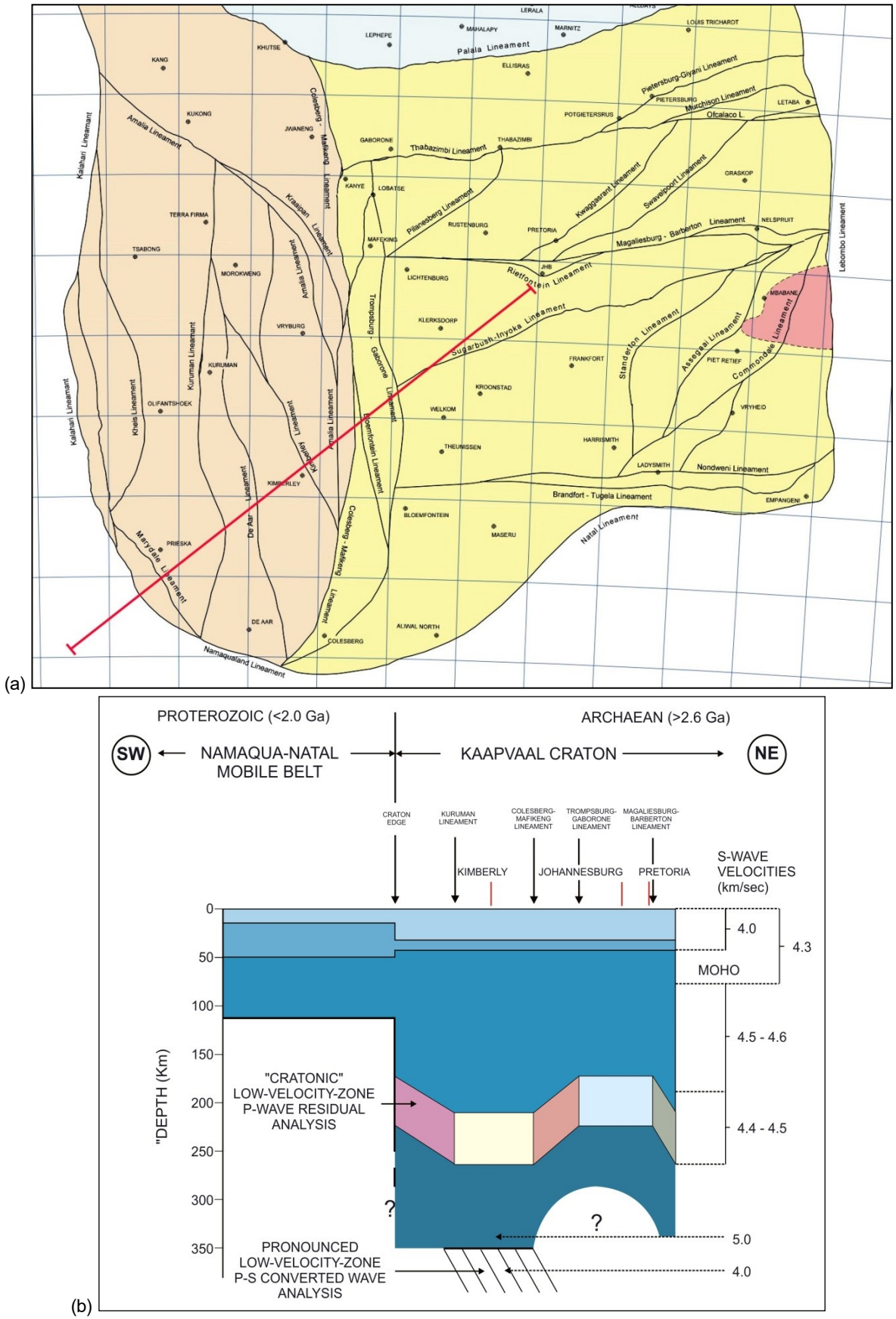
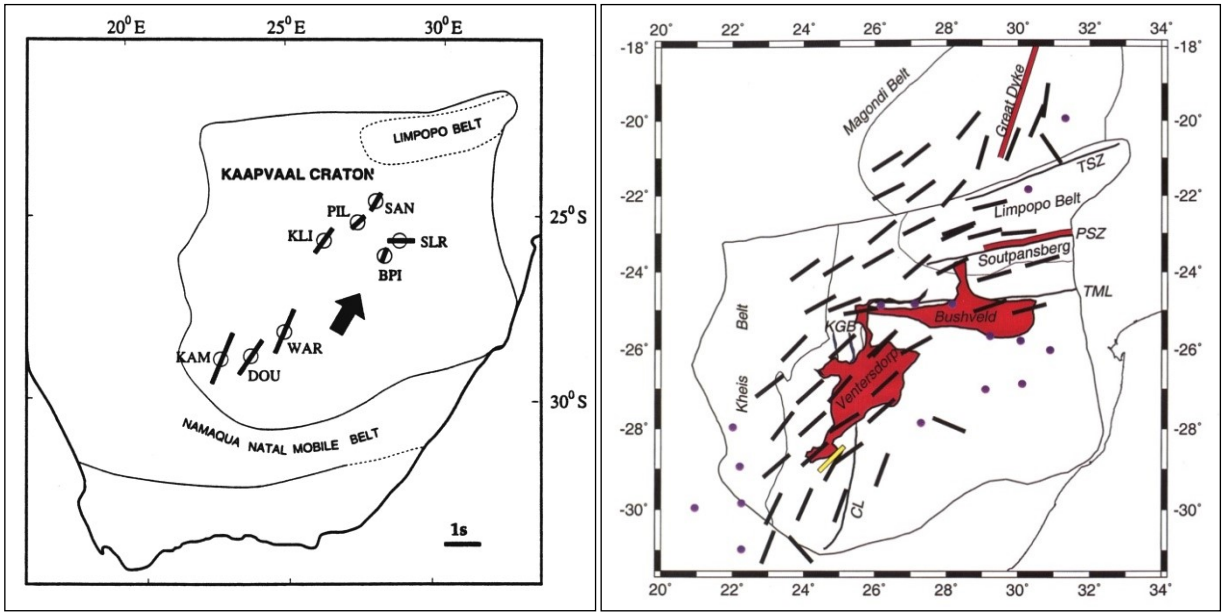


FIGURE 3.4: (a) Reconstruction of the fundamental crustal architecture of the Kaapvaal Craton (this study); (b) Schematic seismic section from data projected onto a deep teleseismic line across the southwestern part of the Kaapvaal Craton (modified after de Wit & Hart, 1993). Lithospheric depths taken from Chichowick & Green (1992), Peberdy (1992) and Vinnik (unpublished) and S-wave velocities and all crustal data from Chichowick & Green (1992), Green & Durrheim (1990) and Vinnik (unpublished). Note: The depth to the top of a low-velocity zone within the lithosphere increases from ~160 km in the Witwatersrand Terrane of the Swazi Subprovince to ~210 km in the Kraaipan Subprovince across the Colesberg-Mafikeng suture.



(a) (b)

FIGURE 3.5: (a) Maps of southern Africa, showing (a) the direction of polarization of the fast split wave (indicated by a straight line; the length of the line is proportional to lapse time δ*t* of the slow wave (see scale bar)) at various stations across the Kaapvaal Craton, as well as the direction of the absolute plate motion of southern Africa since the end of the Jurassic (large arrow) (modified after Vinnik *et al.*, 1996b); and (b) the orientation of shear wave splitting fast polarisation direction across the southern African mantle in relation to relevant geological crustal features (after Silver *et al.*, 2001).

Results of the completed international and multidisciplinary "Kaapvaal Craton Programme" have recently been documented in a series of publications in *Geophysical Research Letters* (*i.e.* Irvine *et al.*, 2001; Shirey *et al.*, 2001; Ben-Ismail *et al.*, 2001; James *et al.*, 2001; Nguuri *et al.*, 2001; Freybourger *et al.*, 2001; Silver *et al.*, 2001) and are summarised by O'Reilly (2001). The most remarkable results of the project came from the deployment of 55 seismometers along a NE-SW profile extending across the Kaapvaal Craton, the Limpopo Province, and the southern Zimbabwe Craton, which captured information from natural seismic events occurring around the world from April 1997 to July 1999. These data have been used to produce three-dimensional images of the present distribution of seismic velocity contrasts (seismic tomography), which in turn were used to obtain a picture of the deep structure in the mantle beneath southern Africa (Fig. 3.6).

James *et al.* (2001) and Stankiewicz *et al.* (2002) have identified high-velocity mantle structures, with seemingly irregular lower surfaces, beneath the Kaapvaal and Zimbabwe cratons and the Limpopo belt, which extend to depths of 250-300 km and represent the buoyant roots of these cratonic regions in southern Africa (Fig. 3.7). By contrast, mantle beneath the Mesoproterozoic Namaqua-Natal and Neoproterozoic/Mesozoic Saldanian-Cape mobile belts to the south of the Kaapvaal Craton is of lower velocity, and probably contains more iron (Fig. 3.7). If the rugged lower surface of the high-velocity volumes is real, it may reflect chemical erosion (by upwelling fluids) of the mantle formed in the Archaean (O'Reilly, 2001).

Above the high-velocity regions, the Moho is sharp and relatively shallow (35-40 km), but beneath the Bushveld Complex and areas of younger crust it is deeper (45-50 km) with a much less defined boundary (Nguuri *et al.*, 2001; see also Stankiewicz *et al.*, 2002 and Niu & James, 2002) (Figs. 3.7 & 3.8). This difference could indicate that processes of crustal formation were different in Archaean and post-Archaean times, or that more complex crust-mantle boundaries are produced by later magmatic or tectonic modification (Nguuri *et al.*, 2001).

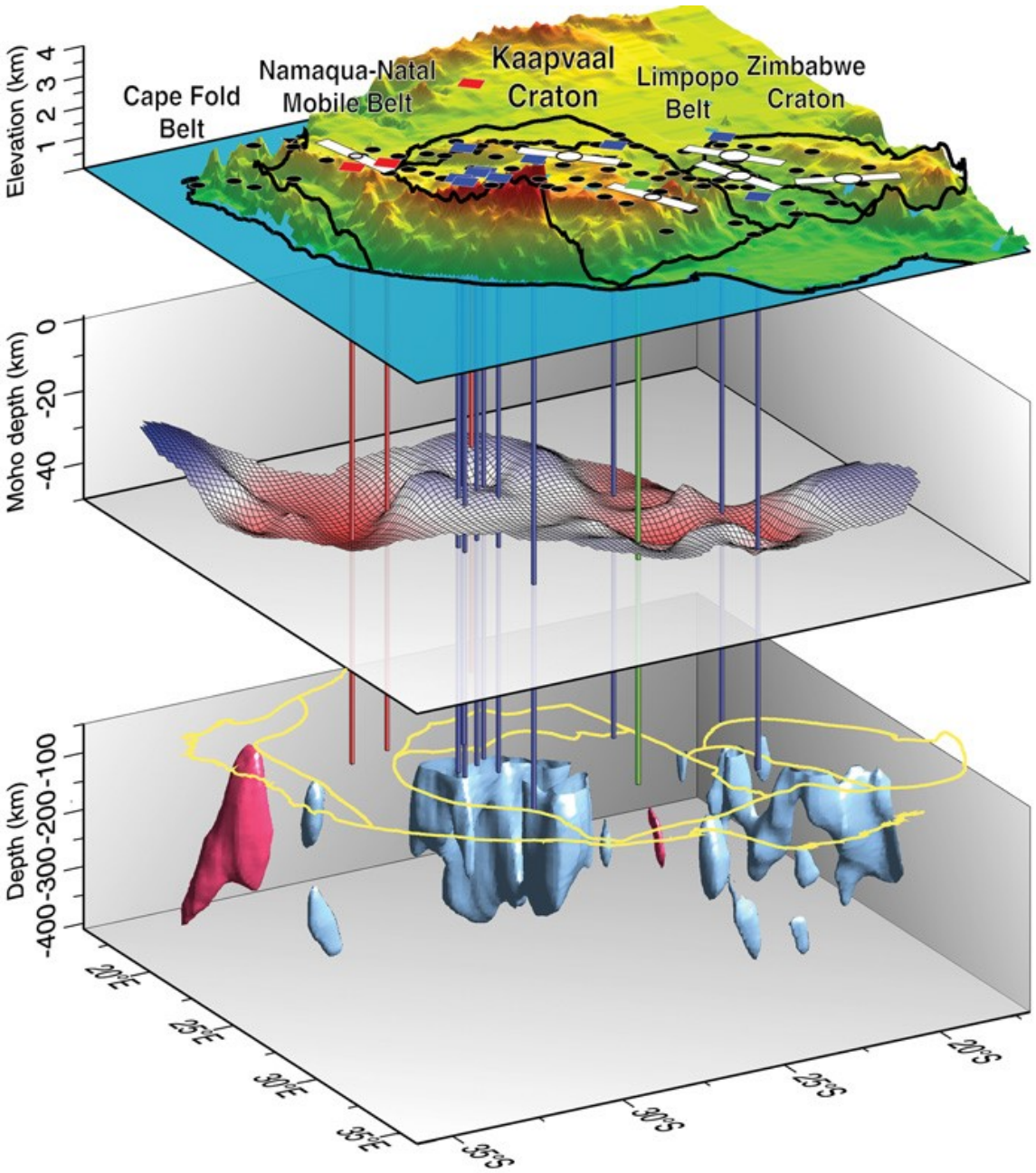


FIGURE 3.6: Three-dimensional image of the deep mantle structure beneath southern Africa, as derived from the present distribution of seismic velocity contrasts (O'Reilly, 2001). Note: Top: Topography and principal geological boundaries (black lines) in southern Africa. Vertical lines connect the surface outcrop of some kimberlite magmas to the deep features revealed by interpretation of the seismic data (blue lines = ~2.5 Gyr; green lines = ~2.5-2.0 Gyr; red lines = <2.0 Gyr.). Centre: Mohorovičić discontinuity (Moho) exhibiting varying depth extent. Bottom: Cratonic cores (blue) reveal themselves as regions of high seismic velocity lying beneath the Kaapvaal and Zimbabwe cratons and the Limpopo Belt. Regions of lower velocity (red) underlie the southern mobile belts and the huge magmatic intrusion of the Bushveld Igneous Complex. Yellow outline shows the surface geological boundaries.

The seismic tomography shows large variations in lithosphere thickness over short lateral distances. A large anomaly of relatively low seismic mantle velocity underlies the Bushveld Complex and extends westwards beneath the unexposed Molopo Farms Complex (Figs. 3.7 & 3.8), confirming previous assumptions that the intrusion of huge magma volumes into the crust has affected the whole lithosphere (O'Reilly, 2001). The lower velocity of the mantle reflects probably modifications of the mantle by fluids, which has resulted in iron enrichment and a consequent decrease in seismic velocity and an increase in density (Griffin *et al.*, 1999).

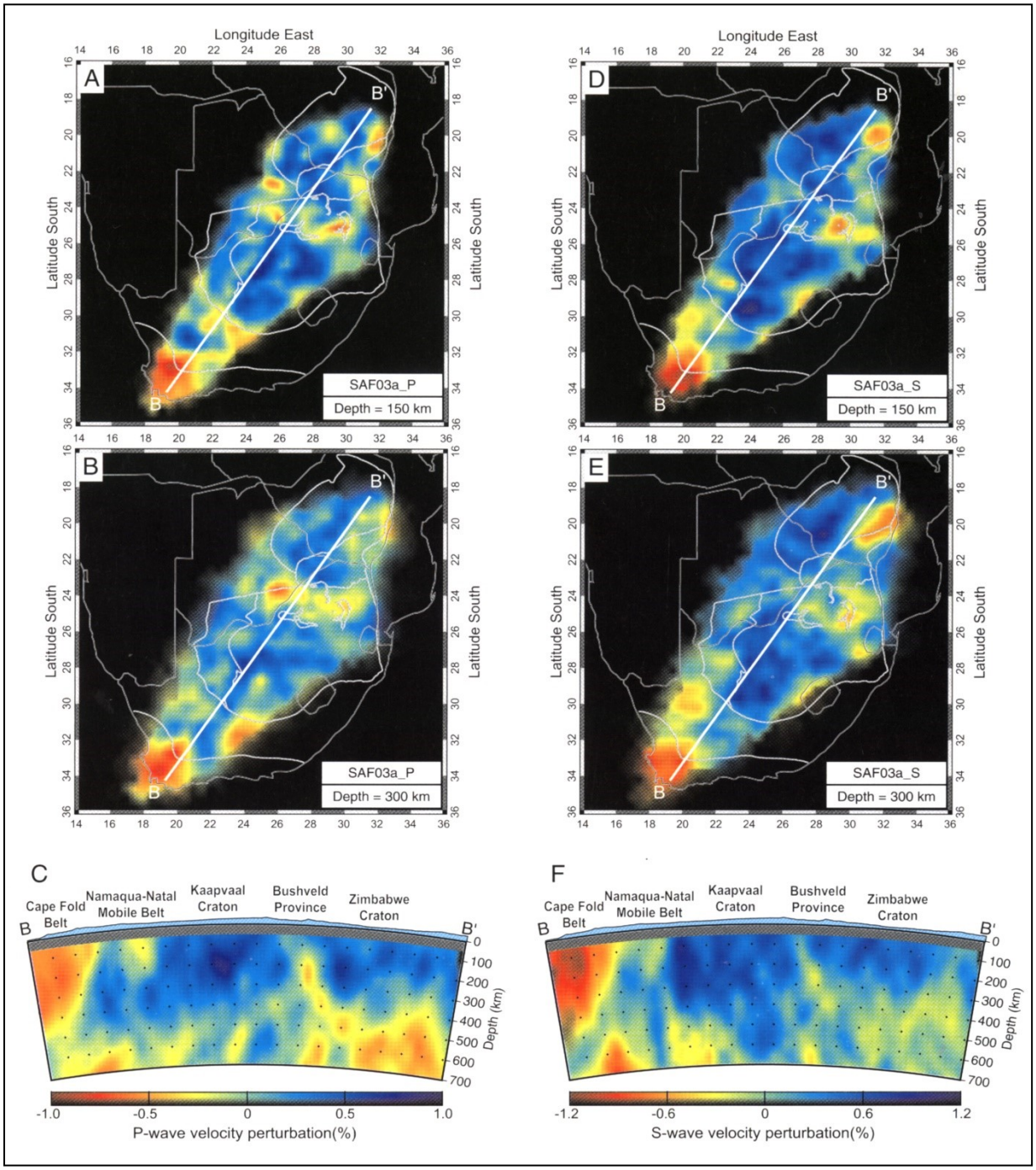


FIGURE 3.7: Horizontal and vertical P- and S-wave velocity perturbation models determined by inversion of delay times after correction for elevation and colour thickness, illustrating (a & b) P-wave and (d & e) S-wave depth slices at 150 km and 300 km respectively, and vertical cross section views of (c) P-wave and (f) S-wave velocity perturbations (after Fouch *et al.*, 2004).

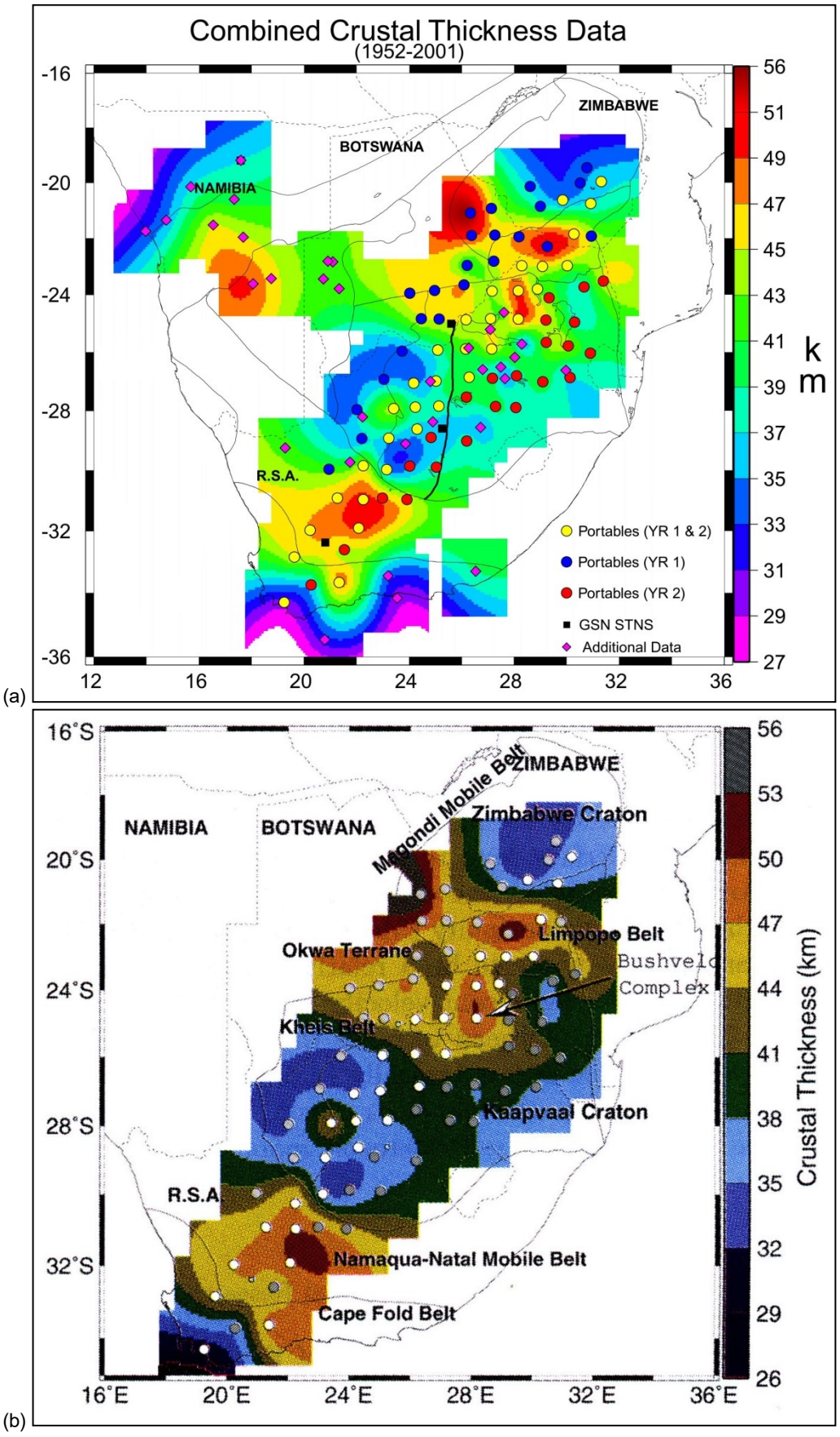


FIGURE 3.8: (a & b) Colour-coded contour map of depth to Moho beneath southern Africa (Nguuri *et al*., 2001). Note: Crustal thickness colour scale is shown on right. Thin crust tends to be associated with undisturbed areas of craton, particularly in the southern and eastern parts of the Kaapvaal craton and in the Zimbabwe craton north of the Limpopo belt. Greater crustal thickness is associated with the Bushveld region and its westward extension into the Okwa and Magondi belts, and with the central zone of the Limpopo belt and the Proterozoic Namaqua–Natal mobile belt.

The Kaapvaal Craton comprises a number of discrete Archaean crustal subdomains/terranes, characterised by distinctive igneous rocks, deformation histories, and tectonic styles (De Wit *et al.*, 1992; de Wit & Hart, 1993; Lowe, 1994, 1999; Poujol & Robb, 1999). Based on current knowledge, the main crustal fragments/blocks/terranes making up the Kaapvaal Craton include the oldest ~3.7-3.1 Ga eastern domain (Barberton Mountain Land comprising the Ancient Gneiss, Southern and Northern Barberton subterranes making up the Swaziland Terrane = Kaapvaal Shield (*i.e.,* earliest nucleus of Kaapvaal Craton)); a ~3.25-2.75 Ga northern domain (Murchison, Giyani, and Pietersburg greenstone belts = Pietersburg Terrane); a ~3.25-3.0 Ga central domain (granitoid domes such as the Johannesburg Dome, Rand anticline and Vredefort Dome = Witwatersrand Terrane); and the western and youngest ~3.0-2.7 Ga domain (Kraaipan, Amalia, Madibe and Marydale greenstone belts = Kraaipan Subprovince) (De Wit *et al.*, 1992a; de Wit & Hart, 1993; Thomas *et al.*, 1993; Lowe, 1994, 1999; Kröner *et al.*, 1996a; Brandl & de Wit, 1997; Poujol & Robb, 1999; Poujol *et al.*, 1999, 2003; Doucouré & de Wit, 2003; Eglington & Armstrong, 2004; Zeh *et al.*, 2009) (Figs. 3.9a & b). The Barberton, Thabazimbi-Murchison and Colesberg-Mafikeng lineaments have been considered to represent suture zones along which the Witwatersrand Terrane, Pietersburg Terrane and Kraaipan Subprovince were accreted successively onto the margins of the Kaapvaal Shield to form the proto-Kaapvaal Craton at ~3.23 Ga, Swazi Subprovince at ~2.985 Ga and Kaapvaal Craton at ~2.87 Ga, respectively (Friese *et al.*, 1995; Friese, 1998a & b, 2001; Schmitz *et al.*, 2004; Eglington & Armstrong, 2004; Zeh *et al.*, 2013).

Recent studies of the Re-Os radiometric system in samples of lithospheric mantle peridotites contained as xenoliths in kimberlites from southern Africa (Walker *et al.*, 1989; Pearson, 1994, 1995, 1998; Janney *et al.*, 1999; Menzies *et al.*, 1999; Irvine *et al.*, 2001; Richardson *et al.*, 2001; Carlson *et al.*, 1999; 2000, 2004) have shown in the broadest sense the general correspondence in timing between major crust building episodes and melt depletion in the underlying lithospheric mantle. A comparison of whole rock Re-Os model age systematics for the mantle from the western and eastern Kaapvaal Craton shows an age difference between these areas. Mean Re-depletion model ages (T_{RD}) for the western Kaapvaal Craton from the Kimberley and Newlands kimberlites are 2.7 Ga and 2.81 Ga, whilst maximum T_{RD} ages for each locality are 1.95 Ga and 3.22 Ga, which compare with average mantle model ages (T_{MA}) of 2.93 Ga and 3.18 Ga respectively (Carlson *et al.*, 1999; Menzies *et al.*, 1999). A mean T_{RD} age of 2.76 ± 0.41 Ga, an oldest T_{RD} age of 3.02 Ga, and a T_{MA} age of 3.25 ± 0.28 Ga for peridotites xenoliths from the Monastery kimberlite are suggestive, but not conclusive evident, of older mantle beneath the older crust of the eastern Kaapvaal Craton (Carlson *et al.*, 2004).

The boundary zones between the subdomains/terranes of the Kaapvaal Craton are exclusively tectonic, characterised by either thrust and/or strike-slip faults, or both, and represent some of the well-known, structural and deep-reaching major lineaments within the craton (*e.g.* Thabazimbi-Murchison and Barberton lineaments) (De Wit *et al.*, 1992a; Vinnik *et al.*, 1995, 1996b; Brandl & de Wit, 1997; de Wit & Ashwal, 1997). Teleseismic P- and PkP-wave travel-time residuals suggest, that the subdomains/terranes are also well defined at depth, and that local changes in depth to the bottom of the lithosphere correspond closely with subdomain/terrane boundaries at surface (Peberdy, 1992; de Wit *et al.*, 1992a; Brandl & de Wit, 1997) (Fig. 3.4). Consequently, the terrane boundaries, observed at surface level as major lineaments, represent fundamental crustal, subvertical, deep lithospheric-asthenospheric breaks within the Kaapvaal Craton. The interpreted subvertical nature of such terrane boundaries is supported by an E-W trending teleseismic profile across the southwestern margin of the São Francisco Craton in Brazil, which illustrates clearly higher and lower P-wave velocities characterising the Archaean São Francisco and Rio de la Plata cratons and intervening Neoproterozoic (Pan-African) Southern Brasiliano Mobile Belt respectively, as well as the subvertical orientation of the craton margins to depths in excess of 400 km (Fig. 3.10).

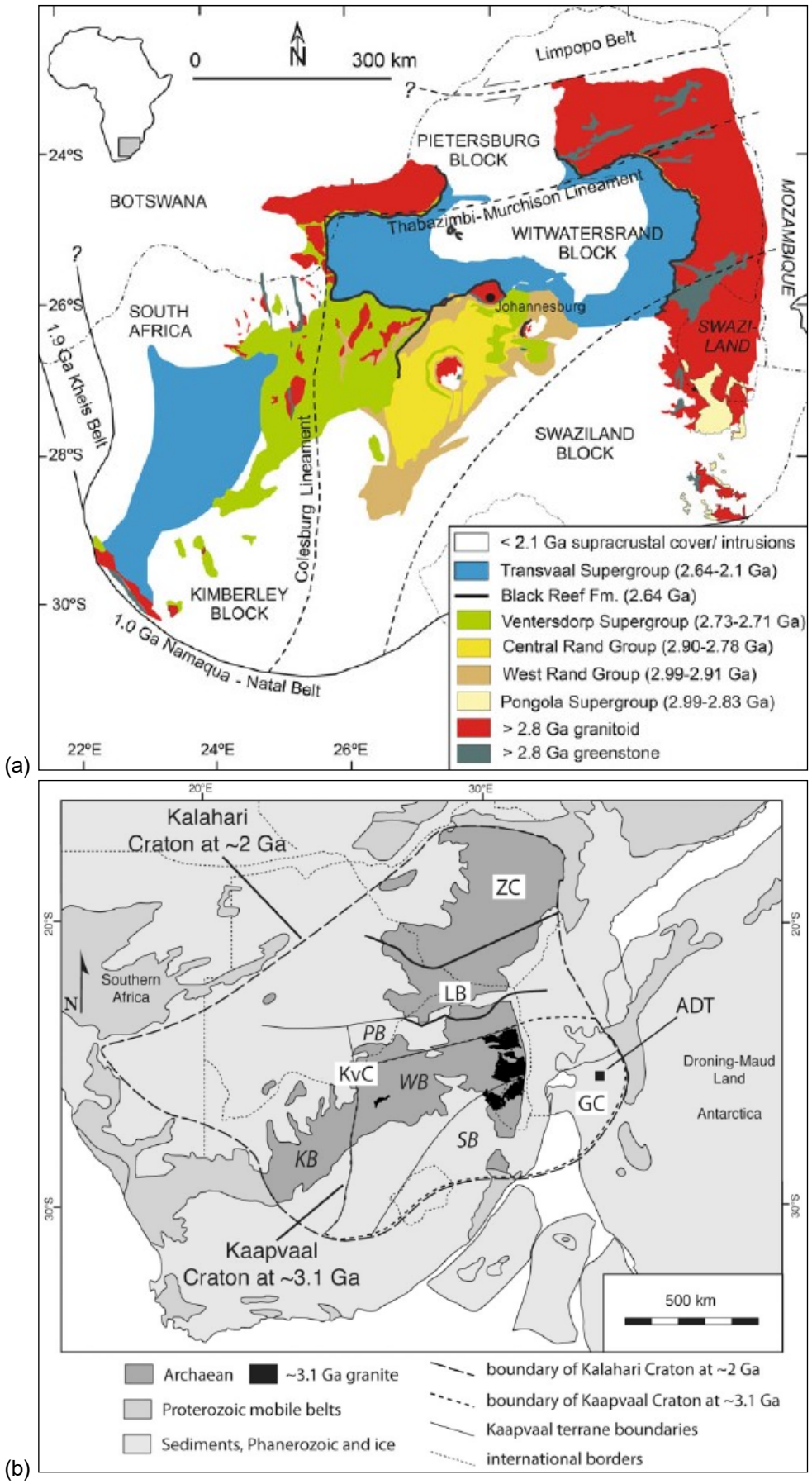


FIGURE 3.9 : (a) Archaean stratigraphic units and different crustal blocks of the Kaapvaal Craton (Frimmel *et al.*, 2014). Note: Bold line outlines the boundary of the Kaapvaal Craton as inferred from aeromagnetic data; (b) Palaeogeographical juxtaposition of the Kalahari Craton (with present-day Africa coordinates) (Marshall *et al.*, 2010). Note: ZC, Zimbabwe Craton; LB, Limpopo Belt; KvC, Kaapvaal Craton (consisting of the following terranes: PB, Pietersburg Block; KB, Kimberley Block; WB, Witwatersrand Block; SB, Swaziland Block).

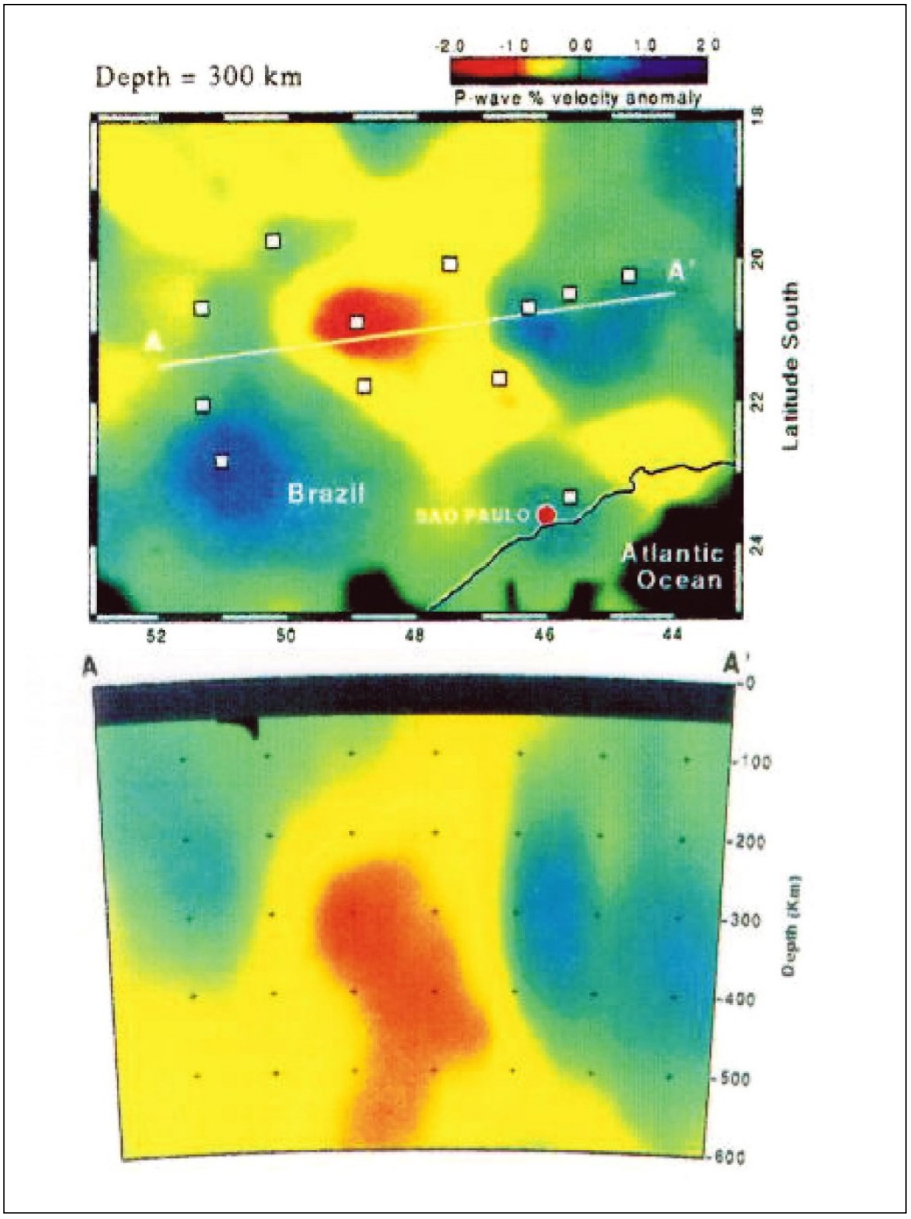


FIGURE 3.10: Deep teleseismic line and section across the southwestern part of the São Francisco Craton in Brazil (provided with courtesy of De Beers Brazil). Note: Clearly higher and lower P-wave velocities characterising the Archaean São Francisco and Rio de la Plata cratons and intervening Neoproterozoic Southern Brasilia Mobile Belt respectively. The cratons extend to depths in excess of 400 km and are characterised by subvertical margins.

Based on the presently available geological data, it is not possible yet to distinguish, whether these subdomains are allochthonous with respect to each other (and thus significantly displaced from their original sites of formation = terranes), or if they were once part of a larger coherent geological province, which has subsequently been tectonically disrupted (De Wit *et al.*, 1992a). To emphasize this lack of knowledge, de Wit *et al.* (1992a) proposed to refer to the individual continental blocks as subdomains or terrains.

However, based on an attempt to synthesize all available geological, geochronological and geophysical data into a reconstruction of the geodynamic evolution of the Kaapvaal Craton from the Neoarchaean to present, strong support for the presence of terranes, rather than subdomains/terrains, is presented in most cases in this study. Furthermore, an attempt was undertaken to refine the initial interpretation of the crustal architecture of the Kaapvaal Craton given by De Wit *et al.* (1992a) (see Appendix 18-V). In this respect, intense literature research and a compilation and reinterpretation of published and unpublished geological, geochronological and

geophysical data were utilised to define and delineate individual terranes and terrane boundaries within the Kaapvaal Craton. Delineation of individual terranes, and constraining the timing and duration of the principal magmatic events within them, is best achieved by the craton-wide application of accurate and precise U–Pb zircon dating (*e.g.*, Kröner & Todt, 1988; Kröner *et al.*, 1989; Armstrong *et al.*, 1990; Robb *et al.*, 1992; Kamo & Davis, 1994; Poujol & Anhaeusser, 2001; Poujol *et al.*, 1996, 2002), together with appropriate tectonic and metamorphic studies. The resultant revised terrane map for the Kaapvaal Craton (including the Central Zone Terrane of the Limpopo Belt and Zimbabwe Craton) is presented in Figure 3.11 and Appendix 26.

Based on this interpretation it can be concluded that most of the identified terrane boundaries coincide with well-known major structural lineaments and greenstone belts within the Kaapvaal Craton, and that there exists a change in the regional tectonic anisotropy as delineated by the greenstone belts, from ENE-WSW to NE-SW trending in the older part of the craton (Swazi Subprovince), to N-S trending in the western part (Kraaipan Subprovince) of the craton (Figs. 3.11a & b). Furthermore, pervasive deformation of the lower crust in continental collisions is now considered to be accompanied by widespread hydration and alteration and reprecipitation of magnetic minerals in the sedimentary cover, thus explaining regional magnetic anomalies of relative high intensity at cratonic collision zones (*e.g.*, Corner, 1989, 1991; Toft *et al.*, 1994; Duane & Saggerson, 1995).

From geophysical data it is apparent that these greenstone belts are not deep synclinal keels, but instead are horizontal thin sheets with large cross-sectional aspect ratios (horizontal : vertical dimensions) (De Beer, 1982; De Beer *et al.*, 1984, 1986, 1988, 1990; Kleywegt *et al.*, 1987; Stettler *et al.*, 1988, 1990; de Beer & Eglington, 1991, de Wit & Ashwal, 1995). The greenstone belts appear as highly tectonised, possibly allochthonous successions with respect to the surrounding sialic crust, and exhibit stratigraphic duplications of 50-75% and more. Stratigraphically and geophysically determined thicknesses of the greenstone belts rarely match, suggesting widespread overestimation of stratigraphic thickness, probably due to overlooking of subtle evidence for structural repetition (De Wit & Ashwal, 1995). A comparison of greenstone belt occurrences worldwide has shown, that greenstone belts are represented throughout Earth history (Condie, 1994; de Wit & Ashwal, 1995) and are not restricted to the Archaean as was previously perceived (*e.g.,* Condie, 1981), and that there exists a wide spectrum of different tectonic environments preserved within greenstone belts, which are nowadays interpreted in the framework of modern plate tectonics. Greenstones are viewed variously as relicts of oceanic crust, generated either in an oceanic (*e.g.*, Engel, 1968; Glikson, 1971; Anhaeusser, 1973, 1982; Glikson & Lambert, 1976; de Wit & Stern, 1981; Condie, 1986; de Wit *et al.*, 1987), or back-arc (*e.g.,* Tarney *et al.*, 1976; Tarney & Windley, 1981) environment, or as having formed in a continental rift environment on thin, primordial crust (*e.g.,* Viljoen & Viljoen, 1969; Anhaeusser *et al.*, 1969; Sutton, 1971; Windley, 1973; Hunter, 1974a; Condie & Hunter, 1976; Compston *et al.*, 1986; Blake & Groves, 1987; Campbell & Hill, 1988). In this respect, the term “greenstone belt” has outgrown its previous restrictive meaning and might now be better viewed as analogous to the more encompassing term “orogenic belt’, because that is in essence what greenstone belts are, given present day understanding (De Wit & Ashwal, 1995).

It will be demonstrated in the following Section that the individual terrane boundaries represent in most cases palaeo-suture zones between Archaean-age accreted terranes, which are deep-reaching, first-order structural discontinuities within the lithosphere of the Kaapvaal Craton. In response to tectonic far-field stresses induced into the lithosphere of the craton during episodically occurring orogenic events around its margins, these translithospheric terrane boundaries as well as prominent crustal fault/shear zones experienced repeatedly reactivation and acted as tectonic relay structures throughout time, thereby influencing and controlling (i) the intra-cratonic pattern and style of stress and deformation, (ii) the formation, position and configuration of intra-cratonic basins and associated sedimentation patterns, as well as (iii) the occurrence of igneous activity within the Kaapvaal Craton since the Neoarchaean until present time.

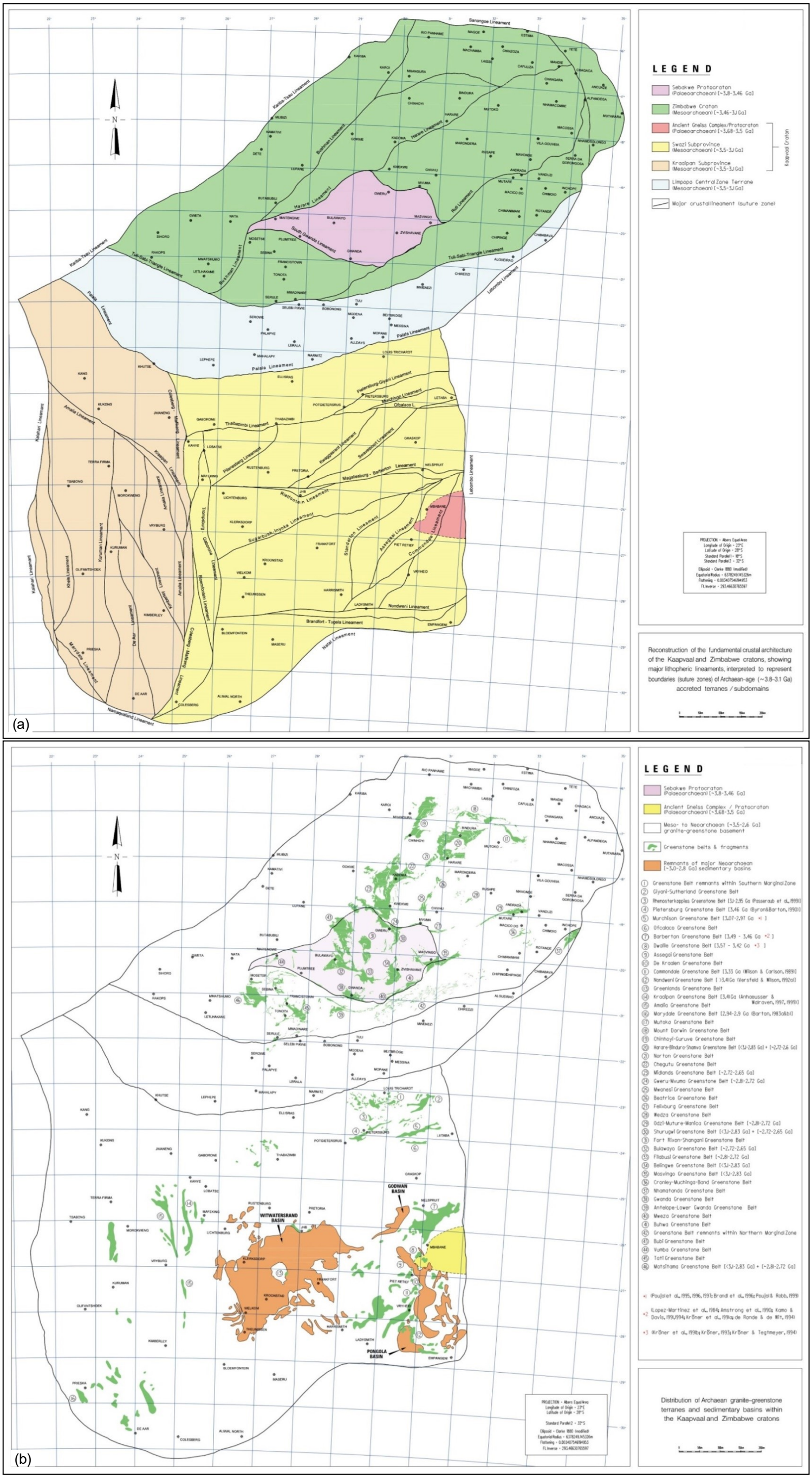


FIGURE 3.11: (a) Reconstruction of the fundamental crustal architecture of the Kaapvaal and Zimbabwe cratons, showing major lithospheric lineaments, interpreted to represent the boundaries of Archaean-age accreted terranes/subdomains (this study). Interpretation is based on unpublished/published geological, geophysical and geochronological data; (b) Distribution of Archaean granite-greenstone terrains and sedimentary basins within the Kaapvaal and Zimbabwe cratons, as based on surface geological and geophysical data (this study). Note the change in regional tectonic anisotropy as delineated by the greenstone belts, from ENE-WSW and NE-SW in the eastern, to N-S in the western, parts of the Kaapvaal Craton.

3.2 ZIMBABWE CRATON

The Meso- to Neoarchaean Zimbabwe Craton underlies most of Zimbabwe as well as parts of northeastern Botswana and westernmost Mozambique, having an exposed area of 1.77 x 10^5 km^2, and a total inferred area of 2.68 x 10^5 km^2. The Zimbabwe Craton is a basement complex consisting of a large number (26) of distinct greenstone belts that constitute about 20% of the craton and comprise mainly ultramafic, mafic and felsic intrusives and volcanics, volcaniclastics, epiclastics, and BIF, as well as undeformed and deformed granitoid and granitoid-gneiss complexes that make up the remainder (Blenkinsop *et al.*, 1997) (Figs. 3.12 & 3.13). Ages of greenstones, granitoids, and gneisses within the craton range from ~3.55-2.53 Ga (see Appendix 21-B for a summary of available geochronological ages). The oldest rocks of the Zimbabwe Craton are tonalitic to trondhjemitic (TTG) gneisses that have been dated between ~3.55 Ga and ~3.35 Ga (*e.g.* Horstwood *et al.*, 1999). Infolded are numerous, up to several kilometres long, narrow remnants of greenstones that are grouped collectively into the Sebakwian Group. Subsequent crust formation events added greenstones that of the ~2.9-2.8 Ga Belingwean and Lower Bulawayan groups, the ~2.7 Ga Upper Bulawayan and Shamvaain groups, and granitoids of the ~2.9-2.8 Ga Chingezi, ~2.7 Ga Sesombi and ~2.6 Ga Chilimanzi suites (Wilson *et al.*, 1995; Jelsma *et al.*, 1996) (Fig. 3.12).

Metamorphic grades and the intensity of deformation vary across the craton from amphibolite to granulite facies grades and generally strong deformation towards the margins of the craton (*e.g.* in the Northern Marginal Zone and Pfunzi Orogenic Belt along the southern and northern craton margins respectively), to lower greenschist facies with only locally intense deformation along proposed intracratonic terrane boundaries (palaeosuture zones) within the craton (*e.g.* Wilson, 1979, 1981; Anhaeusser & Wilson, 1981; Nisbet *et al.*, 1981; Campbell *et al.*, 1992; Jelsma *et al.*, 1996; Blenkinsop *et al.*, 1997).

Along its southern margin, the Zimbabwe Craton is bounded by the Mesoarchaean (~3.5-3.1 Ga) Limpopo Central Zone Terrane, which was accreted onto the craton during the Limpopo Orogeny at ~2.7-2.6 Ga.

The mafic and ultramafic rocks of the Great Dyke and its satellites were emplaced within the craton along NNE-trending extensional fractures zones at ~2.58-2.57 Ga (*e.g.* Mukasa *et al.*, 1998; Armstrong & Wilson, 2000; Oberthür *et al.*, 2002).

The exposed craton is overlain structurally and stratigraphically by relatively unmetamorphosed Proterozoic lithologies to the west, north and east, which show an increase in metamorphic grade and deformation away from the craton. These deposits reflect the development of sedimentary basins around the margins of the Archaean craton, which were subsequently deformed and thrust onto the craton, forming the Magondi (~2.0-1.8 Ga), Zambezi and Mozambique (~1.0-0.5 Ga) belts respectively. Each of these orogenies has affected parts of the Zimbabwe Craton.

The Archaean craton and Proterozoic cover rocks are unconformably overlain by Permian-Cretaceous strata, including the voluminous Karoo flood plateau basalts. Palaeozoic and Mesozoic sedimentation were broadly constrained to extensional basins to the north and northwest (along the Zambezi valley) and to the SSE (within Limpopo Central Zone Terrane). Subsequently Tertiary to Recent sedimentation has been largely related to the expansion and retreat of the Kalahari Desert (which currently lies to the west of the Zimbabwe Craton), leaving a relatively thin veneer of poorly consolidated sands, mainly over the western margin of the Zimbabwe Craton.

Like the Kaapvaal Craton, the Archaean Zimbabwe Craton is composed of a number of distinct tectono-stratigraphic terranes of early to mid-Archaean age (~3.8-3.1 Ga), assembled by plate tectonic processes during several mid- to late-Archaean orogenic cycles (~3.6-3.1 Ga). The Tokwe Subprovince represents the

Zimbabwe protocraton at ~3.35 Ga (Figs. 3.11 & 3.12) and in turn consists of several early- to mid-Archaean terranes, of which some had been amalgamated into an earlier Sebakwe protocraton at ~3.46 Ga. The Sebakwe protocraton represents the oldest crustal fragment within the Tokwe Subprovince and thus the ancient nucleus of the present Zimbabwe Craton (Kusky, 1998; Horstwood *et al.*, 1999; this study).

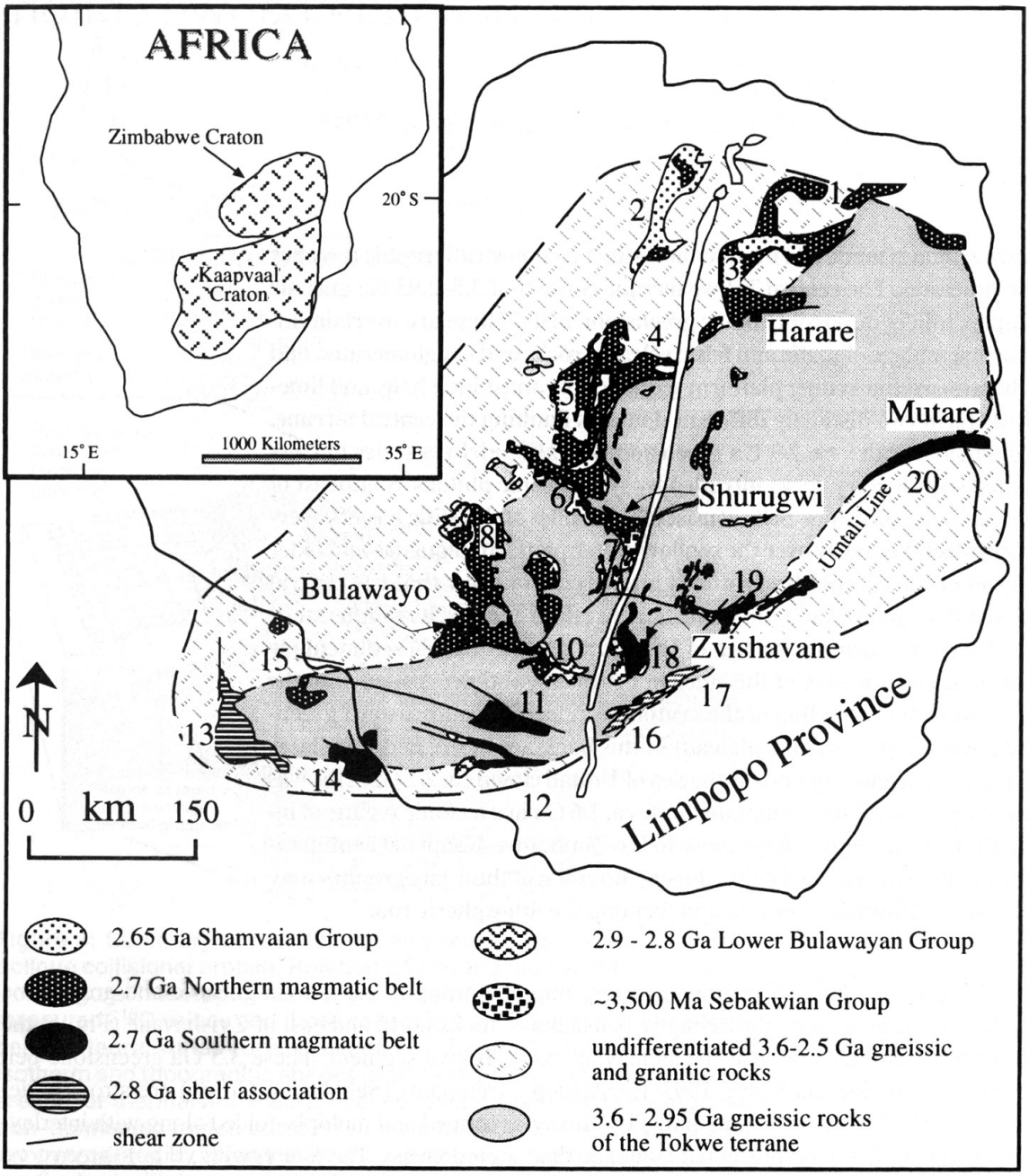


FIGURE 3.12: Archaean terrane interpretation for the Zimbabwe craton, showing the distribution of various greenstone belts and gneissic terrains (after Kusky, 1998). Note: Greenstone belts: 1 = Mount Darwin; 2 = Chipuriro; 3 = Harare; 4 = Chegutu; 5 = Midlands; 6 = Gweru-Mvuma; 7 = Shurugwi; 8 = Bubi; 9 = Bulawayo; 10 = Filabusi; 11 = Gwanda; 12 = Antelope-Lower Gwanda; 13 = Matsitama; 14 = Tati; 15 = Vumba; 16 = Mweza; 17 = Buhwa; 18 = Belingwe; 19 = Masvingo; 20 = Mutare.

Compared to the Kaapvaal Craton, the general lack of detailed geophysical research has not permitted as yet to define the Archaean Zimbabwe Craton at depth, and to identify the boundary (suture) zones between individual terranes of the craton. However, results of the recently completed international and multidisciplinary "Kaapvaal Craton Programme" have provided some information on the structure of the crust and deep mantle beneath the southern Zimbabwe Craton (see Section 3.1; Figs. 3.5b – 3.7).

One of the most important findings is that a NNE-trending mantle fabric producing seismic anisotropy exists across the Zimbabwe Craton (Fig. 3.5b) which was interpreted to have resulted from an unknown pre-2.9 Ga orogenic event and to have undergone reactivation at ~2.6 Ga, thereby facilitating the emplacement of the Great Dykes system (Silver *et al.*, 2001, 2004). Furthermore, the maximum mantle keel thickness beneath the southern Zimbabwe Craton appears to be somewhat less than the one for the Kaapvaal Craton, reaching a local maximum of ~225-250 km (Fouch *et al.*, 2004).

Despite the still limited amount geophysical information an attempt was made in this study to interpret the crustal architecture of the Zimbabwe Craton. Extensive literature research and a compilation and reinterpretation of published and unpublished geological, geochronological and geophysical data were utilised to define individual terranes and terrane boundaries within the Zimbabwe Craton, and the results are presented in Figure 3.11 and Appendix 26.

3.3 LIMPOPO PROVINCE

The Limpopo Province is an east-west trending zone of intensely multi-deformed, high-grade poly-metamorphic Archaean and Palaeoproterozoic crust (see Appendix 21-C for a summary of available geochronological ages) ~700 km in length and between 250 and 320 km wide, located between the Archaean Kaapvaal and Zimbabwe cratons to the south and north respectively (*e.g.* Watkeys *et al.*, 1983; Roering *et al.*, 1992) (Fig. 3.11). The Limpopo Belt has been modelled as a collisional orogen and records a long and complex tectono-metamorphic history, with intermittent episodes of magmatism, metamorphism and deformation spanning from the Palaeoarchaean at ~3.75 Ga (*e.g.* Barton & Key, 1981) to the Palaeoproterozoic at ~2.0 Ga (*e.g.* Hickman & Wakefield, 1975; Watkeys, 1983; Van Reenen *et al.*, 1987; Roering *et al.*, 1992; McCourt & Vearncombe, 1987, 1992; Barton *et al.*, 1992, 1994a; Rollison & Blenkinsop, 1995; Kamber *et al.*, 1995a & b; Berger *et al.*, 1995; Kamber & Biino, 1995; Hisada & Miyano, 1996; Barton & Sergeev, 1997; Holzer *et al.*, 1996, 1997, 1998, 1999; McCourt & Armstrong, 1998; Kröner *et al.*, 1999; Barton *et al.*, 2003, 2006).

The Limpopo Province comprises three shear zone-bounded, distinct tectonic domains/terranes, *viz.* the monometamorphic Northern Marginal Zone (NMZ), the polymetamorphic Limpopo Central Zone (LCZ), and the monometamorphic Southern Marginal Zone (SMZ) (first recognised by Cox *et al.*, 1965 and Mason, 1973) (Fig. 3.13). All three zones are essentially composed of rocks at granulite-facies metamorphic grade (Fig. 3.14). The SMZ is predominantly made of tonalite-trondhjemite-granite assemblages, whereas the NMZ comprises granulite-facies gneisses and charnockites. Both marginal zones represent reworked rocks of the respective cratons. Supracrustal metasedimentary assemblages represent a minor lithological component in the marginal zones but are more prominent in the LCZ.

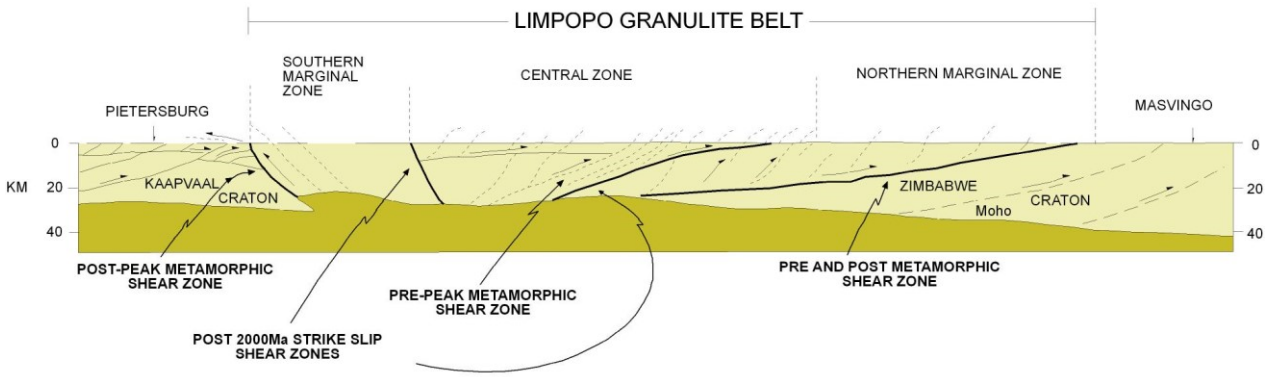


FIGURE 3.13: Schematic crustal cross-section of the Limpopo Belt (after Holzer *et al.*, 1998).

Northern Marginal Zone: The Northern Marginal Zone attains a width of about 30-50 km and exhibits many similarities with the Southern Marginal Zone. It consists mainly of reworked granite-greenstone lithologies of the adjacent Zimbabwe Craton (Robertson, 1968, 1977; Odell, 1975; Robertson & Du Toit, 1981) and is characterised by banded granitic gneiss that surrounds charnockite, enderbite, isolated granulite-grade metasedimentary (metapelitic, BIF and calc-silicate gneisses) and mafic meta-igneous greenstone remnants, and ultramafic-mafic complexes, which are preserved particularly in kilometre-scale isoclinal fold cores (Rollison & Blenkinsop, 1995; Kamber & Biino, 1995; Berger & Rollinson, 1997). The Northern Marginal Zone can be divided into three subunits, reflecting the style and intensity of early Proterozoic tectono-metamorphism superimposed on late Archaean protoliths. In the southernmost unit, *i.e.* the Triangle Shear Zone, a ~2.0 Ga event reached granulite facies and almost completely erased geochronological evidence of older Archaean events (Kamber *et al.*, 1995b).

Southern Marginal Zone: The SMZ (about 60 km wide) is a high-grade gneiss terrane, regarded as reworked extension of the Pietersburg Terrane of the Kaapvaal Craton (Du Toit *et al.*, 1983; Van Reenen *et al.*, 1995; Kreissig *et al.*, 2000, 2001), is composed of tonalitic and trondhjemitic gneisses, *i.e.* the Baviaanskloof Gneiss, and overlain by mafic-ultramafic and pelitic greenstone lithologies and BIFs of the Bandelierkop Formation (*e.g.* du Toit & van Reenen, 1977; du Toit *et al.*, 1983). These lithologies have been intruded by numerous granite, granodiorite, enderbite and charnoenderbite plutons at ~2.72-2.65 Ga (*e.g.* Barton *et al.*, 1991; Barton & van Reenen, 1991b, 1992; Passeraub *et al.*, 1999) which underwent granulite-facies metamorphism and transformation to charnockitic orthogneisses shortly after their intrusion at ~2.675-2.67 Ga (*cf.* Retief *et al.*, 1990; Barton & Van Reenen, 1990). The granulite terrane of the SMZ underwent subsequently retrograde hydration dominated by decompression (Van den Berg & Huizenga, 2001). The SMZ consists of large thrust sheets of complexly folded low-strain gneisses, bounded by an imbricate system of kilometre-wide deep crustal shear zones characterised by the presence of high strain gneisses (*e.g.* Smit *et al.*, 2001).

Limpopo Central Zone: The LCZ is markedly dissimilar to the marginal zones both structurally and lithologically and comprises a ~3.8-3.1 Ga old basement of banded and migmatitic gneisses, which is unconformably overlain by and tectonically interlayered with a >3.31 Ga old, high-grade metasedimentary (*i.e.* marbles and quartzites with minor intercalations of metapelite, amphibolite, carbonate and calc-silicate rocks and intrusive quartzo-feldspathic/granitoid gneisses) succession with shelf-like characteristics (*i.e.* Beit Bridge Complex). Basement and supracrustal succession are intruded by ~3.31-3.18 Ga old precursors of migmatitic and layered granitoid gneisses of tonalitic-trondhjemitic-granodioritic-leucogranitic composition (*i.e.* Sand River TTG Gneiss Suite) (*e.g.* Fripp, 1981, 1982; Barton *et al.*, 1983a; Harris *et al.*, 1987; Retief *et al.*, 1990; Treloar *et al.*, 1992; Tsunogae & Yurimoto, 1995; Jaeckel *et al.*, 1997; Kröner *et al.*, 1998, 1999), as well as by ~3.25 Ga old precursors of meta-gabbroic rocks of the Messina Layered Intrusion (Hor *et al.*, 1975; Barton *et al.*, 1979a; Barton & Key, 1981; Barton, 1983; Barton & Sergeev, 1997; Kröner *et al.*, 1999). All these lithologies are intruded by <~3.1-3.0 Ga old mafic dykes (*e.g.* Barton *et al.*, 1977, 1983b; 1990, 2003, 2006), as well as by ~2.73-2.52 Ga old granitic, granodioritic and enderbitic rocks (orthogneisses) including *e.g.* the Alldays, Singelele, Bulai Zanzibar, Regina and Zandfontein plutons (orthogneisses) (*e.g.* Barton *et al.*, 1979b, 1994a; Jaeckel *et al.*, 1997; Holzer *et al.*, 1998; Kröner *et al.*, 1999; Zeh *et al.*, 2007).

Recently, some of the Mesoarchaean (~3.3 Ga) marbles and metasedimentary rocks of the Beit Bridge Complex have been confirmed by carbon isotope studies and U-Pb zircon geochronology to be <~2.68 - >~2.02 Ga in age and to represent a previously unrecognized Palaeoproterozoic cover sequence (Buick *et al.*, 2003; Barton *et al.*, 2003, 2006). These comparatively little deformed supracrustal rocks have undergone granulite-facies metamorphism (Buick *et al.*, 2003) and upper amphibolite-facies metamorphism

(Barton *et al.*, 2003; Klemd *et al.*, 2003) in the area to the east of Messina and in the area surrounding the Venetia kimberlite pipes respectively, and are likely to represent high-grade metamorphic correlatives to the Transvaal Supergroup within the Kaapvaal Craton.

Hence, the supracrustal paragneisses of the Beit Bridge Complex may be divided into three unconformity bounded successions, dated at >3.1 Ga, 3.1-2.6 Ga, and <2.6 Ga, respectively (Eriksson *et al.*, 1988; Brandl, 1992; Kröner *et al.*, 1998, 1999; Barton *et al.*, 2003; Buick *et al.*, 2003).

Structures and lithologies record a polyphase tectonic and metamorphic evolution respectively (*e.g.* Key, 1977; Fripp, 1981, 1983; Horrocks, 1980, 1983; Brandl, 1981, 1983, 1988, 1990; Watkeys *et al.*, 1983; Barton *et al.*, 1990; Van Reenen *et al.*, 1990; Retief *et al.*, 1990; Roering *et al.*, 1992a & b; Holzer, 1995; Tsunogae & Yurimoto, 1995; Jaeckel *et al.*, 1997; Barton & Sergeev, 1997; Holzer *et al.*, 1996, 1998; Hofmann *et al.*, 1998; Kröner *et al.*, 1998,1999), and cannot be correlated across the bounding shear zones with those in the Southern and Northern Marginal zones except for uplift-related late fabrics (*e.g.* Kamber *et al.*, 1995b). In addition, an anomalously high $^{238}U/^{204}Pb$ ratio of all rocks older than 2.7 Ga in the LCZ compared to those in the marginal zones suggests that the rocks of the LCZ are unrelated to those of the Kaapvaal and Zimbabwe cratons (Barton & Key, 1981; Barton *et al.*, 1983a, 1990).

In view of these contrasting geological features the LCZ has been interpreted as a distinct terrane, *i.e.* the "*Limpopo Central Zone Terrane"* (*e.g.* Barton & Key, 1981; Brandl, 1983; Watkeys, 1984; Eriksson *et al.*, 1988; McCourt & Vearncombe, 1987; Rollinson, 1993). Furthermore, the Limpopo Central Zone Terrane is subdivided into three subterranes, *i.e.*, the Beit Bridge, Mahalapye, and Phikwe terranes (Barton *et al.*, 2006).

The terrane boundaries that separate the three main zones from each other, and also from the surrounding cratons, consist of prominent Neoarchaean shear zones (*e.g.* Cox *et al.*, 1965, Mason, 1973; Watkeys, 1983; Van Reenen *et al.* 1987, 1988, 1990; De Beer & Stettler, 1988, 1991). The NMZ and SMZ respectively adjoin the Zimbabwe and Kaapvaal cratons, have some structural similarities, and are separated from the adjacent cratons by inward dipping thrust zones (*e.g.* McCourt & Vearncombe, 1992). The two marginal zones are regarded as lower crustal high-grade equivalents of the adjacent granite-greenstone terrains of the cratons and have been exhumed mainly in the late Archaean along the northerly North Limpopo Thrust Zone (*e.g.* McCourt & Vearncombe, 1992; Blenkinsop *et al.*, 1995; Mkweli *et al.*, 1995) and the southerly verging Hout River Shear Zone (*e.g.* Smit *et al.*, 1992; Kreissig *et al.*, 2000), respectively (Fig. 3.13). The LCZ is markedly dissimilar both structurally and lithologically and separated from both the SMZ and the NMZ by reactivated ~2 Ga mylonitic strike-slip shear zones (*i.e.*, terrane boundaries), respectively the Palala shear zone and Triangle Shear Zone (*e.g.* James, 1975; Van Reenen *et al.*, 1987; McCourt & Vearncombe, 1987, 1992; Brandl & Reimold, 1990; Roering *et al.*, 1992a & b; Ranganai *et al.*, 2002) (Figs. 3.13 & 3.14). Evidence for both sinistral strike-slip (*e.g.* McCourt & Vearncombe, 1987, 1992) and dextral strike-slip (*e.g.* Schaller, 1997; Schaller *et al.*, 1997, 1999) have been found within the >10 km wide Palala Shear Zone.

The three Limpopo subzones underwent distinct metamorphic histories (summarised by Holzer *et al.*, 1998;) (Fig. 3.14). In the SMZ granulite-facies metamorphism attributed to orogenic tectonics occurred shortly after ~2.7 Ga at ~2.675-2.67 Ga with a clockwise *PT* evolution (*e.g.* Barton & van Reenen, 1990, 1992a & b; Van Reenen *et al.*, 1987, 1990). The SMZ appears to have an Archaean-only history, with no evidence of 2.0 Ga metamorphism (Eriksson *et al.*, 2011). The SMZ is undisputedly characterized by a single P-T path (Stevens & van Reenen, 1992) whose age is directly constrained by U-Pb dating of monazite and zircon dating of melt leucosomes to be 2691 ± 7 Ma and 2643 ± 1 Ma, respectively (Kreissig *et al.*, 2001). Moreover, the granulite facies rocks of the Southern Marginal Zone were thrust onto the adjacent Kaapvaal Craton along the mylonitic oblique-slip Hout River Shear Zone (*e.g.*, Smit *et al.*, 1992). The timing of this

major thrust is constrained by zircon dates from the syn-kinematic Matok Intrusive Complex to be between ca. 2671 and 2664 Ma (Barton & van Reenen, 1992; Barton *et al*., 1992) and by Ar-Ar dating of amphiboles from the Hout River Shear Zone, which yield maximum ages ranging from 2650 to 2620 Ma (Kreissig *et al*., 2001). Collectively, this evidence supports a Kaapvaal Craton-Central Zone amalgamation during the Neoarchean, which is consistent with recent U-Pb and Lu-Hf data from zircons in granitoids that indicate the exotic Central Zone accreted onto the Kaapvaal Craton at 2.67-2.61 Ga (Zeh *et al*., 2009).

In contrast, the granulites in the NMZ are characterised by anticlockwise *PT* evolution and a late thermal peak was reached at ~2.58 Ga, *i.e.* 100 Ma after peak metamorphism in the SMZ (Rollinson, 1989; Kamber & Biino, 1995; Kamber *et al*., 1995b). Closely related to this high-grade metamorphism is the widespread granitoid magmatism in the NMZ (*i.e.* Razi granites), which occurred at ~2.65-2.52 Ga (Blenkinsop & Frei, 1997). An earlier granulite-facies metamorphic event at ~2.87 Ga has been identified within the NMZ, but is geochronologically not well constrained (Treloar *et al*., 1992).

The LCZ has a unique, polytectono-metamorphic-magmatic history and there is an on-going debate in particular about the timing of magmatic and metamorphic events, the significance of polymetamorphism, and the P-T evolution(s) which occurred during the respective events. Geochronological, structural and petrological data provide evidence that the Central Zone has undergone a series of complex and temporally-discrete structural-magmatic-metamorphic events, which included the formation and subsequent anatexis of the Sand River Gneiss during the Palaeo-Mesoarchaean at ~3.24-3.12 Ga (D_1, M_1), structural, metamorphic and magmatic events during the Neoarchaean at 2.66-2.52 Ga (D_2, M_2), and a final ~2.04-2.02 Ga tectono-metamorphic overprint (D_3, M_3) (*e.g.*, Jaeckel *et al*., 1997; Holzer *et al*., 1998, 1999; Kröner *et al*., 1999; Klemd *et al*., 2003; Van Reenen *et al.* 2004; Zeh *et al*., 2004, 2005a & b, 2007; Barton *et al*., 2003, 2006; Kramers *et al*., 2006; Boshoff *et al*., 2006; Perchuk *et al*., 2006, 2008; Zeh *et al*., 2007; Zeh & Klemd, 2008; Rigby *et al*., 2008; Millonig *et al*., 2008; Van Reenen *et al*., 2008; Gerdes & Zeh, 2009; Chudy *et al*., 2009; Rigby, 2009; Rigby & Armstrong, 2010; Brandt *et al*., 2018).

The Palaeoarchaean event is marked by the emplacement of TTGs of the Sand River Gneiss Suite and precursors of meta-gabbroic rocks of the Messina Layered Intrusion at ~3.31-3.18 Ga which all subsequently underwent a first high-grade structural-metamorphic overprint (D_1, M_1) at ~3.1 Ga (*e.g.* Hor *et al*., 1975; Barton *et al*., 1979a; Barton & Key, 1981; Fripp, 1981, 1982; Barton *et al*., 1983a, 1990; Harris *et al*., 1987; Retief *et al*., 1990; Treloar *et al*., 1992; Tsunogae & Yurimoto, 1995; Barton & Sergeev, 1997; Jaeckel *et al*., 1997; Kröner *et al*., 1998, 1999; Barton *et al*., 2003; Zeh *et al*., 2007) prior to the intrusion of basaltic dykes at <~3.1-3.0 Ga (*e.g.* Barton *et al*., 1977, 1983b, 1990, 2003, 2006). The late Archaean history of the LCZ is similar to that of the NMZ. Mainly magmatic activity between ~2.7 and 2.6 Ga (Jaeckel *et al*., 1997; Kröner *et al*., 1999) was followed by high-grade metamorphism (M_2), anatexis and felsic magmatism at ~2.6-2.52 Ga (Holzer *et al*., 1998). A high-pressure granulite metamorphic event (M_3) with a clockwise *PT* evolution and dextral transpressive deformation localised along the bounding strike-slip shear zones of the LZC occurred at ~2.0 Ga (*e.g.* Reenen *et al*., 1987; Barton *et al*., 1994a; Kamber & Biino, 1995; Kamber *et al*., 1995a & b; Hisada & Miyano, 1996; Barton & Sergeev, 1997; Jaeckel *et al*., 1997; Holzer *et al*., 1998, 1999) (Fig. 3.14).

Interpretations of regional gravity data have shown that the Limpopo Province stands out as an arcuate-shaped major gravity high sandwiched between the two cratons due to their predominantly igneous felsic to intermediate crustal rocks (*e.g.* Emenike, 1986; Gwavava *et al*., 1992), with all three Limpopo subzones defining a single gravity anomaly on upward continued maps. The similarity of the gravity anomaly pattern of the three subzones of the Limpopo Province at depth suggests that they represented a single geotectonic entity with the same history during exhumation (Ranganai *et al*., 2002).

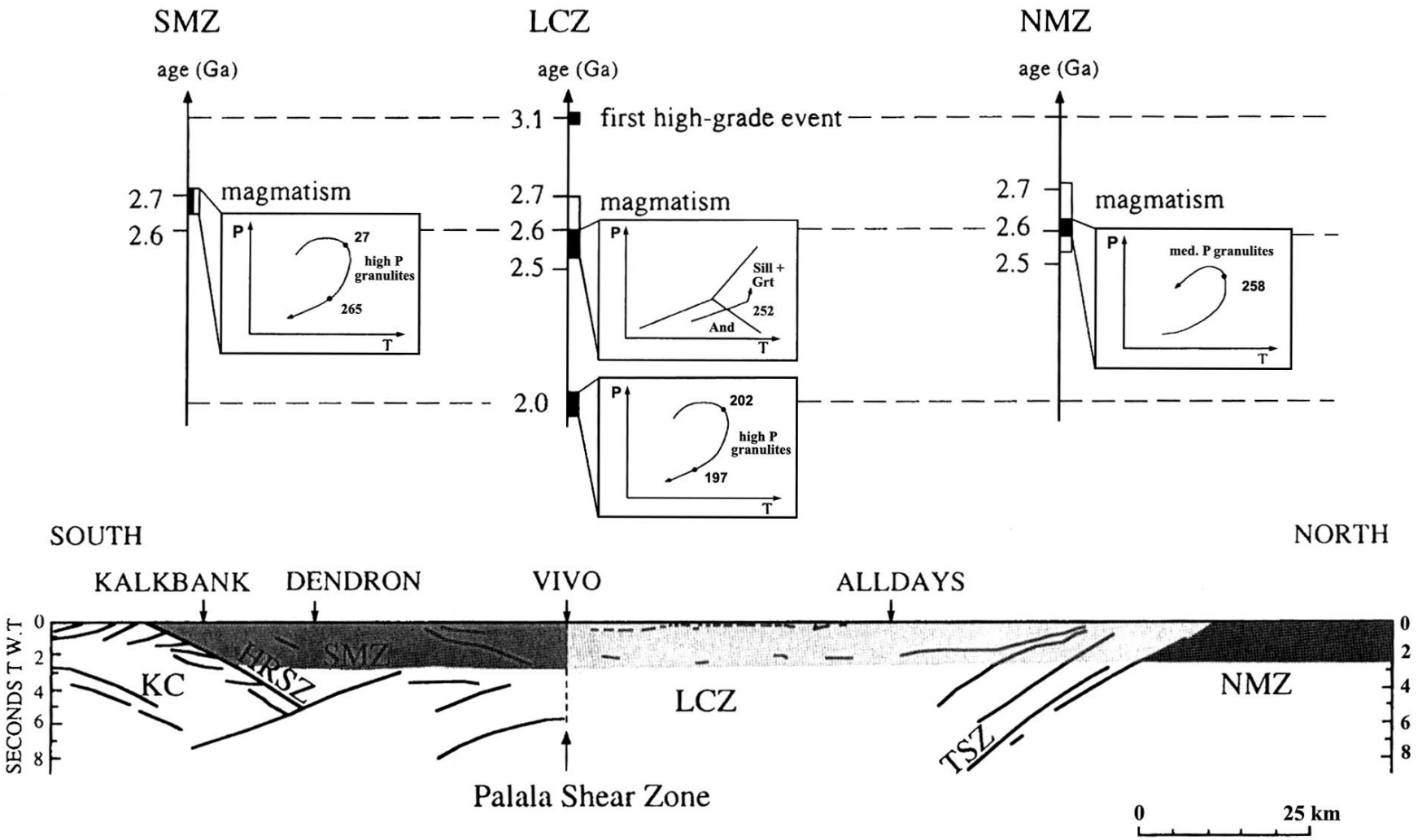


FIGURE 3.14 : Schematic summary of the metamorphic evolution in each of the Limpopo Province subzones (after Holzer *et al.*, 1999) and interpretation of a N-S seismic profile across the Limpopo Province (after De Beer & Stettler, 1992). Note the lack of seismic reflectors within the LCZ, which might be attributed to the existing complex structural pattern produced during polymetamorphism and polyphase ductile folding. Note: SMZ = Southern Marginal Zone; LCZ = Limpopo Central Zone; NMZ = Northern Marginal Zone; KC = Kaapvaal Craton; HRSZ = Hout River Shear Zone; TSZ = Triangle Shear Zone.

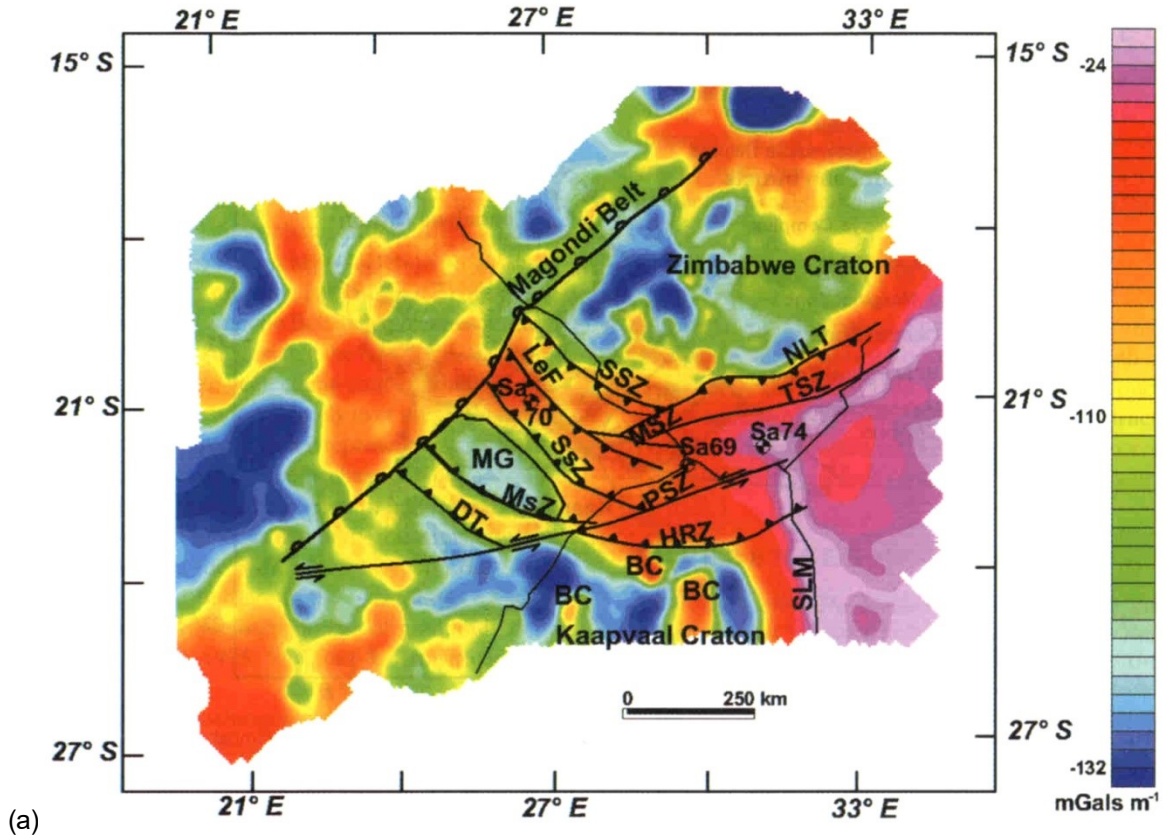
Based on regional gravity data constrained by seismic and geochronological data, Ranganai *et al.* (2002) advocated a much larger Limpopo Province than previously proposed and correlated the Archaean Shashe Belt in Botswana with the LCZ and its northeastern and southwestern marginal zones, which are bounded by the NE-verging Shashe shear (thrust) zone and Lechana fault, as well as the Dinokwe thrust and Mahalapye shear zone, with the NMZ and SMZ of the Limpopo Province respectively (Fig. 3.15). Opposite vergence in the marginal zones bounding the central zone of the Shashe Belt indicates a 'pop-up' structure similar to that documented in the Limpopo Belt (*e.g.* Roering *et al.*, 1992).

The gravity anomaly of the Limpopo Province decreases progressively in amplitude from east to west, correlating with the lateral variation of structural trends and thickness of the crust within the province. Receiver function analysis of broad-band seismic records (Nguuri *et al.*, 2001) show crustal thicknesses of ca. 40-45 km beneath the LCZ, ca. 48-51 at the junction of the Limpopo Province and Shashe Belt, and ca. 50-54 km beneath the central zone of the Shashe Belt (Fig. 3.8). The lower crust is laminated and the Moho poorly defined beneath the LCZ (*cf.* Nguuri *et al.*, 2001). *P-T* estimates based on metamorphic minerals indicate that the present erosional levels were overlain by a lithostatic load of ~25 km and ~15 km in the LCZ and Shashe Belt, respectively. Therefore the pre-exhumation crustal thickness was ~70 km in both the LCZ and Shashe Belt, supporting their linkage and the arc shape of the thickened crust (Ranganai *et al.*, 2002) (Fig. 3.15).

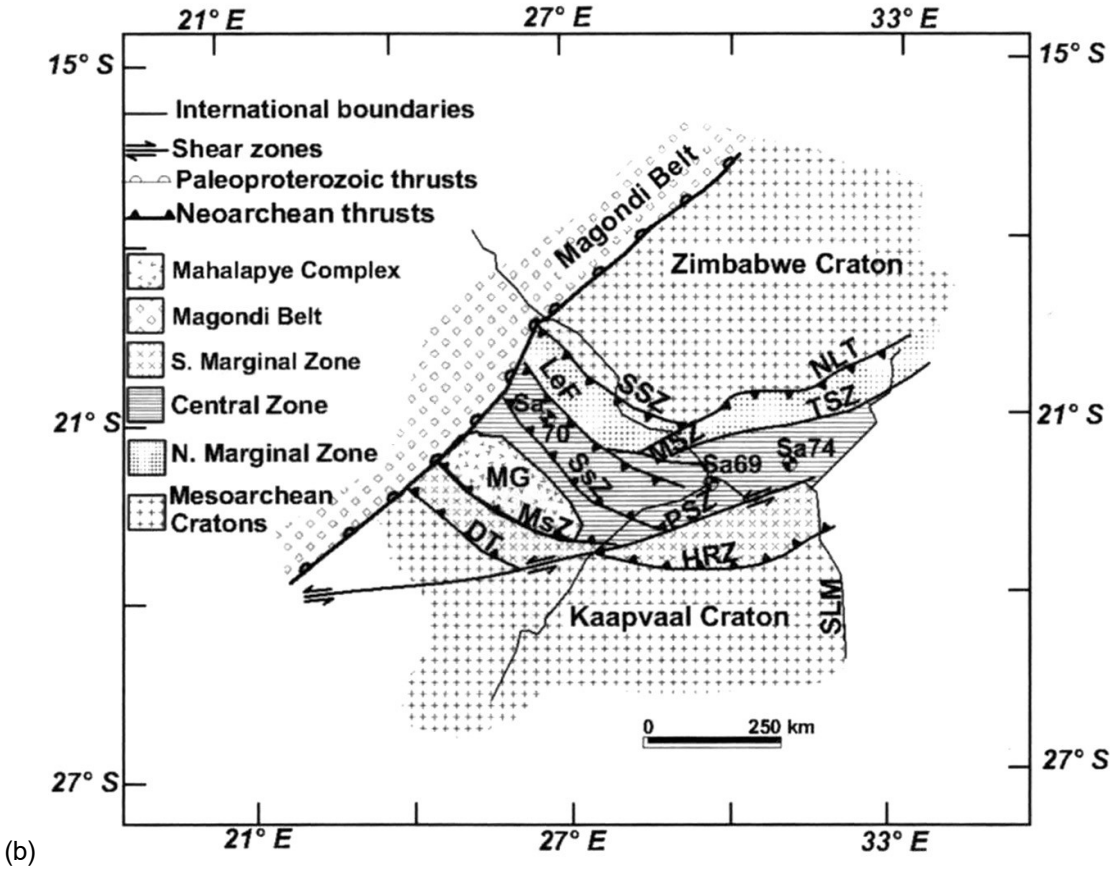
Beneath the LZC a thick cratonic keel is preserved that has been imaged in tomographic models (Figs. 3.6 & 3.7). In this regard, James *et al.* (2001) and Stankiewicz *et al.* (2002) have identified high-velocity mantle structures, with seemingly irregular lower surfaces, not only beneath the Kaapvaal and Zimbabwe cratons, but also beneath the LCZ, which extend to depths of 250-300 km and represent the buoyant roots of these cratonic regions in southern Africa (Figs. 3.6 & 3.7).

These findings are in agreement with carbon isotope distribution and inclusion chemistry of Venetia diamonds which are akin to those of diamonds from most kimberlites located on the Kaapvaal Craton, supporting tectonic models, which postulate that the LCZ is underlain by old thick cratonic lithosphere (Deines *et al.*, 2001; Viljoen, 2002). Furthermore, major and trace-element concentrations in eclogitic and websteritic inclusions in diamonds (Aulbach *et al.*, 2002), and petrological and geochemical data for crustal and upper mantle xenoliths in kimberlite (Pretorius, 1996; Pretorius & Barton, 2003b), supported by experimental compressional wave velocity measurements and calculations of outcropping crustal rocks and xenoliths respectively (Pretorius, 1996; Pretorius & Barton, 2000a) from the Venetia Diamond Mine and a seismic refraction model/profile for the Limpopo Belt (Durrheim *et al.*, 1992) indicate a mixed eclogitic oceanic crustal slab-derived melt and peridotitic mantle source of <~3.0 - >~2.6 Ga. The granulite-facies lithologies that characterise the LCZ end at a *décollement* at a depth of ~10 km and are underlain to a depth of ~56 km (= petrological Moho, where crustal eclogite grades into lherzolites of lithospheric upper mantle) by amphibolite-facies putative protolith (felsic to mafic amphibolite) and restite (garnet-quartz rocks, mafic granulite and crustal eclogite) assemblages in various proportions probably belonging to the Zimbabwe Craton (Pretorius, 1996; Barton & Pretorius, 1998; Pretorius & Barton, 2003a & b; Durrheim *et al.*, 1992) (Fig. 3.13).

The tectonic evolution of the Limpopo Mobile Belt has been the subject of considerable controversy over the years. One traditional school of thoughts advocated that the Limpopo Mobile Belt formed during a single, Neoarchaean, high-grade, tectono-metamorphic event that was initiated by the collision of the Kaapvaal and Zimbabwe cratons. Most tectonic models envisaged high-grade metamorphism in the Limpopo Province to be the product of the "Limpopo Orogeny", resulting from north-south directed continent-continent collision and associated tectonic thickening at ~2.7-2.65 Ga between the Kaapvaal and Zimbabwe cratons (*e.g.* Coward *et al.*, 1973, 1976a,b; Coward, 1976; Barton & Key, 1981; Fripp, 1981, 1982; Light, 1982; Du Toit *et al.*, 1983; Watkeys *et al.*, 1983; Watkeys, 1984; Van Reenen *et al.*, 1987, 1988; 1990; Barton & Van Reenen, 1992a&b; Treloar *et al.*, 1992; Roering *et al.*, 1992b; De Wit *et al.*, 1992a; Rollison, 1993, Windley, 1993; McCourt &



(a)



(b)

FIGURE 3.15: (a) Bouguer anomaly map of the Limpopo-Shashe Belt and adjacent cratons upward continued to 10 km and (b) tectonic interpretation (also as overlay on (a)) based on surface geology and gravity data, showing the distribution of the three tectonic zones of the Archaean Limpopo-Shashe Belt and relations with the Zimbabwe and Kaapvaal cratons and the Palaeoproterozoic Magondi Belt and the Indian Ocean extensional province (after Ranganai *et al.*, 2002).

Armstrong, 1998; Bumby *et al*., 2001; Bumby & van der Merwe, 2004). In this model, the North Limpopo Thrust Zone and Hout River Shear Zone have been interpreted as frontal and back thrusts respectively, along which lower crustal rocks move upwards and spread outwards onto the adjacent cratons from the zone of thickened crust, creating a regional "pop-up-structure" (Treloar *et al.*, 1992; De Wit *et al.*, 1992a).

McCourt & Vearncombe (1987, 1992) presented a different model, invoking east-west collision of the LCZ block with the combined Kaapvaal and Zimbabwe cratons, in which the LCZ was emplaced westwards as a giant allochthonous nappe or exotic thrust she*et al*ong inward dipping lateral ramps (*i.e.* Tuli-Sabi-Triangle and Palala shear zones) and a west-verging frontal ramp. Thrusting of the marginal zones onto the cratons is explained by lateral expulsion during the westward collision.

A combination of the above two scenarios was presented as a third model by Treloar *et al.* (1992). In this model the Limpopo Belt is also related to a "pop-up structure" produced by north-south directed collision. The strike-slip shearing along internal lineaments is explained by lateral extrusion perpendicular to the main shortening direction. In this model the effects of the Limpopo Orogeny are interpreted to extend regionally and over a long period of time. Treloar *et al.* (1992) stressed analogies between the collision-extrusion tectonics of the Limpopo Orogeny and the present day Himalayas.

The other school of thoughts has its beginnings in the mid-1990s with an increasing number of studies (Barton *et al.*, 1994a; Kamber & Biino, 1995; Kamber *et al.*, 1995a & b; Hisada & Miyano, 1996; Barton & Sergeev, 1997; Jaeckel *et al.*, 1997; Kröner *et al.*, 1998; Holzer *et al.*, 1998, 1999; Schaller *et al.*, 1999; Chavagnac *et al.*, 2001; Barton *et al.*, 2003, 2006; Buick *et al.*, 2003, 2006; Zeh *et al.*, 2007; Mouri *et al.*, 2008; Chudy *et al.*, 2009) having identified a Palaeoproterozoic high-pressure granulite metamorphic event at ~2.04-2.02 Ga with associated dextral transpressive tectonism between both cratons along the Tuli-Sabi-Triangle and Palala shear zones which is confined to the Limpopo Central Zone Terrane and interpreted as either reflecting an *anorogenic thermal event*, probably related to the emplacement of the Bushveld Complex at ~2.06 Ga (*e.g.,* McCourt *et al.*, 1995), or to a mantle plume (Treloar *et al.*, 1997), or reflecting a major *orogenic cycle* with associated suturing of the Kaapvaal and Zimbabwe cratons and tectonic crustal thickening (Watkeys, 1983; Barton *et al.*, 1994a; Kamber *et al.*, 1995a & b; Barton & Sergeev, 1997; Jaeckel *et al.*, 1997; Holzer *et al.*, 1996, 1997, 1998, 1999; Schaller, 1997; Schaller *et al.*, 1997, 1999; Kröner *et al.*, 1999; Kreissig *et al.*, 2001; Zeh *et al.*, 2004, 2005; Eriksson *et al.*, 2009).

The controversy about the tectonic setting of the Limpopo Central Zone Terrane culminates in the question whether the collision between the Kaapvaal and Zimbabwe cratons during the Limpopo Orogeny occurred in the Neoarchaean at ~2.7 Ga, or Palaeoproterozoic at ~2.0 Ga (or both). The debate has focussed on whether the identified ~2.0 Ga tectono-metamorphic event represents the actual Limpopo collision (*e.g.* Kamber *et al.*, 1995a & b, Holzer *et al.*, 1997, 1998, 1999; Dorland, 2004, Zeh *et al.*, 2004)), or reactivation within a previously at ~2.7-2.65 Ga assembled Limpopo Belt (*e.g.* McCourt & Armstrong, 1998; Bumby *et al.*, 2001, 2002c; Boshoff *et al.*, 2006; Perchuk *et al.*, 2006, 2007, 2008).

In the latter scenario it is suggested that the entire Central Zone of the Limpopo Belt has been affected by at least two high-grade metamorphic events, with a first penetrative structural-metamorphic overprint during the Neoarchaean, and a shear-zone bounded metamorphic overprint during the Palaeoproterozoic (*e.g.* McCourt & Armstrong, 1998; Bumby *et al.*, 2001, 2002c; Boshoff *et al.*, 2006; Perchuk *et al.*, 2006, 2007, 2008). In contrast, other workers suggested that most parts of the Central Zone underwent their predominant tectono-metamorphic evolution during a Palaeoproterozoic orogenic event, which resulted from oblique collision between the Kaapvaal and Zimbabwe cratons (*e.g.* Kamber *et al.*, 1995a & b, Holzer *et al.*, 1997, 1998, 1999; Dorland, 2004, Zeh *et al.*, 2004). A third model viewed the Limpopo Belt as an assembly of terranes constructed over a period of 700 Ma between ~2.7 and ~2.0 Ga, each with a distinct tectono-metamorphic history (Barton *et al.*, 2006).

In contrast to the first model, the second and third models also take into account the fact that the Central Zone of the Limpopo Belt does not represent a coherent high-grade granulite-facies terrane, but that its centre part (*i.e.* the area around the Venetia kimberlite pipes constituting the so-called Venetia Klippen Complex) underwent only a Palaeoproterozoic amphibolite-facies metamorphic overprint (Barton *et al.*, 2003; Klemd *et al.*, 2003; Zeh *et al.*, 2005a & b) and was affected by horizontal nappe tectonics (Barton *et al.*, 2003). Based on these findings, Zeh *et al.* (2005a & b) suggested that the rocks of the Venetia Klippen Complex represent the roof of the high-grade metamorphic rocks observed in other parts of the Limpopo Belt (*e.g.* Krone Metamorphic Terrane). Both floor rocks of the Krone Metamorphic Terrane and overlying roof rocks of the Venetia Klippen Complex contain relics of the same Palaeoarchaean (~3.3-3.0 Ga) terrane, which was affected by granite intrusions at ~2.65-2.60 Ga, and subsequently exposed and overlain by clastic sediments between ~2.60 and ~2.03 Ga. All rocks then experienced an amphibolite-facies metamorphic overprint in response to thin-skinned fold-and-thrust tectonics during the Palaeoproterozoic at ~2.02 Ga (Chudy *et al.*, 2009).

These days it is generally accepted that the Kaapvaal Craton and Central Zone Terrane-Zimbabwe Craton amalgamation took place during the Neoarchaean Limpopo Orogeny at 2.68-2.64 Ga, and that the M_3 granulite facies metamorphism at ~2.04-2.02 Ga records an intracontinental Palaeoproterozoic transpressional orogeny within the consolidated Kaapvaal-Zimbabwe Craton, which was induced by far-field tectonic processes (*e.g.*, Khoza *et al*., 2013; Xie *et al*., 2017; Brandt *et al*., 2018) (Fig. 3.16).

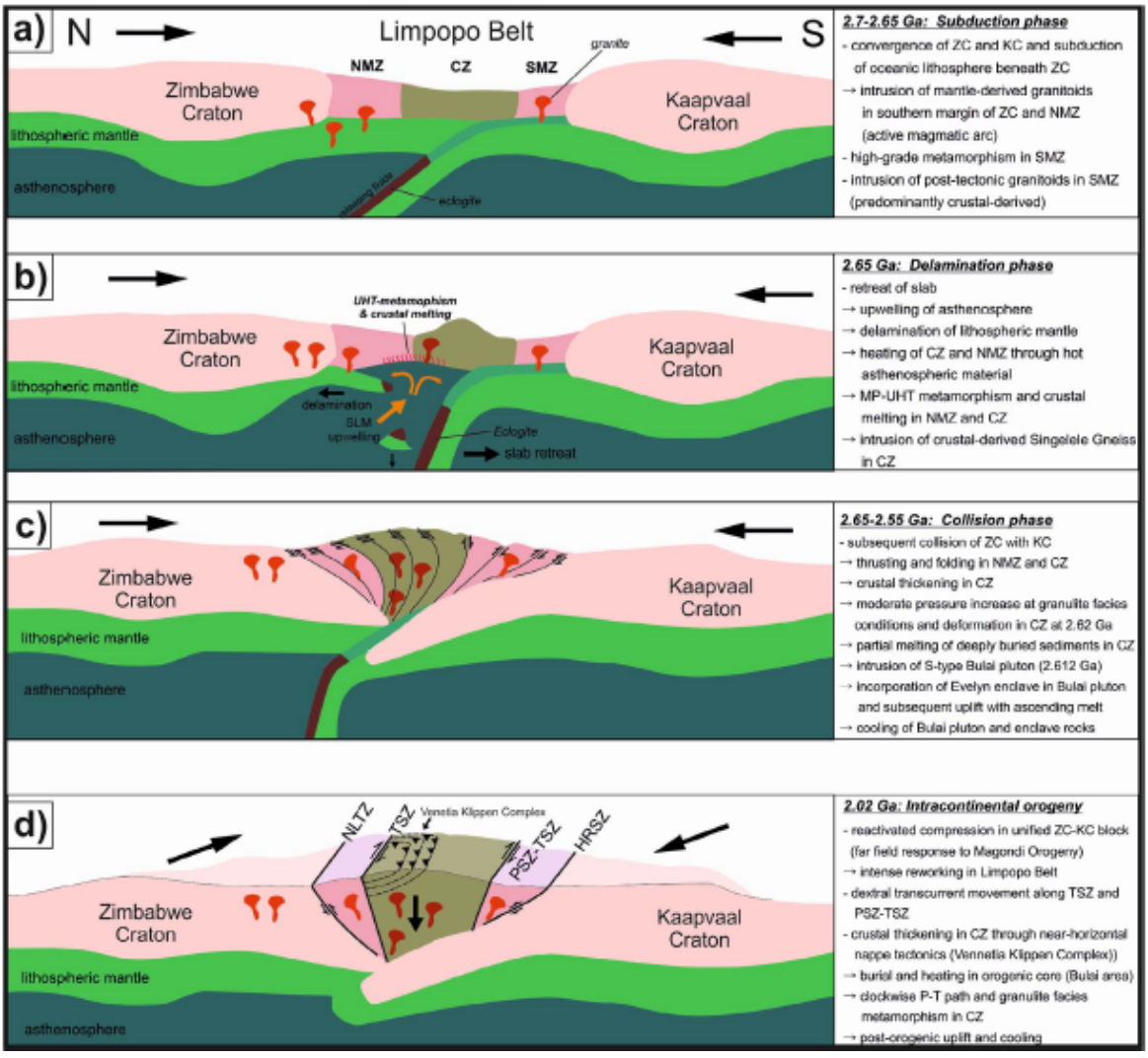


FIGURE 3.16: Schematic model for the geodynamic evolution of the Limpopo Belt from~ 2.7 to 2.0 Ga (Brandt *et al*, 2018). Abbreviations: CZ: Central Zone; NMZ: Northern Marginal Zone; SMZ: Southern Marginal Zone; NLTZ: North Limpopo Thrust Zone; TSZ: Triangle Shear Zone; PSZ-TSZ: Palala Shear Zone-Tshipise Straightening Zone; HRSZ: Hout River Shear Zone.

4 GEODYNAMIC EVOLUTION OF THE KAAPVAAL AND ZIMBABWE CRATONS AND LIMPOPO CENTRAL ZONE TERRANE

Supporting the proposal of de Wit *et al.* (1992a) and de Wit & Hart (1993), the formation of the Kaapvaal Craton during the Archaean is understood, in this study, in terms of lithospheric growth due to processes similar to those of modern-day plate tectonics. Following a brief summary of proposals by de Wit *et al.* (1992a), de Wit & Hart (1993) and Brandl & de Wit (1997), as well as Wilson *et al.* (1995), Kusky (1998) and Horstwood *et al.* (1999) for the Palaeo- to Mesoarchaean (~3.8-3.1 Ga) development of the Kaapvaal and Zimbabwe proto-cratons, respectively, the Mesoarchaean to present (~3.1-0 Ga) evolution of both cratons and the Limpopo Central Zone Terrane will be outlined and discussed in more detail.

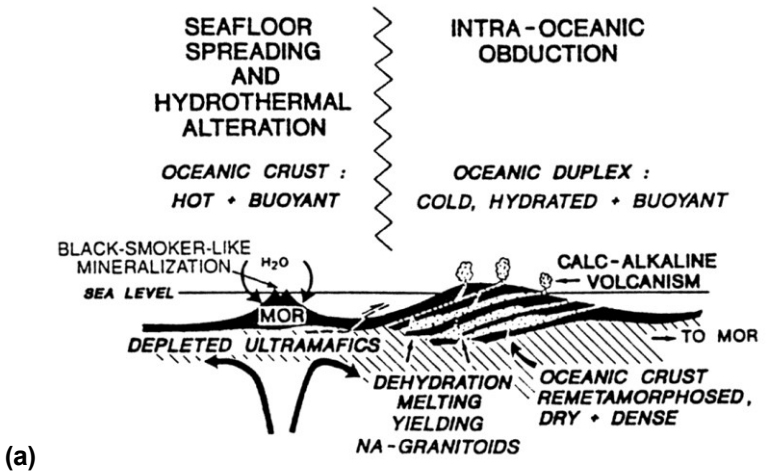
4.1 PALAEOARCHAEAN-MESOARCHAEAN EVOLUTION (~3.8-3.1 GA)

4.1.1 KAAPVAAL GRUNEHOGNA PROTOCRATON

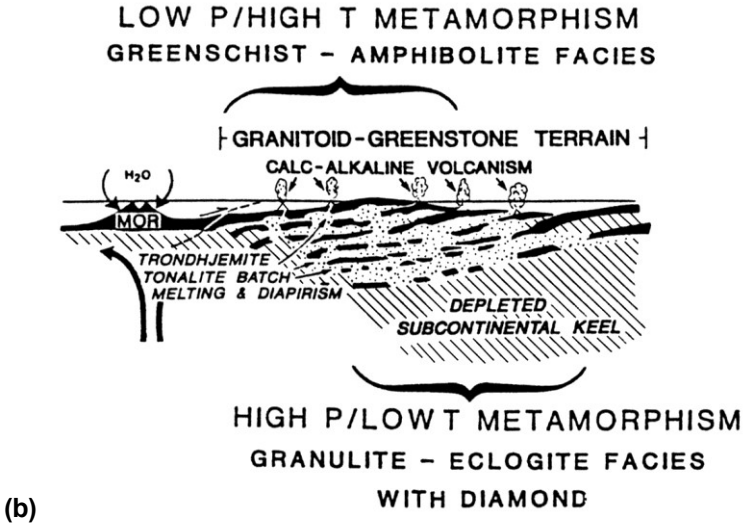
There is as yet no consensus reached as to when the first continental lithosphere emerged and as to the nature of the associated tectonic and thermal processes, operating at that time. (Ashwal, 1990; de Wit *et al.*, 1992a). De Wit *et al.* (1992a) and de Wit & Hart (1993) addressed these fundamental problems by discussing and proposing an evolutionary model for the formation of an Archaean continent, using the Kaapvaal Craton as an example.

In general, this model envisages the earliest continental lithosphere to have formed through linked intra-oceanic processes of spreading and obduction-dominated tectonics (Fig. 1.1a & b). Heat flux and hydrothermal interaction of Archaean MORs (mid-oceanic ridges) was more intense than today, causing the formation of chemically enriched MgO-oceanic crust (due to hotter mantle melts), but physically less dense oceanic lithosphere (due to associated greater degrees of hydration, and silica, iron and magnesium metasomatism), than currently. Such intensely hydrated, low-density, Mg-rich oceanic crust and upper mantle could have resisted a recycling (subduction-like) process, which led to obduction-dominated tectonics. Continuous imbrication of oceanic lithosphere led to the formation of intra-oceanic thrust-stacks (Fig. 1.1a). This resulted in regional load-induced subsidence, which in turn caused *in situ* differentiation and density inversions during dehydration melting of the “wet” oceanic-like rocks to form the vast amounts of tonalite-trondhjemites and associated calc-alkaline extrusives, now present in and around the greenstone belts of the nucleus of the Kaapvaal Shield (De Wit *et al.*, 1992a; de Wit & Hart, 1993) (Fig. 1.1b). Accretion of these early continental fragments formed the larger granite-greenstone terrains or shield areas of the early Archaean cratons, consisting of a mafic-ultramafic keel and an overlying continental-like crust, and thus formed through means of tectonic rather than igneous thickening. Metamorphism during these processes led to vertically stacked “paired metamorphic belts”, *i.e.,* relatively high-P/low-T diamond formation in the keels of the fragments overlain by relatively low-P/high-T greenstone assemblages (De Wit *et al.*, 1992a; de Wit & Hart, 1993).

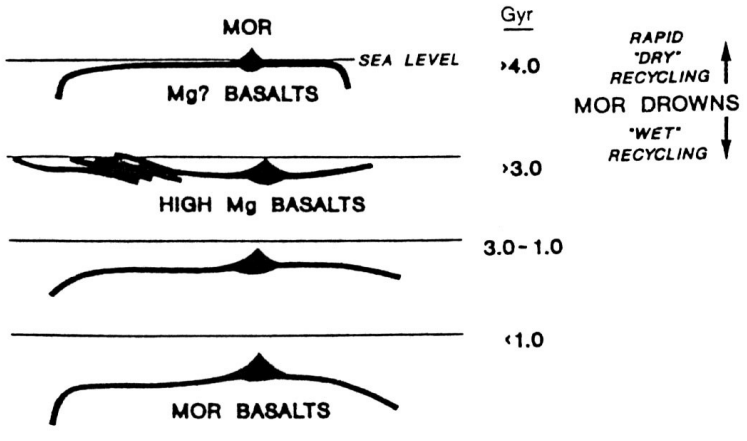
In conclusion, the “essential ingredient” needed to drive this obduction-dominated tectonism and granitoid formation proposed by this model, is an oceanic crust comprising both MgO and H_2O contents. De Wit *et al.* (1992a) and de Wit & Hart (1993) proposed that prior to ~4.0 Ga the average MOR stood above sea level, so that “dry” recycling of the oceanic lithosphere prevailed and that the formation of significant continental crust was therefore inefficient or absent (Fig. 1.1c).



(a)



(b)



(c)

FIGURE 4.1: Schematic model depicting the formation of the earliest continental lithosphere, through linked intra-oceanic processes of spreading and obduction-dominated tectonics. (a) Intra-oceanic obduction and stacking of oceanic lithosphere. (b) Continuous imbrication of oceanic lithosphere leads to tectonic loading and subsidence of hydrated thrust-stacks, which in turn causes *in situ* differentiation and density inversions during dehydration melting of the "wet" oceanic-like rocks to form vast amounts of tonalite-trondhjemites and associated calc-alkaline extrusives. (c) Schematic model for the evolution of oceanic plates with respect to sea level and related formation of the earliest continental crust (granite-greenstone terrains) and associated peridotite-eclogite keels of the continental tectosphere, following gradual "drowning" of mid-oceanic ridges at ~4.1-3.6 Ga (after de Wit *et al.*, 1992a and de Wit & Hart, 1993).

Thus, the formation of the earliest continental crust could only have occurred when the earth's MOR's "drowned" gradually below sea level, triggering for the first time in the history of the Earth, efficient and continuous interaction of the hydrosphere and mantle. Submergence of MOR's was probably related to both (i) the decreasing heat content of the Earth and (ii) ageing of average oceanic lithosphere, and hence reflects a thermally controlled increase in the average depth of the ocean basins. Gradual decline in the Mg-content of the oceanic crust (as a consequence of a decline of the average heat content of the earth) and thus the decrease of the volume of low-density serpentinite, heralds the end of intra-oceanic obduction-dominated tectonics, and the start of modern-day subduction processes of tholeiitic oceanic crust after approximately 3.0 Ga (De Wit *et al.*, 1992a; de Wit & Hart, 1993) (Fig. 1.1c).

With respect to the evolution of the Kaapvaal Shield, the earliest continental core or nucleus of the shield of the Kaapvaal Craton consists of three Palaeo- to Mesoarchaean (~3.7-3.46 Ga) crustal fragments, that is the Ancient Gneiss (~3.7-3.55 Ga) and the Southern and Northern Barberton terranes, of which the two Barberton terranes constitute the Barberton Greenstone Belt (De Wit *et al.*, 1992a).

The comagmatic mafic and ultramafic volcanics and plutonic rocks of the Northern and Southern Barberton Terranes represent Mesoarchaean (~3.55-3.3 Ga) back-arc basin deposits (*e.g.,* Onverwacht Group) and a remnant of Mesoarchaean (~3.49-3.48 Ga) oceanic lithosphere (*i.e.,* Jamestown Ophiolite Complex) respectively (Lopez-Martinez *et al.*, 1984; de Wit *et al.*, 1987b; Armstrong *et al.*, 1990; Kamo & Davis, 1991, 1994; Kröner *et al.*, 1991a, 1996a; de Ronde & de Wit, 1994), the latter which was obducted by thin-skinned thrust tectonics between ~3.46-3.43 Ga (within 50 Ma after its formation), onto an active volcanic, arc-trench like terrain with a trondhjemitic-tonalitic basement dating back to ~3.55-3.52 Ga, by processes similar to those which have emplaced modern ophiolites at convergent margins of Phanerozoic continents (De Wit *et al.*, 1992a; de Wit & Hart, 1993; Brandl & de Wit, 1997).

After a prolonged period of quiescence, the three earliest terranes (*i.e.,* Ancient Gneiss, Southern and Northern Barberton terranes) converged as result of subduction initiation and deposition of deep- to shallow-water clastic sediments of the Fig Tree Group in back-arc basins and were amalgamated during an episode of major northwest-directed thrusting and associated intermediate tonalitic plutonism-volcanism (*e.g.,* Kaap Valley and Nelshoogte plutons) and metamorphism between 3.3- 3.2 Ga (Armstrong *et al.*, 1990; Kamo *et al.*, 1990; Kröner *et al.*, 1991a; Kohler *et al.*, 1993; Byerly *et al.*, 1996), to form the core region of the Kaapvaal Shield (De Wit *et al.*, 1992a; de Ronde & de Wit, 1994; Lowe, 1994, 1999; Brandl & de Wit, 1997). Between ~3.2 and ~3.1 Ga, other slightly younger terranes were accreted onto this nucleus of the Kaapvaal Shield in the south (Natal Terrane), north (Central Terrane) and west (Witwatersrand, Vredefort and Southern terranes) (Appendix 18-V). These accretional tectonics were accompanied by the deposition of the continental-derived alluvial to shallow-marine clastic sequence of the Moodies Group in developing foreland basins at ~3.23-3.17 Ga, and by the emplacement of syn-tectonic (~3.23-3.17 Ga) and post-tectonic (~3.17-3.09 Ga; orogenic collapse-related), voluminous, areally extensive, sheet-like, potassic, granodioritic-adamellitic, composite batholiths (*e.g.,* Kaap Valley, Nelshoogte, Anhalt, Dalmein, Stentor, Mpuluzi, Heerenveen, Nelspruit, Makhutswi, Hebron, Mliba, Halfway House batholiths) and smaller plutons (*e.g.,* Boesmanskop and Salisbury Kop plutons) across the terrane boundaries, with related hydrothermal fluid flow and shear zone-hosted gold mineralisation syn- and post-tectonically at ~3.17-3.09 Ga (*cf.* Anhaeusser & Robb, 1983; Robb, 1983; Robb *et al.*, 1983; Tegtmeyer & Kröner, 1987; Kröner *et al.*, 1989; York *et al.*, 1989; Wilson & Carlson, 1989; Kamo *et al.*, 1990; Armstrong *et al.*, 1990; de Ronde *et al.*, 1991a; Layer *et al.*, 1992; Wendt *et al.*, 1993; Kamo & Davis, 1994; Maphalala & Kröner, 1993; de Ronde & de Wit, 1994; Lowe, 1994, 1999; de Ronde & Kamo, 2000; Elworthy *et al.*, 2000; Carlson *et al.*, 2000). This magmatic event thickened and consolidated (cratonised) the barely stabilised protocontinent, that had

formed by block amalgamation by ~3.2 Ga, to form a stable region at about 3.1 Ga, referred to as the shield of the Kaapvaal Craton (De Wit *et al.*, 1992a; de Wit & Hart, 1993; Carlson *et al.*, 2000).

In summary, the Palaeo-/Mesoarchaean shield of the Kaapvaal Craton is the product of over 500 m.y. of intra-oceanic tectonics (terrain amalgamation) between ~3.64 and 3.1 Ga. The earliest continental nucleus of the shield of the craton may have originated through regional intra-oceanic obduction, giving rise to stacking, tectonic loading and subsidence of hydrated oceanic thrust stacks, which in turn lead to melting in the lower parts of the thrust stack, the generation of tonalite-trondhjemite melts and their intrusion into the oceanic crust to produce the granitoid intrusives and calc-alkaline extrusives presently preserved within the core of the Kaapvaal Shield. Initial amalgamation of the three old terrains at ~3.46-3.43 Ga and at a later stage of other slightly younger terrains between ~3.3 and ~3.1 Ga, led to the formation of the Kaapvaal Shield (proto-craton), which had reached cratonic stability and rigidity by ~3.1 Ga (De Wit, 1986; de Wit & Tredoux, 1988; Tredoux *et al.*, 1989; de Wit *et al.*, 1987, 1990, 1992a; de Wit & Hart, 1988, 1993; de Ronde & de Wit, 1994; Brandl & de Wit, 1997).

4.1.2 ZIMBABWE PROTOCRATON

Like the Kaapvaal Craton, the Archaean Zimbabwe Craton is composed of a number of distinct tectono-stratigraphic terranes of Palaeo- to Mesoarchaean age (~3.8-3.1 Ga), assembled by plate tectonic processes during several Meso- to Neoarchaean orogenic cycles (~3.6-3.1 Ga). The Tokwe Subprovince represents the Zimbabwe proto-Craton at ~3.35 Ga and in turn consists of several Palaeo- to Mesoarchaean terranes, of which some had been amalgamated into an earlier Sebakwe proto-Craton at ~3.46 Ga (Kusky, 1998; Horstwood *et al.*, 1999; this study) (Figs. 3.11 & 3.12).

The Sebakwe proto-Craton consolidated at ~3.46 Ga and represents the oldest crustal fragment within the Tokwe Subprovince and thus the ancient nucleus of the present Zimbabwe Craton. It is composed of the oldest rocks in the Zimbabwe Craton, including amphibolite-facies tonalitic gneisses (representing a combination of ~3.6-3.35 Ga old, syn-(Sebakwian)orogenic emplaced and deformed intrusive granitoids and pre-existing (>3.6-3.8 Ga) granitoid-gneiss basement) and the ~3.6-3.37 Ga old Sebakwian greenstone belt sequence, which consists of a Lower Sequence (ultramafic-mafic volcanic (*i.e.,* komatiites and basalts) and chromitite-bearing intrusive rocks, and minor sediments) and an unconformably overlying Upper Sequence (basal conglomerate (derived from Lower Sequence), quartzites, micaschists and BIFs) (Wilson, 1979, 1981, 1990; Horstwood *et al.*, 1999).

The Lower Sequence of the Sebakwian Supergroup was deposited/intruded possibly in a continental back-arc basin, that formed within a ~3.8-3.6 Ga old continental fragment (*i.e.,* Tokwe Terrane/Segment; Wilson, 1981, 1990) at ~3.6-3.46 Ga, and deformed, metamorphosed and intruded by tonalites at ~3.46 Ga during a tectono-magmatic (orogenic) event, *i.e.,* Sebakwian Orogeny, possibly documenting the collision/amalgamation of the Tokwe Terrane with another continental fragment to form the Sebakwe protocraton. Subsequently, the Upper Sequence of the Sebakwian Supergroup was deposited on the previously deformed and eroded surface of the Lower Sequence (Wilson, 1979, 1981) and basement of the Palaeoarchaean Sebakwe proto-Craton at <3.46-3.37 Ga, possibly representing a molasse-type deposit formed in response to the Sebakwian orogenic event and/or a transgressive marine shelf sequence, overlapping the stabilised Sebakwe proto-Craton in post-(Sebakwian)-orogenic time (this study).

The consolidation of the Tokwe Subprovince occurred during the Tokwe Orogeny at ~3.37-3.35 Ga, which documents possibly the collision and amalgamation of smaller, Palaeoarchaean continental fragments

and/or Mesoarchaean magmatic-arc/back-arc basin-complexes around the Sebakwe protocraton. These collisional tectonics resulted in amphibolite-facies metamorphism and complex and intense deformation of the ~3.6-3.37 Ga Sebakwian greenstone belt sequences and associated granitoid suites, as well as older (>3.6-3.8 Ga) intervening (tightly infolded) tonalitic, locally migmatitic gneissic rocks of the Sebakwe protocratonic nucleus (this study).

The Sebakwian greenstone belt sequence is proposed to have been overturned and thrusted over the older gneissic basement rocks, forming the imbricated and inverted mafic-ultramafic "Selukwe nappe" (Stowe, 1974; Cotterill, 1979). This has been strongly refuted on both structural and stratigraphic grounds (Tsomondo & Blenkinsop, 1991; Tsomondo *et al.*, 1992). However, crustal thickening as a possible combined result of thrust tectonics and magmatic under-/intraplating of mantle-derived magmas, resulted in melting (anatexis) of the Palaeoarchaean (>3.8-3.6 Ga) lower continental crust and led towards the end of the Tokwe Orogeny to the intrusion of late- to post-kinematic, anatectic (S-type) tonalites, granodiorites (*e.g.,* Mont d'Or pluton), pegmatites and leucosomes into deformed Sebakwian Supergroup rocks at ~3.35-3.3 Ga (*e.g.,* Moorbath *et al.*, 1976; Taylor *et al.*, 1984, 1991; Horstwood *et al.*, 1999, this study).

Several smaller terranes, perhaps magmatic arcs or microcontinents, were apparently accreted onto the Tokwe Subprovince during later tectono-thermal (orogenic) event(s) at ~3.3-3.1 Ga, resulting in the formation and stabilisation of the presently preserved Zimbabwe Craton which acted as a coherent unit by ~3.1 Ga (Wilson *et al.*, 1995; Kusky, 1998; this study) (Figs. 3.11 & 3.12).

4.1.3 LIMPOPO CENTRAL ZONE TERRANE

The evolution of the Central Zone Terrane of the Limpopo Province started in the Palaeoarchaean with the deposition of supracrustal successions of the Beit Bridge Complex (comprising metapelite, metaquartzite, magnetite quartzite and amphibolite of the Mount Dowe Group) on a >~3.3 Ga old continental platform in a cratonic environment (*e.g.*, SACS, 1980; Brandl, 1983; Watkeys, 1984; Buick *et al*., 2003) at >~3.3 Ga (Brandl, 1981; Kröner *et al*., 1999; Mouri *et al*., 2009; Zeh *et al*., 2010), or between ~3.1 and ~2.65 Ga (Zeh *et al*., 2008, 2010).

The supracrustal successions of the Beit Bridge Complex were intruded by precursors of meta-gabbroic rocks of the Messina Layered Intrusion at ~3.36-3.5 Ga (Barton, 1996; Mouri *et al*., 2009; Zeh *et al*., 2010) and by TTGs of the Sand River Gneiss Suite at ~3.3 Ga (*e.g.*, Jaeckel *et al.*, 1997; Kröner *et al*., 1998, 1999; Zeh *et al*., 2010).

Subsequently, all Palaeoarchaean lithostratigraphic units underwent a first high-grade structural and metamorphic (anatectic) overprint (D_1, M_1) during the Mesoarchaean at ~3.18-3.1 Ga (*e.g.*, Hor *et al.*, 1975; Barton *et al.*, 1979a; Barton & Key, 1981; Fripp, 1981, 1982; Barton *et al.*, 1983a, 1990; Harris *et al.*, 1987; Retief *et al.*, 1990; Treloar *et al.*, 1992; Tsunogae & Yurimoto, 1995; Barton & Sergeev, 1997; Jaeckel *et al.*, 1997; Kröner *et al.*, 1998, 1999; Barton *et al.*, 2003; Zeh *et al.*, 2007; Gerdes & Zeh, 2009; Mouri *et al*., 2009), prior to the intrusion of basaltic dykes at <~3.1-3.0 Ga (*e.g.* Barton *et al.*, 1977, 1983b, 1990, 2003, 2006).

4.2 MESOARCHAEAN-NEOARCHAEAN EVOLUTION (~3.1-2.53 GA)

Subsequently to the stabilization of the Kaapvaal-Grunehogna and Zimbabwe proto-cratons at ~3.1 Ga, the Meso- to Neoarchaean period (~3.1-2.53 Ga) in the evolution of the cratons was dominated by both intra-continental and continental-margin processes. In response to modern-day plate tectonic processes, continental growth took place during several orogenic cycles mainly along the margins of the cratons through a combination of Cordillera-type tectonic aggregation of crustal fragments (terrane accretion) and subduction-related igneous processes. The geodynamic evolution of the Kaapvaal-Grunehogna and Zimbabwe cratons during the Neoarchaean can be subdivided into the following orogenic cycles, which resulted in tectono-metamorphic, magmatic and sedimentary activity within and around both cratons:

KAAPVAAL-GRUNEHOGNA CRATON:

- Murchison Orogenic Cycle (~3.1-2.97 Ga)
- Limpopo Orogenic Cycle (~2.97-2.64 Ga)
- Bengal Orogenic Cycle (~2.97-2.87 Ga)
- Kraaipan-Vaalbara Orogenic Cycle (~2.95-2.81 Ga)

ZIMBABWE CRATON:

- Bulawayan Orogenic Cycle (~3.1-2.81 Ga)
- Limpopo Orogenic Cycle (~2.81-2.64 Ga)
- Hurungwe Orogenic Cycle (~2.72-2.64 Ga)
- Nyassa Orogenic Cycle (~2.64-2.53 Ga)

INDIAN CRATONS:

- Dharwar Orogenic Cycle (~2.72-2.5 Ga)
- Bundelkhand Orogenic Cycle (~2.72-2.5 Ga)

Note: Despite the fact that some of the orogenic cycles are coeval and geodynamically linked with each other, the presentation of the individual cycles will focus separately on the Kaapvaal-Grunehogna and Zimbabwe cratons for reasons of clarity and simplification. However, as the geodynamic evolution of both cratons is closely linked to each other, especially since the beginning of the second phase of the Limpopo Orogenic Cycle at ~2.81 Ga, tectono-metamorphic, magmatic and sedimentary processes related to the Neoarchaean Limpopo, Hurungwe and Nyassa orogenic cycles will be discussed jointly for the Kaapvaal-Grunehogna and Zimbabwe cratons.

Although not directly related to the geodynamic evolution of the Kaapvaal-Grunehogna Craton, the Dharwar and Bundelkhand orogenic cycles within the Indian subcontinent are discussed here for reasons of completeness.

4.2.1 KAAPVAAL-GRUNEHOGNA CRATON

4.2.1.1 MURCHISON OROGENIC CYCLE (~3.1-2.97 GA)

The development of a southeasterly inclined subduction zone beneath the northern margin of the proto-Kaapvaal-Grunehogna Craton (possibly triggered by the opening/widening of the Limpopo oceanic basin between the Pietersburg and Limpopo Central Zone terranes along an oceanic spreading centre/ridge) initiates the closure of the Murchison oceanic basin between the Pietersburg Terrane and proto-Kaapvaal-Grunehogna Craton and represents the beginning of the Murchison orogenic cycle at ~3.1 Ga (Appendix 20-A). Dehydration of the subducted oceanic lithospheric slab, hydration and melting of the mantle wedge, and magmatic under-/intraplating cause the development of a continental magmatic-arc within the northwestern part of the proto-Kaapvaal-Grunehogna Craton during the period ~3.1-3.0 Ga, which is evident by migmatisation and hydrothermal overprinting of the >3.1 Ga old TTG gneiss-greenstone basement of the northern proto-Kaapvaal-Grunehogna Craton (*e.g.,* in area of Pretoria-Johannesburg Dome (*e.g.,* Barton *et al.*, 1999; Poujol & Anhaeusser, 2001), Vredefort Dome (*e.g.,* Hart *et al.*, 1981, 1999; Kamo *et al.*, 1996), south of the Murchison Greenstone Belt (Makhutswi Migmatite; *e.g.,* Brandl & Kröner, 1993; Poujol & Robb, 1999), and Barberton Mountain Land), the emplacement of I-type granites (*i.e.,* Westerdam, Ottosdal-Coligny and De Pan granites) in the Lichtenburg area (*e.g.,* Robb *et al.*, 1992; Barton *et al.*, 1986) and Harmony Granite to the south of the Murchison Greenstone Belt (*e.g.,* Poujol & Robb, 1999)), and hydrothermal gold mineralisation along dextral transpressional reactivated Mesoarchaean suture zones (*e.g.,* Magaliesburg-Barberton suture zone) in the area of the Barberton Greenstone Belt (*e.g.,* De Ronde *et al.*, 1991a)) (Appendix 20-A).

To the south of the developing intracratonic magmatic arc in the eastern Kaapvaal Craton (*i.e.,* south-central Swaziland), the burial of sediments of the Moodies and Fig Tree groups and equivalents to depths greater than 15 km, led to partial melting, magma generation and the intrusion of low-Ca S-type granite plutons (*e.g.,* Sinceni and Mpuluzi granites) and associated tin-bearing pegmatites, as well as related hydrothermal fluid flow and alteration of greenstone belt lithologies, *e.g.,* in the Dwalile Greenstone Belt, along dextral transtensionally reactivated intracratonic suture zones at ~3.09-3.05 Ga (*cf.,* Maphalala & Kröner, 1993; Wendt *et al.*, 1993; Meyer *et al.*, 1994; Ishihara *et al.*, 2002) (Appendix 20-A).

Along the northern margin of the proto-Kaapvaal-Grunehogna Craton, an oceanic island-arc/back-arc basin complex develops contemporaneously above the active subduction zone, representing the protoliths to the lithologies comprising the Murchison Greenstone Belt. Island-arc magmatism occurs in the form of felsic volcanism (*i.e.,* Rubbervale Formation) and associated granitoid plutonism (*i.e.,* Maranda batholith), whereas volcano-sedimentary sequences (*i.e.,* Weigel, Mackop, La France formations) and VMS-style Cu-Zn deposits accumulate within the adjacent epicratonic back-arc basin at ~3.09-2.98 Ga (*cf.,* Vearncombe, 1986, 1988, 1991, 1992; Vearncombe *et al.*, 1987, 1988, 1992; Brandl & Kröner, 1993; Brandl *et al.*, 1996; Poujol, *et al.*, 1996, 1997; Poujol & Robb, 1999) (Appendix 20-A).

NW-SE directed compressive far field stress, most likely induced into the proto-Kaapvaal-Grunehogna Craton by drag of the subducted oceanic crustal slab along the base of the lithosphere of the overriding craton, which causes the tectonic reactivation of intracratonic Mesoarchaean sutures to sinistral or dextral strike-slip shear zones, depending on their strike orientation relative to the induced maximum compressive stress field axis (σ_1) (Appendix 20-A).

As a result of combined dextral and sinistral strike-slip kinematics along the east-west and north-south striking Magaliesburg-Barberton and Trompsburg-Gaborone suture zones, respectively, the Dominion rift forms either as an intracratonic tectonic escape basin, or as an intracratonic, failed, transtensional back-arc basin to the south of the developing Andean-type magmatic-arc (*cf.,* Bickle & Eriksson, 1982; Tankard *et al.*, 1982; Burke *et al.*, 1986; Crow & Condie, 1987; Clendenin *et al.*, 1988a; Marsh *et al.*, 1989; Stanistreet & McCarthy, 1991; Jackson, 1992, 1994). Rifting between the transtensionally reactivated suture zones leads to the formation of a NNE-SSW striking, westerly dipping, listric, crustal fault system (*e.g.,* Clendenin *et al.*, 1990) to the southeast of the intersection point between, and thereby possibly interlinking, both sutures (Appendix 20-A).

Initial rift-controlled fluvial sedimentation (*i.e.,* Rhenosterspruit Formation) unconformably over Mesoarchaean TTG gneiss-greenstone basement starts at ~3.09 Ga and is terminated by the extrusion of bimodal calc-alkaline volcanics (*i.e.,* initially basaltic andesites derived by partial melting of an upper mantle source without contamination by continental crust, followed by rhyolites derived through direct melting of lower crust) and pyroclastics of the Rhenosterhoek and Syferfontein formations at ~3.074 Ga (*e.g.,* Marsh *et al.*, 1989; Robb *et al.*, 1989, 1990; Clendenin *et al.*, 1990; Jackson, 1992, 1994; Armstrong *et al.*, 1991), and accompanied by the intrusion of comagmatic pre-, syn- and post-Dominion Group I-type granites (*e.g.,* Westerdam, Ottosdal-Coligny and De Pan granites) at ~3.086-3.015 Ga (*e.g.,* Armstrong *et al.*, 1991; Robb *et al.*, 1992; Barton *et al.*, 1999), both as part of the developing intracratonic magmatic-arc.

Felsic, calc-alkaline volcanics extrude along the rifted western continental margin of the Kaapvaal-Grunehogna proto-Craton at ~3.1-3.07 Ga (*cf.,* Robb, 1991; Robb *et al.*, 1991; Poujol *et al.*, 2001; Hirner *et al.*, 2001), representing stratigraphic equivalents to felsic volcanics of the Rhenosterhoek Formation (extruding within the Dominion Group basin) and the comagmatic extrusive phase to syn-Dominion Group I-type granites as part of the developing intracratonic magmatic arc (Appendix 20-A).

Penecontemporaneous crustal extension within the Pietersburg Terrane at ~3.1-2.98 Ga causes mafic volcanism and comagmatic tonalitic-trondhjemitic plutonism (*e.g.,* Makhutswi granitoid, Harmony granite, Vaalpenskraal-type trondhjemite) as well as deposition of clastic sediments (*i.e.,* shales, BIFs, arkoses, sandstones, greywackes) within developing intracontinental rifts (Appendix 20-A). These supracrustal rift-sequences are derived by weathering and erosion of ~3.71-3.4 Ga old TTG/greenstone basement and the penecontemporaneously evolving tonalities and trondhjemites, and represent the protoliths to the greenstone remnants presently preserved within the northern Kaapvaal Craton (including area of future Southern Marginal Zone) (*cf.* Brandl & Kröner, 1993; Poujol & Robb, 1999; Kreissig *et al.*, 1999; Passeraub *et al.*, 1999; Anhaeusser & Poujol, 2004).

Coeval lithospheric extension within the Limpopo Central Zone Terrane, situated north of a possible oceanic spreading centre, leads to the intrusion of basaltic (tholeiitic) dykes at ~3.1-3.0 Ga (*e.g.,* Barton *et al.*, 1977, 1990, 2003), possibly representing feeders to continental flood basalts that might have covered once large areas of the TTG gneiss basement of the Mesoarchaean terrane (Appendix 20-A).

Continued NW-SE convergence between the Pietersburg Terrane and Kaapvaal-Grunehogna proto-Craton leads to closure of the intervening Murchison oceanic basin and culminates in the oblique continent-continent collision between both cratonic fragments along the Thabazimbi-Murchison suture zone at ~2.98 Ga, representing the beginning of the Murchison Orogeny (Appendix 20-B).

The oceanic island-arc/back-arc basin complex becomes accreted onto the northern margin of the Kaapvaal-Grunehogna proto-Craton, thereby experiencing intense compressional deformation (D_1) and metamorphism

(M_1), which is accompanied by the intrusion of syn- to late-orogenic granitoids (*e.g.,* Discovery Granite and Maranda Granodiorite of Maranda Batholith) and related hydrothermal focussed fluid flow and associated epigenetic structurally controlled Mo-W-Be-Sb-Au-B-Hg mineralisation along the Murchison suture zone (*cf.,* Vearncombe, 1986, 1988, 1991, 1992; Vearncombe *et al.*, 1987, 1988, 1992; Brandl & Kröner, 1993; Brandl *et al.*, 1996; Poujol, *et al.*, 1996, 1997; Poujol & Robb, 1999) (Appendix 20-B).

During the early stages of oblique continental collision between the Pietersburg Terrane and Kaapvaal-Grunehogna proto-Craton along the Thabazimbi-Murchison suture zone at ~2.98-2.96 Ga, the Mesoarchaean Pietersburg-Giyani suture zone becomes dextral transpressively reactivated and the site of early (Murchison) orogenic intrusion of syntectonic granites and hypabyssal quartz-/feldspar-porphyries and associated hydrothermal fluid flow/alteration within the Mesoarchaean TTG gneiss-greenstone basement and basal ultramafic-mafic extrusives/intrusives of Pietersburg Greenstone Belt, as well as the location of comagmatic felsic volcanism of the Ysterberg Formation unconformably above the Mesoarchaean TTG gneiss-greenstone basement (Appendix 20-B). A northwest-verging fold-and-thrust belt and associated peripheral foreland basin develops penecontemporaneously with the synorogenic magmatism within the Pietersburg Terrane at ~2.97-2.95 Ga. Progressive tectonic uplift and erosion of the Mesoarchaean metamorphosed and mixed granitoid gneiss-greenstone basement of the most southeastern part of the Pietersburg Terrane leads further north within the developing foreland basin to the deposition of molasses-type deposits (*i.e.,* conglomerates, greywackes and shales) of the Uitkyk Formation unconformably over the slightly earlier (~2.97-2.96 Ga) deposited, deformed and metamorphosed felsic volcanics of the Ysterberg Formation and the older basal mafic-ultramafic extrusive and intrusive rocks of the Pietersburg Greenstone Belt, as well as of the Mesoarchaean TTG gneiss basement of the Pietersburg Terrane at ~2.96-2.95 Ga (*cf.,* de Wit, 1991; de Wit *et al.*, 1993; Kröner *et al.*, 2000) (Appendix 20-B).

The basal extrusive/intrusive units of the Pietersburg and Giyani greenstone belts undergo initially minor deformation during D_1 (*i.e.,* openly folded along northeast-southwest trending axes), progressing to intense northwest-verging thrust deformation during D_2, which was accompanied by greenschist- to lower amphibolite-facies grade metamorphism (M_1) (Jones, 1989; de Wit *et al.*, 1992b; Brandl & de Wit, 1996).

D_1-D_2 deformation (*i.e.,* northwest-verging folding and thrusting) effects also the Mesoarchaean granitoid-gneiss basement and unconformably overlying ~3.1-2.98 Ga old volcano-sedimentary supracrustals (*i.e.,* lateral equivalents to lithologies of Pietersburg and Giyani greenstone belts) within the northern part of the Pietersburg Terrane (*i.e.,* including the area of the future Southern Marginal Zone), which leads to intense crustal thickening and amphibolite-granulite facies grade metamorphism (M_1), and is accompanied by the intrusion of synkinematic tonalities, trondhjemites, granodiorites and pegmatites (Appendix 20-B).

South of the Thabazimbi-Murchison suture zone within the western Kaapvaal-Grunehogna proto-Craton, NW-SE oriented compressive far field stress leads initially to intense transpressive reactivation of intracratonic Mesoarchaean suture zones and the compressive ductile deformation (*i.e.,* southeasterly vergent folding and thrusting (reactivating the basement-Dominion Group contact) of the northern Dominion Group depository (*i.e.,* positive inversion of Dominion Group Basin; *cf.* Van der Merwe, 1994) and the area of the intracratonic magmatic arc in general at ~2.98 Ga (Appendix 20-B).

Subsequently, NW-SE oriented compressive far field stress initiates regional NE-SW oriented crustal extension across the central and southern Kaapvaal-Grunehogna proto-Craton, leading to the formation of the NW-trending Pongola rift as an intracratonic, impactogenal rift, which is accompanied by the intrusion of

the NW-SE striking calc-alkaline, basaltic-andesitic Badplaas-Barberton feeder dyke swarm and gabbro (Piet Retief Suite) and granophyre (Hlelo Suite) of the layered Usushwana Complex along active rift faults and the extrusion of the comagmatic calc-alkaline, basaltic-andesitic Nsuze Group volcanics at ~2.98-2.965 Ga (*cf.*, Armstrong, 1980; Burke *et al.*, 1985; Armstrong *et al.*, 1986; Hunter & Reid, 1987; Hegner *et al.*, 1984; 1994; Havenga, 1996; Uken & Watkeys, 1997; Nhleko, 2003; Olsson *et al.*, 2010; Klausen *et al.*, 2010; Lubnina *et al.*, 2010; Maré & Fourie, 2012; Mukasa *et al.*, 2013; Gumsley *et al.*, 2015), as well as by the intermittent, episodic deposition of continental and marine transgressive (from south and east) sediments (*i.e.,* quartzite, conglomerate, diamictite, siltstone, shale, carbonate) within the intracratonic rift basin unconformably over Mesoarchaean TTG gneiss-greenstone basement (*cf.,* Matthews, 1989; De Beer & Eglington, 1991; Cole & Beukes, 1995; Nhleko, 2003). Coeval granites associated with volcanism within the Nsuze Group include the 2973-2960 Ma Hlatikulu and 2981-2961 Ma Nhlangano plutons (Mukasa *et al.*, 2013; Hofmann *et al.*, 2015), which might reflect increased regional crustal anataxis during a period of rifting-related mantle melting beneath the Pongola impactogenal rift (Appendix 20-B).

Subsequent to continental collision and accretion of the Pietersburg Terrane along the northern margin of the Kaapvaal-Grunehogna proto-Craton during the Murchison Orogeny, which resulted in the assemblage of the Swazi Subprovince of the Kaapvaal Craton and in the formation of a fertile (Au-U mineralised; *cf.,* Kirk *et al.*, 2002) intracratonic magmatic arc province to the north and northwest of the future Witwatersrand Basin by ~2.97 Ga, several subduction zones appear to develop penecontemporaneously around the Kaapvaal-Grunehogna proto-Craton and represent the initial stages of numerous Neoarchaean orogenic cycles (Appendix 20-C*), i.e.*, the Limpopo Orogenic Cycle / Phase 1 (~2.97-2.81 Ga) and Phase 2 (~2.81-2.64 Ga), Bengal Orogenic Cycle (~2.97-2.87 Ga), and Kraaipan-Vaalbara Orogenic Cycle (~2.95-2.81 Ga).

4.2.1.2 LIMPOPO OROGENIC CYCLE/PHASE 1 (~2.97-2.81 GA)

The Limpopo orogenic cycle commences at ~2.97 Ga with the initiation of southwesterly and westerly, shallow subduction of oceanic lithosphere beneath the northern proto-Kaapvaal-Grunehogna Craton and West Dharwar-Antongil Craton (the later defined as combined Mesoarchaean craton by *e.g.,* Agrawal *et al.*, 1992; Collins, 2000; Collins *et al.*, 2001) respectively (Appendix 20-C).

Southwesterly subduction of oceanic lithosphere beneath the northeastern Kaapvaal-Grunehogna proto-Craton initiates the closure of the Limpopo oceanic basin between the Limpopo Central Zone Terrane and Kaapvaal-Grunehogna proto-Craton and represents the beginning of the Limpopo orogenic cycle at ~2.97 Ga (Appendix 20-C). Melting of the subducted oceanic lithospheric slab and magmatic under-/intraplating causes the development of an intracratonic magmatic-arc within the northern Kaapvaal-Grunehogna proto-Craton, which is evident as magmatism in the form of granitoid and comagmatic pegmatite intrusions (*e.g.,* Maranda granodiorite, Melkboomfontein and Mosokgeme granites, Voster Granite Suite (Willie, Baderoukwe and Lekkersmaak granites)) and associated hydrothermal fluid flow/alteration within the ~3.75-2.95 Ga old TTG gneiss-greenstone basement predominantly along the tectonically reactivated and thermally weakened Pietersburg and Murchison suture zones (*cf.* Brandl & Kröner, 1993; Poujol *et al.*, 1996, 1997; Poujol & Robb, 1999; Kröner *et al.*, 2000; Poujol, 2001) and of the Makoppa-type monzogranites in the Makoppa dome area (*cf.* Anhaeusser & Poujol, 2004) at ~2.89-2.81 Ga (Appendices 20-C & 20-D).

Drag of the subducted oceanic crustal slab along the lithospheric base of the overriding cratons induces NE-SW directed compressive far field stress into the Kaapvaal-Grunehogna proto-Craton and causes the

tectonic reactivation of fundamental intracratonic Mesoarchaean sutures to sinistral or dextral strike- to oblique-slip shear zones, depending on their strike orientation relative to the induced maximum compressive stress field axis (σ_1) (Appendix 20-C). The resulting craton-wide transpressional tectonic regime leads to large-scale, SE-directed escape-tectonics, subsidence, and the formation of a large tectonic escape basin (*i.e.,* Witwatersrand Basin) in the area between the Magaliesberg-Barberton, Brandfort-Tugela and Colesberg-Mafikeng suture zones at ~2.97-2.87 Ga, which represents the depository for the West Rand Group and Johannesburg Subgroup (lower Central Rand Group) of the Witwatersrand Supergroup, the former being deposited unconformably above deformed/metamorphosed Dominion Group (Van der Merwe, 1994) and Mesoarchaean TTG gneiss-greenstone basement. Associated with the SE-directed escape (wrench) tectonics along these palaeosuture zones is a tilt of the depositional surface towards southeast and the development of a set of syndepositional, NW-SE trending, *en échelon*, low-amplitude folds or warps within and throughout the depository, which form adjacent to the major lithospheric shear zones and control the basin-internal drainage system and river-dominated sediment dispersal (*e.g.,* McCarthy *et al.*, 1986) (Appendix 20-C). Wrench fault-related, southerly verging and upward-flattening high-angle oblique-reverse faults (*i.e.,* positive "flower structures") form along the northern margin of the Witwatersrand tectonic escape basin in response to transpressive sinistral wrench tectonics along the Rietfontein Fault (*e.g.,* Stanistreet *et al.*, 1986) and Magaliesburg-Barberton suture zone, causing uplift of the Mesoarchaean basement and a steep to locally overturned orientation of the Witwatersrand Supergroup strata to the north and south of these sinistral transpressive reactivated fundamental shear zones respectively.

The sinistral and dextral transpressional tectonics along the northern and western margins of the Witwatersrand Basin respectively occur in discrete pulses, causing episodic uplift and erosion of the adjacent fertile (*i.e.,* Au-U mineralised mainly during Murchison Orogenic Cycle at ~3.1-2.97 Ga) Mesoarchaean TTG gneiss-greenstone basement as evident by the development of numerous angular intra-formational unconformities within the depository. Each unconformity-bounded sequence of the West Rand Group-Johannesburg Subgroup time-interval represents a geomorphological cycle, each beginning with a basal conglomeritic horizon and upward fining into quartzites and shales (*e.g.,* Winter & Brink, 1991). In each case, tectonic uplift of the source area introduces new clastic material to be eroded from the provenance area and deposited as alluvial fans along the shear zone-controlled margins of the basin, followed by the recession of the fans and retreat/denudation of the uplifted source area during cessation of tectonism. In this respect, erosion of Mesoarchaean TTG gneiss-greenstone basement and sedimentary influx (including detrital gold and uraninite) into the depository of the lower Witwatersrand Supergroup occur mainly from peripheral source areas situated to the north and west of the basin (*e.g.,* Poujol *et al.*, 1996, 1999; Kirk *et al.*, 2002), and during relatively short time-intervals from a southern provenance area (discussed further below). At the various basin entry points, sediments are deposited with a radial dispersal pattern as southerly and easterly directed alluvial fans along the northern and western basin margins, respectively. A few kilometres further into the depository, namely in the transition zone between distal fan area and adjacent southeasterly inclined longitudinal braid plain region, the drainage system and river-dominated sediment dispersal swing distinctly into a southeasterly direction, following syndepositionally formed NW-SE trending palaeolows down on a southeasterly inclined braid plain.

Episodic marine transgressions from an open ocean to the west and south of the Witwatersrand depository lead to the interaction of marine shelf and tidal environments with river-dominated fan deltas during the deposition of the West Rand Group and Johannesburg Subgroup. Whereas the lower part of the West Rand Group (laterally extensive fine-grained clastic and chemical sediments, *i.e.,* BIFs, shales, siltstones,

quartz arenites, greywackes, arkoses) is deposited predominantly under shallow marine conditions, deposition of the upper West Rand Group (arenites, greywackes, conglomerates and shales) occurs in more diverse sedimentary environments, ranging from marine, transitional marine to terrestrial, and dominantly subaerial clastic sedimentation during Johannesburg Subgroup time (*e.g.,* Camden-Smith, 1980; Eriksson *et al.*, 1981; Tankard *et al.*, 1982; Stanistreet & McCarthy, 1991; Beukes & Cairncross, 1991; Watchorn & O'Brien, 1991; Winter & Brink, 1991; de Wit *et al.*, 1992a). The general upward shallowing and coarsening of the West Rand Group-Johannesburg Subgroup sequence, as well as the development of progressively more unconformities toward the proximal basin margins, is the result of ocean basin closure and orogenic activity along the southern and eastern margins of the proto-Kaapvaal Craton during the Bengal Orogeny at ~2.92-2.87 Ga (see below) (Appendix 20-C).

In the eastern portion of the greater Witwatersrand depository within the area of the earlier formed impactogenal Pongola (Nsuze) rift basin, the lower Mozaan and Godwan groups (representing stratigraphic equivalents to the West Rand Group and lower Johannesburg Subgroup (*e.g.,* Beukes & Cairncross, 1991; Nelson *et al.*, 1995; Nhleko, 2003) are deposited penecontemporaneously at ~2.97-2.87 Ga during the thermal subsidence stage, following crustal extension and rift development at ~2.98-2.97 Ga (Appendix 20-C).

Shallow westward subduction and melting of hydrated oceanic crustal material beneath the West Dharwar-Antongil Craton, as well as under-/intraplating of mafic-ultramafic magmas (derived from the subducted oceanic crustal slab) into its lithosphere, result in crustal extension and the development of an epicratonic magmatic arc along the eastern margin of the craton, and of an extensive intracratonic back-arc basin, covering most of the West Dharwar-Antongil Craton at ~2.94 Ga (Appendix 20-C). Intracratonic back-arc basin development is accompanied by initial terrestrial fluvial sedimentation (basal oligomictic conglomerates followed by overlying quartzites) and extrusion of subaerial mafic volcanics (basalts) and pyroclastics of the Kalasapura, Allampur and Santavery Formations (*i.e.,* Lower to Middle Bababudan Group, Lower Dharwar Supergroup) (*cf.* Srinivasan & Ojakangar, 1986) unconformably over a ~3.0 Ga old palaeosol cover and underlying Mesoarchaean (~3.5-3.0 Ga) TTG gneiss-greenstone basement within the West Dharwar Craton (*cf.* Chardon *et al.*, 1998) at ~2.94-2.87 Ga.

Continued subduction and magmatic under-/intraplating beneath the West Dharwar-Antongil Craton at ~2.87-2.72 Ga intensifies crustal extension and causes a widening of the intracratonic forming back-arc basin. This results in a marine transgression into the intracratonic back-arc basin and sedimentation of progressively more marine deposits (BIFs and intercalated argillites and greywackes) of the Mulaingiri, Jagar and Mundre Formations (*i.e.,* Upper Bababudan Group, Lower Dharwar Supergroup). Accompanying volcanism within the craton-marginally forming magmatic arc becomes increasingly bimodal with the introduction of felsic components, indicating progressive maturation of the magmatic arc (Appendices 20-D & 20-E).

4.2.1.3 BENGAL OROGENIC CYCLE (~2.97-2.87 GA)

The initiation of southeastward, shallow subduction of oceanic lithosphere beneath the Singhbhum-Bastar-East Dharwar Craton, situated to the southeast of the Kaapvaal-Grunehogna proto-Craton, represents the time of incipient closure of the intervening Bengal oceanic basin between both cratons and marks the beginning of the Bengal orogenic cycle at ~2.97 Ga (Appendix 20-B).

Subduction-related melting of hydrated oceanic crustal material beneath the Singhbhum-Bastar-East Dharwar Craton results in the development of an intracratonic magmatic arc by under- and intraplating of

mafic-ultramafic magmas into the lithosphere of the Singhbhum-Bastar-East Dharwar Craton (derived from the subducted oceanic crustal slab), as well as in lithospheric extension, crustal thinning, and the formation of an adjacent intracratonic back-arc basin (*cf.* Bhattacharji & Saha, 1990; Mukhopadhayay, 1994; Sengupta *et al.*, 1997; Rajamani, 1990; Arora *et al.*, 1995) (Appendix 20-B).

Progressive widening and deepening of the intracratonic back-arc basin at ~2.97-2.87 Ga is accompanied by a marine transgression, resulting in deposition of mainly shallow marine fine siliciclastic sediments (phyllite, shale, chert, Fe-rich jasper and quartzite, minor dolomite and conglomerate) with interbedded mafic-ultramafic, calc-alkaline volcanics (tholeiitic basalts, minor komatiites) of the Younger Iron Ore and Sukma groups unconformably over Neo-/Mesoarchaean (>3.0 Ga) TTG gneiss basement within the Singhbhum and Bastar cratons respectively (*cf.* Sakar, 1982; Bhattacharji & Saha, 1990; Ghosh *et al.*, 1992; Saha, 1994; Mukhopadhayay, 1994; Sengupta *et al.*, 1997; Ramakrishnan, 1990) (Appendix 20-C).

Complete closure of the Bengal oceanic basin, followed by continent-continent collision and accretion of the Singhbhum-Bastar-East Dharwar Craton along the southern and eastern margins of the Kaapvaal-Grunehogna proto-Craton at ~2.92-2.87 Ga, introduces orogenic activity to both cratons during the Bengal Orogeny and results in the formation of the supercontinent "Bengalia". NW-SE compressive far field stress induced into the southern Kaapvaal-Grunehogna proto-Craton results in the extensional reactivation of the NW/SE-striking Pongola rift system and intense lithospheric extension/transtension and active rifting within the central part of the craton (*i.e.,* area of greater Witwatersrand Basin) during the initial stage of continental collision at ~2.92-2.9 Ga, which is accompanied by extrusion of the Crown lavas (*i.e.,* tholeiitic basalts) within the West Rand/Lower Mozaan Group depository (*cf.* Armstrong *et al.*, 1991) and local extensional faulting, block tilting and peneplanation (*cf.* Azazi deformation event of Manzi *et al.* (2013)).

Subsequent orogenic activity causes the dextral transpressive reactivation of the Brandfort-Tugela suture zone and episodic tectonic uplift of the Mesoarchaean TTG gneiss-greenstone basement along and to the south of this Mesoarchaean suture zone during relatively short intermittent time-intervals at ~2.9-2.87 Ga. Associated with the compressive strike- to oblique-slip (wrench) movements along the Brandfort-Tugela suture zone is the development of a set of syndepositional, NE-SW trending, *en échelon*, low-amplitude folds or warps adjacent to the palaeosuture zone which control during short intermitted episodes the basin-internal drainage system and river-dominated sediment dispersal during deposition of the Steyn, Alma and 'B' placers within the extreme southern part of the Witwatersrand depository (Appendix 20-C). Within the southeastern Kaapvaal-Grunehogna proto-Craton, NW-verging thrust tectonics (*i.e.,* D_2-deformation) within the Pongola subbasin occur penecontemporaneously during deposition of the upper portions of the lower Mozaan Group (*i.e.,* stratigraphically equivalent to Johannesburg Subgroup) at ~2.9 Ga (*cf.* Gold, 1993; Hunter & Gold, 1993) (Appendix 20-C).

Within the Indian cratons, compressive stresses induced into the continental lithosphere during the Bengal Orogeny causes regionally extensive regressive deposition of molasses-type lithologies (conglomerates, quartzites, shales) of the Bengpal Group (*cf.* Ramakrishnan, 1990), accumulating within a foreland basin ahead of a southerly verging fold-thrust belt unconformably above supracrustals of the Sukma Group and Mesoarchaean (~3.5 Ga) TTG gneiss basement (Appendices 20-C & 20-D).

4.2.1.4 KRAAIPAN-VAALBARA OROGENIC CYCLE (~2.95-2.81 GA)

Penecontemporaneously with subduction processes along the northern, southern and eastern margins of the Kaapvaal-Grunehogna proto-Craton is the initiation of shallow, westward subduction of oceanic lithosphere beneath the Kraaipan-Narryer-Pilbara Craton at ~2.95 Ga, which leads to the convergence between both cratons and closure of the intervening Kraaipan-Vaalbara oceanic basin, and marks the beginning of the Kraaipan-Vaalbara Orogenic Cycle and final amalgamation process of the Kaapvaal-Grunehogna Craton (Appendix 20-C).

Subduction and melting of hydrated oceanic crustal material beneath the Kraaipan-Narryer-Pilbara Craton during the Kraaipan-Vaalbara Orogenic Cycle at ~2.95-2.87 Ga results in crustal extension and the development of an intracratonic magmatic arc/back-arc basin complex by under- and intraplating of mafic-ultramafic magmas (derived from the subducted oceanic crustal slab) into the lithosphere of the Kraaipan-Narryer-Pilbara Craton. Magmatic under- and intraplating introduces a higher geothermal gradient within and below the overriding craton leading to partial melting and consequent Re-depletion of the older subcontinental lithospheric mantle (*cf*. Richardson *et al.*, 2001, Carlson *et al.*, 1999) and the generation of mixed mantle/crustal-derived (I- and S-type) granitoid magmas intruding into the Kraaipan-Narryer-Pilbara Craton (Appendix 20-C).

Within the Kraaipan Craton, this leads to the emplacement of granodiorites-adamellites and leuco-trondhjemitic dykes, as well as to migmatisation of the Mesoarchaean (>3.25 Ga) TTG gneiss-greenstone basement at ~2.95-2.9 Ga (*cf.* Drennan, 1988; Drennan *et al.*, 1990; Robb *et al.*, 1992; Hoal *et al.*, 1995; Kamo *et al.*, 1995; McCourt *et al.*, 2000; Poujol *et al.*, 2000, 2001a, 2002, 2003; Gericke, 2001; Reimold *et al.*, 2002) (Appendix 20-C).

Within the eastern Pilbara Craton (*i.e.,* the northern part of the craton at present geographic position), crustal extension and the development of the Negri intracratonic back-arc basin is associated with basaltic volcanism, the emplacement of subvolcanic mafic-ultramafic layered intrusions (Millindinna Suite), two phases of granitoid plutons, sills and dykes, and widespread thermotectonic alteration (Krapež & Eisenlohr, 1998) (Appendix 20-C).

Complete closure of the Kraaipan-Vaalbara oceanic basin, followed by continent-continent collision and accretion of the Kraaipan-Narryer-Pilbara Craton along the western edge of Bengalia (= amalgamated Kaapvaal-Grunehogna-Singhbhum-Bastar-East Dharwar Craton) at ~2.87-2.81 Ga, introduces orogenic activity to both cratons during the Kraaipan-Vaalbara Orogeny and results in the formation of the supercontinent “Vaalbara” (*cf.* Cheney *et al.*, 1988; Cheney, 1996).

Within the eastern Pilbara Craton, east-west oriented compressive far field stress conditions, induced by continental collision between the Pilbara and Singhbhum cratons, result in regional lithospheric compression and orogenic folding in a hinterland fold-thrust belt, which is followed by late-stage dextral convergence and uplift (*cf.* Krapež & Eisenlohr, 1998).

Similarly, continental collision between the Kraaipan Craton and Swazi Subprovince of the Kaapvaal-Grunehogna proto-Craton along the Colesberg-Mafikeng suture zone at ~2.87-2.81 Ga induces east-west oriented compressive far field stress into both cratonic regions, resulting in the development of easterly and westerly verging foreland fold-thrust belts and associated peripheral Turffontein Subgroup and retroarc Griquastad foreland basins in the western parts of the Kaapvaal-Grunehogna and Kraaipan cratons respectively (*cf.* Burke *et al.*, 1986; Winter, 1987; Roering *et al.*, 1990) (Appendix 20-D).

In addition to the developing craton-inward migrating thin-skinned fold-thrust belts, Mesoarchaean suture zones within both cratons become compressively/transpressively reactivated to oblique-reserve or strike-slip shear zones, depending on their strike orientation relative to the induced east-west oriented compressive far field stresses (Appendix 20-D).

Continental collision, suturing and orogenic activity at ~2.87-2.81 Ga is accompanied by the intrusion of syn- to late-collisional, peraluminous, uraniferous, I-type granodiorites and adamellites and associated upper mantle-derived hydrothermal fluid circulation along the Colesberg-Mafikeng suture zone, resulting in the formation of hydrothermally altered granitoids (HAGS) (*e.g.,* Drennan *et al.*, 1990; Robb *et al.*, 1992; Anhaeusser & Walraven, 1999; McCourt *et al.*, 2000; Poujol *et al.*, 2000, 2001a, 2002, 2003) and epigenetic gold mineralisation within the Kraaipan and Amalia greenstone belts (Appendix 20-D).

Comparatively less intense NE-SW oriented compressive far field stress (induced into the Kaapvaal-Grunehogna proto-Craton along its northern margin by southwesterly directed shallow subduction of oceanic lithosphere and slab-drag along its lithospheric base since the beginning of the Limpopo orogenic cycle at ~2.97 Ga) becomes subdued and suspended in the western part of the Kaapvaal-Grunehogna proto-Craton during the Kraaipan-Vaalbara Orogeny, but remains operational in the eastern part. As a result of the new stress field conditions within the Kaapvaal-Grunehogna proto-Craton, craton-wide NE-SW transpression and associated development of the lower Witwatersrand Basin as an intracratonic tectonic escape basin during West Rand Group and Johannesburg Subgroup time at ~2.97-2.86 Ga, changes to E-W compression and the formation of the upper Witwatersrand Basin (*i.e.,* Turffontein Subgroup depository) as an craton-inward migrating peripheral foreland basin ahead of an easterly verging fold-and-thrust belt. The development of the easterly verging fold-and-thrust belt is facilitated between strike-slip reactivated E-W and NE-SW striking palaeosuture zones, acting as lateral ramps.

In the foreland of the E-migrating fold-and-thrust belt, *i.e.*, to the east of the western margin of the Witwatersrand Basin across the eastern Kaapvaal Craton, Kraaipan-Vaalbara Orogeny-induced E-directed far field stress causes crustal extensional, leading to rifting and mafic (basaltic-andesitic-dacitic) magmatism across the central and western Witwatersrand Basin, extending to the Pongola Basin in the southeastern Kaapvaal Craton. Mafic magmatism includes the extrusion of the Bird Member lavas across the central and eastern Witwatersrand Basin at ~2.87 Ga (*cf.*, Beukes & Cairncross 1991; Gumsley *et al.*, 2013), the intrusion of mafic-ultramafic sills of the Hlagothi Layered Complex into the Nsuze Group, and potentially the layered mafic-ultramafic Thole Suite and mafic sills pervasive throughout the Mozaan Group possibly coeval with the Tobolsk and Gabela Formation lavas within in the upper Pongola Supergroup (Gumsley *et al.*, 2013, 2015), the Hlelo Suite granophyres of the Usushwana Complex (Walraven & Pape, 1994), and dacitic-rhyolitic volcanic rocks and granophyre of the Amsterdam Formation (Gold, 2006) at ~2.87-2.86 Ga.

Upper-mantle derived gold-bearing hydrothermal fluids (most likely generated by subduction of sediments) are transported upwards into crustal levels along the mantle-tapping Colesberg-Mafikeng suture zone and then focused along the developing easterly verging thrust faults directly into the sedimentary deposits of the western and central Witwatersrand Basin, resulting in epigenetic gold deposition preferably along tectonically reactivated litho-stratigraphic unconformities within conglomeratic horizons of the earlier deposited Johannesburg Subgroup and developing Turffontein Subgroup basins. Easterly migrating fold-thrust belt tectonics and associated hydrothermal fluid flow cause also epigenetic gold mineralisation within older lithologies situated to the west of the developing Turffontein Subgroup peripheral foreland basin, *i.e.,* within Mesoarchaean TTG gneiss-greenstone basement and volcano-sedimentary deposits of Dominion

and West Rand groups, hence resulting in the formation of a fertile western hinterland to the developing peripheral foreland basin coeval with direct epigenetic gold mineralisation within the Central Rand Group deposits. Tectonic uplift of the western hinterland and margin to the Turffontein Subgroup foreland basin causes erosion and reworking of Mesoarchaean TTG gneiss-greenstone basement and Dominion Group, West Rand Group and Johannesburg Subgroup deposits and their accumulation as molasses-type deposits within the peripheral foreland basin during Turffontein Subgroup-time. The erosion/cannibalisation of previously deposited, auriferous Witwatersrand sediments introduces a component of detrital gold to deposits of the Turffontein Subgroup and hence probably contributes significantly to enhancing the gold grades of these younger Witwatersrand placers (*cf.* Blenkinsop & Eriksson, 1995) (Appendix 20-D).

Easterly advancing major fan complexes form along the thrust fault-controlled western margin of the depository, with comparatively smaller westerly and easterly dispersing fan complexes developing on the western and eastern limbs of N-S trending intra-basinal palaeohighs, which form due to low-amplitude folding immediately to the east of the thrust front. Typically radial sediment dispersal patterns within the basin marginal fan complexes swing into linear, southerly dispersal directions within the depository, which are controlled by the intra-basinal warps and a general southerly inclined, longitudinal alluvial braid plain.

Within the central and eastern parts of the Turffontein Subgroup depository (*i.e.,* Central Rand, East Rand and Evander goldfields), input of clastic sediments continues to take place along the tectonically (sinistral strike-slip) reactivated Magaliesburg-Barberton suture zone forming the northern basin margin, with the terrestrial sediments being derived by erosion from a northern source terrain. At various basin entry points, sediments are deposited with a radial dispersal pattern as southerly directed alluvial fans along the northern basin margin. A few kilometres further into the depository, southeasterly sediment dispersal is continuously controlled by NW/SE-trending palaeolows down on a southeasterly inclined braid plain, and not by N-S trending intra-basinal folds or warps that form contemporaneously within the western part of the depository. Due to the absence of easterly migrating fold-thrust tectonics during Turffontein Subgroup-time, hydrothermal fluid flow and associated epigenetic gold mineralisation are less intense in the eastern part of the Turffontein Subgroup basin (*i.e.,* East Rand, South Rand and Evander goldfields), where gold mineralisation in conglomeritic units is predominantly of detrital nature and originally the result of sedimentary processes (Appendix 20-D).

Crustal thickening as a result of NW-directed thrusting and tectonic stacking during the Bengal Orogeny (~2.92-2.87 Ga), as well as of sedimentation during continued thermal subsidence of Nsuze rift at ~2.87-2.84 Ga, causes the generation of anatectic melts in ~3.105-3.074 Ga old TTG basement and their intrusion as post-(D_1)-tectonic, low-Ca, S-type granite plutons (*e.g.,* Mooihoek, Mhlosheni and Godlwayo plutons) and related quartz-porphyry sills into the Pongola Supergroup within the tectonically reactivated Pongola rift basin at ~2.865-2.82 Ga (*e.g.,* Maphalala & Kröner, 1993; Robb *et al.*, 1993; Meyer *et al.*, 1994; Gutzmer *et al.*, 1993; Ishihara *et al.*, 2002).

4.2.1.5 LIMPOPO OROGENIC CYCLE/PHASE 2 (~2.81-2.64 GA)

During continental collision and amalgamation of the Kraaipan-Narryer-Pilbara Craton with Bengalia along the Colesberg-Mafikeng suture zone to form the Kaapvaal-Grunehogna Craton and Vaalbara at ~2.87-2.81 Ga, approximately east-west compressive far field stress conditions dominated in both cratons and resulted in the formation of westerly and easterly verging, thin-skinned fold-thrust belt tectonics during the Kraaipan-

Vaalbara Orogeny within the eastern Kraaipan-Pilbara and western Kaapvaal-Grunehogna cratons respectively (Appendix 20-D).

With cessation of east-west-oriented deviatoric far field stress at the end of the Kraaipan-Vaalbara orogenic event at ~2.81 Ga, NE-SW oriented compressive far field stress, initially induced into the northern Kaapvaal-Grunehogna Craton at ~2.97-2.87 Ga (*i.e.,* during Phase 1 of Limpopo orogenic cycle) due to southwesterly directed, shallow subduction of oceanic lithosphere beneath the northern Kaapvaal-Grunehogna proto-Craton and drag of the subducted oceanic crustal slab along the lithospheric base of the overriding craton, becomes again progressively more prevalent as a result of continuous southwesterly subduction and closure of the Limpopo oceanic basin since ~2.97 Ga.

With the beginning of this second phase of the Limpopo orogenic cycle at ~2.81 Ga, intracratonic Mesoarchaean suture zones within the Kaapvaal-Grunehogna Craton experience renewed tectonic reactivation to sinistral or dextral strike- to oblique-slip shear zones, depending on their strike orientation relative to the induced maximum compressive stress field axis (σ_1) (Appendix 20-E). The resulting craton-wide transpressional tectonic regime leads to the formation of sinistral transpressive shear zones splaying from the sinistral strike-/oblique reverse-slip reactivated Thabazimbi-Murchison and Pietersburg-Giyani sutures within the northern part of the Kaapvaal-Grunehogna Craton, accompanied by pegmatite emplacement along the shear zone system (*cf.*, Barton *et al.*, 1986, 1992; De Wit & Roering, 1990; De Wit *et al.*, 1991; Barton & Van Reenen, 1992). In addition, SE-directed escape-tectonics commence in the northern Kaapvaal Craton, thereby originating from the area of intersection between the east-west and north-south striking Thabazimbi-Murchison and Colesberg-Mafikeng suture zones respectively (Appendix 20-E).

Decompression melting of the upper subcontinental mantle along reactivated Archaean suture zones combined with subduction-related magmatic under- and intraplating of mafic magmas and increased heat flow within the lithosphere of the northern Kaapvaal-Grunehogna Craton, results in partial melting of the lower crust, the formation of comagmatic, bimodal, felsic (I-type granitoid) and mafic (gabbroic) magmas and their ascent, emplacement and accompanying hydrothermal fluid flow/alteration within upper crustal levels predominantly along thermally weekend and tectonically reactivated suture zones, and their extrusion as felsic and mafic volcanics within the area of a developing intracratonic magmatic-arc (*e.g.,* Gaborone Igneous Complex with comagmatic extrusives of Kanye and Lobatse Groups, Rooiwater Complex, Mosita and Mpageni granites, Modipe gabbro with comagmatic mafic (basalt) extrusives of the Derdepoort Formation, Wesselbron Rooibokvlei-type granodiorites/monzogranites, main/older granitoid components of Turfloop Batholith) (*cf.,* Sibiya, 1988, Harmer & Von Gruenewaldt, 1991; Robb *et al.*, 1992; Grobler & Walraven, 1993; Moore *et al.*, 1993; Walraven *et al.*, 1994, 1996, Kamo & Davis, 1994; Henderson, 1996; Poujol *et al.*, 1996, 1997, 2001; Mapeo *et al.*, 1998; Wingate, 1998, Henderson *et al.*, 2000; Kröner *et al.*, 2000; Reimold *et al.*, 2002; Schmitz, 2002; Anhaeusser & Poujol, 2004; Mapeo *et al.*, 2004; Denyszyn *et al.*, 2013) at ~2.81-2.75 Ga (Appendix 20-E). The A-type Gaborone Igneous Complex (including the Mmathethe Granite), composed of alkaline felsic volcanics (*i.e.,* rhyolite lavas) of the Kanye Formation, glacio-volcaniclastic sediments of the Lobatse Group, and a bimodal igneous suite of various types of alkaline rapakivi granites, small diorite/granophyre plutons (*e.g.,* Kgoro Complex), and anorthositic gabbro and norite intrusive as ring complexes into the comagmatic extrusive and glacio-volcaniclastic deposits, are emplaced within the intersection area of the Thabazimbi-Murchison and Colesberg-Mafikeng suture zones at ~2.785-2.78 Ga (*cf.,* Crockett, 1971a; Sibiya, 1988; Grobler & Walraven, 1993; Moore *et al.*, 1993; Walraven *et al.*, 1994, 1996; Wingate, 1998; Modie, 2002; Mapeo *et al.*, 1998, 2004), where SE-directed

tectonic escape and intense crustal extension occur. Comagmatic dolerite dyke swarms are emplaced along ENE-WSE striking extensional faults (*cf.,* Aldiss, 1986; Carney *et al.*, 1994; Modisi, 1994, 1995) which form as interlinking extensional structures in the intersection area between both suture zones in response to SE-directed crustal escape and extension (Appendix 20-E).

Further to the south within the central Kaapvaal-Grunehogna Craton, pull-apart rift tectonics (*i.e.,* transtension) initiated contemporaneously between east-west striking, sinistral strike-slip reactivated Mesoarchaean suture zones at ~2.79Ga, result initially in the extensional reactivation and partial inversion of late Central Rand Group thrust zones and the deposition of siliciclastic sediments of the Ventersdorp Conglomerate Formation unconformably over Witwatersrand Supergroup and Meso-/Neoarchaean TTG gneiss basement in half-grabens at ~2.79-2.789 Ga, which form within the hangingwall block of these extensional reactivated thrust zones and Mesoarchaean sutures (Appendix 20-E). Transtensional tectonics and crustal extension intensify and result eventually in the development of interlinking transtensional fault zones within the area of the Witwatersrand Basin, which is accompanied by the intrusion and extrusion of Klipriviersberg Group tholeiitic feeder dykes and lavas respectively at ~2.789-2.75 Ga (cf. Stamsnijder, 2017; Gumsley *et al*., 2020), thereby terminating the deposition of terrigenous sediments of the Ventersdorp Conglomerate Formation (*cf.* McCarthy *et al.*, 1990b; Van der Westhuizen *et al.*, 1991; Armstrong *et al.*, 1991) (Appendix 20-E).

Lithospheric extension, rifting, flood basalt volcanism, high heat flow and hydrothermal activity within the cratonic crust during Klipriviersberg Group time cause the remobilisation, transport and reprecipitation (*i.e.,* hydrothermal overprint) of the predominantly detrital (syngenetic) gold and uranium mineralisation within the Witwatersrand Supergroup (*cf.,* Robb *et al.*,1997; Drennan *et al.*, 1997, 1999).

Oblique NE-SW convergence between the Limpopo Central Zone Terrane (together with the earlier amalgamated Zimbabwe Craton) and the Kaapvaal-Grunehogna Craton leads to complete closure of the Limpopo oceanic basin and subsequent oblique continent-continent collision between both cratonic blocks along the Palala suture zone at ~2.75 Ga. This introduces NE-SW oriented compressive far field stress and orogenic activity to both colliding cratons during the Limpopo Orogeny at ~2.75-2.64 Ga (Appendix 20-G).

South of the collision zone, *i.e.,* along the northern margin of the Kaapvaal-Grunehogna Craton, mid-crustal rocks undergo prograde granulite-facies metamorphism (M_1) and compressive deformation (D_1) at ~2.72-2.69 Ga. Subsequently, progressive SW-vergent folding and thrusting (D_2) lead to the tectonic uplift, decompression and emplacement of the Southern Marginal Zone (= mid-crustal rocks of northern Kaapvaal Craton/Pietersburg Terrane) as nappe complex onto the northern edge of the Kaapvaal Craton along the southwesterly verging basal Hout River Shear (Thrust) Zone and other overlying crustal thrust zones at ~2.69-2.64 Ga, which was accompanied by syn-decompressional retrograde metamorphism (M_2) and rehydration by deep-seated CO_2-dominated fluids of the uplifted and decompressed mid-crustal, high-grade (granulite-facies) gneissic rocks, but prograde metamorphism in the low-grade (greenschist-facies) overthrusted upper crustal rocks of the northern Kaapvaal Craton. Post-collisional sinistral escape tectonics along the Palala suture zone result within the Southern Marginal Zone in post-decompressional ductile-brittle sinistral strike-slip kinematics (D_3) along the SW-vergent thrust zones (developed during the collisional stage) under amphibolite-facies metamorphic conditions (M_3) at ~2.64 Ga (*cf.* Van Reenen, 1986, Van Reenen *et al.*, 1987, 1988; Roering *et al.*, 1992a&b, Smit *et al.*, 1992, 2001; Smit & Van Reenen, 1997; Kreissig *et al.*, 2000, 2001) (Appendix 20-G).

Post-collisional, lateral, westward tectonic escape of the Zimbabwe Craton/Limpopo Central Zone Terrane along the Palala suture zone relative to the Kaapvaal-Grunehogna Craton at ~2.72-2.64 Ga resulted in sinistral transpressional tectonics (*i.e.,* formation of sinistral strike-slip to oblique-reverse slip shear zones) within the Limpopo Central Zone Terrane and northern Kaapvaal-Grunehogna Craton (*cf.* McCourt & Vearncombe, 1987; Broekhuizen *et al.*, 1995; Broekhuizen, 1998) (Appendix 20-G).

Magmatic activity within the Limpopo Central Zone Terrane in the form of ~2.7-2.6 Ga old granitic, granodioritic and enderbitic intrusions (including *e.g.,* the Singelele and Bulai plutons (*e.g.,* Barton *et al.*, 1979b, 1994a; Jaeckel *et al.*, 1997; Holzer *et al.*, 1998; Kröner *et al.*, 1999) was followed by high-grade metamorphism, anatexis and felsic magmatism at ~2.6-2.52 Ga (Holzer *et al.*, 1998)

As a result of crustal thickening, sinistral transpressional tectonics and subsequent rapid isothermal decompression within the northern Kaapvaal-Grunehogna Craton during this tectonic escape phase of the Limpopo Orogeny, appreciable volumes of granitic magma are generated by partial melting of portions of the upper mantle and lower crust in the subducting plate and by hydration and partial melting of lower portions of the over-riding plate. These granitic magmas intrude as syn- (~2.72-2.65 Ga) to late-orogenic (~2.65-2.63 Ga) granitoid plutons (*e.g.,* Matok, Matlala, Lunsklip, Roodepoort, Mashishimala plutons and younger granite plutons of Turfloop batholith) into higher crustal levels, thereby utilising the tectonically reactivated Pietersburg and Murchison palaeosuture zones, the Hout River Shear (Thrust) Zone, and newly formed sinistral strike-slip shear zones to the south of the Southern Marginal Zone. The shear zone-controlled emplacement of granitoid plutons is accompanied by the continuous infiltration and circulation of CO_2-rich, Au- and S-bearing fluids derived by crustal dehydration and by crystallisation of the granitoid magmas, which leads to shear zone-hosted hydrothermal alteration of and gold mineralisation within the newly emplaced granitoids and older lithologies in both the Southern Marginal Zone and northern Kaapvaal Craton at ~2.72-2.64 Ga (*cf.* Barton, 1984; Van Reenen, 1986; Van Reenen *et al.*, 1987, 1988; Barton *et al.*, 1988, 1990, 1992; Smit *et al.*, 1992; Pretorius & Van Reenen, 1992; Kröner *et al.*, 2000; Poujol, 2001) (Appendix 20-G).

South of the northern sector of the Kaapvaal-Grunehogna Craton dominated by sinistral transpressional tectonics, contemporaneous craton-wide NW-SE crustal extension in response to Limpopo Orogeny-related NE-SW compressive far field stress results in the development of the large NE-SW trending Ventersdorp rift basin as an intracratonic impactogenal rift, which becomes infilled with initial terrestrial-fluvial and later shallow marine sediments (*i.e.,* varying from initial clastic sedimentary and intercalated subaqueous basalts and subaerial extruded rhyolites to overlying calcareous mudrocks, dolomites and sandstones) of the mid- and upper Ventersdorp Supergroup (*i.e.,* Platberg and Pniel groups) and stratigraphic equivalents (*i.e.,* Zoetlief, Buffelsfontein, Wolkberg and Groblersdal groups, Mogobane and Wachteenbeetjie formations, Tshwene-Tshwene and Derdepoort belts, as well as lower Vryburg Formation) at ~2.75-2.64 Ga. Sedimentation takes place in discrete fault-related, possibly interconnected basins, either as small and deep (~3km) pull-apart basins along the sinistral strike-slip reactivated Thabazimbi-Murchison suture zone (*i.e.,* Buffelsfontein, Derdepoort and Tshwene-Tshwene depositories), or larger asymmetrical listric-fault bounded rifts (up to 7km deep) associated with the extensional tectonism (*i.e.,* Zoetlief, Wolkberg, Groblersdal, Mogobane, Wachteenbeetjie, Vryburg depositories) (*cf.* Tyler, 1978a, b, 1979 a, b, c; Tankard *et al.*, 1982; Burke *et al.*, 1985; Clendenin *et al.*, 1988b; Hartzer, 1987, 1989, 1994, 1995; R.E. Myers, 1990; Cheney *et al.*, 1990a; Stanistreet & McCarthy, 1991; Bosch, 1992; Bosch *et al.*, 1993; Eriksson *et al.*, 1993b, 1995; J.M. Barton *et al.*, 1995b; McCourt, 1995; Eriksson & Reczko, 1995; Catuneanu & Eriksson, 1999; Tinker *et al.*, 2002; De Wit & Tinker, 2004) (Appendix 20-G).

Within the eastern portion of the Ventersdorp impactogenal rift (*i.e.,* area of the Witwatersrand Basin), not impactogenal rifting but continued pull-apart rift tectonics (*i.e.,* transtension) between sinistral and dextral strike-slip reactivated, east-west (*i.e.,* Magaliesburg-Barberton, Sugarbush-Inyoka, Brandfort-Tugela) and north-south striking (*i.e.,* Trompsburg-Gaborone) Mesoarchaean suture zones, respectively, intensify and peak at ~2.75 Ga in mid-Ventersdorp time, leading to NW-SE crustal extension and SE-directed tectonic escape of the crustal interior bounded by these suture zones at ~2.75-2.64 Ga (Appendix 20-G).

The interlinking transtensional fault zones, formed during initial rifting at ~2.79-2.75 Ga, facilitate this crustal tectonic escape in the form of major strike-, oblique-, and dip-slip motions within the lateral (*e.g.,* Evander, East Rand, and Central Rand goldfields), oblique (*e.g.,* West Rand and Carletonville goldfields) and frontal ramp areas (*e.g.,* Klerksdorp and Free State goldfields) of these large-scale sigmoidally striking transtensional-extensional fault zones. The continued relaxation of late Central Rand Group thrust zones and the formation of major normal to strike-slip faults (*e.g.,* De Bron, Virginia, Stuirmanspan, Dagbreek faults in the FS Goldfield; Buffelsdoorn and Platberg faults in the Klerksdorp Goldfield; Panvlakte, Roodepoort, Witpoortje faults in the West Rand Goldfield) result in the local development of large grabens and half-graben-like pull-apart basins (*e.g.,* Ireton and Bezuidenhout Valley half-grabens), as well as in roll-over anticlines in the hangingwall block of all these fault zones. The formation of this basin-and-range style horst and graben topography at ~2.75-2.7 Ga is accompanied by deep erosion, denudation and infilling of the grabens with Platberg Group (Kameeldoorns Formation) clastic sediments derived by the erosion of older supracrustal deposits and Mesoarchaean basement lithologies, as well as by intermittent, extensive acid porphyry (Makwassie Formation) and basaltic volcanism (Rietgat Formation) (*cf.* Winter, 1976; Buck, 1980; Minter *et al.*, 1986; Stanistreet *et al.*, 1986; Van Coller, 1988; Meintjes *et al.*, 1989; R.E. Myers *et al.*, 1990a; Charlesworth & McCarthy, 1990; Stanistreet & McCarthy, 1990, 1991; McCarthy *et al.*, 1990a, b & c; Vermaakt & Roering, 1991; R.E. Myers *et al.*, 1992).

The period of craton-wide extension coincides with a punctuated disturbance of the regional geotherm and related extensive high temperature granulite-facies metamorphism and melting in the lowermost crust of the central Kaapvaal Craton at ~2.72 Ga (Schmitz & Bowring, 2001, 2003a & b).

Following a protracted period of erosion and peneplanation, thermal subsidence of the Ventersdorp rift basin at ~2.7-2.66 Ga leads to the extensive, alluvial-plain deposition of terrigenous clastic sediments of the lower Pniel Group (Bothaville Formation) and stratigraphic equivalents within a unitary subsiding intracratonic sag (thermal subsidence) basin unconformably over the Platberg Group and stratigraphic equivalents within the central-southern and northern parts of the Ventersdorp rift basin respectively (see also above) (*cf.* Winter, 1976; Buck, 1980; Minter *et al.*, 1986; Stanistreet *et al.*, 1986; Van Coller, 1988; Meintjes *et al.*, 1989; R.E. Myers *et al.*, 1990a; Charlesworth & McCarthy, 1990; Stanistreet & McCarthy, 1990, 1991; McCarthy *et al.*, 1990a, b & c; Vermaakt & Roering, 1991; R.E. Myers *et al.*, 1992) (Appendix 20-G).

Renewed Limpopo orogenic activity along the northern margin of the Kaapvaal-Grunehogna Craton results in a new pulse of active rifting throughout the Ventersdorp rift basin at ~2.66-2.64 Ga, causing the eruption of extensive basaltic plateau lavas of the upper Pniel Group (Allanridge Formation) and stratigraphic equivalent upper Wolkberg and Buffelsfontein groups (lavas of Abel Erasmus and Witfonteinrand formations respectively) and the termination of alluvial-plain deposition of terrigenous clastic sediments of the lower Pniel Group (Bothaville Formation) and lower Wolkberg and Buffelsfontein groups (see also above) (*cf.* Winter, 1976; Buck, 1980; Button *et al.*, 1981; Tankard *et al.*, 1982; Minter *et al.*, 1986; Stanistreet *et al.*, 1986; Van Coller, 1988; Meintjes *et al.*, 1989; R.E. Myers *et al.*, 1990a; Charlesworth & McCarthy, 1990;

Stanistreet & McCarthy, 1990, 1991; McCarthy *et al.*, 1990a, b & c; Vermaakt & Roering, 1991; R.E. Myers *et al.*, 1992; J.M. Barton *et al.*, 1995b; Eriksson & Reczko, 1995) (Appendix 20-G).

Within the eastern Kaapvaal Craton, dextral transtensional reactivation of faults, forming the central (main) part of the pre-existing (~2.99-2.97 Ga) Pongola rift basin, leads to the generation of I-type mafic and granitic melts by decompressional melting of lower crustal to upper mantle levels, which is followed by their structurally controlled emplacement into upper crustal levels intrusively into Pongola Supergroup deposits in the form of the Usushwana Complex and numerous granitic complexes/plutons (*i.e.,* Sicunusa, Kwetta, Hlatikulu, Ngwempisi, Nzimane, Spekboom and Mbabane granites) at ~2.72-2.67 Ga (*cf.* Layer *et al.*, 1989; Maphalala & Kröner, 1993; Reimold *et al.*, 1993; Robb *et al.*, 1993; Meyer *et al.*, 1994; Thomas *et al.*, 1997; Elworthy *et al.*, 2000) (Appendix 20-G).

4.2.1.6 LATE- TO POST-LIMPOPO OROGENIC PHASE (~2.64-2.585 GA)

A final and short-lived pulse of active rifting occurs within the Ventersdorp basin in late Limpopo orogenic time at ~2.64 Ga, which is preceded by a northwards tilt of the syn-depositional surface within the Transvaal Basin (*cf.* Clendenin *et al.*, 1991; Els *et al.*, 1995; Eriksson & Reczko, 1995) as a result of pre-rift uplift/doming of the crust along the southern margin of the Transvaal basin (NB: The northwards tilt does not require a very short-lived event (<20 m.y.) of orogenic compressive deformation along the southern Transvaal basin margin prior to Black Reef sedimentation (*i.e.,* the so-called pre-Black Reef inversion/Ndebele orogeny) as suggested by *e.g.,* Roering, 1984, 1986; Winter, 1987; Roering & Smit, 1987; Pitts, 1990; Vermaakt & Roering, 1991; Grant, 1992; Hilliard, 1994; Vermaakt, 1995; Coetzee *et al.*, 1995; Hilliard & McCourt, 1995; Els *et al.*, 1995 and Eriksson & Reczko, 1995). WNW-ESE oriented lithospheric extension causes renewed extensional reactivation of mid-Ventersdorp Supergroup age extensional/transtensional faults, late Central Rand Group thrusts and Mesoarchaean suture zones within the Kaapvaal Craton. Furthermore, newly forming NNE-SSW striking extensional fractures and bedding planes within the Witwatersrand Supergroup are intruded by ilmenite-diabase dykes and sills respectively within the area of the Witwatersrand depository, representing feeders to intra-continental tholeiitic lavas, that were once possibly extruded over, and subsequent completely eroded from the central part of the Kaapvaal Craton (*i.e.,* area of Witwatersrand depository) prior to deposition of the Black Reef Formation at ~2.64-2.585 Ga, but were preserved as Rosendal and Waterloo lavas over basal conglomerates of the Lower Vryburg Formation (= Lower Schmidtsdrif Subgroup) within the Griqualand West Basin (*cf.* Beukes, 1978; SACS, 1980; McCarthy *et al.*, 1990b; Harck, 1994; Walraven & Martini, 1995) to the west of the Neoarchaean Colesberg-Mafikeng suture zone (Appendix 20-G).

After cessation of Limpopo Orogeny-related crustal extension and formation of the impactogenal Ventersdorp rift system within the Kaapvaal Craton between ~2.72-2.64 Ga, thermal subsidence and craton-wide erosion and peneplanation of the northerly inclined (within the Transvaal basin) post-Ventersdorp palaeosurface continue, but mid-Ventersdorp age extensional/transtensional faults and extensionally reactivated easterly verging late Central Rand Group thrusts still control the palaeotopography at that time, comprising parallel trending horsts (palaeohighs) and grabens/half-grabens (palaeolows) and forming a palaeorelief of up to 30m (*cf.* Els *et al.*, 1995). Mesoarchaean granitoid gneiss-greenstone basement and Neoarchaean supracrustals (*i.e.,* Dominion Group, Witwatersrand and Ventersdorp supergroups and their lateral equivalents) are eroded from palaeohighs and deposited in alluvial fan and shallow braided stream systems along and within adjacent palaeolows as basal conglomerates, grits and quartzites of the Black Reef Formation and as quartzites of the

Upper Vryburg Formation (*cf.* Button, 1973a; SACS, 1980; Tankard *et al.*, 1982; Key, 1983, 1986; Button, 1986; Clendenin, 1989; Henry *et al.*, 1990; Eriksson *et al.*, 1993b; Harck, 1994; Els *et al.*, 1995; Eriksson & Reczko, 1995) unconformably above older units within the Ventersdorp rift (now the site of an unitary subsiding intracratonic sag (thermal subsidence) basin) to the east and west of the Neoarchaean Colesberg-Mafikeng suture zone respectively at ~2.64-2.62 Ga (Appendix 20-H).

Due to the decay of the asthenospheric upwelling developed during active lithospheric rifting at ~2.72-2.64 Ga, accelerated thermal subsidence and a southwestwards tilt of the depositional surface across the area of the Ventersdorp rift initiates a marine transgression over large parts of the Kaapvaal Craton which advances from the southwest craton-inwards along the Ventersdorp rift and leads to the deposition of increasingly more shallow marine sediments (*i.e.*, quartz-arenites, silt-/mudstones and carbonates) of the upper portions of the Black Reef and Upper Vryburg formations within the unitary subsiding intracratonic sag (thermal subsidence) basin at ~2.62-2.585 Ga (*cf.* Clendenin, 1989; Harck, 1994; Els *et al.*, 1995; Eriksson & Reczko, 1995; Altermann & Nelson, 1998; Catuneanu & Eriksson, 1999) (Appendix 20-H).

4.2.2 ZIMBABWE CRATON

4.2.2.1 BULAWAYAN OROGENIC CYCLE (~3.1-2.81 GA)

Following the stabilisation of the Zimbabwe Craton to a coherent continental block at ~3.1 Ga, northerly directed subduction of oceanic crust beneath the southern margin of the craton marks the beginning of the Bulawayan orogenic cycle at ~3.1 Ga (Appendix 20-A).

In response to these subduction processes, an intracratonic magmatic-arc and adjacent back-arc basin immediately to the north of the arc forms within the southern and central parts of the Zimbabwe Craton, which is accompanied by the extensional reactivation of Mesoarchaean suture zones situated within the zone of intracratonic back-arc basin formation (*e.g.,* Ruti suture zone) and the associated development of individual narrow, elongated rifts along these translithospheric fracture zones (Appendix 20-A).

Ultramafic-mafic layered intrusions, comagmatic ultramafic-mafic (submarine), intermediate, and felsic volcanics, mafic and felsic pyroclastic rocks, and a wide variety of sedimentary rocks of the Lower Bulawayan Supergroup (Blenkinsop *et al.*, 1997) (= Lower Greenstones; Wilson, 1979) are the products of this magmatic-arc/back-arc basin complex, emplaced into and deposited unconformably over the granitoid-gneiss basement of the Zimbabwe Craton at ~3.1-2.87 Ga respectively (*cf.* Taylor *et al.*, 1991; Bickle & Nisbet, 1993; Dougherty-Page *et al.*, 1993; Wilson *et al.*, 1995; Kusky, 1998; Hunter *et al.*, 1998; Horstwood *et al.*, 1999) (Appendices 29-A – 29-C). Lower Bulawayan Supergroup deposits are developed and preserved in the Belingwe, Midlands, Filabusi, Antelope-Lower Gwanda, Shangani, Bubi, Gweru-Mvumba and Odzi-Mutare-Manica (*i.e.,* Macequece Formation) greenstone belts (Figs. 6.36 & 6.37).

Intraplating of mantle-derived magmas, as well as crustal thickening by depositional loading of the magmatic arc, result in partial melting (anatexis) of lower ensialic crust of the Zimbabwe Craton and in the syn-depositional and pre-collisional emplacement of progressively more tonalites and granites of the Chingezi Suite (*e.g.,* Rhodesdale Batholith; Mushadike granitoid, Heaney, Bangala Dam and Nyani tonalites) into the deposits of the Lower Bulawayan Supergroup at ~3.0-2.87 Ga (*cf.* Wilson & Harrison, 1973; Hickman, 1978; Moorbath *et al.*, 1977, 1987; Taylor *et al.*, 1991) (Appendices 20-A – 20-C).

Contemporaneously, crustal extension in the Limpopo Central Zone Terrane results in the intrusion of a basalt dyke swarm at <~3.1-3.0 Ga (*e.g.*, Barton *et al*., 1977, 1983b, 1990, 2003, 2006).

Northerly subduction of oceanic crust beneath the Zimbabwe Craton results in the closure of the Tuli-Sabi oceanic basin between the Zimbabwe Craton and Limpopo Central Zone Terrane in the north and south respectively (Appendix 20-D). Subsequent collision of both continental blocks along the Tuli-Sabi-Triangle suture zone results in crustal thickening due to northerly directed tectonic stacking and intrusion of syn- to late-collisional TTG granitoids of the Chingezi Suite (*e.g.,* Chingezi, Chipinda, Mashaba, Essexdale and Somabula tonalites, Three Fingers and Bulawayo granites) (*cf*. Wilson & Harrison, 1973; Hawkesworth *et al*., 1979; Taylor *et al*., 1991; Wilson *et al*., 1995; Fedo *et al*., 1995; Nägler *et al*., 1997; Jelsma *et al*., 2004), as well as in associated deformation (*i.e.,* E-W folding and N-vergent thrusting), metamorphism (decreasing from granulite- to greenschist-facies from south (near suture zone, *i.e.,* southern margin of craton) to north), and structurally controlled hydrothermal alteration of the Lower Bulawayan Supergroup deposits and associated syn-depositional and syn-collisional granitoids (*cf.* Nägler *et al*., 1997) during the Bulawayan Orogeny at ~2.87-2.81 Ga.

Contemporaneously occurring southerly verging fold-and-thrust tectonics and coeval syn- to late-kinematic intrusion of granitoids are accompanied granulite-facies grade metamorphism within the Limpopo Central Zone Terrane peaking at ~2.87 Ga (*cf.* Treloar *et al*., 1992) (Appendix 20-D).

4.2.2.2 LIMPOPO OROGENIC CYCLE (~2.81-2.64 GA)

Subsequent to the Bulawayan orogenic event, craton-wide, post-orogenic crustal relaxation and extension lead to the formation of intracratonic rifts along extensionally reactivated suture zones within the southern Zimbabwe Craton, *e.g.,* along the Tuli-Sabi-Triangle and Ruti suture zones, accompanied by a marine transgression into these rifts, propagating progressively out of these rifts over the entire southern craton between ~2.81 Ga and ~2.72 Ga (this study) (Appendix 20-E).

Intracratonic rifting along the Tuli-Sabi-Triangle suture zone progressed from east to west and was accompanied by a westward advancing marine incursion/transgression between the diverging Zimbabwe Craton and Limpopo Central Zone Terrane, and the deposition of a shelf-facies rift sequence (*e.g.,* Manjeri Formation of Belingwe Greenstone Belt) under initial fluviatile (alluvial fans and fan-deltas) later shallow-marine conditions (*i.e.,* basal conglomerates, quartzites, shales, marbles, carbonates, cherts, and iron formations) of the Upper Bulawayan Supergroup along the southern margin of the Zimbabwe Craton (*i.e.,* Matsitama, Mweza and Buhwa greenstone belts), unconformably over previously tectonised and metamorphosed greenstone belt successions of the Sebakwian and Lower Bulawayan Supergroups, as well as granite-gneiss basement of the Zimbabwe Craton (Wilson *et al*., 1995; Hunter *et al*., 1998; Kusky, 1998; this study) (Appendix 20-E).

The development of an intra-cratonic rift along the extensionally reactivated Ruti suture zone resulted in the deposition of shallow-water (partially marine) sedimentary succession (basal conglomerates, overlain by grits, arkoses, greywackes, shales and dolomitic limestones) and intermittent felsic rift volcanism of the Mbeza/Vengo Formation (= Upper Bulawayan Supergroup), with sediments derived mostly by erosion of the Lower Bulawayan Supergroup (*i.e.,* Macequece Formation) and the granite-gneiss basement of the Zimbabwe Craton (*cf*. Manuel, 1992; Manhica, 1998) (Appendix 20-E).

The marine transgression propagated out of the intracratonic rift developed along the Tuli-Sabi-Triangle suture zone northwards over the southern Zimbabwe Craton to link up with the intracratonic rift along the Ruti suture zone, leading to widespread deposition of a thin Manjeri-type sequence (up to 1km thick) of clastic and chemical sediments of the Upper Bulawayan Supergroup (Kusky, 1998).

Continued rifting along the Tuli-Sabi-Triangle suture zone progressed finally to the break-up and southerly drift of the Limpopo Central Zone Terrane from the southeastern and southern margins of the Zimbabwe Craton, and in the development of a narrow, wedge-shaped oceanic basin with oceanic crust (*i.e.,* mafic-ultramafic tholeiitic volcanics and intrusives (= pillowed basalts, komatiites and intrusive equivalents)) and shallow-marine sedimentary deposits (*i.e.,* stromatolitic limestones) of Ngezi Group (Belingwe Greenstone Belt) and stratigraphic equivalents forming along a sea-floor spreading centre and as shelf-facies at ~2.71-2.69 Ga respectively (*cf.* Chauvel *et al.*, 1983, 1993; Kusky, 1998; Bolhar *et al.*, 2002). In the southwest, rifting along the Tuli-Sabi-Triangle suture zone did not progress to break-up and drift of the Limpopo Central Zone Terrane from the southwestern Zimbabwe Craton, hence only an intracratonic rift with marine incursions/transgressions from the east developed, which was not accompanied by the formation of oceanic crust (Appendix 20-E).

Oblique NE-SW convergence between the Limpopo Central Zone Terrane to the north (together with the earlier amalgamated Zimbabwe Craton) and the Kaapvaal-Grunehogna Craton to the south leads to complete closure of the Limpopo oceanic basin and subsequent oblique continent-continent collision between both cratonic blocks along the Palala suture zone at ~2.72 Ga (Appendix 20-G). This introduces NE-SW oriented compressive far field stress and orogenic activity to both colliding cratons during the Limpopo Orogeny at ~2.72-2.64 Ga (*cf.* Treloar & Blenkinsop, 1995).

Within the Limpopo Central Zone Terrane and southwestern Zimbabwe Craton, NE-SW compressive far field stress results in sinistral strike-slip and NE-verging fold and thrust tectonics (*e.g.,* Sashe shear/thrust zone within southwestern Zimbabwe Craton) at ~2.72-2.64 Ga, thereby deforming the ~2.81-2.72 Ga old intracratonic shelf sequence (Appendix 20-G) (*cf.* Bagai, 2000; Bagai *et al.*, 2002).

Post-collisional, lateral, westward tectonic escape of the Zimbabwe Craton/Limpopo Central Zone Terrane along the Palala suture zone relative to the Kaapvaal-Grunehogna Craton at ~2.72-2.64 Ga results in sinistral transpressional tectonics (*i.e.,* formation of sinistral strike-slip shear zones) within the Limpopo Central Zone Terrane and northern Kaapvaal-Grunehogna Craton (Appendix 20-G). This tectonic escape phase of the Limpopo Orogeny is accompanied by the intrusion of syn-collisional granitoids into the eastern Limpopo Central Zone Terrane, as well as by continuous infiltration and circulation of CO_2-rich fluids which leads to shear zone-hosted alteration and gold mineralisation in both the Southern Marginal Zone and northern Kaapvaal Craton at ~2.72-2.64 Ga (*cf.* Pretorius & Van Reenen, 1992).

Sinistral strike-slip escape tectonics of the Zimbabwe Craton/Limpopo Central Zone Terrane along the Palala suture zone at ~2.72-2.64 Ga, lead to the initiation of southeasterly directed subduction of oceanic lithosphere beneath the western Zimbabwe Craton and marks the beginning of the Hurungwe Orogenic Cycle at ~2.72 Ga (Appendix 20-G). Consequently, both orogenies are geodynamically linked and related to each other, as the initiation of the Hurungwe Orogenic Cycle was facilitated by processes related to the Limpopo Orogeny.

4.2.2.3 HURUNGWE OROGENIC CYCLE (~2.72-2.64 GA)

SE-directed subduction and melting of hydrated oceanic crustal material beneath the western and northern Zimbabwe during the Hurungwe Orogenic Cycle at ~2.72-2.64 Ga, resulted in the development of an intracratonic magmatic arc by under- and intraplating of mafic-ultramafic magmas into the lithosphere of the western Zimbabwe Craton (derived from the subducted oceanic crustal slab), introducing a higher geothermal gradient and the generation of mixed mantle/crustal-derived (I- and S-type) granitoid magmas through partial melting of the older, lower continental lithosphere (Condie & Harrison, 1976; Wilson *et al.*, 1978; Bickle *et al.*, 1981; Watkeys, 1984; Master, 1991a & b; Bozhko, 1997) (Appendix 20-G)

The major NE-SW trending intra-(Zimbabwe)cratonic magmatic arc (= northern magmatic belt of Upper Greenstones; = Vumba, Bulawayo, Bubi, Gweru-Mvuma, Midlands, Chegutu, Chipuriro, Harare-Shamva, and Mount Darwin greenstone belts) (Figs. 6.35 & 6.37) formed by the extrusion and deposition of initially calc-alkaline felsic volcanics (*i.e.,* andesites, dacite, rhyodacites and rhyolites), pyroclastics and volcaniclastics, later mafic volcanics (*i.e.,* locally pillowed, tholeiitic basalts), and finally again felsic volcanics and volcaniclastics of the Upper Bulawayan Supergroup (Wilson, 1979) unconformably over the ~2.81-2.72 Ga old Manjeri-type shelf sequence in the southwestern part to the craton or older granitoid-greenstone basement units in general, and the intrusion of voluminous, high-level, syn-volcanic mafic to intermediate low evolved magmas (*i.e.,* tonalites, trondhjemites, and granodiorites) of the Sesombi-Wedza granitoid suite as plutons/batholites and subvolcanic porphyries into the comagmatic Upper Bulawayan greenstone volcanics/volcaniclastics at ~2.72-2.64 Ga (*e.g.,* Chauvel *et al.*, 1993; Wilson *et al.*, 1995; Jelsma *et al.*, 1996; Majaule & Davis, 1998; Horstwood, 1999; Bagai, 2000; Bagai *et al.*, 2002) (Appendix 20-G).

This part of the lithosphere in which the formation of this late Archaean intra-cratonic magmatic arc occurred, underwent intense crustal extension (as a result of isostatic uplift of hot, buoyant, and thickened (by magmatic under- and intraplating) lithosphere), which resulted in the development of an extensional to transtensional NE-SW striking fracture/joint system and in the reactivation of pre-existing structures (*e.g.,* NNE-striking Popoteke fracture system, Bushman and Harare suture zones, etc.) (this study) (Appendix 20-G). Inner-arc extensional rifts and basins formed synchronously with the Upper Bulawayan bimodal volcanism and were filled with volcaniclastics, terrigenous sediments (partially derived by unroofing of subvolcanic porphyries) and partial marine sediments (*e.g.,* quartzites, conglomerates, greywackes, phyllites, BIFs, cherts, limestones) (McKenzie, 1978; Wilson *et al.*, 1978, 1995; Wilson, 1979; Nisbet *et al.*, 1981; Foster *et al.*, 1986; Baldock *et al.*, 1991; Blenkinsop *et al.*, 1993).

The magmas of continental tholeiitic composition were derived by melting of the subducted oceanic crustal slab and their ascent through the continental lithosphere of the Zimbabwe Craton, thereby acquiring a crustal contamination component. These relatively primitive magmas extruded as tholeiitic basalts on surface or were emplaced as hyabyssal, sheet-like sill and feeder dyke intrusions at shallow crustal levels. Coeval partial lower crustal melting produced magmas of intermediate composition, which intruded into the magmatic arc as plutons, or erupted as comagmatic intermediate-felsic volcanics/volcaniclastics (= Upper Bulawayan Supergroup) of the Sesombi-Wedza granitoid suite.

The ascent and intrusion of these magmas within higher crustal levels was accompanied by hydrothermal K-feldspar-albite-sericite-pyrite-(□biotite) alteration and skarn formation, as well as porphyry- and shear zone-related copper-gold and copper-deficient gold mineralisation (Buchholz *et al.*, 1998), and both were controlled mainly by extensional/transtensional reactivated major lithospheric suture zones and the magmatic arc internally forming NE-SW-striking extensional/transtensional fracture system (this study).

Southeasterly migration of the intra-cratonic magmatic arc is evident by magmatism progressing spatially in time into the interior of the Zimbabwe Craton, with granitoids of the Sesombi and Wedza suites intruding at ~2.72-2.68 Ga and ~2.68-2.64 Ga into the western and central parts of the craton respectively. Extensional rather than compressional tectonism took place during the Hurungwe Orogenic Cycle and associated development of an intracratonic magmatic arc within the western and northern Zimbabwe Craton (this study).

4.2.2.4 NYASSA OROGENIC CYCLE (~2.64-2.53 GA)

The subduction-related development of an intra-cratonic magmatic arc during the Hurungwe Orogeny (~2.72-2.64 Ga) was terminated by continental collision and accretion between the N-S converging Archaean Nyassa Craton (either amalgamated with, or still separated from the Tanzanian Craton at this time) and Vaalbara along the Sanangoè suture zone, which introduced approximately N-S compressive far field stress to the entire northern part of Vaalbara (*i.e.,* Zimbabwe Craton), resulting in initial compressive, orogenic activity in the northern part of the craton and subsequent craton-wide sinistral transpression during the Nyassa Orogeny (Ngarwe Orogeny of Barton *et al. (*1991), or Pfunzi Orogeny of Vinyu *et al.*, (2001) and Jelsma & Dirks (2002)) at ~2.64-2.585 Ga (Appendix 20-H) (Note: Archaean Sm-Nd whole-rock age data for the Mesoproterozoic Chipera anorthosite/gabbro body, situated north of Sanangoè suture zone, indicate contamination with/assimilation of Archaean crust for the intrusive complex (Evans *et al.*, 1999) and proves the existence of Archaean lithosphere of the proposed Nyassa Craton).

Along the northern margin of the Zimbabwe Craton, peak orogenic activity during the Nyassa Orogeny at ~2.64-2.62 Ga led to pervasive tectonic reworking (*i.e.,* east-west folding and southerly thrusting) (Dirks *et al.*, 1998), migmatisation and retrograde amphibolite-facies metamorphism of older (2947 ±129 Ma - 2937 ±178 Ma; Vail & Snelling, 1971 and Barton *et al.*, 1991 respectively) granulite-facies para- and orthogneisses of the Pfungwe and Mudzi Metamorphic Suites making up the ~2.95 Ga old Pfunzi Orogenic Belt. Migmatisation and amphibolite-facies metamorphism were accompanied by the intrusion of syn- to late-tectonic tonalitic and granitic plutons of the Chilimanzi Suite into the Pfunzi Orogen and resulted in formation of the composite (~2.95 Ga and ~2.62 Ga) Migmatitic Gneiss Terrain (Dirks *et al.*, 2000; Vinyu *et al.*, 2001; Hofmann *et al.*, 2002). The migmatitic gneisses and relict granulites of the Migmatitic Gneiss Terrain were emplaced tectonically onto the northern margin of the Zimbabwe Craton along the southerly verging Pfunzi Boundary Thrust Zone and other synthetic thrust zones, possibly representing pre-existing thrusts formed during the Pfunzi Orogeny at ~2.95 Ga and reactivated during the Nyassa Orogeny at ~2.64-2.585 Ga (Appendix 20-H).

Further south within the northern Zimbabwe Craton, orogenic activity during the Nyassa Orogeny resulted in compressive/transpressive deformation (D_1 and D_2) and synkinematic greenschist-to amphibolite-facies grade metamorphism (M_1 and M_2) of the ~2.72-2.64 Ga old, magmatic arc-related Upper Bulawayan succession and comagmatic Sesombi-Wedza granitoid suite, as well as of Mesoarchaean (>3.1 Ga) TTG gneiss-greenstone basement (Jelsma, 1993; Jelsma *et al.*, 1993; Dirks & Jelsma, 1998a,b; Dirks *et al.*, 2000; Jelsma & Dirks, 2000, 2002; Vinyu *et al.*, 2001).

During the D_1/M_1-event, initial E-W recumbent folding and southerly vergent, thick- and thin-skinned, partially bedding-parallel thrusting/duplexing and large-scale nappe emplacement (with nappe-internal smaller scale imbricate stacking) of Upper Bulawayan greenstones and older TTG gneiss-greenstone basement (*i.e.,* Madziwa gneiss terrain) took place under amphibolite-facies grade metamorphic conditions (M_1) within the northern Zimbabwe Craton at ~2.64-2.62 Ga (Dirks & Jelsma, 1998a & b; Jelsma & Dirks, 2000, 2002) (Appendix 20-H).

The compressive D_1/M_1 imbricate stacking and nappe emplacement event in the northern part of the Zimbabwe Craton was shortly followed by Chilimanzi granite diapirism/doming and related localised (*i.e.,* diapir-marginal), pure-shear D_2-deformation (*i.e.,* refolding of F_1-folds and steepening of D_1-thrusts) and amphibolite- to greenschist-facies grade contact metamorphism (M_2), as well as by contemporaneous, regional sinistral oblique- to strike-slip along the steepened earlier D_1-thrust zones, new forming second- and third-order sinistral strike-slip shear zones converging in a duplex-array (Dirks & Jelsma, 1998a,b; Jelsma & Dirks, 2000, 2002), and reactivated palaeosuture zones (*e.g.,* Bushman and Harare sutures, etc.) across the entire Zimbabwe Craton under greenschist-facies grade metamorphism at ~2.62-2.585 Ga during the sinistral transpressional D_2/M_2-event (this study). Large-scale, arcuate, frontal thrust ramps with southwesterly vergence causing crustal thickening developed as a result of lateral expulsion of compressed crust between the sinistral strike-slip reactivated, NE-SW striking Harare and Ruti suture zones (= lateral ramps) (*cf.* Coward, 1976, 1980; Coward *et al.*, 1973, 1976; Coward & James, 1974; Coward & Daly, 1984; Coward & Treloar, 1990, Treloar *et al.*, 1992; Treloar & Blenkinsop, 1995) (Appendix 20-H).

Both phases of deformation and metamorphism most probably document the collisional/accretional and tectonic escape stages of the continental collision process between the Nyassa and Zimbabwe cratons (this study), and were accompanied by wide-spread, (second- or third-order) shear zone-controlled, hydrothermal alteration and mesothermal lode-gold mineralisation from magmatic fluids within supracrustal greenstone belt lithologies and slightly earlier to synchronously emplaced granodiorites-monzodiorites of the Wedza Suite mainly during the collisional stage at ~2.64-2.62 Ga, and subordinate during the sinistral transpressive phase at ~2.62-2.585 Ga (*e.g.,* Tomschi, 1987; Nutt *et al.*, 1988a & b; Foster, 1989; Wilson & Nutt, 1990; Harley & Charlesworth, 1990; Blenkinsop, 1991; Herrington, 1991; Herrington *et al.*, 1992; Schmidt-Mumm *et al.*, 1993, 1994a,b, 1995a,b; Campbell & Pitfield, 1993, 1994; Frei, 1994; Buchholz *et al.*, 1994; Höppner, 1994; Höppner & Oberthür, 1994; Blenkinsop & Fuchter, 1995; Frei & Kamber, 1995; Pitfield & Campbell, 1993, 1996; Jelsma *et al.*, 1996, 1998; Vinyu *et al.*, 1996; Frei & Pettke, 1996; Darbyshire *et al.*, 1996; Blenkinsop *et al.*, 1996, 1997, 1999, 2000; Oberthür *et al.*, 2000; Selby *et al.*, 2001; Siegesmund *et al.*, 2002; Hofmann *et al.*, 2003).

Continental collision between both cratons was further accompanied by the intrusion of I-type Chilimanzi adamellitic granites (see below) with associated diapiric (doming-related) pure-shear deformation and contact metamorphism (*e.g.,* skarn formation) of the intruded Upper Bulawayan volcano-sedimentary greenstone belt deposits (Ramsay, 1981, 1989; Jelsma, 1993; Jelsma *et al.*, 1993; Dirks & Jelsma, 1998a,b; Jelsma & Dirks, 2000, 2002; Siegesmund *et al.*, 2002) during the tectonic escape stage at ~2.62-2.585 Ga. Synkinematic emplaced granitoid plutons of the Wedza and higher evolved Chilimanzi suites became only marginally deformed (sheared, foliated) under ductile conditions (*i.e.,* acquiring a mylonitic/gneissic outer rim) (*e.g.,* Jelsma, 1993) during the craton-wide sinistral transpressive stage.

Clastic sediments (*i.e.,* conglomerates, sandstones, siltstones) of the Shamwaian Supergroup, derived by erosion of Mesoarchaean TTG gneiss basement and younger greenstone belt successions, were deposited as alluvial fans (*i.e.,* molasses-type deposits) in foreland basins and small pull-apart basins at ~2.64-2.585 Ga, which developed to the south near the front of the southerly verging Nyassa Orogeny-related fold-thrust belt (nappe) within the northern Zimbabwe Craton (*e.g.,* Bindura-Harare-Shamva and Chinhoyi-Guruve greenstone belts) and to the north ahead of the Limpopo Orogeny-related NW-verging Umlali Thrust Zone (= North Limpopo Thrust Zone; NLTZ) and thrust-tectonically emplaced Northern Marginal Zone (nappe) within the southern part of the craton (*e.g.,* Belingwe and Masvingo greenstone belts) (see below), as well as along sinistral strike-/oblique-slip reactivated palaeosuture zones within the central part of the craton (*e.g.,* Midlands

Greenstone Belt) respectively (Kusky & Kidd, 1992; Jelsma, 1993; Wilson *et al.*, 1995; Jelsma *et al.*, 1996; Kusky, 1998; Dirks & Jelsma, 1998a; Hofmann *et al.*, 2001a & b; 2002; this study) (Appendix 20-H).

Penecontemporaneously with deformation and deposition of the Shamwaian Supergroup was the emplacement of voluminous, tabular, crustally derived, adamellitic I-type granites and monzogranites of the Chilimanzi and Razi suites respectively, as well as of comagmatic minor felsic volcanic flows syndepositionally within the sedimentary deposits of the Shamwaian Supergroup at ~2.62-2.585 Ga (Wilson *et al.*, 1995; Jelsma *et al.*, 1996; Blenkinsop & Treloar, 2001), which was controlled in position and style by sinistral strike-slip reactivated intra-cratonic palaeosuture zones within the central and southern Zimbabwe Craton (Kusky, 1998; this study). The generation of the crustally derived granitic magmas was likely caused by two combined processes, *i.e.,* decompression melting (anatexis) of the lower continental crust along these tectonically reactivated translithospheric palaeosuture zones and coeval uprise of the asthenosphere and lithospheric delamination due to subduction slab break-off (*cf.* Kampunzu *et al.,* 2002) (Appendix 20-H). Time-progressive southerly migration of the crustally derived Chilimanzi-Razi magmatism is evident, with granites of the Chilimanzi and Razi suites intruding along suture zones at ~2.62-2.6 Ga and ~2.6-2.53 Ga into the northern to southern and most southeastern parts of the Zimbabwe Craton respectively (this study) (Appendix 20-H).

As a result of closure of the Limpopo ocean and subsequent oblique continental collision between the Limpopo Central Zone Terrane/Zimbabwe Craton and the Kaapvaal Craton during the Limpopo Orogeny at ~2.72-2.64 Ga, as well as Zimbabwe craton-wide N-S compression during the Nyassa Orogeny at ~2.64-2.53 Ga, the narrow, E-W-elongated, wedge-shaped oceanic basin between the Limpopo Central Zone Terrane in the south and the Zimbabwe Craton to the north started to close progressively from west to east (zipper-like) at ~2.64 Ga, initiating southerly inclined subduction of oceanic lithosphere beneath the eastern Limpopo Central Zone Terrane (Appendix 20-H). Subduction-related magmatic underplating and slab-melting beneath the Limpopo Central Zone Terrane at that time is supported by major and trace-element concentrations in eclogitic and websteritic inclusions in diamonds (Aulbach *et al.*, 2002) and crustal and upper mantle xenoliths in kimberlite (Pretorius & Barton, 2003b) from the Venetia Diamond Mine indicating a mixed eclogitic oceanic crustal slab-derived melt and peridotitic mantle source of <~3.0 - >~2.6 Ga.

Subduction-related generation and intrusion of I-type tonalitic-trondhjemitic-granitic magmas within the eastern Limpopo Central Zone Terrane as plutonic complexes (*e.g.,* Verbaard, Singelele and Alldays plutons) occurs at ~2.64-2.62 Ga (Jaeckel *et al.*, 1997; Kröner *et al.*, 1999) in post-Limpopo Orogeny time during the initial stages of the ensuing Nyassa Orogeny.

The easterly advancing, diachronous closure of the wedge-shaped oceanic basin at ~2.64-2.585 Ga results in the formation of a N- and NNW-verging fold-thrust belt, and culminates in the obduction of the ~2.7 Ga old oceanic lithosphere/plateau (= tholeiitic mafic-ultramafic dominated Upper Bulawayan greenstones of southern magmatic belt; *e.g.,* Ngezi Group) as ophiolite nappe complex along northerly verging thrust zones over the ~2.81-2.7 Ga old, para-autochthonous Manjeri-type shelf-sequence and older TTG-gneiss/greenstone basement along the southern margin of the Zimbabwe Craton (Kusky & Kidd, 1992; Kusky & Winsky, 1995; Kusky, 1998) (Appendix 20-H). Furthermore, granulite-facies ~2.72-2.62 Ga old granite gneisses (= crustally derived enderbites and charnockites of predominantly granitic and tonalitic composition), minor, ~3.1-2.87 Ga old supracrustal Lower Bulawayan greenstone formations (metasediments and mafic to ultramafic metavolcanics) and granitoids, and >3.1 Ga old granitoid gneiss basement from mid-crustal levels of the most southeastern Zimbabwe Craton (*i.e.,* Umtali Terrane) (Ridley, 1992; Rollinson & Blenkinsop, 1995; Blenkinsop *et al.*, 1995; Berger *et al.*, 1995; Kamber *et al.*, 1995;

Berger & Rollinson, 1997; this study) were tectonically uplifted (vertically by up to ~20km) and emplaced diachronously from west to east as large-scale nappe (= Northern Marginal Zone; NMZ) along the NNW-verging Umlali Thrust Zone (= North Limpopo Thrust Zone; NLTZ) onto the low- to medium metamorphic granite-greenstone Umtali Terrane at ~2.62-2.585 Ga (Ridley, 1992; Blenkinsop *et al.*, 1995; Mkweli *et al.*, 1995; Kisters *et al.*, 1998, Kusky, 1998) (Appendix 20-H).

Diachronous thrusting within the southeastern part of the craton along the NLTZ and exhumation of the NMZ progressing from west to east, was accompanied by peak-reaching (amphibolite to granulite-facies) metamorphism of the >2.62 Ga old lithologies of the NMZ, sinistral transpressive reactivation of the Ruti and Triangle suture zones, and gold and associated sulphide mineralisation within the NMZ in second-order structures related to the NLTZ, as well as by the synkinematic intrusion of first porphyritic granites, later charnockites and enderbites of the Razi suite as sheet-like bodies into the NMZ along fundamental structures such as the Ruti Suture Zone, North Limpopo Thrust Zone, as well as northern and southern margins of the Triangle Suture Zone (*e.g.,* Ridley, 1992; Tsunogae *et al.*, 1992; Berger *et al.*, 1995; Mkweli *et al.*, 1995; Kamber *et al.*, 1995a&b; 1996; Blenkinsop & Frei, 1996; Mkweli, 1998; Kisters *et al.*, 1998; Frei *et al.*, 1999; Kolb *et al.*, 2000; Kolb & Meyer, 2002; this study) (Appendix 20-H).

Contemporaneously within the eastern Limpopo Central Zone Terrane, mainly syntectonic magmatic activity during the Limpopo Orogeny between ~2.72 and 2.62 Ga (Jaeckel *et al.*, 1997; Kröner *et al.*, 1999) was followed by high-grade (low-P/high-T) metamorphism (granulite-facies), anatexis and intrusion of granitic, granodioritic and enderbitic plutons (*e.g.,* Bulai and Singelele plutons) at ~2.62-2.53 Ga (Barton *et al.*, 1979b, 1994a; Jaeckel *et al.*, 1997; Holzer *et al.*, 1998; Kröner *et al.*, 1999) during the Nyassa Orogeny (Appendix 20-H).

Late-(Nyassa)-orogenic NNE-SSW compression resulted in craton-wide, southerly advancing crustal extension and the diachronous formation/propagation (this study) of the NNE-SSW striking Popoteke (Nyassa) fracture systems (J.F. Wilson, 1990, A.H. Wilson, 1992, 1996) as part of a failed, intra-cratonic, impactogenal rift at ~2.585 Ga (Appendix 20-I). Rapid decompression melting along the fractures of the asthenospheric mantle (hydrated and enriched in incompatible elements by Nyassa-orogenic subduction processes and earlier melted and metasomatised during production of Chilimanzi granitoid suite) and uprise of the asthenosphere as a result of subduction slab break-off (*cf.* Kampunzu *et al.,* 2002) led to the formation of large volumes of depleted mantle-derived ultramafic-mafic magmas of the Great Dyke suite (*i.e.,* dunite, harzburgite, peridotite, pyroxenite, norite, gabbro) (Wilson & Wilson, 1981; Wilson *et al.*, 1987; Podmore & Wilson, 1987; Wilson & Prendergast, 1989; A.H. Wilson, 1982, 1992, 1996), which invaded the fracture system over a short period of about 10 Ma at ~2.585-2.575 Ga (Mukasa *et al.*, 1998; Wingate, 2000; Armstrong & Wilson, 2000; Oberthür *et al.*, 2002; Söderlund *et al.*, 2010). Crustal extension, fracture development and associated dyke intrusions extended across the NLTZ into the Limpopo Central Zone Terrane, after cessation of northerly verging thrust movements along this thrust zone at ~2.585 Ga (Appendix 20-I). The fracture/dyke-system of the Great Dyke suite might represent a feeder system to an extensive flood basalt province, which subsequently had been completely removed by erosion.

The final phase of the Nyassa Orogeny is dominated by orogenic escape tectonics leading to a 30°anticlockwise rotation of the main compressive stress direction (σ_1) from NNE-SSW to NNW-SSE and a gradual change from crustal extension to sinistral transtension across the Popoteke impactogenal rift (Friese, 2016, 2018).

While tectono-magmatic activity had ceased within most parts of the Zimbabwe Craton at ~2.575 Ga and protoliths of the Kariba, Chipisa, Chitumbi and Charoti paragneisses were deposited in rifts along the western passive margin of the craton at ~2.585-2.46 Ga (this study), late- to post-tectonic porphyritic granite and pegmatite/quartz vein emplacement, hydrothermal activity/skarn-type alteration of older lithologies under greenschist-facies metamorphic conditions (retrograde in NMZ), and occasional granite-/shear zone-hosted gold mineralisation (= late-stage Razi granite magmatism) continued until ~2.53 Ga within the southeastern Zimbabwe Craton, *i.e.,* within the Northern Marginal Zone and Umtali Terrane, and predominantly along the Ruti Suture Zone and North Limpopo Thrust Zone (Manuel, 1992; Schmidt-Mumm *et al.*, 1993, 1994; Frei, 1995; Frei & Kamber, 1995; Kempen, 1997; Kempen *et al.*, 1997; Frei *et al.*, 1999; Kolb & Meyer, 2002), as well as within the central (Buchholz *et al.*, 1998) and southern (Holzer *et al.*, 1999) parts of the craton along, or in close vicinity, of the sinistral transpressive reactivated Harare suture zone and other crustal shear zones respectively (this study) (Appendix 20-I)

This indicates diachronism and younging of tectono-thermal activity during the Nyassa Orogeny from north to south across the Zimbabwe craton, as well as the end of the Nyassa Orogenic Cycle at ~2.53 Ga, by which time cratonisation of the Zimbabwe Craton is completed.

4.2.3 INDIAN CRATONS

4.2.3.1 BUNDELKHAND OROGENIC CYCLE (~2.775-2.5 GA)

Penecontemporaneously with subduction processes along the northern margin of the supercontinent Vaalbara (*i.e.* Kaapvaal-Grunehogna Craton) during the second phase of the Limpopo Orogenic Cycle is the initiation of shallow, northward subduction of oceanic lithosphere beneath the southern margin of Vaalbara (*i.e.* Pilbara, Singhbhum, Bastar and East Dharwar cratons) at ~2.775 Ga, which leads to the convergence between Vaalbara and the Aravalli-Bundelkhand Craton (*cf.* Sharma, 1998) and to progressive closure of the intervening Central Indian oceanic basin, and marks the beginning of the Bundelkhand Orogenic Cycle (Appendix 20-E).

Subduction and melting of hydrated oceanic crustal material beneath southern Vaalbara during the Bundelkhand Orogenic Cycle at ~2.775-2.5 Ga results in crustal extension and the development of an intracratonic magmatic arc/back-arc basin complex by under- and intraplating of ultramafic magmas (derived from the subducted oceanic crustal slab) within the lithosphere of southern Vaalbara.

Upper mantle-derived ultramafic magmas ascend relatively quickly through the continental lithosphere and are emplaced within the developing intracratonic back-arc basin initially as ultramafic plutons and komatiitic lavas, later as progressively more differentiated mafic to felsic extrusives (basalts, porphyries) and comagmatic plutons (gabbros, granites) together with minor amounts of clastic sediments of the lower Fortescue Group within the Pilbara Craton at ~2.775-2.72 Ga (*cf.* Arndt *et al.*, 1991; Trendall *et al.*, 1995; Nelson *et al.*, 1999) (Appendix 20-E). Further east within the Singhbhum and Bastar cratons, concomitant marine transgressions from the Central Indian oceanic basin into the developing intracratonic back-arc basin results in the shallow marine to shelf deposition of BIFs, cherts, mudrocks, shales, minor coarse siliciclastics with intercalated komatiitic-basaltic volcanics of the Younger Iron Ore Group (Singhbhum Craton) and Bailadila Group (Bastar Craton). (Appendix 20-E).

Continued magmatic under- and intraplating introduces a progressively higher geothermal gradient and eventually the generation of mixed mantle/crustal-derived (I- and S-type) granitoid magmas through partial melting

of the older, lower continental lithosphere within the overriding Vaalbara supercontinent, which for example intrude as monzogranites, syenites and porphyries (*e.g.* Dongargarh Granite) and extrude as calc-alkaline volcanics (*i.e.* andesites, tholeiitic basalts, rhyolites, dacites) and felsic pyroclastics of the Upper Fortescue and Nandagao Groups within the intracratonic magmatic arc in the Pilbara and Bastar cratons at ~2.72-2.62 Ga respectively, leading to considerable thickening of the cratonic crust (*cf.* Mahadeven, 1998) (Appendices 20-G & 20-H).

Penecontemporaneously with intracratonic magmatic arc plutonism and volcanism in southern Vaalbara, granitoid magmas form by partial melting of lower crustal levels of the ~3.3-2.83 Ga old TTG gneiss-greenstone basement of the Aravalli Craton and intrude the latter as large granitoid bodies (*e.g.* Untala trondhjemite, Jagat granitoid, Gingla granite) at ~2.66-2.62 Ga (Roy & Kröner, 1996).

Complete closure of the Central Indian oceanic basin and continent-continent collision between Vaalbara and the Aravalli-Bundelkhand Craton along the Central Indian tectonic/suture zone, marks the beginning of the Central Indian Orogeny and the closing stages of the Bundelkhand Orogenic Cycle at ~2.58-2.5 Ga (*cf.* Radhakrishna, 1983, 1989; Radhakrishna & Naqvi, 1986; Radhakrishna & Ramkrishnan, 1988; Harris, 1993; Roy, 1998; Acharyya, 1998; Bhowmik *et al.*, 1999; Mazumder *et al.*, 2000) (Appendix 20-I).

Concomitant with collision-related tectonothermal activity and granulite-facies metamorphism within the Central Indian suture zone (Roy, 1998; Bhowmik *et al.*, 1999), approximately north-south oriented compressive far field stress induced into the lithosphere of both colliding continents, results in east-west crustal extension and thinning within the overriding Vaalbara continent and the development of major intracratonic (impactogenal?) rift basin(s) within the Singhbhum and Bastar cratons. Initial sedimentation of fluvio-terrestrial, coarse siliciclastics (basal glacial conglomerates, quartzites, arkoses) unconformably above the Younger Iron Ore Group and Nandagao Group is followed by the deposition of pelites, cherts, Fe formations and the concomitant extrusion of large volumes of bimodal volcanics (komatiites, basaltic komatiites, basalts, rhyolites) of the Danhjori and Sakoli groups within the Singhbhum and Bastar cratons respectively at ~2.58-2.45 Ga (*cf.* Posamantier & Veil, 1988; Bandyopadhyaya *et al.*, 1995; Bose *et al.*, 1997; Eriksson *et al.*, 1999; Mazumder *et al.*, 2000) (Appendix 20-I). Anorogenic, K-rich granite intrusions at ~2.6-2.5 Ga (Sarkar *et al.*, 1990, 1993; Friend & Nutman, 1991; Chadwick, 1994) accompany the rift basin development within the Bastar Craton.

Presumably as a consequence of considerable crustal thickening by tectonic stacking within a southerly migrating fold-thrust belt, anatectic melting of lower crustal rocks in the Aravalli-Bundelkhand craton leads to the generation of large volumes of S-type granitic magmas which intrude syn- to post-tectonically (*i.e.* phases of low-angle thrusting and shearing) into higher crustal levels as Bundelkhand Granite and other related K-rich granitic complexes at ~2.55-2.45 Ga, accompanied by the extrusion of associated rhyolites (*cf.* Sarkar *et al.*, 1984; Gopalan *et al.*, 1990; Friend & Nutman, 1991; Rahman & Zainuddin, 1993; Chadwick, 1994; Roy & Kröner, 1996; Wiedenbeck *et al.*, 1996; Sharma, 1998) (Appendix 20-I).

4.2.3.2 DHARWAR OROGENIC CYCLE (~2.72-2.5 GA)

Penecontemporaneously with subduction processes along the southern margin of the supercontinent Vaalbara during the Bundelkhand Orogenic Cycle is the initiation of shallow, eastward subduction of oceanic lithosphere beneath the West Dharwar-Antongil Craton at ~2.72 Ga, which leads to the convergence between Vaalbara and the West Dharwar-Antongil Craton and to closure of the intervening Dharwar oceanic basin, and marks the beginning of the Dharwar Orogenic Cycle (Appendix 20-G).

The accretion of the Aravalli-Bundelkhand and West-Dharwar cratons onto the southern eastern margins of Vaalbara at ~2.58-2.5 Ga respectively completes the formation of the late Neoarchaean to early Palaeoproterozoic supercontinent “Afrindalia” (Appendix 20-I).

4.3 LATE NEOARCHAEAN-PALAEOPROTEROZOIC EVOLUTION (~2.585-1.73 GA)

4.3.1 POST-LIMPOPO AND LATE-TO POST-NYASSA (~2.585-2.47 GA) OROGENIC PERIOD

The period between the end of the Limpopo Orogenic Cycle at ~2.585 Ga and the beginning of tectono-magmatic activity during the Mtshingwe-Kalahari-Gascoyne Orogenic Cycle at ~2.47-2.22 Ga, is characterised by relative tectonic quiescence and stability, as well as low freeboard and high sea level conditions (*cf.* Eriksson *et al.*, 1999) within the western and central parts of the supercontinent Afrindalia, *i.e.* Kaapvaal and Pilbara cratons (Appendix 20-I).

Within the Kaapvaal Craton, ongoing decay of the asthenospheric upwelling (developed during active lithospheric rifting at ~2.72-2.64 Ga) in the form of accelerated thermal subsidence and formation of an unitary subsiding sag basin across the area of the impactogenal Ventersdorp rift, accompanied by tectonic tilting/flexuring of the depositional surface from northwards during Lower Black Reef Formation-time (Clendenin *et al.*, 1991; Els *et al.*, 1995; Eriksson & Reczko, 1995) to southwestwards (Clendenin *et al.*, 1988b; Clendenin, 1989; Altermann & Herbig, 1991; Hälbich *et al.*, 1993), causes the marine transgression (initiated during Upper Black Reef/Vryburg Formation-time at ~2.62-2.585 Ga) to advance further craton-inwards from the craton’s passive western margin northeastwards along the Ventersdorp rift and to establish shallow marine epeiric sea conditions over as much as 90% of the Kaapvaal Craton. Carbonate platform sedimentation at ~2.585-2.55 Ga results in a thick carbonate succession of the Lower Ghaap, Taupone and Chuniespoort groups (Martin *et al.*, 1998) which is followed by a second major transgression at ~2.516-2.43 Ga (Altermann & Nelson, 1998), during which banded iron formation (BIF) platform deposits of the Upper Ghaap, Taupone and Chuniespoort groups develop over much of the Kaapvaal Craton within three structural basins (bounded by reactivated suture zones and crustal faults of the Pongola and Ventersdorp rift basins), *i.e.* the Griqualand West, Kanye and Transvaal basins respectively (Button, 1973a,b, 1976a; Beukes, 1980, 1983; Key, 1983; Button, 1986; Clendenin *et al.*, 1988a, b & c; Clendenin, 1989; Klein & Beukes, 1990; Eriksson *et al.*, 1995; Eriksson & Reczko, 1995; Eriksson & Altermann, 1998; Altermann & Nelson, 1998; Catuneanu & Eriksson, 1999; Nelson, 1999) (Appendix 20-I).

Episodic and alternating minor extensional (normal-slip) and compressional (reverse-slip) reactivation of palaeosuture zones (*e.g.* Thabazimbi-Murchison and Magaliesberg-Barberton suture zones) within the northern and central Kaapvaal Craton during Lower Chuniespoort Group (Malmani Subgroup) depositional time (~2.585-2.55 Ga), influencing sedimentation along the northern margin of, and within, the intracratonic Chuniespoort Group depository (as indicated by alluvial-fan deposits, subaqueous slump breccias and diamictites along the northern margin and rhythmites further south within the basin) (Clendenin, 1989; Martin, 1990; Martin *et al.*, 1990; Henry *et al.*, 1993) and accompanied by transgressions and regressions, as well as the craton-wide southwestwards tectonic tilt of the depositional surface, is related to the combined effects of thermal subsidence of the Ventersdorp impactogenal rift and NNE-SSW compressive far field stress conditions (Clendenin *et al.*, 1988b & c; Clendenin, 1989; Martin, 1990; Martin *et al.*, 1990) induced during late Nyassa orogenic activity along the northern margin of the Zimbabwe Craton, causing differential uplift of the Zimbabwe Craton, Central Zone Terrane and northern Kaapvaal-Grunehogna Craton until ~2.53 Ga (Appendix 20-I).

Tectonic uplift of the Zimbabwe Craton relative to contemporaneous subsidence of the Kaapvaal Craton further south results in accelerated erosion of lithologies mainly of the ~2.72-2.64 Ga old intracratonic magmatic arc formed during the Hurungwe Orogenic Cycle and subordinately of older Archaean basement of the Zimbabwe Craton, and their southward transport and deposition as molasses-type clastic sediments (*i.e.* quartzites of the Lower Gumbu Group/Beit Bridge Complex) syntectonically and unconformably above multiphase deformed and metamorphosed Archaean basement within the southern part of the Limpopo Central Zone Terrane at <~2.64 Ga, hence representing a stratigraphic correlative to the Black Reef/ Vryburg Formation (*cf.* Buick *et al.*, 2003; Barton *et al.*, 2003) (Appendix 20-H).

Subsequent marine transgressions extend from the south intermittently further north beyond the Palala suture zone into the southern parts of the Limpopo Central Zone Terrane, leading to shallow marine epeiric sea conditions and the deposition of carbonate and sedimentary rocks (*i.e.* marbles and metasediments of middle and Upper Gumbu Group/Beit Bridge Complex) above the initial molasses-type clastic deposits of the Lower Gumbu Group, hence representing stratigraphic correlatives to deposits of the ~2.585-2.43 Ga "Chuniespoort-Ghaap-Taupone Group" (*cf.* Buick *et al.*, 2003; Barton *et al.*, 2003) (Appendix 20-I).

Similarly within the southwestern part of Afrindalia, *i.e.* over large portions of the Pilbara Craton, a major marine transgression, continental drowning and lowered continental freeboard conditions are initiated at ~2.6 Ga and the result of ongoing decay of the asthenospheric upwelling (developed during active lithospheric rifting at ~2.775-2.62 Ga) in the form of accelerated thermal subsidence across the area of the intracratonic back-arc basin/magmatic arc complex. The marine transgression establishes shallow marine epeiric sea conditions over much of the Pilbara Craton which results in continuous chemical sedimentation (BIFs, carbonates) with very little clastic disturbance (shales) of the Hamersley Group at ~2.6-2.43 Ga into the intracratonic, deep, shelf-type (back-arc) basins formed during deposition of the Fortescue Group, conformably over deposits of the Jeerinah Formation (Upper Fortescue Group) (*cf.* Trendall *et al.*, 1998; Nelson *et al.*, 1999; Jahn & Simonson, 1995; Barley *et al.*, 1998; Martin *et al.*, 1998, 1999; Pickard, 2002) (Appendix 20-I).

Penecontemporaneously with large-scale marine transgressions and lowered freeboard levels over the western and central parts of the supercontinent Afrindalia (*i.e.* over the Kaapvaal-Grunehogna and Pilbara cratons), eustatic sea level fall and marine regression due to glacial climate, as well as penecontemporaneous intracratonic extension within the southern part of Afrindalia (*i.e.* within Singhbhum and Bastar cratons) in response to continental collision along the Central Indian Tectonic Zone (suture) during the Central Indian Orogeny at ~2.55-2.5 Ga (see above), results in the deposition of basal glacial diamictites, conglomerates and poorly sorted arkosic terrestrial sediments of alluvial fan origin, and profuse mafic/ultramafic volcanism of the Dhanjori Formation (within Singhbhum Craton) and Sakoli Group (within Bastar Craton) unconformably above the Younger Iron Ore Group and Nandagao Group in intracratonic (impactogenal?) rifts at ~2.55-2.43 Ga respectively (Posamantier & Veil, 1988; Bandyopadhyaya *et al.*, 1995; Bose *et al.*, 1997; Eriksson *et al.*, 1999; Mazumder *et al.*, 2000) (Appendix 20-I).

Relative tectonic quiescence and thermal subsidence of the intracratonic Dhanjori rift basin and a marine transgression (due to high atmospheric CO_2 build-up from volcanism and restricted weathering under glacial cover) over the Singhbhum Craton, results in the deposition of mainly marine sediments (sand-, silt-, mudstone, shale) of the Chaibasa Formation above the Dhanjori Formation and older lithologies at ~2.4-2.3 Ga (Bose *et al.*, 1997; Mazumder *et al.*, 2000) (Appendix 20-J).

Within the Zimbabwe Craton, tectono-magmatic activity during the Nyassa Orogeny, with crustal extension and the development of the intracratonic, impactogenal Popoteke failed rift, had ceased within most parts of the craton at ~2.585 Ga. Thermal uplift related to the Great Dyke intrusion and concomitant rifting results in high freeboard conditions and substantial erosion and/or non-deposition of supracrustals between ~2.585 and ~2.22 Ga. In comparison, passive margin rifting and marine transgression along the western edge of the Zimbabwe Craton resulted in deposition of the protoliths (*i.e.* from base to top: arkoses, greywackes, marls, carbonates, arenites, turbidites) of the Kariba, Chipisa, Chitumbi and Charoti paragneisses in epicratonic rifts and as shelf sequence under initial shallow, later deeper marine conditions at ~2.585-2.47 Ga (*cf.* Master, 1991a & b) (Appendix 20-I).

Towards the end of the post-Nyassa tectonic stable period, predominantly Mesoarchaean intracratonic suture zones within the entire Zimbabwe Craton experience increasingly more intense tectonic reactivation in the form of transtension under brittle conditions (this study), which is accompanied by minor felsic magmatism (*i.e.* porphyries and granites) and associated hydrothermal fluid flow with structurally controlled gold-sulphide-tungsten mineralisation and alteration/isotopic resetting of older lithologies along these trans-lithospheric structures and newly formed shear zones at ~2.49-2.47 Ga, heralding the beginning of the Mtshingwe-Kalahari-Gascoyne Orogenic Cycle and Mtshingwe Orogeny at ~2.47 Ga. Minor hydrothermal activity and associated alteration/isotopic resetting of older lithologies, and possibly felsic magmatism extends southwards into the Limpopo Central Zone Terrane and north-central Kaapvaal Craton (for details see below) (Appendix 20-I).

Penecontemporaneously with renewed minor tectono-magmatic and hydrothermal activity within the Zimbabwe Craton, LCZ and northern Kaapvaal Craton at ~2.49-2.47 Ga during the early pre-orogenic stage of the Mtshingwe Orogeny is subtle tectonic activity in the form of uplift along the western margins of the Kaapvaal and Pilbara cratons, which results in regressive marine conditions, decreasing sea levels and elevated continental freeboard. This leads to a decrease in chemical marine sedimentation (*i.e.* BIFs, carbonates) within the Kaapvaal Craton and in deposition of increasingly more clastic sediments with minor intermittent (~2.47-2.46 Ga old) volcanism of the Koegas Subgroup (upper Ghaap Group) and Duitschland Formation (upper Chuniespoort Group) within the intracratonic Griqualand West and Transvaal subbasins respectively. Comparatively high sea level and low freeboard conditions prevail within the Pilbara Craton at this time, resulting in the continued deposition of deep shelf chemical sediments (*i.e.* BIFs) of the Boolgeda Iron Formation (uppermost Hamersley Group). However, felsic volcanism either subaerial (tuffs) or subaqueous (lavas) of the underlying Upper Brockman Iron and Woongarra formations at ~2.46-2.45 Ga respectively, indicates the beginning of tectonic activity in the form of uplift/doming also within the Pilbara Craton (*cf.* Clendenin, 1989; Eriksson & Reczko, 1995; Eriksson *et al.*, 1999; Barley *et al.*, 1998; Pickard, 2002) (Appendix 20-I).

Lowered sea level and elevated continental freeboard conditions within the Kaapvaal and Pilbara cratons peak in the time interval ~2.43-2.35 Ga, creating a regional hiatus of approximately 80 m.y. During this period considerable southeastwards crustal tilting, differential uplift, weathering and erosion (more intense in the west) of BIF and the underlying carbonate platform rocks, and/or non-deposition is taking place as a result of pre-rift doming preceding active rifting with the onset of Pretoria and Turee Creek groups deposition at ~2.35 Ga within the Kaapvaal and Pilbara cratons respectively (*cf.* Eriksson *et al.*, 1999; Catuneanu & Eriksson, 1999) (Appendix 20-J).

4.3.2 MTSHINGWE-KALAHARI-GASCOYNE OROGENIC CYCLE (~2.47-2.22 GA)

Following a period of relative tectonic quiescence and crustal stability within the central part of the supercontinent Afrindalia (*i.e.* within Kaapvaal-Grunehogna and Pilbara cratons) for approximately 120 million years, *i.e.,* since the end of the Limpopo Orogenic Cycle at ~2.585 Ga, as well as penecontemporaneous with intracratonic extension in the southern part of Afrindalia (*i.e.* within Singhbhum and Bastar cratons) during and after the Central Indian Orogeny at ~2.58-2.5 Ga, the initiation of westward subduction (*cf.* Stettler *et al.*, 1997) of oceanic lithosphere beneath the Archaean Yilgarn-Rehoboth Craton and composite Bamilimu Craton (comprises the smaller Archaean **Ba**ngweulu, **Mi**nga, **Li**kasi and **Mu**kingwe terranes/cratons; *cf.* Petters, 1991; Renault *et al.*, 2002) leads to convergence between Afrindalia and these two continents and to closure of the intervening Mtshingwe-Kalahari-Gascoyne oceanic basin, marking the beginning of the Mtshingwe-Kalahari-Gascoyne Orogenic Cycle at ~2.47 Ga (Appendix 20-I).

Oceanic basin closure, followed by continental collision and orogenic activity takes place first along the northwestern margin of the supercontinent Afrindalia, *i.e.* western edge of Zimbabwe Craton, where the Bamilimu continent is accreted onto Afrindalia during the Mtshingwe Orogeny at ~2.47-2.43 Ga. This results in the deformation and metamorphism of the ~2.585-2.47 Ga old passive margin rift/shelf sequence and its obduction onto the Neoarchaean (~2.72-2.64 Ga) Hurungwe Gneiss basement (= intracratonic magmatic arc of Upper Bulawayan greenstones) of the western Zimbabwe Craton (*cf.* Loney, 1969; Master, 1991) (Appendix 20-J).

NW-SE compressive far field stress induced into the western Zimbabwe Craton during this orogenic activity results the transtensional reactivation of predominantly Mesoarchaean intracratonic suture zones and formation of new shear zones under brittle conditions, as well as in NE-SW oriented crustal extension and development of the NW-SE striking, extensional Mtshingwe fracture system across the entire craton. Intracratonic extensional/transtensional tectonism is accompanied by structurally controlled minor felsic magmatism (*e.g.* Hatchland porphyry/Midlands Greenstone Belt (Pitfield & Campbell, 1993), post-tectonic granite in NMZ (Berger *et al.*, 1993)) and hydrothermal fluid flow with gold-sulphide-tungsten mineralisation (Tomschi *et al.*, 1989; Darbyshire *et al.*, 1996; Frei & Pettke, 1996; Oberthür *et al.*, 2000) and alteration/partial isotopic resetting of older lithologies (*cf.* Davies *et al.*, 1970; Hawkesworth *et al.*, 1975, 1979; Jahn & Condie, 1976; Hahn *et al.*, 1991; Kent *et al.*, 1996; Mukasa *et al.*, 1998; Oberthür *et al.*, 2000; Wingate, 2000; McCourt *et al.*, 2001) along the reactivated sutures and newly formed shear zones across large parts of the craton, extending across the Tuli-Sabi-Triangle suture zone into the eastern part of the Limpopo Central Zone Terrane (*cf.* Barton *et al.*, 2003) (Appendix 20-J). Structurally controlled hydrothermal activity, leading to alteration and partial isotopic resetting of older lithologies, and possibly minor felsic magmatism (*e.g.* Palmietfontein Granite situated immediately to the south of SMZ) extend also beyond the Palala suture zone into the northern and central Kaapvaal Craton as far south as to the northern margin of the Witwatersrand Basin (*cf.* Key & Wright, 1982; Barton *et al.*, 1983; Armstrong *et al.*, 1986; Vearncombe *et al.*, 1987; Poujol *et al.*, 1998, 1999; Barton *et al.*, 1999) (Appendix 20-J).

Further south along the western margin of Afrindalia, continuing subduction-related melting of hydrated oceanic crustal material beneath the Yilgarn-Rehoboth Craton and under- and intraplating of mafic-ultramafic magmas into the craton results in craton-wide lithospheric (back-arc basin) extension and formation of an extensional fracture system, accompanied by intrusion of mafic magmas along the extensional fracture zones as the Widgiemootha dyke swarm at ~2.42 Ga (Appendix 20-J).

The end of the Mtshingwe-Kalahari-Gascoyne Orogenic Cycle is characterised by complete closure of the Kalahari-Gascoyne oceanic basin and continental collision and accretion of the Yilgarn-Rehoboth Craton

onto the western margin of Afrindalia (*i.e.* western margins of Pilbara, Narryer and Kaapvaal-Grunehogna cratons) along the Kalahari-Gascoyne suture zone to form the Palaeoproterozoic supercontinent “Afrindalia” during the Kalahari-Gascoyne Orogeny at ~2.43-2.35 Ga (Appendix 20-K).

Approximately east-west and northwest-southeast oriented compressive far field stresses are induced into the Kaapvaal-Grunehogna and Pilbara cratons causing the development of the thin-skinned east- and southeast-verging, craton-inwards migrating Kalahari (*i.e.* Uitkomst thrust event = pre-Makganyene Formation deformation, *cf.* Altermann & Hälbich, 1990, 1991; = pre-Segwagwa Group deformation, *cf.* Mapeo,1995) and Ophthalmian (*cf.* Powell, 1997) fold-thrust belts respectively, as well as the formation of intracratonic, peripheral foreland basins ahead of both fold-thrust belts. Thrust-related uplift and erosion of the western margins of the Kaapvaal-Grunehogna and Pilbara cratons provides terrigenous detritus which is deposited within the foreland basins as molasse-type sand-/siltstones and greywackes of the lower Segwagwa, lower Postmasburg and Turee Creek groups (Appendix 20-K). The northeast-southwest configuration of the Chuniespoort-Ghaap-Taupone Group depository (controlled by the Ventersdorp impactogenal rift) changes to a configuration with uplift of the western Kaapvaal Craton and deepening towards the east during Pretoria Group time (*cf*. Dorland, 2004).

As a result of the thin-skinned thrust tectonics within the Kalahari and Ophthalmian fold-thrust belts, supracrustals of the Hamersley Supergroup (Pilbara Craton) and Ventersdorp Supergroup and Ghaap Group (Kaapvaal Craton) are transported in an southeasterly and easterly direction over Archaean granite-greenstone basement along their basal unconformable contact with the basement, as well as internally predominantly along bedding and unconformity planes (*cf.* Tinker *et al.*, 2002). Compressive far field stress conditions extend further eastward to the central parts of the Kaapvaal Craton, where they result in positive inversion of late Central Rand Group thrusts and mid-Ventersdorp extensional faults, as well as formation of new easterly verging thrust faults and N-trending, low-amplitude, open folds along the western margin of the Witwatersrand Basin (*cf.* Clendenin *et al.*, 1990; van der Merwe, 1994; see Section 6.3.3.2.) (Appendix 20-K).

Further continent-inwards within the central part of the supercontinent Afrindalia and to the east and ahead of the compressive fold-thrust belts, *i.e.* central Kaapvaal and Singhbhum cratons, lithospheric extension results in the tectonic rejuvenation of Archaean suture and crustal fault zones.

Within the central Kaapvaal Craton, the periodically transtensional reactivated Palala and Thabazimbi-Murchison suture zones and crustal faults of the Neoarchaean Pongola rift basin control erosion from a relatively elevated source area to the north of the suture zones (*i.e.* Pietersburg and Central Zone terranes of northern Kaapvaal Craton and Limpopo Province respectively), as well as alluvial fan and fan delta deposition of coarse terrigenous clastics (arkoses, quartz arenites and shales) along the northern margin of the Pretoria Basin, grading southward into shallow-marine, less to non-clastic rocks (siltstones, quartz arenites, carbonates and jasper) of the Lower Pretoria Group (Rooihoogte – Timeball Hill formations) in fault-controlled (pull-apart) basins within the rejuvenated Pongola rift basin to the south at ~2.35-2.22 Ga.

Large asymmetric, easterly vergent, upright and recumbent to highly inclined folds without an associated axial planar cleavage form most probably as roll-over anticlines/synclines above extensionally reactivated listric Pongola rift faults in post-Timeball Hill to pre-Boshoek Formation time (*i.e.* between 2263 ± 85 and 2222 ± 13 Ma) for example in the Mpumalanga Province, which is accompanied by the deposition of coarse clastic sediments (arkoses, quartzites, conglomerates, diamictites) of the Boshoek Formation unconformably over folded shales of the Timeball Hill Formation (*cf.* Harley *et al.*, 1990).

Intensified rifting within the Kaapvaal Craton in the closing stages of the Kalahari-Gascoyne Orogeny at ~2.22 Ga, results in voluminous mafic volcanism (*i.e.* lavas of Hekpoort Formation) within the reactivated Pongola rift basin (*cf.* Sharpe, 1981; Tankard *et al.*, 1982; Schreiber, 1990; Harmer & Von Gruenewaldt, 1991; Schreiber *et al.*, 1992; Eriksson *et al.*, 1991, 1993b, 1994b, 1995, 1996; Eriksson & Reczko, 1995; Reczko *et al.*, 1995; Bumby, 1997; Bumby *et al.*, 1998; Catuneanu & Eriksson, 2002) (Appendix 20-K).
Penecontemporaneously, intracratonic rifting and relative sea level fall within the Singhbhum Craton results in the fluvial and aeolian deposition of poorly sorted gritty quartzites and finer siliciclastics, as well as in profuse bimodal volcanism of the Dhalbhum Formation unconformably above the Chaibasa Formation and older lithological units at ~2.3-2.22 Ga (Ray *et al.*, 1996; Mazumder, 1996; Singh, 1997, 1998) (Appendix 20-K).

Tectonic reactivation of suture and crustal shear zones within the Kaapvaal-Grunehogna Craton during the Kalahari-Gascoyne Orogeny is accompanied by easterly directed migration of hydrocarbon-bearing hydrothermal fluids, leading to associated alteration/isotopic resetting of older Archaean and Proterozoic lithologies along such structural discontinuities (see Appendix 23 for a summary of isotopic resetting ages) and remobilisation of older lode-type gold into younger, or reactivated older shear zones at ~2.35-2.22 Ga (*cf.* Barton *et al.*, 1990; Drennan *et al.*, 1997, 1999). However, magmatic activity within Afrindalia appears to have been minimal during this period and is restricted to the occasional intrusion of crustally derived granites, such as the Messica Granite, into the eastern Zimbabwe Craton (western Mozambique) along a possible Archaean suture zone between the Tokwe and Barue terranes at ~2.35 Ga (Appendix 20-K).

In the period between ~2.32 Ga and ~2.24 Ga occurs the change from a reducing to an oxidising atmosphere (Dorland *et al.*, 2002; Dorland, 2004; Bekker *et al.*, 2004), which is approximately 50 Ma earlier than the Cloud-Holland model for the history of atmospheric oxygen suggests (Holland, 1984; Rye & Holland, 1998; Ohmoto, 1996, 1997; Dorland, 1999; Beukes *et al.*, 2002a & b), and coincides with the deposition of the glacial diamictites of the Rooihoogte/Makganyene and Timeball Hill formations and volcanism of Hekpoort/Ongeluk Formation during the second and third glacial event in the Palaeoproterozoic (Wing *et al.*, 2002; Bekker *et al.*, 2004).

4.3.3 UBENDIAN OROGENIC CYCLE (~2.22-1.86 GA)

Initiation of easterly subduction of oceanic lithosphere under the western margin of Afrindalia at ~2.22 Ga, marks the beginning of the Ubendian Orogenic Cycle with convergence between the Congo Craton and Afrindalia, progressive closure of the intervening Ubendian oceanic basin, as well as rifting and opening of the Magondi and Gordonia oceanic basins between Afrindalia and the Bamilimu Craton and Afrindalia and the Yilgarn-Pilbara Craton due to slab roll-back respectively (Appendix 20-L).

Opening of the Magondi oceanic basin is associated with the development of epi-/continental rift basins along the northwestern margin of Afrindalia, *i.e.* along the western margins of the Zimbabwe and Nyassa cratons. Along the western edge of the Zimbabwe Craton, the basal, continental, volcano-sedimentary Deweras Group of the Magondi Supergroup (including Malaputese Formation of Dete-Kamativi Inlier as correlative) (predominantly arenaceous red-bed succession with tuffs, agglomerates, subalkaline basalts and associated feeder dykes and sills) is deposited unconformably over Archaean basement in the east and the Palaeoproterozoic Hurungwe gneisses in the west. Deposition occurs in a shallow water environment within pull-apart basins developing along extensional/transtensional reactivated faults and fractures of the Popoteke fault/fracture system at ~2.22-2.1Ga (*cf.* Bliss, 1970, 1971; Tennick & Phaup, 1976, Newham,

1986; Leyshon & Tennik, 1988; Treloar, 1988; Höhndorf *et al.*, 1989; Master, 1991a & b, 1994; Bartholomew, 1999; Hahn & Steiner, 2001; Hahn, 2002) (Appendix 20-L). Contemporaneously further north along the western margin of the Nyassa Craton, volcano-sedimentary protoliths of the Mkushi Gneiss (central Zambia) are deposited in epi-/continental rift basins (Appendix 20-L).

Further east within the interior of Afrindalia, contemporaneous lithospheric extension due to subduction-related slab roll-back commences at ~<2.22 Ga and leads to episodic extensional/transtensional reactivation of Archaean and older Palaeoproterozoic suture and crustal fault/shear zones (Appendix 20-L):

- Within the Kaapvaal Craton, lithospheric extension results in the combined extensional reactivation and post-orogenic collapse (negative inversion) of the Palaeoproterozoic (~2.35-2.22 Ga) Kalahari fold-thrust belt, as well as in the continuous extensional rejuvenation of the Neoarchaean (~2.98-2.97 Ga) Pongola rift basin to the east.

- Intracratonic pull-apart rift basins develop within the area of the transtensionally reactivated (inverted) Kalahari fold-thrust belt in the western Kaapvaal Craton at ~2.22-2.05 Ga, forming the depositories for siliciclastic sediments and mafic volcanics of the Upper Postmasburg Group (Ongeluk & Voëlwater Formations) and Upper Segwagwa Group (Tsatsu Formation – Gatespane & Mogapinyana Formations; Ditlhojana Volcanic Formation – Sengoma Quartzite Formation) (Appendices 20-L & 20-M).

- Lithospheric extension within the northern and central parts of the Kaapvaal Craton is responsible for continuous erosion of the Central Zone and Pietersburg terranes as relatively elevated source terrains to the north of the reactivated Palala and Thabazimbi-Murchison suture zones respectively, for alluvial fan and fan delta deposition of coarse terrigenous clastics (arkoses, quartz arenites and shales) along the northern margin of the Pretoria Basin, grading southward into shallow-marine, less to non-clastic rocks (siltstones, quartz arenites, carbonates and jasper), as well as for the eruption of minor mafic volcanic intervals of the Upper Pretoria Group (Dwaalheuwel – Houtbek/Rayton/Lower Woodlands formations) in fault-controlled (pull-apart) basins within the rejuvenated Pongola rift basin to the south at ~2.22-2.1 Ga (*cf.* Sharpe, 1981; Tankard *et al.*, 1982; Schreiber, 1990; Schreiber *et al.*, 1992; Harmer & Von Gruenewaldt, 1991; Eriksson *et al.*, 1991, 1993b, 1994b, 1995, 1996; Eriksson & Reczko, 1995; Reczko *et al.*, 1995; Bumby, 1997; Bumby *et al.*, 1998) (Appendix 20-L).

- Subduction-related slab roll-back and related lithospheric extension within the southwestern part of Afrindalia causes intense intercontinental rifting, progressing to continental break-up and formation of the Gordonia oceanic basin between the Rehoboth-Kaapvaal and Yilgarn-Pilbara cratonic blocks at ~2.2-2.05 Ga. Contemporaneously, rifting and extensional reactivation (negative inversion) of the Palaeoproterozoic (~2.35-2.22 Ga) Ophthalmian fold-thrust belt in the southern Pilbara Craton and its counter-part in the northern Yilgarn Craton is accompanied by intracratonic rift basin deposition of siliciclastic sediments of the Lower Wyloo Group and Yerrida Group respectively, which advances to continental break-up and opening of the Capricorn oceanic basin between the Yilgarn and Pilbara cratons (Appendix 20-L).

- Penecontemporaneously within the southern part of Afrindalia, *i.e.* within the Singhbhum and Bastar cratons, a rise in relative sea level and a marine transgression result in the deposition of initially terrestrial sediments (arkosic and quartzitic sandstones, shales and minor conglomerates), but later progressively more marine carbonate-dominated lithologies of the Kolhan and Sausar groups at ~2.2-2.1 Ga (Gosh & Chatterjee, 1990; 1994; Saha, 1994) (Appendix 20-L).

Continental rifting and widening of the Magondi oceanic basin is reversed with the initiation of southeasterly subduction of oceanic lithosphere under the western edge of Afrindalia, heralding the convergence between the Bamilimu Craton and Afrindalia and the closure of the Magondi oceanic basin at ~2.1 Ga (Appendix 20-M).

First compressive stress induced into the overriding western leading edge of Afrindalia at ~2.1 Ga results in tilting and erosion of the supracrustal rift sequences of the Deweras Group and correlatives within the western Zimbabwe Craton, which precedes deposition of the subsequent Lomagundi and Piriwiri groups (*cf.* Bliss, 1970, 1971; Tennick & Phaup, 1976, Newham, 1986; Leyshon & Tennik, 1988; Treloar, 1988; Höhndorf *et al.*, 1989; Master, 1991a & b, 1993, 1994; Bartholomew, 1999; Hahn & Steiner, 2001; Hahn, 2002) (Appendix 20-M).

Thermal subsidence and associated deepening and widening of the Deweras rift basin at ~2.1-2.05 Ga leads to a marine transgression into, and drowning of the rift basin, and to the deposition of synchronous eastern continental shelf (basal conglomerate, dolomites, quartzites, arkoses) and western equivalent deep water deposits (slates and quartzites) of the Lomagundi and Piriwiri groups respectively (including Inyantue, Tshontanda & Kamativi formations of Dete-Kamativi Inlier) (*cf.* Bliss, 1970, 1971; Stowe, 1978; Stagman, 1981; Leyshon & Tennik, 1988; Treloar, 1988; Master, 1991a & b, 1993, 1994; Schidlowski & Todt, 1998; Bartholomew, 1999; Höhndorf & Vetter, 1999; Hahn & Steiner, 2001; Hahn, 2002) (Appendix 20-M).

Subduction-related magmatic under- and intra-plating results in the development of an oceanic to intracratonic magmatic arc and adjacent back-arc basin complex to the southeast at ~2.1-2.05 Ga along the western margin of Afrindalia, *i.e.* western margins of the Nyassa, Zimbabwe, Kaapvaal and Rehoboth cratons (Appendix 20-M). Pre-orogenic magmatic-arc calc-alkaline granitoids (*e.g.* Miami and Kubu Island granites) intrude into adjacent back-arc basin deposits of the Magondi Supergroup within the western Zimbabwe Craton, whereas intra-cratonic magmatic arc deposits in the form of calc-alkaline granites intrusive into clastic sediments and porphyritic felsic volcanics and volcanoclastics (ignimbrites and tuffs) of the Lower Okwa Group (Okwa Inlier) develop within the extreme northwestern Kaapvaal Craton (*cf.* Loney, 1969; Priem *et al.*, 1972; Aldiss & Carney, 1992; Carney *et al.*, 1994; Ramokate, 1996; Ramokate *et al.*, 1996, 1997; Hanson *et al.*, 1998b). The development of a magmatic arc/back-arc basin complex along the western edge of the Rehoboth Craton occurs penecontemporaneously but over a much longer period at ~2.05-1.86 Ga, and is represented by the deposition of the Metamorphic Suite, *i.e.* volcano-sedimentary successions of the Abbabis and Neuhof formations and Hohewarte and Mooiriver/Kairab complexes (= back-arc basin), as well as predominantly pre-orogenic calc-alkaline granitoids of the Rucana Gneiss Complex (Angola), Epupa and Grootfontein complexes and Huab Formation (Namibia) (= magmatic-arc) (*cf.* Jacob *et al.*, 1978; Burger & Walraven, 1979; SACS, 1980; Tegtmeyer & Kröner, 1985; Reid, 1988; Ziegler & Stössel, 1991, 1993; Becker *et al.*, 1996; Becker & Brandenburg, 2000, 2002; Becker *et al.*, 2000) (Appendices 20-M & 20-N).

In response to NW-SE compressive far stress field conditions within the northern Kaapvaal Craton induced during the early stages of the Magondi Orogeny at ~2.1-2.05 Ga, approximately E-W striking, Meso- to Neoarchaean (>2.7 Ga) translithospheric suture zones (*e.g.* Palala, Pietersburg, Thabazimbi-Murchison and Magaliesberg-Barberton suture zones and Neoarchaean (~2.81-2.64 Ga), Limpopo Orogeny-related shear zones within the northern Kaapvaal Craton experience initially dextral strike-slip (at ~2.1-2.06 Ga), later during the main and late phases of the Magondi & Okwa orogenies (~2.05-1.86 Ga) progressively more dextral oblique reverse-slip reactivation (*i.e.* progressing from transtensional to transpressional reactivation). Generally NW-SE striking extensional faults of the Neoarchaean (~2.97-2.95 Ga) Pongola impactogenal rift basin undergo normal dip- to oblique-slip reactivation (*i.e.* extensional-transtensional reactivation), whereas NE-SW striking extensional faults of the Neoarchaean (~2.71-2.64 Ga) Ventersdorp rift basin and the Mesoarchaean (>3.1 Ga) Pilanesberg,

Kwaggasrand-Wonderkop and Swavelpoort-Steelpoort suture zones of similar strike orientation, experience sinistral strike-/normal oblique-slip reactivation (Appendix 20-M).

Reactivational faulting along these pre-existing suture and crustal shear/fault zones is accompanied by large-scale, low-amplitude, open, upright, symmetrical folding of the Transvaal Supergroup, Woodlands Formation and Rooiberg Group along two different, but contemporaneously developing trends prior to and during the emplacement of the RLS at ~2.1-2.06 Ga. NE-SW to ENE-WSW folding is confined to the northern Kaapvaal Craton (*i.e.* western Transvaal Basin) and develops directly in response to NW-SE oriented compressive *in situ* far field stress, whereas NW-SE to NNW-SSE folding is spatially and genetically related to extensional faulting along the NW-SE striking Pongola rift faults (*i.e.* fault-bend folding) (*cf.* Crockett, 1969a, b, 1971b, 1972; Key, 1983; Dietvorst, 1988; Crockett & Key, 1989; Hartzer, 1987, 1989, 1994, 1995; Eriksson *et al.*, 1998). Hence, an interference pattern between both groups of folds develops only in the western Transvaal Basin, whereas for the remainder of the basin an interference pattern develops between fault-bend folds associated with reactivated NW-SE striking Pongola rift faults and the NE-SW striking Pilanesberg, Kwaggasrand-Wonderkop and Swavelpoort-Steelpoort suture zones (*cf.* Sharpe & Chadwick, 1982; Harmer & von Gruenewaldt, 1991; Odgers *et al.*, 1993; Hartzer, 1995; Bumby *et al.*, 1998) (Appendix 20-M).

The initial transtensional reactivation of Archaean suture zones/terrane boundaries in combination with the transtensional rejuvenation of the Pongola rift basin within the northern Kaapvaal Craton during the early stages of the Magondi Orogeny at ~2.1-2.05 Ga, results in decompressional melting of the subcontinental lithospheric upper mantle and the formation of vast amounts of ultramafic-mafic magmas. Their ascent through the continental crust is facilitated primarily along the deep-seated, translithospheric suture zones and partly along extensional faults of the Pongola rift basin (Appendix 20-M).

Pre- to early Magondi orogenic magmatism in the northern and central Kaapvaal Craton at ~2.1-2.06 Ga commences with the intrusion of pre-Bushveld granophyric sills, their E-W striking feeder dykes (Rykoppies dyke swarm) and of the Marico Hypabyssal Suite (mafic sills) into supracrustals of the Chuniespoort and Pretoria groups, and the extrusion of mafic and felsic magmas of the Lower Rooiberg Group within the northern part of the craton (*e.g.* Harmer & von Gruenewaldt, 1991; Schweitzer *et al.*, 1995a & b, 1997; Buchanan *et al.*, 1999, 2002, 2004), the emplacement of small igneous complexes within the central part of the craton (*e.g.* Losberg, Lindequesdrift and Roodekraal complexes, as well as Schurwedraai, Baviaanskraal and Rietfontein alkaline granites within Vredefort Dome area; felsites and porphyritic felsite dykes in East Rand Goldfield), hydrothermal infiltration along reactivated pre-existing fault systems, and thermal overprinting within a large variety of stratigraphic units (*cf.* Willemse, 1959 1969; Fumerton, 1978; Cawthorn *et al.*, 1981; Sharpe, 1981, 1984; Hargraves, 1987; Engelbrecht, 1988, 1990; Walraven & Elsenbroek, 1991; Allsopp *et al.*, 1991; Moser & Hart, 1996; Moser, 1997; this study) (Appendices 25, 20-M & 20-0).

During this pre-Bushveld magmatic and tectonic instable period, the reactivation of Archaean fault and suture zones and concomitant interference folding cause the formation of a dome-and-basin topography in the northern and northwestern Kaapvaal Craton, *i.e.* to the north and northwest of the reactivated Pongola rift basin. Rapid crustal uplift, erosion of Pretoria/Segwagwa Group rocks and gravitational tectonic sliding of units of the Transvaal Supergroup from the dome areas south and eastwards into the rapid subsiding Pongola rift basin, results in the syn-tectonic deposition of the Upper Woodlands Formation (chaotic and very coarse-grained slump and talus debris) and Otse Group (conglomerates, shale-clast deposits and mudrocks) in fault-bounded basins developing within the confines of the reactivated western part of the Ventersdorp rift basin, coeval with Lower Rooiberg Group volcanism within the rejuvenated Pongola rift to the east at ~2.075-2.061 Ga (*cf.* Crockett, 1969a, b, 1971b, 1972; De Waal, 1970; Key, 1983; Engelbrecht,

1986, 1988; Dietvorst, 1988; Dietvorst *et al.*, 1991; Cheney & Twist, 1991; Hartzer, 1994, 1995; Eriksson & Reczko, 1995; Eriksson *et al.*, 1995, 1998; Bumby *et al.*, 1998) (NB: Deposition of the Otse Group occurs during emplacement of the BIC at ~2.061-2.05 Ga and represents the continuation of initial Upper Woodlands Formation sedimentation) (Appendix 20-M).

Intermediate to felsic magmas, generated during decompressional melting of the subcontinental lithospheric upper mantle and hence comagmatic to the mafic-ultramafic mantle derived magmas of the Rustenburg Layered Suite (RLS) of the Bushveld Igneous Complex (BIC), ascend comparatively fast through the cratonic lithosphere along deep-seated, translithospheric suture zones and partly along extensional faults of the Pongola rift basin and extrude as basaltic, andesitic to dacitic and rhyolitic lavas (with minor intercalated volcaniclastic and clastic units) of the Lower Rooiberg Group (Dullstroom Formation) unconformably over Pretoria Group deposits, as well as intrude as dykes and sills (*e.g.* Marble Hall diorite sills and epidiorite/norite dykes and sills within Witwatersrand Basin) prior to and during the emplacement of the RLS at ~2.075-2.056 Ga (*cf.* Twist & French, 1983; Cheney & Twist, 1991; Eriksson *et al.*, 1994a; Hatton & Schweitzer, 1995; Eales & Cawthorn, 1996; Walraven, 1997; Schweitzer *et al.*, 1995a, b, 1997; Schweitzer, unpubl.; Martini, 1998; De Waal & Armstrong, 2000; De Waal *et al.*, 2002) (Appendices 20-M & 20-O). Penecontemporaneously within the northwestern Kaapvaal Craton, the lower Kukong felsites and overlying conglomerates (stratigraphic equivalents to the Rooiberg Group felsic volcanics and chaotic rudaceous Upper Woodlands slump deposits) are deposited unconformably over sedimentary deposits of the Segwagwa Group prior to and during the intrusion of the Molopo Farms Complex at ~2.075-2.058 Ga (*cf.* Key *et al.*, 1996; Eriksson *et al.*, 1998; Lock *et al.*, 2002) (Appendices 20-M & 20-O).

This initial magmato-thermal activity culminates in the intraplating of vast amounts of upper mantle-derived mafic-ultramafic magmas into the subcontinental lithosphere of the northern Kaapvaal Craton, their ascent through the cratonic lithosphere primarily along the suture and rift fault zones, and in their structurally controlled emplacement as RLS of the BIC and related satellite intrusions (*e.g.* Molopo Farms, Koringkoppies, Modipe, Uitkomst, Uitloop, Dwarsfontein, Kaffirskraal, Losberg, Roodekraal, Vereeniging, Vogelstruisfontein, and Phalaborwa complexes) at ~2.061-2.05 Ga (*cf.* Schutte *et al.*, 1960; Hanekom, 1965; Verwoerd, 1967; Willemse, 1969; Tyler, 1979a; Nell, 1984; Eriksson, 1984; Gould & Rathbone, 1985; Kenyon *et al.*, 1986; Gould *et al.*, 1987; Kruger, 1989; Von Gruenewaldt *et al.*, 1989; Coetzee & Kruger, 1989; Eriksson, 1989; McCarthy *et al.*, 1990; Walraven *et al.*, 1990; Du Plessis, 1990; Du Plessis & Walraven, 1990; Harmer & von Gruenewaldt, 1991; Verwoerd, 1993; Von Gruenewaldt & Harmer, 1993; Reichhardt, 1994; Reischmann, 1995; Gauert *et al.*, 1995, 1996; Von Zyl, 1996; Gauert, 1998, 2001; De Waal & Armstrong, 2000; De Waal *et al.*, 2001; Curl, 2001) (Appendices 20-M & 20-O).

The emplacement of the RLS occurs at a critical level in the crust (~4km), where the magmatic pressure equalises and exceeds the overburden pressure, and the upper mantle-derived mafic-ultramafic magmas (original magma volume $>1x10^6$ km^3; Cawthorn & Walraven, 1998) are emplaced by lifting of overlying strata as sill-like, *ca.* 7000-9000 m thick laccolith with a slight discordance within deposits of the Transvaal Supergroup and Lower Rooiberg Group between the major suture zones and rift faults of the Pongola basin at ~2.061-2.059 Ga (*cf.* Kruger & Corner, 1987; Walraven *et al.,* 1990; Du Plessis & Levitt, 1987; Du Plessis, 1990; Du Plessis & Walraven, 1990; Walraven & Hattingh, 1993; Eales *et al.*, 1993; Eales & Cawthorn, 1996; Cawthorn, 1998; Cawthorn & Walraven, 1998; Cawthorn *et al.*, 1998; Good, 1999; Clarke *et al.*, 2000; Cawthorn & Webb, 2001; Buick *et al.*, 2001) (Fig. 4.2). The mechanical reactivation of these suture zones is accompanied and accelerated by thermal softening due to a higher geothermal gradient caused by the intraplating of these magmas (*cf.* Good, 1999). Intrusion loci or feeders to magmas of the RLS for each individual compartment develop at the intersection points between suture zones and Pongola rift faults (*cf.* Walraven, 1974; Sharpe *et al.*, 1981).

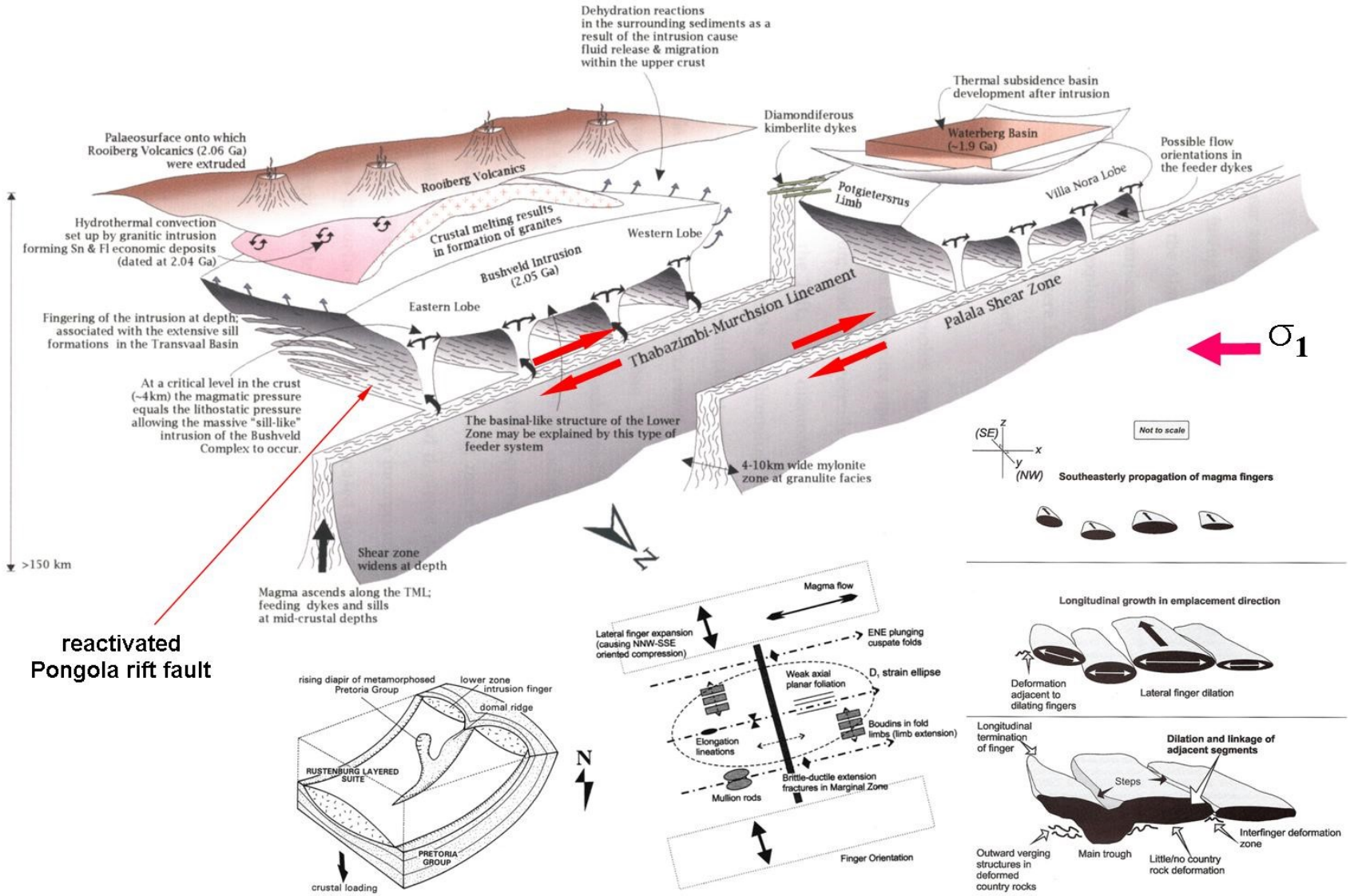


FIGURE 4.2 : Proposed Bushveld Complex intrusion mechanism utilising the Thabazimbi-Murchison, Barberton-Magaliesberg and Palala suture zones as conduits for ascending magmas of Rustenburg Layered Suite (RLS) along these translithospheric shear zones. At a critical level in the crust, the magmatic pressure equals the lithostatic pressure, which allows the massive "sill-like" RLS intrusion of the Bushveld Complex to occur (modified after Good, 1999). Insert: Sketch models illustrating the emplacement of the RLS as initial SE-advancing finger system to final sill system (Clarke *et al.*, 2000, 2009) and formation of diapirs/domes of metamorphosed Pretoria Group between coalescing intrusive fingers (Uken & Watkeys, 1997) proposed to be controlled by NW-SE striking, reactivated Pongola rift faults (this study).

Emplacement of the RLS-magmas within the Transvaal Supergroup occurs by lateral flow of finger-like sills in a local WSW–ENE (Spruitfontein inlier) but regionally NW-SE direction, thereby causing NNW-SSE and NE-SW oriented compression and folding in the interfinger areas and parallel to sill propagation direction, respectively (Clarke *et al.*, 2000, 2005, 2009), as well as the formation of diapirs/domes of metamorphosed Pretoria Group between coalescing intrusive fingers (Uken & Watkeys, 1997) (Figure 4.2). Within the main compartment of the BIC, the Pilanesberg, Kwaggasrand-Wonderkop and Swavelpoort-Steelpoort suture zones, as well as pre-RLS interference fold domes (*e.g.* Rooiberg and Stavoren fragments, Crocodile River and Denilton domes) and Pongola rift faults act as physical barriers and cause further compartmentalisation and variations regarding extent, thickness, and lithostratigraphy of the RLS (*cf.* Hatton & von Gruenewaldt, 1987; Du Plessis & Levitt, 1987; Bristow & Wilson, 1989; Du Plessis, 1990; Du Plessis & Walraven, 1990; Davey, 1992; Odgers *et al.*, 1993; Scoon & Teigler, 1994; Hartzer, 1995; Lea, 1996). In other words, the emplacement, geometry and position of the E-W trending main compartment, and of the separate NW-SE trending northern and southern compartments of the BIC are controlled by the Thabazimbi-Murchison and Magaliesberg-Barberton suture zones, as well as by the Palala and Sugarbush suture zones and rift faults of the central/main part of the Pongola rift (Appendix 20-M).

Similarly, decompression melting of the subcratonic lithospheric upper mantle at the intersection point of the transtensionally reactivated Mesoarchaean Kuruman and Amalia suture zones with the western marginal rift fault of the Neoarchaean Ventersdorp Basin results in the generation, ascent and intrusion of ultramafic-mafic magmas of the layered Molopo Farms Complex within the Griqualand West Supergroup at ~2.056-2.055 Ga (*cf.* Von Gruenewaldt *et al.*, 1987; Kruger, 1989; Wilhelm *et al.*, 1990; Du Plessis, 1990; Du Plessis & Walraven, 1990) (Appendix 20-M).

The dextral transtensional reactivation of ENE-trending translithospheric Archaean suture zones in the northern Kaapvaal Craton, decompressional melting of the subcontinental lithospheric upper mantle, generation of vast amounts of RLS ultramafic-mafic magmas and ascent through the continental crust along them is proposed to have occurred episodically in response to rhythmically induced pulses of SSE-directed compressive far field stress, causing the rhythmic emplacement of first-order layered magmatic cycles (*i.e.*, Marginal, Lower, Critical, Main and Upper zones) and numerous second- and third-order magmatic cycles (*i.e.*, subzones and units). The relatively short period (ca. 1 million years) of RLS magmatic activity took place at the end of peak-reaching extensional-transtensional stress field conditions and tectonics in the northern Kaapvaal Craton during the initial phase of the Magondi Orogeny at ~2.15-2.055 Ga.

Dehydration reactions in the surrounding sediments of the Transvaal Supergroup as a result of the intraplating of RLS magmas, cause fluid release and circulation and associated hydrothermal alteration in an contact-metamorphic aureole around the cooling RLS within the Transvaal Supergroup floor rocks, as well as non-pervasively and retrogressively within the RLS itself at ~2.059-2.056 Ga (*cf.* Nell, 1984; Schiffries & Rye, 1989, 1990; Kaneko & Miyano, 1990; Wallmach *et al.*, 1989, 1995; Schweitzer & Hatton, 1995; Good, 1999; Buick *et al.*, 2000, 2001). Furthermore, contact metamorphism, gravitational loading and heating of argillaceous and arenaceous floor rocks of the Transvaal Supergroup initiates diapirism and the formation of large country-rock domal structures (*e.g.* Phepane, Malope, Zaaikloof, Katkloof, Schwerin, Derde Gelid and Steelpoort domes) on the margin of, and within the RLS in the northeastern part of the BIC, where isostatic subsidence was greater than in any other part of the BIC (Button, 1978; Uken & Watkeys, 1997b; Uken, 1998).

After its emplacement, cooling and thermal collapse/subsidence of the RLS results in tilting of the continuous sill-like intrusion towards its centre by 10-25º, which is also imposed on the Transvaal Supergroup and older strata beneath (*cf.* Tweedie, 1981; Leeb du Toit, 1986; Harmer & Von Gruenewaldt, 1991). The

emplacement of the RLS within the Transvaal Supergroup and its isostatic subsidence creates load stresses and space problems which results in space accommodation by compressional tectonics in the form of radially outward-verging fold and thrust structures (the latter preferentially developed along prominent unconformities) with extensive duplication within the Transvaal Supergroup around the periphery of the BIC (*e.g.* Mhlapitsi Belt) (*cf.* Bastin, 1968; Button,1973a; Roering *et al.*, 1987; Key, 1983; Andreoli, 1988a & b; Potgieter, 1992; Andreoli *et al.*, 1993; Harley, 1993; Harley & Charlesworth, 1990, 1992, 1994, 1995; Mapeo, 1995; Key *et al.*, 1996; Bumby, 1997). Concurrent heat-induced generation of hydrothermal cells and syn-tectonic fluid focussing (see also below) along the radially outward-verging, bedding-parallel thrusts and reactivated pre-existing NNE-SSW striking mid-Ventersdorp extensional faults results in mesothermal Au-Cu-(Bi-As-Sb-W) mineralisation and formation of economic gold deposits along both structures (*i.e.* steep and flat reefs) mainly within carbonaceous shales of the Chuniespoort Group, and subordinately within the Pretoria Group, Black Reef Formation, Wolkberg Group, and Archaean granitic basement in the Sabie-Pilgrim's Rest goldfield (*cf.* Zietsman, 1967; Meyer *et al.*, 1986; Maske *et al.*, 1986; Tyler, 1986, 1989; Anderson, 1992; Anderson *et al.*, 1992; Harley, 1993; Harley & Charlesworth, 1990, 1992, 1994, 1995; Boer & Harley, 1994; Boer *et al.*, 1995b). Analogous epigenetic, mesothermal gold mineralisation occurs along northerly and southerly verging thrust systems within the Chuniespoort Group along the NW- and SW-margins of the Western BIC Limb (*e.g.* Dwalboom and Swartruggens gold deposits) respectively (*e.g.* Duane *et al.*, 1991 and references therein) (Appendix 20-M).

A significantly higher geothermal gradient, caused by the intrusion of the sill-like RLS, results in anatexis of the Transvaal Supergroup lithologies immediately above the Rustenburg Layered Suite intrusion. A-type granitic magmas formed during anatectic melting extrude as rhyolitic lavas of the Upper Rooiberg Group (Damwal, Kwaggasnek and Schrikkloof formations) and become emplaced as a shallow-level, *ca*. 1500 m thick, tabular (sheet-like), composite granitoid batholith (*i.e.* Lebowa Granite Suite (LGS; Nebo, Klipkloof and Makhutso granites) and Rashoop Granophyre Suite) above the RLS within lithologies of the Transvaal Supergroup and lower Rooiberg Group at ~2.056-2.052 Ga (*cf.* Coertze *et al.*, 1978; Twist & French, 1983; MacCaskie, 1983; Walraven, 1985, 1988; Kleeman & Twist, 1989; Walraven & Hattingh, 1993; Hatton & Schweitzer, 1995; Eales & Cawthorn, 1996; Hill *et al.*, 1996; Walraven, 1997; Schweitzer *et al.*, 1995a, b, 1997; Schweitzer, unpubl.; Martini, 1998), which is accompanied by the formation of early orthomagmatic (formed during the crystallisation of the granites at 600-400°C) polymetallic Sn-W-Mo-F-(iron oxide) ore deposits within the granites (endogranitic; *e.g.* Zaaiplaats tin deposit; *e.g.* Groves & McCarthy, 1978; Ollila, 1981; Crocker, 1986; Pollard *et al.*, 1991; Freeman, 1998; Robb *et al.*, 2000) and Rooiberg Group (exogranitic; *e.g.* Vergenoeg fluorite deposit; Borrok *et al.*, 1998) (Fig. 4.2; Appendix 20-M).

Similarly, the higher geothermal gradient, caused by the emplacement of the Molopo Farms Complex, results in anatexis of lithologies of the Taupone and Segwagwa groups above the complex. Anatectic granitic magmas are emplaced as granites (*e.g.* Moshaneng Granite) into lower Kukong felsites and extruded as upper Kukong felsites coeval with the deposition of volcaniclastic sediments at ~2.056-2.052 Ga (*cf.* Key *et al.*, 1996; Lock *et al.*, 2002) (Appendices 20-M & 20-O).

Hydrothermal convection of late magmatic fluids (interacting with wall rocks and mixing with externally derived connate or meteoric fluids) caused by the granitic intrusions, continues less than 4 Ma after the emplacement of the LGS (*cf.* Cathles *et al.*, 1997) and results in the formation of several, relative small but economic, structurally controlled (*i.e.* predominantly along and within the intersection area between reactivated Pongola rift faults and sutures zones) late-stage magmato-hydrothermal (at 400-200°C), polymetallic sulphide Cu-Pb-

Zn-As-Ag-Au ore deposits within the granites (endogranitic; *e.g.* Spoedwel, Rooibokkop-Boschhoek, Albert and Gras Valley deposits) and within Pretoria and Rooiberg groups (exogranitic; *e.g.* Rooiberg and Union deposits) at ~2.052-2.048 Ga (*cf.* Hunter, 1973c; Stear, 1977; Smits, 1986; Walraven *et al.*, 1982; Pringle, 1986; Rozendaal *et al.*, 1986; Crocker, 1986; Crocker *et al.*, 1988; Walraven, 1988; Walraven & Hattingh, 1993; McNaughton *et al.*, 1993; von Gruenewaldt, 1993; Freeman, 1998; Good, 1999; Robb *et al.*, 1994a, 2000; Nomade *et al.*, 2004). Orthomagmatic PGE mineralisation of the Platreef within the northern BIC compartment and occasionally of the Merensky Reef along the Thabazimbi-Murchison suture zone is remobilised, transported and reprecipitated in litho-structural traps within the Platreef itself and underlying contact-metamorphosed footwall lithologies (Friese, 2003b; Friese & Chunnett, 2004) and as PGE-Au-chromium-bearing rare earth fluorcarbonate quartz-(carbonate)-hematite veins in brecciated and metasomatically silicified felsites of the Rooiberg Group (*i.e.* Waterberg deposit; *cf.* Wagner & Trevor, 1923; McDonald *et al.*, 1995, 1999; Distler *et al.*, 2000; Distler & Yudovskaya, 2002) respectively.

Abnormally high heat flow within the crust accompanying the emplacement of the RLS causes a fluid flux with associated alkali metasomatism, silicification and quartz veining, as well as regionally persistent greenschist facies metamorphism (~2-3 kbar; 350°C) and the formation of peak-metamorphic mineral assemblages within West and Central Rand Group lithologies in the northern and central Witwatersrand Basin at ~2.061-2.054 Ga (*cf.* Tweedie, 1986; Frimmel, 1994, 1997a & b). Associated with this thermal event is gold and uranium remobilisation within deposits of the Central Rand Group (*e.g.* Rundle & Snelling, 1977; Frimmel, 1997b; Kositcin *et al.*, 2001; England *et al.*, 2001).

Upper Rooiberg Group felsic volcanism is succeeded immediately by the conformable to unconformable deposition of volcano-sedimentary deposits of the Loskop, Glentig and Selons River formations, indicating a waning and the final stage of BIC-related magmatism at ~2.05 Ga (Appendices 20-M & 20-O).

After consumption by subduction of the intervening oceanic lithosphere between the Bamilimu Craton and Afrindalia and closure of the Magondi oceanic basin, the first phase of the Ubendian Orogenic Cycle culminates in the Magondi Orogeny at ~2.05-1.93 Ga, which documents the continental collision between the Bamilimu Craton and Afrindalia. Continent-continent collision during the Magondi Orogeny results in SE-directed thick- and thin-skinned thrusting and folding in the internal and external zones of the Magondi orogenic belt respectively, whereby the Piriwiri is thrusted over the Lomagundi Group, and the latter onto the Deweras Group. Coeval with thrusting, associated crustal thickening and magmatic underplating is high-grade metamorphism (grade decreasing from granulite-facies in western hinterland to greenschist-facies in eastern foreland), migmatisation, and the intrusion of enderbites and charno-enderbites during peak-metamorphic conditions and of late syn- to post-collisional/tectonic granitoids (*e.g.* Hurungwe Granite) at deeper and higher crustal levels into the Magondi fold-thrust belt respectively at ~2.0-1.93 Ga (Clifford *et al.*, 1967; Loney, 1969; Stagman, 1981; Leyshon & Tennick, 1988; Treloar, 1988; Treloar & Kramers, 1989; Master, 1991a & b, 1994; Carney *et al.*, 1994; Munyanyiwa *et al.*, 1995; Ramokate, 1996; Hanson *et al.*, 1998b; Munyanyiwa & Maaskant, 1998; McCourt *et al.*, 2001) (Appendix 20-N).

Orogenic activity and compressive tectonism along the western margin of Afrindalia induces progressively increasing SSE-directed compressive far field stress into the lithosphere of the supercontinent, leading to considerable tectonic reactivation of pre-existing Archaean, and formation of new structural elements at ~2.05-1.93 Ga (Appendix 20-N):

- Approximately east-west striking Neoarchaean (~2.72-2.64 Ga) terrane boundaries (= suture zones) between the Kaapvaal Craton, Limpopo Central Zone Terrane, and Zimbabwe and Nyassa cratons (*i.e.* Palala, Tuli-Sabi-Triangle, and Sanangoè sutures zones) experience dextral transpressive (strike-/oblique reverse-slip) reactivation, as well as coeval syntectonic granitoid magmatism and high-T amphibolite-to-granulite-facies metamorphism within the adjacent lithosphere at ~2.02-1.97 Ga, progressing to retrograde greenschist-facies conditions at ~1.97-1.93 Ga (*cf.* Kamber *et al.*, 1995a & b; Holzer *et al.*, 1997,1998,1999; Schaller, 1997; Schaller *et al.*, 1997, 1999; Belluso *et al.*, 2000) (Appendix 20-N).

- Within the Zimbabwe Craton, NW-SE oriented compressive far field stress results in the sinistral and dextral strike-slip reactivation of the Popoteke and Mtshingwe fracture systems respectively. Neoarchaean (~2.72-2.57 Ga) sinistral shear zones and intracratonic Mesoarchaean (~3.46-3.1 Ga) suture zones undergo dextral transpressive reactivation (Appendix 20-N).

- A second phase of structurally controlled hydrothermal gold-sulphide-tourmaline mineralisation occurs within the Zimbabwe Craton along brittle, dextrally reactivated Mesoarchaean suture zones and ductile Neoarchaean (~2.65-2.585 Ga) sinistral shear zones at ~2.02-1.93 Ga, due to remobilisation of Neoarchaean (~2.64-2.585 Ga) gold-scheelite-tourmaline vein mineralisation by crustal-derived metamorphic fluids along the same shear zones (Frei & Pettke, 1996), as well as partly along extensional fractures of the Sebanga-Mashonaland fracture/dyke system forming at ~1.93-1.86 Ga (see below).

- Dextral oblique-reverse (transpressive) reactivation of the NLTZ and the development of a new system of low-grade thrusts parallel to the NLTZ within the NMZ, facilitate the second and final uplift and exhumation of the NMZ which is accompanied by decompression and greenschist-facies retrogression of the high-grade NMZ lithologies (Kamber & Biino, 1995; Kamber *et al.*, 1996; Blenkinsop & Frei, 1996) (Appendix 20-N).

- Dextral strike-/oblique reverse slip (transpressive) reactivation of E-W to NW-SE striking Archaean shear zones within the Central Zone Terrane takes place under peak-metamorphic granulite-facies conditions (>10 kbar, ~825°C) at ~2.025-~2.02 Ga and is followed by near-isothermal decompression (<3-5 kbar, 600-750°C) and wide-spread anatexis at ~2.005-2.0 Ga. Anatexis, migmatisation and tectonic reworking under high-grade (low-P/high-T) metamorphic (granulite-facies) conditions of the Archaean granulitic basement gneisses results within the western part of the terrane in the formation of the igneous Mahalapye Complex (Carney *et al.*, 1994) with anatexis and intrusion of the Mokgware Pluton and Mahalapye Granite into the complex at ~2.025-2.0 Ga (Chavagnac *et al.*, 1997; McCourt & Armstrong, 1998; Holzer *et al.*, 1999, Mapeo *et al.*, 2000), contemporaneously with upper amphibolite- to granulite-facies metamorphism, anatexis and related granitic plutonism in the central and eastern parts of the Limpopo Central Zone Terrane (Layer *et al.*, 1996; Kröner *et al.*, 1999; Schaller, 1997; Holzer *et al.*, 1997, 1998, 1999; Schaller *et al.*, 1997, 1999; Belluso *et al.*, 2000; Barton *et al.*, 2003) (Appendix 20-N).

- Within the northern Kaapvaal Craton, progressively increasing SSE-directed compressive far field stress causes a changeover to compressive-transpressive stress field conditions and tectonics, shutting down the RLS magmatic plumbing system and heralding the end of Bushveld magmatic activity at ~2.055 Ga. Dextral strike-/oblique reverse-slip (transpressive) reactivation of E-W striking Limpopo Orogeny-generated (~2.78-2.64 Ga) crustal shear zones and Archaean suture zones (*e.g.* Palala, Thabazimbi-Murchison and Pietersburg suture zones), combined with thermal subsidence of the BIC and Molopo

Farms Complex and extensional reactivation of NW-SE striking Pongola rift faults, result in the development of pull-apart and thermal subsidence basins and associated deposition of siliciclastic continental red-bed sediments (sandstones, grits, rare conglomerates, minor quartz porphyry lavas) of the Blouberg Formation (up to 1.4km thick) and unconformably overlying (up to 3.6km thick) Lower Waterberg Group (Nylstroom & Lower Matlabas subgroups) at ~2.05-1.93 Ga (*cf.* Bruiyn & Andrew, 1972; Tickell, 1975; Jansen, 1975, 1976, 1982; Walraven, 1981; Cheney & Twist, 1986; Callaghan, 1986; Du Plessis, 1987; Du Plessis & Clendenin, 1988; Du Plessis & Walraven, 1990; Callaghan & Brandl, 1991; Callghan *et al.*, 1991; Van der Neut *et al.*, 1991; Eriksson *et al.*, 1997; Dorland, 2004). Deposits of the Blouberg Formation and Lower Waterberg Group were tilted and overturned along their basin margins, formed by the dextral transpressive reactivated Palala and Thabazimbi-Murchison suture zones, prior to the deposition of the Lower and Upper Waterberg groups respectively (*cf.* Callaghan, 1986; Bumby *et al.*, 2002). Dextral strike- to oblique reverse-slip (transpressive) reactivation of the Palala and Thabazimbi-Murchison suture zones causes the marginal deformation of the BIC along these suture zones (*e.g.* Brandl, 1986; Callaghan, 1986) (Appendix 20-N).

- Contemporaneously with granulite-facies grade metamorphism and anatexis in the Limpopo Central Zone Terrane and deposition of the Blouberg Formation and lower Waterberg Group in the northern Kaapvaal Craton is the emplacement of the Entabeni Granite along a reactivated Neoarchaean Pongola rift fault at ~2021 Ma (*cf.* Dorland, 2004; Cheney *et al.*, 1990b; Barton *et al.*, 1995a). Late anatectic granitic crustal melts intrude syntectonically into the Koedoesrand Formation (= correlative to Pretoria Group) as Palala Granite along the Palala suture zone at ~1972 Ma (*cf.* McCourt, 1983; McCourt & Vearncombe, 1987; Brandl, 1986; Brandl & Reimold, 1990; Broekhuizen *et al.*, 1995; Broekhuizen, 1998) (Appendix 20-N).
- Within the western and central Kaapvaal Craton, NE-SW lithospheric extension results in the continued sinistral transtensional and extensional reactivation of the Palaeoproterozoic (~2.35-2.22 Ga) Kalahari fold-thrust belt and Neoarchaean (~2.98-2.97 Ga) Pongola rift basin respectively at ~2.05-1.93 Ga. Intracratonic pull-apart rift basins continue to develop within the area of the transtensionally reactivated (inverted) Kalahari fold-thrust belt, forming the depositories for fluvial to shallow marine sediments (shale, quartzite, minor dolomite) of the Lower Olifantshoek Supergroup (Lucknow & Mapedi formations) and stratigraphically equivalent Lower Vaalkoppies Group (Dagbreek Formation). Shallow marine conditions within the rifted terrain are established by marine incursions from the Gordonia oceanic basin situated to the south of the Rehoboth and Kaapvaal cratons (Appendix 20-M).
- Subduction-related metasomatism of the subcontinental lithospheric mantle within the western parts of Afrindalia (*i.e.* western Nyassa, Zimbabwe, Kaapvaal and Rehoboth cratons, Limpopo Central Zone Terrane) at ~2.0 Ga leads to the destruction/reabsorption of diamonds and resetting of the isotopic system of Archaean-age lithospheric mantle (*cf.* Cohen *et al.*, 1984; Richardson *et al.*, 1985).

At the time of intracratonic rifting within the rejuvenated Archaean Pongola rift basin and thermal subsidence of the crust above the cooling BIC and Molopo Farms Complex with concurrent rift-controlled deposition of the Lower Waterberg Group within the central Kaapvaal Craton, the impact of a large meteorite occurs approximately within the centre of the presently preserved Witwatersrand Basin at ~2.02 Ga, forming the Vredefort Dome as central uplift and an associated multi-ring crater of 250-300km in diameter (for detail see Section 6.3.3.1) (Appendix 20-N).

Shortly after, or partly overlapping in time with, the final stages of the Magondi orogenic activity, closure of the Ubendia oceanic basin, accretion of the oceanic magmatic arc and continental collision between the converging Archaean Angola (Congo) Craton (*e.g.* Cahen *et al.*, 1984; Caen-Vachette *et al.*, 1988; Delhal, 1991; Tack *et al.*, 1999) and Afrindalia, marks the beginning of the Okwa Orogeny and the main phase of the Ubendian orogenic cycle at ~1.93 Ga (Appendix 20-P). Orogenic activity and compressive tectonism along the western margin of Afrindalia during the Okwa Orogeny induces compressive SE-directed *in situ* far field stress into the lithosphere of the supercontinent, leading to considerable tectonic reactivation of pre-existing Archaean, and formation of new, structural elements at ~1.93-1.86 Ga:

- Intense SE-directed thrusting, associated NE-trending folding and accompanying amphibolite-facies metamorphism of the Okwa Group results in the development of the Okwa River Gneiss Complex representing a nappe complex that is thrusted against the Kaapvaal Craton (*e.g.* Thomas *et al.*, 1993a).

- Resultant NE-SW oriented crustal extension within the Zimbabwe Craton leads to the development of NW-SE striking extensional fracture zones, which is accompanied by the intrusion of dolerite dykes and sills of the Sebanga-Mashonaland dyke system at ~1.93-1.86 Ga (*cf.* Charlton, 1973, 1975; Compston & McElhinny, 1975; Stagman, 1978; Bates & Jones, 1996; Evans, 2001; Wingate, 2004 unpubl. data). Doleritic magmas partly intrude also along the extensional/transtensional reactivated Mtshingwe fracture system (*e.g.* Mazowe river dyke swarm within area of Harare-Bindura-Shamva greenstone belt) (Appendix 20-P).

- Dextral strike-/ to oblique-slip (transtensional) reactivation of Neoarchaean shear zones within the Limpopo Central Zone Terrane is accompanied by fault-controlled deposition of mainly clastic (shallow lacustrine to fluvial) sediments with minor andesitic volcanics of the Lower Palapye Group (Selika and Moeng formations) in fault-bounded basins unconformably over Archaean basement lithologies at ~1.93-1.86 Ga (Ermanovics *et al.*, 1978; Ermanovics, 1980; Key *et al.*, 1983; Carney *et al.*, 1994; Dorland, 2004), which continues until ~1.8 Ga during Kheis Orogeny-induced far field stress conditions (see below) (Appendix 20-P).

- Dextral strike- to oblique reverse-slip (transpressive) reactivation of the Palala and Thabazimbi-Murchison suture zones continues after the emplacement of the Bushveld Igneous Complex until ~1.86 Ga, causing the marginal deformation of the complex along these suture zones (*e.g.* Brandl, 1986; Callaghan, 1986; Brandl & Reimold, 1990) and is the result of NW-SE oriented compressive far field stress conditions induced during two successive orogenies, *i.e.* Magondi and Okwa orogenies at ~2.05-1.93 Ga and ~1.93-1.86 Ga respectively (Appendix 20-P).

- On-going dextral strike- to oblique reverse-slip reactivation of E-W striking Limpopo Orogeny-generated (~2.78-2.64 Ga) crustal shear zones and Archaean suture zones (*e.g.* Palala, Thabazimbi-Murchison and Pietersburg suture zones) within the northern Kaapvaal Craton result in the continued development of intracratonic pull-apart rift basins and associated deposition of siliciclastic continental red-bed sediments of the Upper Waterberg Group (Upper Matlabas & Kransberg subgroups) (*e.g.* Jansen, 1976, 1982; Cheney & Twist, 1986; Du Plessis, 1987; Du Plessis & Clendenin, 1988; Du Plessis & Walraven, 1990; Callaghan & Brandl, 1991; Callaghan *et al.*, 1991; Eriksson *et al.*, 1997) at ~1.93-1.86 Ga (Appendix 20-P).

- Isolated minor alkaline magmatism within the northern Kaapvaal Craton occurs penecontemporaneously with active crustal extension and the development of intracratonic pull-apart rift basins and associated

Upper Waterberg Group deposition at ~1.88-1.86 Ga. This short period of alkaline magmatism is represented by the structurally controlled emplacement of the Klipspringer kimberlite dyke swarm (C.B. Smith, pers. comm.., 1997) and Schiel Alkaline Complex (Barton *et al.*,1996), heralding intense and peak-reaching active crustal extension, rifting and mafic volcanism during Lower Soutpansberg Group (Sibasa Formation) time at ~1.83-1.8 Ga (see below) (Appendix 20-P).

- Intensifying NE-SW lithospheric extension within the Kaapvaal Craton results in the continued sinistral transtensional and extensional reactivation of the Palaeoproterozoic (~2.35-2.22 Ga) Kalahari fold-thrust belt and Neoarchaean (~2.98-2.97 Ga) Pongola rift basin respectively at ~1.93-1.86 Ga. Intensified intracratonic pull-apart rift basin development within the area of the transtensionally reactivated (inverted) Kalahari fold-thrust belt leads to volcanism, intrusion of dykes and sills and deposition of andesitic lavas and pyroclastics of the Middle Olifantshoek Supergroup (Hartley Formation) (*cf*. Cornell *et al.*, 1998) and siliciclastic sediments of the stratigraphically equivalent Upper Vaalkoppies Group (Sultanaoord Formation) and Brulpan Group (Uitdraai/Prynnsberg & Groblershoop formations) (Appendix 20-P).
- The extensional/sinistral transtensional reactivation of Archaean suture zones within the southwestern Kaapvaal Craton is accompanied by a short-lived episode of alkaline magmatism between ~1.93-1.91 Ga and contemporaneously with Hartley Formation volcanism in the extensionally reactivated Kalahari fold-thrust belt in the form of the emplacement of the Keikamspoort Carbonatite along the Marydale suture zone near Prieska, Trompsburg Complex along the Trompsburg-Gaborone suture zone and picrite dykes along the Kimberley suture zone near Kimberley (*cf*. Cornell *et al.*, 1998; Maier *et al.*, 2003; Clement *et al.*, 1979) (Appendix 20-P).

Convergence between the southern Congo (Angola) and Rehoboth cratons results in intense compressive deformation, metamorphism (amphibolite-facies), as well as northwesterly and southeasterly vergent folding and overthrusting of deposits of the magmatic-arc/back-arc basin complexes onto the margins of both cratons respectively at ~1.93-1.86 Ga (Appendix 20-P). Intracratonic retroarc and peripheral foreland basins develop ahead of the craton-inwards migrating fold-thrust belts along the northwestern and southeastern margins of the Rehoboth and Congo cratons, representing evolving depositories for volcano-sedimentary terrestrial and shallow marine deposits of the Rehoboth Sequence and Khoabendus Group (and Okapuka & Elim formations) respectively (*cf.* Burger *et al.*, 1976; Burger & Walraven, 1979; Mailing, 1981; Seifert, 1986; Nagel *et al.*, 1996; Ziegler & Stössel, 1993; Becker *et al.*, 1996; Becker *et al.*, 2000) (Appendix 20-P).

4.3.4 ARAVALLI OROGENIC CYCLE (~2.2-1.73 GA)

Following an extensive period of approximately 300 million years. of intense erosion and denudation of the Archaean basement of the Aravalli-Bundelkhand Craton since the end of the Bundelkhand Orogenic Cycle at ~2.5 Ga, the initiation of subduction of oceanic lithosphere beneath the southeastern margin of Afrindalia at ~2.2 Ga causes crustal extension and the development of an intracratonic back-arc basin within the Aravalli Craton. Initial deposition of fluvio-terrestrial siliciclastics (*i.e.* conglomerates, quartzites and minor arkoses) interbedded with high alumina tholeiitic basalts, komatiites, picrites and pyroclastics, is followed by a marine transgression into the back-arc basin and the shallow marine deposition of dolomites of the Lower Aravalli Supergroup unconformably over polydeformed/-metamorphosed, weathered Archaean (~3.3-2.5 Ga)gneiss-migmatite basement and a regional extensive palaeosol at ~2.2-2.1 Ga (*cf.* Vinogradov *et al.*, 1964; Naha &

Halyburton, 1974; Naha & Roy, 1983; Sinha Roy, 1988; Deb *et al.*, 1989; Deb & Sarkar, 1990; Roy, 1988, 1990; Roy *et al.*, 1988, 1993; Gopalan *et al.*, 1990; Ahmad & Rajamani, 1991; Upadhyaya *et al.*, 1992; Ahmad & Tarney, 1994; Banerjee & Bhattacharya, 1994; Tobisch *et al.* 1994; Wiedenbeck & Goswami, 1994; Wiedenbeck *et al.*, 1996; Roy & Kröner, 1996; Verma, 1998; Bhattacharya, 1998) (Appendix 20-L).

Episodic phases of increased rifting followed by periods of relative tectonic quiescence within the developing intracratonic Aravalli back-arc basin causes repeatedly marine transgressions into the basin, which is expressed by the deposition of numerous fining-upward cycles of the Middle and Upper Aravalli Supergroup at ~2.1-2.05 Ga and ~2.05-1.93 Ga respectively, comprising basal coarse siliciclastics (conglomerates, quartzites, arkoses), followed by dolomites, and pelites (phyllites, slates) at the top (*cf.* Roy *et al.*, 1993; Mazumder *et al.*, 2000) (Appendices 20-M & 20-N).

Possibly micro-plate accretion causes deformation and metamorphism under greenschist to lower amphibolite facies conditions of the Aravalli Supergroup which is accompanied by the emplacement of the Darwal Granite and related K-rich granites, as well as associated hydrothermal quartz veining on a large scale within the Aravalli Supergroup at ~2.0-1.9 Ga (Chaudhary *et al.*, 1984; Sharma, 1998). Dolerite dykes intrude the deformed and metamorphosed Aravalli Supergroup late- to post-kinematically (Roy & Kröner, 1996).

4.3.5 KHEIS OROGENIC CYCLE (~2.05-1.73 GA)

Initiation of westerly subduction of oceanic lithosphere beneath the eastern margins of the Sao Francisco-Rio de la Plata-Gawler Craton at ~2.05 Ga marks the beginning of the Kheis Orogenic Cycle with east-west convergence between the Congo and Sao Francisco-Rio de la Plata-Gawler cratons, as well as between the Yilgarn-Pilbara and Rehoboth-Kaapvaal cratons and closure of the intervening Kheis and Gordonia oceanic basins respectively, which results in the development of an extensive oceanic magmatic arc/back-arc basin belt during the time interval ~2.05-1.83 Ga (Appendices 20-N & 20-P). Calc-alkaline, I-type volcanism and plutonism and sedimentation within the oceanic or continental margin magmatic arc and adjacent back-arc basins is represented by lithologies of the Tandilia System (Argentina) (Teixeira *et al.*, 2002), Francevillian Supergroup (Gabon) (*cf.* Bonhomme *et al.*, 1982; Hein & Bolton, 1993), Orange River and Grunau/Onseepkan groups and Vooilsdrif Igneous Suite of the Richtersveld and Namaqua provinces (South Africa/Namibia) (*cf.* Reid & Barton, 1983; Watkeys, 1986; Colliston & Schoch, 1998), and by igneous and sedimentary precursors to para-/orthogneisses of the Rudall/Northhampton Complex (Western Australia). Volcano-sedimentary deposits of the Bryah-Padbury and Upper Wyloo groups accumulate in intracratonic back-arc rift basins developing within the Yilgarn and Pilbara cratons respectively (Appendices 20-N & 20-P).

Complete closure of the Gordonia and Kheis oceanic basins and subsequent continental collisions between the converging Yilgarn-Pilbara and Rehoboth-Kaapvaal cratons in the east and the Sao Francisco-Rio de la Plata-Gawler and Yilgarn-Pilbara-Congo cratons further to the west respectively, is initiated penecontemporaneously at ~1.83 Ga, leading to crustal shortening, intense deformation and metamorphism and the formation of orogenic belts along the suture zones, *i.e.* Tandilia, Gabon, Richtersveld-Bushmanland and Capricorn orogenic belts, during the Kheis Orogeny at ~1.83-1.73 Ga (*cf.* Onstott & Hargraves, 1981; Shackleton, 1986; Ledru *et al.*, 1989; D'Agrella-Filho *et al.*, 1996; Teixeira *et al.*, 2002).

Within the western interior of Afrindalia, *i.e.* in the area of the extensionally reactivated ~2.35-2.22 Ga old Kalahari fold-thrust belt and Kalahari suture zone, near colinear compressive reactivation of thrust faults of the fold-thrust belt, in addition to the development of a new system of thin-skinned NE- to ENE-verging

thrusts at ~1.83-1.73 Ga, lead to the formation of the Kheis fold-thrust belt and deposition of siliciclastic rocks (conglomerates, quartzites, greywackes) of the Upper Olifantshoek Supergroup (Matsap and Brulsand formations = Volop Group) within an associated retroarc foreland basin developing to the east and ahead of the fold-thrust belt (Appendix 20-Q). Lower and mid Olifantshoek Supergroup lithologies (Lucknow, Mapedi and Hartley formations) and stratigraphic equivalents (Vaalkoppies and Brulpan groups) deposited at ~2.05-1.83 Ga, and older rock units of the Griqualand West Supergroup and Archaean basement are thrusted east-northeastwards over the cratonic cover in a series of five major nappes, thereby being intensely deformed (sheared and isoclinally and recumbently folded) and metamorphosed, with the metamorphic grade increasing westwards towards the Kalahari suture zone. Below the sole thrust (Blackridge thrust fault) of the thin-skinned Kheis fold-thrust belt, lithologies of the Griqualand West and Ventersdorp supergroups undergo relative minor deformation (*cf.* Coward & Potgieter, 1983; Stowe, 1983, 1986; Hartnady *et al.*, 1985; Beukes & Smit, 1987; Schlegel, 1986, 1988; Altermann & Hälbich, 1990, 1991; Humphreys *et al.*, 1991; Van Bever Donker, 1991; Cornell *et al.*, 1998; Hilliard, 1999; Moen, 1999; Tinker *et al.*, 2002).

Further craton-inward within the west-central Kaapvaal Craton, decreasingly intense ENE-directed compressive far field stress results mainly in ENE-directed bedding-parallel thrusting, ramping and duplexing within supracrustals of the Witwatersrand, Ventersdorp and Transvaal supergroups (this study), minor reactivation of east-verging late Central Rand Group thrusts and mid-Ventersdorp Supergroup transtensional/extensional faults (*cf.* Clendenin *et al.*, 1990), sinistral transpressive reactivation of E-W striking Archaean suture zones and Limpopo Orogeny-generated (~2.78-2.64 Ga) crustal shear zones (*e.g.* Palala, Thabazimbi-Murchison and Magaliesburg-Barberton suture zones) (*cf.* Du Plessis, 1987; Du Plessis & Clendenin, 1988; Du Plessis & Walraven, 1990), as well as in NNW-trending, low-amplitude, open folding of Archaean-Palaeoproterozoic supracrustals (*i.e.* Ventersdorp and Transvaal supergroups), syn-BIC units (*i.e.* Upper Woodlands Formation, Otse Group, Rooiberg Group), and of the western BIC (*cf.* Crockett, 1969a&b, 1971b, 1972; Key, 1983; Dietvorst, 1988; Crockett & Key, 1989; Swartz, 1991; Hartzer, 1987, 1989, 1994, 1995; Mapeo, 1995; Courtnage, 1996; Eriksson *et al.*, 1998) at ~1.83-1.73 Ga (Appendix 20-Q).

To the east of the front of compressive deformation, *i.e.* within the central and eastern parts of the Kaapvaal Craton and Limpopo Central Zone Terrane, approximately north-south extensional stress field conditions and lithospheric extension dominate at ~1.83-1.8 Ga, resulting in the extensional/transtensional reactivation of the Palala suture zone and Neoarchaean crustal shear zones within the northern Kaapvaal Craton and Limpopo Central Zone Terrane and associated development of the transtensional (pull-apart) Palapye and extensional (half-graben) Soutpansberg failed rift basins within the Limpopo Central Zone Terrane and immediately to the south of the Palala suture zone respectively (*e.g.* Holzer *et al.*, 1999; Bumby, 2000; Bumby *et al.*, 2001, 2002a). Within the Soutpansberg rift basin, initial fluvial deposition of terrestrial clastic sediments (shale, greywacke and locally derived conglomerate of the basal (up to 9 m thick) Tshifhefhe Formation/Lower Soutpansberg Group) unconformably over granitoid basement and Waterberg Group deposits (*e.g.* Jansen, 1975, 1976, 1982; Brandl, 1986, 1987; Bumby *et al.*, 2001, 2002b; Gutzmer *et al.*, 2002a), is followed by the extrusion of voluminous (up to 3.3km), subaerial basaltic/andesitic magmas and deposition of intercalated pyroclastic and sandstone lenses (200-400 m thick) of the Sibasa Formation (*e.g.* Jansen, 1975, 1976; Barker, 1976, 1979, 1983; Meinster, 1977; SACS, 1980; Barker *et al.*, in press) at ~1.83-1.8 Ga (*e.g.* Cheney *et al.*, 1990b; Barton & Pretorius, 1997). Feeder magmas to the Sibasa tholeiitic lavas ascend along reactivated Archaean shear zones and newly forming east-west striking extensional fracture zones and become emplaced as comagmatic feeder dykes and sills within Waterberg Group deposits and at depth (~10km) as small gabbroic plutons over an extensive region mainly within the Pietersburg Terrane and partly

in the southern portion of the central-eastern Limpopo Central Zone Terrane (*cf.* Barton, 1979; Pretorius, 1996; Barton & Pretorius, 1997; Barton *et al.*, 2003). Subsequent to peak-reaching active crustal extension, rifting and volcanism during Sibasa Formation time, progressively increasing thermal subsidence during decelerated active rifting is accompanied by the deposition of up to 2.8km of predominantly siliciclastic (arenaceous and argillaceous) rocks with rare intercalated pyroclastic horizons and basalts of the Funduzdi Formation at ~1.8 Ga (*cf.* Dorland, 2004; Barker *et al.*, in press) (Appendix 20-Q).

Within the Limpopo Central Zone Terrane, pull-apart rift tectonics and associated deposition of mainly clastic (shallow lacustrine to fluvial) sediments (conglomerate, quartzite, shale, limestone) with minor andesitic-rhyolitic volcanics of the Lower Palapye Group (Selika and Moeng formations) in developing fault-bounded basins (*cf.* Ermanovics *et al.*, 1978; Key, 1980; Cheney *et al.*, 1990b; Carney *et al.*, 1994; Dorland, 2004) and basin development (*e.g.* Palapye Basin) along reactivated Archaean shear zones within the Limpopo Central Zone Terrane continue after cessation of Okwa Orogeny-induced far field stress conditions at ~1.86 Ga until ~1.8 Ga (Appendix 20-Q).

Continental collisions between the converging Yilgarn-Pilbara and Rehoboth-Kaapvaal cratons in the east and the Sao Francisco-Rio de la Plata-Gawler and Yilgarn-Pilbara-Congo cratons further to the west respectively during the Kheis Orogeny at ~1.83-1.73 Ga induces regional pervasive deformation of the lower crust and accompanied crustal thickening, extensive tilting, heating, hydration and large-scale tectonic fluid expulsion and penetrative fluid flow into and through the cover rocks of the western and central Kaapvaal-Rehoboth Craton from the west-southwest, decreasing in an easterly direction, *i.e.* away from the orogenic front craton-inwards (Appendix 20-Q).

Structural ground penetration and migration of tectonically overpressured intrabasinal connate brines/hydrothermal fluids (<240°C, low salinity) occur mainly along thrust-reactivated pre-existing Kalahari Orogeny (~2.35-2.22 Ga)-related thrusts and unconformities within the Neoarchaean-Palaeoproterozoic supracrustals of the Dominion Group, Witwatersrand, Ventersdorp and Griqualand West-Transvaal supergroups, as well as along newly forming easterly verging thrusts and reactivated older, moderate to steeply dipping fault/shear and suture zones within the Mesoarchaean basement and overlying supracrustals, resulting in extensive karsting of the Campbell Group dolomites in the Griqualand West Basin (Appendix 20-Q).

This structurally controlled hydrothermal activity causes extensive or partial isotopic resetting and alteration of rocks and minerals of the Neoarchaean-Palaeoproterozoic supracrustal formations and parts of the Mesoarchaean cratonic basement within the western and central Kaapvaal Craton (see Appendix 25-B for a summary of Palaeoproterozoic isotopic resetting ages within the Kaapvaal Craton), and results in the formation of epigenetic ore-deposits (*i.e.* hydrothermally altered syngenetic Fe-Mn ores in the Heynskop Formation (Koegas Subgroup), Hotazel Formation (Postmasburg Group), and along Postmasburg Group-Olifantshoek Group unconformity; see below) including low temperature carbonate-hosted Mississippi Valley-type (MVT) Pb-Zn(F) deposits (*e.g.* Pering, Bushy Park, Witkop, Balloch, Zeerust) in structural traps (*e.g.* palaeokarsts with associated palaeokarstic brecciation) mainly along reactivated Mesoarchaean suture zones and NW-SE striking Neoarchaean Pongola rift faults within the Ghaap and Chuniespoort groups (Griqualand West and Transvaal supergroups respectively) (*cf.* Stowe, 1986; Ryan, 1986; Wheatley *et al.*, 1986a & b; Beukes & Smit, 1987; Duane & de Wit, 1988; Duane & Kruger, 1991; Duane *et al.*, 1991; Cain & Clague, 2000; Greyling, 2000; Poetter, 2001; Schaefer, 2002; Greyling *et al.*, 2002) (Appendix 20-O). Source rocks, from which Pb and Zn are leached/remobilised by hot, saline bituminous hydrocarbon “oilfield” brines, are most likely Mesoarchaean basement lithologies, the Ventersdorp Supergroup bimodal volcano-sedimentary succession, and the host

carbonates. Orogenic tectonism expels fluids out of the deeper parts (high-grade cores) of the orogen and Griqualand West subbasin along tectonic décollements through the rocks of the Ventersdorp Supergroup and into lower-metamorphic, cooler marginal deposits of the Transvaal Supergroup, where precipitation in associated structurally controlled karsts is caused by mixing with oxidising groundwater (simultaneously expelled from red-bed sequences of the overlying Olifantshoek Supergroup) along tectonically active fault and shear zones (Duane *et al.*, 1991).

Regional low-grade metamorphism and structurally controlled hydrothermal fluid flow and alteration along easterly verging bedding- and non-bedding-parallel thrusts and dextral transtensionally reactivated NNE-SSW striking, Neoarchaean (~2.72-2.64 Ga) Ventersdorp rift faults within the Hotazel Formation (Upper Postmasburg Group) results in a weak metamorphic overprint and hydrothermal upgrading/enrichment (metasomatic transformation) of syngenetic (early diagenetic), low-grade, carbonate-rich Mamatwan-type manganese ore (*e.g.* Kleyenstüber, 1984; Nel *et al.*, 1986; Beukes, 1993; Cornell & Schütte, 1995; Cairncross *et al.*, 1997) to high-grade oxide-rich Wessels-type ore in the Kalahari manganese field around Hotazel at ~1.8-1.73 Ga (*cf.* Dixon, 1989; Beukes *et al.*, 1995; Gutzmer & Beukes, 1995, 1996, 1997; Gutzmer *et al.*, 1995; Tsikos & Moore, 1998; Lüders *et al.*, 1999; Tsikos *et al.*, 2000; Evans *et al.*, 2001; Gutzmer *et al.*, 2002c) (Appendix 20-Q).

Fe-dominated hydrothermal fluid flow within the area of the BIC leads to the formation of the structurally controlled, epigenetic hydrothermal-metasomatic, high-grade Thabazimbi iron (hematite) ore deposits within the Penge Iron Formation (here along the faulted contact between basal carbonaceous shale and overlying iron formation) (Gutzmer *et al.*, 2002b) along the sinistral transtensionally reactivated Thabazimbi-Murchison suture zone, to structurally controlled iron replacement within the RLS predominantly along igneous layering (this study), and earlier formed magmato-hydrothermal polymetallic deposits within the BIC become partially hydrothermally overprinted/superimposed by low temperature Fe-F-U oxide ores (*e.g.* Robb *et al.*, 2000) (Appendix 20-Q).

With active intracratonic lithospheric extension diminishing during the final stages of the Kheis Orogeny at ~1.8 Ga, previously rifted lithospheric sections within the central and eastern parts of the northern Kaapvaal Craton and Limpopo Central Zone Terrane undergo progressively more thermal subsidence, resulting in the deposition of a thick (up to a few kilometres) and laterally extensive post-rift sequence of predominantly fluvial to shallow-marine siliciclastic red-bed sediments (sandstone with oncolitic manganese deposits, shale, conglomerate) and minor basaltic and pyroclastic intercalations of the Upper Palapye (Tswapong, Lotsane and Shoshong formations) and Upper Soutpansberg (Wylliespoort, Ngwanedsi and Nzhelele formations) groups unconformably over and laterally overstepping pull-apart rift basin deposits of the Lower Palapye and Soutpansberg groups (and Roodeberg Formation as correlative to Wylliespoort Formation) at ~1.8-1.73 Ga respectively (*cf.* Ermanovics *et al.*, 1978; Barker, 1983; Cheney *et al.*, 1990b; Gutzmer *et al.*, 2002a; Dorland, 2004; Barker *et al.*, in press) (Appendix 20-Q).

Predominantly active extensional tectonism and Sibasa mafic magmatism, and to a lesser degree subsequent lithospheric thermal subsidence, are accompanied by fault-controlled hydrothermal fluid flow and metasomatic alteration of Archaean and Palaeoproterozoic lithologies within the Limpopo Central Zone Terrane and northern Kaapvaal Craton, leading to hydrothermal copper mineralisation in deposits of the Soutpansberg rift (*i.e.* sedimentary and mafic volcanic rocks of the Lower Soutpansberg Group) and along extensionally reactivated shear and fault zones (*e.g.* Messina and Dowe-Tokwe faults and related splays) within the Singelele Gneiss in the southern part of the eastern Limpopo Central Zone Terrane (*e.g.* copper

deposits near Messina), or within the Waterberg Group (*e.g.* Nooitgedacht Mine) (*cf.* Söhnge, 1946; Van Graan, 1964; De Bruiyn, 1972; Jacobsen *et al.*, 1975; Barton, 1979; Barton *et al.*, 1979b, 1983b; Ryan *et al.*, 1983; Callaghan, 1986; Cheney *et al.*, 1990b; Bahnemann, 1986; Barton & Pretorius, 1997; Barton *et al.*, 2003), as well as to the enrichment of primary stratiform manganese mineralisation in the Palapye Group (*cf.* Key, 1980; Schaefer *et al.*, 1999) at ~1.83-1.73 Ga (Appendix 20-Q).

Late- to post-compressional crustal relaxation within the western and central Kaapvaal Craton at ~1.75-1.73 Ga is accompanied by minor mafic magmatism in the form of isolated intrusion of dolerite dykes along reactivated crustal fault/shear zones (*e.g.* Mamutlan dolerite intrusive into Hartley basalts/Mamutlan, Botswana (Cornell *et al.*, 1998) and Ottosdal dolerite/Ottosdal, South Africa (Burger & Walraven, 1980)).

In summary: The Kheis orogenic event at ~1.83-1.73 Ga documents continent-continent collision and accretion between cratons of western Afrindalia (from north to south: West African, Congo, Rehoboth and Yilgarn cratons) and most probably at this stage already amalgamated cratons of another continent (today parts of South America and Australia), comprising among others the Guyana, Sao Francisco, Rio de la Plata and Gawler cratons. This orogeny represents the final stage in the formation of the late Palaeoproterozoic supercontinent 'Atlantica' or 'Columbia' through amalgamation of Archaean continental fragments (cratons) and accretion of intervening juvenile Palaeoproterozoic crust (oceanic island arcs, fore- and back-arc basins), with the amalgamation process being completed globally by ~1.73 Ga (Zhao *et al.*, 2003, 2004; Eriksson *et al.*, 2005; Yakubchuk, 2008).

The intra-(Afrindalia)continental Kheis and Capricorn orogenies in South Africa and Western Australia respectively at ~1.83-1.73 Ga occur penecontemporaneously to, and are associated with the Kheis orogenic event, and are part of a series of continental collision events which resulted in the amalgamation of this late Palaeoproterozoic supercontinent.

Earlier mid-Palaeoproterozoic (~2.1-1.93 Ga) orogenic event, *i.e.* Eburnean Orogeny in West Africa, Ubendian Orogeny in Tanzania and Zambia, and the Magondi and Okwa orogenies in Zimbabwe, Botswana and Namibia (and time-equivalent collisional orogenies between cratons of South America), represent synchronous to diachronous continental collision and accretion events within Afrindalia, *i.e.* preceded the final amalgamation between cratons of Africa and South America during the Kheis Orogeny.

Orogenically-expelled hot, reactive ore fluids (brines) out of the deeper parts (high-grade cores) of the orogen and driven along tectonic décollements through and into lower-metamorphic, cooler marginal supracrustal rocks of the colliding and amalgamating cratons, results in epigenetic hydrothermal mineralisation where precipitation in associated karsts is caused by mixing with oxidising groundwater along tectonically active fault and shear zones (*cf.* Hughes, 1987; Duane & de Wit, 1988; Duane & Saggerson, 1995).

4.4 MESOPROTEROZOIC EVOLUTION (~1.73-0.82 GA)

4.4.1 POST-KHEIS OROGENIC CRUSTAL EXTENSION (~1.73-1.4 GA)

After the assembly of the late Palaeoproterozoic supercontinent Atlantica (Columbia) at ~1.73 Ga (of which the proto-Kalahari Craton (Jacobs *et al*., 2008) forms part of it) and a period of some 60 million years of relative tectono-magmatic quiescence and continental stability between ~1.73-1.67 Ga, break-up and dispersal of this supercontinent took place during the early Mesoproterozoic at ~1.67-1.4 Ga, marking the beginning of the Kibaran orogenic cycle. During this break-up and dispersal period, active continental margin rifting with associated sedimentation, volcanism and formation of juvenile oceanic crust takes place within the southern part of Atlantica in response to rifting and drifting of the amalgamated Yilgarn and Pilbara cratons and cratons of India from the southern margin of the Rehoboth-Kaapvaal-Grunehogna Craton(= proto-Kalahari Craton), which resulted in the opening of the Lomanian oceanic basin. Within the supercontinent Atlantica itself, continent-wide extensional reactivation occurs predominantly along Archaean suture zones and Archaean-Palaeoproterozoic crustal fault systems shear zones, which led to rifting and basin formation, was accompanied by minor but wide-spread, structurally controlled magmatism and associated hydrothermal activity at ~1.67-1.6 Ga (Appendices 20-R, 25-A & 25-B).

Continent marginal rift basins, such as the Bijawar and Gwalior basins, form within the Aravalli-Bundelkhand Craton (Sharma, 1998), while penecontemporaneously, passive continental margin rifting and associated sedimentation occurs along the eastern margin of Atlantica (*i.e.* of the Kaapvaal-Grunehogna, Zimbabwe, Nyassa and Tanzanian cratons), where open oceanic conditions exist, and continue most probably until the beginning of the accretionary/collisional stage of the Mozambique (Lomanian) Orogenic Cycle at ~1.15 Ga.

Within the supercontinent Atlantica itself, continent-wide extensional reactivation occurs predominantly along pre-existing fundamental Archaean and Palaeoproterozoic structural discontinuities, *i.e.* suture zones and prominent crustal shear zones. Extensional reactivation takes place predominantly within the Ubendian orogenic belt (= suture zone between Afrindalia and Bamilimu and Congo continents), as well as mainly along Archaean suture zones between individual Archaean cratons amalgamated within Atlantica (*e.g.* Sanangoè, Tuli-Sabi-Triangle, Palala, and Kalahari sutures). Craton-internal suture zones (= sutures between individual Archaean terranes) and other major crustal shear zones within the Archaean cratons of Atlantica experience comparatively less extensional reactivation.

This results in the development of mainly intra-continental rifts and basins (with rifting generally not progressing to continental break-up and oceanic basin formation) predominantly along the margins of the Archaean cratons within Atlantica, as well as partially in the superimposition of new rifts and basins over reactivated pre-existing rifts within the cratons. Intracontinental red-bed rift sequences are deposited in grabens and basins, which form above extensional reactivated Archaean suture and crustal fault zones, such as deposits of the Wilgenhoutsdrift Group, which accumulate above the Palaeoproterozoic Kalahari suture zone along the western margin of the Kaapvaal Craton.

The extensional reactivation of the Sanangoè suture zone between the Nyassa and Zimbabwe cratons results in the formation of an intracontinental rift with shallow marine incursions, and in the deposition of the Fingoè and Chíduè groups as shelf sequences onto the rifted passive margins of the southern Nyassa and northern Zimbabwe cratons respectively. Continued rifting along the Sanangoè suture zone progresses to break-up and drift between both cratons, resulting in the formation of juvenile oceanic crust (Oliver *et al.*,

1994) and deposition of the Angónia, Luia and Zámbuè groups in a marine shelf to deeper-water environment within a forming oceanic basin ("Zambezi Ocean") at ~1.4 Ga.

Within the Kaapvaal Craton and neighbouring Limpopo Central Zone Terrane, intracratonic reactivation of Archaean suture zones and Archaean-Palaeoproterozoic crustal fault systems leads to rifting and basin formation, was accompanied by minor but wide-spread, structurally controlled magmatism and associated hydrothermal activity at ~1.67-1.6 Ga. Examples are the emplacement of kimberlites in the Kuruman area at ~1.67-1.6 Ga (Shea *et al*., 1986; C.B. Smith, pers. comm. 1997), high-Ti dioritic dykes within the Vredefort Dome at ~1.62 Ga (Reimold *et al*., 1988) and of the first intrusive phase (white syenite) of the Pilanesberg alkaline complex at ~1.6-1.58 Ma (Lee, 2016) at, or near, the intersection point of the prominent, NW/SE-striking, Pongola-age (~2.98-2.96 Ga) Rustenburg Fault and the Pilanesberg suture zone, the deposition of felsic tuffs in the Palapye area within the Limpopo Central Zone Terrane at ~1.6 Ga (Mapeo *et al*., 2000), as well as hydrothermal fluid flow and isotopic resetting of older strata along extensionally reactivated fault/shear zones within the Bushveld Complex at ~1.67-1.53 Ga (Lebowa Granite Suite and Rooiberg Group; Coertze *et al*., 1978, Walraven 1982, 1987, Walraven *et al*., 1982, 1983; mafic dykes (Letts *et al*., 2004); NE/SW-striking granite dykes of Lebowa Granite Suite cross-cutting the Platreef pyroxenite at Mogalakwena Platinum Mine (Friese, unpubl.)), in the northern Kaapvaal Craton at ~1.615 Ga (*e.g.* Entabeni Granite; Cheney *et al*., 1990) and Limpopo Central Zone Terrane at ~1.63-1.6 Ga (Venetia area; Barton *et al*., 2003) (Appendices 20-R, 21-C, 25-A & 25-B).

4.4.2 KIBARAN AND LOMANIAN OROGENIC CYCLES (~1.4-0.82 GA)

On a global scale, the beginning of worldwide orogenic activity during the Mesoproterozoic Orogenic Cycle at ~1.4 Ga is characterised by a cascade of continental collisions and amalgamations of numerous continental fragments that subsequently construct the supercontinent "Rodinia" at ~900 Ma (*e.g.* Dalziel, 1991, 1992a; Hoffman 1991, 1992; Moores, 1991). Thereafter basin formation and deformation were intracratonic and controlled by reactivation of old lines of weakness.

In central and southern Africa, this worldwide orogenic activity commences with the Kibaran Orogenic Cycle at ~1.4-1.25 Ga, which gives rise predominantly to the development of supracrustal belts and granitoid plutonism formed and emplaced respectively between ~1.4 and 0.95 Ga. While juvenile crust is being formed at this time around the individual cratons in central and southern Africa, the craton interiors undergo flexuring and fracturing which is accompanied by intracratonic mafic (tholeiitic) magmatism in the form of mafic dykes/sills and basalt lava flows.

Recent studies have shown that the Mesoproterozoic orogenic cycle within the African continent occurred in two distinct tectono-thermal events, *viz*. the predominantly intracontinental **Kibaran orogenic cycle** at ~1.4-1.25 Ga (*e.g.* Cahen & Snelling, 1966, 1984; Daly & Unrug, 1982; Klerks *et al.*, 1984; Pohl, 1987, 1990, 1994; Tack *et al.*, 1993; Friese *et al.*, 1995), and the mainly continent-marginal **Lomanian orogenic cycle** at ~1.25-0.82 Ga (*e.g.* Cahen & Snelling, 1984; Piper, 1987; Pohl, 1990; Theunissen & Lavreou, 1990; Thomas *et al.*, 1994; Jacobs *et al.*, 1993; Jacobs & Thomas, 1994; Friese *et al.*, 1995).

4.4.2.1 KIBARAN OROGENIC CYCLE (~1.4-1.25 GA)

After ca. 330 million years of apparent quiescence around the margins of the proto-Kalahari Craton, renewed tectonic activity during the Mesoproterozoic heralded a major period of crustal growth. The Kibaran Orogenic Cycle commences with the initiation of subduction around and beneath the southern, western and northwestern margins of the proto-Kalahari Craton which leads to the formation of juvenile island arc/back arc basin terranes ~1.45-1.35 Ga (*i.e.*, Kairab-Kumbis Metamorphic Complex of the Sinclair-Ghanzi-Chobe Belt, Choma-Kalomo Block and the Namaqua-Natal Belt; Hanson *et al*., 1988; Hoal, 1990; Hoal & Heaman, 1995; Hanson, 2003; Singletary *et al*., 2003; Becker *et al*., 2006; Bulambo *et al*., 2006; Pettersson *et al*., 2007; Jacobs *et al*., 2008; Miller, 2012; Bial *et al*., 2015a; Cornell *et al*., 2015) (Appendix 20-T). Contemporaneous with active margin development around the proto-Kalahari Craton, Archaean suture zones and NW/SE-striking faults of the Neoarchaean Pongola rift system within the interior of the Kaapvaal Craton undergo extensional-transtensional reactivation (*e.g.*, pre-Pilanesberg extensional (normal dip-slip) reactivation of the Bobbejaanswater fault system, *i.e.*, Thabazimbi-Murchison suture zone (Du Plessis &Clendenin, 1988; Martin, 1990), which was accompanied by intraplate alkaline and carbonatite magmatism (*e.g.*, Leeuwfontein, Leeuwkraal, Rondawel, Franspoort, Buffelsdrift, Klipdrift, Haakdoornfontein and Roodeplaat complexes of the Piennars River Complex, Brandfort, Spitskop, Stukpan complexes, first intrusive phase (~1.45 Ga) of the Timbavati Gabbro Complex; second intrusive phase (white syenite) of the Pilanesberg alkaline complex) predominantly along them at 1.43-1.31 Ga (cf., Oosthuyzen & Burger, 1964; Bristow *et al*., 1982; Harmer, 1985, 1993; Harmer & Armstrong, unpubl.; Brandt *et al*., 1996) (Appendices 20-S & 25-A). The structurally controlled, intracratonic, alkaline magmatism was accompanied by hydrothermal activity and isotopic resetting as evident by several geochronological studies (see Appendix 25-B).

Subsequent to active margin development around the proto-Kalahari Craton and associated Kaapvaal Craton-wide extension and alkaline magmatism at ~1.45-1.35 Ga, island arc/back arc basin-continent collision occurred along the southern margin of the Kaapvaal Craton at ~1.35-1.25 Ga during the Kibaran Orogeny. The Archaean basement and overlying Pongola Supergroup of the southern Kaapvaal Craton underwent compressional deformation in the form of folding and thrusting (*i.e.*, the temporally weakly constrained pre-Ntingwe (D4) deformation of Matthews (1990)) (Appendix 20-T).

The Kibaran orogenic event induced N-directed far field stress into the lithosphere of the Swazi Subprovince of the Kaapvaal Craton east of the Colesberg-Mafikeng suture zone caused regional E-W crustal extension, which led to the dextral transtensional reactivation of the Neoarchaean (~2.98-2.96 Ga), NW/SE-striking Pongola rift system, resulting in the initiation of the Pilanesberg rift system at ~1.3 Ga as a dextral pull-apart rift superimposed onto the Pongola rift system, and to the development of N/S-striking, extensional fault and fracture zones. Structurally controlled alkaline magmatism along the newly formed N/S-striking Kibaran extensional fault system was accompanied by hydrothermal fluid flow and alteration along these rift zones (Appendices 20-S & 20-T). Widespread geological and geochronological evidence for Swazi Subprovince-wide, E-W crustal extension and extensional-transtensional tectonism related to Kibaran orogenic activity at ~1.35-1.25 Ga can be found across the Witwatersrand Basin, Johannesburg Dome and Bushveld Complex (Appendices 24 & 25).

Penecontemporaneously with the orogenic processes along the southern margin of Afrindalia begins orogenic activity within Atlantica, *i.e.* along the suture zone between the Afrindalia, Bamilimu and Congo continents, which had been rifted from each other since the start of break-up of Atlantica at ~1.67 Ga. During the intracratonic Kibaran orogenic event at ~1.35-1.25 Ga, the intracontinental rift and its deposits,

that formed along the extensionally reactivated Ubendian-age suture zone between the Afrindalia, Bamilimu and Congo continents, undergo inversion, deformation and metamorphism, thereby partially reworking older, Ubendian-age orogenic belts and forming, from north to south, the ensialic Kibaran-age Karangwe-Ankole, Kibaran, Irumide, and Ghanzi-Chobe orogenic belts along the western margin of the Tamazilika continent (*cf.* Hartnady *et al.*, 1985; Borg, 1988).

4.4.2.2 LOMANIAN OROGENIC CYCLE (~1.25-1.0 GA)

After cessation of Kibaran orogenic activity at ~1.25 Ga, the Kaapvaal Craton underwent a period of ca. 50 million years of relative tectono-magmatic quiescence, which coincided with rifting and juvenile oceanic crust formation around the southern margin. Initiation of possibly numerous, either diachronously and contemporaneously formed, northeasterly and southeasterly inclined subduction zones off the continent's southwestern and southeastern margins, manifests the beginning of the Lomanian Orogenic Cycle and the final episode in the closure process of the Lomanian oceanic basin through NW-SE plate convergence between Afrindalia and an Indo-Antarctic continent at ~1.25 Ga. During the Lomanian Orogenic Cycle at ~1.25-1.0 Ga, subduction-related crustal growth occurs in the form of the formation of an extensive oceanic magmatic-arc terrane, consisting of numerous oceanic volcanic-arc/fore-and back-arc basin complexes, between both continents at ~1.25-1.04 Ga and ~1.25-0.95 Ga to the south and east of Afrindalia respectively (*e.g.* Andreoli, 1984; Pinna *et al*., 1993; Jacobs *et al*., 1993; Jacobs & Thomas, 1994; Thomas *et al*., 1994).

NE-directed subduction beneath the southwestern craton margin (Namaqua sector) resulted in the formation of juvenile crust in the form of island arc calc-alkaline granitoid magmatism (*e.g.*, Keimoes batholith) and back-arc basin deposition of volcano-sedimentary sequences (*e.g.*, Areachap terrane) at ~1.25-1.2 Ga (Geringer *et al*., 1986, 1988, 1994 Cornell *et al*., 1990, 1992), while penecontemporaneous rifting and juvenile Mesoproterozoic oceanic crust formation (= Tugela terrane) and subduction away (southeastwards) from the craton along the southeastern craton margin (Natal sector) caused magmatism (felsic and mafic volcanics and calc-alkaline granitoids) and sedimentation in an oceanic island-arc/back-arc basin setting and resulted in the formation of the Mzumbe and Margate terranes at ~1.25-1.18 Ga (*e.g.*, Matthews 1972, 1981; Reid, 1979; Barton, 1983; Barton & Burger, 1983; Hartnady *et al*., 1985; Stowe, 1986; Joubert, 1986; Thomas 1989; Eglington *et al*., 1989; Thomas & Eglington, 1990; Jacobs *et al*., 1993, 1997; Thomas *et al*., 1992, 1994, 1999; Johnston *et al*., 1997, 2001, 2003; Eglington, 2006; Cornell *et al*., 1996, 2006; McCourt *et al*., 2006) (Appendix & 20-T).

NE-directed collision, accretion and obduction of Palaeoproterozoic microcontinents/island arc terranes (*i.e.*, Richtersveld Subprovince, Bushmanland Terrane/Subprovince, Kakamas and Kaaien terranes) and juvenile Mesoproterozoic crust (*i.e.*, Areachap Terrane) along the southwestern margin of the Kaapvaal Craton took place at ~1.2-1.18 Ga during the early phase of the Lomanian Orogeny, while successive NW-directed, oblique collision, accretion and obduction of the juvenile Tugela ophiolite terrane (Tugela allochthon) and Mzumbe and Margate island arc/back-arc basin terranes onto the southeastern margin of the Kaapvaal Craton took place at ~1.18-1.08 Ga during the main phase of the Lomanian Orogeny, which caused successive deformation and metamorphism of the accreted and obducted terranes and significant structural crustal thickening along the craton's southern margin (*e.g.*, Matthews, 1972; Scogings, 1989; Thomas, 1989; Eglington *et al*., 1989; Thomas & Eglington, 1990; Thomas *et al*., 1994; Jacobs & Thomas, 1994; Jacobs *et al*., 1997, Johnston *et al*., 1997, 2001, 2003; de Wit & Tinker, 2004; Cornell *et al*., 2006; Eglington, 2006; McCourt *et al*., 2006; Spencer *et al*., 2015) (Appendix 20-U).

NE- and NW-directed compression during arc-continent collision along the southwestern (Namaqua sector) and southeastern (Natal sector), respectively, gradually changes to dextral and sinistral transpression and the development of major, ductile, dextral and sinistral transpressive shear zones parallel to the craton's southern margin as part of the ensuing late-tectonic crustal escape phase of the Lomanian Orogeny at ~1.08-1.0 Ga, respectively (Coward & Potgieter, 1983; Harris, 1988; Eglington *et al*., 1989; Thomas *et al*., 1990a, 1992b & c; Van Bever Donker, 1991; Colliston *et al*., 1991; Van Bever Donker, 1991; Jacobs *et al*., 1993; Jacobs & Thomas, 1994; Eglington *et al*., 2010). This event is accompanied by the widespread intrusion of rapakivi-textured granitoids and charnockites associated with high-T, moderate-P granulite-grade metamorphism in the transcurrent tectonic setting, and the deposition clastic sediments and bimodal volcanic rocks of the Koras and Sinclair Groups in dextral pull-apart rift basins in the Namaqua sector (*e.g.*, Botha *et al*., 1979; Hoal *et al*., 1989; H6rstmann *et al*., 1990; Jacobs *et al*., 1993; Thomas *et al*., 1993, 1994, 2003; Johnston *et al*., 1997, 2001, 2003; Eglington *et al*., 2003; Eglington & Armstrong, 2004; Eglington, 2006; McCourt *et al*., 2006; Cornell *et al*., 2006; Jacobs *et al*., 2008; Mendonidis *et al*., 2002, 2015; Spencer *et al*., 2015; Oriolo & Becker, 2018). Late- to post-orogenic hydrothermal activity within the Lomanian (Namaqua-Natal) orogenic belt continues until ~0.9 Ga (Jacobs *et al*., 1997) (Appendix 20-U).

Lomanian orogenic activity along the southern margin of the Kalahari Craton induces NW-directed compressive far field stress into the lithosphere of the Kaapvaal Craton, which results in the development of a NW-migrating, thin-skinned fold-and-thrust belt within the craton interior and the compressive and transpressive reactivation of Mesoarchaean suture zones and Neoarchaean-Palaeoproterozoic crustal fault zones (see Section 6.4.4.7 for details). The NW/SE-striking Neoarchaean (~2.98-2.96 Ga) Pongola rift system undergoes sinistral-transtensional reactivation to the north of the Magaliesburg-Barberton suture zone system in the foreland ahead of the Lomanian fold-and-thrust belt. This causes the continued formation of the Pilanesberg rift system, since its initiation at ~1.3 Ga as a dextral transtensional (pull-apart) rift during the Kibaran Orogeny at ~1.35-1.25 Ga, to a sinistral transtensional (pull-apart) rift during the Lomanian Orogeny at ~1.2-1.05 Ga by superimposition onto the Neoarchaean Pongola rift. Pilanesberg rift development is accompanied by a phase of alkaline magmatic activity, closely associated with, and confined to, the Mesoproterozoic pull-apart rift (Appendices 20-S & 20-U).

Deformation and associated structurally controlled alkaline magmatism and hydrothermal fluid flow, alteration and isotopic resetting linked to Lomanian-age, NW-directed compressive far field stress extend beyond the northern margin of the Witwatersrand Basin into the northern Kaapvaal Craton where an extensional-transtensional tectonic regime dominates (Friese *et al*., 1995) (Appendix 20-U).

4.5 NEOPROTEROZOIC-LATE PALEOZOIC EVOLUTION (~1000-320 MA)

4.5.1 PAN-AFRICAN OROGENIC CYCLE (~1000-480 GA)

Following the formation of the Kalahari Craton as integral part in the assembly process of the supercontinent Rodinia during the Lomanian (Grenville) Orogeny at the end of the Mesoproterozoic at ~1.0 Ga (Hartnady *et al*., 1985; Jacobs *et al*., 2008; Oriolo & Becker, 2018; cf., Clifford, 1970) and post-Lomanian orogenic collapse (uplift, denudation and cooling) of the late-Mesoproterozoic orogenic belts until the early Neoproterozoic at ~900 Ma, which was accompanied by the emplacement of granitoids and pegmatites, the succeeding the Pan-African orogenic cycle commenced at ~900 Ma with rifting along the margins of the Kalahari Craton and associated sedimentation and alkaline and bimodal volcanism in the rift zones during the early Neoproterozoic Tonian period (~900-720 Ma). Extensive rifting, sedimentation and magmatism around the Kalahari Craton were superseded, in some cases, by drifting and ocean basin formation, leading to the break-up of Rodinia (Appendix 20-V). Intracontinental rifting and continental break-up of Rodinia into three major Pan-African lithospheric plates, *i.e.*, East-, West- and South-Gondwana occurred partially along Mesoproterozoic (Kibaran- and Lomanian-age) and older suture zones (Appendix 20-W).

Subduction, initiated around the Kalahari Craton towards the end of the Tonian period at ~720 Ma, continued for ca. 85 million years during the mid-Neoproterozoic Cryogenian period (~720-635 Ma) and resulted in the formation of island arc terranes (Jacobs *et al*., 2008 and references therein). In the Gariep Belt, the Richtersveld Suite records anorogenic intrusions at ~840-770 Ma (Frimmel *et al*. 2001; Miller 2008), whereas metavolcano-sedimentary sequences of comparable age are recorded in the lower portions of the Gariep Supergroup (*e.g.,* Frimmel *et al*., 2002). In the Damara Belt, rifting is recorded by several Cryogenian metavolcano-sedimentary rocks (Foster *et al*., 2014 and references therein), whereas evidences of late Tonian-Cryogenian magmatism and sedimentation were documented in the Zambezi Belt (*e.g.*, Vinyu *et al*., 1999; Hargrove *et al*., 2003). Glacio-sedimentary rocks of the Geci and Cobué groups were deposited unconformably over the granulitic basement of the Mozambique Metamorphic Province at <820-600 Ma During the Tonian-Cryogenian period of Rodinia break-up, no significant intracratonic tectono-magmatic activity occurred within the interior of the Kalahari Craton (this study) (Appendix 20-V).

Subduction around the Kalahari Craton was followed by inversion of the craton-marginal rift zones and crustal reworking of the craton's margin as a result of arc-continent accretion and continent-continent collision, culminating in the collision of the three Pan-African lithospheric plates and amalgamation into the supercontinent Gondwana in the late Neoproterozoic-Palaeozoic (Ediacaran-Cambrian) in a series of successive, diachronous Pan African orogenies at ~640-480 Ma (*e.g.*, Pinna *et al.,* 1993; Kröner *et al*., 1997; Grantham *et al*., 2003; Gray *et al*., 2008; Bingen *et al*., 2009; Lehmann *et al*., 2015) (Appendix 20-W). Along the collision zones, the East Africa-Antarctica, West Congo-Kaoko-Gariep, Damara-Lufilian-Zambezi and Saldania-Ross-Delamerian orogens formed by convergence and collision between East and West Gondwana at ~640-590 Ma, Amazonian-Rio de la Plata Craton and Congo-São Francisco Craton at ~630-560 Ma, North and South Gondwana at ~560-520 Ma, and island arcs along the southern margin of Gondwana at ~515-480 Ma, respectively (*e.g.*, Pinna *et al*., 1993; Kröner *et al*., 1997; Grantham *et al*., 2003; Jacobs *et al*., 2006; Boger & Miller, 2004; Foden *et al*., 2006; Gray *et al*., 2008; Bingen *et al*., 2009; Lehmann *et al*., 2015; Shannan *et al*., 2018) (see Appendices 19 & 20-W). A peripheral foreland basin developed inboard (on the western edge of the Kalahari Craton) of the Damaran, Gariep and Saldania belts as a result of lithospheric flexure in response to thrust loading, in which synorogenic flysch-like sediments of the Nama and Vanrhyynsdorp Groups and molasse-type sediments of the Klipheuwel Group were

deposited in two subbasins and late-orogenic (tectonic escape) strike-slip-related pull-apart basins, respectively, unconformably over syn- to late-orogenic I-type granites of the Cape Granite Suite at ~630-520 Ma (Germs, 1983; Le Roux & Gresse, 1983; Hörstmann *et al*., 1990; Gresse, 1986, 1992a; Gresse *et al*., 1988; Germs & Gresse, 1991; Saylor, 1992; Gresse & Germs, 1993). A foreland basin developed to the north of the Saldania-Ross-Delamerian orogenic belt at ~515-480 Ma in which molasse deposits (*e.g.*, Natal Group) were laid down derived from the erosion of the Saldania-Ross-Delamerian fold-and-thrust belt (cf., Thomas et a/., 1992d).

Consumption of the Mozambique Ocean between 841 and 632 Ma (Cutten & Johnson, 2006) and collision and amalgamation of West Gondwana (comprising most of the Central Africa Craton) and East Gondwana (was composed of juvenile crust, now attributed to the Arabian-Nubian Shield, and older crystalline basement of the Dharwar Craton of southern India, Madagascar and the eastern granulites of Kenya and Tanzania) at ~640-530 Ma gave rise to the development of the N-S trending, 6,000 km long East Africa Orogen (EAO) (Hoffman, 1991; Pinna *et al*., 1993; Grunow *et al*., 1996; Dalziel, 1992, 1997, Shackleton, 1993, 1996; Stern, 1994; Shackleton, 1994, 1996; Wilson *et al*.,1997; Kröner *et al*., 2001; Fritz *et al*., 2018), or, stressing its southernmost continuity, East Africa-Antarctica Orogen (EAAO) (Jacobs *et al*., 2006) (Appendix 20-W).

Penecontemporaneously and possibly driven by W-directed compressive far field stresses induced by the East Africa-Antarctica Orogeny, convergence and collision between the united Amazonian-Rio de la Plata Craton and the united Congo-São Francisco Craton at ~630-560 Ma led to the formation of the West Congo-Kaoko-Gariep-Saldania Belts along the present western margin of southern Africa (see Appendix 20-W).

Subsequently, closure and destruction of the Zambezi-Adamastor oceanic basin (Johnson *et al*., 2005), which might have been a series of linked rifts and narrow ocean basins (*e.g.*, Jacobs *et al*., 2008), was driven by far field stresses from the collisional plate margins and resulted in the collision and amalgamation of South Gondwana (composed of the Kalahari and East Antartic cratons, amalgamated since the ~1.0 Ga Grenvillian orogenic cycle) with the already united East and West Gondwana plates along the Kuunga suture zone at ~560-520 Ma forming the Damara-Lufilian-Zambezi Belt (DLZ) (cf. Burke *et al*., 1977; Pinna *et al*., 1993; Oliver *et al*., 1998; Porada & Berhorst, 2000; John *et al*., 2003; Johnson & Oliver, 2000, 2004; Lehmann *et al*. 2015; Oriolo *et al*., 2016, 2017) (Appendix 20-W). Consequently, the N-S trending suture of the EAO impinges on the E-W trending Kuunga Orogen suture, comprising (from west to east) the Damara-Lufilian-Zambezi Belt, the Lúrio Thrust Belt and, further eastwards, thrust belts of Sri Lanka (Appendix 20-W). Mafic and ultramafic rock fragments in Neoproterozoic metasediments (Roan Group, Katanga Supergroup) of the Lufilian and Zambezi segments of the DLZ Belt supposedly represent relics of obducted ocean floor rocks, forming a tectonic mélange. The Chewore Ophiolite in the Chewore Inliers represents a larger fragment of oceanic crust. Amphibolites in the Damara segment of the DLZ Belt show MORB tholeiitic affinities (Breitkopf & Maiden, 1988) and are supposedly also derived from ocean floor protoliths.

Pan-African, subduction-related HP-LT metamorphism is reflected by eclogites and whiteschists (kyanite+talc+yoderite) in ophiolite and by kyanite in metapelite (Vrána & Barr, 1972; Vrána *et al*., 1975), and manifest peak metamorphic conditions with T estimated at 630-690 °C and P ranging from >13 to 26-28 kb (John & Schenk, 2003; John *et al*., 2004). Sm-Nd whole rock-garnet and Lu-Hf whole rock garnet dating yield ages ranging from 659 ± 14 Ma to 595 ± 10 Ma, interpreted as indicating the age of Pan-African eclogite-facies metamorphism (John & Schenk, 2003; John *et al*., 2004).

The Lufilian and Zambezi segments of the DLZ Belt can be described as a thin- and thick-skinned, double-verging orogen with thrust transport to the NNE-NE (Wilson *et al*., 1993; Hanson *et al*., 1994; Johnson & Oliver, 2004) and SSE (Barton *et al*., 1991; Dirks *et al*., 1999; Vinyu *et al*., 1999; Müller *et al*., 2001), respectively. Transport directions and sinistral shear along the Mwembeshi Dislocation suggest oblique convergence between West and South Gondwana. The spatial arrangement of metamorphic ages and range in timing of peak metamorphic conditions indicate that the closure of the Zambezi-Adamastor Ocean and amalgamation of South and West Gondwana was not a simple collision between two large lithospheric plates, but rather a series of collisional events among several cratonic fragments, taking place between ~615 Ma and 520 Ma, a period of almost 100 Ma.

One of the cratonic fragments in the DLZ Belt was the rigid Choma-Kalomo block, which supposedly acted as an indentor when it became caught between West and South Gondwana. Its presence within the collision zone changed the geometry of compression and thrusting, resulting in the arcuate shape of the Lufilian segment (*i.e.*, the Lufilian Arc) of the DLZ Belt (Bulambo *et al*., 2006), comprising Neoproterozoic folded and north-thrusted metasediments of the Katanga Supergroup.

Although the DLZ collisional event is well documented by Neoproterozoic metamorphic U-Pb data of older rocks, the scarcity of juvenile TTG suites having ages between ~616 and 520 Ma is notable. In Zambia, the few known examples of syn-kinematic felsic igneous rocks include the Hook Granite (~566-533 Ma) and nearby Mwembeshi Rhyolite (~551 Ma).

Late Pan-African final docking of the three lithospheric plates during the Ross-Delamarian Orogeny at ~500-480 Ma induced NW-directed compressive far field stress into Gondwana, which caused the sinistral strike-slip reactivation of the East Africa-Antarctica Orogen and West Congo-Kaoko-Gariep-Saldania Orogen and sinistral transtensional tectonic (Appendix 20-W). This was followed by post-Pan-African orogenic collapse (uplift, denudation and cooling) of the Pan African orogens at ~480-430 Ma, which was accompanied by the emplacement of granitoids and pegmatites (Goscombe *et al*., 2000; Macey & Armstrong, 2005; Grantham *et al*., unpublished data, in Macey *et al*., 2006; Cronwright & Roberts, unpublished CHIME data, in Macey *et al*., 2006).

Minor Palaeozoic (~533-491 Ma) kimberlite-lamprophyre magmatism occurred across the Kalahari Craton in an apparent younging direction from NE to SW, *i.e.*, in the Zimbabwe Craton (Colossus kimberlite cluster (~533 Ma); Allsopp *et al*., 1985; Phillips *et al*. 1998), in the Limpopo Central Zone Terrane (kimberlite clusters of Mwenezi (~520 Ma) (Phillips *et al*., 1997), Venetia (~519 Ma) (Allsopp *et al*., 1995; Phillips *et al.,* 1998) and River Ranch (Jelsma *et al*., 2004)), in the Kaapvaal Craton (The Oaks kimberlite cluster (~505 Ma) (Phillips *et al*., 1998), and in the Namaqua orogenic belt (Garub lamprophyre cluster (491 Ma) (Allsopp *et al*., 1979). The intracratonic kimberlite-lamprophyre magmatism coincided with, and was likely triggered by far field stress induced into the Kalahari Craton during the Pan-African Kuunga Orogeny at ~560-520 Ma and Ross-Delamarian Orogeny at ~500-480 Ma, which caused the generation and ascend of kimberlite-lamprophyre magmas by decompressional upper mantle melting along tectonically reactivated translithospheric suture zones and their crustal emplacement along crustal fault zones (this study) (Appendix 20-W).

4.5.2 LATE-TO POST-PAN-AFRICAN OROGENIC RELAXATION AND COLLAPSE (~480-320 GA)

Pan-African orogenic activity is followed by post-orogenic relaxation and collapse (extensional tectonism, rapid uplift, denudation and cooling) of the Pan African orogens at ~480-430 Ma, which is accompanied by

the emplacement of granitoids and late-stage pegmatites (*e.g.*, Goscombe *et al*., 2000; Macey & Armstrong, 2005; Macey *et al*., 2006; Foden *et al*., 2006) (Appendix 20-W). Intracontinental basins develop in response to extensional tectonism during the post-orogenic relaxation and collapse within the Pan-African orogens. Over a protracted period of ca. 160 million years from the Ordovician to Mid-Carboniferous (~480-320 Ma), passive continental margin basin sedimentation along the southern edge of Gondwana results in the deposition of the 10 km thick Cape Supergroup, which is deposited as beach, deltaic and shallow marine clastic sediments on a broad, relatively stable platform from a granitic source to the north (*e.g.*, Tankard *et al*., 1982; Johnson, 1991; Broquet, 1992; Thamm & Johnson, 2006; Tankard *et al*., 2009).

Aside from the emplacement of the Beitbridge kimberlite into the Limpopo Central Zone at ~430 Ma (Kramers & Smith, 1983), no significant intracratonic tectono-sedimentary and magmato-hydrothermal activity occurs within the interior of the Kaapvaal Craton and Kalahari Craton overall during the post-Pan-African Cycle period from Early Ordovician to Mid-Carboniferous at ~480-320 Ma (this study) (Appendix 20-V).

4.6 LATE PALEOZOIC-RECENT EVOLUTION (~320-0 MA)

While at least the central parts of Gondwana remained stable through most of the Palaeozoic era, crustal extension and rifting processes take place during the Late Palaeozoic until present time (~320-0 Ma), extending through present-day Africa, Madagascar, India and parts of Antarctica. Extension and rifting occur predominantly along the margins of, and between individual Precambrian continental terranes along lines of Proterozoic and Archaean crustal weakness (*e.g.* Dingle *et al.*, 1983; Martin & Hartnady, 1986; Watkeys & Sweeney, 1988), leading to the formation of narrow basins and grabens and associated sedimentation and magmatism. The Late Palaeozoic to Recent structural and stratigraphic evolution of southern Africa can be separated into two stages, *viz*. a **late-Gondwana** ("Karoo"/Carboniferous-Jurassic; ~320-157 Ma) **stage**, characterised by last orogenic activity (Gondwanide Orogeny) during the final amalgamation phase of Gondwana (~320-205 Ma) and the subsequent rift (fragmentation) phase of the supercontinent (~205-157 Ma), which are associated with the development of intracontinental basins (*e.g.* Zambezi, Maniamba-Lugenda and Save-Limpopo basins) within Gondwana, and a **post-Gondwana** (Mesozoic-Recent; ~157-0 Ma) **stage**, documenting the drift (dispersal) phase of Gondwana which is associated with the opening of the Indian and Atlantic oceans and associated formation of ocean continental margin basins (*e.g.* Mozambique & Ruvuma basins).

Note: The last ~35 Ma of the post-Gondwana stage are regarded nowadays as a separated evolutionary phase, *i.e.* the **Neotectonic** (Oligocene-Recent; ~35-0 Ma) **phase**, which is presented in Section 4.7.

4.6.1 LATE-GONDWANA ("KAROO") STAGE (~320-157 MA)

The late-Gondwana ("Karoo") stage can be divided into two distinct episodes, *i.e.* an early (~320-205 Ma) and late (~205-157 Ma) to post (~157-0 Ma) Gondwana rifting phase.

4.6.1.1 EARLY GONDWANA RIFTING PHASE/GONDWANIDE OROGENIC CYCLE (~320-205 MA)

The early Gondwana rifting phase (~320-205 Ma) (Late Carboniferous-Triassic) coincides with the onset of southward subduction of the Gondwanan beneath the Palaeo-Pacific plate along the southern Panthalassan (Pacific/Iapetus) margin of Gondwana. This marks the start of the Gondwanide orogenic cycle in the Early Carboniferous at ~330 Ma. Approximately 40 million years later, accretion of island arcs and microcontinents along the southern margin of Gondwana marks the start of the Permo-Triassic Gondwanide Orogeny at ~290-230 Ma, leading to the final amalgamation of the Gondwana (Pangea) supercontinent by ~230 Ma and causing the development of an extensive, E/W-trending retroarc foreland basin system to the north of the Gondwanide fold-and-thrust belt that can be traced over a distance of 13,000 km across the southern margin of the supercontinent from South America, southern Africa, Antarctica and into eastern Australia (*e.g.*, Du Toit, 1937; Hälbich *et al*., 1983; Gresse &Theron, 1992; Veevers & Morgan, 2000; Curtis, 2001; Torsvik & Cocks, 2002, 2004; Veevers, 2004; Cawood, 2005; Vaughan & Pankhurst, 2008; Boger, 2011; Hansma *et al*., 2016) (Appendix 20-X).

Along the southern (Panthalassan) margin of Gondwana, orogenic activity, both in the form of magmatic-arc development and episodic accretion of terranes, was intermittently present from the very start of Gondwana existence in Cambrian times until its break-up in the Middle and Late Jurassic (~550-205 Ma) (Appendix 20-X).

Late Precambrian to Late Palaeozoic (~650-450 Ma) tectono-magmatic activity during the Pan African Orogenic Cycle along the southern margin of the forming Gondwana supercontinent, is represented by the Precambrian-Cambrian (~650-520 Ma) and Ordovician-Devonian (~490-320 Ma) Pampean and Famatinian orogenic cycles in South America respectively (*e.g.* Pankhurst & Rapela, 1998), the Precambrian-Cambrian (~650-500 Ma) Saldanian Orogenic Cycle in South Africa, as well as the Early to Middle Palaeozoic (~560-450 Ma) Ross Orogenic Cycle in Antarctica (*e.g.* Collinson *et al.*, 1994; Curtis & Storey, 1996). The terrane accretion along the southern margin of Gondwana during the Palaeozoic might be causally related with the contemporaneous calving of terranes along the northern (Tethyan) margin (*e.g.* Smith, 1999), by continental-scale stress transmission (De Wit & Ransome, 1992; Trouw & De Wit, 1999).

Subsequent to the Pan-African Orogenic Cycle, the Permo-Triassic (~320-240 Ma) Gondwanide Orogenic Cycle along the southern margin of Gondwana represents the final, and hence just one in a series of intermittent tectono-magmatic events leading to the amalgamation of Gondwana (Trouw & De Wit, 1999).

Not continental collision, but rather oblique plate convergence associated with northerly flat slab subduction of oceanic crust of the palaeo-Pacific plate beneath the southern margin of Gondwana, leads to the formation of a ~1000 km wide oceanic to intracontinental Andean-type magmatic-arc and adjacent retro-arc foreland basin to the north within the southern part of the supercontinent, as well as induces compressional to dextral transpressional far field stresses in the overriding plate (= Gondwana continent) (*e.g.* Trouw & De Wit, 1999; Johnston, 2000) (Appendix 20-X).

The induction of compressional to dextral transpressional far field stresses within Gondwana, possibly generated by enhanced friction caused by low angle subduction, results in the development of dextral transpressional, northwesterly to northerly verging fold-and-thrust belts along the southern margin of Gondwana (*i.e.,* Pan Gondwanian Mobile Belt or Gondwanide Orogen comprising the Ventana Fold Belt/South America, Cape Fold Belt/South Africa, Falkland Fold Belt/Falkland Island crustal block, Ellsworth-Whitemore Fold Belt/Haag Nunataks crustal block, Pensacola Fold Belt/Antarctica and intracontinental foreland basins (*i.e.* Paraná, Karoo, Transantarctica/Beacon and East Australian/Bowen basins) to the north

(*e.g.* Trouw & De Wit, 1999 and references therein), as well as in rifting, strike-slip and compressional deformation in the interior of the supercontinent (Daly *et al.*, 1991) (Appendix 20-X).

Within the African portion of Gondwana, Palaeozoic (~500-310 Ma) passive rifted margin deposits (*e.g.* Cape Supergroup) were folded, synkinematically low-grade (diagenesis to greenschist-facies) metamorphosed, and northerly thrusted towards the interior of the Kalahari Craton. The Cape Orogeny develops along Late Proterozoic trends following the weakest and most deformed zones of the continental lithosphere (Tankard *et al.*, 1982; Thomas *et al.*, 1993a). The Late Carboniferous-Middle Jurassic Karoo Basin develops in front of the Cape Fold Belt and above the northerly inclined subducting slab as an alternating large continental cratonward migrating retroarc foreland basin (with an initial underfilled, later filled phase of deep, later shallow marine sedimentation = Dwyka, Ecca and Beaufort groups) in Late Carboniferous-Middle Triassic time (~310-240 Ma) in response and simultaneously to supralithospheric loading generated as a result of crustal shortening and thickening in the Cape Fold Belt, and as orogenward migrating foresag-basin (with overfilled phase of nonmarine sedimentation = Stormberg Group) in Late Triassic-Middle Jurassic time (~230-183 Ma) during orogenic unloading (de Wit *et al.* 1988; Johnson, 1991; de Wit & Ransome, 1992; Cole, 1992; Johnson & Beaumont, 1995; Johnson *et al.*, 1997; Trouw & de Wit, 1999; Catuneanu *et al.*, 1998, 2002, 2005) (Appendix 20-X). Crustal thickening occurs either as a result of accretion of an oceanic magmatic-arc (*e.g.* Catuneanu *et al.*, 1997), or merely in response to combined low-angle oblique subduction and magmatic under-/intra-plating during the development of an intracontinental magmatic-arc (Trouw & De Wit, 1999).

Contemporaneously, Precambrian orogenic belts, developed along the margins of individual cratons within southern Africa, experienced extensional/transtensional reactivation, resulting in the formation of extended rift structures, which were linked with the broad platform depression (= main Karoo Basin) within the interior of the Kalahari Craton. Both, main Karoo foreland/sag-basin and rifts were filled by thick sequences of terrigenous and carbonate formations of the Karoo Supergroup (*e.g.* Bordy & Catuneanu, 2002). In the north, an incursion of palaeo-Tethys seawaters along the axial part of a major depression between Africa and Madagascar occurred, that formed above the extensionally reactivated East African Orogen (= suture/collision zone between East and West Gondwana) (Appendix 20-X).

4.6.1.2 LATE (~205-157 MA) TO POST (~157-0 MA) GONDWANA RIFTING PHASE

Following the Gondwanide Orogeny and related extension of Precambrian orogenic belts within southern Africa at ~310-205 Ma, crustal extension continues and intensifies, marking the end of the Gondwana supercontinent (as southern part of the supercontinent Pangea) and the beginning of Gondwana break-up into separate continental blocks during the late Gondwana rifting phase at ~205-157 Ma (Early to Middle Jurassic) (*e.g.*, Scotese *et al.*, 1988).

The terrestrial deposition of the Karoo Supergroup in the Karoo Basin was terminated with the extensive extrusion of felsic volcanics and plateau (flood) basalts (*e.g.*, Erlank, 1984; Jourdan *et al.*, 2007) and the intrusion of dolerite dykes and sills of the Drakensberg Basalt and Lebombo Groups and Bumbeni Complex as part of the Karoo Igneous Province, representing a classic continental flood basalt province, within southern Africa over a very short time span of ca. 5 Ma at the onset of Gondwana fragmentation at ~183-178 Ma (McDougall, 1963; Fitch & Miller, 1971, 1984; Siedner & Mitchell, 1976; Allsopp *et al*., 1984a & b; Eales *et al*., 1984; Stratten, 1986; Sweeney & Watkeys, 1990; Campbell & Griffiths, 1990; Hooper *et al*., 1993; Marsh *et al*., 1995; Encarnacion *et al*., 1996; Duncan *et al*., 1997; Le Gall *et al*., 2002; Duncan &

Marsh, 2006, 2007), caused either by high-volume mantle plume head activity impinging on the Kaapvaal lithosphere (*e.g.*, Campbell & Griffiths, 1990; Bristow & Hatton, 1992; Antoine & Moyes, 1992; Storey, 1995; White & McKenzie, 1995; Storey & Kyle, 1997; White, 1997), subduction (Cox, 1978, 1992), or lithospheric stretching (Gallagher & Hawkesworth, 1992) with the subsequent breakup of the Gondwana supercontinent.

The actual start of Gondwana break-up with initial crustal extension within the Kalahari Craton, however, occurred at ~205 Ma, *i.e.*, ca. 22 million years prior to the establishment of the Karoo continental flood province at ~183 Ma, as indicated by minor kimberlite magmatism within the Zimbabwe Craton (*i.e.*, Dorowa carbonatite (205 Ma; Nicolaysen *et al*., 1962; recalculated by Jelsma *et al*., 2004)) and Kaapvaal Craton (*i.e.*, Dokolwayo kimberlite/Swaziland (200 Ma; Allsopp & Roddick, 1984) and Ramatseliso kimberlite/Lesotho (194 Ma; Davis, 1978)).

The breakup of Gondwana and dispersion of the fragments that surrounded southern Africa is proposed to have occurred in five successive stages and induced strain into the African plate, which was marked repeatedly by brittle failure and dyke injection (*e.g.*, Watkeys, 2006) (Appendix 20-Z).

The break-up of Gondwana which commenced with crustal extension during an initial rift phase at ~205 Ma, intensified in late-Jurassic time at ~157 Ma and corresponds to the period of active Gondwana break-up and dispersal into separate continental blocks (drift phase), and associated opening of the South Atlantic in the west and the late stage of separation of East and West Gondwana in the east of the African continent, as well as the formation of Indian Ocean marginal basins during the drift phase at ~157-0 Ma. Both the western and eastern African regions were linked through the Central African shear zones, but in contrast to the west coast of Africa, where extension predominated, the opening of the Indian Ocean was facilitated mainly by transtensional movements.

Along the east coast of Africa, the break-up of Gondwana comprised a period of active sea-floor spreading in the western Somalia Basin and Mozambique Channel Basin. During this period, Gondwana separated into two major blocks, *i.e.* West Gondwana (Africa and South America) and East Gondwana (Antarctica, India and Sri Lanka, Madagascar, Seychelles and Australia). Drift of continental blocks occurred along a series of transform faults located parallel to Davies Ridge, Mozambique Escarpment and Explora Escarpment (Antarctica) (Lawver *et al*., 1992).

Towards the end of the late Gondwana rifting stage (~175-157 Ma), volcanic activity in the Afro-Antarctic part of Gondwana gradually diminished, while a deep depression formed between Africa and Madagascar, along which the palaeo-Tethys transgression further developed, creating a marine seaway separating the African and Indo-Madagascar blocks.

During the Late Jurassic (~157-142 Ma), the drift of Madagascar and Antarctica relative to Africa was initiated and sea-floor spreading was accompanied by the wide extension of the palaeo-Tethys marine transgression over the eastern margin of the African block and western Madagascar, resulting in discordant deposition of Upper Jurassic marine shale and limestone in the northeastern African coastal basins (*i.e.*, Kenya-Somalia and Tanzania basins), including the Ruvuma basin and northern part of the Mozambique basin. In the central and southern part of the Mozambique basin, a rift system was formed and thick syn-rift, red-coloured sedimentary sequences accumulated (Salman & Abdula, 1995).

The first half of the Early Cretaceous period (~142-130 Ma) was marked by continuing sea-floor spreading in the Somali and Mozambique Channel basins. The marine transgression reached the southern end of the

African block. On the southeastern margin of Africa, the development of rift structures and accumulation of thick sedimentary sequences continued, accompanied by a partial regression.

The second half of the Early Cretaceous period (~130-97 Ma) was characterised by a new transgression onto the African continent, probably related to the break-up of West Gondwana, separation of South America and opening of the South Atlantic. At the end of the Early Cretaceous, Madagascar had virtually stopped rifting with respect to Africa, and the formation of the main structures of the East African continental margin had been completed (Lawver *et al*., 1992; Salman & Abdula, 1995).

The Late Cretaceous to Eocene (~97-35 Ma) represents a period of stabilisation of the East African continental margin. Further development of the marginal sedimentary basins was limited to progradational extension of the sedimentary section towards the ocean and development of compensatory depressions (Salman & Abdula, 1995). The Late Cretaceous (~97-65 Ma) was typified by a development of widespread transgression within Eastern Africa. Along the entire continental margin, rather uniform, marl/clay sequences accumulated prograding onto the continental slope. In the southern portion of the Madagascar/Indian block and the adjacent Mozambique Channel and Mascarene basins, volcanic activity was common, with deposition of thick volcanogenic and volcanogenic-sedimentary sequences. This was related to the beginning of sea-floor spreading within the Mascarene Basin in the second half of the Late Cretaceous and the separation of India and the Seychelles from Madagascar. The widespread deposition of Palaeocene and Eocene (~65-35 Ma) shallow-water shelf carbonate sediments with reefal facies along the outer edge of the shelf, completed the stabilisation phase of the East African continental margin (Salman & Abdula, 1995).

Gondwana break-up was accompanied by episodic kimberlite magmatism which was triggered by, and is genetically linked to major plate reorganisation events that affected the supercontinent. The onset of kimberlite magmatism was closely associated with thermal perturbations (either caused by thermal insulation or mantle upwelling) beneath a stagnant or sluggish supercontinent. These perturbations have caused uplift and the onset of continental break-up through fracture zones propagating into the supercontinent, as well as the formation of Large Igneous Provinces (LIPs) (*e.g.*, Jelsma *et al*., 2009).

With focus on the African Plate, and more specifically on the southern African lithosphere, episodic kimberlite magmatism was triggered by, and is genetically linked to (1) apparent variation in direction and velocity in the relative plate motion paths of the African versus Eurasian plate and African versus Antarctica plate) (Marsh, 1973; Hargraves & Onstott, 1980; Jelsma *et al*., 2004; Moore *et al*., 2008), (2) stages of uplift and erosion, and the formation of unconformities in the offshore and onshore stratigraphic record documenting episodic tectonic instability (cf., Jelsma & Smith, 2004; Moore *et al*., 2008) and (3) Large Igneous Province (LIP) manifestation (Jelsma *et al*., 2009).

In southern Africa, kimberlite magmatism followed (1) the break-up of West and East Gondwana with the opening of the Weddell Sea and Somali Basin and the eruption of the Karoo-Ferrar basalts at ~180 Ma, (2) the break-up of South America and Africa with the opening of the South Atlantic and the eruption of the Parana-Etendeka basalts at 135 Ma, (3) seafloor spreading in the South Atlantic which caused rifting of Africa and South America at ~135-115 Ma, and (4) continental break-up between Southern Africa and South America with concomitant magmatism at ~95-80 Ma, which heralded major plate reorganisation (Jelsma *et al*., 2009).

A close temporal association is also apparent between Large Igneous Province magmatism (the Karoo-Ferrar Province at ~180 Ma, the Parana-Etendeka Province at ~135 Ma and perhaps the Reunion Province

at ~85 Ma) and the coinciding and subsequent main pulses of kimberlite magmatism (~180-145 Ma, ~135-115 Ma, ~95-80 Ma) (Jelsma *et al*., 2004, 2009).

The thermal perturbations beneath the southern African continental lithosphere responsible for thermal expansion, uplift, erosion, fracturing and LIP magmatism during the break-up of Gondwana since the Early Jurassic at ~205 Ma was proposed by Sears (2001) to have been caused by a stalling in plate motion of Gondwana, which resulted in thermal insulation of the underlying mantle beneath the stagnant or sluggish supercontinent, thereby driving its own break-up. Alternatively, Bristow & Hatton (1992), Antoine & Moyes (1992), Storey (1995), Storey & Kyle (1997) and White (1997) argued for active mantle upwelling to have been the cause for the thermal perturbations beneath Gondwana and its break-up.

In line with the proposal of an active mantle upwelling process, Friese (1998b, 2004a, 2007a) argued for the presence of the African Superplume beneath the southern African continent since at least the Early Jurassic at ~205 Ma to have been responsible for thermal expansion, uplift, erosion, extensional reactivation of translithospheric Archaean suture zones and pre-Jurassic crustal fault zones, new formation of translithospheric and crustal extensional-transtensional fault and fracture systems, LIP and kimberlite magmatism, and the break-up of the Gondwana supercontinent (see Section 6.4.5.5 for details). With regard to the distribution and orientation of Jurassic-Cretaceous kimberlite pipes and dykes within South Africa and the Kaapvaal Craton, some fundamental conclusions can be drawn:

Post-Karoo dyke intrusions of various age and composition exhibit different trends across southern Africa and there appears to exist a systematic and age-progressive change in orientation from ENE-trending Mid-Jurassic (~200-170 Ma) dolerite dykes, via E-trending Late Jurassic (~170-150 Ma) hornblende-granophyre dykes and WNW-trending Early Cretaceous (~150-120 Ma) dolerite dykes, to NW-trending Mid- to Late Cretaceous (~120-78 Ma) kimberlite dykes (see Appendix 20-Y). This time-progressive change in orientation of brittle extensional fracture zones and dykes can be explained by assuming an anti-clockwise rotation of about 45° of the African plate since the beginning of Gondwana fragmentation above the African plume, which appears to represent a stationary convection cell in the lower asthenosphere and inducing extensional stresses into the overlying lithosphere since at least the Early Jurassic at ~205 Ma (see Appendix 20-Y). All post-Karoo fracture/dyke systems formed initially as extensional fracture/dyke systems which subsequently underwent progressively more dextral strike-slip as they were rotated anti-clockwise into an oblique position to the constant NW-SE horizontal compressive stress field. All post-Karoo fracture systems are proposed to be of translithospheric nature, which formed at the base of and propagated through the lithosphere to surface, thereby being accompanied by injection and ascend of mantle-derived magmas, representing feeder dykes to the Mesozoic and Cenozoic lavas preserved in southern Africa. The majority of kimberlite pipe clusters occur at the intersection of NW/SE- and NE/SW-trending fractures belonging to the post-Karoo-recent Ceres-Prince Edward/Trans Indian Fracture Zone and Cape-Tzaneen Fracture Zone, respectively. Some kimberlite pipe clusters occur at the intersection of these Phanerozoic fractures zones with major Archaean terrane boundaries/sutures or Archaean crustal fault systems within the Kaapvaal Craton (see Appendix 20-Y).

In summary, it is proposed in this study that active mantle upwelling within the African Superplume caused uplift and the induction of NW-SE oriented, horizontal compressive far field stress into the continental lithosphere of southern Africa by basal drag at least since the Jurassic at ~205 Ma, which led to the development of the NW/SE-striking, translithospheric Ceres-Prince Edward/Trans Indian fracture zone system at the onset of continental break-up. Subsequent spreading and ocean floor development is marked by apparent variation in direction and velocity in the relative plate motion paths of the African versus

Eurasian plate and African versus Antarctica plate. Stress induced into the southern African continent by ridge push resulted in the formation of translithospheric, NE/SW-striking, dextral transtensional continental continuation of oceanic transform fault corridors (*e.g.*, Cape-Tzaneen fracture zone) propagating into the supercontinent, and the extensional-transtensional reactivation of translithospheric Archaean suture zones and pre-Jurassic crustal fault systems with episodic uplift and erosion and focused kimberlite melt migration. The association of kimberlite occurrences with the translithospheric discontinuities indicates kimberlite melt production through upper mantle decompressional melting and melt migration and emplacement into crustal levels along these high strain zones. A progressive age variation of kimberlite magmatism in southern Africa may be attributed to stress propagation along the translithospheric discontinuities.

4.7 NEOTECTONIC EVOLUTION (~35-0 MA)

Neotectonics, the study of young typically Neogene and Quaternary deformation, has been a long neglected discipline on its own and has its roots in seminal geomorphologic investigations (*e.g.* Du Toit, 1933; King, 1963; Partridge & Maud, 1987). In recent years, however, the distribution of in situ stress, seismicity and neotectonic activity across the subcontinent has attracted increasing attention and intense research (*e.g.* McCarthy *et al.*, 1993; Andreoli *et al.*, 1996; Brandt, 1998; Stacey & Wesseloo, 1998; Partridge & Maud, 2000; De Kock, 2000; Spönemann & Hagedorn, 2000; and references therein) especially as a result of major hydroelectric, nuclear engineering and mining projects. Such investigations have begun to identify a pattern of neotectonic history that was much more extensive than was ever imagined possible within a "stable" cratonic environment. Furthermore, a multidisciplinary set of data has emerged which allows today to develop and better constrain geodynamic models for the geologic evolution of the African subcontinent over its recent past, thus providing a framework for long-term seismic risk assessment in southern Africa.

The break-up of Gondwana since the Early-Jurassic (~205 Ma) is generally accepted as the last major tectonic episode to have effected southern Africa. Because of the continuation of the Gondwana fragmentation process during the Cretaceous and Cenozoic until present time, the beginning of the neotectonic period in South Africa has never been formally established (*cf.* Becker, 1993). In the past, the term neotectonics has been used to imply a generic Cenozoic (especially Quaternary) crustal deformation (*cf.* Hartnady, 1985; Andreoli *et al.*, 1990; Ransome & De Wit, 1992) and Andreoli *et al.* (1996) proposed neotectonic activity in South Africa to have been initiated in the Miocene (~25 Ma). Nowadays, the beginning of neotectonic activity in southern Africa is envisaged to have started with the beginning of the Oligocene at ~35 Ma which coincides with the African continent to have become stationary over the so-called African Superplume (*cf.* Burke, 1996).

The behaviour of the African Plate has changed during the Oligocene at ~35-30 Ma and many, if not all of the phenomena that have characterised Africa over the past ~35-30 Ma have been induced by the cessation of plate motion (*i.e.* a reduction to below a velocity of ~10 mm/year). Significant erosional and depositional changes on the African Plate over the past ~35-30 Ma have been dominated by responses to changes in topography induced by the action of underlying plumes (Burke, 1996). Burke's (1996) proposal is based on the idea that if a plate is not moving over a plume or plume population, then the plume (population) has time to interact with the overlying plate. If the plate is moving, then interaction is limited because the plate moves

away from the site of interaction too fast for the consequences, whether they be thermal, magmatic, or topographic, to develop.

Two possible causes or "triggers' for the change in the behaviour of the African Plate have been proposed by Burke (1996). Either intensified collision of the African Plate with the Eurasian Plate at ~35-30 Ma, or the impingement of the Afar plume alone or together with other coeval plumes on the base of the lithosphere, which was associated with the entrainment of a large mass of fertile or potential magma source material from a large neighbouring volume of the upper mantle and causing an increase of the viscosity of the asthenosphere beneath an extensive region of the African Plate, sufficed to arrest the motion of the African Plate with respect to the underlying mantle circulation. It is also possible that both processes of collision with Eurasia and plume impingement could have happened at the same time and acted together.

In recent years, intense research regarding neotectonic activity in Southern Africa has revealed, that there is a striking match between the tectonic fabric of the southeast Atlantic and southwest Indian Ocean and the tectonic fabric of the African subcontinent (*e.g.* Andreoli *et al.*, 1989, 1990, 1993, 1994, 1995, 1996).

It is evident that a number of major oceanic transform faults or fracture zones, *e.g.* the Cape/False Bay, Falkland-Agulhas, Trans-Indian/Ceres-Prince Edward and Mozambique-Madagascar fracture zones, continue into on-shelf and on-shore joints/faults of the South African continent (Figs. 6.38 & 6.39b).

In addition, neotectonic activity in Southern Africa has been analysed in terms of known stress fields and it is clear today, that the African plate south of the equator appears divided in two zones of compressive stress orientation: one zone of predominant NNE-directed trends which corresponds to the East African Rift system, and a second zone in southern and southwestern Africa, but including the southwest Indian Ocean, characterized by NW-WNW trends (Zoback *et al.*, 1989, Zoback, 1992; Andreoli *et al.*, 1996) (Fig. 6.39a).

In South Africa, the boundary between these two zones coincides with the apparent southern termination of the Rift System in southern Mozambique, near Richards Bay, and in the Northern Transvaal. Most of South Africa, Namibia and the ocean floor between the Bredasdorp Basin and the Southwest Indian ridge is dominated by this pervasive, NW-WNW-trending, horizontal compressive stress field of deep-seated, undetermined origin for which the term Wegener Stress Anomaly (WSA) was proposed (Andreoli *et al.*, 1996). The WSA appears to have existed already in the Jurassic, before the break-up of Gondwana, which is indicated by the orientation of major Jurassic dyke swarms in South America, South Africa and in Botswana, and persisted during the south Atlantic break-up phase in the Cretaceous (indicated by WNW-trending Cretaceous kimberlite dykes in Lesotho) until today. Offshore fault zones caused by the WSA include the WNW-trending, so-called Ceres-Prince Edward and Trans Indian Fractures Zones in the southwest Indian Ocean (Figs. 2.4a & b).

Short periods of waning during the Late Cretaceous caused the stress field to be dominated by NE-directed ridge push, which led to strike-slip along the Falkland-Agulhas Fracture Zone and the formation of the Cape-Tzaneen Fracture Zone, the on-shore continuation within the South African continent of the False Bay Fracture Zone (Andreoli *et al.*, 1996) (Figs. 2.4a & b).

Pavoni's (1997) proposed model of bicellular, whole-mantle convection and associated global geotectonic and geophysical bipolarity explains both, the orientation and the deep-seated, until now undetermined origin of the WSA. According to this model, two torus-like convection cells, the Pacific cell and the African cell, with ascending flow in the mantle underneath the central Pacific and African plates respectively, and converging and descending flow beneath Indonesia and Central America, are responsible for the formation of two large-

scale zones of both, lithospheric divergence (marked by growth of the Pacific and African plates from two spreading centres) and convergence (marked by the belt of young folded mountains) since the Mid-Jurassic (see Section 2.1).

It is proposed that upwelling hotter than average and buoyant mantle material, after impinging at the base of the lithosphere of the African Plate, exercises basal drag in a southeasterly to east-southeasterly direction, thereby inducing horizontal compressive stress into the entire lithosphere. In addition, the lithosphere above the African plume experienced uplift, extension and magmatism. The elevated topography has developed over time, with much of the uplift estimated by most studies to have occurred since the breakup of Gondwana with a significant amount occurring during the Cenozoic (see Section 6.4.2.7). A range of observations show that Africa experienced and is currently still experiencing active interplate rifting and volcanism for at least the past~200 Ma (Burke, 1996). The eruption of the Jwaneng kimberlite cluster at ~245 Ma might be the earliest evidence for the effects of the African Superplume

The effects of large-scale mantle convection beneath the African plate is nowadays believed to be responsible for the tectono-magmatic and geomorphological development of southern Africa since the beginning of the break-up and dispersal process of the Gondwana supercontinent at ~205 Ma, which continues until present time and is responsible for neoseismicity and neotectonic activity, controlling the neomorphological development of the southern African landscape. The current in situ stress field present in southern Africa is of composite nature and comprises both NW-SE and NE-SW compressive stress orientations, which are the result of a complex interplay between mantle convection and lithospheric basal drag, thermally induced continental uplift and ridge-push forces.

APPENDIX 20

PALAEOGEOGRAPHIC RECONSTRUCTION MAPS DEPICTING THE GEODYNAMIC EVOLUTION OF THE SOUTHERN AFRICAN LITHOSPHERE FROM THE NEOARCHAEAN TO PRESENT (~3.1-0 Ga)

APPENDIX 20-A : Geodynamic evolution of southern Africa during the period ~3.1-3.0 Ga.

APPENDIX 20-B : Geodynamic evolution of southern Africa during the period ~3.0-2.97 Ga.

APPENDIX 20-C : Geodynamic evolution of southern Africa during the period ~2.97-2.87 Ga.

APPENDIX 20-D : Geodynamic evolution of southern Africa during the period ~2.87-2.81 Ga.

APPENDIX 20-E1: Geodynamic evolution of the Kaapvaal Craton during the period ~2.81-2.75 Ga.

APPENDIX 20-E2: Conceptual model for escape tectonics in the area of the Gaborone Granite Complex.

APPENDIX 20-F : Limpopo Orogenic Cycle-related magmatism within the Kaapvaal Craton during the period ~2.786-2.64 Ga.

APPENDIX 20-G : Geodynamic evolution of southern Africa during the period ~2.75-2.64 Ga.

APPENDIX 20-H : Geodynamic evolution of southern Africa during the period ~2.64-2.585 Ga.

APPENDIX 20-I : Geodynamic evolution of southern Africa during the period ~2.585-2.43 Ga.

APPENDIX 20-J : Geodynamic evolution of southern Africa during the period ~2.43-2.35 Ga.

APPENDIX 20-K : Geodynamic evolution of southern Africa during the period ~2.35-2.22 Ga.

APPENDIX 20-L : Geodynamic evolution of southern Africa during the period ~2.22-2.1 Ga.

APPENDIX 20-M1: Geodynamic evolution of southern Africa during the period ~2.1-2.05 Ga.

APPENDIX 20-M2: Tectono-structural setting of the Bushveld Complex.

APPENDIX 20-N : Geodynamic evolution of southern Africa during the period ~2.05-1.93 Ga.

APPENDIX 20-O : Ubendian (~2.1-1.86 Ga) and Kheis (~1.83-1.73 Ga) Orogenic Cycle-related magmatism within the Kaapvaal Craton.

APPENDIX 20-P : Geodynamic evolution of southern Africa during the period ~1.93-1.83 Ga.

APPENDIX 20-Q : Geodynamic evolution of southern Africa during the period ~1.83-1.73 Ga.

APPENDIX 20-R : Geodynamic evolution of southern Africa during the period ~1.73-1.4 Ga.

APPENDIX 20-S : Kibaran (~1.4-1.25 Ga) and Lomanian (~1.2-1.0 Ga) Orogenic Cycle-related magmatism within the Kaapvaal Craton.

APPENDIX 20-T : Geodynamic evolution of the proto-Kaapvaal Craton during the period ~1.4-1.25 Ga.

APPENDIX 20-U : Geodynamic evolution of the Kalahari Craton during period ~1.2-1.0 Ga.

APPENDIX 20-V : Geodynamic evolution of the Kalahari Craton during the period ~900-650 Ma.

APPENDIX 20-W : Geodynamic evolution of supercontinent Gondwana during the period~650-450 Ma.

APPENDIX 20-X : Geodynamic evolution of supercontinent Gondwana during the period ~290 - 215 Ma.

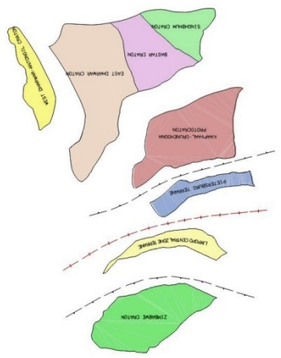
APPENDIX 20-Y : Geodynamic evolution of southern Africa during the period ~200-80 Ma.

APPENDIX 20-Z : Geodynamic evolution of southern Africa during the period ~190-120 Ma.

APPENDIX 20-A

GEODYNAMIC EVOLUTION OF SOUTHERN AFRICA
DURING THE PERIOD ~3.1–3.0 GA

0 50 100 150 200
KILOMETRES



LEGEND

- PROTEROZOIC - INTRACRATONIC MAGMATIC-ARC (MAFIC TO FELSIC) AND / OR (HYPER)ALKALIC DEPOSITS (LATE 2.1 TO 0.6 GA) BASEMENT
- ARCHEAN CRATON
  - LOWER GRANODIORITE - TONALITE (~ LOWER BULAWAYAN EQUIVALENTS)
  - GREENSTONES 3.1–2.9 GA)
- PETROGRAPHIC TERRANE
- MAFIC & ULTRAMAFIC GREENSTONE BELTS (~3.1–2.96 GA)
- MAFIC-SUN CRITICAL BELT (~3.07–2.9 GA)
- DUTOIT / POSSOLT SUPRACRUST DISTRIBUTION OF DEEP-SEA GROUP (~2.96–2.871 GA)
- PROTEROZOIC - INTRACRATONIC MAGMATIC-ARC (MAFIC TO FELSIC) WITHIN NORTHERN PROTO-KAAPVAAL CRATON (~2.06–2.015 GA)
- S-TYPE GRANITES (E.G. SUKENI GRANITE, ~2.871 GA)
- AREA OF INTRACRATONIC MAGMATIC-ARC AND BACK-ARC BASIN DEVELOPMENT
- AREA OF OLDEST MAGMATIC ISLAND-ARC AND BACK-ARC BASIN DEVELOPMENT
- PROPOSED PALAEO-SUBDUCTION ZONE (TEETH ON SUBDUCTED OCEANIC SLAB)
- PROPOSED ACCRETIONARY OROGENIC CONTACT
- OBLIQUE - / STRIKE-SLIP FAULT
- CRUSTAL SUTURE ZONE / TERRANE BOUNDARY
- MAJOR MANTLE CONVECTIVE FAR FIELD STRESS ORIENTATION (E.)

APPENDIX 20-B

GEODYNAMIC EVOLUTION OF SOUTHERN AFRICA DURING THE PERIOD ~3.0 – 2.97 GA

0 100 200 300 400 500 KILOMETRES

LEGEND

PREDOMINANTLY INTRACRATONIC MAGMATIC-ARC (BANDITOS ARC/OR HYDROTHERMALLY OVERPRINTED OLDER ~2.67 GA) BASEMENT

- LOWER GREENSTONES (~3.1–2.87 GA)
- LOWER BULAWAYAN (GREENSTONES)

ZIMBABWE CRATON

- OUTCROP/POSSIBLE SUBSURFACE DISTRIBUTION OF DOMAIN ON GAOUP
- OUTCROP DISTRIBUTION OF NSUZE GROUP

KAAPVAAL–ZIMBABWEAN PROTO-CRATON

- BADPLAAS–BARBERTON DYKE SWARM
- YOUNGER IRON ORE GROUP (BONAU GROUP) (~3.0–2.55 GA)

SINOMBANE CRATON

- ARKOSAAL CANOPYMINE, MURRIBWAU GNAIS TE & EQUIVALENTS
- SUKWA GROUP (~3.1–2.95 GA)
- GNAIS TES

BASTIAN CRATON

- GNAIS TES (OLDER SUITE)
- GNAIS TES (YOUNGER SUITE)

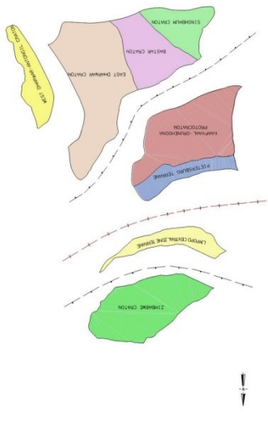
EAST DAMARAN CRATON

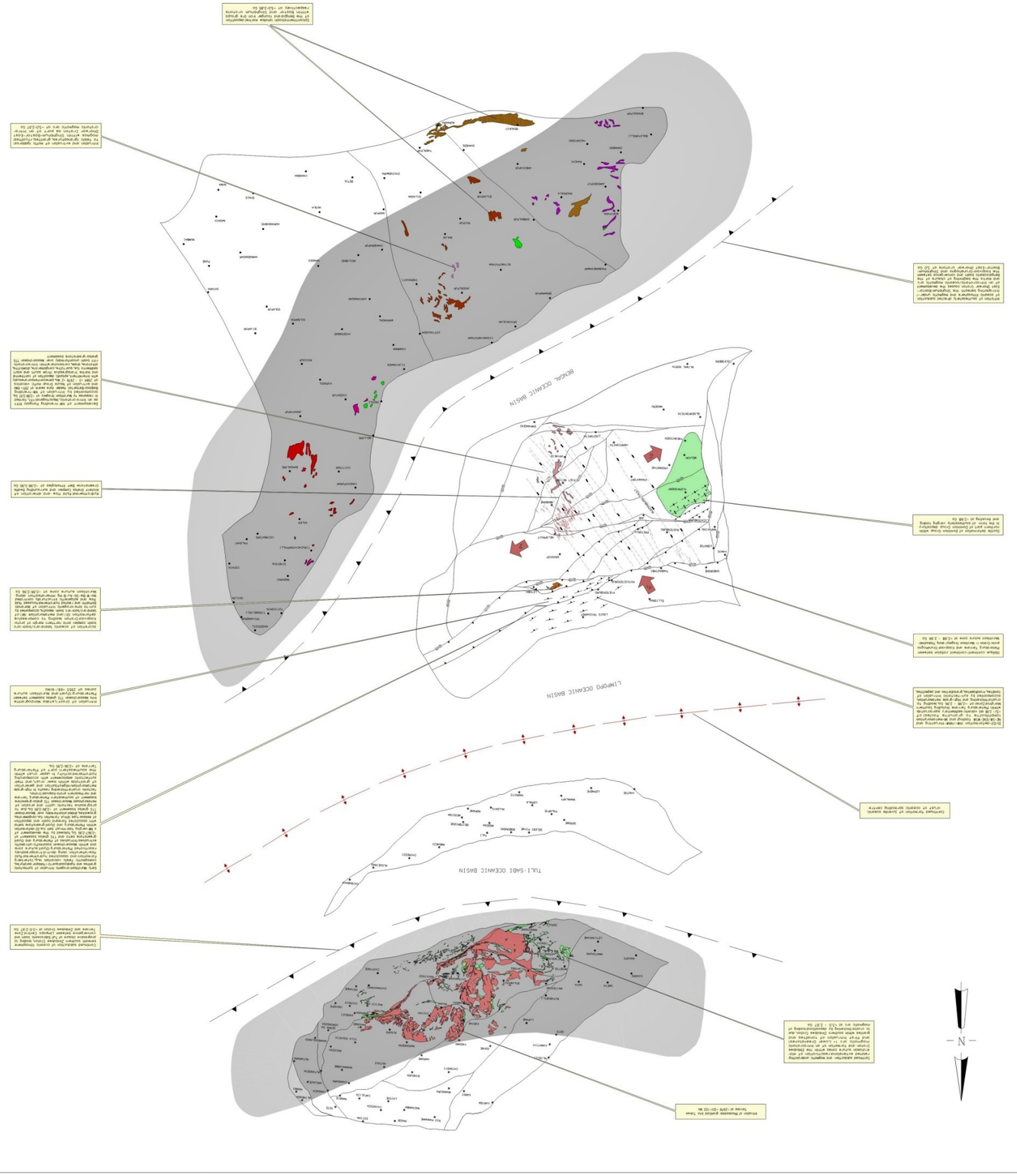
- CARBONATES AND AMPHIBOLITES

SINOMBANE, BASTIAN AND EAST DAMARAN CRATON

- AREA OF INTRACRATONIC MAGMATIC-ARC AND BACK-ARC BASIN DEVELOPMENT
- AREA OF OCEANIC MAGMATIC ISLAND-ARC AND BACK-ARC BASIN DEVELOPMENT

- PROPOSED SUBDUCTED CRUSTAL SLAB (TEETH ON SUBDUCTED CRUSTAL SLAB)
- PROPOSED FAILED-SUBDUCTION ZONE
- PROPOSED OCEANIC FAILED-SPREADING CENTRE
- THRUST FAULT
- BEDDING-PARALLEL THRUST FAULT
- OBLIQUE REVERSE-SLIP FAULT
- STRIKE-SLIP FAULT
- NORMAL FAULT
- SYNCLINE
- ANTICLINE
- CRUSTAL SUTURE ZONE / TERRANE BOUNDARY
- MAJOR HORIZONTAL COMPRESSIVE FAR FIELD STRESS ORIENTATION (σ_1)
- MAJOR HORIZONTAL EXTENSIONAL FAR FIELD STRESS ORIENTATION (σ_1)



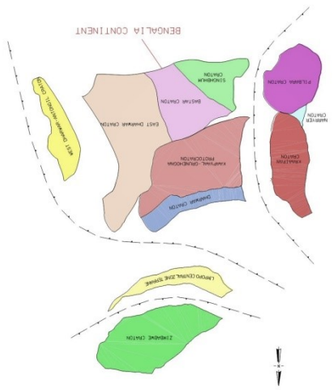


GEODYNAMIC EVOLUTION OF SOUTHERN AFRICA DURING THE PERIOD ~2.97 - 2.87 GA

APPENDIX 20-C

0 100 200 300 400
KILOMETRES

BENGALIA CONTINENT



LEGEND

PRE-ORDOVICIAN - INTRACRATONIC MAGMATIC-ARC
- DEFORMED GRANITOIDS AND GNEISSES (~2.97 GA) BASEMENT
- (= LOWER BULAWAYAN) GREENSTONES (~2.87 GA)

ZIMBABWE CRATON
- LOWER GREENSTONES (~2.7-2.87 GA)
- WEST RAND GROUP & JOHANNESBURG SUBGROUP, CHUNIAN GROUP & MOLOPO FORMATION (KHOMAN AND GEMSBULT INTERMEDIATE)
- APPROXIMATE AREAL EXTENT OF MAIN NSUZE GROUP BELT-BASIN

KAAPVAAL-GRUNEHOGNA PROTO-CRATON

YOUNGER IRON ORE GROUP (BOOMI GROUP) (~2.8-2.95 GA)

SINGHBHUM CRATON

BENGPAL GROUP (~2.95-2.75 GA)

BASTAR CRATON

BARBERTON GROUP (~2.95-2.85 GA)

WEST DHARWAR-ANTONDIL CRATON
- MAFIC INTRUSIONS (I.E. GABBROS)

GRANOPHYRE / PORPHYRY / GRANITIC INTRUSIONS

MAFIC-ULTRAMAFIC INTRUSIONS / EXTRUSIONS

PILBARA CRATON

SHALKEPUT GRANITE

LOCATION OF SUPERACE BOREHOLE TA2

KHAAIFAN CRATON

LOCATION OF BLATTANTIN DIAMOND MINE

AREA OF INTRACRATONIC MAGMATIC-ARC AND BACK-ARC BASIN DEVELOPMENT

AREA OF OCEANIC MAGMATIC (ISLAND-ARC AND BACK-ARC BASIN DEVELOPMENT

PROPOSED PALAEO-SUBDUCTION ZONE (TEETH ON SUBDUCTED CRUSTAL SLAB)

THRUST FAULT

OBLIQUE REVERSE-SLIP FAULT

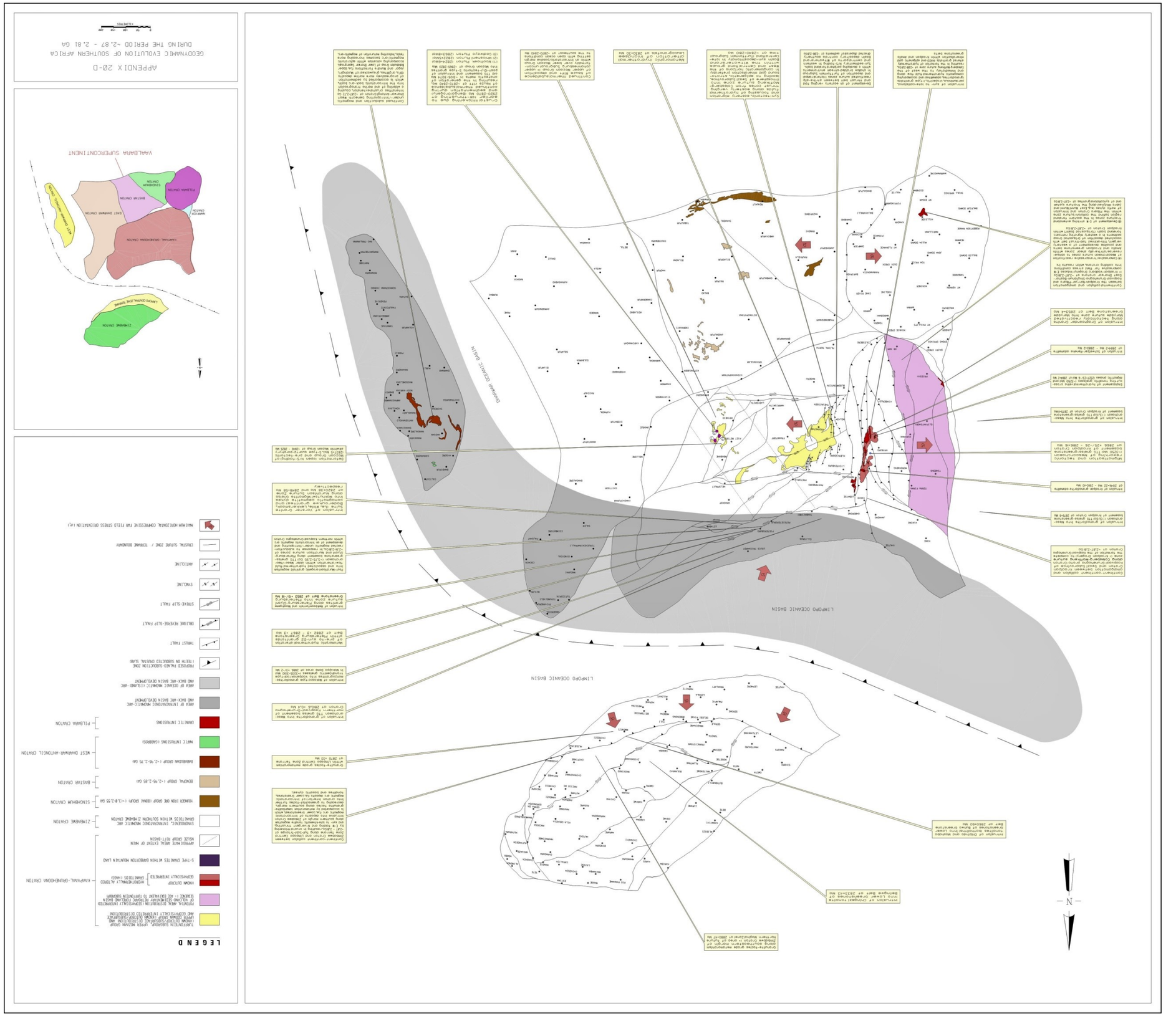
STRIKE-SLIP FAULT

SYNCLINE

ANTICLINE

CRUSTAL SUTURE ZONE / TERRANE BOUNDARY

MAXIMUM HORIZONTAL COMPRESSIVE FAR FIELD STRESS ORIENTATION (σ1)



APPENDIX 20-D

GEODYNAMIC EVOLUTION OF SOUTHERN AFRICA DURING THE PERIOD ~2.87 - 2.81 GA

0 100 200 300 400
KILOMETERS

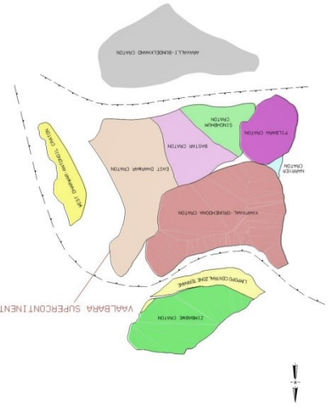
LEGEND

- TUFF/PYRITE SUBGROUP, UPPER MAZAWA GROUP AND OLDTSPRUIT FORMATION, LOWER TRANSVAAL SUPERGROUP
- EXTENSIONAL ANGULAR UNCONFORMITY BETWEEN UPPER TRANSVAAL SUPERGROUP AND OLDER CRATONIC BASIN
- PITSTRUCTURAL ANGULAR UNCONFORMITY BETWEEN UPPER TRANSVAAL SUPERGROUP AND OLDER CRATONIC BASIN
- KAAPVAAL-ZIMBABWE CRATON
- KOMATIITE/BASALT, LOWER MAZAWA GROUP
- KOMATIITE/BASALT, UPPER MAZAWA GROUP
- S-TYPE GRANITES WITHIN AMBERTON MOUNTAIN LAND
- APPROXIMATE ANGULAR EXTENT OF MAJOR SCOUT GROUP (UPPER) UNCONFORMITY
- ANTICLINE
- SYNCLINE
- STRIKE-SLIP FAULT
- OBLIQUE REVERSE-SLIP FAULT
- THRUST FAULT
- TEETH ON SUBDUCTED OCEANIC SLAB
- PROTEROZOIC PLANETARY-SUBDUCTION ZONE AND BACK-ARC BASIN DEVELOPMENT
- AREA OF OCEANIC MAGMATIC ARC AND BACK-ARC BASIN DEVELOPMENT
- INTRACONTINENTAL MAGMATIC ARC
- GRANITIC INTRUSIONS
- PILBARA CRATON
- MAFIC INTRUSIONS (~2080MOS)
- BARBERTON GREENSTONE BELT (~3.55-3.23 GA)
- WEST DHARWAR GRANITOIDS (~3.3-3.0 GA)
- MAFIC INTRUSIONS (~2.79-2.75 GA)
- BASTAR CRATON
- BENGPAL GROUP (~2.95-2.85 GA)
- YOUNGER IRON ORE GROUP IRONS (GROUP (~1.3-2.55 GA)
- SINGHBHUM CRATON
- SINGHBHUM CRATON
- ZIMBABWE CRATON
- ZIMBABWE CRATON
- GWANI TIOLS W THIN SOUTHERN ZIMBABWE CRATON
- ARROWHEAD ANGULAR UNCONFORMITY BETWEEN ARCHEAN CRATON AND PROTEROZOIC SUPERGROUP
- SCOUT GROUP (UPPER) - SCOUT
- MAJOR CRATONIC UNCONFORMITY BETWEEN ARCHEAN CRATON AND PROTEROZOIC SUPERGROUP
- KAAPVAAL-ZIMBABWE CRATON
- KOMATIITE/BASALT, LOWER MAZAWA GROUP
- KOMATIITE/BASALT, UPPER MAZAWA GROUP
- S-TYPE GRANITES WITHIN AMBERTON MOUNTAIN LAND
- APPROXIMATE ANGULAR EXTENT OF MAJOR SCOUT GROUP (UPPER) UNCONFORMITY
- ANTICLINE
- SYNCLINE
- STRIKE-SLIP FAULT
- OBLIQUE REVERSE-SLIP FAULT
- THRUST FAULT
- TEETH ON SUBDUCTED OCEANIC SLAB
- PROTEROZOIC PLANETARY-SUBDUCTION ZONE AND BACK-ARC BASIN DEVELOPMENT
- AREA OF OCEANIC MAGMATIC ARC AND BACK-ARC BASIN DEVELOPMENT
- INTRACONTINENTAL MAGMATIC ARC
- GRANITIC INTRUSIONS
- PILBARA CRATON
- MAFIC INTRUSIONS (~2080MOS)
- BARBERTON GREENSTONE BELT (~3.55-3.23 GA)
- WEST DHARWAR GRANITOIDS (~3.3-3.0 GA)
- MAFIC INTRUSIONS (~2.79-2.75 GA)
- BASTAR CRATON
- BENGPAL GROUP (~2.95-2.85 GA)
- YOUNGER IRON ORE GROUP IRONS (GROUP (~1.3-2.55 GA)
- SINGHBHUM CRATON
- SINGHBHUM CRATON
- ZIMBABWE CRATON
- ZIMBABWE CRATON
- GWANI TIOLS W THIN SOUTHERN ZIMBABWE CRATON
- MAJOR MORE ZONAL COMPRESSIVE FAR FIELD STRESS ORIENTATION (~)

APPENDIX 20-E

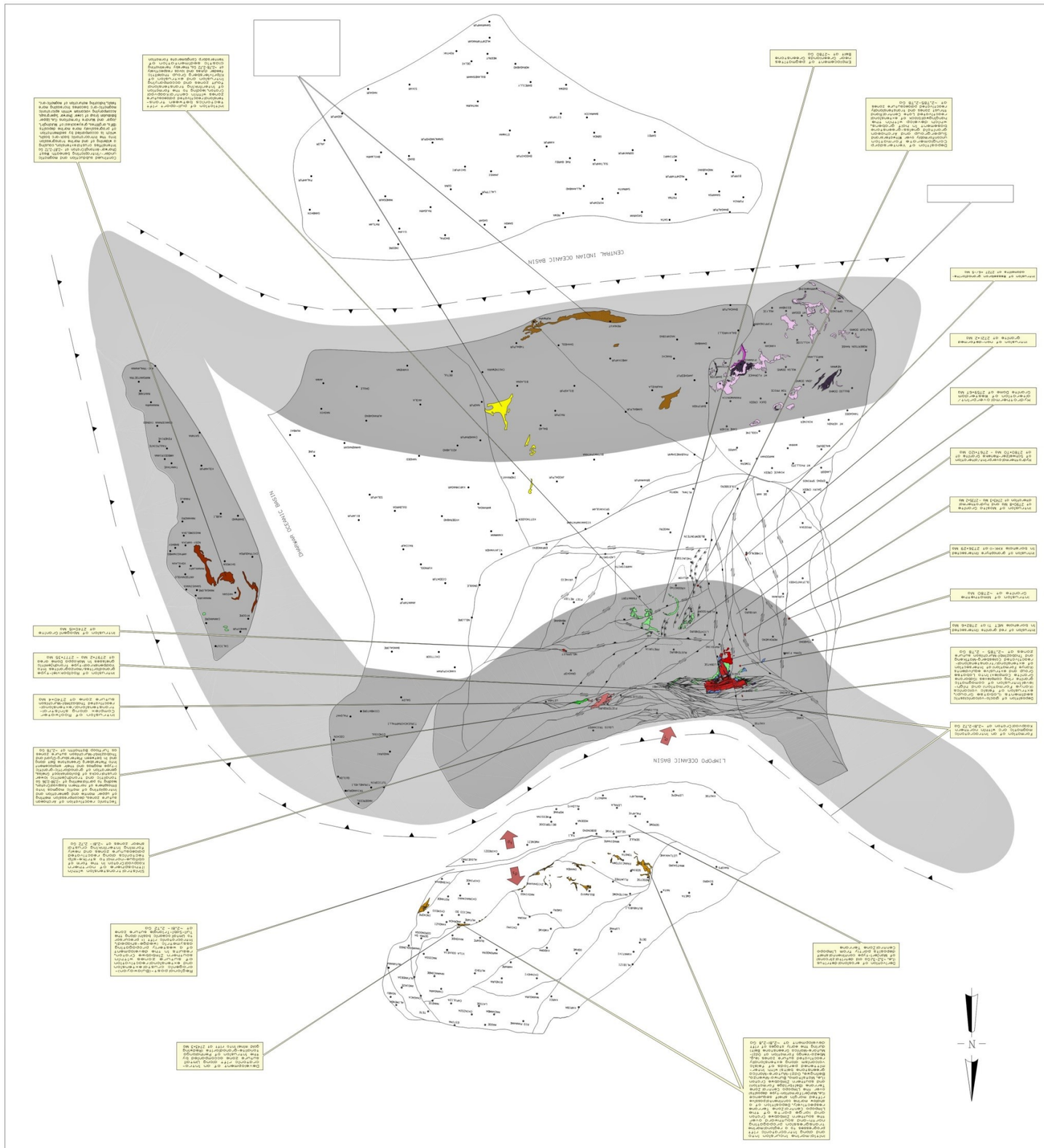
GEODYNAMIC EVOLUTION OF SOUTHERN AFRICA
DURING THE PERIOD ~2.81 - 2.72 GA

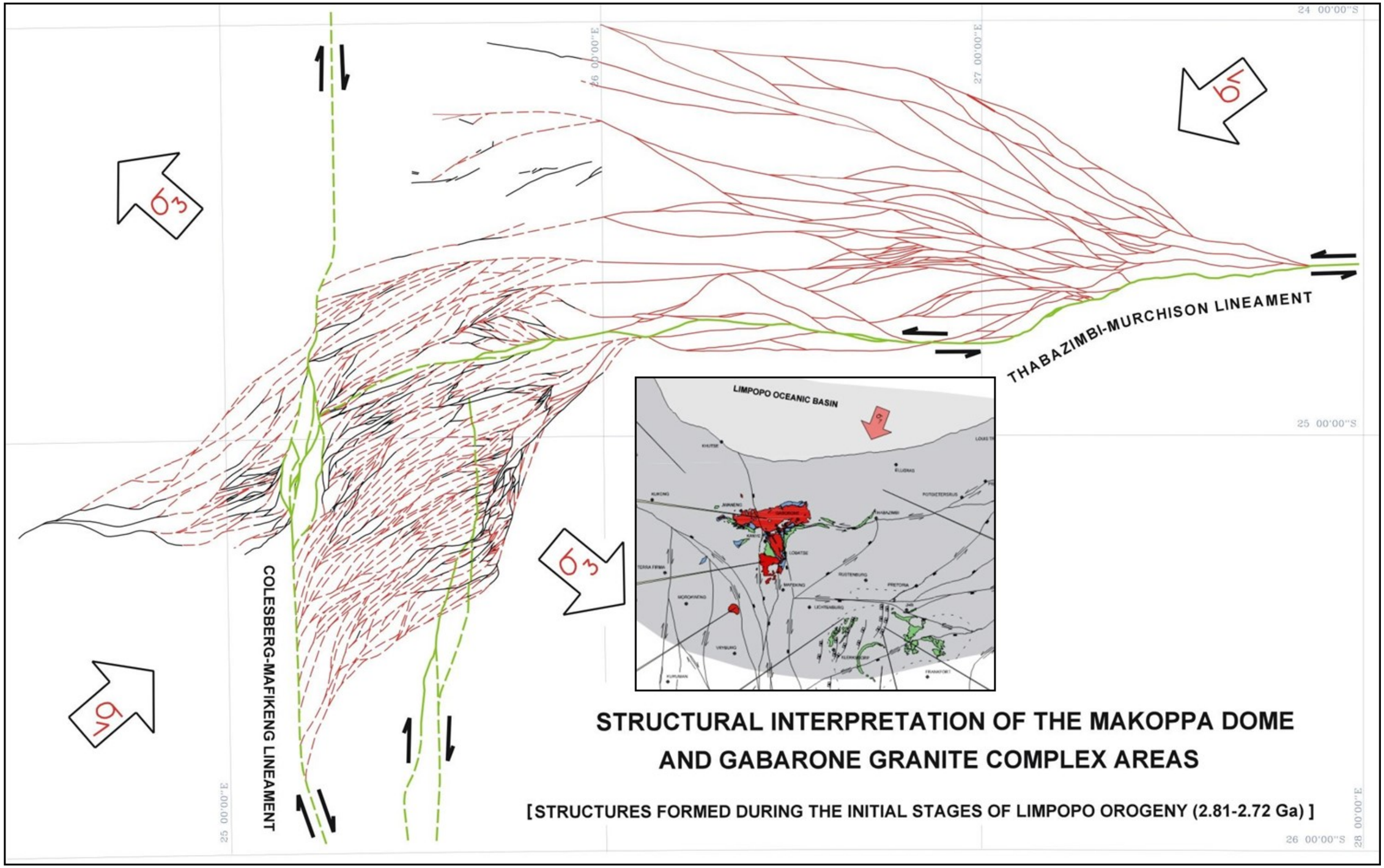
0 50 100 150 200
KILOMETERS



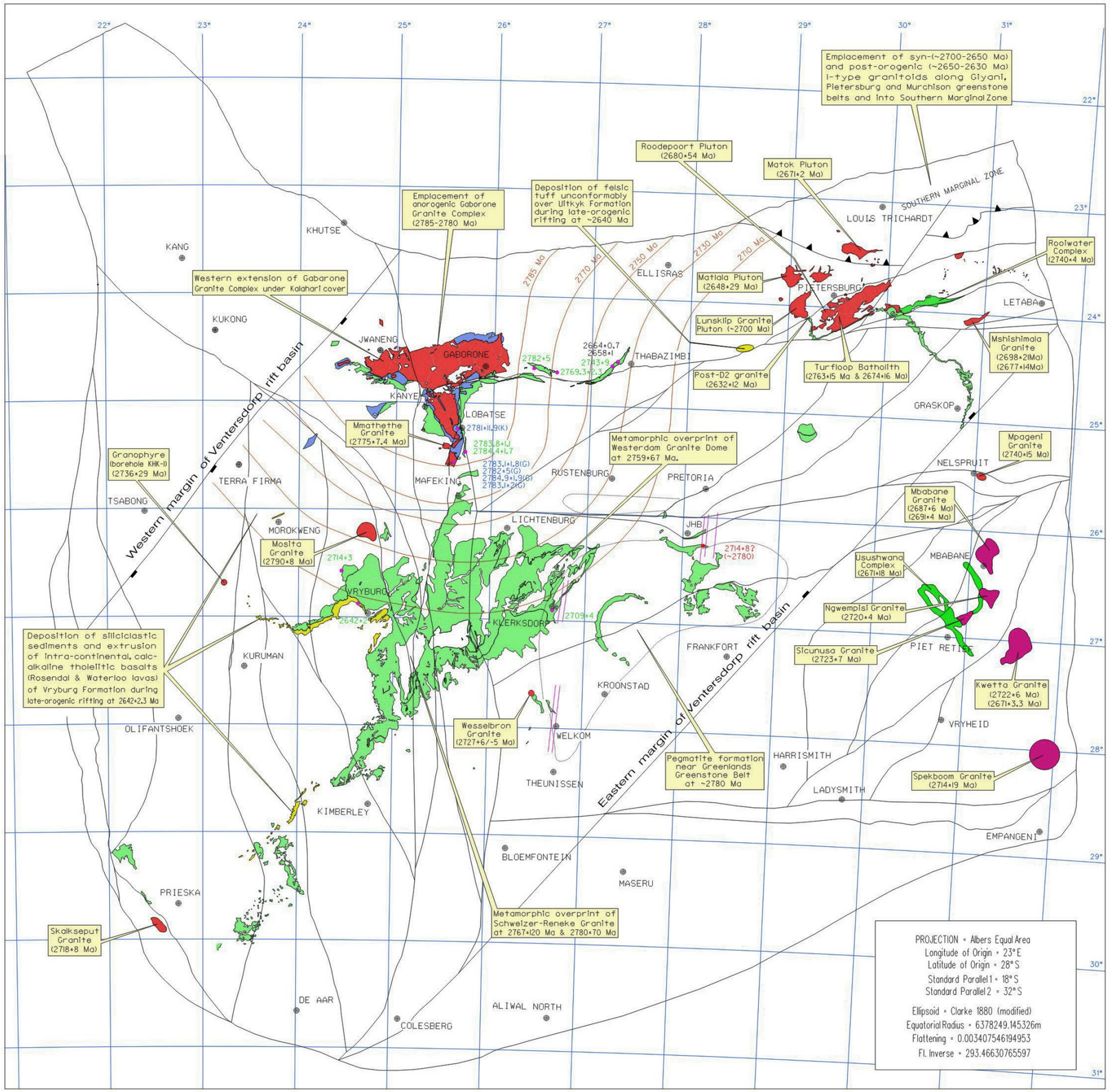
LEGEND

- OUTCROP / POSSIBLE SUBCROP DISTRIBUTION OF VENTERSDORP CONGLOMERATE FORMATION
- OUTCROP OF LOBATSE, BUFFELSFONTEIN AND KLIPRIVIERSBERG GROUPS
- KAAPVAAL CRATON
- PRE-OBSERVED INTRUSIONS
- MAGMATIC-ARC GRANITOIDS
- POSSIBLE SUBCROP DISTRIBUTION OF KLIPRIVIERSBERG GROUP
- ZIMBABWE CRATON
- (= CONTINENTAL SHELF) DEPOSITS
- WAVEDEY FORMATION-TYPE
- TOKWEE IRON BE GROUP IRONAY GROUP (~2.9-2.55 GA)
- SINOMBHUM CRATON
- BALIHOLLA GROUP (~2.85-2.7 GA)
- BASTAR CRATON
- BARABUDAN GROUP (~2.95-2.75 GA)
- MAFIC INTRUSIONS (GABBROS)
- WEST DHARWAR-ANTONOLL CRATON
- MAFIC EXTRUSIONS (BASALT) AND FELSIC CLASTIC SEDIMENTS AND FELSIC LAVAS (PORPHYRY & BLATED GRANITES)
- ULTRAMAFIC EXTRUSIONS (KOMATIITIC BASALTS)
- MAFIC-ULTRAMAFIC INTRUSIONS
- PILGARA CRATON
- LOWER PORPHYRIC GROUP (~2.775-2.72 GA)
- AREA OF INTRACRATONIC MAGMATIC-ARC AND BACK-ARC BASIN DEVELOPMENT
- AREA OF OCEANIC MAGMATIC ISLAND-ARC AND BACK-ARC BASIN DEVELOPMENT
- PROPOSED PALAEO-SUBDUCTION ZONE
- TITTH ON SUBDUCTED CRUSTAL SLAB
- INVERTED THRUST FAULT
- OBLIQUE-NORMAL (TRANSTENSIONAL) FAULT
- STRIKE-SLIP FAULT
- NORMAL FAULT
- RIFTED CONTINENTAL MARGIN
- CRUSTAL SUTURE ZONE / TERRANE BOUNDARY
- MAJOR MORE ZONAL COMPRESSIVE FAR FIELD STRESS ORIENTATION (σ1)
- MAJOR MORE ZONAL EXTENSIONAL FAR FIELD STRESS ORIENTATION (σ3)





APPENDIX 20-E2 : Conceptual model for escape tectonics in the area of the Gaborone Granite Complex. Kinematic model is used as an analogy for the development of the Witwatersrand Basin as an intracratonic tectonic escape basin during deposition of the West Rand Group and Johannesburg Subgroup at ~2.99-2.87 Ga, in response to combined sinistral and dextral strike-/oblique-slip tectonics along E-W- (*i.e.*, Magaliesburg-Barberton suture) and N-S-striking (*i.e.*, Trompsburg-Gaborone suture) Mesoarchaean suture zones, respectively (this study).



LEGEND

- OUTCROP OF VENTERSDORP SUPERGROUP AND STRATIGRAPHIC EQUIVALENTS (LOBATSE, ZOETLIEF, BUFFELSFONTEIN, WOLKBERG AND GROBLERSDAL GROUPS)
- VRYBURG FORMATION
- GRANITE COMPLEX
- KANYE FORMATION
- OUTCROP / POSSIBLE SUBCROP DISTRIBUTION OF VENTERSDORP SUPERGROUP AND STRATIGRAPHIC EQUIVALENTS
- OUTCROP / POSSIBLE SUBCROP DISTRIBUTION OF KLIPRIVIERSBERG GROUP
- LATE- TO POST-OROGENIC ILMENITE-DIABASE DYKES (±2640 MA)
- 2770 Ma — ISOCHRONE OF VENTERSDORP-AGE MAGMATISM

GEOCHRONOLOGICAL DATA (IN MA):

- PNIEL GROUP (ALLANRIDGE FORMATION), BUFFELSFONTEIN GROUP (WITFONTEINRAND FORMATION)
- PLATBERG GROUP (MAKWASSIE FORMATION), ZOETLIEF GROUP (KAREEFONTEIN FORMATION), BUFFELSFONTEIN GROUP (WATERVAL FORMATION), LOBATSE GROUP (NNYWANE FORMATION) AND VRYBURG FORMATION
- KLIPRIVIERSBERG GROUP (ALBERTON FORMATION)
- ANOROGENIC GRANITE COMPLEX (G), KANYE FORMATION (K)

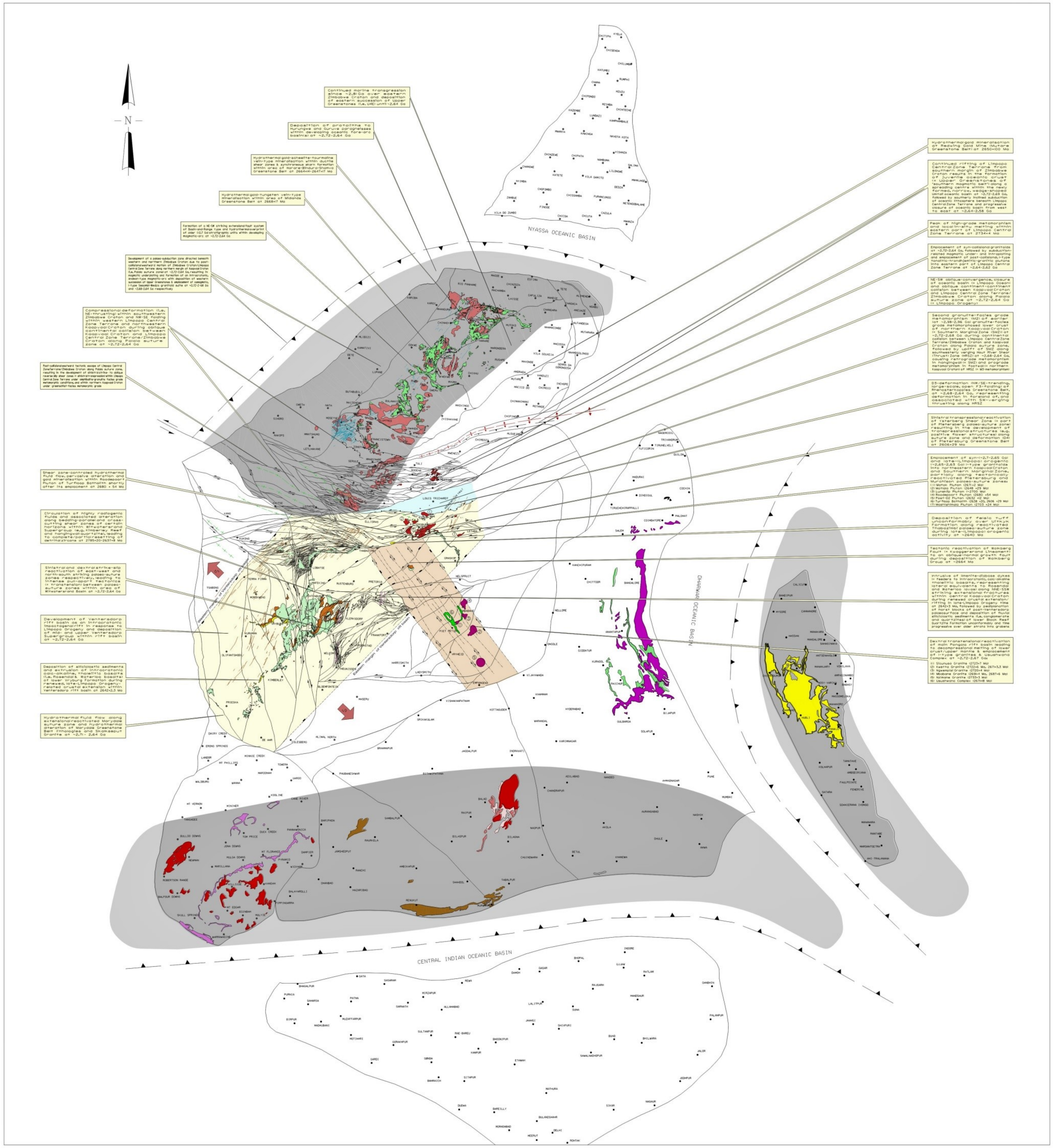
NOTE: SEE APPENDIX 21-A FOR A SUMMARY OF GEOCHRONOLOGICAL DATA

PROJECTION = Albers Equal Area
Longitude of Origin = 23°E
Latitude of Origin = 28°S
Standard Parallel 1 = 18°S
Standard Parallel 2 = 32°S
Ellipsoid = Clarke 1880 (modified)
Equatorial Radius = 6378249.145326m
Flattening = 0.003407546194953
Fl. Inverse = 293.46630765597

APPENDIX 20-F

Limpopo Orogenic Cycle-related magmatism within the Kaapvaal Craton during the period ±2.785 - 2.64 GA

0 50 100 150 200
KILOMETRES



LEGEND

Zimbabwe Craton
- UPPER GREENSTONES OF "NORTHERN MAGMATIC ARC" (~2.72-2.65 GA) (= UPPER BULAWAYAN GREENSTONES)
- PREOROGENIC (~2.68-2.65 GA), INTRACRATONIC MAGMATIC-ARC GRANITOIDS (= SESOMBI-WEDZA SUITE)
- PREOROGENIC (~2.68-2.65 GA), INTRACRATONIC MAGMATIC-ARC PORPHYRIES (= SESOMBI-WEDZA SUITE)
- CONTINENTAL INTRA-MAGMATIC ARC EXTENSIONAL FAULT SYSTEM OF BASIN-AND-RANGE TYPE

Kaapvaal Craton & Limpopo Central Zone
- SYN- AND POST-OROGENIC, I-TYPE GRANITOIDS WITHIN NORTHEASTERN KAAPVAAL CRATON AND EASTERN LIMPOPO CENTRAL ZONE TERRANE
- I-TYPE GRANITES WITHIN EXTENSIONALLY REACTIVATED ARCHAEAN (~2.97-2.95 GA) PONGOLA IMPACTOGENAL RIFT WITHIN SOUTHEASTERN KAAPVAAL CRATON

Kaapvaal-Grunehogna Craton
- OUTCROP OF MID- & UPPER VENTERSDORP SUPERGROUP & STRATIGRAPHIC EQUIVALENTS (~2.72-2.64) (I.E. PLATBERG, ZOETLIEF, PNIEL, BUFFELSFONTEIN, WOLKBERG, GROBLERSDAL GROUPS, NNYWANE, MOGOBANE & WACHTEENBEETJIE FORMATIONS, TSHWENE-TSHWENE & DERDEPOORT BELTS)
- LOWER VRYBURG FORMATION (~2.64 GA)
- APPROXIMATE AREAL EXTENT OF INTRACRATONIC, IMPACTOGENAL VENTERSDORP RIFT BASIN
- APPROXIMATE AREAL EXTENT OF MAIN PONGOLA / NSUZE GROUP RIFT-BASIN
- APPROXIMATE AREAL EXTENT OF SOUTHERN MARGINAL ZONE
- SCHEMATIC POSITION / ORIENTATION OF LATE- TO POST-(LIMPOPO) OROGENIC (~2.64 GA) ILLMENITE-DIABASE DYKES
- EXTENSIONAL FAULTS OF VENTERSDORP RIFT BASIN

Singhbhum Craton
- YOUNGER IRON ORE GROUP (BONAI GROUP) (~3.0-2.55 GA)

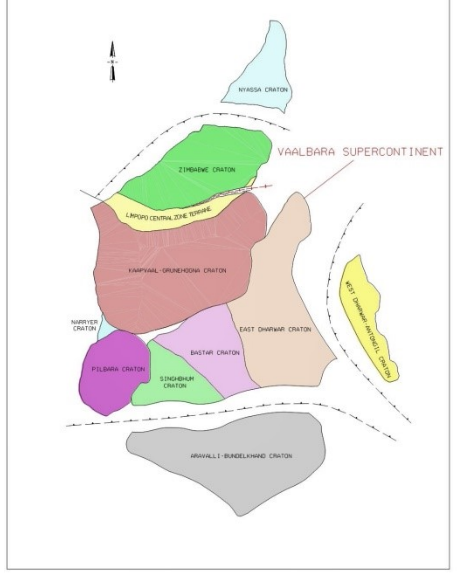
Bastar Craton
- DONGARGARH GRANITE AND OTHER GRANITES
- BIJLI RHYOLITE
- NANDAGAO GROUP (PITEPANI ANDESITE) (~2.7-2.6 GA)

East Dharwar Craton
- EASTERN GREENSTONES (~2.72-2.55 GA)
- CLOSEPET GRANITE AND RELATED GRANITES (~2.72-2.55 GA)

West Dharwar-Antongil Craton
- CHITRADURGA GROUP (~2.75-2.5 GA)

Pilbara Craton
- GRANITE INTRUSIONS (~2.7-2.65 GA)
- LOWER JEERINAH FORMATION (~2.69-2.64 GA); MADDINA BASALT, BUNJINAH, TUMBIANA & PYRADIE FORMATIONS (~2.72-2.69 GA) — UPPER FORTESCUE GROUP

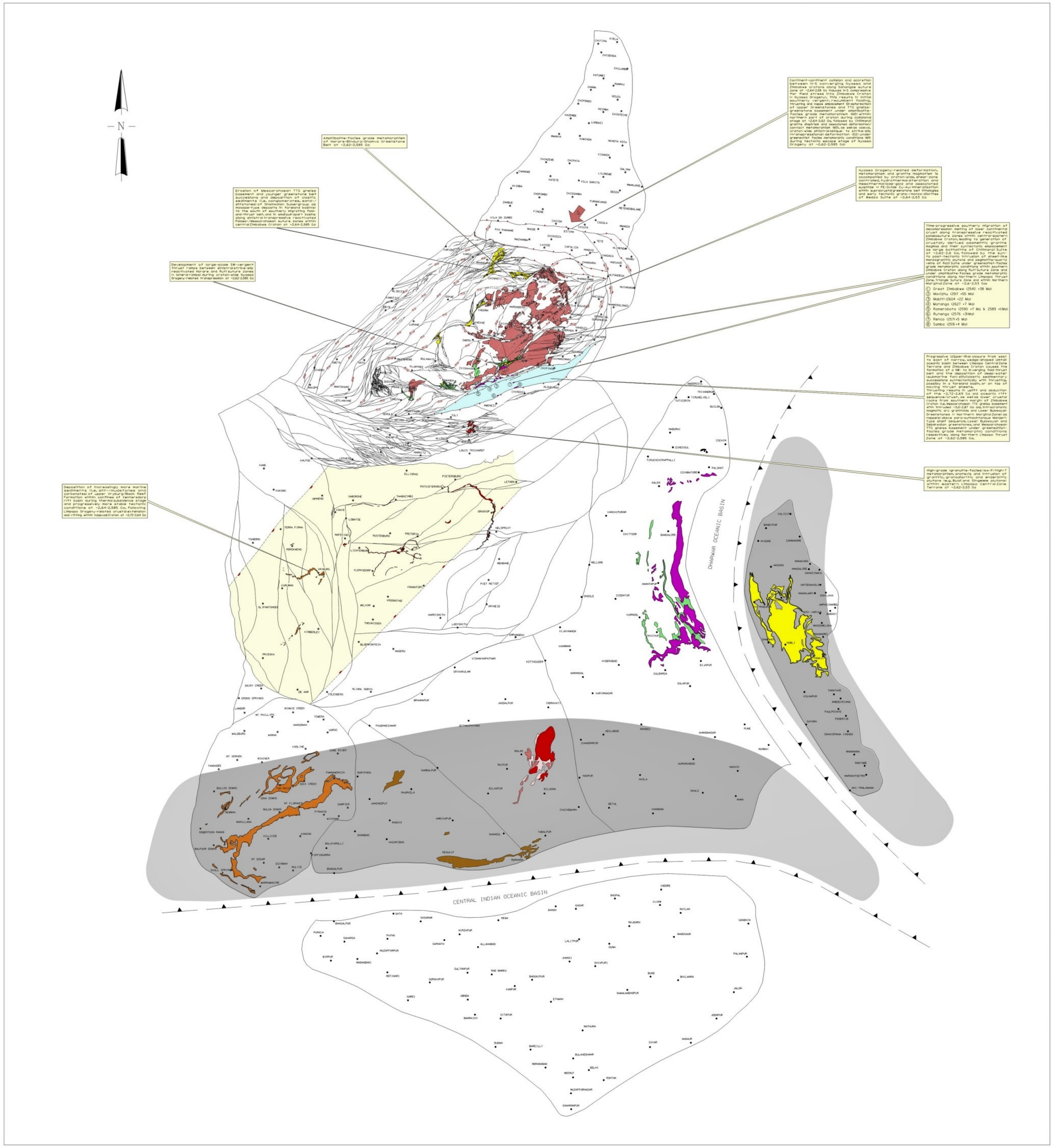
- AREA OF INTRACRATONIC MAGMATIC-ARC AND BACK-ARC BASIN DEVELOPMENT
- AREA OF OCEANIC MAGMATIC (ISLAND)-ARC AND BACK-ARC BASIN DEVELOPMENT
- PROPOSED PALAEO-SUBDUCTION ZONE (TEETH ON SUBDUCTED CRUSTAL SLAB)
- PROPOSED OCEANIC PALAEO-SPREADING CENTRE
- THRUST FAULT
- INVERTED (EXTENSIONALLY REACTIVATED) THRUST FAULT OF LATE CENTRAL RAND GROUP-AGE
- STRIKE-SLIP FAULT
- OBLIQUE-REVERSE FAULT
- OBLIQUE-NORMAL FAULT
- SYNCLINE
- ANTICLINE
- CRUSTAL SUTURE ZONE / TERRANE BOUNDARY
- MAXIMUM HORIZONTAL COMPRESSIVE FAR FIELD STRESS ORIENTATION (σ_1)
- MAXIMUM HORIZONTAL EXTENSIONAL FAR FIELD STRESS ORIENTATION (σ_3)



APPENDIX 20-G

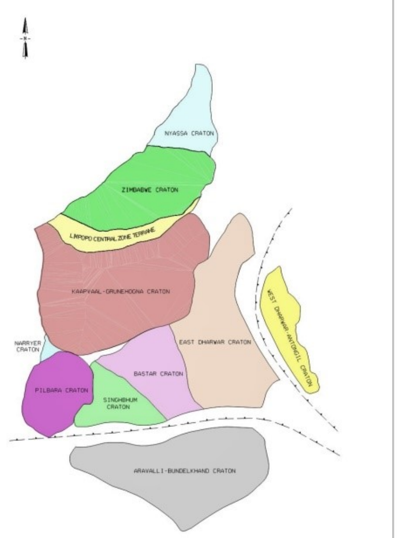
GEODYNAMIC EVOLUTION OF SOUTHERN AFRICA DURING THE PERIOD ~2.72 - 2.64 GA

0 50 100 150 200
KILOMETRES



LEGEND

UPPER GREENSTONES OF "SOUTHERN MAGMATIC ARC" (~2.72-2.69 GA) (= UPPER BULAWAYAN GREENSTONES)		ZIMBABWE CRATON
SHAMWAIAN SUPERGROUP (~2.64-2.585 GA)		ZIMBABWE CRATON
SYN-OROGENIC (~2.62-2.6 GA), ADAMELLITES-GRANITES OF CHILIMANZI SUITE		ZIMBABWE CRATON
SYN- TO POST-OROGENIC (~2.6-2.53 GA) MONZOGRANITES AND PEGMATITE/QUARTZ VEINS OF RAZI SUITE		ZIMBABWE CRATON
APPROXIMATE AREAL EXTENT OF NORTHERN MARGINAL ZONE		ZIMBABWE CRATON
BLACK REEF FORMATION (~2.64-2.585 GA)		KAAPVAAL-GRUNEHOGNA CRATON
UPPER VRYBURG FORMATION (~2.64-2.585 GA)		KAAPVAAL-GRUNEHOGNA CRATON
APPROXIMATE AREAL EXTENT OF INTRACRATONIC, IMPACTOGENAL VENTERSDORP RIFT BASIN		KAAPVAAL-GRUNEHOGNA CRATON
YOUNGER IRON ORE GROUP (BONAI GROUP) (~3.0-2.55 GA)		SINGHBHUM CRATON
DONGARGARH GRANITE AND OTHER GRANITES		BASTAR CRATON
BIJLI RHYOLITE		BASTAR CRATON
NANDAGAO GROUP (PITEPANI ANDESITE) (~2.7-2.6 GA)		BASTAR CRATON
EASTERN GREENSTONES (~2.72-2.55 GA)		EAST DHARWAR CRATON
CLOSEPET GRANITE AND RELATED GRANITES (~2.72-2.55 GA)		EAST DHARWAR CRATON
CHITRADURGA GROUP (~2.75-2.5 GA)		WEST DHARWAR-ANTONGIL CRATON
UPPER JEERINAH FORMATION (~2.64-2.62 GA)	UPPER FORTESCUE GROUP	PILBARA CRATON
AREA OF INTRACRATONIC MAGMATIC-ARC AND BACK-ARC BASIN DEVELOPMENT		
AREA OF OCEANIC MAGMATIC (ISLAND)-ARC AND BACK-ARC BASIN DEVELOPMENT		
PROPOSED PALAEO-SUBDUCTION ZONE (TEETH ON SUBDUCTED CRUSTAL SLAB)		
THRUST FAULT		
STRIKE-SLIP FAULT		
OBLIQUE-REVERSE FAULT		
OBLIQUE-NORMAL FAULT		
CRUSTAL SUTURE ZONE / TERRANE BOUNDARY		
MAXIMUM HORIZONTAL COMPRESSIVE FAR FIELD STRESS ORIENTATION (σ_1)		
MAXIMUM HORIZONTAL EXTENSIONAL FAR FIELD STRESS ORIENTATION (σ_3)		



APPENDIX 20-H

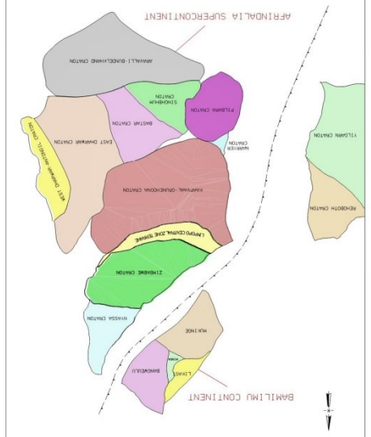
GEODYNAMIC EVOLUTION OF SOUTHERN AFRICA
DURING THE PERIOD ~2.64 - 2.585 GA

0 50 100 150 200
KILOMETRES

APPENDIX 20-I

GEODYNAMIC EVOLUTION OF SOUTHERN AFRICA
DURING THE PERIOD ~2,585 - 2,47 GA

0 50 100 150 200
KILOMETERS



LEGEND

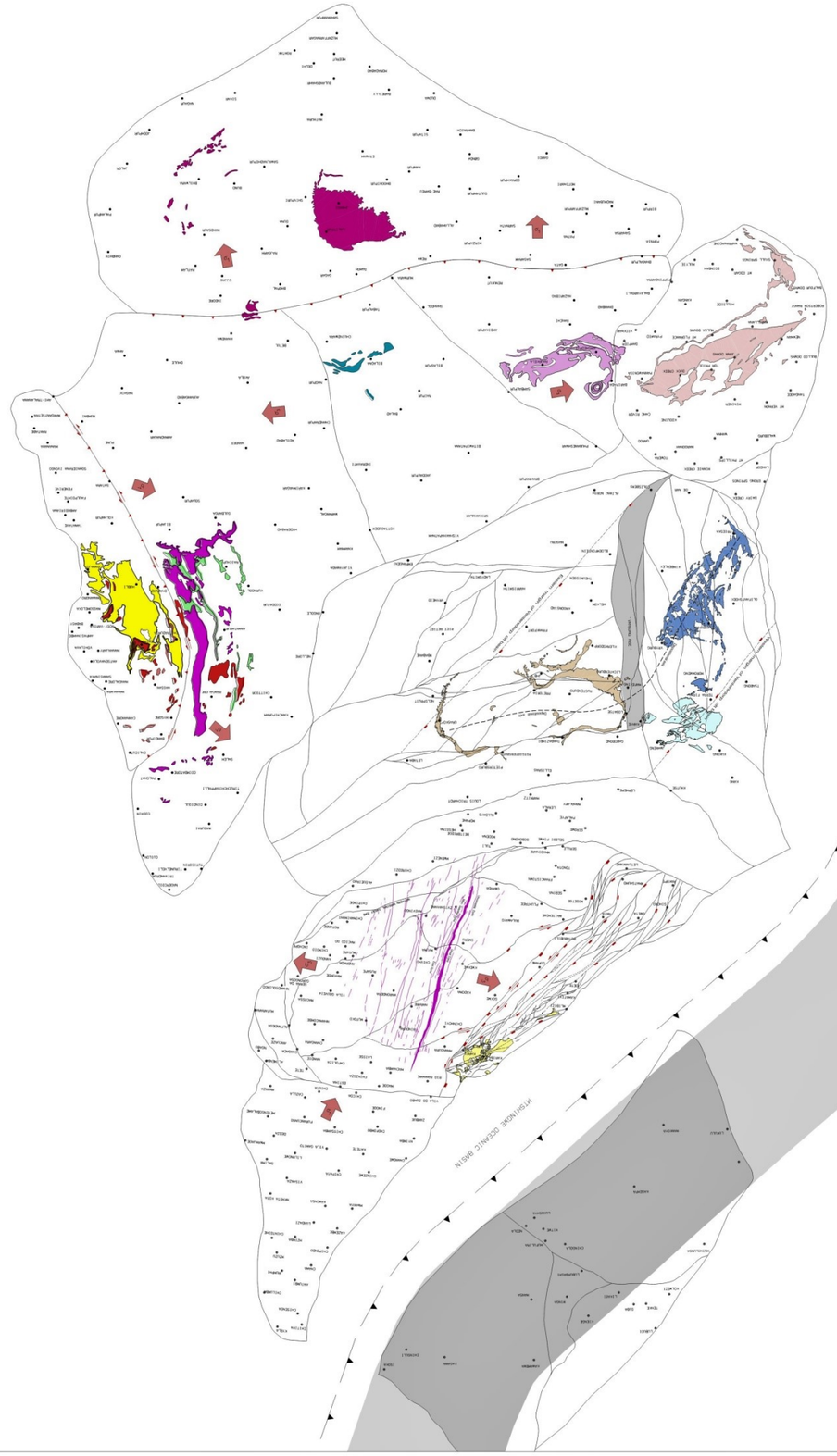
- ZIMBABWE CRATON
  - KAAPVAAL-GRUNEHOGNA CRATON
    - CHUNDESPOORT GROUP
    - TAUPONE GROUP
    - OMMEP GROUP
  - SINOBHEM CRATON
    - DHANJORI FORMATION (~2,55-2,43 GA)
  - BHUTAN CRATON
    - SAMJOL GROUP (~2,55-2,5 GA)
  - EAST DHARWAR CRATON
    - ELDIPET GNAWI RELATED GNAWI TES (~2,72-2,55 GA)
    - EASTERN AREEKSTONES (~2,72-2,55 GA)
    - GNAWI TES (UNDIFFERENTIATED)
  - WEST DHARWAR-ANTUNDU CRATON
    - CHITADOKSA GROUP (~2,75-2,5 GA)
    - ERUMPUR GNAWI TE
    - GNAWI TES (UNDIFFERENTIATED)
  - PILGARA CRATON
    - HAMERSLEY GROUP (~2,6-2,4 GA)
  - AFRINDALI-BANDELAMAND CRATON
    - BANDELAMAND GNAWI TE (~2,55-2,5 GA)

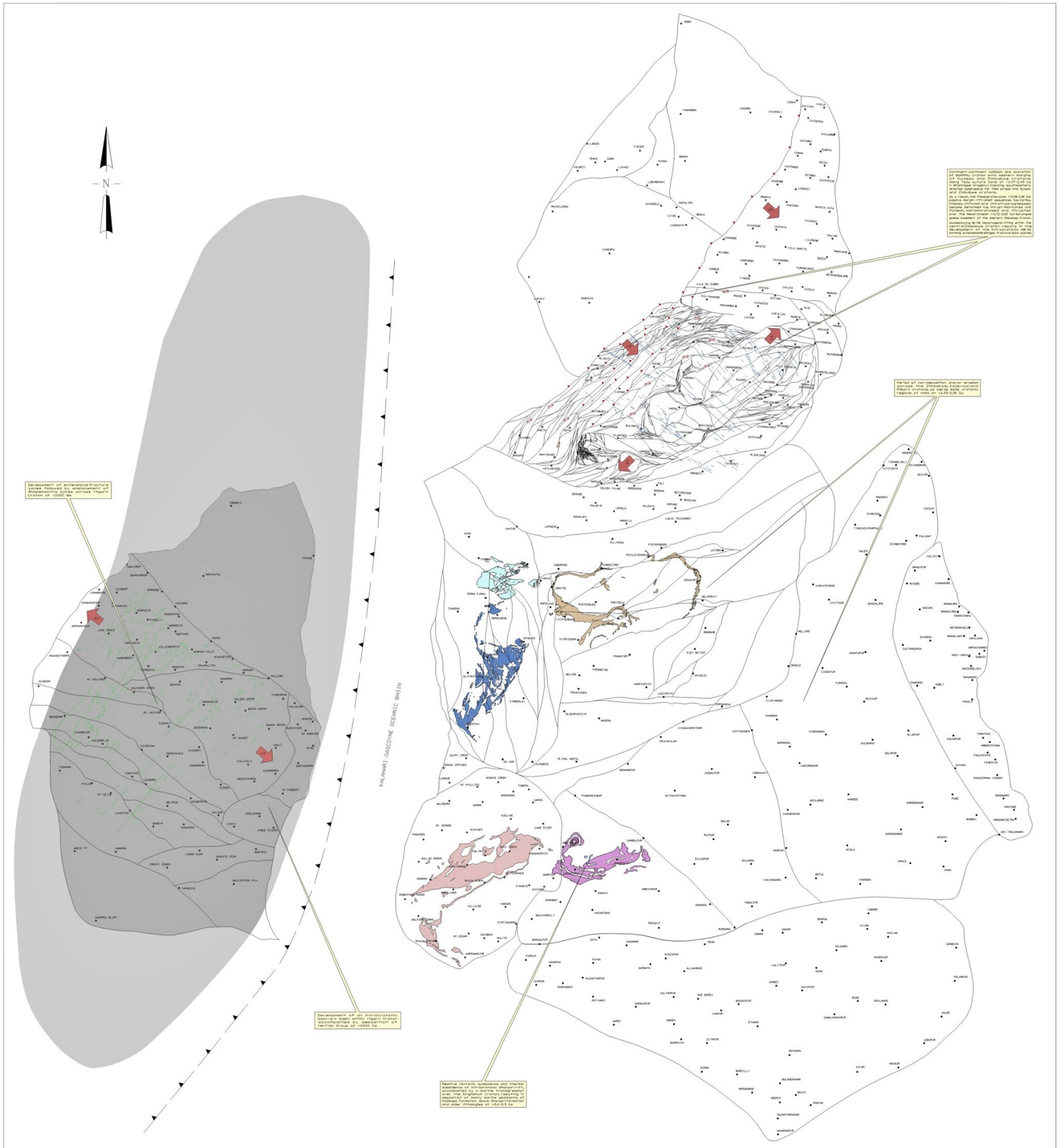
AREA OF INTRACRATONIC METAMORPHIC AND BACK-ARC BASIN DEVELOPMENT

AREA OF OCEANIC METAMORPHIC-SUBDUCTION ZONE AND BACK-ARC BASIN DEVELOPMENT

- KAAPVAAL CRATON AND ZIMBABWE CRATON (~2,585-2,575 GA)
- GREAT DYKE AND SATELLITE INTRUSIONS (~2,59-2,47 GA)
- KAAPVAAL CRATON AND ZIMBABWE CRATON (~2,71-2,64 GA)
- CHUNDESPOORT GROUP
- TAUPONE GROUP
- OMMEP GROUP
- SINOBHEM CRATON
- DHANJORI FORMATION (~2,55-2,43 GA)
- BHUTAN CRATON
- SAMJOL GROUP (~2,55-2,5 GA)
- EASTERN DHARWAR CRATON
- ELDIPET GNAWI RELATED GNAWI TES (~2,72-2,55 GA)
- GNAWI TES (UNDIFFERENTIATED)
- WESTERN DHARWAR-ANTUNDU CRATON
- CHITADOKSA GROUP (~2,75-2,5 GA)
- ERUMPUR GNAWI TE
- GNAWI TES (UNDIFFERENTIATED)
- PILGARA CRATON
- HAMERSLEY GROUP (~2,6-2,4 GA)
- ARMHALI-BANDELAMAND CRATON
- BANDELAMAND GNAWI TE (~2,55-2,5 GA)

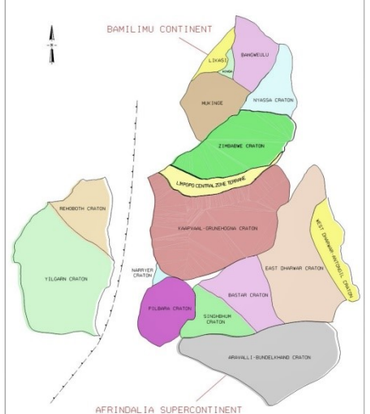
- PROPOSED SUBDUCTION ZONE (TEETH ON SUBDUCTED SLAB)
- KIRK-SLIP FAULT
- DELGAE-NEGESE FAULT
- DELGAE-NORWE FAULT
- THRUST FAULT
- NORWE FAULT
- CRUSTAL SUTURE ZONE / TERRANE BOUNDARY
- MAJOR MOBILE ZONAL COMPRESSIVE FAR FIELD STRESS ORIENTATION (σ_H)
- MAJOR MOBILE ZONAL EXTENSIONAL FAR FIELD STRESS ORIENTATION (σ_H)





LEGEND

- GHAAP GROUP
- TAUPONE GROUP
- CHUNIESPOORT GROUP
  - ~2.59 - 2.43 GA — KAAPVAAL-GRUNEHOGNA CRATON
- HAMERSLEY GROUP (~2.6-2.43 GA) — PILBARA CRATON
- DHANJORI FORMATION (~2.55-2.43 GA)
- CHAIBASA FORMATION (~2.43-2.35 GA)
  - SINGHBHUM CRATON
- AREA OF INTRACRATONIC MAGMATIC-ARC AND BACK-ARC BASIN DEVELOPMENT
- AREA OF OCEANIC MAGMATIC (ISLAND)-ARC AND BACK-ARC BASIN DEVELOPMENT
- WIDGIEMOOTHA DYKES (~2.42 GA)
- MTSHINGWE FRACTURE SYSTEM (~2.47-2.35 GA)
- SINISTRAL STRIKE-SLIP REACTIVATED SEGMENT OF NEOARCHAEAN (~2.705-2.64 GA) SHEAR ZONE
- THRUST FAULT
- STRIKE-SLIP FAULT
- OBLIQUE-REVERSE FAULT
  OBLIQUE-NORMAL FAULT
- SYNCLINE
  ANTICLINE
- PROPOSED PALAEO-SUBDUCTION ZONE (TEETH ON SUBDUCTED CRUSTAL SLAB)
- CRUSTAL SUTURE ZONE / TERRANE BOUNDARY
- MAXIMUM HORIZONTAL COMPRESSIVE FAR FIELD STRESS ORIENTATION (σ_1)
- MAXIMUM HORIZONTAL EXTENSIONAL FAR FIELD STRESS ORIENTATION (σ_3)



APPENDIX 20-J

GEODYNAMIC EVOLUTION OF SOUTHERN AFRICA DURING THE PERIOD ~2.47 - 2.43 GA

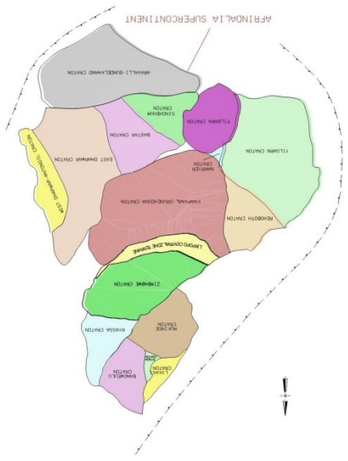
0 50 100 150 200 KILOMETRES

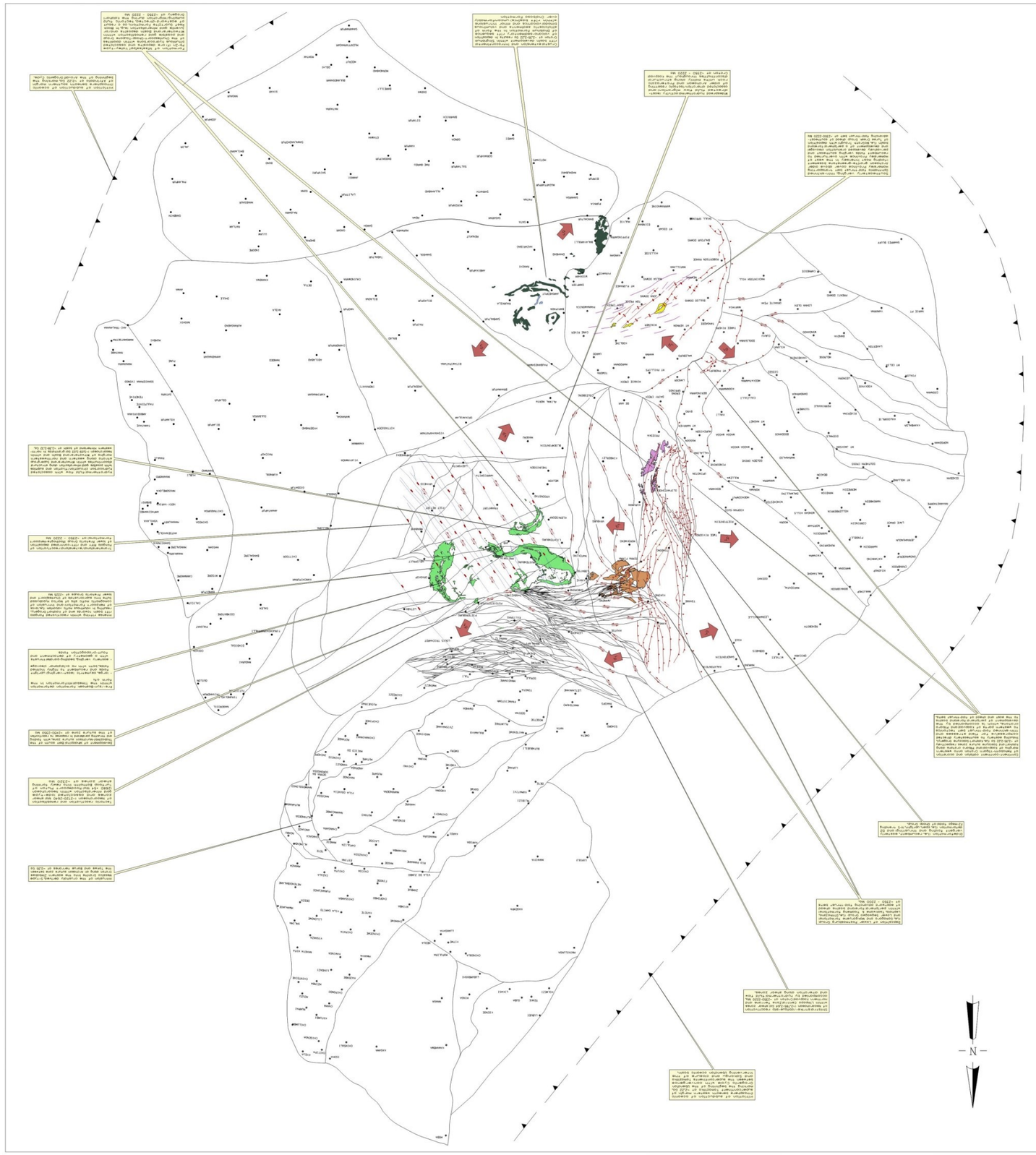
APPENDIX 20-K

GEODYNAMIC EVOLUTION OF SOUTHERN AFRICA DURING THE PERIOD ~2.43 - 2.35 GA

0 50 100 150 200

KILOMETERS





LEGEND

- LOWER PRETORIA GROUP (CARBONATE & MARGARITIFERA FORMATIONS)
- LOWER SILVERTON GROUP (LEPHALALA, TSOMAHAE & TLHAMENG FORMATIONS)
- LOWER PRETORIA GROUP (ROOIHOOGTE FORMATION - TIMEBALL HILL FORMATION)
- SILICICLASTICS
- MAFIC EXTRUSIVES AND INTRUSIVES
- TUBEE CREEK GROUP
- THRUST FAULT
- STRIKE-SLIP FAULT
- DOLOMITE-REVERSE FAULT
- DOLOMITE-NORMAL FAULT
- SYNCLINE
- ANTICLINE
- PROPOSED PALAEO-SUBDUCTION ZONE (TEETH ON SUBDUCTED CRUSTAL SLAB)
- CRUSTAL SUTURE ZONE / TERRANE BOUNDARY
- MAJOR MAPPED ZONAL CONTINUATION (c.)
- MAJOR MAPPED ZONAL EXTENSIONAL FAR FIELD STRESS ORIENTATION (c.)
- EXTENSIONAL / TRANSTENSIONAL REACTIVATED NORMAL FAULT OF NEBOCHAEAN (~2.72-2.65 Ga PHALA RIFT BASIN
- REACTIVATED (INVERTED) SEGMENT OF NORMAL FAULT OF NEBOCHAEAN (~2.72-2.64 Ga VENTERSDORP RIFT BASIN
- SINISTRAL STRIKE-SLIP REACTIVATED SEGMENT OF NEBOCHAEAN (~2.715-2.64 Ga SHEAR ZONE
- AREAL EXTENT OF CENTRAL ARCH PART OF PHALA RIFT BASIN
- AREAL EXTENT OF LEBOER PHALA RIFT BASIN
- AREAL EXTENT OF NORTHERN-EXTENDED PART OF PHALA RIFT BASIN

APPENDIX 20-L

GEODYNAMIC EVOLUTION OF SOUTHERN AFRICA
DURING THE PERIOD ~2.35 - 2.1 GA

0 500 1000 1500 2000
KILOMETRES

AFRINDALIA SUPERCONTINENT

ANNAMALAI-BHADRACHAND CRATON
YILGARN CRATON
PILBARA CRATON
SINGHBHUM CRATON
BASTAR CRATON
EAST DHARWAR CRATON
KAAPVAAL-ZIMBABWE CRATON
WEST DHARWAR CRATON
NEOARCHEAN (~2.8-2.5 Ga) GRANITE-GREENSTONE TERRANE
PALEOPROTEROZOIC (~2.5-2.2 Ga) SUPRACRUSTAL BELT
ZIMBABWE CRATON
NYANKANDE CRATON
LIMPOPO CENTRAL ZONE GRANULITE
MAKHADO CRATON
MAN CRATON
LEO-KENEMA CRATON
BANGWEULU CRATON
REGIMBITI CRATON
TANZANIA CRATON

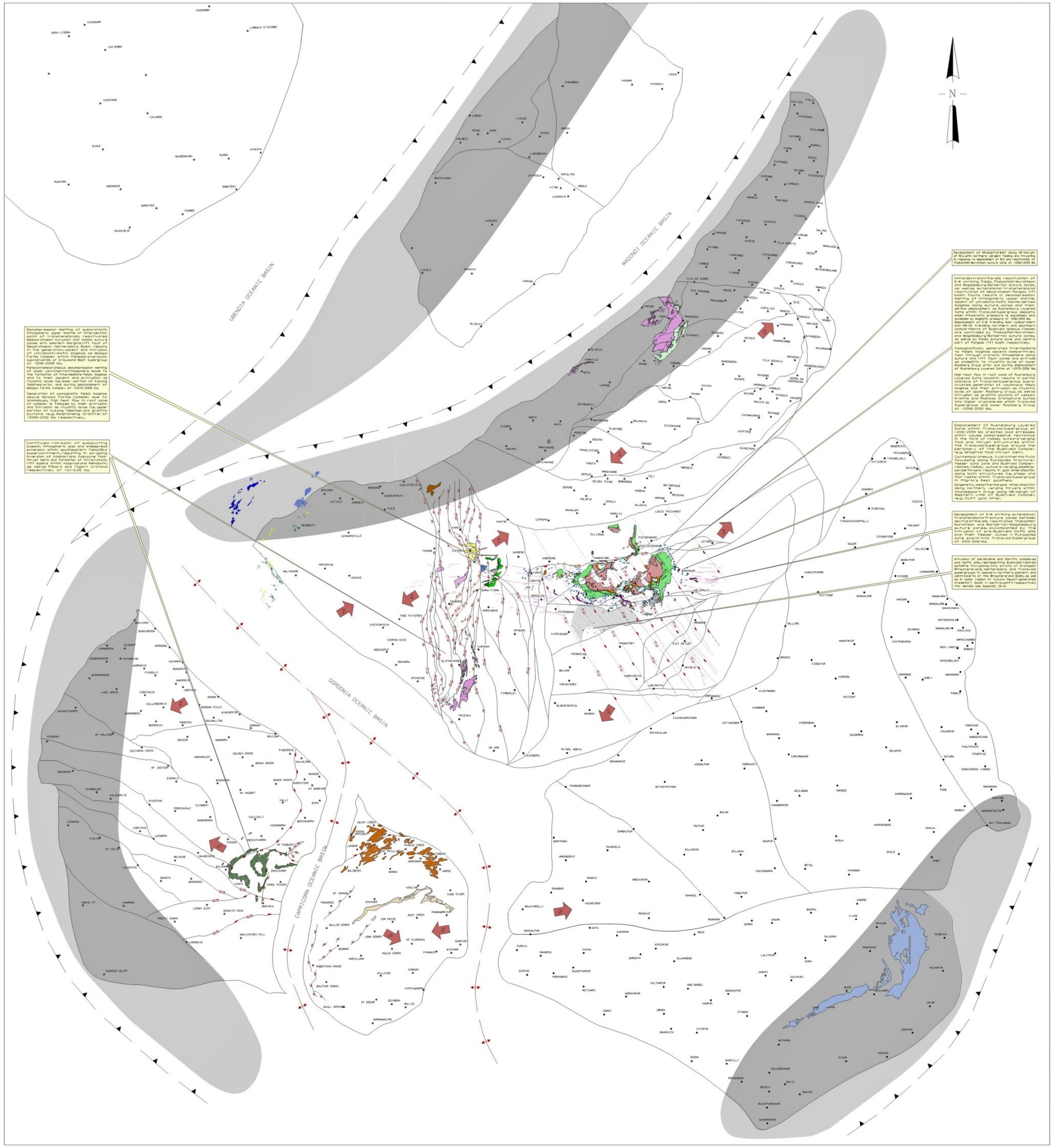
LEGEND

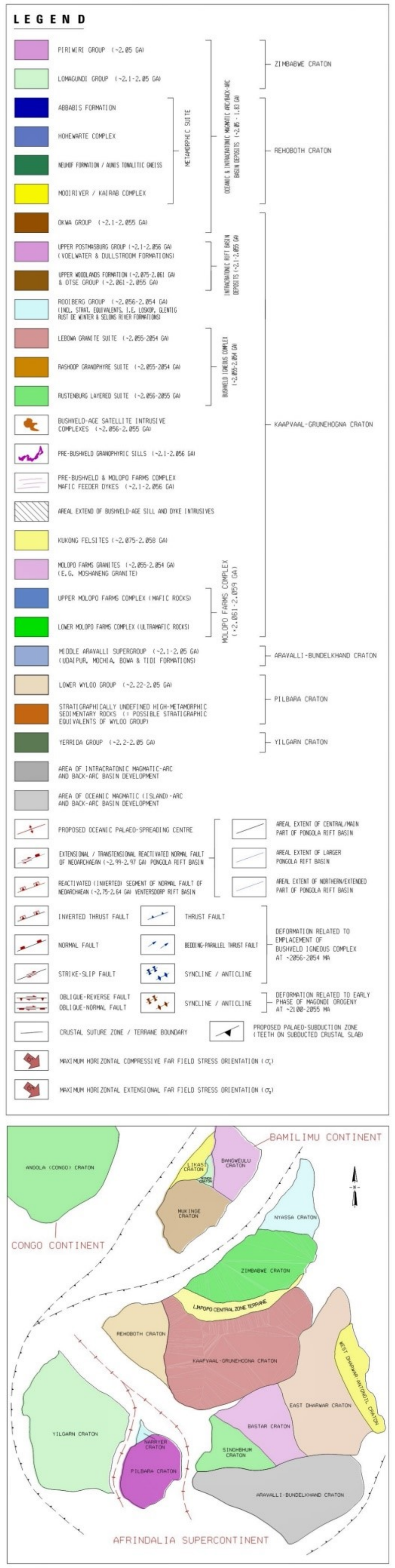
INCL. MAFIC/FELSIC IGNEOUS OF RIFT-RELATED MAGMATISM
DEVONIAN GROUP (~2.2-2.1 Ga)
UPPER POSTMASBURG GROUP (~2.22-2.05 Ga)
OLIFANTSHOEK & MOKALANYEN FORMATIONS
TRANSVAAL SUPERGROUP - BOOMPLAAS QUARTZITE FORMATION
UPPER DEWDROP GROUP (~2.22-2.1 Ga)
TAIHUA - GAOJIAYAN & MOUNT YOUNG FORMATIONS
UPPER PRETORIA GROUP (~2.22-2.1 Ga)
HEKPOORT FORMATION TO TOP?
KOLANA GROUP (~2.2-2.12 Ga)
SAUSAR GROUP (~2.2-2.1 Ga)
CHUARIAN GROUP (~2.2-2.1 Ga)
LOWER HAVAKALI SUPERSEQUENCE (~2.2-2.1 Ga)
CHELMURA & JUMANDIAN FORMATIONS
LOWER VALOZ GROUP (~2.22-2.05 Ga)
STABILISED MAGMATIC ACTIVITY RELATED TO RIFTING
SEDIMENTARY ROCKS (+ POSSIBLE STABILISATION)
EARLIEST OF VALOZ GROUP)
VERDICA GROUP (~2.2-2.05 Ga)
ARCHEAN OF INDIVIDUAL MAGMATIC-ARC AND BACK-ARC BASIN DEVELOPMENT
AREA OF OCEANIC MAGMATIC-ARC AND BACK-ARC BASIN DEVELOPMENT
PROPOSED PALAEO-SUBDUCTION ZONE (METIN ON SUBDUCTED CRUSTAL SLAB)
PROPOSED OCEANIC PALAEO-SPREADING CENTRE
EXTENSIONAL / TRANSTENSIONAL REACTIVATED NORMAL FAULT OF NEOARCHEAN (~2.7-2.5 Ga) PONDAUA RIFT BASIN
REACTIVATED (INVERTED) SEGMENT OF NORMAL FAULT OF NEOARCHEAN (~2.72-2.64 Ga) VENTERSDORP RIFT BASIN
AREAL EXTENT OF CRUSTAL PART OF PONDAUA RIFT BASIN
AREAL EXTENT OF LAVACRS PONDAUA RIFT BASIN
AREAL EXTENT OF NORTHEASTWARDS PART OF PONDAUA RIFT BASIN

CRUSTAL SUTURE ZONE / TERRANE BOUNDARY
MAJOR MORE ZONAL COMPRESSIVE FAR FIELD STRESS ORIENTATION ( )
MAJOR MORE ZONAL EXTENSIONAL FAR FIELD STRESS ORIENTATION ( )
DOLLGUE-NORNAL FAULT
DOLLGUE-REVERSE FAULT
STRIKE-SLIP FAULT
NORMAL FAULT
INVERTED THRUST FAULT

CAPRICORN OROGENIC BELT
LIBERIAN OCEANIC BASIN
MOGONDI OCEANIC BASIN
GONDWANA OCEANIC BASIN

N

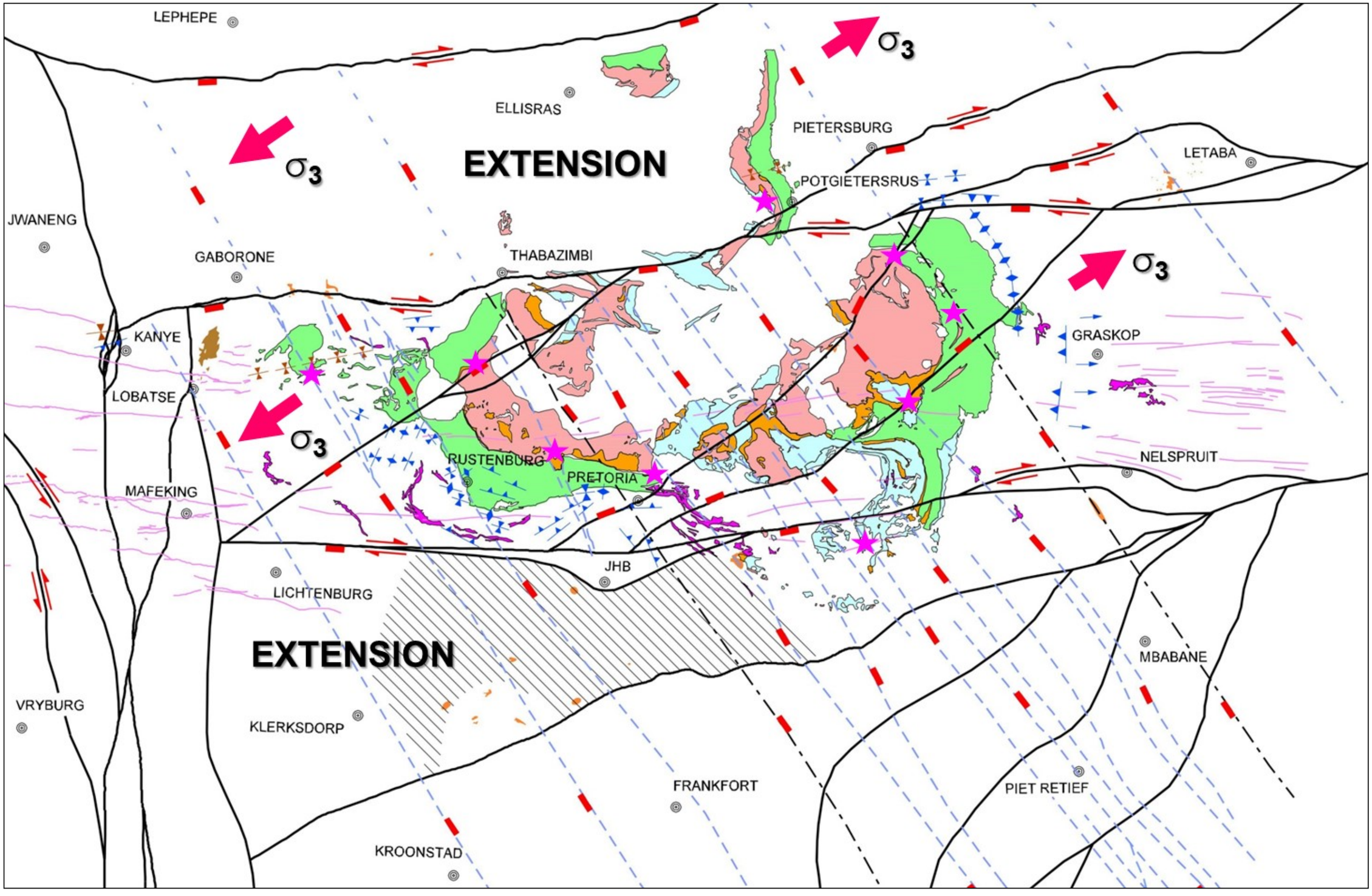




APPENDIX 20-M

GEODYNAMIC EVOLUTION OF SOUTHERN AFRICA DURING THE PERIOD ~2.1 - 2.055 GA

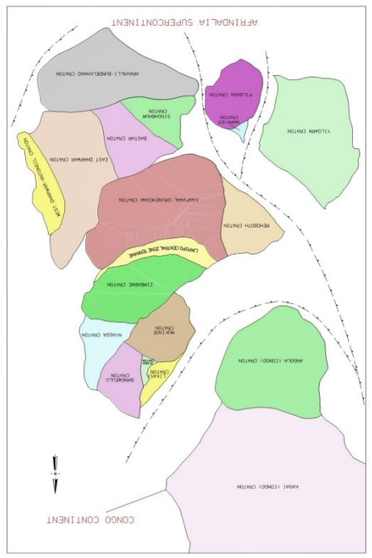
0 50 100 150 200 KILOMETRES

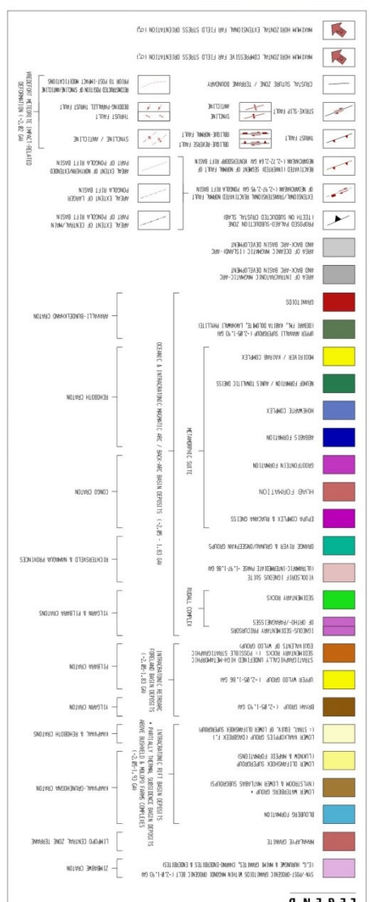


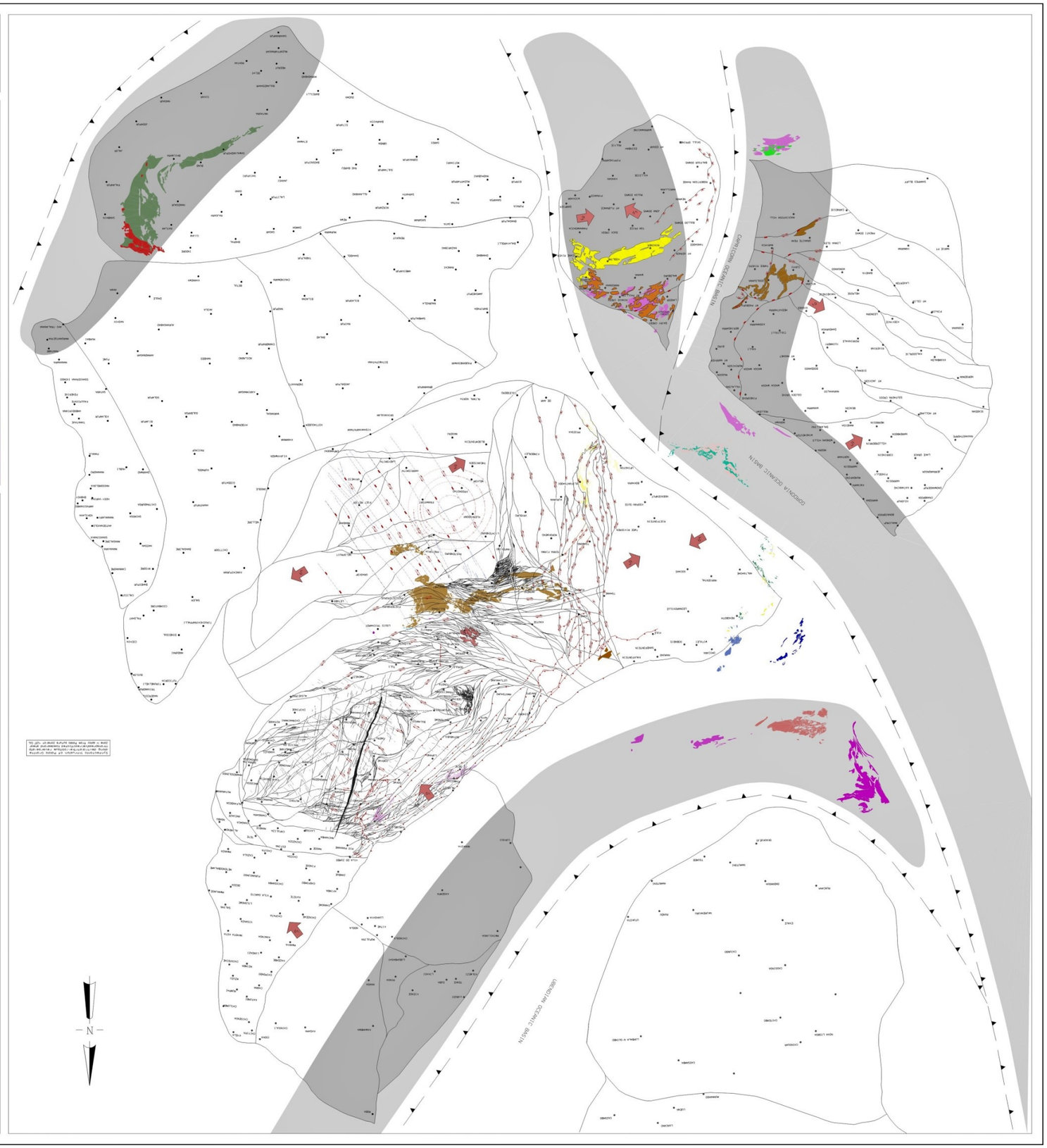
APPENDIX 20-M2 : Tectono-structural setting of the Bushveld Complex. Kinematic model for the emplacement of the Bushveld Complex at ~2.056-2.054 Ga, proposing SSE-directed compressive far field stress induced by the Magondi Orogeny causing the combined dextral transtensional and extensional reactivation of E/W-striking translithospheric suture zones and NW/SE-striking crustal Pongola rift faults, respectively. Suture zones controlled the generation of ultramafic-mafic magmas at depth through decompression melting of the upper mantle and their ascend into the crust, while Pongola rift faults facilitated their crustal emplacement within the reactivated Neoarchaean Pongola impactogenal rift.

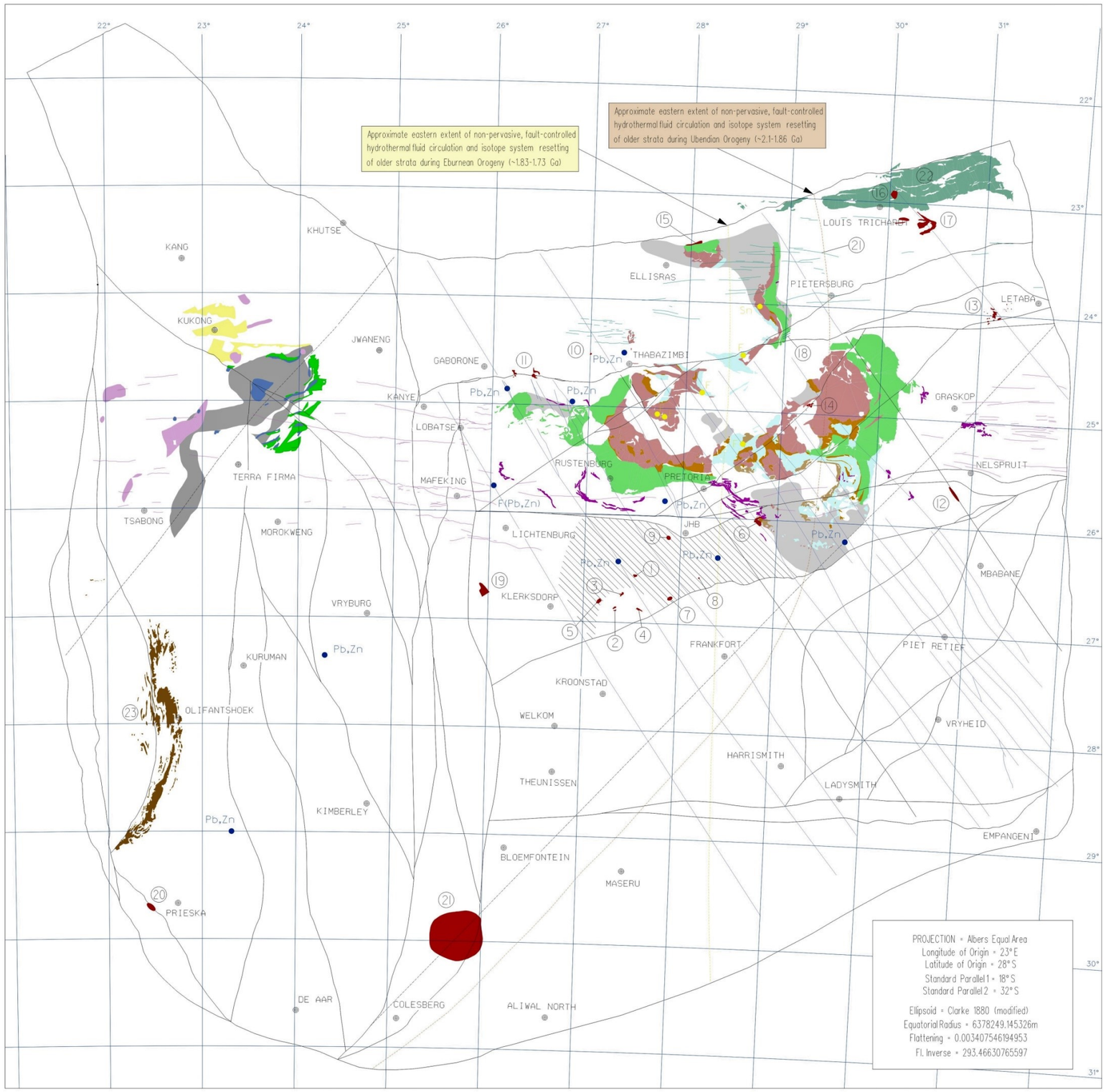
APPENDIX 20-N

GEODYNAMIC EVOLUTION OF SOUTHERN AFRICA
DURING THE PERIOD ~2.05 - 1.93 GA









LEGEND

- Loskop, Glentig, Rust de Winter, Selons River Formations (= Rooiberg Group strat. equivalents)
- Rooiberg Group (2061 ± 2 Ma – 2057 ± 4 Ma)
- Lebowa Granite Suite (Nebo, Klipkloof & Makhutso Granites 2054 ± 2 Ma)
- Rashopp Granophyre Suite (Stavoren Granophyre Suite 2056 ± 1 Ma – 2053 ± 12 Ma)
- Rustenburg Layered Suite (2056 ± 0.3 Ma – 2055 ± 0.4 Ma)
- Subcrop (geophysically inferred)

OUTCROP — BUSHVELD COMPLEX (~2056-2054 MA)

- Kukong felsites (2074 ± 4 Ma – 2058 ± 3 Ma)
- Molopo Farms Granites (e.g. Moshaneng Granite 2054 ± 2 Ma)
- Upper Molopo Farms Complex (mafic rocks)
- Lower Molopo Farms Complex (ultramafic rocks)
- Subcrop (geophysically inferred)

OUTCROP — MOLOPO FARMS COMPLEX (~2056-2054 MA)

- Pre-Bushveld & Molopo Farms Complex dyke and sill intrusions (~2100-2060 Ma)
- Aerial extent of Bushveld-age dyke and sill intrusions within the Witwatersrand Basin
- PB, ZN — Mississippi Valley-type mineralisation within Transvaal/ Griqualand West Sequence (~2050-2000 Ma and/or ~1830-1730 Ma)
- Areal extent of main Pongola rift basin
- Areal extent of larger Pongola rift basin
- Areal extent of Ventersdorp rift basin
- Areal extent of Pilanesberg Graben System (= northern extension of Pongola rift basin)

BUSHVELD SATELLITE INTRUSIVE COMPLEXES (~2060-2050 MA)

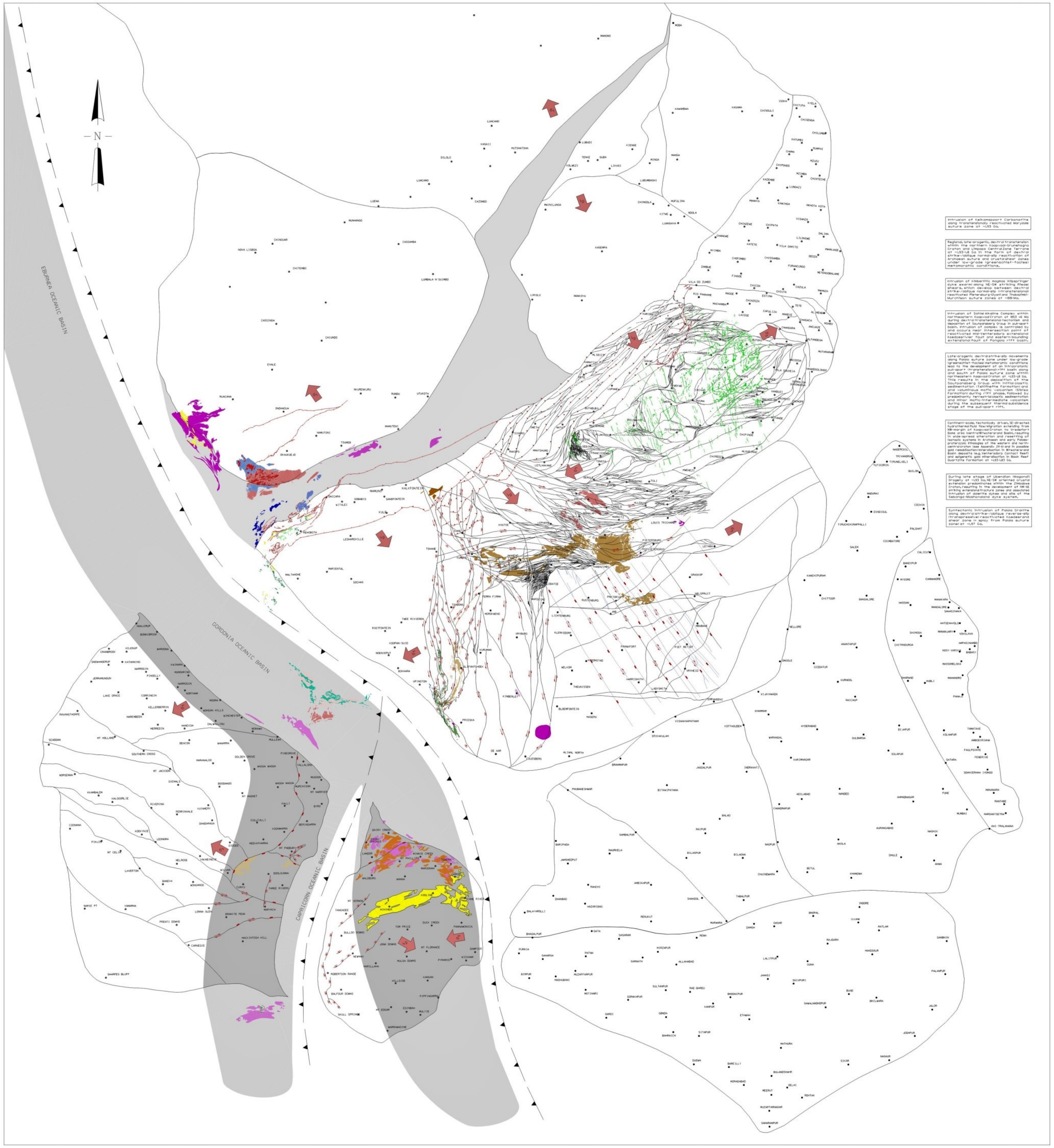
1. Losberg Complex (2041 ± 41 Ma)
2. Schurwedraai & Baviaanskraal Alkali Granites/Syenites (2052 ± 14 Ma)
3. Rietfontein Alkaline Granite (>2008 ± 10 Ma)
4. Lindequesdrift Complex (2055 ± 6 Ma)
5. Roodekraal Complex (2053 ± 9 Ma)
6. Dwarsfontein Complex
7. Vereeniging Gabbroid
8. Kaffirskraal Complex
9. Vogelstruisfontein Gabbroid
10. Koringkoppies Complex
11. Modipe Gabbro Complex
12. Uitkomst Complex (2054 ± 7 Ma)
13. Phalaborwa Carbonatite Complex (2060 ± 0.5 Ma)
14. Marble Hall Diorite Sill (2062 ± 8 – 2055.6 ± 3.1 Ma)
15. Palala Granite (~1972 Ma)
16. Entabeni Granite (2021 ± 5 Ma)
17. Schiel Complex (1853 ± 6 Ma)
18. Klipspringer kimberlite dyke swarm (~1881 Ma)
19. Dolerite/Ottosdal (1740 ± 13 Ma)
20. Keikamspoort Carbonatite Complex (~1930 Ma)
21. Trompsburg Layered Complex (1915 ± 6 Ma)
22. Sibasa Formation basalts and feeder dykes (Soutpansberg Group) (~1830-1800 Ma)
23. Hartley Formation basalts (Olifanshoek Group) (1928 ± 4 Ma)

NOTE : For references regarding geochronological data, see Appendix 25-A

APPENDIX 20-0

UBENDIAN (~2.1-1.86 GA) AND EBURNEAN (~1.83-1.73 GA) OROGENIC CYCLE-RELATED WITHIN THE KAAPVAAL CRATON

0 50 100 150 200
KILOMETRES



LEGEND

- LOWER PALAPYE GROUP (SELIKA & MOENG FORMATIONS)
- BRULPAN GROUP (UITDRAAI/PRYNNSBERG & GROBLERSHOOP FORMATIONS)
- UPPER WATERBERG GROUP (~1.93-1.86 GA) (UPPER MATLABAS & KRANSBERG SUBGROUPS)
- MIDDLE OLIFANSHOEK SUPERGROUP (HARTLEY FORMATION)
- UPPER VAALKOPPIES GROUP (SULTANAOORD F.) (= STRAT. EQUIV. OF MIDDLE OLIFANSHOEK SUPERGROUP)

INTRACRATONIC PULL-APART RIFT BASIN DEPOSITS (~1.93 - 1.83 GA) — LIMPOPO CENTRAL ZONE TERRANE; KAAPVAAL-GRUNEHOGNA CRATON

- PADBURRY GROUP (~1.93-1.83 GA)
- LOWER ELIM FORMATION (~1.87-1.83 GA)
- LOWER OKAPUKA FORMATION (~1.87-1.83 GA)
- LOWER KHOABENDUS GROUP (~1.87-1.83 GA)
- UPPER WYLOO GROUP (~2.05-1.87 GA)
- STRATIGRAPHICALLY UNDEFINED HIGH-METAMORPHIC SEDIMENTARY ROCKS (= POSSIBLE STRATIGRAPHIC EQUIVALENTS OF WYLOO GROUP)

INTRACRATONIC RETROARC FORELAND BASIN DEPOSITS (~1.93 - 1.83 GA) — YILGARN CRATON; REHOBOTH CRATON; CONGO CRATON; PILBARA CRATON

- IGNEOUS-SEDIMENTARY PRECURSORS OF ORTHO-/PARAGNEISSES
- GLADKOP GRANITOID SUITE (~1.93-1.73 GA)
- VIOOLSDRIF IGNEOUS SUITE (INTERMEDIATE TO FELSIC PHASE ~1.86-1.83 GA)
- ORANGE RIVER & GRUNAU/ONSEEPKAN GROUPS (~2.05-1.86 GA)
- FRANSFONTEIN GRANITOID SUITE (~1.86-1.73 GA)
- EPUPA COMPLEX & RUACANA GNEISS
- HUAB FORMATION
- GROOTFONTEIN FORMATION
- ABBABIS FORMATION
- HOHEWARTE COMPLEX
- NEUHOF FORMATION / AUNIS TONALITIC GNEISS
- MOOIRIVER / KAIRAB COMPLEX

METAMORPHIC SUITE

OCEANIC & INTRACRATONIC MAGMATIC ARC/BACK-ARC BASIN DEPOSITS (~2.05 - 1.83 GA) — YILGARN & PILBARA CRATONS; RICHTERSVELD & NAMAQUA PROVINCES; CONGO CRATON; REHOBOTH CRATON

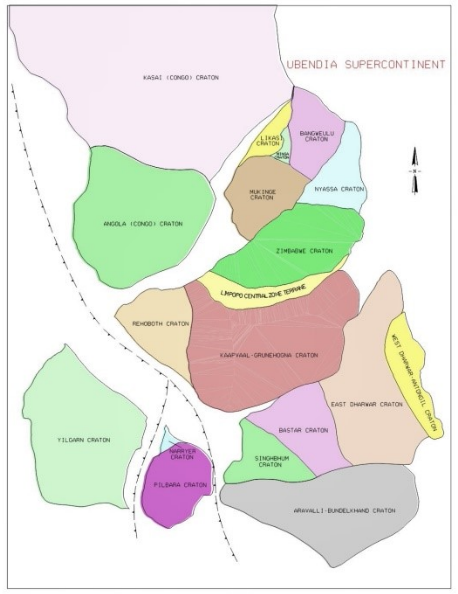
- JUVENILE PALAEOPROTEROZOIC LITHOSPHERE (~2.1-1.83 GA)
- AREA OF INTRACRATONIC MAGMATIC-ARC AND BACK-ARC BASIN DEVELOPMENT
- AREA OF OCEANIC MAGMATIC (ISLAND)-ARC AND BACK-ARC BASIN DEVELOPMENT
- PROPOSED PALAEO-SUBDUCTION ZONE (TEETH ON SUBDUCTED CRUSTAL SLAB)
- MAFIC SILLS POSSIBLY COMAGMATIC WITH LAVAS OF SIBASA FORMATION (~1.92-1.83 GA)
- POSSSIBLE FEEDER DYKES TO MAFIC LAVAS OF SIBASA FORMATION (~1.92-1.83 GA)

— KAAPVAAL-GRUNEHOGNA CRATON

- SEBANGA-MASHONALAND SILLS (~1.92-1.83 GA)
- SEBANGA-MASHONALAND FRACTURE/DYKE SYSTEM (~1.92-1.83 GA)

— ZIMBABWE CRATON & LIMPOPO CENTRAL ZONE TERRANE

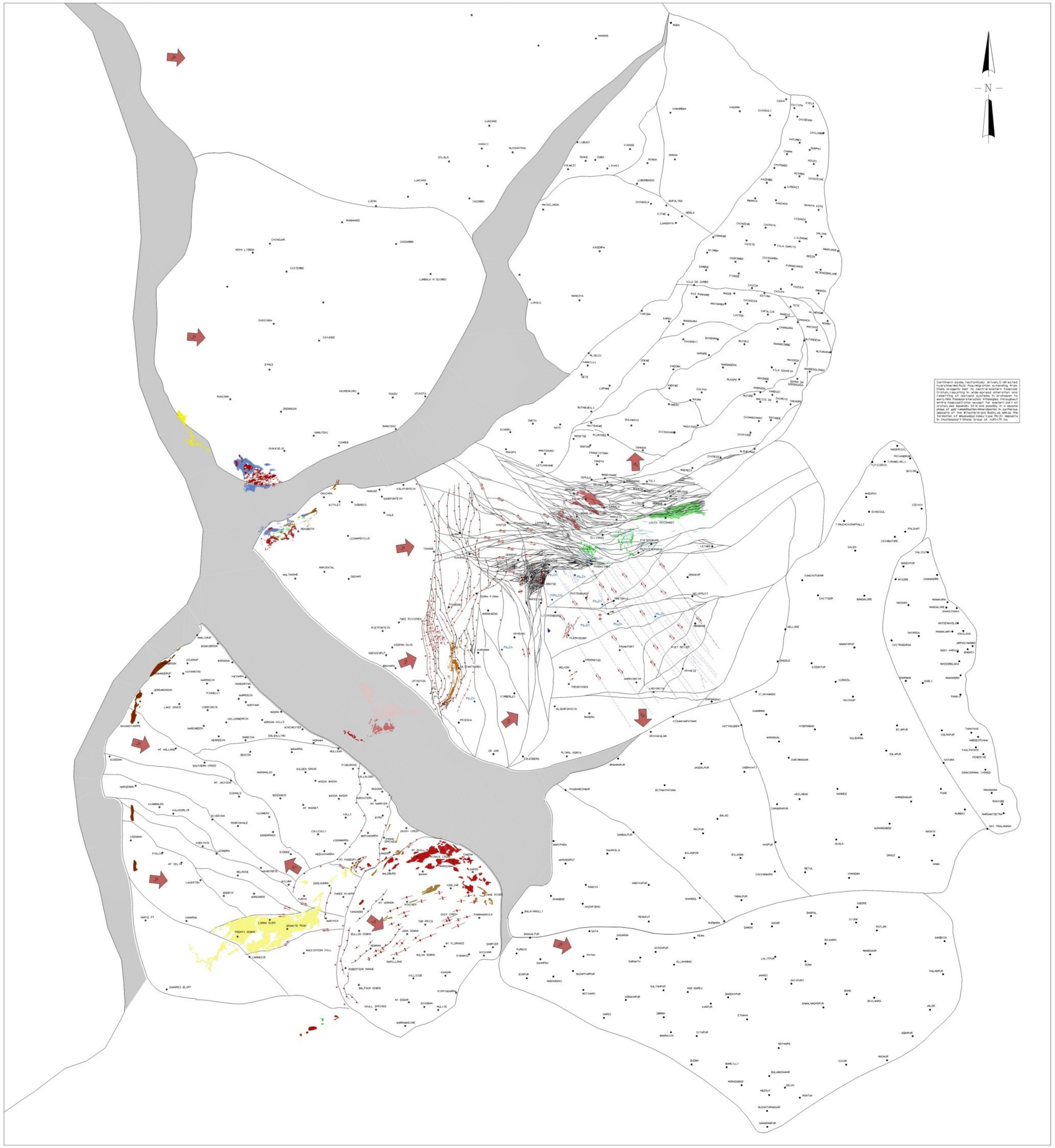
- REACTIVATED (INVERTED) SEGMENT OF NORMAL FAULT OF NEOARCHAEAN (~2.72-2.64 GA) VENTERSDORP RIFT BASIN
- OBLIQUE-REVERSE FAULT
- OBLIQUE-NORMAL FAULT
- THRUST FAULT
- SYNCLINE
- ANTICLINE
- STRIKE-SLIP FAULT
- CRUSTAL SUTURE ZONE / TERRANE BOUNDARY
- MAXIMUM HORIZONTAL COMPRESSIVE FAR FIELD STRESS ORIENTATION (σ_1)
- MAXIMUM HORIZONTAL EXTENSIONAL FAR FIELD STRESS ORIENTATION (σ_3)



APPENDIX 20-P

GEODYNAMIC EVOLUTION OF SOUTHERN AFRICA DURING THE PERIOD ~1.93 - 1.83 GA

0 50 100 150 200 KILOMETRES

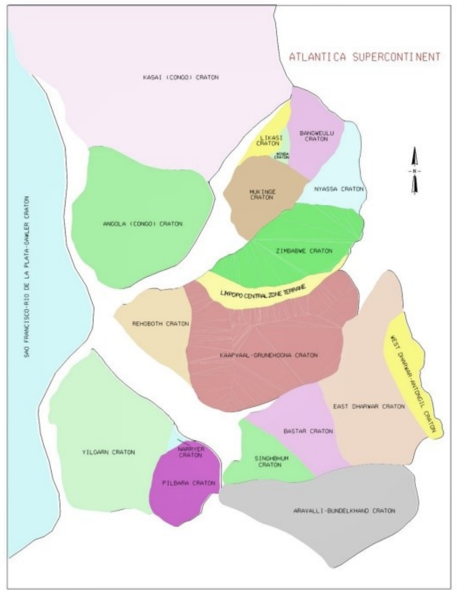


LEGEND

- UPPER PALAPYE GROUP (TSWAPONG, LOTSANE & SHOSHONG FORMATIONS)
- UPPER SOUTPANSBERG GROUP (~1.8-1.73 GA) (WYLLIES POORT & NZHELELE FORMATIONS)
- LOWER SOUTPANSBERG GROUP (~1.83-1.8 GA) (TSHIFHEFHE, SIBISA & FUNDUZI FORMATIONS)
- MAFIC SILLS POSSIBLY COMAGMATIC WITH LAVAS OF SIBASA FORMATION (~1.83-1.8 GA)
- POSSSIBLE FEEDER DYKES TO MAFIC LAVAS OF SIBASA FORMATION (~1.83-1.8 GA)
- UPPER OLIFANSHOEK SUPERGROUP (MATSAP & BRULSAND FORMATIONS = VOLOP GROUP)
- GAUB VALLEY & BILLSTEIN FORMATIONS
- MARIENHOF FORMATION
- UPPER ELIM FORMATION (~1.83-1.73 GA)
- EARAHEEDY GROUP
- MOUNT BARREN GROUP
- CAPRICORN FORMATION
- UPPER KHOABENDUS GROUP (~1.83-1.73 GA)
- UPPER OKAPUKA FORMATION
- FRANSFONTEIN GRANITOID SUITE (~1.86-1.73 GA)
- OPETJIE GRANODIORITE (PIKSTEEL INTRUSIVE SUITE) (~1.78 GA) WEENER IGNEOUS COMPLEX (~1.77-1.74 GA) NAUB DIORITE (~1.725 GA)
- VIOOLSDRIF IGNEOUS SUITE (FELSIC PHASE ~1.83-1.73 GA)
- GLADKOP GRANITOID SUITE (~1.93-1.73 GA)
- GRANITOIDS
- ULTRAMAFIC-MAFIC-INTRUSIONS
- JUVENILE PALAEOPROTEROZOIC LITHOSPHERE (~2.1-1.83 GA)
- REACTIVATED (INVERTED) SEGMENT OF NORMAL FAULT OF NEOARCHAEAN (~2.72-2.64 GA) VENTERSDORP RIFT BASIN
- THRUST FAULT
- BEDDING-PARALLEL THRUST FAULT
- STRIKE-SLIP FAULT
- OBLIQUE-REVERSE FAULT
- OBLIQUE-NORMAL FAULT
- SYNCLINE
- ANTICLINE
- CRUSTAL SUTURE ZONE / TERRANE BOUNDARY
- MAXIMUM HORIZONTAL COMPRESSIVE FAR FIELD STRESS ORIENTATION (σ_1)
- MAXIMUM HORIZONTAL EXTENSIONAL FAR FIELD STRESS ORIENTATION (σ_3)
- PB,ZN — MISSISSIPPI VALLEY-TYPE MINERALIZATION WITHIN CHUNIESPOORT/GHAAP GROUP (TRANSVAAL/GRIQUALAND WEST SUPERGROUP)

Groupings: REHOBOTH SEQUENCE; THERMAL SUBSIDENCE BASIN DEPOSITS (~1.83-1.73 GA); INTRACRATONIC RIFT BASIN DEPOSITS (~1.83 - 1.8 GA); INTRACRATONIC RETROARC FORELAND BASIN DEPOSITS (~1.83-1.75 GA); INTRACRATONIC PERIPHERAL FORELAND BASIN DEPOSITS (~1.83-1.73 GA); SYN- TO POST-OROGENIC GRANITOID MAGMATISM (~1.83 - 1.73 GA)

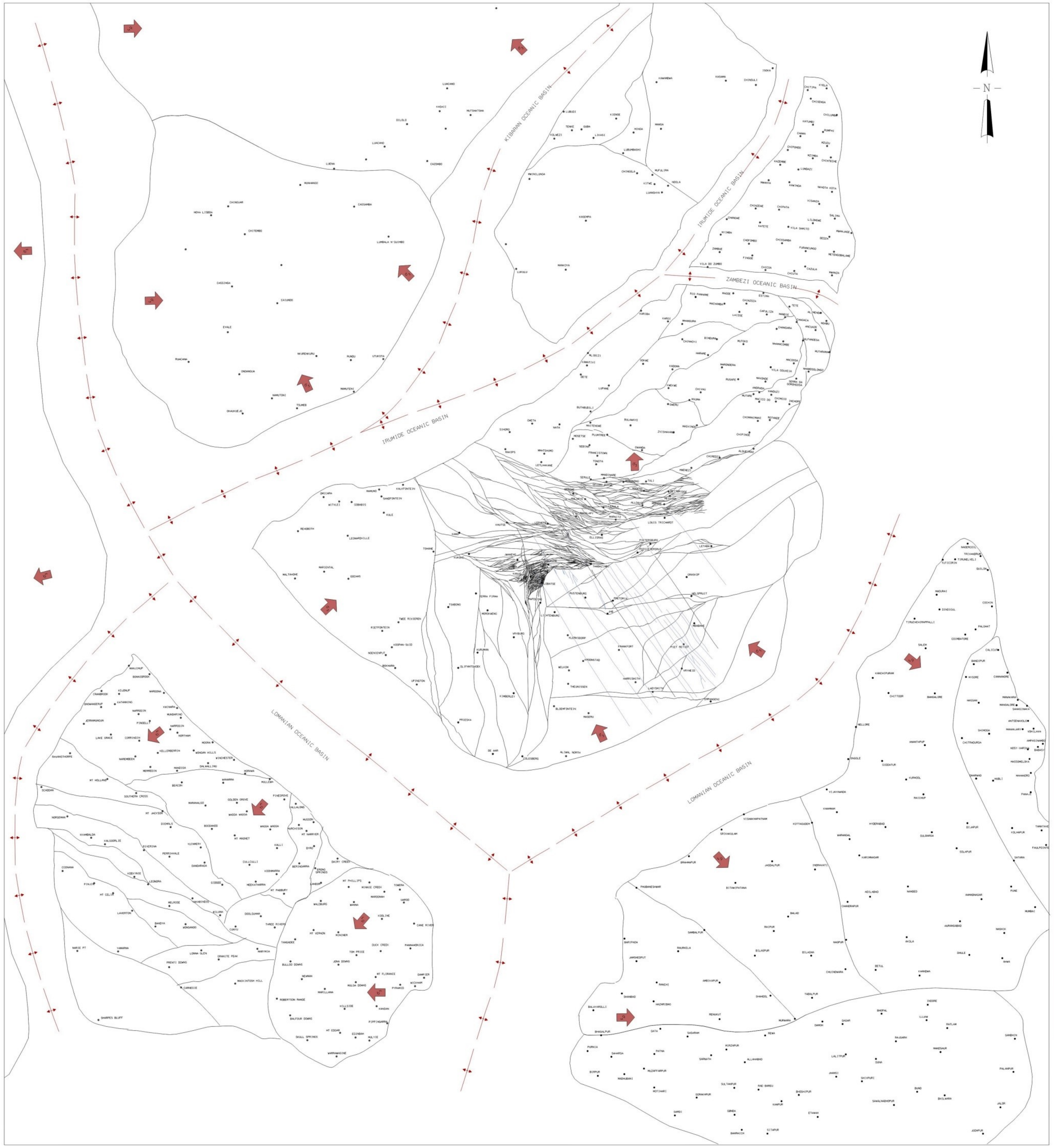
Terranes: LIMPOPO CENTRAL ZONE TERRANE; KAAPVAAL-GRUNEHOGNA CRATON; REHOBOTH CRATON; YILGARN CRATON; PILBARA CRATON; CONGO CRATON; REHOBOTH CRATON; RICHTERSVELD PROVINCE/TERRANE; YILGARN & PILBARA CRATONS



APPENDIX 20-Q

GEODYNAMIC EVOLUTION OF SOUTHERN AFRICA DURING THE PERIOD ~1.83 - 1.73 GA

0 50 100 150 200 KILOMETRES



LEGEND

- UPPER PALAPYE GROUP (TSWAPONG, LOTSANE & SHOSHONG FORMATIONS)
- UPPER SOUTPANSBERG GROUP (~1.8-1.73 GA) (WYLLIES POORT & NZHELELE FORMATIONS)
- LOWER SOUTPANSBERG GROUP (~1.83-1.8 GA) (TSHIFHEFHE, SIBISA & FUNDUZI FORMATIONS)
- MAFIC SILLS POSSIBLY COMAGMATIC WITH LAVAS OF SIBASA FORMATION (~1.83-1.8 GA)
- POSSSIBLE FEEDER DYKES TO MAFIC LAVAS OF SIBASA FORMATION (~1.83-1.8 GA)
- UPPER OLIFANSHOEK SUPERGROUP (MATSAP & BRULSAND FORMATIONS = VOLOP GROUP)
- GAUB VALLEY & BILLSTEIN FORMATIONS
- MARIENHOF FORMATION
- UPPER ELIM FORMATION (~1.83-1.73 GA)
- EARAHEEDY GROUP
- MOUNT BARREN GROUP
- CAPRICORN FORMATION
- UPPER KHOABENDUS GROUP (~1.83-1.73 GA)
- UPPER OKAPUKA FORMATION
- FRANSFONTEIN GRANITOID SUITE (~1.86-1.73 GA)
- OPETJIE GRANODIORITE (PIKSTEEL INTRUSIVE SUITE) (~1.78 GA) WEENER IGNEOUS COMPLEX (~1.77-1.74 GA) NAUB DIORITE (~1.725 GA)
- VIOOLSDRIF IGNEOUS SUITE (FELSIC PHASE ~1.83-1.73 GA)
- GLADKOP GRANITOID SUITE (~1.93-1.73 GA)
- GRANITOIDS
- ULTRAMAFIC-MAFIC-INTRUSIONS
- JUVENILE PALAEOPROTEROZOIC LITHOSPHERE (~2.1-1.83 GA)
- REACTIVATED (INVERTED) SEGMENT OF NORMAL FAULT OF NEOARCHAEAN (~2.72-2.64 GA) VENTERSDORP RIFT BASIN
- THRUST FAULT
- BEDDING-PARALLEL THRUST FAULT
- STRIKE-SLIP FAULT
- OBLIQUE-REVERSE FAULT
- OBLIQUE-NORMAL FAULT
- SYNCLINE
- ANTICLINE
- CRUSTAL SUTURE ZONE / TERRANE BOUNDARY
- MAXIMUM HORIZONTAL COMPRESSIVE FAR FIELD STRESS ORIENTATION (σ_1)
- MAXIMUM HORIZONTAL EXTENSIONAL FAR FIELD STRESS ORIENTATION (σ_3)
- PB-ZN: MISSISSIPPI VALLEY-TYPE MINERALIZATION WITHIN CHUNIESPOORT/GHAAP GROUP (TRANSVAAL/GRIQUALAND WEST SUPERGROUP)

REHOBOTH SEQUENCE

THERMAL SUBSIDENCE BASIN DEPOSITS (~1.83-1.73 GA)

INTRACRATONIC RIFT BASIN DEPOSITS (~1.83 - 1.8 GA)

INTRACRATONIC RETROARC FORELAND BASIN DEPOSITS (~1.83-1.75 GA)

INTRACRATONIC PERIPHERAL FORELAND BASIN DEPOSITS (~1.83-1.73 GA)

SYN- TO POST-OROGENIC GRANITOID MAGMATISM (~1.83 - 1.73 GA)

LIMPOPO CENTRAL ZONE TERRANE

KAAPVAAL-GRUNEHOGNA CRATON

REHOBOTH CRATON

YILGARN CRATON

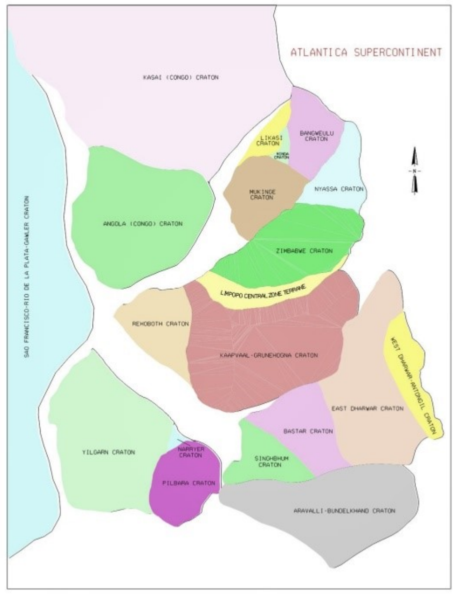
PILBARA CRATON

CONGO CRATON

REHOBOTH CRATON

RICHTERSVELD PROVINCE/TERRANE

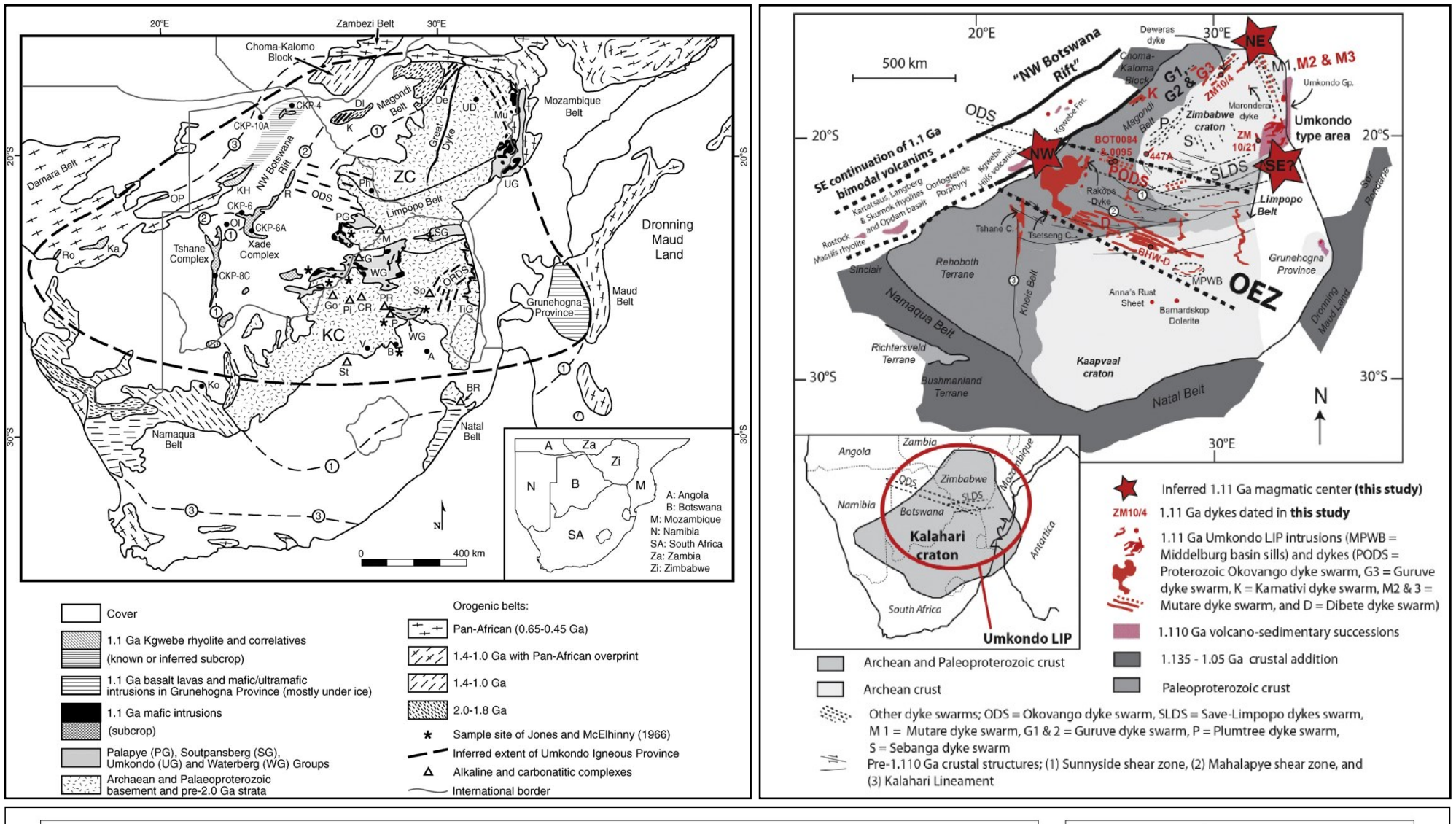
YILGARN & PILBARA CRATONS

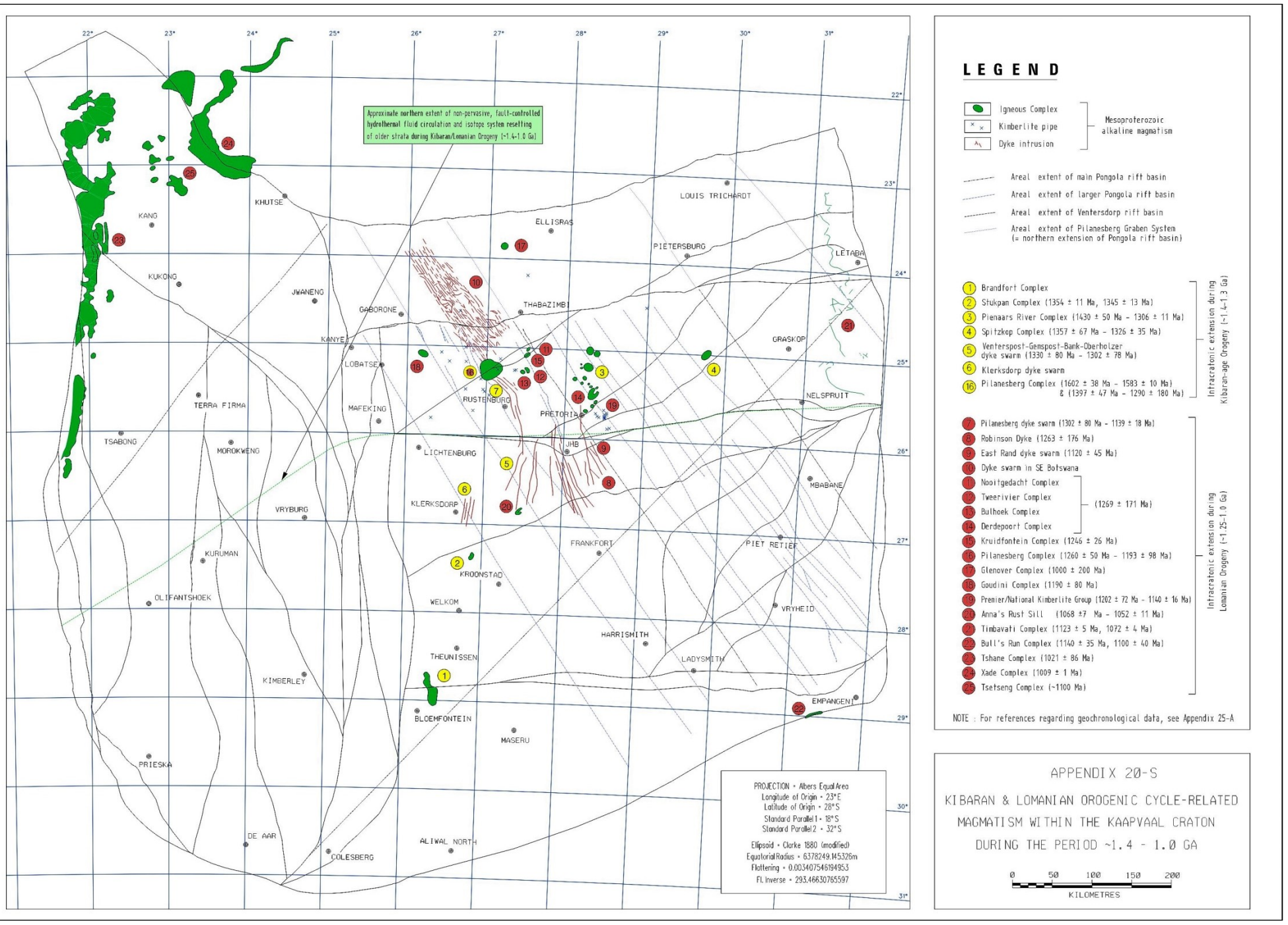


APPENDIX 20-R

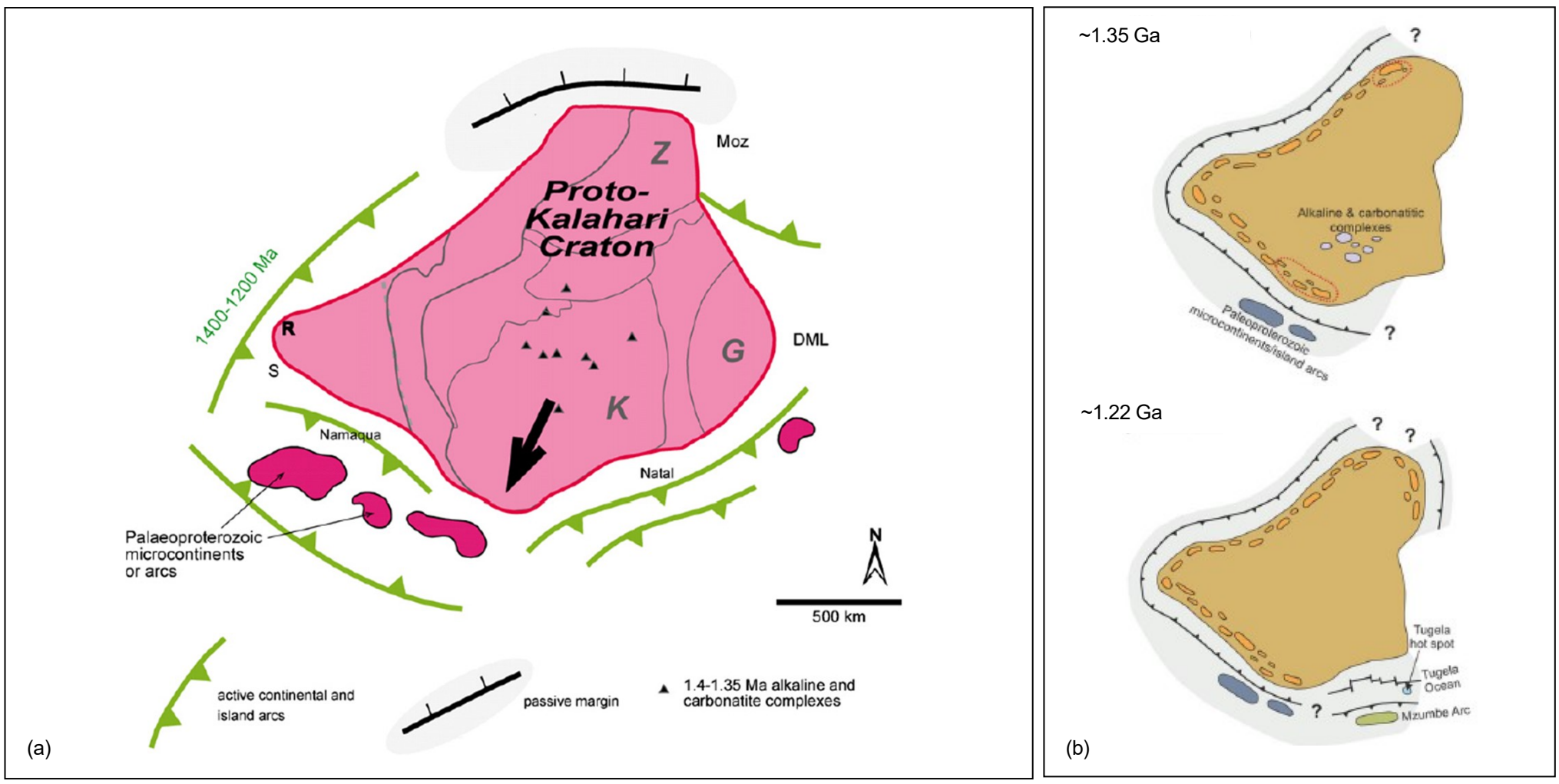
GEODYNAMIC EVOLUTION OF SOUTHERN AFRICA DURING THE PERIOD ~1.73 - 1.4 GA

0 50 100 150 200
KILOMETRES

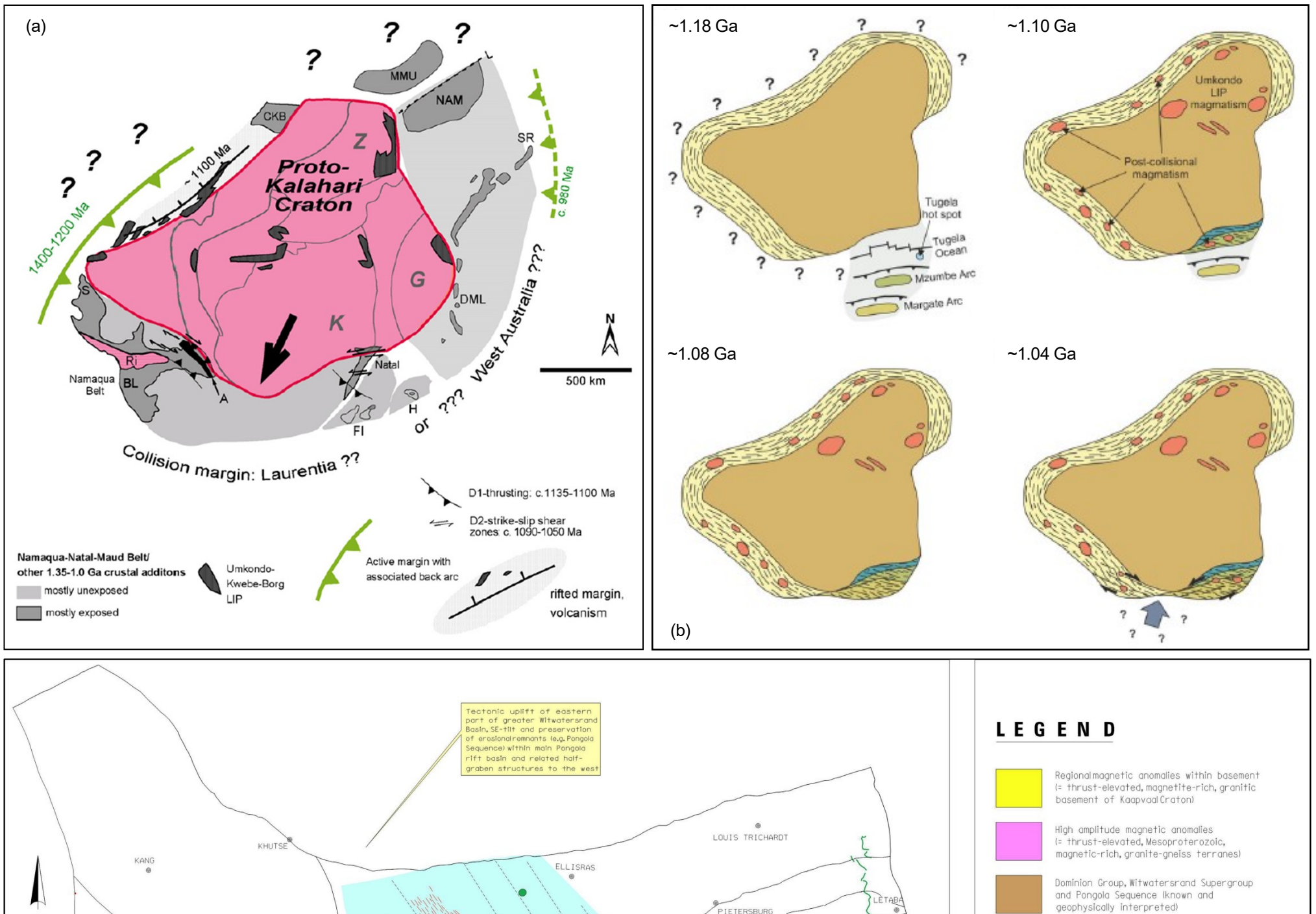


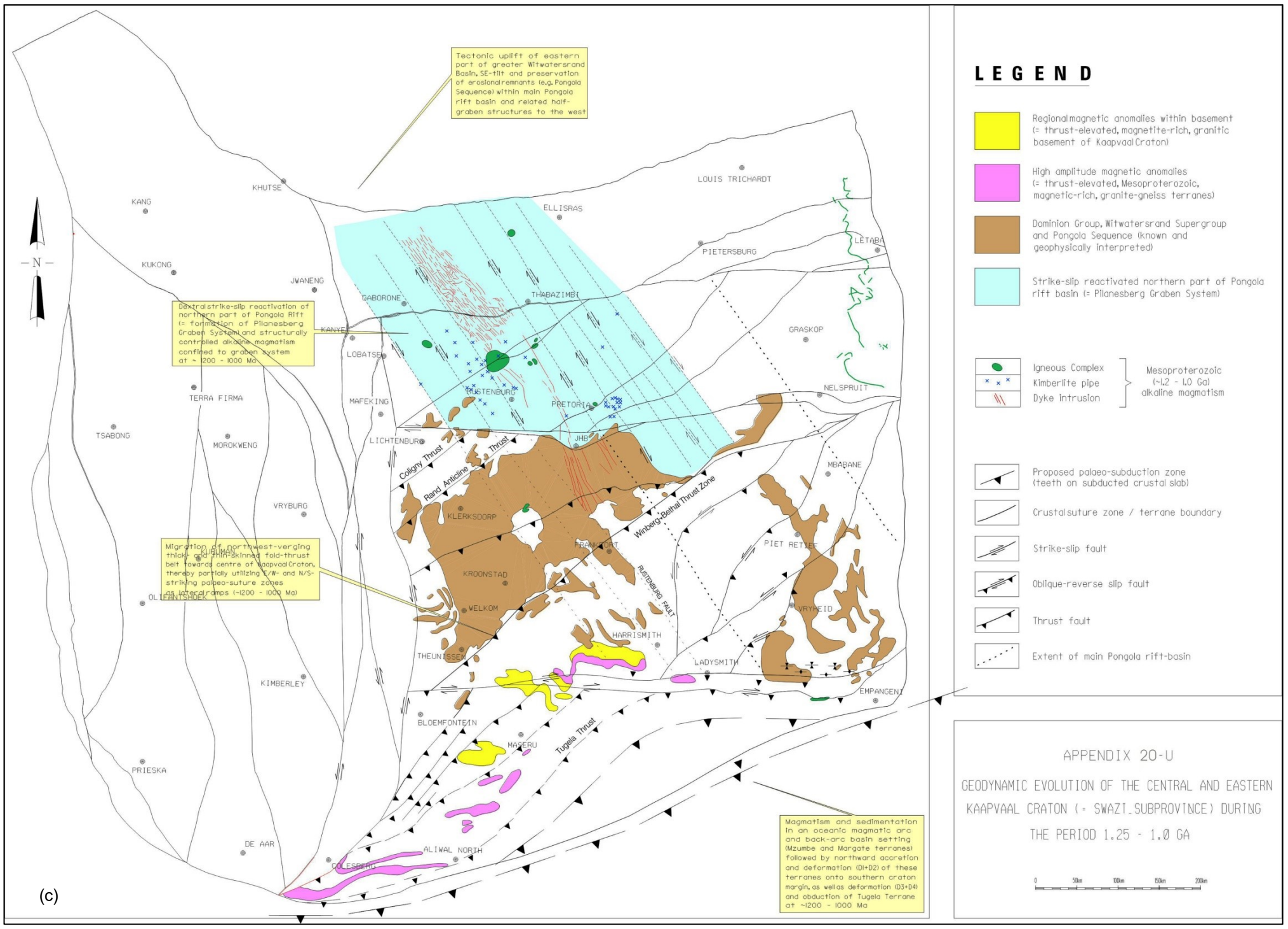


APPENDIX 20-S : Kibaran (~1.4-1.25 Ga) and Lomanian (~1.2-1.0 Ga) Orogenic Cycle-related magmatism within the Kaapvaal Craton. (a) Mesoproterozoic intraplate magmatic rocks in the Kalahari Craton in southern Africa and Dronning Maud Land, Antarctica (restored to pre- Mesozoic position after Reeves *et al*., 2002) (Hanson *et al*., 2006). Present-day coordinates are shown for Africa. Covered tectonic boundaries: 1: edge of Archaean cratonic basement; 2: boundary between Palaeoproterozoic terrains and Northwest Botswana Rift; 3: boundaries between Mesoproterozoic and Pan-African orogens. Alkaline and carbonatitic complexes: BR: Bull's Run; CR: Crocodile River complexes; G: Glenover; Go: Goudini; M: Martin's Drift kimberlite cluster; P: Premier kimberlite cluster; Pi: Pilanesberg; PR: Pienaars River complexes; Sp: Spitskop; St: Stukpan. Inferred extent of Umkondo Igneous Province shown by bold dashed lines. Known or probable members of Umkondo Province: B: dolerite at Barnardskop; De: Deweras and associated dykes in Guruve area; K: Kamativi dykes; Ka: Kartatsaus, Langberg and Skumok rhyolites and Opdam basalts; Mu: Mutare dykes; OP: Oorlogsende Porphyry; R: Rakops Dyke; Ro: rhyolite at Rostock massifs; TiG: Timbavati Gabbro; UD: dolerite dyke correlated with Umkondo dolerites by Wilson *et al*. (1987) and Allsopp *et al*. (1989b); V: dolerite intruding Vredefort Dome. Deweras and associated dykes and Kamativi and Mutare dyke suites are shown schematically; all three dyke suites may contain dykes unrelated to Umkondo Province, as discussed in text. Other labelled features: A: Amersfoort; DI: Dete Inlier; KC: Archaean Kaapvaal Craton; KH: Kgwebe Hills; Ko: Koras Group; ODS: Okavango Dyke Swarm; OI: Okwa Inlier; ORDS: Olifants River Dyke Swarm; Ph: Phoenix leucogranites; ZC: Archaean Zimbabwe Craton. Locations of boreholes CKP-8C in Tshane Complex, CKP-6 and 6A in Xade Complex, CKP-4 in Kgwebe Formation and CKP-10A in subsurface gabbro farther west are also shown. Modified from Hanson *et al*. (1998) and references therein. Distribution of Umkondo mafic intrusions from Mortimer (1984), Zimbabwe Geological Survey (1994) and Keyser (1997). (b) Distribution of the Mesoproterozoic Umkondo Group and Umkondo-related volcanics, shallow intrusions, sills and dykes, and magmatic centres as defined by Umkondo dykes (De Kock *et al*., 2014). (c) Kibaran (~1.4 - 1.25 Ga) and Lomanian (~1.2 - 1.0 Ga) Orogenic Cycle-related magmatism within the Kaapvaal Craton (Friese *et al*., 1995 & this study).

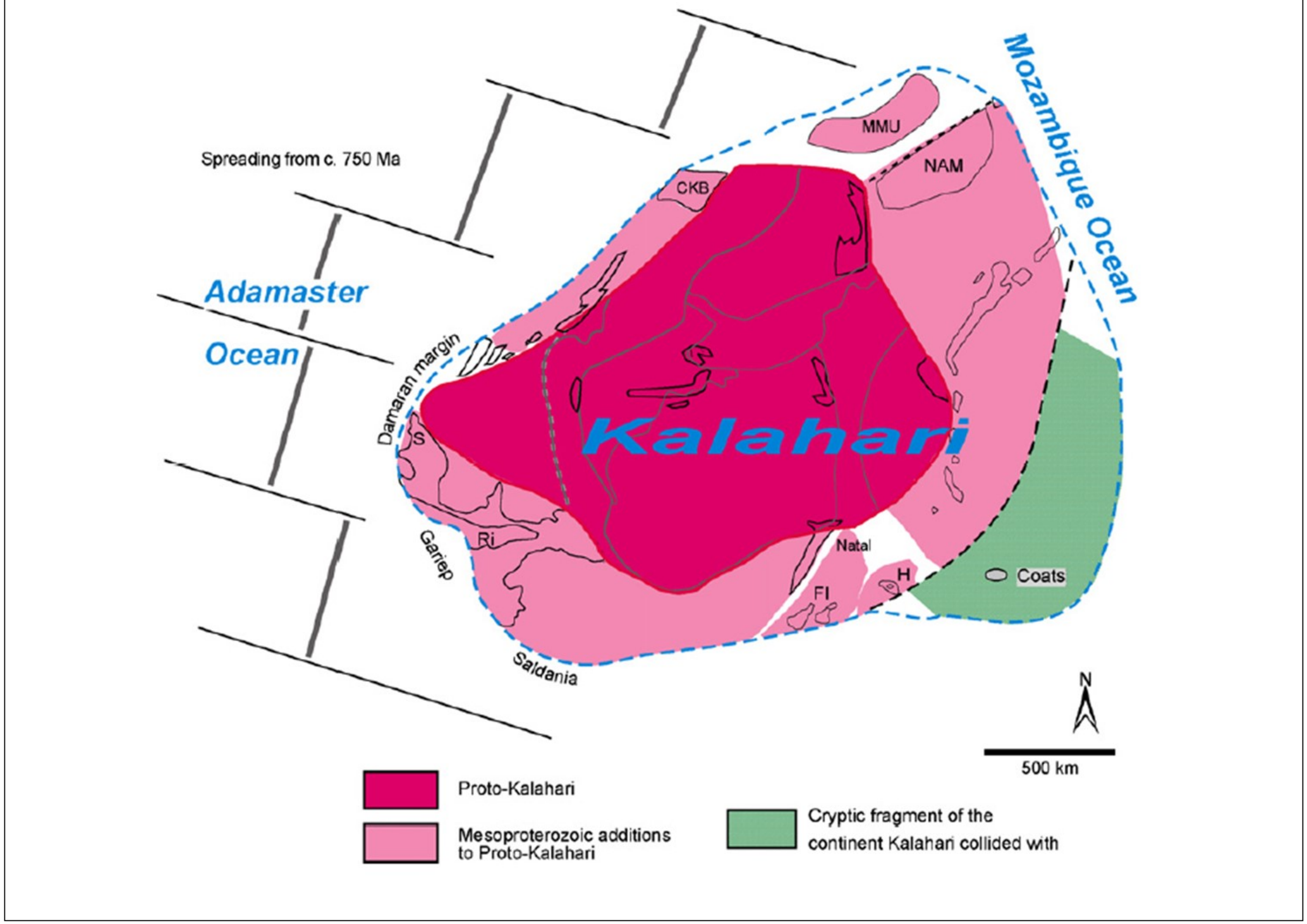


APPENDIX 20-T : Geodynamic evolution of the proto-Kalahari Craton during the period ~1.4-1.25 Ga. (a) Passive and active continental margin and island arc terrane development around proto-Kalahari Craton at ~1.4-1.2 Ga, followed by northwestward accretion of island arcs and Palaeoproterozoic microcontinents along the craton's southern margin at ~1.2-1.08 Ga (Jacobs *et al*., 2008). Abbreviations: G, Grunehogna Craton; DML, Dronning Maud Land; K, Kaapvaal Craton; Moz, northern Mozambique; R, Rehoboth; S, Sinclair; Z, Zimbabwe Craton. Black triangles refer to Mesoproterozoic intraplate alkaline to carbonatite intrusions at ca. 1.3 Ga (after Hanson *et al*., 2006). (b) Schematic Mesoproterozoic tectonic evolution of the proto-Kalahari Craton at ~1.35-1.2 Ga (Oriolo & Becker, 2018; modified after Watters (1976), Hoal (1990), Jacobs & Thomas (1994), Kampunzu *et al*. (1998), Becker *et al*. (2005, 2006), McCourt *et al*. (2006), Jacobs *et al*. (2008), Miller (2008), and Spencer *et al*., 2015). Note: Subduction along the margin of the proto-Kalahari Craton at ~1.35-1.22 Ga. Red dashed lines indicate areas where it is unclear whether magmatism was arc- or extension-related (northeastern area: Choma-Kalomo Block, southwestern area: Namaqua Belt). Coeval alkaline and carbonatitic complexes are recorded at ~1.4-1.35 Ga in the southern proto-Kalahari Craton (Hanson *et al*., 2006). (c) Geodynamic evolution of the Kaapvaal Craton during the Kibaran Orogeny at ~1.35-1.25 Ga (this study).

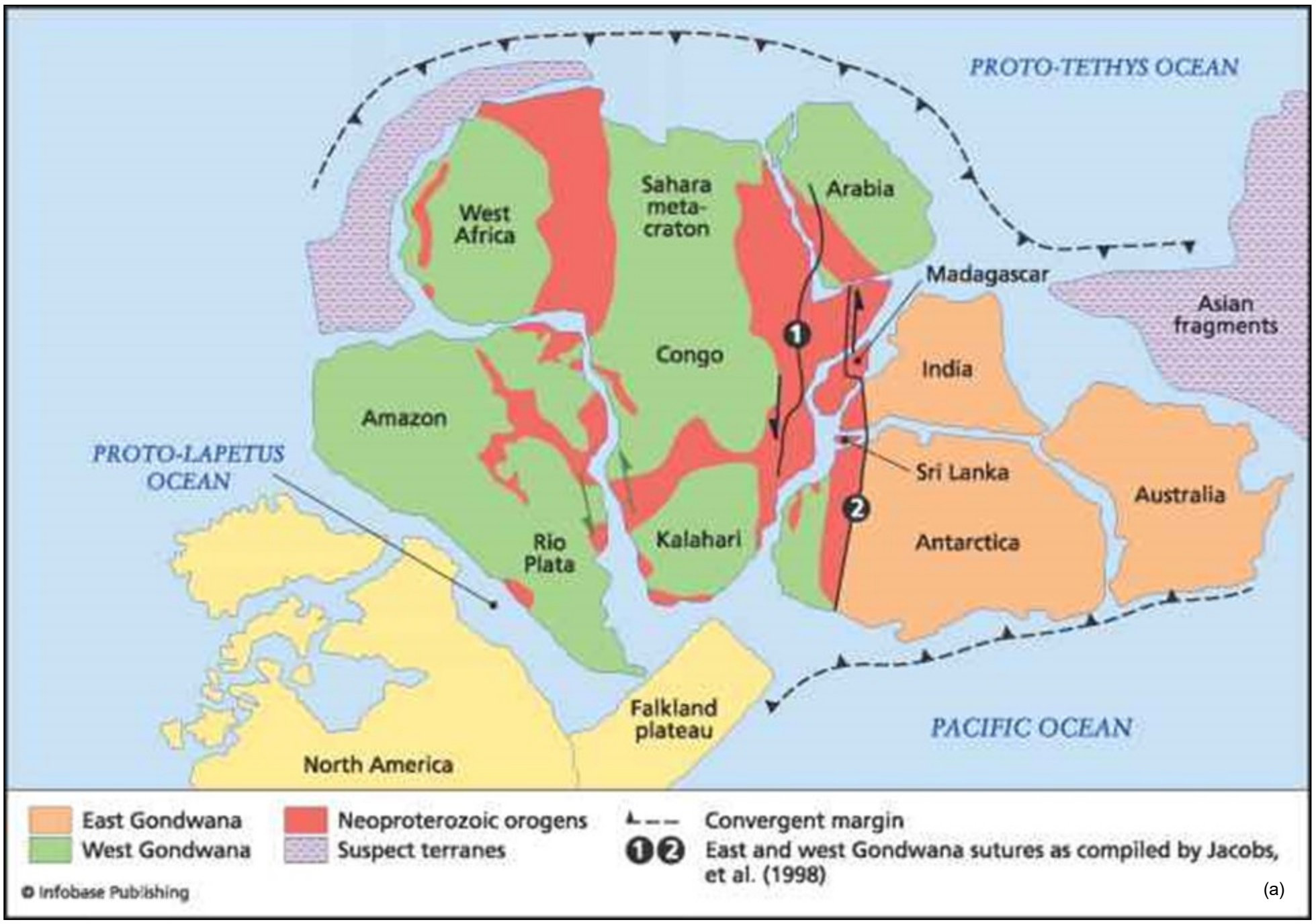


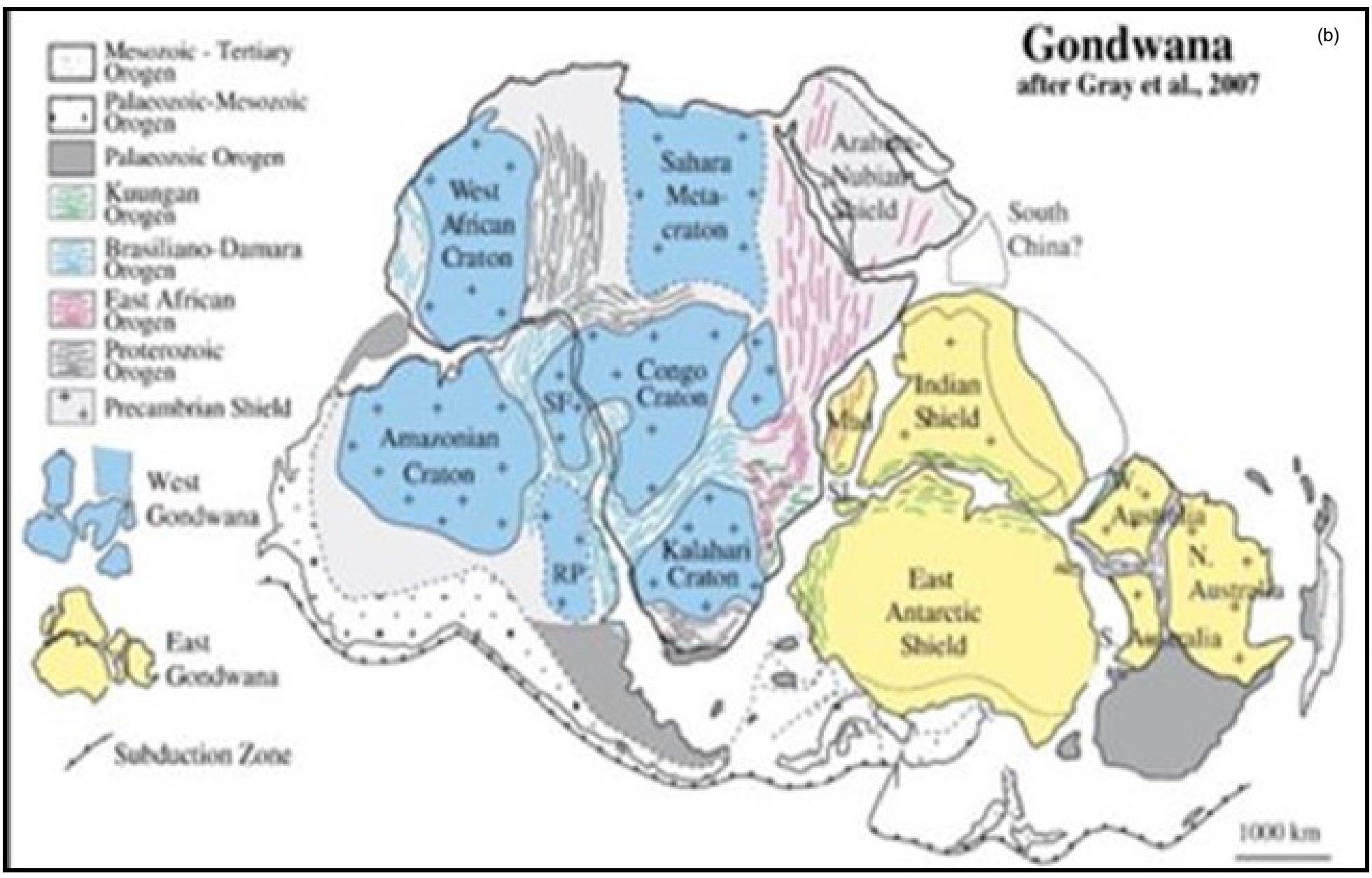


APPENDIX 20-U : **Geodynamic evolution of the Kalahari Craton during the period ~1.2-1.0 Ga.** (a) Geodynamic development of the Kalahari Craton at 1135-1050 Ma (Jacob *et al*., 2008). Subsequent to active margin development along the northwestern craton margin and emplacement of the Umkondo-Kwebe-Borg large igneous province, collision and indentation tectonic processes continued along the southern craton margin. Whilst large amounts of juvenile crust had accreted along the SE, E and NW margins, major components of older crust were accreted along the Namaqua Belt. Abbreviations: A, Areachap terrane; BL, Bushmanland Terrane; CKB, Choma-Kaloma Block; FI, Falkland Islands; G, Grunehogna Craton; DML, Dronning Maud Land; H, Haag Nunatak; K, Kaapvaal Craton; L, Lurio Belt; MMU, Marupa–Malawi–Unango terrane; NAM, Nampula Province; S, Sinclair; SR, Sør Rondane; R, Rehoboth; Ri, Richtersveld; Z, Zimbabwe Craton. (b) Schematic Mesoproterozoic tectonic evolution of the proto-Kalahari Craton at ~1.22-1.04 Ga(Oriolo & Becker, 2018; modified after Watters (1976), Hoal (1990), Jacobs & Thomas (1994), Kampunzu *et al*. (1998), Becker *et al*. (2005, 2006), McCourt *et al*. (2006), Jacobs *et al*. (2008), Miller (2008), and Spencer *et al*., 2015). Note: Widespread deformation and metamorphism during the collisional phase of the Namaqua Orogeny at ~1.22-1.1 Ga along the SW margin of Kalahari Craton, while subduction continued along SE craton margin. Post-collisional magmatism coeval with the Umkondo LIP magmatism at ~1.1 Ga. Post-collisional magmatism after the obduction of the Tugela ophiolite and the accretion of the Mzumbe Terrane at ~1.1-1.08 Ga. Accretion of the Margate Terrane in the Natal Belt at ~1.08-1.04 Ga. Strike-slip deformation along the Namaqua-Natal Belt at ~1.04-1.0 Ga. (c) Geodynamic evolution of the Kaapvaal Craton during the Lomanian Orogeny at ~1.2-1.0 Ga (this study).

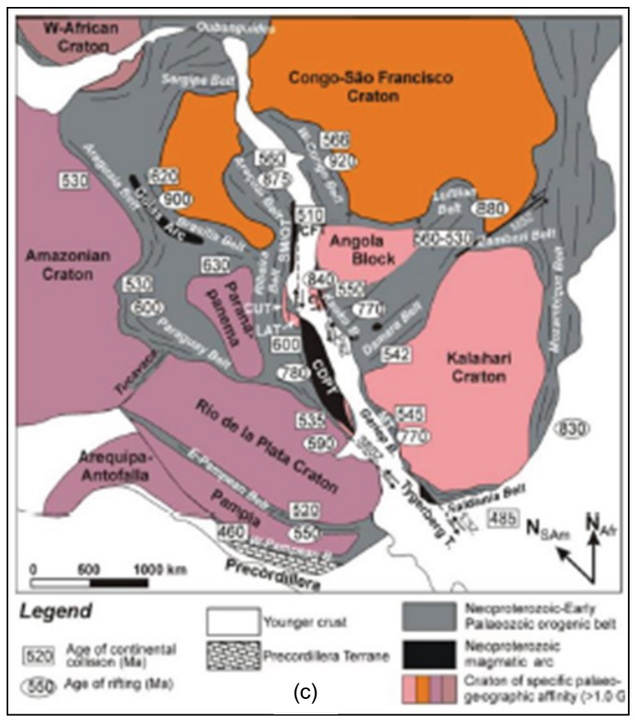


APPENDIX 20-V : **Geodynamic evolution of the Kalahari Craton during the period ~900-700 Ma (Jacob *et al.*, 2008).** Breakup of supercontinent Rodinia and rifting of Kalahari Craton from Rodinia at ~0.9-0.7 Ga. A fragment of the colliding counterpart of Kalahari (Laurentia?, Australia?) remained attached and is now possibly preserved in Coats Land (East Antarctica). Abbreviations: CKB, Choma Kaloma Block; FI, Falkland Islands; H, Haag Nunatak; L, Lurio Belt; MMU, Marupa–Malawi–Unango terrane; NAM, Nampula Province; S, Sinclair; Ri, Richtersveld.

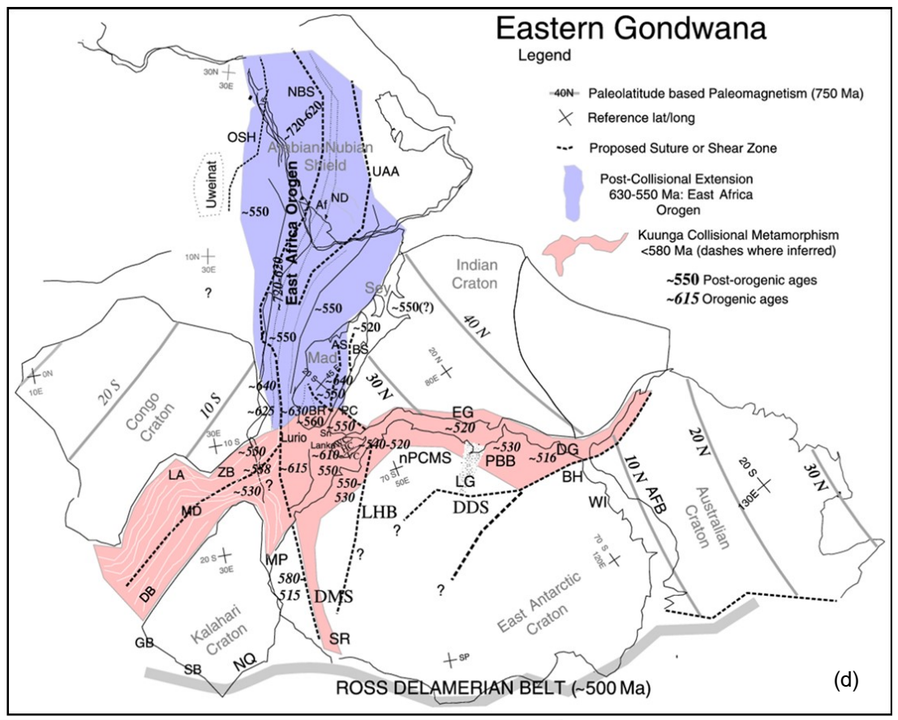




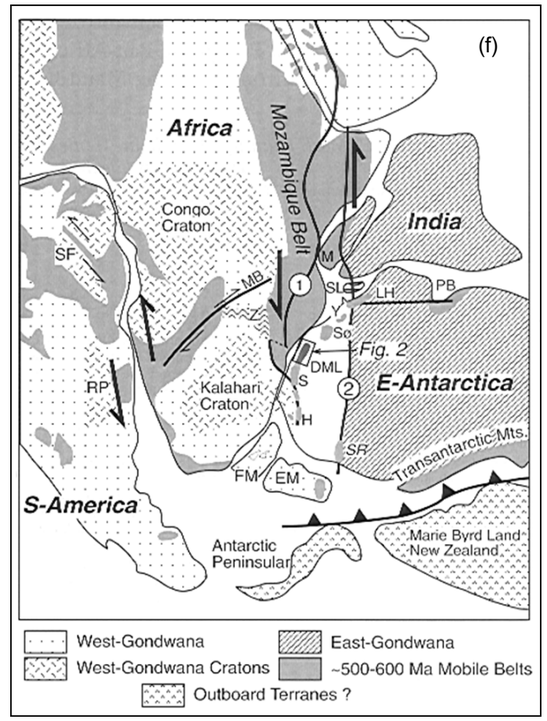
APPENDIX 20-W : Geodynamic evolution of supercontinent Gondwana during the period~650-450 Ma. Palaeo-reconstructions of the supercontinent Gondwana after (a) Kusky *et al*. (2003) and (b) Grey *et al*. (2007), illustrating continental components and Neoproterozoic orogenic belts, the latter formed as a result of successive continental collisions and amalgamations during the Pan-African orogenic event at ~640-480 Ma.

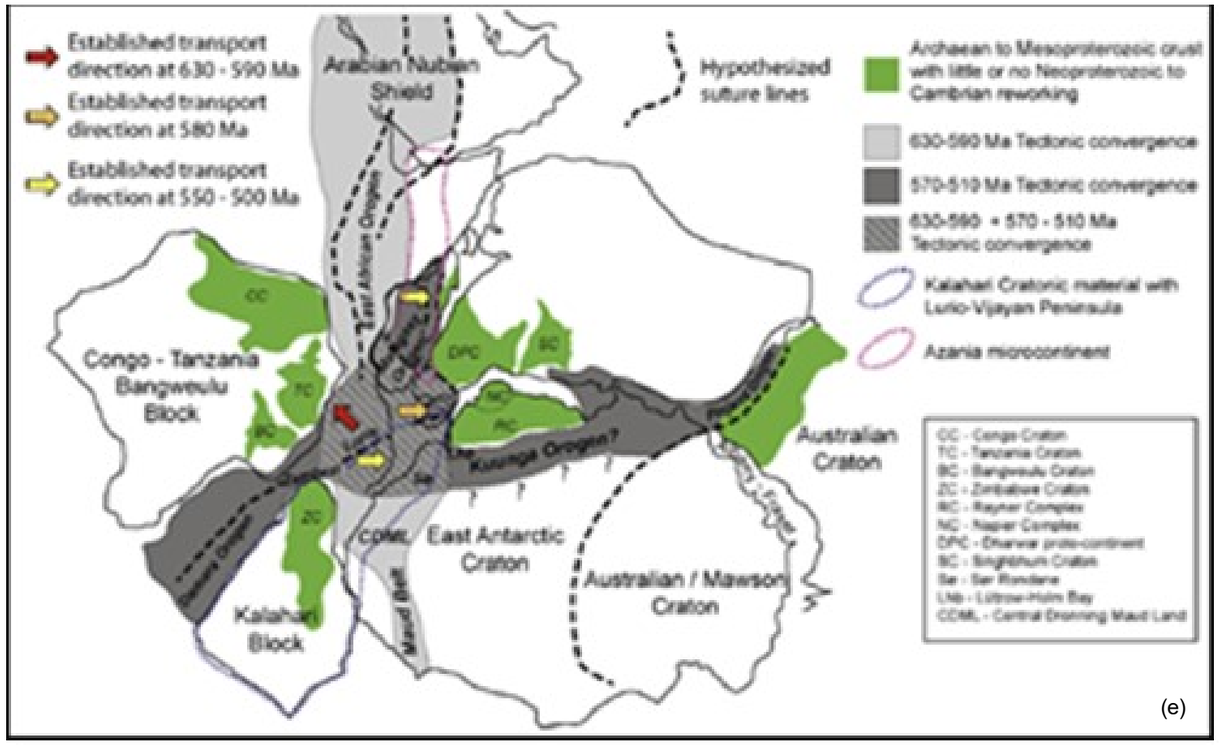


(c)

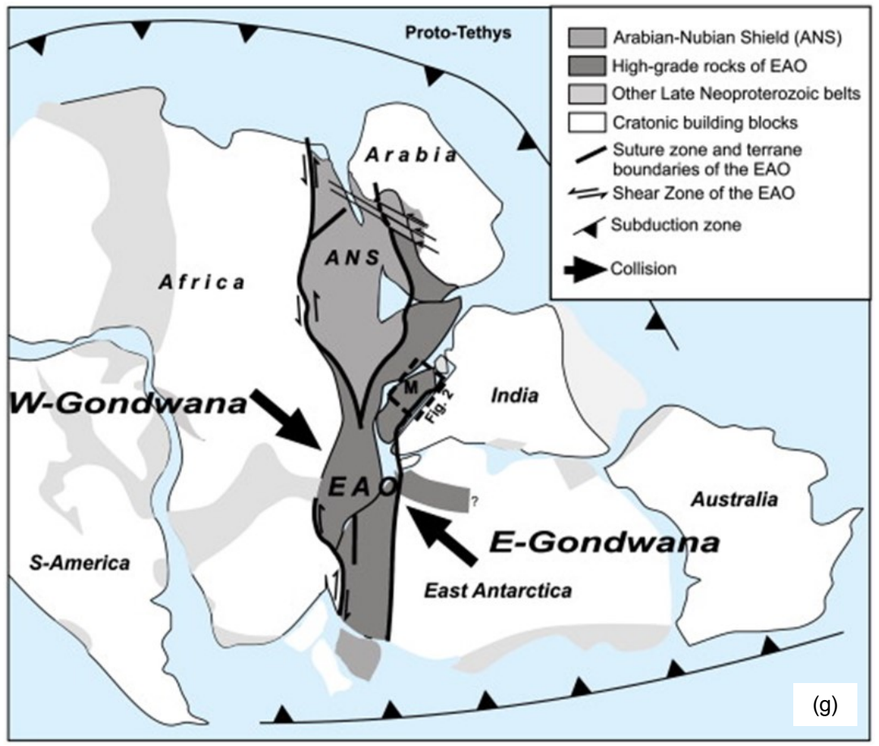


(d)



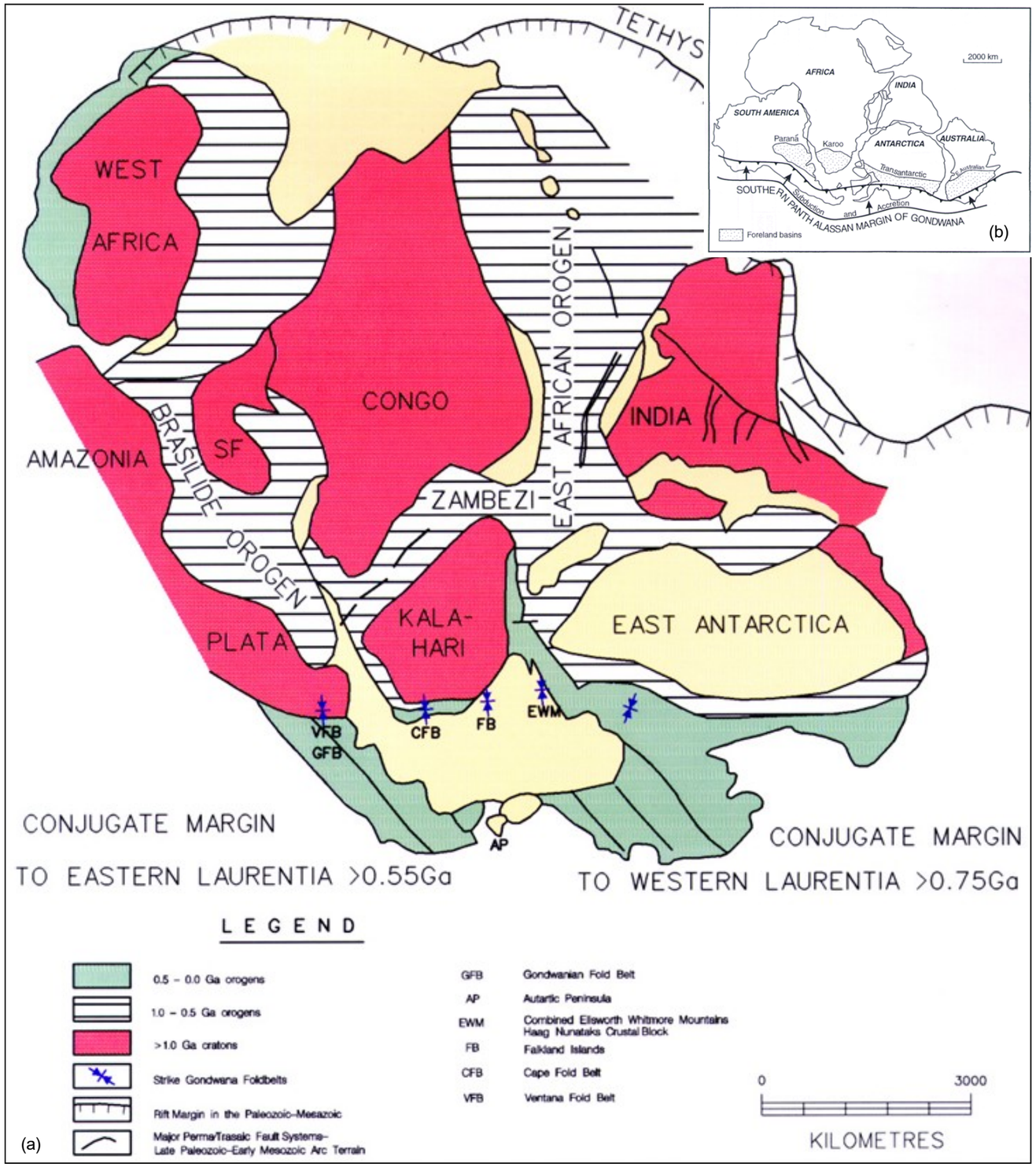


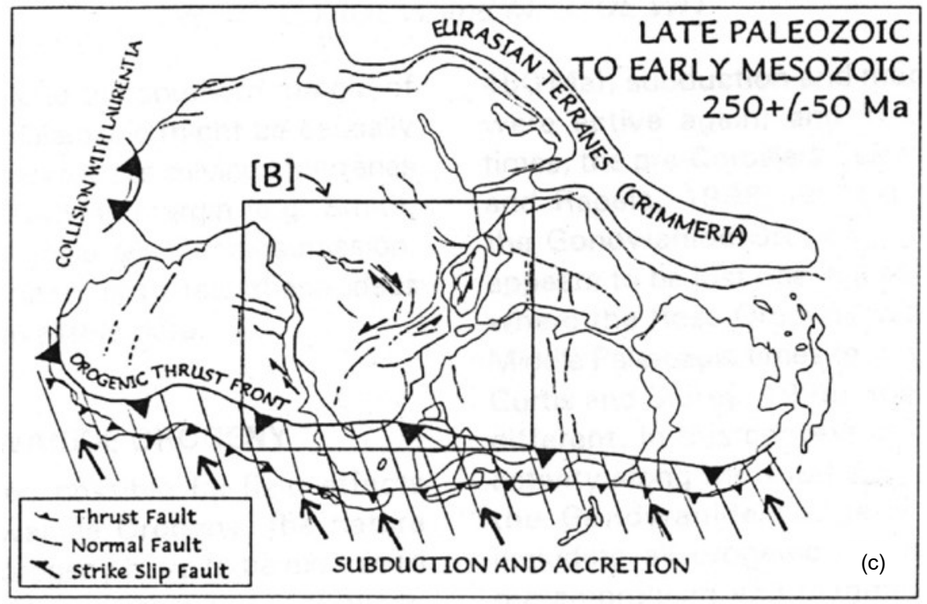
(e)

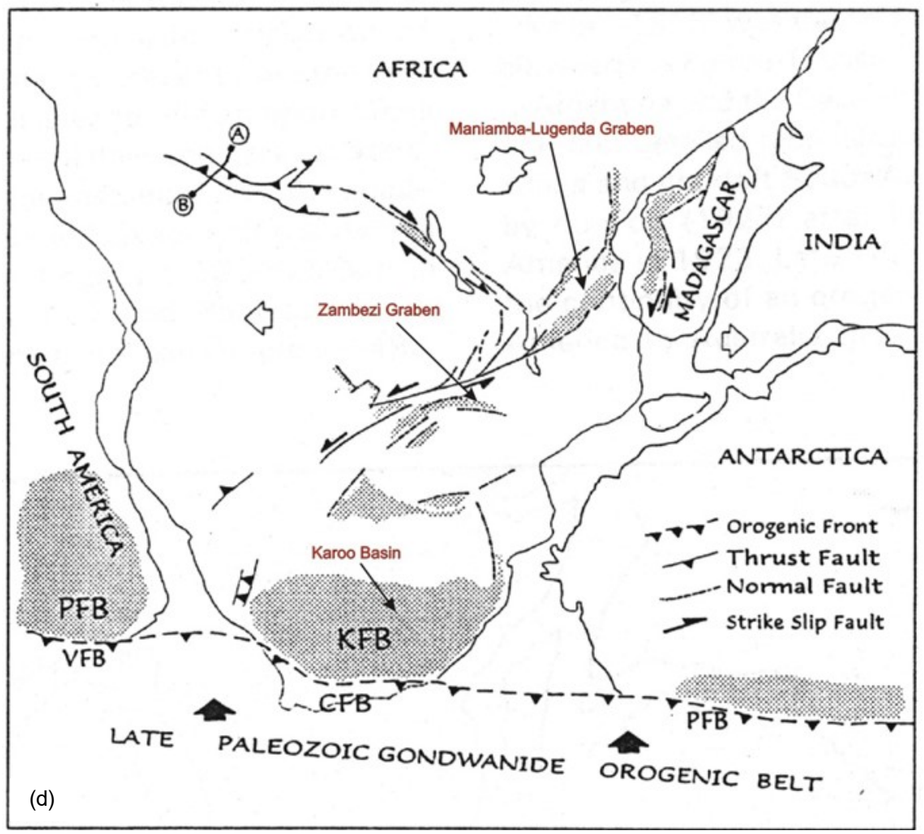


(g)

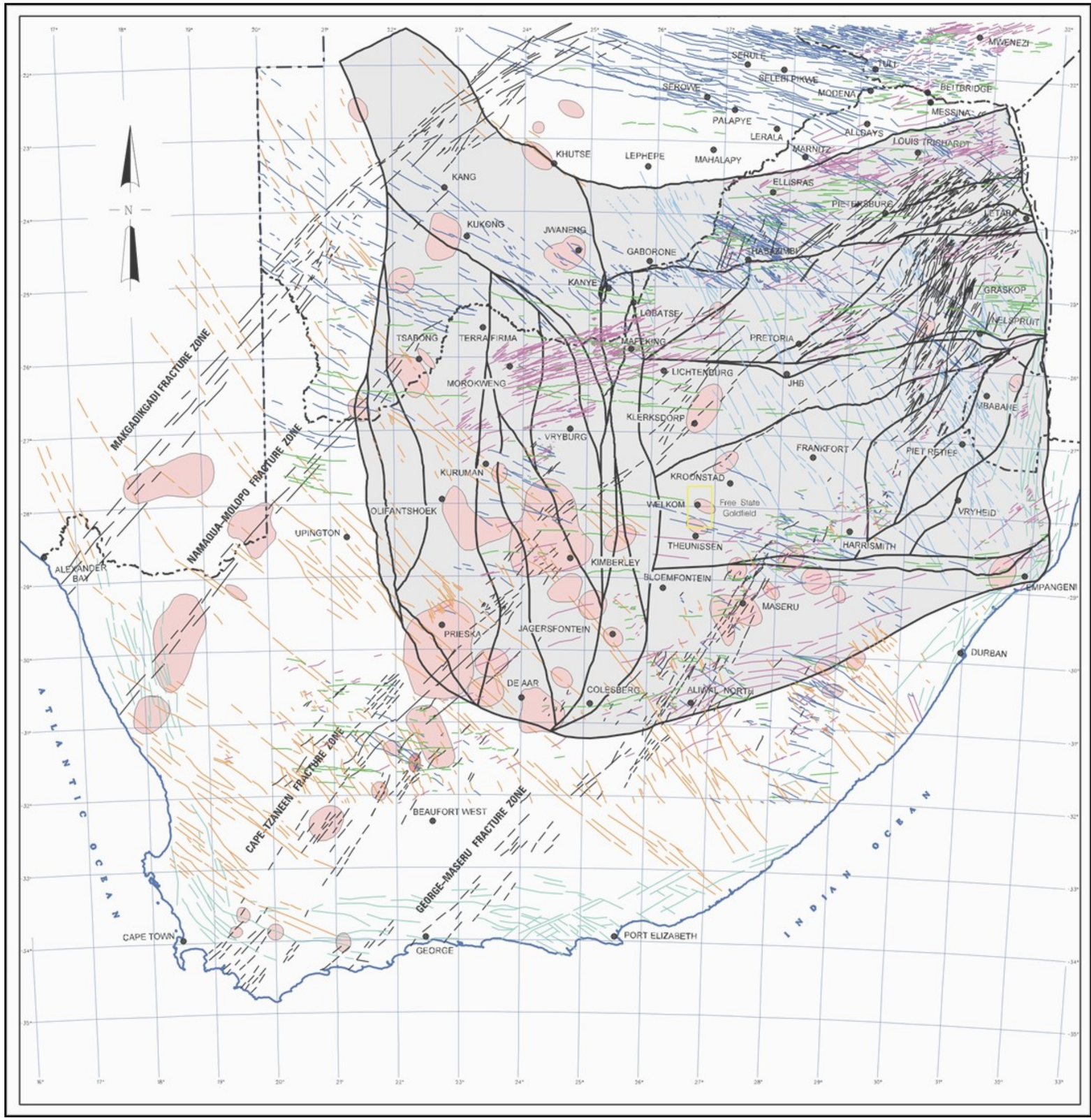
APPENDIX 20-W : **Geodynamic evolution of supercontinent Gondwana during the period~640-480 Ma (continued).** Palaeo-reconstructions of the supercontinent Gondwana after (c) Gaucher *et al*. (2009) and (d) Meert (2003), illustrating continental components and Neoproterozoic orogenic belts, the latter formed as a result of successive continental collisions and amalgamations during the Pan-African orogenic event at ~640-480 Ma. (f & g) Late Pan-African final docking of the three lithospheric plates during the Ross-Delamarian Orogeny at ~500-480 Ma induced NW-directed compressive far field stress into Gondwana, which caused the sinistral strike-slip reactivation of the East Africa-Antarctica Orogen and West Congo-Kaoko-Gariep-Saldania Orogen and sinistral transtensional tectonic (Jacobs & Thomas, 2004; Thomas *et al*., 2009).

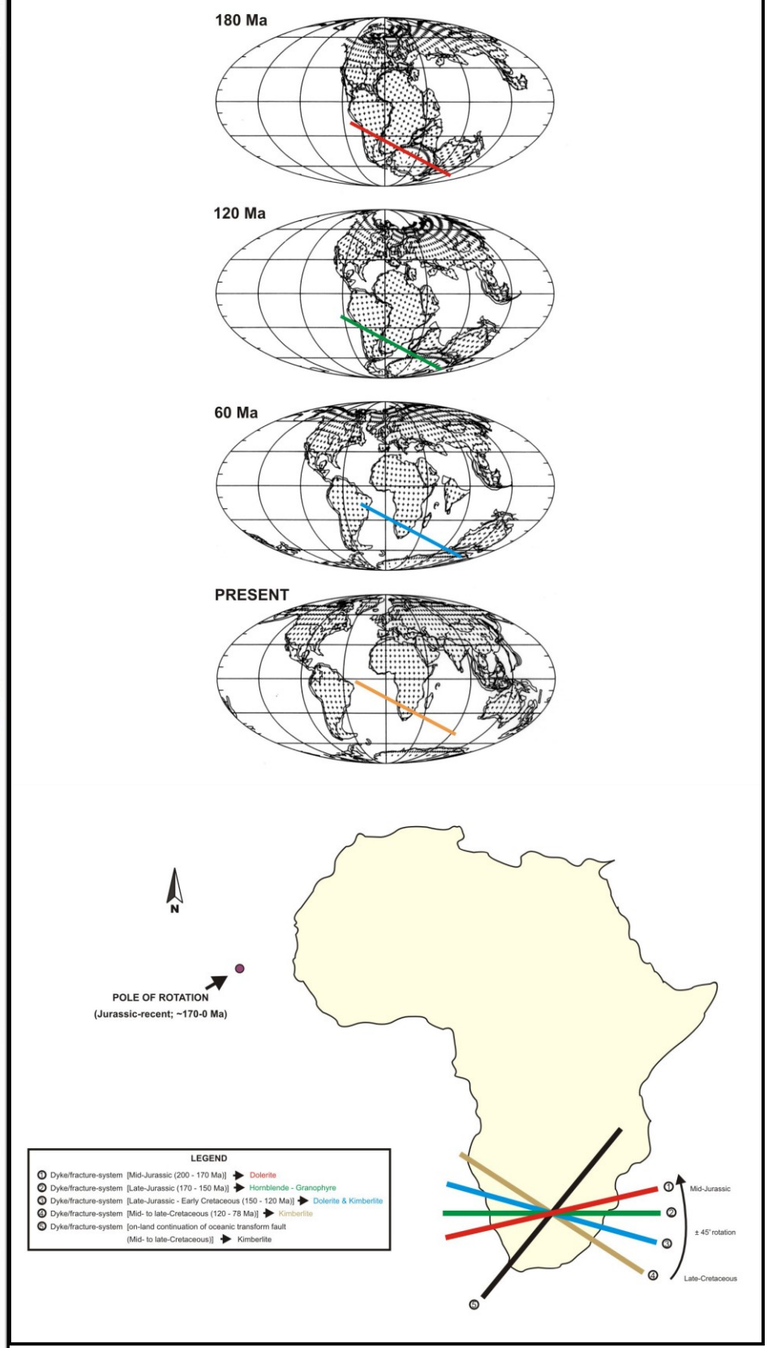




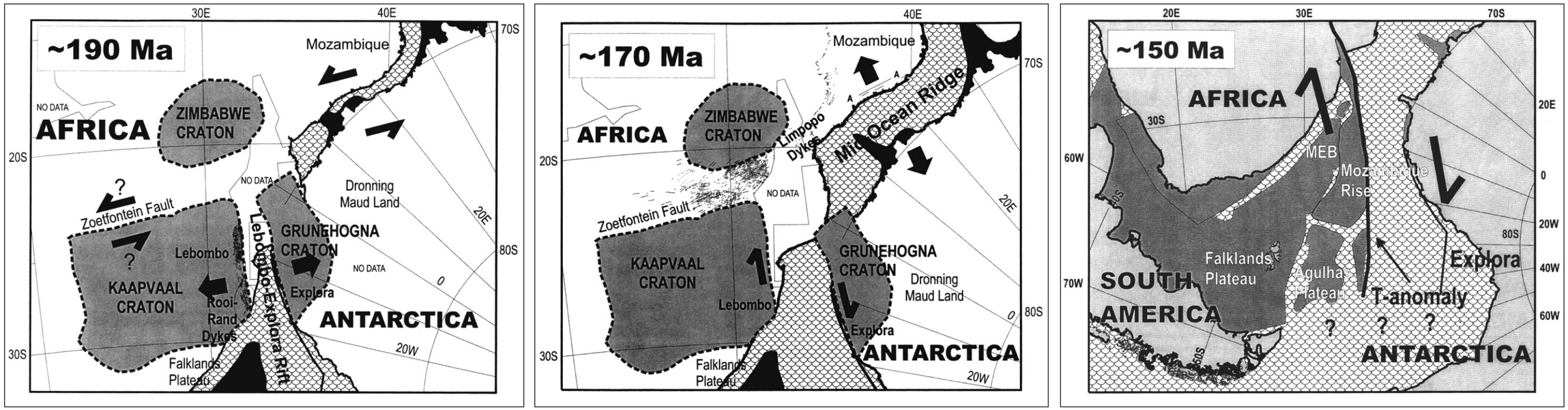


APPENDIX 20-X : Geodynamic evolution of supercontinent Gondwana during the period ~290-215 Ma. (a) Gondwana reconstruction at ~0.5 Ga showing the distribution of Pan-African mobile belts (~0.8-0.5 Ga) and older shields (modified after Trouw & De Wit, 1999); (b) Palaeoreconstruction of the Gondwanide Orogen and related foreland basins within the southern Gondwana supercontinent (De Wit, 1992). (c) Schematic diagram showing large-scale Late Palaeozoic fracturing of the Gondwana lithosphere. The orientation of the various fault systems is compatible with stress induced failure due to 'impact' tectonics along the southern margin of Gondwana during terrane accretion (modified by Trouw & De Wit (1999) from de Wit & Ransome (1992)). (d) Gondwana reconstruction showing the major Permo-Triassic structures of central Africa and adjacent Madagascar. Note the mixture of normal, strike-slip and thrust structures. Stippled areas are Permo-Triassic ("Karoo") foreland basin and rift sedimentation (modified by Trouw & De Wit (1999) from Daly *et al.* (1991)).





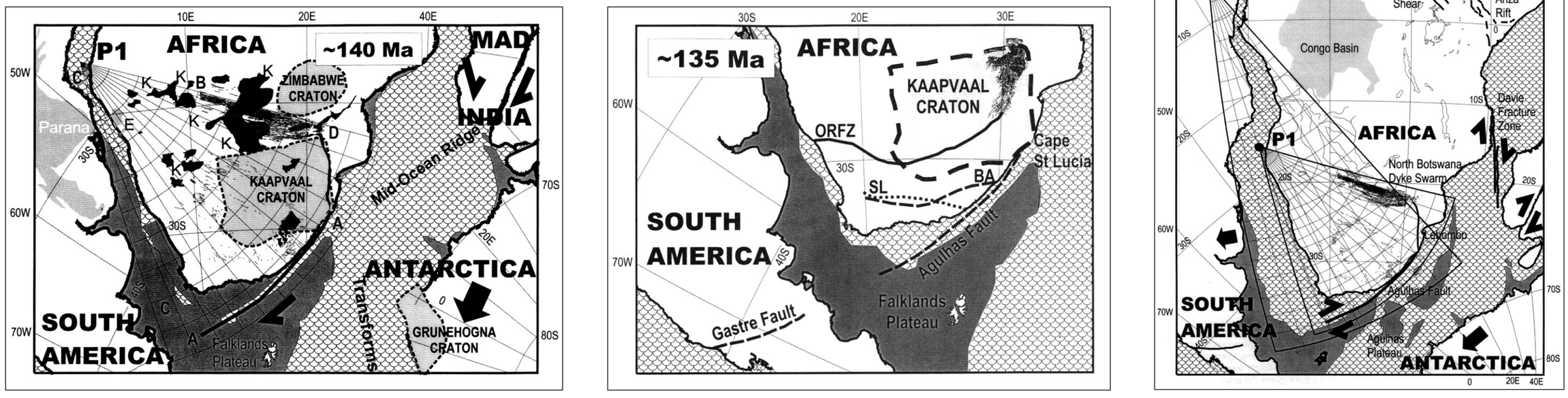
APPENDIX 20-Y: Geodynamic evolution of southern Africa during the period ~200-80 Ma. (a) Successive development of extensional-transtensional fault/fracture and dyke systems across Southern Africa during the Mesozoic (Friese, 1998b). Note: Kaapvaal Craton (grey shaded area), craton-internal Archaean suture zones (solid black lines), Jurassic-Cretaceous kimberlite fields/clusters (red-shaded areas). (b) Proposed sequential development of extensional fault/fracture zones and associated emplacement of dykes across the southern African continent in response to Gondwana supercontinent break-up and dispersal tectonics at ~200-80 Ma (Friese, 1998b).



(a) (b) (c)

LEGEND: Dark grey = Archaean craton; Black = plateau; Pillow pattern = juvenile ocean floor; Light grey = sub-marine crustal fragment (*e.g.* Falklands Plateau); K = basalt (geophysically interpreted Karoo beneath Kalahari sand cover); E = Etendeka basalt/Namibia; B–D = Botswana/Okawango dyke swarm

All diagrams in orthographic projection centred at 25^0S, 35^0E (a & b), 30^0S, 35^0E (c), 25^0S, 30^0E (d), 24^0S, 25^0E (e) and 10^0S, 20^0E (f).



(d) (e) (f)

APPENDIX 20-Z: Geodynamic evolution of southern Africa during the period ~190-120 Ma. Palaeogeographic time-slice interpretation maps, illustrating sequential rifting and drifting stages in the geodynamic evolution of southern Gondwana during the Mesozoic (after Reeves, 2000): (a) E-W rifting, development of the first rupture (= Lebombo-Explora Rift) and separation of Grunehogna Province from Kaapvaal Craton, accompanied by the intrusion of rift-parallel dykes (*e.g.* Rooi Rand dykes) between East and West Gondwana in early Jurassic time; (b) N-S drifting succeeds E-W rifting as West Gondwana starts to rotate anti-clockwise with East Gondwana moving south along the Davie Fracture Zone, causing a transtensional regime in the Lebombo-Explora Rift and opening of the Mozambique proto-Ocean with associated intrusion of Limpopo dykes in mid-Jurassic time; (c) - (e) N-S motion of East Gondwana becomes clockwise rotation (about an Euler pole (P1) west of southern Africa) around southern Africa, utilising initially the T-anomaly later the Agulhas fault for dextral strike-slip of Antarctica against Africa in Late Jurassic to Early Cretaceous time. Orange River fracture zone (= precursor to Agulhas fault) serves as a line of some stress release. Initiation of South Atlantic rifting/opening accompanied by the extrusion of Etendeka and Paraná basalts in Namibia and Brazil respectively, intrusion of coast/rift-parallel dykes, Okavango dyke swarm and sigmoidal dykes in northernmost South Africa; (f) Rifting and drifting propagate northwards through the southern Atlantic in Early Cretaceous time, while dextral strike-slip motion of the Falkland Plateau and Antarctica with respect to Africa continues along the Agulhas fault and intracontinental extensional/transtensional rifting takes place within the African continent.

APPENDIX 21

SUMMARY OF SELECTED GEOCHRONOLOGICAL DATA PERTINENT TO SOUTHERN AFRICA, WESTERN AUSTRALIA, INDIA AND EAST ANTARCTICA

APPENDIX 21-A : Summary of selected geochronological data pertinent to the Kaapvaal Craton

APPENDIX 21-B: Summary of selected geochronological data pertinent to the Zimbabwe Craton

APPENDIX 21-C : Summary of selected geochronological data pertinent to the Limpopo Central Zone Terrane

APPENDIX 21-A: Summary of selected geochronological data pertinent to the Kaapvaal Craton.

Period	Reference	Lithology / Locality	Age (Ma)	Method	Interpretation by author(s)
SWAZI TERRANE [PALAEO- / MESOARCHAEAN (~3.7-3.1 Ga)]	Kröner *et al.* (1996)	Weakly foliated porphyritic granodiorite (Vlakplaats Granodiorite) / Ancient Gneiss Complex (Swaziland)	3702 ± 1	Pb-Pb evapor.; zircon	Xenocrysts = age of source rock
	Kröner & Tegtmeyer (1994)	Tonalitic gneiss (Ngwane Gneiss) / Ancient Gneiss Complex (Swaziland)	3683 ± 10 3490 ± 3	U-Pb; zircon Pb-Pb evapor.; zircon	Xenocrysts = age of source rock Formation/crystallization age of igneous protolith
	Compston & Kröner (1988)	Banded tonalitic gneiss (Ngwane Gneiss) / north of Piggs Peak, Ancient Gneiss Complex (Swaziland)	3644 ± 4 ~4200 – 3800 3504 ± 6	U-Pb; zircon Sm-Nd; T_{DM} whole-rock U-Pb; zircon	Formation/crystallization age of igneous protolith Age of crust into which igneous protolith intruded Age of recrystallisation/metamorphism
	Kröner *et al.* (1989)	Banded tonalitic gneiss (Ngwane Gneiss) / south of Tshaneni, Ancient Gneiss Complex (Swaziland) Tonalitic gneiss (Ngwane Gneiss) / Ngwempisi River, Ancient Gneiss Complex (Swaziland) Banded leucocratic gneiss (Ngwane Gneiss) / Ancient Gneiss Complex (Swaziland) Tsawela tonalitic gneiss / Ancient Gneiss Complex (Swaziland)	3505 ± 24 3563 ± 3 3455 ± 22 3458 ± 3 – 3436 ± 6, 3362 ± 22 ~3700 - 3500	U-Pb; zircon U-Pb; zircon U-Pb; zircon Pb-Pb evapor.; zircon Sm-Nd; T_{DM} whole-rock	Formation/crystallization age of igneous protolith Formation/crystallization age of igneous protolith Formation/crystallization age of igneous protolith Formation/crystallization age of igneous protolith Age of crustal source rock
	Wendt (unpubl.) in Kröner *et al.* (1991)	Banded tonalitic gneiss (Ngwane Gneiss) / Ancient Gneiss Complex (Swaziland) Banded tonalitic gneiss (Ngwane Gneiss) / Ancient Gneiss Complex (Swaziland) Banded tonalitic gneiss (Ngwane Gneiss) / Ancient Gneiss Complex (Swaziland) Banded tonalitic gneiss (Ngwane Gneiss) / Ancient Gneiss Complex (Swaziland) Banded tonalitic gneiss (Ngwane Gneiss) / ENE of Mankayane, Ancient Gneiss Complex (Swaziland) Banded tonalitic gneiss (Ngwane Gneiss) / Ancient Gneiss Complex (Swaziland) Banded trondhjemitic gneiss (Ngwane Gneiss) / Ancient Gneiss Complex (Swaziland) Foliated granitoid gneiss (Ngwane Gneiss) / Ancient Gneiss Complex (Swaziland) Trondhjemitic gneiss (Tsawela Gneiss) / Ancient Gneiss Complex (Swaziland) Deformed Mpuluzi granite / Ancient Gneiss Complex (Swaziland)	3392 +74/-50 3328 +66/-53 3308 ± 34 3508 ± 3 3306 ± 6 3304 ± 11 3263 ± 97 3222 ± 15 3362 ± 22 3049 ± 25	U-Pb; zircon U-Pb; zircon U-Pb; zircon U-Pb; zircon U-Pb; zircon U-Pb; zircon U-Pb; zircon U-Pb; zircon U-Pb; zircon U-Pb; zircon	 Formation/crystallisation age
	Maphalala (1998)	Quartz-monzonite gneiss enclaves (= possibly erosional remnants of Ancient Gneiss Complex) / (Swaziland) Quartz-monzonite gneiss enclaves (= possibly erosional remnants of Ancient Gneiss Complex) / (Swaziland) Granodiorite of Usuthu Suite / south-central Swaziland	3401 ± 181 3412 ± 4 3360 ± 4	Rb-Sr; whole-rock Pb-Pb evapor.; zircon Pb-Pb evapor.; zircon	Formation/crystallisation age Formation/crystallisation age Formation/crystallisation age
	Barton *et al.* (1983d)	Granodiorite suite (gabbro – trondhjemite) / Ancient Gneiss Complex (Swaziland) Tsawela Gneiss / Ancient Gneiss Complex (Swaziland)	3350 ± 57 3323 ± 86	Rb-Sr; whole-rock Rb-Sr; whole-rock	Formation/crystallisation age; Over-estimated age Kröner *et al.*. (1991) Formation/crystallisation age; Over-estimated age (Hunter, 1991)
	Barton *et al.* (1980)	Orthogneisses of Ngwane Gneiss (Bimodal Suite) / Njoli Dam, Ancient Gneiss Complex (Swaziland)	3555 ± 110	Rb-Sr; whole-rock	Formation/crystallization age of igneous protolith
	Carlson *et al.* (1983)	Ngwane (Bimodal Suite) gneisses, Dwalile metavolcanics and younger granitoids / AGC (Swaziland)	3417 ± 34	Sm-Nd; T_{DM} whole-rock	Formation/crystallization age of igneous protolith
	Kröner *et al.* (1988)	Dwalile Metamorphic Suite (schists, amphibolites, serpentinites, metapelites, quartzites, BIFs, gneisses; =possible correlative to Onverwacht Group of Barberton Greenstone Belt) / Ancient Gneiss Complex (Swaziland)	~3450	; zircon, garnet	Age of metamorphism
	Kröner & Compston (unpubl.) in Kröner *et al.* (1991)	Xenocrystic zircon in 3521 ± 10 Ma old tonalitic gneiss / Dwalile area, Ancient Gneiss Complex (Swaziland) Trondhjemitic gneiss (Ngwane Gneiss) / Ancient Gneiss Complex (Swaziland) Metaquartzite of Dwalile Supracrustal Suite / Ancient Gneiss Complex) / (Swaziland) Quartzofeldspathic gneiss (Mahamba Gneiss) / Ancient Gneiss Complex (Swaziland)	3683 ± 10 3521 ± 23 3566 ± 33 – 3524 ± 17 3566 ± 21 – 3423 ± 30 3553 ± 12	U-Pb; zircon U-Pb; zircon U-Pb; zircon U-Pb; zircon U-Pb; zircon	Generation of igneous protolith at ~3.52 Ga by melting of a ~3.68 Ga old crustal source Age of heterogeneous source terrain, with youngest zircon defining upper age of Dwalile Supracrustal Suite
	Dziggel *et al.* (2002)	Arkose of Onverwacht Group / Barberton Greenstone Belt (SA)	3521 ± 5.6	U-Pb; zircon	Age of source terrain = max. age of deposition
	Davis & Allsopp (1976)	Tsawela tonalitic gneiss / Ancient Gneiss Complex (Swaziland)	3323 ± 168	Rb-Sr; whole-rock	Formation/crystallization age of igneous protolith
	Kröner *et al.* (1991)	Granodioritic gneiss (Ngwane Gneiss) close to contact with Dwalile supracrustal suite / AGC (Swaziland) Banded tonalitic gneiss (Ngwane Gneiss) / Ancient Gneiss Complex (Swaziland) Banded trondhjemitic gneiss (Ngwane Gneiss) / Ancient Gneiss Complex (Swaziland) Banded tonalitic gneiss (Ngwane Gneiss) enclave in Mpuluzi Batholith / Ancient Gneiss Complex (Swaziland) Tsawela tonalitic gneiss / Ancient Gneiss Complex (Swaziland) Tsawela tonalitic gneiss / Ancient Gneiss Complex (Swaziland) Metaquartzite (Mahamba Gneiss) / Ancient Gneiss Complex (Swaziland) Metapelite (Mahamba Gneiss) / Ancient Gneiss Complex (Swaziland) Weakly foliated granodiorite (Usutu Suite) / Ancient Gneiss Complex (Swaziland) Weakly foliated granodiorite (Usutu Suite) / Ancient Gneiss Complex (Swaziland) Unfoliated granodiorite (Usutu Suite) / Ancient Gneiss Complex (Swaziland) Banded gneiss (Ngwane Gneiss) / ENE of Mankayane, Ancient Gneiss Complex (Swaziland)	3213 ± 10 3215 ± 4 3449 ± 4 3412 ± 8 3455 ± 3 3436 ± 6 3300 ± 3 3297 ± 8 3220 ± 8 3231 ± 3 3306 ± 4 3372 ± 30	Pb-Pb evapor.; zircon U-Pb; zircon U-Pb; zircon U-Pb; zircon U-Pb; zircon U-Pb; zircon U-Pb; zircon U-Pb; zircon U-Pb; zircon U-Pb; zircon U-Pb; zircon Pb-Pb; whole-rock	Resetting event = hydrothermal alteration (this study) Resetting event = hydrothermal alteration (this study) Formation/crystallisation age of igneous protolith Formation/crystallisation age of igneous protolith Formation/crystallisation age of igneous protolith Formation/crystallisation age of igneous protolith Age of granulite-facies grade metamorphism Age of granulite-facies grade metamorphism Resetting event = hydrothermal alteration (this study) Resetting event = hydrothermal alteration (this study) Formation/crystallisation age of igneous protolith Formation/crystallisation age of igneous protolith or resetting during intrusion of a granitoid phase at ~3.3 Ga

APPENDIX 21-A: Summary of selected geochronological data pertinent to the Kaapvaal Craton.

Period	Reference	Lithology / Locality	Age (Ma)	Method	Interpretation by author(s)
SWAZI TERRANE *[PALAEO- / MESOARCHAEAN (~3.7-3.1 Ga)]*	Compston & Kröner (1988)	Ngwane Gneiss (Ancient Gneiss Complex	3644 ± 2	U-Pb; zircon	Formation/crystallisation age
	Tegtmeyer (1989) and Kröner *et al.* (1991)	Zircons from metaquartzite of Dwalile Supracrustal Suite / Ancient Gneiss Complex (Swaziland)	3494 ± 6 – 3459 ± 1	U-Pb; zircon	Age of heterogeneous source terrain
		Metavolcanics (peridotitic and basaltic komatiite and basal) of Dwalile Supracrustal Suite / Ancient Gneiss Complex (Swaziland)	3618 ± 18	Sm-Nd; T_{DM} whole-rock	Age of source rock for Dwalie Supracrustal Suite
		Metasediments of Dwalile Supracrustal Suite / Ancient Gneiss Complex (Swaziland)	3470 ± 100 ~3800-3650	Sm-Nd; T_{DM} garnet Sm-Nd; T_{DM} model	Age of metamorphic event Age of source rock
		Banded calc-silicate rock of Dwalile Supracrustal Suite / Ancient Gneiss Complex (Swaziland)	3220 ± 220	Sm-Nd; T_{DM} whole-rock	Resetting event = hydrothermal alteration during granitoid emplacement
		Dwalile Suite and Ngwane, Tsawela and Mahamba Gneisses / Ancient Gneiss Complex (Swaziland)	3625 ± 94	Sm-Nd; T_{DM} whole-rock	Combined age of protolith(s) of rocks analysed
		Detrital zircons of quartzofeldspathic gneiss interlayered with metaquartzite and pelitic gneiss (Mahamba Gneiss) / Ancient Gneiss Complex (Swaziland)	3581 ± 20 – 3505 ± 7, 3553 ± 12(mean) ~3600	U-Pb; zircon Sm-Nd; T_{DM} whole-rock	Age of pre-Mahamba basement (= one of the older members of Ngwane Gneiss) and depositional age of Mahamba supracrustal Suite shortly after ~3550 Ma
	Kröner & Compston (1988)	Zircons from granitic pebbles and granitoid gneiss clasts in basal conglomerate and quartzite of Moodies Group / Barberton Greenstone Belt (SA)	3570 ± 6, 3531 ± 4, 3518 ± 11	U-Pb; zircon	Formation/crystallisation age of igneous protolith to granitoid gneisses & granites (= age of underlying AGC & Onverwacht Group as source terranes)
	Kröner (2007)	Tonalite gneiss (Ancient Gneiss Complex)	3563 ± 3	U-Pb; zircon	Formation/crystallisation age
	Armstrong *et al*. (1990)	Xenocrystic zircons from the Theespruit Formation (L. Onverwacht Gr.) / Barberton Greenstone Belt (SA)	3531 ± 10	U-Pb; zircon	Age of pre-Onverwacht Group basement
	Byerly *et al*. (1996)	Xenocrystic zircons from the Hooggenoeg Formation (U. Onverwacht Gr.) / Barberton Greenstone Belt (SA)	3559 ± 27	U-Pb; zircon	Age of pre-Onverwacht Group basement
	Kröner *et al*. (1991a)	Xenocrystic zircons from dacitic tuff of Hooggenoeg Formation (U. Onverwacht Gr.) / Barberton Greenstone Belt (SA) Xenocrystic zircons in dacitic volcaniclastics of Fig Tree Group / Barberton Greenstone Belt (SA) Xenocrystic zircons in strongly foliated trondhjemitic gneiss (Steynsdorp pluton) / Barberton Greenstone Belt (SA)	3504 ± 4 3522 ± 4 – 3323 ± 4 3533 ± 4, 3531 ± 3	Pb-Pb evapor.; zircon Pb-Pb evapor.; zircon Pb-Pb evapor.; zircon	Age of pre-Onverwacht Group basement Age of pre-Fig Tree Group basement/source terrain Age of basement
	Kröner & Tegtmeyer (1994)	Xenocrystic zircons in greywacke of Fig Tree Group / Barberton Greenstone Belt (SA)	3523 ± 13	U-Pb; zircon	Age of pre-Onverwacht Group basement/source terrain
	Armstrong *et al*. (1990)	Xenocrystic zircons in metagabbro intruding Komati Formation (L. Onverwacht Gr.) / Barberton Greenstone Belt (SA)	3523 ± 6	U-Pb; zircon	Age of pre-Onverwacht Group basement/source terrain
	Armstrong *et al.* (1990), Kamo *et al.* (1990), Kamo & Davis (1994)	Thrust slice of tonalitic gneiss tectonically emplaced within Theespruit Formation (Lower Onverwacht Group)/ Barberton Greenstone Belt (SA)	3538 ± 6 3538 ± 6	U-Pb; zircon U-Pb; zircon	Formation/crystallisation age or age of metamorphism & deformation of igneous protolith prior to Onverwacht Gr.
	Kamo *et al.* (1990), Kamo & Davis (1994)	Steynsdorp gneissic trondhjemitic pluton tectonically emplaced / Barberton Greenstone Belt (SA)	3509 +8/-7	U-Pb; zircon	Formation/crystallisation age or age of metamorphism & deformation of igneous protolith
	Kröner *et al.* (1996)	Steynsdorp gneissic trondhjemitic pluton / Barberton Greenstone Belt (SA) Steynsdorp gneissic granodioritic pluton / Barberton Greenstone Belt (SA) Strongly foliated felsic schist of Theespruit Formation close to intrusive contact with Steynsdorp pluton/ Barberton Greenstone Belt (SA) Vlakplaats granodiorite pluton / Barberton Greenstone Belt (SA) Xenocrystic zircons in Steynsdorp gneissic trondhjemitic pluton / Barberton Greenstone Belt (SA)	3510 ± 4, 3509 ± 4, 3505 ± 5, 3502 ± 2 3510 ± 3 3540 ± 3 3553 ± 4 3538 ± 9	Pb-Pb evapor.; zircon Pb-Pb evapor.; zircon Pb-Pb evapor.; zircon Pb-Pb evapor.; zircon U-Pb; zircon	Formation/crystallisation age Formation/crystallisation age Grain growth (= contact metamorphism) related to Steynsdorp pluton intrusion Age of pre-Onverwacht Group basement/source terrain Age of pre-Onverwacht Group basement/source terrain
	Xie *et al*. (2012)	Greenstones / Nondweni Greenstone Belt	3532 ± 4, 3520 ± 6, 3418 ± 5	U-Pb; zircon	Formation/crystallisation age
	Kröner *et al*. (1991a, 1992) Kröner & Tegtmeyer (1994)	Steynsdorp gneissic trondhjemitic pluton tectonically emplaced / Barberton Greenstone Belt (SA)	3496 ± 3, 3490 ± 4, 3490 ± 3	Pb-Pb evapor.; zircon	Formation/crystallisation ages or ages of metamorphism & deformation of igneous protolith
	Kamo *et al.* (1990), Kamo & Davis (1994)	Stolzburg Pluton (trondhjemite) / Barberton Greenstone Belt (SA)	3458 +5/-4	U-Pb; zircon	Formation/crystallisation age
	Kröner *et al.* (1991a)	Stolzburg Pluton (trondhjemite) / Barberton Greenstone Belt (SA)	3445 ± 4	Pb-Pb evapor.; zircon	Formation/crystallisation age
	Barton *et al*. (1983c)	Stolzburg Pluton (trondhjemite) / Barberton Greenstone Belt (SA)	3481 ± 92	Rb-Sr; whole-rock	Formation/crystallisation age
	Dziggel *et al.* (2002)	Stolzburg Pluton (trondhjemite) / Barberton Greenstone Belt (SA)	3431 ± 11	U-Pb; zircon	Formation/crystallisation age
	Robb *et al.* (1986)	Stolzburg Pluton (trondhjemite) / Barberton Greenstone Belt (SA)	3408 +89/-95	Pb-Pb; whole-rock	Formation/crystallisation age
	Kamo *et al.* (1990), Kamo & Davis (1994)	Doornhoek Pluton (trondhjemite) / Barberton Greenstone Belt (SA)	3448 ± 4	U-Pb; zircon	Formation/crystallisation age
	Armstrong *et al.* (1990)	Theespruit Pluton (trondhjemite) / Barberton Greenstone Belt (SA)	3437 ± 6	U-Pb; zircon	Formation/crystallisation age
	Kröner *et al.* (1991a)	Theespruit Pluton (trondhjemite) / Barberton Greenstone Belt (SA)	3440 ± 5	Pb-Pb evapor.; zircon	Formation/crystallisation age
	Kamo *et al.* (1990), Kamo & Davis (1994)	Theespruit Pluton (trondhjemite) / Barberton Greenstone Belt (SA)	3443 +4/-3	U-Pb; zircon, titanite	Formation/crystallisation age
	Robb *et al.* (1986)	Theespruit Pluton (trondhjemite) / Barberton Greenstone Belt (SA)	3475 +148/-165	Pb-Pb; whole-rock	Formation/crystallisation age
	Barton *et al.* (1983c)	Theespruit Pluton (trondhjemite) / Barberton Greenstone Belt (SA)	3432 ± 135	Rb-Sr; whole-rock	Formation/crystallisation age
	Armstrong *et al*. (1990)	Volcaniclastic sediment of Theespruit Formation (Lower Onverwacht Group) tectonically emplaced / BGB (SA)	3453 ± 6	U-Pb; zircon	Formation/crystallisation age
	Kröner *et al*. (1996)	Felsic volcanic (tuff) schist of Theespruit Formation (Lower Onverwacht Group) / Barberton Greenstone Belt (SA)	3548 ± 1.3, 3547 ± 2, 3544 ± 3	Pb-Pb evapor.; zircon	Formation/crystallisation age
	Lopez-Martinez *et al*. (1984)	Komatiitic metabasalt from Komati Formation (Lower Onverwacht Group) / Barberton Greenstone Belt (SA)	3489 ± 34	$^{40}Ar/^{39}Ar$; w.-r. & amphib.	Formation/crystallisation age
	Brévart *et al*. (1986)	Komatiitic basalt from Komati Formation (Lower Onverwacht Group) / Barberton Greenstone Belt (SA)	3460 ± 70	Pb-Pb; whole-rock	Formation/crystallisation age
	Armstrong *et al*.. (1990)	Volcaniclastic sedimentary unit (Middle Marker) in Komati Formation (Lower Onverwacht Group) separating Komati and Hooggenoeg formations / Barberton Greenstone Belt (SA) Metagabbros intruding Komati Formation (Lower Onverwacht Group) / Barberton Greenstone Belt (SA)	3472 ± 5 3352 +6/-5 3482 ± 5, 3357 ± 5	U-Pb; zircon U-Pb; baddeleyite U-Pb; zircon	Formation/crystallisation age (= maximum age for Komati Formation) Formation/crystallisation Formation/crystallisation
	Kamo *et al.* (1990) Kamo & Davis (1994)	Felsic (porphyry) dyke cutting Komati Formation (L. Onverwacht Group) / Barberton Greenstone Belt (SA) Pegmatitic gabbro intrusive into Komati Formation (L. Onverwacht Group) / Barberton Greenstone Belt (SA)	3470 +39/-9, 3467 +12/-7, 3458 ± 1.6, 3457 ± 3, 3454 ± 9.6 3352 +6/-5, 3347 ± 3	U-Pb; zircon U-Pb; zircon	Formation/crystallisation age (= minimum age for Komati Formation) Formation/crystallisation age
	Kröner & Todt (1988)	Felsic volcaniclastic metaquartzite of Hoogenoeg Formation (Upper Onverwacht Group) / BGB (SA)	3451 ± 15 – 3438 ± 12	Pb-Pb evapor.; zircon	Formation/crystallisation age

APPENDIX 21-A: Summary of selected geochronological data pertinent to the Kaapvaal Craton.

Period	Reference	Lithology / Locality	Age (Ma)	Method	Interpretation by author(s)
SWAZI TERRANE *[PALAEO- / MESOARCHAEAN (~3.7-3.1 Ga)]*	Tegtmeyer & Kröner (1987)	Granite pebble in conglomerate (Moodies Group) / Barberton Greenstone Belt (SA)	3474 +35/-31	U-Pb; zircon	Minimum age for granite emplacement for the
	Armstrong *et al*. (1990)	Dacitic volcanic of Hoogenoeg Formation (Upper Onverwacht Group) / Barberton Greenstone Belt (SA)	3445 ± 8	U-Pb; zircon	Formation/crystallisation age
	Kröner *et al.* (1991a)	Dacitic tuff of Hoogenoeg Formation (Upper Onverwacht Group) / Barberton Greenstone Belt (SA)	3445 ± 3 – 3416 ± 5	Pb-Pb evapor.; zircon	Formation/crystallisation age
	Kröner & Compston (1988)	Detrital zircons of greywacke (Fig Tree Group) / Barberton Greenstone Belt (SA)	3453 ± 9	U-Pb; zircon	Age of underlying Onverwacht Group as source terrane
	Kröner *et al.* (1989)	Tsawela Gneiss	3458 ± 6	Pb-Pb evapor.; zircon	Formation/crystallisation age
	Kröner & Tegtmeyer (1994)	Tsawela Gneiss	3436 ± 6	Pb-Pb evapor.; zircon	Formation/crystallisation age
	Mukasa *et al*. (2013)	Tsawela Gneiss (Ancient Gneiss Complex) / on north side of Pongola Supergroup depository	3428 ± 22	U-Pb; zircon	Formation/crystallisation age
	Carlson *et al*. (1983)	Ancient Gneiss Complex (including Tsawela Gneiss)	3417 ± 34	Sm-Nd, whole rock	Formation/crystallisation age
	Byerly *et al*. (1996)	Rhyodacitic tuff in Hoogenoeg Formation (Upper Onverwacht Group) / Barberton Greenstone Belt (SA) Tuffaceous chert layer in uppermost part of Kromberg Formation (Upper Onverwacht Group) / BGB (SA) Tuff in Mendon Formation (Upper Onverwacht Group) / Barberton Greenstone Belt (SA)	3452 ± 3 3334 ± 3 3298 ± 3	Pb-Pb evapor.; zircon Pb-Pb evapor.; zircon Pb-Pb evapor.; zircon	Formation/crystallisation age Formation/crystallisation age Formation/crystallisation age
	Wilson & Carlson (1989)	Greenstones / Commondale Greenstones Belt	3316 ± 16	Sm–Nd; whole rock	Formation/crystallisation age
	Nhleko (2003)	Rhyolite of Ntambo Member (Nsuze Group; Pongola Supergroup) / (Swaziland)	3303 ± 25	U-Pb; zircon	Inherited zircons = age of basement rock to Nsuze Group
	Byerly *et al.* (1996)	Dacitic tuff (Fig Tree Group) / Barberton Greenstone Belt (SA) Tuffaceous sandstone (Fig Tree Group) / Barberton Greenstone Belt (SA)	3258 ± 3 3253 ± 3	Pb-Pb evapor.; zircon Pb-Pb evapor.; zircon	Formation/crystallisation age Formation/crystallisation age
	Kröner *et al.* (1991a)	Dacitic tuffs and agglomerates (Fig Tree Group) / Barberton Greenstone Belt (SA)	3259 ± 5 – 3225 ± 3	Pb-Pb evapor.; zircon	Duration of felsic volcanism
	Kohler *et al*. (1993)	Silicic metavolcanics (Upper Fig Tree Group) / Barberton Greenstone Belt (SA)	3256 ± 1	U-Pb; zircon	Formation/crystallisation age
	Farrow *et al*. (1990)	Anhalt leucotonalite (Piet Retief)	3250 ± 39	Rb–Sr; whole rock	Formation/crystallisation age
	Kamo *et al.* (1990)	Syndepositional ignimbrite between Fig Tree and Moodies groups / Barberton Greenstone Belt (SA)	3227 ± 1	U-Pb; zircon	Formation/crystallisation age
	Kröner *et al.* (1991a)	Moodies Group / Barberton Greenstone Belt (SA)	~3227	inferred	Age of deposition as a result of tectonism associated with thrusting and intrusion of Kaap Valley & Dalmein plutons
	Kröner *et al.* (1991a)	Dacitic dyke intrusive into Fig Tree Group / Barberton Greenstone Belt (SA)	3241 ± 6	Pb-Pb evapor.; zircon	Formation/crystallisation age
	Byerly *et al.* (1996)	Felsic intrusion into Onverwacht Group / Barberton Greenstone Belt (SA)	3237 ± 3	Pb-Pb evapor.; zircon	Formation/crystallisation age
	Armstrong & Retief (unpubl.)	Granitoid forming the basement to Godwan Formation / west of Barberton Greenstone Belt (SA)	3230 ± 3	U-Pb; zircon	Formation/crystallisation age
	Layer *et al*. (1998)	Feldspar porphyry dyke intrusive into Moodies Group / Barberton Greenstone Belt (SA)	3224.5 ± 0.4	U-Pb; zircon	Formation/crystallisation age
	Kamo & Davis (1994)	Kaap Valley tonalite (interior phase) / Barberton Greenstone Belt (SA) Kaap Valley tonalite (border phase) / Barberton Greenstone Belt (SA)	3227 ± 2 3227 ± 1	U-Pb; zircon U-Pb; zircon	Formation/crystallisation age pre-dating D_2-early Formation/crystallisation age pre-dating D_2-early
	Armstrong *et al*. (1990)	Kaap Valley tonalite / Barberton Greenstone Belt (SA)	3226 ± 14	U-Pb; zircon	Formation/crystallisation age
	Tegtmeyer & Kröner (1987)	Kaap Valley tonalite / Barberton Greenstone Belt (SA)	3229 ± 5	U-Pb; zircon	Formation/crystallisation age
	Layer *et al*. (1992)	Kaap Valley tonalite / Barberton Greenstone Belt (SA)	3226 ± 5; 3223 ± 4 3214 ± 4 (interior) 3142 ± 20 (margin)	U-Pb; zircon $^{40}Ar/^{39}Ar$; hornblende $^{40}Ar/^{39}Ar$; biotite	Formation/crystallisation age Post-crystallisation time span of cooling of pluton between ~3225 and ~3142 Ma
	Layer (1991)	Kaap Valley tonalite / Barberton Greenstone Belt (SA)	3212 ± 12	$^{40}Ar/^{39}Ar$; hornblende	Formation/crystallisation age
	Robb *et al.* (1986)	Kaap Valley tonalite / Barberton Greenstone Belt (SA)	3211 +94/-102 3191 +77/-81	Pb-Pb; whole-rock Pb-Pb; whole-rock	Formation/crystallisation age Formation/crystallisation age
	Maphalala & Kröner (1993)	Granodiorite of Usuthu Suite / north-central Swaziland	3231 ± 4	Pb-Pb evapor.; zircon	Formation/crystallisation age
	Mukasa *et al*. (2013)	Granitoid / Hoopwell area Granitoid / Piet Retief area	3267 ± 21 3147 ± 13	U-Pb; zircon U-Pb; zircon	Formation/crystallisation age Formation/crystallisation age
	Elworthy *et al*. (2000)	Anhalt leucotonalite / near Nondweni, southeastern Kaapvaal Craton (SA) Mvunyana granodiorite / near Nondweni, southeastern Natal (SA) Natal Spa granitoid / ~65 km south of Piet Retief, southeastern Kaapvaal Craton (SA)	3254 ± 39 3295 ± 34 3288 ± 139	Rb-Sr; whole-rock Rb-Sr; whole-rock Rb-Sr; whole-rock	Formation/crystallisation age Formation/crystallisation age Formation/crystallisation age
	Schoene & Bowring (2010)	Usutu granitoid suite	3265.5 ± 0.5, 3236.1 ± 0.5, 3221.6 ± 0.5	U–Pb zircon	Formation/crystallisation age
	De Ronde & Kamo (2000)	Nelshoogte Trondhjemite Pluton with pronounced S_2-foliation / Barberton Greenstone Belt (SA) Mafic meso-tonalite intrusion with S_2-foliation / Barberton Greenstone Belt (SA) Mafic meso-tonalite intrusion without S_2-foliation / Barberton Greenstone Belt (SA) Tonalite dyke cross-cutting S_2 -fabric and are folded by F_3-folds/ near contact between greenstone belt and Kaap Valley Tonalite Pluton; Barberton Greenstone Belt (SA)	3236 ± 1 3229 ± 1 3229 ± 1 3228 ± 2	U-Pb; zircon U-Pb; zircon U-Pb; zircon U-Pb; zircon	Formation/crystallisation age Formation/crystallisation age and lower age limit of D_2-early Formation/crystallisation age and lower age limit of D_2-early Formation/crystallisation age, upper age limit of D_2 & lower age limit of D_3
	Kamo & Davis (1994)	Feldspar-quartz porphyry folded by F_2-folds/ ~9km E of Stolzburg Syncline; Barberton Greenstone Belt (SA) Porphyry folded by F_3 Stolzburg Syncline / Barberton Greenstone Belt (SA)	3229 +4/-3 3222 +10/-4	U-Pb; zircon U-Pb; zircon	Formation/crystallisation age and lower age limit of D_2-early Formation/crystallisation age
	York *et al*. (1989)	Nelshoogte Trondhjemite Pluton / Barberton Greenstone Belt (SA)	3212 ± 2	Pb-Pb evapor.; zircon	Formation/crystallisation age
	De Ronde *et al.* (1991a)	Feldspar-quartz porphyry cutting F_2-folds in Fig Tree Formation / ~4km E of Stolzburg Syncline; BGB (SA) Volcaniclastic ignimbrite of Fig Tree Formation folded by large F_3 Stolzburg Syncline / BGB (SA)	3227 ± 3 3226 ± 1	U-Pb; zircon U-Pb; zircon	Formation/crystallisation age and upper age limit of D_2-early Formation/crystallisation age and lower age of D_2-late
	Meyer *et al*. (1993)	Natal Spa granite	3223 ± 2	U-Pb; zircon	Formation/crystallisation age and upper age of D2-late
	Kamo *et al.* (1990), Kamo & Davis (1994)	Dalmein Pluton (monzonite) / Barberton Greenstone Belt (SA)	3216 +2/-1	U-Pb; zircon	Formation/crystallisation age and upper age of D_2-late
	Barton *et al*. (1983c)	Dalmein Pluton / Barberton Greenstone Belt (SA)	3201 ± 43	Rb-Sr; whole-rock	Formation/crystallisation age

APPENDIX 21-A: Summary of selected geochronological data pertinent to the Kaapvaal Craton.

Period	Reference	Lithology / Locality	Age (Ma)	Method	Interpretation by author(s)
SWAZI TERRANE *[PALAEO- / MESOARCHAEAN (~3.7-3.1 Ga)]*	Kröner *et al.* (1989)	Granodiorite / Ancient Gneiss Complex (Swaziland) Tonalitic gneiss / Ancient Gneiss Complex (Swaziland) Leucogranite veins / Ancient Gneiss Complex (Swaziland)	3216 ± 3 3214 ± 20 3166 ± 4	Pb-Pb evapor.; zircon U-Pb; zircon U-Pb; zircon	Formation/crystallisation age Formation/crystallisation age Formation/crystallisation age
	Kamo & Davis (1994)	Doornhoek Pluton (trondhjemite) / Barberton Greenstone Belt (SA) Stolzberg Pluton (trondhjemite) / Barberton Greenstone Belt (SA) Steynsdorp Pluton (trondhjemite) / Barberton Greenstone Belt (SA)	3215 ± ? 3201 ± 1.6 3190 ± 1.6	U-Pb; zircon U-Pb; zircon U-Pb; zircon	Resetting event = hydrothermal alteration (this study) Resetting event = hydrothermal alteration (this study) Resetting event = hydrothermal alteration (this study)
	Reimold *et al.* (1993)	Granite / Natal (SA)	3210 ± 25	Pb-Pb evapor.; zircon	Formation/crystallisation age
	Saha *et al.* (2010)	Anhalt granite Anhalt trondhjemite	3193 ± 8 3222 ± 8	U-Pb; zircon U-Pb; zircon	Formation/crystallisation age Formation/crystallisation age
	Elworthy *et al.* (2000)	Nkandla granitoid / southeastern Kaapvaal Craton (SA) Mhlatuze granitoid / southeastern Kaapvaal Craton (SA) Nseleni granitoid / southeastern Kaapvaal Craton (SA)	3184 ± 1937 3177 ± 199 3162 ± 80	Rb-Sr; whole-rock Rb-Sr; whole-rock Rb-Sr; whole-rock	Formation/crystallisation age Formation/crystallisation age Formation/crystallisation age
	Allsopp (1961unpubl.)	G4 Granite White Mfolozi granite / ~20 km east of Nondweni, southeastern Kaapvaal Craton (SA)	3163 ± 103 3162 ± 80	Rb-Sr; whole-rock Rb-Sr; whole-rock	Formation/crystallisation age Formation/crystallisation age
	De Ronde *et al.* (1991a)	Quartz porphyry dyke cut by an Au-mineralised shear and rutile associated with hydrothermal alteration and Au mineralisation within same shear / Fairview Gold Mine; Barberton Greenstone Belt (SA)	3126 ± 21 - 3084 ± 18	U-Pb; zircon, rutile	Age bracket for D3 gold mineralising event
	Kamo *et al.* (1990), Kamo & Davis (1994)	Stentor Pluton (trondjemite) / Barberton Greenstone Belt (SA) Boesmanskop Pluton (syeno-granitic) / Barberton Greenstone Belt (SA) Mpuluzi Pluton (granodiorite) / Barberton Greenstone Belt (SA) Nelspruit Pluton / Barberton Greenstone Belt (SA) Hebron Pluton (granodiorite) / Barberton Greenstone Belt (SA) Salisbury Kop Pluton / Barberton Greenstone Belt (SA)	3108 ± 4 3107 ± 1 3107 +4/-2 3105 +3/-2 3104 +3/-2 3109 +10/-8	U-Pb; zircon U-Pb; zircon, titanite U-Pb; zircon, titanite U-Pb; zircon, titanite U-Pb; zircon, titanite U-Pb; zircon	Formation/crystallisation age Formation/crystallisation age Formation/crystallisation age Formation/crystallisation age Formation/crystallisation age Formation/crystallisation age
	Wendt *et al.* (1993)	Salisbury Kop Pluton (undeformed homogeneous granodiorite) / Barberton Greenstone Belt (SA) Mliba Granodiorite Pluton / south-central Swaziland	3079 ± 39 3100 ± 11	U-Pb; zircon U-Pb; zircon	Formation/crystallisation age Formation/crystallisation age
	Maphalala & Kröner (1993)	Mliba Granodiorite Pluton / south-central Swaziland	3105 ± 5	Pb-Pb evapor.; zircon	Formation/crystallisation age
PIETERSBURG TERRANE *[PALAEO- / MESOARCHAEAN (~3.7-3.1 Ga)]*	Poujol *et al.* (1996, 1997)	French Bob TTG along southern contact of Murchison Greenstone Belt (SA) Oldest detrital zircon in metaconglomerate (MacKop Formation) / Murchison Greenstone Belt (SA) Detrital zircon in metaconglomerate (MacKop Formation) / Murchison Greenstone Belt (SA)	3228 ± 12 3364 ± 18 3168 ± 11	U-Pb; zircon U-Pb; zircon U-Pb; zircon	Formation/crystallisation age Min. crystallisation age of igneous protolith to TTG gneiss basement (this study) Age of one of the source areas for conglomerate
	Barton (1984)	TTG gneiss / southeast of Murchison Greenstone Belt (SA)	~3270	Rb-Sr; whole-rock	
	Brandl & Kröner (1993)	Migmatitic tonalitic gneiss / north of Pietersburg Greenstone Belt (SA) Felsic metavolcanic / Giyani Greenstone Belt (SA) Groot Letaba granitoid gneisses / north of Murchison Greenstone Belt, south of Giyani (SA)	3333 ± 5 3203 ± 4 3171 ± 6	Pb-Pb evapor.; zircon Pb-Pb evapor.; zircon Pb-Pb evapor.; zircon	Formation/crystallisation age Formation/crystallisation age Formation/crystallisation age
	De Wit *et al.* (1993)	Pre- to syn-(D_2) tectonic granitoid intrusive (= 2958 ± 2 Ma) into basal mafic-ultramafic sequence of Pietersburg Greenstone Belt / Pietersburg Greenstone Belt (SA)	3160 ± 14	U-Pb; zircon	Xenocryst = age of granitoid gneiss basement
	Arakawa *et al.* (1992)	Mafic supracrustal rocks / Rhenosterkoppies Greenstone Belt (SA)	3187 ± 104	Rb-Sr; whole rock	Formation/crystallisation age
	Kreissig *et al.* (1999)	Tonalitic-trondhjemitic basement gneisses/ Southern Marginal Zone & northern Kaapvaal Craton (SA)	~3750-3400	Sm-Nd; whole-rock	Formation/crystallisation age of precursor TTG basement
	Byron & Barton (1990)	Mafic metavolcanics / Eersteling Gold Mine, Pietersburg Greenstone Belt (SA)	3455 +120/-128	Pb-Pb; 2nd isochron	Age of metamorphic overprint
	Kröner *et al.* (2000)	Metaandesite / near the town of Giyani, Giyani Greenstone Belt (SA) Well-foliated tonalitic gneiss / near Tshivhulana Hill, ~10km NW from Giyani Greenstone Belt (SA) Well-foliated migmatitic, granodioritic gneiss / south of Giyani Greenstone Belt (SA)	3203.3 ± 0.2 3282.6 ± 0.4 3170.5 ± 0.3	Pb-Pb evapor.; zircon Pb-Pb evapor.; zircon Pb-Pb evapor.; zircon	Formation/crystallisation age Formation/crystallization age of igneous protolith Formation/crystallization age of igneous protolith
	Crampton (1972)	Migmatitic granitoid gneisses / Derdepoort area (SA)	3493 ± 38	Rb-Sr; whole-rock	Formation/crystallisation age
WITWATERSRAND TERRANE *[PALAEO- / MESOARCHAEAN (~3.7-3.1 Ga)]*	Anhaeusser & Burger (1982)	Tonalitic gneiss / Johannesburg Dome (SA)	3170 ± 34	U-Pb; zircon	Formation/crystallisation age
	Allsopp (1961, 1964) recalc. by Layer *et al.* (1988)	Granodioritic orthogneiss / Johannesburg Dome (SA)	3200 ± 65, 3132 ± 64 3066 ± 65	Rb-Sr; whole-rock	Formation/crystallisation age of granodiorite
	Barton *et al.* (1999)	Tonalite / Johannesburg Dome (SA) Granodiorite, granite and leucosome from migmatite / Johannesburg Dome (SA) Granodiorite, granite and leucosome from migmatite, tonalite / Johannesburg Dome (SA)	~3170 3135 ± 51 3112 ± 14 ~3300-3500 & ~4000-4300	Rb-Sr; whole-rock Rb-Sr; whole-rock Pb-Pb; whole-rock Sm-Nd; whole-rock	Formation/crystallisation age Formation/crystallisation age Formation/crystallisation age Age of source rock
	Poujol & Anhaeusser (1999; 2001)	Mafic-ultramafic greenstone remnants/xenoliths in trondhjemite gneisses /Johannesburg Dome (SA) Trondhjemite gneiss / Johannesburg Dome (SA) Tonalite gneiss / Johannesburg Dome (SA) Porphyritic granodiorites / Johannesburg Dome (SA) Mafic dykes with associated granitic veins within dykes / Johannesburg Dome (SA)	> 3340 3340 ± 3.3 3201 ± 5, 3199.9 ± 2 3121.2 ± 5, 3114.2 ± 2.4 3117 ± 12	Inferred U-Pb; zircon U-Pb; zircon U-Pb; zircon U-Pb; zircon	Inferred age of formation/crystallisation Formation/crystallisation age Formation/crystallisation age Formation/crystallisation age Formation/crystallisation age
	Armstrong *et al.* (1991)	Xenocrystic zircon in quartz-feldspar porphyry (Makwassie Formation; Platberg Group) / Klerksdorp Goldfield (SA) Xenocrystic zircon in highly amygdaloidal volcanic horizon of Crown lava (West Rand Group) / (SA) Basement granitoid to Dominion Group / Klerksdorp Goldfield (SA)	3480 ± 7 (core) 3259 ± 9, 3230 ± 8, 3121 ± 6; 3103 ± 9 3120 ± 5	U-Pb; zircon (mean) U-Pb; zircon U-Pb; zircon	Age of granitoid-gneiss basement Xenocrysts = Ages of granitoid-gneiss basement Formation/crystallisation age
	Robb *et al.* (1992)	Peraluminous granodiorite-adamellite / Hartbeesfontein Dome (SA) Low-Ca granite / south of Vredefort Dome (SA)	3174 +9/-7 3101 ± 2	U-Pb; zircon U-Pb; zircon	Formation/crystallisation age Formation/crystallisation age
	Kamo *et al.* (1996)	Xenocrystic zircon in Lesutaskraal pseudotachylitic breccia / Vredefort Dome (SA)	~3310, 3172 ± 2	U-Pb; zircon	Xenocryst = Age of granitoid-gneiss basement
	Hart *et al.* (1999)	Granulitic Paragneiss / Centre of Vredefort Dome (SA) Granulitic Paragneiss / Centre of Vredefort Dome (SA)	≥ 3425 3107 ± 9	U-Pb; zircon U-Pb; monazite	Min. estimate for average detrital zircon age (= average age of deposition) Age of granulite-facies grade metamorphism
	Tredoux *et al.* (1999)	Metaperidotites / Centre of Vredefort Dome (SA)	~3500-3300	Re-Os; model ages	Model ages for granitoid-gneiss basement
	Reimold *et al.* (1988)	Actinolite-chlorite schist of granitoid-gneiss basement / Southeastern sector of Vredefort Dome (SA)	3340 ± 40	Rb-Sr; whole-rock	Formation/crystallisation age
	Flowers *et al.* (2003)	Granitoid-gneiss basement / Centre of Vredefort Dome (SA)	~3313		Formation/crystallisation age

APPENDIX 21-A: Summary of selected geochronological data pertinent to the Kaapvaal Craton.

Period	Reference	Lithology / Locality	Age (Ma)	Method	Interpretation by author(s)
KRAAIPAN TERRANE *[PALAEO- / MESOARCHAEAN (~3.7-3.1 Ga)]*	Hirner *et al.* (2001)	Felsic Schist of Western and Eastern Succession / Madibe Greenstone Belt (SA) Felsic Schist of Western and Eastern Succession / Madibe Greenstone Belt (SA)	3428 ± 11, ~3180 3201 ± 4	U-Pb; zircon U-Pb; zircon	Xenocryst = Age of granitoid-gneiss basement Xenocryst = Age of granitoid-gneiss basement
	Anhaeusser & Walraven (1999)	Tonalitic-trondhjemitic basement gneisses intrusive into Kraaipan G.B./Kraaipan granite-greenstone belt BIF of Gold Ridge & Ferndale formations (Kraaipan Group) / Kraaipan granite-greenstone terrane (SA)	3162 ± 8 3410 +61/-64	Pb-Pb evapor.; zircon Pb-Pb; whole-rock	Minimum age for crystallisation Age of deposition or complete resetting during metamorphism
	Gericke (2001)	Volcaniclastic unit / Kraaipan granite-greenstone terrane (SA)	3191.1 ± 7.9	U-Pb; zircon	Formation/crystallisation age?
	Poujol *et al.* (2001a)	Fine-grained leuco-trondhjemitic gneiss / Amalia granite-greenstone terrane (SA)	3178 ± 10	U-Pb; zircon	Xenocryst = Age of granitoid-gneiss basement
	Schmitz (2002)	Tonalitic gneiss / Kimberley area (SA)	3170 ± 32	U-Pb; zircon	Xenocryst = Age of granitoid-gneiss basement
	McCourt *et al.* (2000)	Xenocrystic zircons in Draghoender Granite / Marydale Greenstone Belt (SA) Xenocrystic zircons in Skalkseput Granite / Marydale Greenstone Belt (SA)	~3125 ~3111	U-Pb; zircon U-Pb; zircon (core)	Minimum age of basement or protolith of granite Minimum age of basement or protolith of granite
	Drennan *et al.* (1990), Drennan (1988)	Basement tonalitic gneisses & migmatites from Bultfontein Diamond Mine / Kimberley area (SA)	~3250 (core)	U-Pb; zircon	Age of metamorphism
SWAZI TERRANE *[NEOARCHAEAN (~3.1-2.95 Ga)]*	Toulkeridis *et al.* (1994)	Carbonate of Mapepe Formation (Fig Tree Group) / Barberton Greenstone Belt (SA)	3102 ± 64	Sm-Nd; clay minerals	Partial resetting event = hydrothermal alteration
	Kamo & Davis (1994)	Stentor Pluton (trondjemite) / Barberton Greenstone Belt (SA)	3082 ± 3	U-Pb; zircon	Minimum age of metamorphism/alteration
	Maphalala & Kröner (1993)	Sinceni Granite Pluton / south-central Swaziland Lochiel (Mpuluzi) Granodiorite-Adamellite Batholith / south-central Swaziland	3074 ± 4 3074 ± 6	Pb-Pb evapor.; zircon Pb-Pb evapor.; zircon	Formation/crystallisation age Formation/crystallisation age
	Kamo & Davis (1994)	Undeformed intrusive felsic sill within Komati Formation / Barberton Greenstone Belt (SA)	3080 ± 3	U-Pb; zircon	Maximum limit of formation/crystallisation age of sill
	Wendt *et al.* (1993)	Lochiel (Mpuluzi) Granodiorite-Adamellite Batholith / south-central Swaziland	3074 ± 4	Pb-Pb evapor.; zircon	Formation/crystallisation age
	Wendt (unpubl.) in Kröner *et al.* (1991)	Deformed Mpuluzi granite / Ancient Gneiss Complex (Swaziland)	3049 ± 25	U-Pb; zircon	Formation/crystallisation age
	Layer *et al.* (1992)	Kaap Valley tonalite / Barberton Greenstone Belt (SA)	3035 ± 9	40Ar/39Ar; biotite	Partial thermal resetting age/event along pluton margin
	Allsopp *et al.*. (1968)	Pegmatite cross-cutting lode-type gold deposit at New Consort Mine/Barberton Greenstone Belt (SA)	3030 ± 40	Rb-Sr; whole-rock	Formation/crystallisation age =minimum age for gold mineralisation
	Nhleko (2003)	Rhyolite of Ntambo Member (Nsuze Group; Pongola Supergroup) / (Swaziland)	3014 ± 12	U-Pb; zircon	Inherited zircons = age of basement rock to Nsuze Group
	Kröner *et al.* (1989)	Trondhjemitic gneiss / Ancient Gneiss Complex (Swaziland)	3005 ± 6	U-Pb; zircon	New zircon growth = Partial thermal resetting age/event
	Kröner & Compston (unpubl.) in Kröner *et al.* (1991)	BIF (Dwalile Supracrustal Suite) / Dwalile area, Ancient Gneiss Complex (Swaziland) Komatiitic basalt (Dwalile Supracrustal Suite) / Dwalile area, Ancient Gneiss Complex (Swaziland)	3095 ± 20 2949 ± 95	Pb-Pb; whole-rock Pb-Pb; whole-rock	Resetting event = hydrothermal alteration Resetting event = hydrothermal alteration
	Wendt (unpubl.) in Kröner *et al.* (1991)	Banded tonalitic gneiss (Ngwane Gneiss) / Ancient Gneiss Complex (Swaziland)	2981 ± 30	U-Pb; zircon	Resetting event = hydrothermal alteration due to intrusion of Mpuluzi Batholith
	Burger & Coertze (1973)	Nsuze Group	3090 ± 90 3083 ± 150	U-Pb; zircon Rb-Sr; whole rock	Formation/crystallisation age
	Mukasa *et al.* (2013)	Andesite volcanic layer in lowest unit of Nsuze Group / (Swaziland & SA) Rhyolite (middle volcanic layer) in middle unit of Nsuze Group / (Swaziland & SA) Andesite (volcanic layer) in highest unit of Mozaan Group / (Swaziland & SA)	2980 ± 10 2966 ± 10, 2968 ± 6, 2967 ± 9 2954 ± 9	U-Pb; zircon	Period of deposition for the Pongola Supergroup
	Nhleko (2003)	Rhyolite of Ntambo Member (Nsuze Group; Pongola Supergroup) / (Swaziland)	2977 ± 5	U-Pb; zircon	Formation/crystallisation age
	Hegner *et al.* (1994)	Basalt-rhyolite suite (Nsuze Group; Pongola Supergroup) / (Swaziland)	2985 ± 1, 2984 ± 2.6, 2940 ± 22 2934 ± 114	U-Pb; zircon Sm-Nd; whole rock	Formation/crystallisation age =maximum age for Mozaan Group
	Walraven (unpubl.)	Rhyolite (Nsuze Group; Pongola Supergroup) / (Swaziland)	2978 ± 2	U-Pb; zircon	Formation/crystallisation age =maximum age for Mozaan Group
	Olsson (2012)	Usushwana Complex	2989.2 ± 0.8, 2989.8 ± 1.7	U-Pb; baddeleyite	Formation/crystallisation age
	Gumsley *et al.* (2015)	Piet Retief Suite of Usushwana Complex SE-trending dolerite dyke of Badplaas dyke swarm	2990 ± 2, 2989 ± 1, 2978 ± 2 2980 ± 1	U-Pb; zircon U-Pb; zircon	Formation/crystallisation age Formation/crystallisation age (feeder to lower Pypklipberg (Nhlebela) Formation of Nsuze Group)
	Olsson *et al.* (2010)	SE-trending dolerite dykes of Badplaas dyke swarm	2966 ± 1, 2967 ± 1	U-Pb; zircon	Formation/crystallisation age (feeders to upper Agatha Formation of Nsuze Group; Gumsley *et al.* (2015))
	Havenga (1996)	SE-trending dolerite dykes of Badplaas dyke swarm / Barberton Greenstone Belt (SA)	2972 ± 11	Pb-Pb;	Formation/crystallisation age
	Mukasa *et al.* (2013)	Nhlangano gneiss (post-Pongola Supergroup) Hlatikulu granite (post-Pongola Supergroup) Kwetta Granite (post-Pongola Supergroup)	2963 ± 9 2973 ± 31, 2960 ± 11, 2742 ± 22 2911 ± 50, 2721 ± 16, 2720 ± 10	U-Pb; zircon U-Pb; zircon U-Pb; zircon	Formation/crystallisation age Formation/crystallisation age Formation/crystallisation age
PIETERSBURG TERRANE *[NEOARCHAEAN (~3.1-2.95 Ga)]*	Brandl & Kröner (1993)	Makhutswi granitoid gneiss / north of Murchison Greenstone Belt (SA)	3118 ± 5, 3112 ± 5, 3078 ± 6	Pb-Pb evapor.; zircon	Formation/crystallisation age
	Saager & Köppel (1976)	Galena associated with gold in carbonated mafic volcanics / Murchison Greenstone Belt (SA)	3020 ± 50	Pb-Pb; galena	
	Vearncombe *et al.* (1992)	Galena & pyrite from Cu-Zn-line & pyrite associated with gold / Murchison Greenstone Belt (SA)	~3100	Pb-Pb; galena, pyrite	
	Poujol (2001)	Baderoukwe trondhjemitic gneiss / Murchison Greenstone Belt (SA) Dacite (Rubbervale Formation) / Murchison Greenstone Belt (SA) Discovery Granite from Gravelotte Mine (Maranda Batholith) / Murchison Greenstone Belt (SA)	3018 ± 15 2969 ± 20 2969 ± 17	U-Pb; zircon U-Pb; zircon U-Pb; zircon	Formation/crystallisation age Formation/crystallisation age Formation/crystallisation age
	Poujol & Robb (1999)	Makhutswi migmatitic gneiss / Murchison Greenstone Belt (SA) Harmony granite gneiss / Murchison Greenstone Belt (SA)	3063 ± 12 3091 ± 5	U-Pb; zircon U-Pb; zircon	Formation/crystallisation age Formation/crystallisation age
	Poujol *et al.* (1996, 1997)	Sediments and felsic volcanics (Weigel Formation) / Murchison Greenstone Belt (SA) Metaconglomerate (MacKop Formation) / Murchison Greenstone Belt (SA) Rhyolite (Rubbervale Formation) / Murchison Greenstone Belt (SA) Granodiorite from Malati Pump Mine (Maranda Batholith) / Murchison Greenstone Belt (SA) Discovery Granite from Gravelotte Mine (Maranda Batholith) / Murchison Greenstone Belt (SA) Maranda Granodiorite (Maranda Batholith) / Murchison Greenstone Belt (SA) Pyrite from Malati Pump Mine Granodiorite, felsic schist (Weigel Formation) and rhyolite (Rubbervale Formation) / Murchison Greenstone Belt (SA)	3087 ± 21 3364 ± 18 - 3076 ± 4 2971 ± 10 2970 ± 15 2960 ± 43 2901 ± 20 (~2970) 2979 ± 25	U-Pb; zircon U-Pb; zircon U-Pb; zircon U-Pb; zircon U-Pb; zircon U-Pb; zircon Pb-Pb; pyrite	Average age = maximum age of deposition Youngest detrital zircon = maximum age of deposition Formation/crystallisation age Formation/crystallisation age Formation/crystallisation age Formation/crystallisation minimum age (interpreted age; this study) Age of epigenetic Mo-W-Be-Sb-Au-B-Hg and syngenetic base metal (Cu-Zn) mineralisation
	Vearncombe *et al.* (1987)	Lower Rubbervale Formation / Murchison Greenstone Belt (SA)	2953 +29/-38	Pb-Pb; whole-rock	Formation/crystallisation age or deformation age?

APPENDIX 21-A: Summary of selected geochronological data pertinent to the Kaapvaal Craton.

Period	Reference	Lithology / Locality	Age (Ma)	Method	Interpretation by author(s)
PIETERSBURG TERRANE *[NEOARCHAEAN (~3.1-2.95 Ga)]*	Brandl *et al.* (1996)	Rhyolite (Rubbervale Formation) / Murchison Greenstone Belt (SA)	2967.5 ± 1.3 2965.2 ± 1.4	Pb-Pb evapor.; zircon U-Pb; zircon	Formation/crystallisation age Formation/crystallisation age
	De Wit *et al.* (1993)	Pre- to syn-(D_2) tectonic granitoid intrusive into basal mafic-ultramafic sequence of Pietersburg Greenstone Belt / Pietersburg Greenstone Belt (SA)	2958 ± 2	U-Pb; zircon	Formation/crystallisation age of granitoid, age of D_2 & minimum age for basal sequence of Pietersburg Greenstone Belt
		Conglomerate (Uitkyk Formation) / Pietersburg Greenstone Belt (SA)	2957 ± 1	U-Pb; zircon	Youngest zircon = beginning of deposition of Uitkyk Formation
	Kröner *et al.* (2000)	Metaquartzporphyry of Ysterberg Formation / Pietersburg Greenstone Belt (SA)	2949.7 ± 0.2	Pb-Pb evapor.; zircon	Formation/crystallisation age
		Homogeneous monzogranitic gneiss (Groot-Letaba Gneiss) / ~4 km northwest of Ka-Makhuva Village, between Murchison and Giyani greenstone belts (SA)	2953 +68/-61	U-Pb; zircon	Formation/crystallization age of igneous protolith
	Passeraub *et al.* (1999)	Tonalitic gneiss / Rhenosterkoppies Greenstone Belt (SA) Fuchsite-bearing schist / Rhenosterkoppies Greenstone Belt (SA) Kyanite-bearing schist / Rhenosterkoppies Greenstone Belt (SA)	~3000 ~3100 ~2950	Sm-Nd; whole-rock Sm-Nd; whole-rock Sm-Nd; whole-rock	Formation/crystallisation age Formation/crystallisation age Formation/crystallisation age
	Kreissig *et al.* (1999)	Greenstone belt metapelites / Southern Marginal Zone and northern Kaapvaal Craton (SA)	~3000-2950	Sm-Nd; whole-rock	Age of deposition of supracrustals (greenstone belts) derived by erosion from coeval granitoids and older TTG basement
	Anhaeusser & Poujol (2004)	Vaalpenskraal-type trondhjemitic gneisses / Makoppa Dome (SA)	3034 ± 64, 3013 ± 11	U-Pb; zircon	Formation/crystallisation age
WITWATERSRAND TERRANE *[NEOARCHAEAN (~3.1-2.95 Ga)]*	Robb *et al.* (1992)	Low-Ca granite of Westerdam Dome / northwest margin of Witwatersrand Basin (SA)	3086 ± 3	U-Pb; zircon	Formation/crystallisation age
		Low-Ca granite of Ottosdal-Coligny granite / northwest margin of Witwatersrand Basin (SA)	3031 +11/-10	U-Pb; zircon	Formation/crystallisation age
	Barton *et al.* (1999)	Granodiorite, granite and leucosome from migmatite / Johannesburg Dome (SA)	3093 ± 3.2 3081 ± 33 3062 ± 26	Pb-Pb evapor.; zircon Rb-Sr; whole-rock Pb-Pb; whole-rock	Formation/crystallisation age Formation/crystallisation age Formation/crystallisation age
	Robb *et al.* (1989, 1990)	Rhenosterspruit Formation (basal member of Dominion Group) unconformably overlying granite of Westerdam Dome / northwest margin of Witwatersrand Basin (SA)	< 3086 ± 3	U-Pb; zircon	Formation/crystallisation age Westerdam Dome granite = maximum age of Rhenosterspruit Formation (Dominion Group)
	Armstrong *et al.* (1991)	Xenocrystic zircon in highly amygdaloidal volcanic horizon of Crown Lava (West Rand Group) / Klerksdorp Goldfield (SA)	3087 ± 5, 3083 ± 8, 3083 ± 12	U-Pb; zircon	Xenocryst = Age of granitoid-gneiss basement
		Quartz-feldspar porphyry (Syferfontein Formation; Dominion Group) / Klerksdorp Goldfield (SA)	3074 ± 6	U-Pb; zircon	Formation/crystallisation age
		Xenocrystic zircon in Makwassie Quartz Porphyry (West Rand Group) / Klerksdorp Goldfield (SA)	3068 ± 39	U-Pb; zircon	Xenocryst = Age of granitoid-gneiss basement
	Hart *et al.* (1981)	Outer Granite Gneiss / Vredefort Dome (SA)	3080 ± 40	U-Pb; zircon	Formation/crystallisation age
	Hart *et al.* (1999)	Mafic granulite / Centre of Vredefort Dome (SA)	3079 ± 1 - 3017 ± 6	U-Pb; zircon	No interpretation given
	Kamo *et al.* (1996)	Xenocrystic zircon in charnockitic gneiss / Vredefort Dome (SA)	3083 ± 8, 3060 ± 12	U-Pb; zircon	Formation/crystallisation age of xenocryst or metamorphism
		Xenocrystic zircon in Lesutaskraal pseudotachylitic breccia / Vredefort Dome (SA)	3073 ± 4, ~3065, 3045 ± 2, 3040 ± 2, 3037 ± 2, 3016 ± 4	U-Pb; zircon	Formation/crystallisation age of xenocryst or metamorphism
		Xenocrystic zircon in granophyre / Vredefort Dome (SA)	3055 ± 2	U-Pb; zircon	Formation/crystallisation age of xenocryst or metamorphism
	Kirk *et al.* (2002)	Gold (authigenic in appearance) and pyrite (detrital, diagenetic and authigenic) from Vaal and Steyn reefs & VCR / Klerksdorp & Welkom goldfields (SA)	3030 ± 20	Re-Os; gold, zircon	Combined formation/crystallisation age = age of cogenetic Au & U mineralisation in mantle or mantle-derived igneous source rock(s)/ terrane(s) = major Au-U & crust-forming event in Kaapvaal Craton = gold & uraninite in Witwatersrand Supergroup are detrital
	Reimold *et al.* (1988)	Migmatite of granitoid-gneiss basement / Southeastern sector of Vredefort Dome (SA)	3010 ± 10 (errochron) 2970 ± 4 (isochron) 3105 ± 151	U-Pb; whole-rock U-Pb; whole-rock Rb-Sr; whole-rock	Age of upper amphibolite-granulite facies metamorphism and associated partial melting (Lana *et al*., 2003)
	Poujol & Anhaeusser (2001)	Granodiorites / Johannesburg Dome (SA) Trondhjemite gneiss / Johannesburg Dome (SA)	3101 ± 5; 3091 ± 3; 3086 ± 16; 3078 ± 3 2997 ± 7; 2947 ± 57	U-Pb; zircon U-Pb; zircon	Partial thermal resetting ages/events Partial thermal resetting ages/events
	Armstrong *et al.* (1991)	Xenocrystic zircon in quartz-feldspar porphyry (Makwassie Formation; Platberg Group) / Klerksdorp Goldfield	3068 ± 39 (mantle)	U-Pb; zircon (mean)	Age of hydrothermal overprint of ~3.48 Ga old granitoid-gneiss basement
	Barton *et al.* (1999)	Tonalite / Johannesburg Dome (SA)	3001 +132/-146	Pb-Pb; whole-rock	Partial thermal resetting age/event
	Allsopp (1961)	Halfway-House granite / Johannesburg Dome (SA) Halfway-House pegmatite / Johannesburg Dome (SA)	3060 ± 100 3010 ± 30, 3000 ± 40	Rb-Sr; feldspar Rb-Sr; biotite, feldspar	Partial thermal resetting age/event Partial thermal resetting age/event
KRAAIPAN TERRANE *[NEOARCHAEAN (~3.1-2.95 Ga)]*	Poujol *et al.* (2000, 2001a)	Trondhjemitic basement gneiss / ~7km south of Amalia; Amalia granite-greenstone terrane (SA)	3008 ± 4	U-Pb; zircon	Formation/crystallisation age of igneous protolith
	Anhaeusser & Walraven (1999)	Tonalitic-trondhjemitic basement gneisses intrusive into Kraaipan Greenstone Belt / Kraaipan granite-greenstone terrane (SA)	3162 ± 8 - 3070 ± 7	Pb-Pb evapor.; zircon	Minimum ages for crystallisation
	Poujol *et al.* (2001a)	Volcanics from Madibe and Kraaipan greenstone belts /Kraaipan granite-greenstone terrane (SA)	3098.4 ± 7.6, 3082.5 ± 5.9, 3083 +40/-14	U-Pb; zircon	Formation/crystallisation age
	Hirner *et al.* (2001)	Felsic volcanic schist of Western Succession / Madibe Greenstone Belt (SA) Felsic volcanic schist of Eastern Succession / Madibe Greenstone Belt (SA)	3097.4 ± 8.8 3082.5 ± 5.9	U-Pb; zircon U-Pb; zircon	Formation/crystallisation age Formation/crystallisation age
	Robb (1991)	Felsic volcanic schist of Kraaipan Group / near Kraaipan; Kraaipan granite-greenstone terrane (SA)	3083 +40/-14	U-Pb; zircon	Formation/crystallisation age
	Robb *et al.* (1991)	Felsic volcanics of Kraaipan Group / near Kraaipan; Kraaipan granite-greenstone terrane (SA)	3066 ± 32	U-Pb; zircon	Formation/crystallisation age
	Harris *et a*.. (1987)	Granites and sediments / outcropping within Kheis Belt along & to the west of Kalahari Line (SA)	~3000	Sm-Nd; whole rock	Formation/crystallisation age; (proof for Archaean-age of Rehoboth Craton west of Kalahari suture zone (this study))
	Barton *et al.* (1986)	BIF of Marydale Group / Marydale Greenstone Belt (SA)	~3000	Pb-Pb; whole-rock	Age of greenschist-facies grade metamorphism; (minimum age of deposition of BIF (this study))
	Cornell & Barton (1979)	Modderfontein iron formation of Marydale Group / Marydale Greenstone Belt (SA)	2990 ± 120	Pb-Pb, whole-rock	Minimum age of Marydale Group
	Armstrong (1987)	Marydale Group / Marydale Greenstone Belt (SA)	2901 +82/-84	Pb-Pb; whole-rock	Formation/crystallisation age; Partial thermal resetting age/event (this study)

APPENDIX 21-A: Summary of selected geochronological data pertinent to the Kaapvaal Craton.

Period	Reference	Lithology / Locality	Age (Ma)	Method	Interpretation by author(s)
SWAZI TERRANE *NEOARCHAEAN(~2.95-2.72 Ga)]*	Hegner *et al*. (1994)	Pyroxenite of Usushwana Complex / Mpumalanga Province (SA) Basalt-rhyolite suite (Nsuze Group; Pongola Supergroup) / (Swaziland)	2871 ± 30 2883 ± 69	Sm-Nd; whole-rock Rb-Sr; whole rock	Formation/crystallisation age; Age of basement rocks from which mafic rocks of Usushwana Comp/ex were derived by partial melting (this study) Partial thermal resetting age/event
	Layer *et al*. (1988)	Usushwana Complex	2875 ± 40	Rb-Sr; w.-r. & Sm-Nd min.	Formation/crystallisation age; thermal resetting age/event (this study)
	Gumsley *et al*. (2015)	Dolerite sill intruding into the Mozaan Group (Pongola Supergroup) coeval with Hlagothi Layered Complex	2869 ± 5	U-Pb; zircon	Formation/crystallisation age
	Gumsley *et al*. (2013)	NW-trending feeder dyke coeval with Hlagothi Complex Meta-peridotite, pyroxenite, gabbro sills of Hlagothi Layered Complex intrusive into Pongola Supergroup	2874 ± 2 2866 ± 2	U-Pb; baddeleyite U-Pb; baddeleyite	Formation/crystallisation age Formation/crystallisation age
	Gutzmer *et al*. (1999)	Pre-tectonic quartz-porphyry sill in Mozaan Group / Mooihoek-Kubuta area (Swaziland)	2837 ± 5 2837 ± 5	U-Pb; zircon U-Pb; zircon	Formation/crystallisation age & min. depositional age of Mozaan Group Xenocryst = age of granitoid basement
	Robb *et al*. (1993)	Godlwayo Pluton / south-central Swaziland	2863 ± 5	U-Pb; zircon	Formation/crystallisation age & min. depositional age of Mozaan Group
	Walraven & Pape (1994)	(Schurwerand Formation) Lower Mozaan Group (SA)	2860 ± 26	Pb-Pb; whole-rock	Minimum depositional age of Mozaan Group
	Maphalala & Kröner (1993)	Nhlangano Granitoid Pluton / south-central Swaziland Mooihoek Granite Pluton / south-central Swaziland Mhlosheni Granite Pluton / south-central Swaziland	2929 ± 5 2824 ± 6 2822 ± 5	Pb-Pb evapor.; zircon Pb-Pb evapor.; zircon Pb-Pb evapor.; zircon	Formation/crystallisation age Formation/crystallisation age Formation/crystallisation age = minimum age for Mozaan Group
	Mukasa *et al*. (2013)	Mswati (Mhlosheni Pluton) (post-Pongola Supergroup granitoid intrusion) / (Swaziland & SA) Mswati (Sicunusa Pluton) (post-Pongola Supergroup granitoid intrusion) / (Swaziland & SA)	2838 ± 10, 2837 ± 6 2717 ± 11	U-Pb; zircon U-Pb; zircon	Formation/crystallisation age = minimum age for Mozaan Group Formation/crystallisation age = minimum age for Mozaan Group
	Compston & Kröner (1988)	Mkhondo Metamorphic Suite (quartzites, BIFs, gneisses, amphibolites) / Ancient Gneiss Complex (Swaziland)	~2748	Sm-Nd; TDM whole-rock	Age of metamorphism and/or hydroth. alteration/resetting (Hunter, 1991)
	Kröner *et al*. (1989)	Biotite-rich quartzofeldspathic gneiss / Ancient Gneiss Complex (Swaziland)	2745 ± 6	U-Pb; zircon	Age of crystallisation or recrystallisation of zircons
	Kamo *et al*. (1990),Kamo & Davis(1994)	Mpageni Pluton (syenite) / Barberton Greenstone Belt (SA)	2740 ± 15	U-Pb; zircon	Formation/crystallisation age
	Thomas *et al*. (1997)	Nzimane Granite intrusive into Pongola Group / Nzimane Inlier, northeastern KwaZulu-Natal (SA)	2733 ± 3	U-Pb; zircon	Formation/crystallisation age
	Schoene & Bowring (2010)	Hlatikulu Granite	2729.8 ± 0.4, 2728.9 ± 0.5	U-Pb; zircon	Formation/crystallisation age
	Maphalala & Kröner (1993)	Sicunusa Granitoid Pluton / south-central Swaziland Kwetta Granitoid Pluton / south-central Swaziland Hlatikulu Granitoid Batholith / south-central Swaziland Ngwempisi Granitoid Pluton / south-central Swaziland	2723 ± 7 2722 ± 6 2722 ± 7 2720 ± 4	Pb-Pb evapor.; zircon Pb-Pb evapor.; zircon Pb-Pb evapor.; zircon Pb-Pb evapor.; zircon	Formation/crystallisation age Formation/crystallisation age Formation/crystallisation age Formation/crystallisation age
PIETERSBURG TERRANE *[NEOARCHAEAN (~2.95-2.72 Ga)]*	Brandl & Kröner (1993)	Banded tonalitic gneiss / north of Pietersburg Greenstone Belt (SA) Discordant leucosome band / north of Pietersburg Greenstone Belt (SA)	2886 ± 4 2885 ± 4	Pb-Pb evapor.; zircon Pb-Pb evapor.; zircon	Formation/crystallisation age Formation/crystallisation age
	Poujol & Robb (1999)	Pegmatite intrusive into Makhutswi gneiss / Murchison Greenstone Belt (SA)	2848 ± 58	U-Pb; zircon	Formation/crystallisation age
	Poujol *et al*. (1996, 1997)	Willie Granite (undeformed porphyritic granite) / Murchison Greenstone Belt (SA)	2820 ± 38	U-Pb; zircon	Formation/crystallisation age
	Kröner *et al*. (2000)	Weakly foliated feldspar porphyry / near settlement of Ka-Homu, Giyani Greenstone Belt (SA) Strongly foliated Melkboomfontein Granite intrusive into Pietersburg Greenstone Belt / near village of GaMothiba, Pietersburg Greenstone Belt (SA) Turfloop Granite / near Mankweng, Pietersburg Greenstone Belt (SA) Homogeneous granodioritic gneiss / near Mphego Village, north of Giyani Greenstone Belt (SA)	2874.1 ± 0.2 2853 +19/-18 2883.6 ± 0.6 2810.6 ± 0.4	Pb-Pb evapor.; zircon U-Pb; zircon Pb-Pb evapor.; zircon Pb-Pb evapor.; zircon	Formation/crystallisation age Formation/crystallisation age of granite; minimum age for greenstones of Pietersburg Greenstone Belt, and maximum age of deformation affecting both granite and greenstones Inherited older gneiss component within Turfloop Granite Formation/crystallization age of igneous protolith
	Anhaeusser & Poujol (2004)	Makoppa-type granodiorite-monzogranite / Makoppa Dome (SA)	2886 +3/-2	U-Pb; zircon	Formation/crystallisation age
	Vearncombe *et al*. (1987)	Lower Rubbervale Formation / Murchison Greenstone Belt (SA)	2837 ± 25	Rb-Sr; whole-rock	Resetting event =hydrothermal alteration (this study)
	Barton *et al*. (1995a)	Entabeni Granite / Northern Province (SA)	~2810	Sm-Nd; whole-rock	Age of tonalitic-trondhjemitic basement rocks (derived from a mafic mantle source) from which the Entabeni Granite was derived by partial melting
	Poujol *et al*. (1996, 1997)	Hornblende tonalite of Rooiwater Complex / Murchison Greenstone Belt (SA)	2740 ± 4	U-Pb; zircon	Formation/crystallisation age
	Burger & Walraven (1975/76, 1979, 1980); Walraven *et al*. (1981)	Gneisses / northwest of Murchison Greenstone Belt (SA)	2780 - 2660	U-Pb; ?	
	Henderson (1996) Henderson *et al*. (2000)	Turfloop Granite Batholith / Pietersburg Greenstone Belt (SA)	2777 ± 10 2763 ± 15 2720 ± 40 2785 ± 15	U-Pb, zircon U-Pb; titanite Sm-Nd; whole-rock Rb-Sr; whole-rock	2777 ± 10 = Formation/crystallisation age of older component of possibly heterogeneous Turfloop Granite Batholith
	Kröner *et al*. (2000)	Turfloop Granite Batholith / Pietersburg Greenstone Belt (SA)	2763 ± 15	U-Pb, zircon	Formation/crystallisation age in agreement with Henderson *et al*. (2000)
	Anhaeusser & Poujol (2004)	Rooibokvlei-type granodiorite / Makoppa Dome (SA)	2797 ± 2, 2777 ± 35	U-Pb; zircon	Formation/crystallisation age
	Sibiya (1988)	Majwana granites (Gaborone Granite Suite) / Kubung area, Gaborone Granite Complex (SA)	2830 ± 10	U-Pb; zircon	Formation/crystallisation age
	Burger & Coertze (1975)	Granite (Gaborone Granite Suite) / Gaborone Granite Complex (SA)	2825 ± 100	U-Pb; zircon	Formation/crystallisation age
	Moore *et al*. (1993)	Rhyolite of Kanye Formation / Gaborone Granite Complex (SA) Microgranophyre of Kgale Granite (Gaborone Granite Suite) / Gaborone Granite Complex (SA) Leucocratic granite of Kgale Granite (Gaborone Granite Suite) / Gaborone Granite Complex (SA)	2787.7 ± 1.7, 2784.8 ± 1.8 2784.9 ± 1.9 2783.1 ± 2.0	U-Pb; zircon U-Pb; zircon U-Pb; zircon	Formation/crystallisation age Formation/crystallisation age Formation/crystallisation age
	Grobler & Walraven (1993)	Rhyolite (Kanye Formation) / Gaborone Granite Complex, Mafikeng (Botswana) Granite phase (Kgale Granite) / Gaborone Granite Complex, Mafikeng (Botswana) Granite phase (Thamaga Granite) / Gaborone Granite Complex, Mafikeng (Botswana) Granophyric granite (Kgale Granite) / Gaborone Granite Complex, Mafikeng (Botswana) Sperulitic microgranophyre (Kgale Granite) / Gaborone Granite Complex, Mafikeng (Botswana)	2784.8 ± 1.1 2783.2 ± 1.8 2783.1 ± 1.8 2782 ± 5 2779.1 ± 2.8	Pb-Pb evapor.; zircon Pb-Pb evapor.; zircon Pb-Pb evapor.; zircon Pb-Pb evapor.; zircon Pb-Pb evapor.; zircon	Formation/crystallisation age Formation/crystallisation age Formation/crystallisation age Formation/crystallisation age Formation/crystallisation age
	Armstrong & Robb (unpubl.)	Granophyre / Gaborone Igneous Complex (Botswana)	2778 ± 7	U-Pb; zircon	Formation/crystallisation age
	Walraven *et al*. (1994)	Mafic lava of Lobatse Group (overlying Gaborone Granite Complex and Kanye Formation) / Derdepoort (SA)	2769.3 ± 2.3	U-Pb; zircon	Formation/crystallisation age
	Walraven *et al*. (1996)	Plantation Porphyry (Lobatse Group) / Kanye area (Botswana)	2781.7 ± 1.9	Pb-Pb evapor.; zircon	Formation/crystallisation age
	Mapeo *et al*. (2004)	Undeformed red granite / Borehole MET 7 ~50 km SW of Kanye, Amalia-Kraaipan greenstone belt (Botswana)	2782 ± 6	U-Pb; zircon	Formation/crystallisation age
	Mapeo *et al*. (1998)	Mmathethe Granite / Gaborone Igneous Complex (Botswana)	2775.2 ± 7.4	Pb-Pb evapor.; zircon	Formation/crystallisation age
	Wingate (1998)	Rhyolite (Derdepoort Formation) / Derdepoort (SA) Basalt (Derdepoort Formation) / Derdepoort (SA)	2781.12 ± 2.2 2782 ± 5	U-Pb; zircon U-Pb; zircon	Formation/crystallisation age Formation/crystallisation age

APPENDIX 21-A: Summary of selected geochronological data pertinent to the Kaapvaal Craton.

Period	Reference	Lithology / Locality	Age (Ma)	Method	Interpretation by author(s)
WITWATERSRAND TERRANE *[NEOARCHAEAN (~2.95-2.72 Ga)]*	Poujol *et al*. (1998, 1999)	Kimberley Reef (Turffontein Subgroup) / Evander Goldfield (SA) Main Bird Quartzite (MBQ2) (Johannesburg Subgroup) / Evander Goldfield (SA)	2828 ± 39 2894 ± 10	U-Pb; zircon U-Pb; zircon	Youngest detrital zircon = maximum age of deposition Youngest detrital zircon = maximum age of deposition
	Kositcin *et al*. (2001) England *et al*. (2001)	Mapaiskraal Member quartzite (Upper Johannesburg Subgr.) / Vaal Reef No. 8 Shaft, Klerksdorp Goldfield (SA) Mapaiskraal Member quartzite (Upper Johannesburg Subgr.) / Vaal Reef No. 8 Shaft, Klerksdorp Goldfield (SA) Zanpan Pebble Marker (Johannesburg Subgroup) / Vaal Reef no. 8 Shaft, Klerksdorp Goldfield (SA) Zanpan Pebble Marker (Johannesburg Subgroup) / Vaal Reef no. 8 Shaft, Klerksdorp Goldfield (SA)	~3075, ~2925, ~2885 2764 ± 5 (diagenetic) 2873 ± 5 (detrital or diagenetic?) ~3031 – 2976 (detrital)	U-Pb; zircon U-Pb, xenotime U-Pb, xenotime U-Pb, xenotime	Youngest detrital zircon population = max. age of deposition Oldest authigenic xenotime = min. depositional age Max. (if detrital) or min. (if diagenetic) depositional age Youngest detrital xenotime = max. age of deposition
	Armstrong *et al*. (1991)	Crown lava (West Rand Group) / Klerksdorp Goldfield (SA)	2914 ± 8	U-Pb; zircon	Formation/crystallisation age
	Kamo *et al*. (1996)	Xenocrystic zircon in Granophyre / Vredefort Dome (SA)	2924 ± 4	U-Pb; zircon	Xenocryst = age of granitoid-gneiss basement
	Hart *et al*. (1999)	Granulitic Paragneiss / Centre of Vredefort Dome (SA) Granulitic Paragneiss / Centre of Vredefort Dome (SA)	2914 ± 3 2890 ± 3	U-Pb; monazite U-Pb; zircon	No interpretation given No interpretation given
	Kamo *et al*. (1996)	Xenocrystic zircon in Granophyre / Vredefort Dome (SA)	2800 ± 19	U-Pb; zircon	Xenocryst = age of granitoid-gneiss basement
	Allsopp (1961)	Corlett Drive pegmatite / Johannesburg Dome (SA)	2800 ± 30	Rb-Sr; feldspar	Partial thermal resetting age/event
	Poujol *et al*. (1998, 1999)	Altered Kimberley Reef & Hangingwall Quartzite (HW2) (Johannesburg Subgroup) cut by shear zones / Evander Goldfield (SA)	2785 ± 20 - 2637 ± 8	U-Pb; zircon	Fluid circulation along shear zones and total isotopic resetting of detrital zircon grains during Ventersdorp rifting/magmatism
	Good (1999)	Mica-quartz pegmatite within sheared granite / Mt. Welkom Mine (SA)	2775.03, 2740.98	Rb-Sr; mica model ages	Time of hydrothermal fluid flow /mineralisation and tectonic reactivation along Thabazimbi-Murchison Lineament
	Kositcin *et al*. (2001) England *et al*. (2001)	Diagenetic and hydrothermal (no detrital) xenotimes in Mapaiskraal Member quartzite, Vaal Reef conglomerate & Zanpan Pebble Marker (Lower Johannesburg Subgroup) / Vaal Reef no. 8 Shaft, Klerksdorp Goldfield (SA)	~2735 - 2710	Pb-Pb, xenotime	Peak at ~2717 Ma = age of lithospheric extension, high heat flow, flood-basalt volcanism during Ventersdorp Supergroup deposition & hydrothermal xenotime growth possibly associated with Au mineralisation or remobilisation
	Van Niekerk & Burger (1969) recalc. by Cahen *et al*. (1984)	Volcanics of Dominion Group / (SA)	2725 ± 75	Pb-Pb; sulphides, apatite	Resetting event =hydrothermal alteration (this study)
	Armstrong *et al*. (1991)	Klipriviersberg Group basaltic lava (Ventersdorp Supergroup) / Central Rand Goldfield (SA)	2714 ± 8	U-Pb; zircon	Formation/crystallisation age; Partial thermal resetting age/event (this study)
	Robb *et al*. (1992)	Wesselbron Granodiorite-adamellite / Borehole 1633 west of Welkom, Free State goldfield (SA)	2727 +6/-5	U-Pb; zircon	Formation/crystallisation age
KRAAIPAN TERRANE *[NEOARCHAEAN (~2.95-2.72 Ga)]*	Mapeo *et al*. (2004)	Mildly deformed pink granite / Borehole MET 6 ~63 km SW of Kanye, Amalia-Kraaipan greenstone belt (Botswana) Granitic biotite gneiss / Borehole MET 1 ~75 km SW of Kanye, Amalia-Kraaipan greenstone belt (Botswana)	2943 ± 9 2939 ± 9	U-Pb; zircon U-Pb; zircon	Formation/crystallisation age Formation/crystallisation age of igneous precursor
	Schmitz (2002)	Rhyolite / Kraaipan granite-greenstone terrane (SA) Granitoid gneiss / Kimberley area (SA) Granitoid gneiss / Kimberley area (SA) Granitoid gneiss / Kimberley area (SA) Pegmatite / Kimberley area (SA)	2940 ± 2 2932 ± 1 2928 ± 2 2927 ± 1 2926 ± 2	U-Pb; zircon U-Pb; zircon U-Pb; zircon U-Pb; zircon U-Pb; zircon	Formation/crystallisation age Formation/crystallisation age Formation/crystallisation age Formation/crystallisation age Formation/crystallisation age
	Gericke (2001)	Granodiorite / Kraaipan granite-greenstone terrane (SA)	2941 ± 2	U-Pb; zircon	Formation/crystallisation age
	Poujol *et al*. (2000, 2001a, 2002)	Fine-grained leuco-trondhjemitic gneiss / Amalia granite-greenstone terrane (SA) Leuco-trondhjemite dyke intrusive into trondhjemitic basement gneiss / ~7km south of Amalia; Amalia granite-greenstone terrane (SA) Granodiorite (MAD1) / in Kraaipan area; Kraaipan granite-greenstone terrane (SA) Granodiorite-adamellite (KP5) / in Madibogo-Kraaipan area; Kraaipan granite-greenstone terrane (SA) Granodiorite (DG6) / east of Disaneng Dam; Kraaipan granite-greenstone terrane (SA) Granodiorite (KHUN1) / in river section near Khunwana; Kraaipan granite-greenstone terrane (SA)	2939 ± 9.6 2943 ± 14 2917 ± 9, 2913 ± 17 2915 ± 12, 2913 ± 15 2879 ± 9 2879 ± 11	U-Pb; zircon U-Pb; zircon U-Pb; zircon U-Pb; zircon U-Pb; zircon U-Pb; zircon	Formation/crystallisation age Formation/crystallisation age Formation/crystallisation age Formation/crystallisation age Formation/crystallisation age Formation/crystallisation age
	Anhaeusser & Walraven (1997, 1999)	Kraaipan granodiorite-adamellite / Kraaipan granite-greenstone terrane (SA) Tonalitic-trondhjemitic basement gneisses intrusive into Kraaipan Greenstone Belt / (SA)	2846 ± 22 2921 +71/-74; 2866 +25/-26 - 2816 ±16	Pb-Pb evapor.; zircon Pb-Pb evapor.; zircon	Minimum formation/crystallisation age Ages of migmatisation and crustal reworking
	Reimold *et al*. (2002)	Granitoid in KHK-1 drill core / ~40km southwest of Ganyesa Dome (Morokweng impact structure)	2878 ± 8	U-Pb; zircon	Formation/crystallisation age
	Drennan *et al*. (1990) and Drennan (1988)	Basement tonalitic gneisses & migmatites from Bultfontein Diamond Mine / Kimberley area (SA)	~2940 (rim)	U-Pb; zircon	Age of migmatisation of gneiss
	Robb *et al*. (1992)	Basement tonalitic gneisses & migmatites (borehole TA2) / near Schweizer-Reneke, west of Amalia (SA) Hydrothermal vein cutting sample TA2 / Amalia granite-greenstone terrane (SA) Adamellite of Schweizer-Reneke Dome (borehole TBK2) /Amalia granite-greenstone terrane (SA)	2927 +23/-6 2884 ± 2 2880 ± 2	U-Pb; zircon U-Pb; rutile U-Pb; monazite	Age of migmatisation of gneiss Exogenous hydrothermal manifestation of Schweitzer Reneke Dome Formation/crystallisation age
	McCourt *et al*. (2000)	Draghoender Granite (intrusive into Marydale G. B.) / Marydale granitoid-greenstone terrane (SA) Skalkseout Granite (porphyritic biotite-muscovite granite) / Marydale granitoid-greenstone terrane (SA)	2853 ± 4 2938 ± 5, 2930 ± 9	U-Pb; zircon U-Pb, zircon (cores)	Formation/crystallisation age Interpretation unclear; (Formation/crystallisation age (this study))
	Vajner (1974a&b)	Draghoender Granite (intrusive into Marydale Greenstone Belt) / Marydale granitoid-greenstone terrane (SA)	~2900	U-Pb; zircon	Formation/crystallisation age
	Kamo *et al*. (1995)	Hydrotherm. altered granitoid gneiss (Mabuasehube North borehole) / ~50km N of Mabuasehube pan (Botswana)	2928 ± 4	U-Pb; zircon, titanite	Formation/crystallisation age of igneous precursor
	Hoal *et al*. (1995)	Basement gneiss / borehole intersection along Kalahari Line (SA)	2926 ± 2	U-Pb; sphene	Formation/crystallisation age of igneous precursor
	Richardson *et al*. (2001)	Sulfide inclusions in eclogitic diamonds / Kimberley kimberlite (SA)	2890 ± 60	Re-Os, sulfides	Formation/crystallization age of diamonds during subduction
	Carlson *et al*. (1999)	Peridotitic xenolith in kimberlite / Kimberley Diamond Mine (SA)	2930 ± 300	Re-Os, whole-rock	Average T_{MA} Re-Os model age of mantle underlying Kimberley
	Poujol *et al*. (2001a)	Coarse-grained biotite-trondhjemite gneiss / Amalia granite-greenstone terrane (SA)	2859 ± 4	U-Pb; zircon	Age of metamorphism?
	Poujol *et al*. (2000, 2001a, 2002)	Mosita adamellite / ~40km west of Setlagole; Kraaipan granite-greenstone terrane (SA)	2790 ± 8	U-Pb; zircon	Formation/crystallisation age
	Denyszyn *et al*. (2013)	Modipe Gabbro (sill-like body) / southern Botswana & northern South Africa	2784 ± 1	U-Pb; baddeleyite	Formation/crystallisation age
	Barton *et al*. (1986)	Adamellite of Schweizer-Reneke Dome / Amalia granite-greenstone terrane (SA)	2780 ± 70 2767 ± 110	Pb-Pb; whole-rock Rb-Sr; whole-rock	Resetting event = hydrothermal alteration (this study) Resetting event = hydrothermal alteration (this study)
	Reimold *et al*. (2002)	Granophyre in KHK-1 drill core / ~40km southwest of Ganyesa Dome (Morokweng impact structure)	2736 ± 29	U-Pb; zircon	Possible formation/crystallisation age

APPENDIX 21-A: Summary of selected geochronological data pertinent to the Kaapvaal Craton.

Period	Reference	Lithology / Locality	Age (Ma)	Method	Interpretation by author(s)
KRAAIPAN TERRANE *[NEOARCHAEAN (~2.95-2.72 Ga)]*	Poujol *et al*. (2005)	Accretionary lapilli tuff, agglomerate and quartz-chlorite schist / Amalia Greenstone Belt (SA)	2750 ± 5	U-Pb; zircon	Formation/crystallisation age of Platberg Group-age volcanics
	Schmitz (2002)	Unfoliated granite / Kimberley area (SA)	2724 ± 2	U-Pb; zircon	Formation/crystallisation age
	Poujol *et al*. (2001b)	Lapilli tuff / Amalia Greenstone Belt (SA) Quartz-chlorite-sericite volcanic schist / Amalia Greenstone Belt (SA)	2754 ± 5 2740 ± 13	U-Pb; zircon U-Pb; zircon	Formation/crystallisation age; Resetting event = hydrothermal alteration (this study)
	Gericke (2001)	Quartz-chlorite-sericite volcanic schist / Amalia Greenstone Belt (SA)	2728 ± 25	U-Pb; zircon	Formation/crystallisation age; Resetting event = hydrothermal alteration (this study)
	Allsopp (1961, 1964)	Adamellite of Schweizer-Reneke Dome / Amalia granite-greenstone terrane (SA)	2700 ± 55	Rb-Sr; whole-rock	Resetting event =hydrothermal alteration (this study)
	Poujol *et al*. (2000)	Granodiorite-adamellite / in Madibogo-Kraaipan area; Kraaipan granite-greenstone terrane (SA)	2720 ± 31	U-Pb; zircon	Resetting event = hydrothermal alteration
	Anhaeusser & Walraven (1999)	Mosita adamellite / Kraaipan granite-greenstone terrane (SA)	2749 ± 3	Pb-Pb evapor.; zircon	Formation/crystallisation age; Resetting event = hydrothermal alteration (this study)
	Burger & Walraven (1979)	Mosita adamellite / 60km southwest of Phitshane-Molopo; Kraaipan granite-greenstone terrane (SA) Granite intrusive into basement granitoid gneisses / ~60km southwest of Phitshane-Molopo; Kraaipan granite-greenstone terrane (SA)	2718 ± 65 2691 ± 65	U-Pb; zircon U-Pb; zircon	Formation/crystallisation age; Resetting event = hydrothermal alteration (this study) Formation/crystallisation age; Resetting event = hydrothermal alteration (this study)
	Reimold *et al*. (2002)	Granophyre and ~2880 Ma old granitoid in KHK-1 drill core / ~40km southwest of Ganyesa Dome (Morokweng impact structure) (SA)	2689 ± 5 & 2690 ± 16	U-Pb; zircon	Minimum formation/crystallisation ages; Resetting event = hydrothermal alteration (this study)
	Harding *et al*. (1974)	Gaborone Granite Complex / (Botswana)	2685 ± 70	Rb-Sr; whole-rock	Partial thermal resetting age/event
	Cahen *et al*. (1984)	Gaborone Granite Complex / (Botswana)	2616 ± 18	Rb-Sr; whole-rock	Formation/crystallisation age?; Partial thermal resetting age/event (this study)
	Fipke *et al*. (1995) ?	Xenolith of metamorphic basement rock in kimberlite / Kimberley area (SA)	2647 ± 9	Pb-Pb; tourmaline	Partial thermal resetting age/event of basement (this study)
	Schmitz & Bowring (2002)	Eclogite xenolith in kimberlite / Kimberley area (SA)	2630 ± 1	U-Pb; zircon	Age of metamorphism
	Elworthy *et al*. (2000)	Anhalt leucotonalite / near Piet Retief, southeastern Kaapvaal Craton (SA) Natal Spa granitoid / ~65 km south of Piet Retief, southeastern Kaapvaal Craton (SA) Mvunyana granodiorite / near Nondweni, southeastern Kaapvaal Craton (SA)	2671 ± 82 2638 ± 80 2611 ± 80	Rb-Sr; biotite Rb-Sr; biotite Rb-Sr; biotite	Partial thermal resetting age/event Partial thermal resetting age/event Partial thermal resetting age/event
SWAZI TERRANE *[NEOARCHAEAN-PALAEO-PROTEROZOIC (~2.72-2.22 Ga)]*	Meyer *et al*. (1993)	Spekboom Granite / south-central Swaziland Granite of Kwetta Granitoid Pluton / south-central Swaziland	2714 ± 19 2671 ± 3	Pb-Pb evapor.; zircon Pb-Pb evapor.; zircon	Formation/crystallisation age Formation/crystallisation age
	Layer *et al*. (1989)	Mbabane Granite Pluton / Barberton Greenstone Belt (Swaziland)	2691 ± 4 2687 ± 6	Pb-evapor.; zircon ^{40}Ar-^{39}Ar; hornblende	Formation/crystallisation age Formation/crystallisation age
	Barton *et al*. (1983)	Kwetta Granite Hlatikulu Granite Mswati (Mshlosheni) Granite Nhlangano Granite	2520 ± 422 2417 ± 148 2286 ± 304 2244 ± 355	Rb–Sr whole rock	Formation/crystallisation age; thermal resetting age/event (this study)
	Layer *et al*. (1988)	Usushwana Complex	2386 ± 58	^{40}Ar/^{39}Ar	Thermal resetting age/event
	Armstrong (1987)	Godwan Formation (basic lava)	2325 +69/-73	Pb-Pb; whole-rock	Formation/crystallisation age (Thermal resetting event (this study))
	Walraven *et al*. (1987)	Godwan Formation (basic lava)	2326 +65/-66	Pb-Pb; whole-rock	Formation/crystallisation age (Thermal resetting event (this study))
PIETERSBURG TERRANE *[NEOARCHAEAN-PALAEOPROTEROZOIC (~2.72-2.22 Ga)]*	Poujol *et al*. (2001b)	Mashishimala Granite / Murchison Greenstone Belt (SA)	2698 ± 21	U-Pb; zircon	Formation/crystallisation age
	Poujol *et al*. (1996, 1997)	Mashishimala Granite / Murchison Greenstone Belt (SA) Pyrite from Discovery Gold Mine and Gravelotte Emerald Mine / Murchison Greenstone Belt (SA)	2677 ± 14 2690 ± 35	U-Pb; zircon Pb-Pb; pyrite	Formation/crystallisation age Age of structurally controlled, hydrothermal gold mineralisation
	Burger & Walraven (1975/76, 1979, 1980); Walraven *et al*. (1981)	Gneisses / northwest of Murchison Greenstone Belt (SA)	~2780 – 2660	U-Pb;	
	Barton & van Reenen (1992)	Pegmatites / along northern margin of Pietersburg Greenstone Belt (SA) Pegmatites / cross-cutting Giyani Greenstone Belt (SA) Two-mica granite / south of Lwaji arm of Giyani Greenstone Belt (SA) Pegmatite in Shamiriri Granite / Giyani Greenstone Belt (SA)	~2757, ~2717 ~2692 – 2297 ~2650 ~2651	Rb-Sr; muscovite Rb-Sr; muscovite Rb-Sr; muscovite Rb-Sr; muscovite	Formation/crystallisation age Formation/crystallisation age Formation/crystallisation age Formation/crystallisation age
	Passeraub *et al*. (1999)	Syntectonic titanite within amphibolite / Rhenosterkoppies Greenstone Belt (SA) Syntectonic titanite from porphyritic tonalite biotite gneiss / Rhenosterkoppies Greenstone Belt (SA) Post-tectonic epidote and titanite from granodiorite gneiss intrusive into tonalite gneiss / / Rhenosterkoppies GB (SA) Kyanite in quartz-muscovite/fuchsite schist / Rhenosterkoppies Greenstone Belt (SA)	2729 ± 19 2754 ± 2 2743 ± 21 2634 ± 49	Pb-Pb; titanite Pb-Pb; titanite Pb-Pb; titanite Pb-Pb; kyanite	Minimum age of D_2-deformation & amphibolite-facies metamorphism Maximum age of D_2-deformation and formation of fabric Age of late D_2-deformation Age of tectonism, amphibolite metamorphism & hydrothermal fluid flow / metasomatism along Hout River Shear Zone
	Barton *et al*. (1992)	Charnoenderbite of Matok Pluton / Pietersburg Greenstone Belt (SA)	2671 ± 2	U-Pb; zircon	Formation/crystallisation age
	Burger & Walraven (1975/76)	Turfloop Granite Batholith / Pietersburg Greenstone Belt (SA)	2660 ± 50 2616 ± 50	U-Pb; zircon U-Pb; zircon	Formation/crystallisation age; Resetting/hydrothermal alteration (this study) Formation/crystallisation age; Resetting/hydrothermal alteration (this study)
	Barton *et al*. (1990)	Turfloop Granite Batholith / Pietersburg Greenstone Belt (SA)	2638 ± 20 2660 +13/-12	Rb-Sr; whole-rock Pb-Pb; isochron	Formation/crystallisation age; Resetting/hydrothermal alteration (this study) Formation/crystallisation age; Resetting/hydrothermal alteration (this study)
	Kröner *et al*. (2000)	Turfloop Granite Batholith / near Mankweng, Pietersburg Greenstone Belt (SA)	2674 ± 16	U-Pb; zircon	Younger component of possibly heterogeneous Turfloop Granite
	De Wit *et al*. (1992)	Granite intrusive into Uitkyk Formation / Pietersburg Greenstone Belt (SA)	2687 ± 2	U-Pb; zircon	Formation/crystallisation age
	Barton *et al*. (1995b)	Witfonteinrand lavas of Buffelsfontein Group / Makoppa Dome, west of Thabazimbi (SA)	2664 ± 0.7	U-Pb; zircon	Formation/crystallisation age (= correlatives to Allanridge lavas / Pniel Group)
	SACS (unpubl.) and Eriksson & Reczko (1995)	Witfonteinrand lavas of Buffelsfontein Group / Makoppa Dome, west of Thabazimbi (SA)	2658 ± 1	U-Pb; zircon	Formation/crystallisation age (= correlatives to Allanridge lavas / Pniel Group)
	Dorlan (2004)	Youngest detrital zircon in Schelem Formation (Wolkberg Group) overlying unconformably mafic lavas of Abel Erasmus Formation (Wolkberg Group) representing source of zircon / farm Rietfontein 34KS, Button Kop area (SA)	2635 ± 18	U-Pb; zircon	Approximate age of Abel Erasmus lavas; (= correlatives to Witfonteinrand lavas (Buffelsfontein Group) and Allanridge lavas (Pniel Group) (this study))
	Barton *et al*. (1983e)	Palmietfontein Granite / Southern Marginal Zone (SA)	2456 ± 78	Rb-Sr; whole-rock	Formation/crystallisation age
	Barton *et al* (1990)	Roodepoort Pluton (SA)	2343 +69/-73 2307 ± 46	Pb-Pb; whole-rock Rb-Sr; muscovite	Second phase of hydrothermal alteration and remobilisation of ~2.66 Ga old lode-type gold along shear zones within and along margins of pluton
	Barton & van Reenen (1992)	Pegmatites / cross-cutting Giyani Greenstone Belt (SA)	~2297	Rb-Sr; muscovite	Formation/crystallisation age; Hydrothermal alteration/resetting (this study)
	Byron & Barton (1990)	Maltz Reef / Pietersburg Greenstone Belt (SA)	2208 ± 26	Rb-Sr; whole-rock	Hydrothermal alteration phase with no affect to distribution of gold
	Vearncombe *et al*. (1987)	Rooiwater Complex / Murchison Greenstone Belt (SA)	2544 +29/-31 2490 ± 35	Pb-Pb; whole-rock Rb-Sr; whole-rock	Resetting event = hydrothermal alteration Resetting event = hydrothermal alteration
	Burger & Walraven (1977-78)	Meinhardskraal Granite / ~40 SW of Pietersburg (SA)	2255 ± 45	U-Pb; zircon	Formation/crystallisation age; Hydrothermal alteration/resetting (this study)

APPENDIX 21-A: Summary of selected geochronological data pertinent to the Kaapvaal Craton.

Period	Reference	Lithology / Locality	Age (Ma)	Method	Interpretation by author(s)
WITWATERSRAND TERRANE *[NEOARCHAEAN-PALAEOPROTEROZOIC (~2.72-2.22 Ga)]*	Walraven *et al*. (1991)	Kareefontein Quartz Porphyry (Zoetlief Group, Ventersdorp Supergroup) / (SA)	2714 ± 3, 2714 +28/-30	Pb-Pb evap.; zircon U-Pb; zircon	Formation/crystallisation age
	Walraven *et al*. (1987)	Makwassie Quartz Porphyry (Zoetlief Group, Ventersdorp Supergroup) / (SA)	2693 +60/-59	U-Pb; zircon	Formation/crystallisation age
	Gericke (2001)	Makwassie Quartz Porphyry (Zoetlief Group, Ventersdorp Supergroup) / (SA)	2706 ± 22	U-Pb; zircon	Formation/crystallisation age
	Armstrong *et al*. (1991)	Quartz-feldspar porphyry (Makwassie Formation; Platberg Group) / Klerksdorp Goldfield (SA)	2709 ± 4	U-Pb; zircon	Formation/crystallisation age
	Armstrong *et al*. (1986)	Township Quartz Porphyry (Makwassie Formation) / Klerksdorp (SA)	2699 ± 16	U-Pb; zircon	Formation/crystallisation age
	Retief (unpubl.)	Township Quartz Porphyry (Makwassie Formation) / Klerksdorp (SA)	2693 +60/-59	U-Pb; zircon	Formation/crystallisation age
	Van Niekerk & Burger (1978)	Township Quartz Porphyry (Makwassie Formation) / Klerksdorp (SA)	2643 ± 80	U-Pb; zircon	Formation/crystallisation age; Partial thermal resetting age/event (this study)
	Allsopp (1961)	Witkoppen pegmatite / Johannesburg Dome (SA)	2620 ± 60	Rb-Sr; feldspar	Partial thermal resetting age/event
	Zeh *et al*. (2020)	Detrital zircons from quartzite of Black Reef Formation / Graskop (SA)	2618 ± 11	U-Pb, zircon	Youngest detrital zircon = maximum age of deposition
	Martin *et al*. (1998)	Tuff bed in upper Oak Tree Formation (Transvaal Sequence) / Kromdraai & Berlyn Forest (SA)	2588 ± 7, 2583 ±5	U-Pb; zircon	Formation/crystallisation age (= maximum age/begin of marine transgression/carbonate deposition)
	Walraven & Martini (1995)	Tuff horizon at top of upper Oak Tree Formation (Transvaal Sequence) / near Johannesburg (SA)	2550 ± 3	Pb-Pb evapor.; zircon	Formation/crystallisation age
	Hart *et al*. (1999)	Dolerite dyke / Centre of Vredefort Dome (SA)	2584 ±10, 2564±16	U-Pb; zircon	Formation/crystallisation age
	Walraven (unpublished data)	Bushy Bend Lava Member at base of Timeball Hill Formation of Pretoria Group (Transvaal Supergroup) / (SA)	~2350	U-Pb; zircon	Formation/crystallisation age (= lower age limit of Pretoria Group)
	Hannah *et al*. (2002)	Pyrite from shales of lower Timeball Hill Formation (Pretoria Group, Transvaal Supergroup / (SA)	2322 ± 15	Re/Os; pyrite	Age of deposition
	Hunter & Hamilton (1978)	Shales of Timeball Hill Formation of Pretoria Group (Transvaal Supergroup) / (SA)	2263 ± 85	Pb-Pb; whole-rock	Formation/crystallisation age
	Dorland (2004)	Hekpoort Andesite Formation of Pretoria Group (Transvaal Supergroup) / Borehole EBA1 (near Fochville) and borehole RHK1 (near Potchefstroom) (SA)	~2240; 2225 ± 3	Pb-Pb; zircon	Formation/crystallisation age (= ~2240 Ma)
	Cornell *et al*. (1996)	Hekpoort Andesite Formation of Pretoria Group (Transvaal Supergroup) / (SA)	2222 ± 13	Pb-Pb; whole-rock	Formation/crystallisation age
	Hamilton (1977)	Hekpoort Andesite Formation of Pretoria Group (Transvaal Supergroup) / (SA)	2224 ± 21	Rb-Sr; whole-rock	Formation/crystallisation age
	Burger & Coertze (1974)	Hekpoort Andesite Formation of Pretoria Group (Transvaal Supergroup) / (SA)	2224 ± 21	Rb-Sr; whole-rock	Formation/crystallisation age
	Van Niekerk & Burger (1964)	Township Quartz Porphyry (Makwassie Formation) / Klerksdorp (SA)	2286 +40/-41 2300 ± 100	Pb-Pb; zircon U-Pb; zircon	Formation/crystallisation age Formation/crystallisation age
	Van Niekerk (1968)	Township Quartz Porphyry (Makwassie Formation) / Klerksdorp (SA)	2238 ± 100, 2245 ± 90	U-Pb; zircon	Formation/crystallisation age
	Walraven *et al*. (1987)	Township Quartz Porphyry (Makwassie Formation) / Klerksdorp (SA)	2352 +160/-184	Pb-Pb; whole-rock	Formation/crystallisation age
	Walraven *et al*. (1990)	Zoetlief Group / Vryburg (SA)	2313 ± 5.8	Pb-Pb; zircon	Partial thermal resetting age/event
	Armstrong *et al*. (1986)	Township Quartz Porphyry (Makwassie Formation) / Klerksdorp (SA) Mafic lavas (Klipriviersberg Group) / Central Rand Goldfield (SA)	2350 +160/-180 2430 ± 50	Pb-Pb; whole-rock Pb-Pb; whole-rock	Partial thermal resetting age/event Partial thermal resetting age/event
	Armstrong *et al*. (1987)	Mafic lavas (Klipriviersberg Group) / Johannesburg (SA) Township Quartz Porphyry (Makwassie Formation) / Klerksdorp (SA)	2370 ± 70 2371 +102/-106	Pb-Pb; whole-rock Pb-Pb; whole-rock	Partial thermal resetting age/event Partial thermal resetting age/event
	Armstrong *et al*. (1991)	Mafic lavas (Klipriviersberg Group) / Central Rand Goldfield (SA) Township Quartz Porphyry (Makwassie Formation) / Klerksdorp (SA)	2369 ± 35, 2341 ± 21, 2295 ± 20, 2203 ± 17 2358 ± 8, 2330 ± 8, 2152 ± 9	U-Pb; zircon U-Pb; zircon	Partial thermal resetting ages/events Partial thermal resetting ages/events
	Armstrong *et al*. (1991)	Syferfontein Formation (Dominion Group) / Klerksdorp (SA)	2317 ± 31	U-Pb; zircon	Partial thermal resetting age/event
	Giusti (1988)	Varkenskraal Granite / Rand Anticline (SA)	~2200	U-Pb; pyrite	Partial thermal resetting age/event (Pb-mobilization and/or U-depletion)
	Allsopp (1961, 1964)	Halfway-House Granite / Johannesburg Dome (SA)	2310 ± 40, 2261 ± 80	Rb-Sr; biotite	Partial thermal resetting age/event
	Barton *et al*. (1986)	Linden Tonalite / Johannesburg Dome (SA)	2268 ± 94	Rb-Sr; whole-rock	Partial thermal resetting age/event
	Allsopp *et al*. (1986)	Kerogen from Carbon Leader & Vaal reefs / Carletonville & Klerksdorp goldfields (SA)	2320 ± 50	U-Pb; kerogen	Formation/crystallisation age of kerogen; thermal resetting age/event
	Robb *et al*. (1994)	Kerogen from Carbon Leader & Vaal reefs / Carletonville & Klerksdorp goldfields (SA) Bitumen nodules from peraluminous granites adjacent to the northwest of Witwatersrand Basin (SA)	2329 + 69/-60 2380 +441/-91	U-Pb; kerogen U-Pb; bitumen	Hydrocarbon circulation and fixation age Hydrocarbon circulation and fixation age; thermal resetting age/event
	Poujol *et al*. (1998, 1999)	Authigenic pyrite from altered Kimberley Reef / Evander Goldfield (SA)	2380 ± 25, 2373 ± 18, ~2487, ~2448	Pb-Pb; pyrite	Formation/crystallisation age of pyrite
	Kositcin *et al*. (2001) England *et al*. (2001)	Vaal Reef conglomerate (Johannesburg Subgroup) / Vaal Reef No. 8 Shaft, Klerksdorp Goldfield (SA)	~2382 - 2039	U-Pb; .xenotime	Post-diagenetic thermo-tectonic events (~2040 Ma = Au & U remobilisation during Bushveld and/or Vredefort events)
	Barton *et al*. (1999)	Leucosome from migmatite / Johannesburg Dome (SA) Tonalite / Johannesburg Dome (SA) Granodiorite and granite (SA)	2430 ± 50 2385 ± 127, 2321 ± 23 2240 ± 53, 2202 ± 56, 2188 ± 44, 2158 ± 47, 2117 ± 47, 2110 ± 45	Rb-Sr; whole-rock Rb-Sr; whole-rock Rb-Sr; biotite	Partial thermal resetting age/event Partial thermal resetting age/event Partial thermal resetting age/event
	Lana *et al*. (2003e)	Quartz-sericite-biotite schist / Greenlands Greenstone Complex of Vredefort Dome (SA)	2202 ± 3	U-Pb; rutile	Time of hydrothermal activity
	Flowers *et al*. (2003)	High-grade migmatite / Central part of Vredefort Dome (SA)	~2260	U-Pb ; monazite	
	Robertson (1988)	Various lithologies of Broodkop Migmatite Complex within D_4 Shear Zone / SE sector of Vredefort Dome (SA)	~2200	Rb-Sr; whole-rock	Time of hydrothermal activity during shearing along D_4 Shear Zone (this study)
	Reimold *et al*. (1990)	Pseudotachylite / Vredefort Dome (SA)	2250 ± 0.04	K-Ar	Time of pseudotachylite formation
	Gibson *et al*. (2000)	Greenschist-amphibolite facies metasediments of Witwatersrand Supergroup and mafic meta-lava of Dominion Group / Vredefort Dome	2169 ± 7	^{40}Ar-^{39}Ar; sericite	M1 and M2 metamorphism accompanying the Bushveld magmatic and Vredefort Impact events at ~2.06 and 2.02 Ga, respectively
	Barton *et al*. (1988)	Galena in extension fractures within VCR / Carletonville Goldfield	~2150	Pb-Pb; galena	Formation/crystallization age of galena; thermal resetting age/event

APPENDIX 21-A: Summary of selected geochronological data pertinent to the Kaapvaal Craton.

Period	Reference	Lithology / Locality	Age (Ma)	Method	Interpretation by author(s)
KRAAIPAN TERRANE [NEOARCHAEAN-PALAEOPROTEROZOIC (~2.72-2.22 Ga)]	McCourt *et al*. (2000)	Skalkseput Granite (porphyritic) / Marydale granitoid-greenstone terrane (SA)	2718 ± 8	U-Pb, zircon	Interpretation unclear; Resetting/hydrothermal alteration event (this study)
	Walraven *et al*. (unpubl.)	Rosendal and Waterloo lavas within Vryburg Formation (Transvaal Supergroup?; Ventersdorp Supergroup = this study) / Vryburg (SA)	2642 ± 2	U-Pb; zircon	Formation/crystallisation age (= lower age limit of Transvaal Sequence.); Upper age limit of Ventersdorp Supergroup (this study)
	Vajner (1974a&b)	Skalkseput Granite (porphyritic) / Marydale granitoid-greenstone terrane (SA)	~2640	U-Pb; zircon	Formation/crystallisation age; Resetting/hydroth. alteration event (this study)
	Altermann (1996) & Altermann & Nelson (1998)	Tuff bed in lower Nauga Formation of Campbellrand Supergroup (Griqualand West Sequence) / (SA)	2588 ± 6	U-Pb; zircon	Formation/crystallisation age (= maximum age/begin of marine transgression/carbonate deposition)
	Altermann & Nelson (1998)	Tuff bed in upper Monteville Formation of Campbellrand Subgroup (Griqualand West Sequence) / (SA)	2555 ± 19	U-Pb; zircon	Formation/crystallisation age
	Barton *et al*. (1994)	Tuff horizon in lower Nauga Formation of Campbellrand Supergroup (Griqualand West Sequence) / near Prieska (SA)	2552 ± 11	U-Pb; zircon	Formation/crystallisation age
	Altermann & Nelson (1998)	Tuff horizon in lower Nauga Formation of Campbellrand Supergroup (Griqualand West Sequence) / near Prieska (SA)	2549 ± 7	U-Pb; zircon	Formation/crystallisation age
	Jahn *et al*. (1990)	Stromatolitic carbonates of Reivilo Formation of lower Campbellrand Supergroup (Griqualand West Sequence) / (SA)	2557 ± 49	Pb-Pb; carbonate	Age of dolomitisation of lower Campbellrand Subgroup
	Summer & Bowring (1996)	Tuff bed in upper part of Gamohaan Formation (top of Campbellrand Subgroup / Griqualand West Sequence) / (SA)	2521 ± 3	U-Pb; zircon	Formation/crystallisation age (=minimum age of Ghaap carbonates)
	Altermann & Nelson (1998)	Tuff bed in upper part of Gamohaan Formation (top of Campbellrand Subgroup / Griqualand West Sequence) / (SA)	2516 ± 4	U-Pb; zircon	Formation/crystallisation age (=minimum age of Ghaap carbonates)
	Armstrong (unpublished data)	Tuff bed at top of Kuruman Iron Formation (Griqualand West Sequence) / (SA)	2465 ± 7	U-Pb; zircon	Formation/crystallisation age
	Pickard (2003)	Felsic tuffaceous mudrocks at top of Riries Member (top of Kuruman Iron Formation (Griqualand West Sequence)) / (SA)	2460 ± 5	U-Pb; zircon	Age of deposition
	Trendall *et al*. (1990)	Tuff bed in lower part of Griquatown Iron Formation (Griqualand West Sequence) / (SA)	2432 ± 31	U-Pb; zircon	Formation/crystallisation age (= upper age limit for deposition of Chuniespoort/Ghaap Group)
	Walraven *et al*. (1982)	Ongeluk Andesite Formation of Postmasburg Group (Griqualand West Supergroup) / (SA)	2240 ± 57	Pb-Pb; whole-rock	Formation/crystallisation age; Thermal resetting age/event (this study)
	Armstrong (1987)	Ongeluk Andesite Formation of Postmasburg Group (Griqualand West Supergroup) / (SA)	2239 +69/-72	Pb-Pb; whole-rock	Formation/crystallisation age; Thermal resetting age/event (this study)
	Cornell *et al*. (1996)	Ongeluk Andesite Formation of Postmasburg Group (Griqualand West Supergroup) / (SA)	2236 ± 38	Pb-Pb; whole-rock	Formation/crystallisation age; Thermal resetting age/event (this study)
	Reimold *et al*. (2002)	Granophyre (~2740 Ma) and granitoid (~2880 Ma) in KHK-1 drill core / ~40km southwest of Ganyesa Dome (Morokweng impact structure)	2363 ± 19, 2298 ± 12, 2232 ± 15, 2352 ± 20	U-Pb; zircon	No interpretation given; Resetting event = hydrothermal alteration (this study)
	Armstrong (1987)	Intercalated lava flow within Vryburg Formation (Griqualand West Sequence) / Griqualand West Basin (SA)	2357 +115/-121	Pb-Pb; whole-rock	Formation/crystallisation age; Thermal resetting age/event (this study)
	Burger & Coertze (1973)	Plantation Porphyry (Lobatse Volcanic Group)	2230 ± 120, 2215 ± 100, 2200 ± 100	Rb-Sr; whole-rock	Formation/crystallisation ages; Thermal resetting ages/event (this study)
	Burger & Coertze (1975)	Correlates of Gaborone Granite Complex & Kanye Volcanic Formation / south of Derdepoort (SA)	2318 ± 17	Rb-Sr; whole-rock	No interpretation given; Thermal resetting ages/event (this study)
	Harding & Snelling (1972)	Gaborone Granite Complex	2305 ± 100 2331 ± 44, 2302 ± 133	K-Ar; whole-rock Rb-Sr; whole-rock	Partial thermal resetting age/event Partial thermal resetting ages/events
	Key & Wright (1982)	Gaborone Granite Complex	2428 ± 55, 2394 ± 26	Rb-Sr; whole-rock	Partial thermal resetting ages/events
	McElhinny (1966)	Gaborone Granite Complex	2290 ± 44	Rb-Sr; whole-rock	No interpretation given; Thermal resetting ages/event (this study)
	Burger (1974)	Gaborone Granite Complex	2318 ± 17	Rb-Sr; whole-rock	Partial thermal resetting age/event
	Harding *et al*. (1974)	Gaborone Granite Complex	2328 ± 44	Rb-Sr; whole-rock	Partial thermal resetting age/event
	Grobler & Walraven (1993)	Gaborone Granite Complex	2341 ± 289	Rb-Sr; whole-rock	Partial thermal resetting age/event
	Walraven *et al*. (1991)	Kareefontein Quartz Porphyry (Zoetlief Group)	2301 ± 28	Pb-Pb; zircon	Partial thermal resetting age/event
	SACS (1980)	Kareefontein Quartz Porphyry (Zoetlief Group)	~2310	U-Pb; zircon	Formation/crystallisation age; Thermal resetting ages/event (this study)
	Barton *et al*. (1986)	BIF from Marydale Group / Marydale Greenstone Belt (SA)	~2200	Pb-Pb; whole-rock	Partial resetting event = age of amphibolite-facies metamorphism

APPENDIX 21-B: Summary of selected geochronological data pertinent to the Zimbabwe Craton.

Period	Reference	Lithology / Locality	Age (Ma)	Method	Interpretation by author(s)
TOKWE TERRANE AND SEBAKWIAN GREENSTONES *[PALAEO-/MESOARCHAEAN (~3.8-3.1 Ga)]*	Horstwood *et al*. (1999)	Sebakwe River gneiss / within Midlands Greenstone Belt Kwekwe gneiss (= western marginal unit of Rhodesdale granitoid-gneiss complex) / Midlands area Tokwe River gneiss / Tokwe Segment Leucosome crosscutting Tokwe River gneiss / Tokwe Segment	3565 ± 21 3456 ± 6 3455 ± 2 3368 ± 9	U-Pb; zircon U-Pb; zircon U-Pb; zircon U-Pb; zircon	Formation/crystallization age Formation/crystallization age Formation/crystallization age Formation/crystallization age
	Dodson *et al*. (2001)	Mushandike granite gneiss / Tokwe Segment	3374 ± 7, 3368 ± 11	U-Pb; zircon	Formation/crystallization age of igneous precursor
	Taylor *et al*. (1991)	Tokwe River migmatitic gneiss / Tokwe Segment Mushandike granodiorite gneiss / Tokwe Segment Shabani gneiss / Tokwe Segment Mont d'Or tonalite-granodiorite gneiss / Tokwe Segment	3475 +87/-93 ~3540 ~3460 ~3670, ~3640	Pb-Pb; whole-rock Sm-Nd; (t_{DM}) Sm-Nd; (t_{DM}) Sm-Nd; (t_{DM})	Formation/crystallization age Age of crustal source rock of Mushandike granodiorite Formation/crystallization age Age of crustal source rock of Mont d'Or tonalite
	Taylor *et al*. (1984)	Mont d'Or tonalite-granodiorite gneiss / Tokwe Segment	3345 ± 55	Pb-Pb; whole-rock	Formation/crystallization age
	Cahen *et al*. (1984)				
	Barton *et al*. (1993)				
	Manuel (1992)	North Vumba granitoid gneiss / Manica Greenstone Belt (Mozambique)	3385 ± 255	Rb-Sr; whole-rock	Formation/crystallization age
	Hawkesworth & Bickle (1977)	Ngezi River gneiss / southeast of Belingwe Ngezi tonalite / southeast of Belingwe	3230 ± 60 3426 ± 40	Rb-Sr; whole-rock Rb-Sr; whole-rock	Formation/crystallization age Formation/crystallization age
	Moorbath *et al*. (1986)	Tokwe River migmatitic gneiss / Tokwe Segment Shabani gneiss / Tokwe Segment	~3600, ~3560 ~3460	Sm-Nd; (t_{DM}) Sm-Nd; (t_{DM})	Age of crustal source rock of Tokwe River gneiss Formation/crystallization age
	Moorbath *et al*. (1977)	Shabani gneiss / Tokwe Segment	3495 ± 120	Rb-Sr; whole-rock	Formation/crystallization age
	Moorbath *et al*. (1976)	Mont d'Or tonalite-granodiorite gneiss / Tokwe Segment	3350 ± 120, 3325 ± 47	Rb-Sr; whole-rock	Formation/crystallization age
	Hawkesworth *et al*. (1975)	Tokwe River migmatitic gneiss / Tokwe Segment Shabani gneiss / Tokwe Segment Mashaba tonalite gneiss / west of Fort Victoria	3500 ± 400 3476 ± 50 3288 ± 150	Rb-Sr; whole-rock Rb-Sr; whole-rock Rb-Sr; whole-rock	Formation/crystallization age Formation/crystallization age Formation/crystallization age
	Hickman (1974a & b)	Mushandike granodiorite gneiss / Tokwe Segment Tonalitic gneisses east of Mushandike granodiorite gneiss / Tokwe Segment	3369 ± 72, 3445 ± 260 3602 ± 290	Rb-Sr; whole-rock Rb-Sr; whole-rock	Age of crustal source rock (Taylor *et al*., 1991) Formation/crystallization age
	Vail & Dodson (1969)	Pegmatite in Que Que gneiss (= unit of the Rhodesdale Batholith) Granite boulder in basal Bulawayan conglomerate / Sebakwe River	3332 ± 70 3259 ± 100	K-Ar; muscovite K-Ar; muscovite	Formation/crystallization age Formation/crystallization age
	Dougherty-Page (1994)	TTG clast in Shamvaian Group / Harare-Bindura-Shamva Greenstone Belt	3197 ± 10	Pb-Pb; zircon	Age of crustal source rock (provenance)
	Dodson *et al*. (1988)	Detrital zircons from conglomerate of Wanderer Formation (= Sebakwaian Group) / Shurugwi Greenstone B. & quartzite of Buhwa sequence (= Lower Bulawayan Group)/Mweza Greenstone B.	abundance peaks at: ~3.8-3.75, 3.6, 3.46, 3.35 and 3.2 Ga	U-Pb; zircon	Age of crustal source rock (provenance) and tectono-magmatic / -metamorphic events

APPENDIX 21-B: Summary of selected geochronological data pertinent to the Zimbabwe Craton.

Period	Reference	Lithology / Locality	Age (Ma)	Method	Interpretation by author(s)
LOWER BULAWAYAN GREENSTONES AND RELATED GRANITOIDS *[NEOARCHAEAN (~3.1-2.81 Ga)]*	Jelsma *et al.* (2004)	Banded migmatitic gneiss / Shangani Batholith	2837.2 ± 0.3	Pb-Pb; zircon	Age of trondhjemite protolith
	Wilson *et al.* (1995)	Koodoovale Formation (Mtshingwe Group) / Belingwe Greenstone Belt Chingezi tonalite / Shangani Batholith Felsic volcanics of Hokonui Formation / Belingwe Greenstone Belt	2904 ± 9 2833 ± 43 2904 ± 9	U-Pb; zircon U-Pb; zircon U-Pb; zircon	Age of inherited zircon (this study) Formation/crystallization age Formation/crystallization age
	Dougherty-Page (1994)	TTG clast in Shamvaian Group / Harare-Bindura-Shamva Greenstone Belt	2925 ± 10, 2800 ± 20 ~2980-3200	Pb-Pb; Sm-Nd; (t_{DM})	Age of crustal source rock (provenance) Age of crustal source rock (provenance)
	Taylor *et al.* (1991)	Rhodesdale gneiss / Rhodesdale Batholith Mushandike granodiorite / Tokwe Segment Chingezi tonalite / Shangani Batholith Cardiff Hill rhyolite of Arcturus Formation / Harare-Bindura-Shamva Greenstone Belt Maliyami Formation / Midlands Greenstone Belt Mafic volcanics / Bulawayo area	~2990 2946 +125/-135 2917 ± 171 2874 ± 32, 2825 +94/-100, 2800 +76/-72, 2686 +88/-94 2818 ± 91, 2723 ± 102, 2684 ± 102 ~3050, ~2980, ~2950 ~2800 2867 +171/-195 2867 +77/-81	Sm-Nd; (t_{DM}) Pb-Pb; whole-rock Pb-Pb; whole-rock Pb-Pb; whole-rock Rb-Sr; whole-rock Sm-Nd; (t_{DM}) Sm-Nd; (t_{DM}) Pb-Pb; whole-rock Rb-Sr; whole-rock	Formation/crystallization age Formation/crystallization age Formation/crystallization age Formation/crystallization age Formation/crystallization age Age of crustal source rock (provenance) Age of crustal source rock (provenance) Formation/crystallization age Formation/crystallization age
	Baldock & Evans (1988)	Metadacites (Upper Bulawayan Group) / Harare-Bindura-Shamva Greenstone Belt Umwindsi gneiss / Harare-Bindura-Shamva Greenstone Belt Passaford Formation / Harare-Bindura-Shamva Greenstone Belt Iron Mask Formation / Harare-Bindura-Shamva Greenstone Belt	~2870, ~2853, ~2812 2865 ± 135 ~2870-2810 ~3050-2910	Sm-Nd; (t_{DM}) Rb-Sr; whole-rock Sm-Nd; (t_{DM}) Sm-Nd; (t_{DM})	Age of crustal source rock (provenance) Formation/crystallization age Age of crustal source rock (provenance) Age of crustal source rock (provenance)
	Moorbath *et al.* (1987)	Mushandike granodiorite	2917 ± 171 2946 +125/-135	Rb-Sr; whole-rock Pb-Pb; whole-rock	Formation/crystallization age Formation/crystallization age
	Hawkesworth *et al.* (1979)	Mashaba tonalite Chingezi tonalite / Shangani Batholith	2860 ± 60, 2870 ± 160 2817 ± 35, 2810 ± 70	Rb-Sr; whole-rock Rb-Sr; whole-rock	Formation/crystallization age Formation/crystallization age
	Hickman (1978)	Bangala Dam gneisses and Nyani gneisses / Northern Marginal Zone	2930 ± 60	Rb-Sr; whole-rock	Formation/crystallization age
	Moorbath *et al.* (1977)	Rhodesdale gneiss / Rhodesdale Batholith	2976 +121/-132	Pb-Pb; whole-rock	Formation/crystallization age
	Wilson & Harrison (1973)	Heaney tonalite / between Bulawayo and Fort Rixon Bulawayo porphyritic granite / between Bulawayo and Fort Rixon Mashaba tonalite Essexdale tonalite / between Bulawayo and Fort Rixon Somabula tonalite / between Fort Rixon and Great Dyke Three Fingers porphyritic granite / between Fort Rixon and Great Dyke	2936 ± 59 2875 ± 87, 2822 ± 85 2882 ± 58 2826 ± 57 2812 ± 57 2796 ± 84	K-Ar; hornblende K-Ar; hornblende K-Ar; biotite K-Ar; hornblende K-Ar; biotite K-Ar; biotite	Formation/crystallization age Formation/crystallization age Formation/crystallization age Formation/crystallization age Formation/crystallization age Formation/crystallization age
	Nägler *et al.* (1997)	Synkinematic, metamorphic titanites from supracrustals (*e.g.* quartzites, amphibolites) of Sebakwaian Group /Hormet mine (Tokwe Segment) Synkinematic migmatitic supracrustal boudins of Sebakwian Group / Hormet mine (Tokwe Segment)	2868 ± 21, 2863 ± 26, 2856 ± 20 2852 ± 64, 2848 ± 26	Pb-Pb; titanite Pb-Pb; zircon	Age of penetrative, amphibolite-facies metamorphic and deformation event within Tokwe Segment
		Quartzites and pelites of basal supracrustal succession / Shurugwi Greenstone Belt	<3.1 - >2.86 Ga	Pb-Pb; zircon	Youngest zircon ~3.1 Ga = maximum age of deposition (= Lower Bulawayan Group, this study)
		Shurugwi Ultramafic Complex intrusive into <3.1 Shurugwi supracrustals / Shurugwi Greenstone Belt	<3.1 - >2.86 Ga		Age constrained by maximum age of deposition (<3.1Ga) and metamorphism/deformation at 2.86Ga
	Vail & Snelling (1971)	Biotite gneiss of Pfungwe Metamorphic Suite / Pfunzi Orogenic Belt	2947 ± 129	Rb-Sr; whole-rock	Age of granulite-facies metamorphism
	Barton *et al.* (1991)	Partly retrogressed felsic granulite pods within orthogneiss of Mudzi Metamorphic Suite (Migmatitic Gneiss Terrain) / Pfunzi Orogenic Belt	2937 ± 178	Rb-Sr; whole-rock	Age of granulite-facies metamorphism

APPENDIX 21-B: Summary of selected geochronological data pertinent to the Zimbabwe Craton.

Period	Reference	Lithology / Locality	Age (Ma)	Method	Interpretation by author(s)
MANJERI FORMATION AND EQUIVALENTS (= MIDDLE GREENSTONES) *[NEOARCHAEAN (~2.81-2.72 Ga)]*	Wilson *et al*. (1995)	Dacite clast in reworked volcanic breccia (Koodoovale Formation, Mtshingwe Group) / Belingwe Greenstone Belt Rhyolite of Arizona Formation / Gweru Greenstone Belt Felsic volcanic of Eldorado Formation / Filabusi Greenstone Belt	2831 ± 6 2805 ± 6 2799 ± 9, 2788 ± 10	U-Pb; zircon U-Pb; zircon U-Pb; zircon	Formation/crystallization age Formation/crystallization age Formation/crystallization age
	Bolhar *et al*. (2002)	Limestone of Manjeri Formation / Belingwe Greenstone Belt	2706 ± 49	Pb-Pb; whole-rock	Age of early diagenesis (= minimum age of deposition)
	Moorbath *et al*. (1987)	Limestone of Marbel Formation (= correlative to Manjeri Formation; this study) / Masvingo Greenstone Belt	2839 ± 33	Pb-Pb; whole-rock	Age of early diagenesis (= minimum age of deposition)
	Manhica (1998)	Felsic tuffaceous schist (Mbeza-Vengo Formation/ Manica Group) / Manica Greenstone Belt (Mozambique)	2801 ± 42	Rb-Sr; whole-rock	Formation/crystallization age
	Manuel (1992)	Felsic tuffaceous schist (Mbeza-Vengo Formation/ Manica Group) / Manica Greenstone Belt (Mozambique)	2810 ± 36	Rb-Sr; whole-rock	Formation/crystallization age
UPPER BULAWAYAN GREENSTONES *[NEOARCHAEAN (~2.72-2.64 Ga)]*	Jelsma *et al*. (1996)	Rhyodacite of Iron Mask Formation / Harare-Bindura-Shamva Greenstone Belt	2715 ± 15	U-Pb; zircon	Formation/crystallization age
	Wilson *et al*. (1995)	Andesite of Maliyami Formation / Midlands Greenstone Belt Felsic Volcanic of Surprise Formation / Shurugwi Greenstone Belt Tuffite of Maparu Formation (intercalated with Arcturus Formation) / Harare-Shamva Greenstone Belt Rhyodacite of Avalon Formation / Bulawayan Greenstone Belt Felsic clast in reworked volcanic breccia of What Cheer Formation / Midlands Greenstone Belt Rhyolite of Iron Mask Formation / Harare-Bindura-Shamva Greenstone Belt Volcaniclastic sediments of Passaford Formation / Harare-Shamva Greenstone Belt	2702 ± 6 2698 ± 27 2697 ± 9 2696 ± 7 2683 ± 8 2645 ± 4 2643 ± 8	U-Pb; zircon U-Pb; zircon U-Pb; zircon U-Pb; zircon U-Pb; zircon U-Pb; zircon U-Pb; zircon	Formation/crystallization age Formation/crystallization age Formation/crystallization age Formation/crystallization age Formation/crystallization age Formation/crystallization age Formation/crystallization age
	Chauvel *et al*. (1993)	Komatiitic metabasalts of Reliance Formation / Belingwe Greenstone Belt Metabasalt / Bulawayo Greenstone Belt	2692 ± 9 2675 ± 173	Pb-Pb; whole-rock Pb-Pb; whole-rock	Formation/crystallization age Formation/crystallization age
	Taylor *et al*. (1991)	Gwenoro Dam migmatitic gneisses Cardiff Hill rhyolite of Arcturus Formation / Harare-Bindura-Shamva Greenstone Belt	2705 + 60/-63 2721 ± 60 2659 +38/-39	Pb-Pb; whole-rock Rb-Sr; whole-rock Pb-Pb; whole-rock	Formation/crystallization age Formation/crystallization age Formation/crystallization age (mixed age)
	Baldock & Evans (1988)	Felsic volcanics / Bulawayo Greenstone Belt Felsic volcanics of Iron Mask Formation / Harare-Bindura-Shamva Greenstone Belt Metadacites of Upper Bulawayan Group / Harare-Bindura-Shamva Greenstone Belt	2615 ± 28 2512 ± 168 ~2742 ~2717, ~2662, ~2616	Rb-Sr; whole-rock Rb-Sr; whole-rock Sm-Nd; (t_{CHUR}) Sm-Nd; (t_{CHUR})	Formation/crystallization age Formation/crystallization age Age of crustal source rock (provenance) Age of crustal source rock/Formation/crystallization age
	Chauvel *et al*. (1983)	Upper Bulawayan Group / Belingwe Greenstone Belt	2690 ± 26	Pb-Pb; whole-rock	Formation/crystallization age
	Bolhar *et al*. (2002)	Limestone of Cheshire Formation (Ngezi Group) / Belingwe Greenstone Belt	2601 ± 49	Pb-Pb; whole-rock	Age of early diagenesis (= minimum age of deposition)
	Shimizu *et al*. (2001)	Komatiite (Zeederbergs Formation, Ngezi Group) / Belingwe Greenstone Belt Komatiitic basalt (Zeederbergs Formation, Ngezi Group) / Belingwe Greenstone Belt Enriched basalt (Zeederbergs Formation, Ngezi Group) / Belingwe Greenstone Belt	2634 ± 425 2649 ± 89 2654 ± 28	Pb-Pb; whole-rock Pb-Pb; whole-rock Pb-Pb; whole-rock	Formation/crystallization age Formation/crystallization age Formation/crystallization age
	Hamilton *et al*. (1977)	Mixed suite of mafic volcanics / Kwekwe, Bulawayo and Masvingo greenstone belts	2640 ± 140	Sm-Nd	Formation/crystallization age (mixed age)
	Jahn & Condie (1976)	Komatiitic metabasalts of Reliance Formation / Belingwe Greenstone Belt Metabasalts / Bulawayo and Kwekwe areas Mafic-intermediate volcanics of Arcturus Formation / Harare-Bindura-Shamva Greenstone Belt Harare-Bindura-Shamva Greenstone Belt Upper Bulawayan Group / Bulawayo Greenstone Belt	2700 ± 70 2690 ± 90 2670 ± 60 2730 ± 60 2629 ± 78	Rb-Sr; whole-rock Rb-Sr; whole-rock Rb-Sr; whole-rock Rb-Sr; whole-rock Rb-Sr; whole-rock	Formation/crystallization age Formation/crystallization age (mixed age) Formation/crystallization age Formation/crystallization age Formation/crystallization age
	Hawkesworth *et al*. (1975)	Gwenoro Dam migmatitic gneiss Maliyami Formation / Midlands Greenstone Belt Bulawayo Greenstone Belt	2730 ± 24 2660 ± 70, 2680 ± 74 2540 ± 180	Rb-Sr; whole-rock Rb-Sr; whole-rock Rb-Sr; whole-rock	Formation/crystallization age Formation/crystallization age Formation/crystallization age
	Wilson & Harrison (1973)	Mpopoti porphyritic granite / between Fort Rixon and Great Dyke	2715 ± 82	K-Ar; biotite	Formation/crystallization age

APPENDIX 21-B: Summary of selected geochronological data pertinent to the Zimbabwe Craton.

Period	Reference	Lithology / Locality	Age (Ma)	Method	Interpretation by author(s)
SESOMBI-WEDZA GRANITOID SUITE *[NEOARCHAEAN (~2.72-2.64 Ga)]*	Bagai *et al*. (2002)	Mafic xenolith from G2 migmatitic gneiss / Sebina village, Vumba granite-greenstone terrain	2733 ± 5	U-Pb; zircon	Formation/crystallization age of lower mafic-ultramafic volcanics
		G4 Vumba dioritic granitoid / Vumba granite-greenstone terrain	2696 ± 4	U-Pb; zircon	Formation/crystallization age
		G2 Maebe granitic gneiss/migmatite / Vumba granite-greenstone terrain	2690 ± 4	U-Pb; zircon	Formation/crystallization age of igneous precursor
		G1 tonalitic orthogneiss (Mashawe pluton) / Nswazwi village, Vumba granite-greenstone terrain	2686 ± 6	U-Pb; zircon	Formation/crystallization age of igneous precursor
		G5 granitoid (Domboshaba monzogranite) / Vumba granite-greenstone terrain	2647 ± 4	U-Pb; zircon	Formation/crystallization age
	Jelsma *et al*. (1996) and Vinyu *et al*. (1996)	Granodiorite (Wedza suite) / Harare-Bindura-Shamva Greenstone Belt	2667 ± 4	U-Pb; zircon	Formation/crystallization age (mixed age)
		Mazowe (Jumbo) granodiorite (Wedza suite) / Harare-Bindura-Shamva Greenstone Belt	2664 ± 15 ~2780, ~2640	U-Pb; zircon Sm-Nd; (t_{DM})	Formation/crystallization age (mixed age) Age of crustal source rock, mantle derivation age
		Shear zone-hosted gold-scheelite-tourmaline hydrothermal veins within Mazowe (Jumbo) granodiorite and calc-silicate skarn / Harare-Bindura-Shamva Greenstone Belt	2664 ± 14, 2659 ± 13	Pb-Pb; minerals	Age of hydrothermal gold mineralisation within ductile shear zone and synchronous skarn formation
		Bindura granodiorite (Wedza suite) / Harare-Bindura-Shamva Greenstone Belt	2649 ± 6 ~2780, ~2620-2640	U-Pb; zircon Sm-Nd; (t_{DM})	Formation/crystallization age (mixed age) Age of crustal source rock, mantle derivation age
		Chishawasha granodiorite	2646 ± 36	Pb-Pb; whole-rock	Formation/crystallization age
		Porphyries / Harare-Bindura-Shamva Greenstone Belt	2641 +57/-76	Pb-Pb; whole-rock	Formation/crystallization age
	Horstwood (1999)	Sesombi tonalite / Midlands Greenstone Belt	2668 ± 17	U-Pb; zircon	
	Darbyshire *et al*. (1996)	Scheelites from gold-tungsten veins oblique or near parallel to S1 / Midlands Greenstone Belt	2668 ± 64	Sm-Nd; scheelite	Age of hydrothermal gold mineralisation
	Mkweli *et al*. (1995)	Tshaba River granite (Sesombi-Wedza suite, this study) / south of West Nicholson along Ruti Shear Zone (= Umtali suture)	2669 ± 67	U-Pb; zircon	Formation/crystallization age
	Dougherty-Page (1994)	Granodiorite (Sesombi suite) / Harare-Bindura-Shamva Greenstone Belt	2673 ± 5		
	Taylor *et al*. (1991)	Somabula tonalite / between Fort Rixon and Great Dyke	2752 +50/-52 ~2740	Pb-Pb; whole-rock Sm-Nd; (t_{DM})	
		Sesombi tonalite / Midlands Greenstone Belt	2579 +154/-173 ~2680	Pb-Pb; whole-rock Sm-Nd; (t_{DM})	
	Hawkesworth *et al*. (1975)	Somabula tonalite / between Fort Rixon and Great Dyke	2720 ± 60, 2650 ± 80	Rb-Sr; whole-rock	
		Sesombi tonalite / Midlands Greenstone Belt	2690 ± 140, 2633 ± 140, 2602 ± 50	Rb-Sr; whole-rock	
		Umniati gneiss / from Rhodesdale batholith near Que Que	2686 ± 33	Rb-Sr; whole-rock	
	Hickman (1974a)	Somabula tonalite / between Fort Rixon and Great Dyke	2650 ± 80		
	Baldock & Evans (1988)	Denda granodiorite (Wedza suite) / Harare-Bindura-Shamva Greenstone Belt	2680 ± 104	Rb-Sr; whole-rock	
	Schmidt-Mumm *et al* (1993)	Tonalite-granodiorite at Penhalonga (Redwing Gold Mine) / Mutare Greenstone Belt	2742 ± 3	U-Pb; zircon	Formation/crystallization age
		Gold mineralization at Redwing Gold Mine / Mutare Greenstone Belt	2650 ± 100	estimated model age	Age of hydrothermal gold mineralisation
	Frei & Pettke (1996)	Shear zone-hosted gold-sulphide-tourmaline hydrothermal veins / Kimberley mine (Harare-Bindura-Shamva Greenstone Belt)	2647 ± 9	Pb-Pb; tourmaline	Age of hydrothermal gold mineralisation within ductile shear zone
	Hanson *et al*. (1998)	Xenocrystic zircon from Kubu Island granite / Sua Pan; southwestern Zimbabwe Craton (Botswana)	~2670	Pb-Pb; zircon	Emplacement of Kubu Island granite within lithosphere with a Neoarchaean component
	Majaule & Davis (1998)	Leucocratic granodiorite gneiss / east of Bushman shear zone in Mosetse area (Botswana)	2648 ± 2	U-Pb; zircon	Formation/crystallization age
		Megacrystic, migmatitic monzodiorite / east of Bushman shear zone in Mosetse area (Botswana)	2646 ± 2.5 2639 ± 2	U-Pb; zircon U-Pb; titanite	Formation/crystallization age Formation/crystallization age
		Intensely altered migmatitic tonalite gneiss / east of Bushman shear zone in Mosetse area (Botswana)	2710 ± 19	U-Pb; zircon	Estimated formation/crystallization age
		Tonalitic gneiss / east of Bushman shear zone in Mosetse area (Botswana)	2648 ± 2.5	U-Pb; zircon	Formation/crystallization age
SHAMVAIAN GROUP, CHILIMANZI-RAZI GRANITOID SUITE AND GREAT DYKE *[NEOARCHAEAN (~2.72-2.64 Ga)]*	Jelsma *et al*. (1996)	TTG clast in Shamvaian Group / Harare-Bindura-Shamva Greenstone Belt	3030 ± 37	Pb-Pb; whole-rock	Age of crustal source rock (provenance)
			~3040-2720	Sm-Nd; w-r	Age of crustal source rock (provenance)
		Black Cat porphyry (Shamvaian Group) / Harare-Bindura-Shamva Greenstone Belt	2672 ± 12	U-Pb; zircon	Formation/crystallization age (mixed age)
		Shamva porphyries / Harare-Bindura-Shamva Greenstone Belt	2641 ± 64	Pb-Pb; whole-rock	Formation/crystallization age
			~2830-2710	Sm-Nd; w-r	Age of crustal source rock
	Wilson *et al*. (1995)	Felsic volcanics of Shamvaian Group / Masvingo Greenstone Belt	2661 ± 17	U-Pb; zircon	Formation/crystallization age
		Felsic volcanics of Shamvaian Group / Harare-Bindura-Shamva Greenstone Belt	2645 ± 4, 2643 ± 8	U-Pb; zircon	Formation/crystallization age
	Dougherty-Page (1994)	Pre-sedimentary metamorphic age of TTG clast in conglomerate of Shamvaian Group	~2680-2650	Pb-Pb; whole-rock	Youngest detrital component = maximum age of deposition
	Armstrong & Wilson (2000)	Granitic wall-rock of Darwendale Subchamber / Great Dykes	2647 ± 9	U-Pb; zircon	Formation/crystallization age
	Vinyu *et al*. (2001)	Granitic leucogneiss intruding paragneisses / Pfunzi Orogenic Belt	~2623	U-Pb; zircon	Formation/crystallization age; age of amphibolite-facies metamorphism and migmatisation
		Makachi granitoid / Pfunzi Orogenic Belt	2625.1 ± 1.4	U-Pb; zircon	
		Tonalitic orthogneiss / Pfunzi Orogenic Belt	~2620	U-Pb; zircon	
	Dirks *et al*. (2000)	Quartzofeldspathic gneisses of Migmatitic Gneiss Terrain / Pfunzi Orogenic Belt	~2620-2571	Pb-Pb; zircon	Formation/crystallisation age
		Porphritic granites intrusive into Migmatitic Gneiss Terrain / Pfunzi Orogenic Belt	~2570-2559	Pb-Pb; zircon	Formation/crystallisation age

APPENDIX 21-B: Summary of selected geochronological data pertinent to the Zimbabwe Craton.

Period	Reference	Lithology / Locality	Age (Ma)	Method	Interpretation by author(s)
SHAMVAIAN GROUP, CHILIMANZI-RAZI GRANITOID SUITE AND GREAT DYKE *[NEOARCHAEAN (~2.72-2.64 Ga)]*	Hofmann *et al*. (2002)	Light grey, porphyritic Chirwa dome granite / Makaha Greenstone Belt Granite clasts in strongly foliated metaconglomerate / Makaha Greenstone Belt Medium grey, xenolith-rich granodioritic gneiss / Makaha Greenstone Belt Pale grey, leucocratic granitic gneiss cross-cutting xenolith-rich granodioritic gneiss / Makaha G. B.	2569.6 ± 0.3 2628.6 ±0.3–2613.1 ±0.5 2601.3 ± 0.5 2593.3 ± 0.3	Pb-Pb evapor.; zircon Pb-Pb evapor.; zircon Pb-Pb evapor.; zircon Pb-Pb evapor.; zircon	Formation/crystallization age Formation/crystallization age of granite source Formation/crystallization age of igneous precursor Formation/crystallization age of igneous precursor
	Jelsma *et al*. (1996) and Vinyu *et al*. (1996)	Glendale tonalite (Chilimanzi suite) / Harare-Bindura-Shamva Greenstone Belt Murehwa granite batholith (Chilimanzi suite) / Harare-Bindura-Shamva Greenstone Belt	2618 ± 6 ~2650-2620 2601 ± 14	U-Pb; zircon Sm-Nd; w-r U-Pb; zircon	Formation/crystallization age Mantle derivation age Formation/crystallization age (mixed age)
	Frei & Kamber (1995)	Garnet from an auriferous calc-silicate skarn / (Jumbo/Mazowe Mine) Harare-Bindura-Shamva Greenstone Belt	2618 ± 19 2611 ± 17	Pb-Pb; garnet Pb-Pb; garnet, diopsite & pyrite	Age of shear-zone hosted gold mineralisation and adjacent skarn alteration/mineralisation
	Baldock & Evans (1988)	Felsic volcanics / Bulawayo Greenstone Belt	2615 ± 28	Rb-Sr; whole-rock	Formation/crystallization age
	Hickman (1974b)		2620 ± 80, 2610 ± 60		
	Frei (1994)	Pyrite from quartz-gold veins, and garnet, diopside and pyrite from auriferous calc-silicate skarn / (Mazowe Mine) Harare-Bindura-Shamva Greenstone Belt	2609 ± 37	Pb/Pb; pyrite, garnet, diopside	Age of hydrothermal gold mineralisation
	Oberthür *et al*. (2000)	Scheelite in gold-pyrite-quartz-carbonate veins / (Stori's Golden Shaft Mine) Harare-Bindura-Shamva Greenstone Belt	2604 ± 84	Sm-Nd; scheelite	Age of hydrothermal gold mineralisation
	Kamber *et al*. (1996)	Samba charnockite (Razi suite) / Northern Marginal Zone along S-contact of Triangle Shear Zone	2591 ± 4	U-Pb; zircon	Formation/crystallization age and age of peak metamorphism in Northern Marginal Zone
	Mkweli *et al*. (1995) recalculated by Frei *et al*. (1999)	Mataga porphyritic granite (Razi suite) / along and within North Limpopo Thrust Zone Syn- to late-tectonic granites (Razi Suite) / within Northern Limpopo Thrust Zone	2627 ± 7 2587 ± 51	U-Pb; zircon Rb-Sr; whole-rock	Formation/crystallization age Formation/crystallization age
	Hickman (1978) recalculated by Frei *et al*. (1999)	Chibi granite batholith (Chillimanzi suite)	2630 ± 30 2574 ± 15	Rb-Sr; whole-rock recalculated	Formation/crystallization age (mixed age) Formation/crystallization age
	Siegesmund *et al*. (2002)	Boudinaged pegmatite within mafic schists in contact zone between Chinamora & Murehwa batholith and wedge-shaped Shamva greenstone belt / Shamva area (Harare-Bindura-Shamva Greenstone Belt)	2619 +28/-24	U-Pb, apatite	Formation/crystallization; age of syntectonic plutonism
	Selby *et al*. (2001)	Gold-sulphide-bearing quartz-molybdenite veins cross-cutting foliated porphyroblastic granodiorite (Eureca granitoid) / Eureca Gold Mine (Harare-Bindura-Shamva Greenstone Belt)	2620 ± 9.4 2620 ± 9.3 2622.6 ± 9.3 2612 ± 9	Re-Os, molybdenite	Age of shear zone-hosted quartz-gold-sulphide mineralisation associated with pegmatitic/aplitic dykes
	Kamber *et al*. (1992)	Granite (Razi suite) / Masvingo	2583 ± 52	Rb-Sr; whole-rock	Formation/crystallization age
	Blenkinsop & Frei (1996)	Renco porphyritic granite (Razi suite)/Northern Marginal Zone along N-contact of Triangle Shear Zone	2571 ± 6 2570 ± 25	U-Pb; zircon Pb-Pb; zircon	Formation/crystallization age Formation/crystallization age
	Hickman (1976) recalculated by Frei *et al*. (1999)	Victoria porphyroblastic granite batholith Chishawasha granite batholith (Razi suite) / Masvingo Great Zimbabwe granite batholith Chilimanzi granite batholith	2604 ± 70 2574 ± 14 2554 ± 60 2554 ± 60	Rb-Sr; whole-rock Rb-Sr; whole-rock Rb-Sr; whole-rock Rb-Sr; whole-rock	Formation/crystallization age Formation/crystallization age Formation/crystallization age Formation/crystallization age
	Frei *et al*. (1999)	Matibi porphyritic granite (Razi suite) / Northern Marginal Zone Romorehoto porphyritic granite (Razi suite) / along and within North Limpopo Thrust Zone Rutenga porphyritic granite (Razi suite) / Northern Marginal Zone along S-contact of Triangle Shear Z. Great Zimbabwe porphyritic granite (Razi suite) / S of Masvingo along Ruti Shear Z. (= Umtali suture) Mavizhu porphyritic granite (Razi suite) / Northern Marginal Zone along N-contact of Triangle Shear Z.	2604 ± 22 2590 ± 7, 2589 ± 11 2576 ± 31 2540 ± 38 2517 ± 55	U-Pb; zircon U-Pb; zircon U-Pb; zircon U-Pb; zircon U-Pb; zircon	Formation/crystallization age Formation/crystallization age Formation/crystallization age Formation/crystallization age Formation/crystallization age
	Mukasa *et al*. (1998)	Darwendale, Sebakwe and Wedza subchambers / Great Dyke	2596 ± 14 2587 ± 8 2586 ± 16, 2572 ± 43	Pb-Pb; w-r & min. U-Pb; rutile Sm-Nd; w-r & min.	Formation/crystallization age Formation/crystallization age Formation/crystallization age
	Wingate (2000)	Umvimeela Dyke, East Dyke and Darwendale Subchamber / Great Dyke Darwendale Subchamber / Great Dyke	2574 ± 2 2571 ± 9	U-Pb; baddeleyite U-Pb; zircon	Formation/crystallization age Formation/crystallization age
	Armstrong & Wilson (2000)	Websterite pegmatoid of Selukwe Subchamber / Great Dyke Granitoid anatectic dyke of Darwendale Subchamber / Great Dyke	2579 ± 3 2574 ± 7	U-Pb; zircon U-Pb; zircon	Formation/crystallization age Formation/crystallization age
	Oberthür *et al*. (2002)	Bronzitites of P1 pyroxenite layer / Great Dyke	2575.4 ± 0.7	U-Pb; zircon, rutile	Formation/crystallization age
	Kempen *et al*. (1997)	Synkinematic pegmatites emplaced along gold-sulphide mineralised NNW-verging thrust zones and ENE/WSW-striking steep shear zones / Renco Mine (Northern Marginal Zone) Shear zone-hosted chalcopyrite associated with gold mineralisation / Renco Mine (Northern Marginal Zone)	2553 ± 114 2580 ± 10; 2560 ± 10	Rb-Sr; whole-rock Pb-Pb; chalcopyrite	Formation/crystallization age Formation/crystallization age; age of gold mineralisation
	Buchholz *et al*. (1998)	Ford porphyritic granite / Midlands Greenstone Belt	2541 ± 17	Pb-Pb; zircon	Formation/crystallization age of granite and age of associated granite-/shear-zone-hosted gold mineralisation
	Frei & Kamber (1995)	Clinopyroxene from skarn-type alteration in auriferous thrust/shear zones / Renco Mine (Northern Marginal Zone)	2532 ± 35	Pb-Pb; clinopyroxene	Age of skarn-type alteration & assoc. gold-sulphide miner.
	Schmidt-Mumm *et al*. (1993)	St. Augustine granite at Penhalonga (Redwing Gold Mine) / Mutare Greenstone Belt	2522 ± 36	Rb-Sr; whole-rock	Formation/crystallization age
	Holzer *et al*. (1999)	Shashe granite (Motlutse Complex) / Bobonong area, Botswana	2497 ± 19	U-Pb; zircon	Formation/crystallization age

APPENDIX 21-B: Summary of selected geochronological data pertinent to the Zimbabwe Craton.

Period	Reference	Lithology / Locality	Age (Ma)	Method	Interpretation by author(s)
PALAEOPROTEROZOIC (~2.53-1.75 Ga)	Darbyshire *et al.* (1996)	Scheelites from gold-tungsten veins crosscutting S1 / (Lily-Whitewaters area) Midlands Greenstone Belt Scheelites from gold-tungsten veins crosscutting S1 / (Rhodesdale terrane) Midlands Greenstone Belt	2413 ± 71 2444 ± 102	Sm-Nd; scheelite Sm-Nd; scheelite	Age of hydrothermal gold mineralisation Age of hydrothermal gold mineralisation
	Frei & Pettke (1996)	Shear zone-hosted gold-sulfide-tourmaline hydrothermal veins / Kimberley mine (Harare-Bindura-Shamva Greenstone Belt)	~2415-2285	Ar-Ar; biotite	
	Pitfield & Campbell (1993)	Hatchland porphyry / Midlands Greenstone Belt	2457 ± 65	Rb-Sr; whole-rock	Formation/crystallization age
	Berger *et al.* (1993)	Post-tectonic granite intrusive into Northern Marginal Thrust Zone	2428 ± 7	U-Pb; zircon	Formation/crystallization age
	Tomschi *et al.* (1989)	Galena in hydrothermal veins in Jumbo/Mazowe pluton / Harare-Bindura-Shamva Greenstone Belt	2410 ± 20	Pb-Pb; galena	
	Oberthür *et al.* (2000)	Scheelite in gold-pyrite-quartz-carbonate veins / (Mazowe Mine) Harare-Bindura-Shamva Greenstone Belt	2430 ± 460 2410 ± 200	Rb-Sr; scheelite Sm-Nd; scheelite	Resetting event = hydrothermal alteration; age of hydrothermal gold mineralisation (this study)
	McCourt *et al.* (2001)	Hurungwe granite (intrusive into Piriwiri Group) / Magondi Orogenic Belt	1997.5 ± 2.6 2742 ± 12, 2454 ± 12, 2198 ± 5	U-Pb; zircon (rims & magmatic) U-Pb; zircon (cores)	Formation/crystallization age of Hurungwe Granite Inherited zircons = ages of basement units
	Clifford *et al.* (1967)	Urungwe (=Hurungwe) granite (intrusive into Piriwiri Group) / Magondi Orogenic Belt	2153 ± 125	Rb-Sr; whole-rock	Formation/crystallization age
	Priem *et al.* (1972)	Syn-orogenic granodiorite (Dete-Kamativi inlier) / Magondi Orogenic Belt Post-orogenic granite (Dete-Kamativi inlier) / Magondi Orogenic Belt	2195 ± 100 2000 ± 80	Rb-Sr; whole-rock Rb-Sr; whole-rock	Formation/crystallization age Formation/crystallization age
	Schidlowski & Todt (1998)	Dolomites of Lomagundi Group / Magondi Orogenic Belt	~2130	Pb-Pb; whole-rock	Formation/crystallization age
	Höhndorf & Vetter (1999)	Galena from Piriwiri Group / Magondi Orogenic Belt	2122 ± 14	Pb-Pb; galena	Age of Pb-Zn mineralisation?
	Treloar (1988)	Mafic lavas near the base of Deweras Group / Magondi Orogenic Belt Galena from Copper Queen massive sulphide deposit (Piriwiri Group) / Magondi Orogenic Belt	2170 ± 100 ~2100	Rb-Sr; whole-rock Pb-Pb; galena	Formation/crystallization age Minimum age of deposition of Piriwiri Group
	Loney (1969)	Miami granite intrusive into pelitic gneisses/schists of Piriwiri Group / eastern end of Lake Kariba Syn- to post-kinematic granitoids intrusives into gneisses / Kariba area; Magondi Orogenic Belt	2049 ± 32 1980 ± 80	Rb-Sr; whole-rock Rb-Sr; whole-rock	Formation/crystallization age Formation/crystallization age
	Munyanyiwa *et al.* (1995)	Charno-enderbite intrusive into gneisses of internal zone of Magondi Belt / Magondi Belt Enderbite intrusive into gneisses of internal zone of Magondi Belt / Magondi Belt	1959 ± 3 1960 ± 39 1933 ± 4 1932 ± 17	Pb-Pb evapor.; zircon U-Pb; zircon Pb-Pb evapor.; zircon U-Pb; zircon	Formation/crystallization age of enderbite and charno-enderbite and age of peak-metamorphism
	Hanson *et al.* (1998)	Kubu Island granite / Sua Pan, southwestern Zimbabwe Craton (Botswana)	2038 ± 15	U-Pb; zircon	Formation/crystallization age
	Frei & Pettke (1996)	Shear zone-hosted gold-sulfide-tourmaline hydrothermal veins / Kimberley mine (Harare-Bindura-Shamva Greenstone Belt)	2021 ± 17 1936 ± 26 1915 ± 19	Pb-Pb; pyrrhotite Pb-Pb; tourmaline Rb-Sr; biotite	Age of multistage hydrothermal gold mineralisation within cataclastically reactivated Late Archaean (~2.65 Ga) shear zones at ~2.02-1.93 Ga
	Compston & McElhinney (1975)	Mashonaland dolerite dykes	1920 ± 73 1921 ± 75 1808 ± 23	Rb-Sr; mean age Rb-Sr; whole-rock, min. Rb-Sr; whole-rock, min.	Formation/crystallization age Formation/crystallization age Formation/crystallization age
	Charlton (1973, 1975)	Mashonaland dolerite dykes	1840 ± 30 ~1764	K-Ar; feldspar K-Ar; whole-rock	Formation/crystallization age Formation/crystallization age
	Wingate (2004, unpubl. data)	Mashonaland dolerite dykes	1860	U-Pb; baddeleyite	Formation/crystallization age
MESOPROTEROZOIC (~1.75-1.0 Ga)	Hahn *et al.* (1991)	Deweras dyke / south and east of Chinhoyi	1100 ± 270	Rb-Sr; whole-rock	Formation/crystallization age
	Allsopp *et al.* (1989)	Mafic lavas and sills (Umkondo Group)	1080 +140/-25	Rb-Sr; whole-rock	Formation/crystallization age
	Munyanyiwa (1997) recalculated by Wingate (2001)	Granophyre horizon within an Umkondo dolerite sill / Chimanimani area	1105 ± 2 1107 ± 6	U-Pb; zircon recalculated	Formation/crystallization age Formation/crystallization age
	Wingate (2001)	Felsic gabbro near upper contact of a Umkondo dolerite sill / Nyanga area	1098 ± 10 1103 ± 32 1099 ± 9	Pb-Pb; baddeleyite Pb-Pb; zircon Estimated/combined	Formation/crystallization age Formation/crystallization age Best estimated combined age of formation/crystallization
	Dirks *et al.* (2000)	Hornblende-bearing tonalitic and porphyritic granodioritic gneisses (Masoso Suite) / Zambezi Belt	~1018-1005	Pb-Pb; zircon	Formation/crystallization ages of igneous precursors

APPENDIX 21-B: Summary of selected geochronological data pertinent to the Zimbabwe Craton.

Period	Reference	Lithology / Locality	Age (Ma)	Method	Interpretation by author(s)
METAMORPHIC OVERPRINT	Taylor, *et al*. (1991)	Shabani gneiss / Tokwe Segment	3088 +44/-46 ~3240	Pb-Pb; whole-rock Sm-Nd; (t_{DM})	Resetting event = hydrothermal alteration Resetting event = hydrothermal alteration
		Northern Marginal Zone	2880 ± 47		Age of granulite-facies metamorphism
	Moorbath *et al*. (1977)	Rhodesdale gneiss	2700 ± 80	Rb-Sr; whole-rock	Resetting event = hydrothermal alteration (Taylor *et al*., 1991)
	Siegesmund *et al*. (2002)	Late kinematic garnets from contact metamorphosed greenstone belt wall rocks in contact zone to Chinamora & Murehwa batholith / Shamva area (Harare-Bindura-Shamva Greenstone Belt) Mafic schists throughout greenstone belt / Shamva area (Harare-Bindura-Shamva Greenstone Belt)	2623 ± 8 2621-2498	Pb-Pb, garnet Ar-Ar; hornblende	Age of metamorphism related to syntectonic plutonism Mixed metamorphic and cooling ages
	Manuel (1992)	South Vumba granitoid gneiss / Manica Greenstone Belt (Mozambique)	2527 ± 632	Rb-Sr; whole-rock	Formation/crystallization age; Resetting event = hydrothermal alteration (this study)
	Hawkesworth *et al*. (1979)	Heaney tonalite / between Bulawayo and Fort Rixon Mashaba tonalite Lower Bulawayan Group / Belingwe Greenstone Belt	2653 ± 100 2545 ± 80 2556 ± 41	K-Ar; biotite K-Ar; biotite Rb-Sr; whole-rock	Resetting event = hydrothermal alteration (Cahen *et al*., 1984) Resetting event = hydrothermal alteration (Cahen *et al*., 1984) Resetting event = hydrothermal alteration (Cahen *et al*., 1984)
	Jelsma *et al*. (1996) and Vinyu *et al*. (1996)	Bindura granodiorite (Wedza suite) / Harare-Bindura-Shamva Greenstone Belt	2617 ± 23	U-Pb; zircon	Resetting event = metamorphism
	Van Dijk & Kater (1996)	Amphibolite of Arcturus Formation / Harare-Bindura-Shamva Greenstone Belt	2621 ± 60 2606 ± 4 2571 ± 44	Ar-Ar; whole-rock U-Pb; garnet Ar-Ar; whole-rock	Age of metamorphic overprint Age of metamorphic overprint Age of metamorphic overprint
	Majaule & Davis	Megacrystic, migmatitic monzodiorite (Sesombi suite, this study) / east of Bushman shear zone in Mosetse area (Botswana) Intensely altered migmatitic tonalite gneiss / east of Bushman shear zone in Mosetse area (Botswana)	2595 ± 6 2638 ± 3.2	U-Pb; titanite U-Pb; titanite	Resetting event = metamorphism Resetting event = metamorphism
	Pitfield & Campbell (1993)	Sesombi tonalite / Midlands Greenstone Belt	2579 ± 42	Rb-Sr; whole-rock	Resetting event = hydrothermal alteration
	Selby *et al*. (2001)	2.62 Ga old gold-sulphide-bearing quartz-molybdenite veins cross-cutting foliated porphyroblastic granodiorite (Eureca granitoid) / Eureca Gold Mine (Harare-Bindura-Shamvaian Greenstone Belt)	2578 ± 9	Re-Os, molybdenite	Resetting event = hydrothermal alteration (this study)
	Moorbath *et al*. (1977)	Somabula tonalite / between Fort Rixon and Great Dyke	2594 ± 80, 2568 ± 73	Rb-Sr; whole-rock	Resetting event = hydrothermal alteration (Taylor *et al*., 1991)
	Jahn & Condie (1976)	Upper Bulawayan Group / Harare-Bindura-Shamva Greenstone Belt Upper Bulawayan Group / Bulawayo Greenstone Belt	2472 ± 156 2383 ± 119	Rb-Sr; whole-rock Rb-Sr; w.-r. & min.	Resetting event = hydrothermal alteration (Cahen *et al*., 1984) Resetting event = hydrothermal alteration (Cahen *et al*., 1984)
	Bolhar *et al*. (2002)	Limestone of Cheshire Formation (Ngezi Group) / Belingwe Greenstone Belt	2543 ± 70	Pb-Pb; whole-rock	1. Late-stage diagenesis, or 2. Resetting event = hydrothermal alteration, or 3. Tectonic activity along Mtshingwe Fault
	Hawkesworth *et al*. (1975)	Upper Bulawayan Group / Bulawayo Greenstone Belt Mixed Lower and Upper Bulawayan Group / Belingwe Greenstone Belt Mafic volcanics / Bulawayo area Mafic volcanics / Kwekwe area Lower Bulawayan Group (pre-Maliyama Formation) / Midlands Greenstone Belt Maliyami Formation (Upper Bulawayan Group) / Midlands Greenstone Belt	2532 ± 70 2507 ± 110 2485 ± 90 2480 ± 140 2452 ± 84 2403 ± 42 2397 ± 91	Rb-Sr; whole-rock Rb-Sr; whole-rock Rb-Sr; whole-rock Rb-Sr; whole-rock Rb-Sr; whole-rock Rb-Sr; w.-r. & min. Rb-Sr; whole-rock	Resetting event = hydrothermal alteration (Cahen *et al*., 1984) Resetting event = hydrothermal alteration (Cahen *et al*., 1984) Resetting event = hydrothermal alteration Resetting event = hydrothermal alteration Resetting event = hydrothermal alteration (Cahen *et al*., 1984) Resetting event = hydrothermal alteration (Cahen *et al*., 1984) Resetting event = hydrothermal alteration (Cahen *et al*., 1984)
	Taylor *et al*. (1991)	Mafic volcanics / Kwekwe area	2380 +309/-394	Pb-Pb;	Resetting event = hydrothermal alteration
	Van Breemen & Dodson (1972)	Volcanics / Tati Greenstone Belt	2523 ± 33	Rb-Sr; whole-rock	Resetting event = hydrothermal alteration (Cahen *et al*., 1984)
	Hamilton (1977) recalculated by Cahen *et al*. (1984) recalculated by Mukasa *et al*. (1998)	Picrite and gabbro of Hartley and Wedza complexes / Great Dyke	2514 ± 16, 2461 ± 16 2452 ± 14 2455 ± 16	Rb-Sr; whole-rock	Resetting event = hydrothermal alteration (this study) Resetting event = hydrothermal alteration (this study) Resetting event = hydrothermal alteration (Mukasa *et al*., 1998)
	Davies *et al*. (1970)	Picrite and gabbro of Hartley, Selukwe and Wedza complexes / Great Dyke	2478 ± 87	Rb-Sr; whole-rock	Resetting event = hydrothermal alteration (this study)
	Robertson & Van Breemen (1970)	Dykes of southern satellite complex / Great Dyke	2533 ± 54	Rb-Sr; whole-rock	Resetting event = hydrothermal alteration (this study)
	Hahn *et al*. (1991)	West and Umvimeela dykes / gabbroic satellites of Great Dyke	2490 ± 120	Rb-Sr; whole-rock	Resetting event = hydrothermal alteration (this study)
	Allsopp (1965) recalculated by Mukasa *et al*. (1998)	Picrite of Hartley and Wedza complexes / Great Dyke	2505 ± 50 2478 ± 100 2476 ± 30	K-Ar; biotite K-Ar; pyroxene K-Ar; pyroxene	Resetting event = hydrothermal alteration (this study) Resetting event = hydrothermal alteration (this study) Resetting event = hydrothermal alteration (Mukasa *et al*., 1998)
	Mukasa *et al*. (1998)	Darwendale Subchamber / Great Dyke	2467 ± 85	Rb-Sr; w-r & min.	Resetting event = hydrothermal alteration
	Bagai *et al*. (2002)	G2 Sebina granitic gneiss/migmatite / Vumba granite-greenstone terrain G5 granitoid (Domboshaba granite) / Vumba granite-greenstone terrain	2489 ± 9, 2478 ± 46, 2466 ± 8, 2464 ± 9, 2464 ± 5, 2339 ± 4, 2318 ± 6, 2305 ± 4, 2303 ± 38 2455 ± 16	U-Pb; zircon U-Pb; zircon	Formation/crystallization age of igneous precursor; Resetting event = hydrothermal alteration (this study) Formation/crystallization age; Resetting event = hydrothermal alteration (this study)

APPENDIX 21-B: Summary of selected geochronological data pertinent to the Zimbabwe Craton.

Period	Reference	Lithology / Locality	Age (Ma)	Method	Interpretation by author(s)
METAMORPHIC OVERPRINT	Loney (1969) recalculated by Master (1991)	Kariba paragneisses (part of Hurungwe paragneisses) / Hurungwe area	2420 ± 100, 2287 ± 92 2368 ± 92	Rb-Sr; whole-rock	Age of metamorphism Age of metamorphism = minimum age of deposition (Master, 1991)
	Loney (1969) recalculated by Master (1991)	Chipisa paragneisses (part of Hurungwe paragneisses) / Hurungwe area	2500 ± 100, 2360 ± 90 2443 ± 90	Rb-Sr; whole-rock	Age of metamorphism Age of metamorphism = minimum age of deposition (Master, 1991)
	Loney (1969)	Pelitic gneisses (correlatives to Piriwiri Group? (= correlatives to Kariba, Chipisa, Chitumbi, Chiroti paragneisses; this study)) / eastern end of Lake Kariba	2465 ± 54	Rb-Sr; whole-rock	Age of deposition Age of metamorphism = minimum age of deposition (this study)
	Vail & Snelling (1971)	Pyroxene-gneiss / Nyamanji (northern Zimbabwe Craton)	2406 ± 170	Rb-Sr; whole-rock	Resetting event = hydrothermal alteration
	Hawkesworth *et al*. (1979)	Chibi batholith / southeast of Belingwe Greenstone Belt near Mukwakwe	2400 ± 170	Rb-Sr; whole-rock	Resetting event = hydrothermal alteration (this study)
	Wingate (2000)	Darwendale Subchamber / Great Dyke and Umvimeela and East dykes Darwendale Subchamber / Great Dyke	2351 ± 20 2466 ± 22 - 2327 ± 11	U-Pb; baddeleyite U-Pb; zircon	Resetting event = hydrothermal alteration Resetting event = hydrothermal alteration
	Selby *et al*. (2001)	~2.62 Ga old gold-sulphide-bearing quartz-molybdenite veins cross-cutting foliated porphyroblastic granodiorite (Eureca granitoid) / Eureca Gold Mine (Harare-Bindura-Shamvaian G. B.)	2219.2 ± 9.1	Re-Os, molybdenite	Resetting event = hydrothermal alteration (this study)
	Bagai *et al*. (2002)	G1 tonalitic orthogneiss (Mashawe pluton) / Vumba granite-greenstone terrain G2 Sebina granitic gneiss/migmatite / Vumba granite-greenstone terrain	2106 ± 10 1733 ± 4	U-Pb; zircon U-Pb; zircon	Formation/crystallization age of igneous precursor; Resetting event = hydrothermal alteration (this study)
	Höhndorf *et al*. (1989)	Mafic lavas (Deweras Group) / Magondi Orogenic Belt	2060 ± 100	Rb-Sr; whole-rock	Resetting event = metamorphism (Master, 1991)
	Jones *et al*. (1975)	Southern satellite dyke complex of Great Dyke/ Northern Marginal Zone	~1950	palaeomagnetics	Resetting event = metamorphism
	Faure *et al*. (1963)	Great Dyke	1950 ± 150	Rb-Sr; whole-rock	Resetting event = hydrothermal alteration (Mukasa *et al*., 1998)
	Wingate (2000)	Darwendale Subchamber / Great Dyke	1992 ± 10 - 1773 ± 11 1350 ± 64 - 1085 ± 8	U-Pb; zircon U-Pb; zircon	Resetting event = hydrothermal alteration Resetting event = hydrothermal alteration
	Vail *et al*. (1968)	Phyllites of Piriwiri Group / Magondi Orogenic Belt Slates of Lomagundi Group / Magondi Orogenic Belt	1753 ± 65, 1659 ± 50 1974 ± 70, 1905 ± 70	K-Ar; whole-rock K-Ar; whole-rock	Resetting event = metamorphism (Cahen *et al*., 1984) Resetting event = metamorphism (Cahen *et al*., 1984)
	Treloar & Kramers (1989)	Granulites (Piriwiri Group) / Magondi Orogenic Belt	1890 ± 260 1780 ± 280	Rb-Sr; whole-rock Rb-Sr; whole-rock	Resetting event = metamorphism Resetting event = metamorphism
	Munyanyiwa *et al*. (1995)	Charno-enderbite intrusive into gneisses of internal zone of Magondi Orogenic Belt	1663 ± 58	U-Pb; zircon	Resetting event = local thermal event
	Vail & Dodson (1969)	Mashonaland dolerites Umkondo dolerites	1642 ± 26 1527 ± 21 1440 ± 22 ~1146 - 650, ~500	K-Ar; whole-rock K-Ar; whole-rock K-Ar; whole-rock K-Ar; whole-rock	Resetting event = hydrothermal alteration Resetting event = hydrothermal alteration Resetting event = hydrothermal alteration Resetting event = hydrothermal alteration
	Clifford *et al*. (1967)	Urungwe (= Hurungwe) granite (intrusive into Piriwiri Group) / Magondi Orogenic Belt	1666 ± 90 1211 ± 40 948 ± 40 843 ± 40	Rb-Sr; microcline Rb-Sr; muscovite K-Ar; muscovite K-Ar; biotite	Resetting event = metamorphism (Cahen *et al*., 1984) Resetting event = metamorphism (Cahen *et al*., 1984) Resetting event = metamorphism (Cahen *et al*., 1984) Resetting event = metamorphism (Cahen *et al*., 1984)
	De Kock *et al*. (2014)	NW-trending Divuli Ranch dyke in Magondi belt / SE Zimbabwe NE-trending Deweras dyke from Guruve swarm in Magondi belt / NW Zimbabwe NE-trending dyke (possible SW extension of Guruve swarm) in Magondi belt /Botswana NW-trending dyke of Okavango swarm in Magondi belt / Botswana	1110 ± 19 1112 ± 8, 1109 ± 13, 1104 ± 12 1111 ± 5 1109 ± 13, 1104 ± 12	U-Pb; baddeleyite	Formation/crystallization age
	Van de Wel *et al*. (1998)	G5 granite and pegmatite veins/dykes / Tati granite-greenstone terrain (Botswana)	1022 ± 6	U-Pb; zircon	Formation/crystallization age; Resetting event = hydrothermal alteration (this study)
	Wingate (2000)	Darwendale Subchamber / Great Dyke	816 ± 24 - 708 ± 62	U-Pb; zircon	Resetting event = hydrothermal alteration
	Mukasa *et al*. (1998) recalc. by Wingate (2000)	Darwendale Subchamber / Great Dyke	823 ± 91, 813 ± 86	U-Pb; zircon & rutile	Resetting event = hydrothermal alteration
	Thole & Robinson (1976)	Piriwiri Group phyllites and Lomagundi Group slates / Shamrock Mine	~550	K-Ar; biotites	Resetting event = hydrothermal alteration
	Vinyu *et al*. (1999)	Migmatitic gneisses (Pfungwe Metamorphic Suite) / Pfunzi Orogenic Belt, south of Rushinga	507.9 ± 2.5, 491.3 ± 2.1	Ar^{40}/Ar^{39}; hornblende	Resetting event = hydrothermal alteration

APPENDIX 21-C: Summary of selected geochronological data pertinent to the Limpopo Central Zone Terrane.

Period	Reference	Lithology / Locality	Age (Ma)	Method	Interpretation by author(s)
MESOARCHAEAN (~3.8-3.1 Ga)	Zeh *et al.* (2010)	Messina Suite (anorthosite) Sand River Gneiss Suite	3358 ± 14 3268 ± 8 - 3283 ± 7	U-Pb; zircon (LA-ICP-MS) U-Pb; zircon (LA-ICP-SF-MS)	Formation/crystallization age of igneous protolith Formation/crystallization age of igneous protolith
	Mouri *et al.* (2009)	Messina Suite (anorthosite)	3344 ± 3.6	U-Pb; zircon (Cameca 1270)	Formation/crystallization age of igneous protolith
	Kröner *et al.* (1999)	Trondhjemitic-granodioritic gneiss of Sand River Granitoid Suite/Causeway Locality near Messina (RSA)	3314 +2/-5 ~3260	U-Pb; zircon (mean) (SHRIMP) Sm-Nd; whole-rock (SHRIMP)	Formation/crystallization age of igneous protolith Mean crustal residence age of igneous protolith
		Trondhjemitic layered gneiss (previously mapped as Alldays Gneiss) of Sand River Granitoid Suite / Bellevue farm ~10 km west of Mopane (RSA)	3297 ± 6.5 ~3410	U-Pb; zircon (mean) (SHRIMP) Sm-Nd; whole-rock (SHRIMP)	Formation/crystallization age of igneous protolith Mean crustal residence age of igneous protolith
		Granodioritic gneiss (previously mapped as Alldays Gneiss) of Sand River Granitoid Suite / Macloutse farm near Swartwater (RSA)	3293 ± 2	U-Pb; zircon (mean) (SHRIMP)	Formation/crystallization age of igneous protolith
		Quartz-monzonitic augen-gneiss (Sand River Granitoid Suite)/Vrouenroom farm at Limpopo River (RSA)	3292 ± 4	U-Pb; zircon (mean) (SHRIMP)	Formation/crystallization age of igneous protolith
		Trondhjemitic gneiss (previously mapped as part of Malala Drift Group/Beit Bridge Complex) of Sand River Granitoid Suite / Esmefour farm east of Messina (RSA)	3205 +69/-62	U-Pb; zircon (mean) (SHRIMP)	Formation/crystallization age of igneous protolith
		Trondhjemitic layered gneiss cutting D_1-fabric in Sand River Granitoid Suite / at Sand River ~3 km east of National Road N1 near Pangbourne farm (RSA)	3197 ± 30	U-Pb; zircon (mean) (SHRIMP)	Formation/crystallization age of igneous protolith
	Kröner *et al.* (1998)	Granodioritic gneisses of Sand River Granitoid Suite / Sand River area near Messina (RSA)	3239 ± 2, 3240 ± 7	U-Pb; zircon	Formation/crystallization age of igneous protolith
	Jaeckel *et al.* (1997)	Tonalitic gneisses of Sand River Granitoid Suite / Causeway Locality near Messina (RSA)	3181 ± 44	U-Pb; zircon	Formation/crystallization age of igneous protolith
		Trondhjemitic gneisses of Sand River Granitoid Suite / Causeway Locality near Messina (RSA)	3169 ± 40	U-Pb; zircon	Formation/crystallization age of igneous protolith
	Barton *et al.* (2003)	Quartzfeldspathic gneiss in Unit 1 of Venetia Klippe / Venetia kimberlite pipe cluster (RSA)	3209 ± 49	U-Pb; zircon	Maximum age of deposition of sedimentary precursor
		Quartzfeldspathic gneiss in Unit 1 of Venetia Klippe / Venetia kimberlite pipe cluster (RSA)	~3300-3200	U-Pb; zircon	Formation/crystallization age of igneous protolith (if orthogneiss), or age of source rock & max deposition age of ~3.2 Ga (if paragneiss)
	Tsunogae & Yurimoto (1995)	Tonalitic-trondhjemitic gneisses of Sand River Granitoid Suite / Causeway Locality near Messina (RSA)	3230 +70/-60	U-Pb; zircon	Formation/crystallization age of igneous protolith
	Treloar *et al.* (1992)	Tectonic lenses of pelitic metasediment in Sand River Gneiss / Causeway Locality near Messina (RSA)	3128 ± 212	Sm-Nd; garnet, whole-rock	Age of high-grade metamorphism effecting gneiss
	Retief *et al.* (1990)	Tonalitic-trondhjemitic gneisses of Sand River Granitoid Suite / Causeway Locality near Messina (RSA)	~3290-3200	U-Pb; zircon	Formation/crystallization age of igneous protolith
	Harris *et al.* (1987)	Sand River Gneiss / Causeway Locality near Messina (RSA)	~3200-3000	Sm-Nd; whole-rock	
	Barton *et al.* (1979)	Anorthositic and leucogabbroic gneisses of Messina Suite (Layered Intrusion) / Messina area (RSA)	3270 +105/-112	Rb-Sr; whole-rock	Formation/crystallization age of igneous protolith (Barton, 1983)
	Barton *et al.* (2003)	Ortho-amphibolite in Unit 1 of Venetia Klippe / Venetia kimberlite pipe cluster (RSA)	3099 ± 37	U-Pb; zircon	Age of high-grade metamorphism, or inherited grain = age of magmatism (preferred interpretation)
	Barton *et al.* (1977, 1983b, 1990)	Mafic dykes / Messina area (RSA)	~3000	Rb-Sr, Pb-Pb, Sm-Nd	Various formation/crystallization ages
	Treloar *et al.* (1992)	/ Bangala dam area (Zimbabwe)	2870 ± 33		Granulite-facies grade metamorphism
NEOARCHAEAN (2.72-2.52 Ga)	Kröner *et al.* (1999)	Quartz monzonitic augen-gneiss of Sand River Granitoid Suite / Vrouenroom farm at Limpopo River (RSA)	2734 ± 4	U-Pb; zircon (SHRIMP)	Peak of high-grade metamorphism and local in-situ melting
		Granitic (dacite) layered granulite-facies gneiss intrusive into supracrustals of Beit Bridge Complex / Hoogeveld farm between Doreen and Messina (RSA)	2717 ± 3	U-Pb; zircon (SHRIMP)	Formation/crystallization age of igneous protolith
		Granodioritic layered gneiss / Nwanedzi River in Sigonde Nature Reserve ~60km east of Messina (RSA)	2716 ± 2	U-Pb; zircon (SHRIMP)	Formation/crystallization age of igneous protolith
		Granite gneiss (Singelele Gneiss) interlayered with supracrustals of Beit Bridge Complex / Ostend farm between Doreen and Messina (RSA)	2681 ± 8, 2669 +58/-55	U-Pb; zircon (SHRIMP)	Formation/crystallization age of igneous protolith emplaced in multiple magmatic phases
		Porphyroblastic granite gneiss (Alldays Gneiss) / south of Alldays at type locality (RSA)	2650 ± 21	U-Pb; zircon (SHRIMP)	Formation/crystallization age of igneous protolith
		Tonalitic-trondhjemitic gneiss (Alldays Gneiss) / Ceon farm northeast of Alldays (RSA)	2637.9 ± 0.3 ~3010	U-Pb; zircon (SHRIMP) Sm-Nd; whole-rock (SHRIMP)	Formation/crystallization age of igneous protolith Mean crustal residence age of igneous protolith
		Trondhjemitic gneiss (Alldays Gneiss) / Ceon farm northeast of Alldays (RSA)	2638.3 ± 0.4	U-Pb; zircon (SHRIMP)	Formation/crystallization age of igneous protolith
		Porphyroblastic granite augen-/flaser-gneiss (Alldays Gneiss Suite) / Worcester farm (RSA)	2677 ± 13 - 2610 ± 75	U-Pb; zircon (SHRIMP)	Formation/crystallization age of igneous protolith
		Tonalitic gneiss intrusive into Verbaard Gneiss / Verbaard farm (RSA)	2629 ± 3	U-Pb; zircon (SHRIMP)	Formation/crystallization age of igneous protolith
		Granodioritic phase of Zanzibar Gneiss / Taphalapata River (Botswana)	2614 ± 13	U-Pb; zircon (SHRIMP)	Formation/crystallization age of igneous protolith
		Quartzmonzonitic phase of Zanzibar Gneiss / Taphalapata River (Botswana)	2653 ± 5	U-Pb; zircon (SHRIMP)	Formation/crystallization age of igneous protolith
		Granite gneiss cutting foliated pelitic gneiss of Beit Bridge Complex / Boston farm ~500 m north of Three Sisters hill, northwest of Messina (RSA)	2620 ± 8	U-Pb; zircon (SHRIMP)	Formation/crystallization age of igneous protolith
	Buick *et al.* (2003)	Ortho-amphibolite gneiss	2692 ± 8	U-Pb; zircon (SHRIMP)	Formation/crystallization age of igneous protolith
	Jaeckel *et al.* (1997)	Tonalitic gneiss (Verbaard Gneiss) interlayered with gneisses of Sand River Granitoid Suite / at Sand River on Verbaard farm ~12 km SSW of Messina (RSA)	2647 ± 0.4, 2615.6 ± 0.2	U-Pb; zircon	Formation/crystallization age of igneous protolith
	Barton *et al.* (2003)	Quartzite in Unit 3 of Venetia Klippe / Venetia kimberlite pipe cluster (RSA)	2665 ± 13	U-Pb; zircon	Maximum age of deposition from a uniform source of ~2.67 Ga & other minor sources older than ~2.8 Ga
	Layer *et al.* (1996)	Trondhjemitic gneiss / eastern part of Central Zone Terrane (RSA)	2658 ± 2 Ma	U-Pb; zircon	Formation/crystallization age of igneous protolith
	Boshoff (2003)	Avoca gneiss Avoca gneissose granite	2651 ± 8 2626.8 ± 4.5	U-Pb; zircon (SHRIMP) U-Pb; zircon (SHRIMP)	Formation/crystallization age of protolith Formation/crystallization age

APPENDIX 21-C: Summary of selected geochronological data pertinent to the Limpopo Central Zone Terrane.

Period	Reference	Lithology / Locality	Age (Ma)	Method	Interpretation by author(s)
NEOARCHAEAN (2.72-2.52 Ga)	Watkeys & Armstrong (1985)	Lamprophyric dykes intruding Bulai Gneiss pluton / west of Messina (RSA)	2671 ± 163 2641 +125/-138	Rb-Sr; whole-rock Pb-Pb; errorchron	Formation/crystallization age Formation/crystallization age
	Hickman & Wakefield (1975)	Anorthositic and granitoid gneisses / Phikwe Complex (Botswana)	2660 ± 40	Rb-Sr, whole-rock	Age of deformation (D_1) under granulite-facies grade metamorphism (M_1)
	Zeh *et al.* (2007)	Alldays Gneiss Suite (Regina gneiss) Singelele Gneiss Zanzibar Gneiss (granite) Zanzibar Gneiss (granodiorite) Bulai Gneiss Suite (granite)	2649 ± 9 2647 ± 12 2614 ± 9 2613 ± 7 2612 ± 7	U-Pb; zircon (LA-ICP-MS) U-Pb; zircon (LA-ICP-MS) U-Pb; zircon (LA-ICP-MS) U-Pb; zircon (LA-ICP-MS) U-Pb; zircon (LA-ICP-MS)	Formation/crystallization age of igneous protolith Formation/crystallization age of igneous protolith Formation/crystallization age of igneous protolith Formation/crystallization age of igneous protolith Formation/crystallization age of igneous protolith
	Van Reenen *et al.* (2008)	Singelele Gneiss	2627 ± 3	U-Pb; zircon (SHRIMP)	Formation/crystallization age of igneous protolith
	Xie *et al.* (2017)	Mafic dykes in Sand River Gneiss	2607 - 2604	U-Pb; zircon (SHRIMP)	Formation/crystallization age
	Barton *et al.* (1994)	Enderbitic phase of Bulai Gneiss pluton / west of Messina (RSA) Granitic phase of Bulai Gneiss pluton / west of Messina (RSA)	2605 ± 2 2572 ± 4	U-Pb; zircon (ID-TIMS) U-Pb; zircon (ID-TIMS)	Formation/crystallization ages (Bulai is composite pluton emplaced over a period of ~30 Ma; Kröner *et al.* (1999))
	Jaeckel *et al.* (1997)	Granodioritic gneiss (Singelele Gneiss) / near Messina (RSA) Quartz-monzonitic gneiss (Singelele Gneiss) / ~5 km southeast of Messina (RSA) Metapelite of Beit Bridge Complex / east of Messina (RSA) Quartz-monzonite gneiss (possibly part of Singelele pluton) intrusive into anorthosite gneiss of Messina Suite / Bokveld farm east of Messina (RSA)	2582.5 ± 0.3 2569 ± 0.3 2575 ± 4 2551.6 ± 0.2	Pb-Pb evaporation Pb-Pb evaporation U-Pb; zircon Pb-Pb evaporation	Formation/crystallization age of igneous protolith emplaced in multiple magmatic phases Age of low-P/high-T metamorphism Formation/crystallization age of igneous protolith
	Barton *et al.* (1979b)	Granitoid gneiss (Singelele Gneiss) / near Messina (RSA)	~2598	Rb-Sr; whole-rock	Formation/crystallization age of igneous protolith
	Kröner *et al.* (1999)	Sillimanite-rich granite gneiss (Zoetfontein Gneiss) / Zoetfontein farm southeast of Swartwater (RSA) Weakly foliated granite interlayered with metapelite of Beit Bridge Complex / Causeway Locality near Messina (RSA) Enderbitic (granodioritic) gneiss of Bulai Pluton / between Messina and Venetia Mine (RSA) Leucogranitic veins in tonalitic gneiss / Verbaard farm (RSA) Leucocratic garnetiferous gneiss (= anatectic melt product of metapelite of Beit Bridge Complex) / at Limpopo River ~2 km west of Beit Bridge border post (RSA/Zimbabwe) Foliated tonalitic gneiss (Tshipise Gneiss) interlayered with Beit Bridge Complex / near Tshipise (RSA)	2608 ± 2 2604 ± 9 2587.1 ± 0.4 2570 ± 4 2557 ± 5 2512 ± 7	U-Pb; zircon (SHRIMP) U-Pb; zircon (SHRIMP) Evaporation and Vapour Digestion U-Pb; zircon (SHRIMP) U-Pb; zircon (SHRIMP) U-Pb; zircon (SHRIMP)	Formation/crystallization age of igneous protolith Formation/crystallization age of igneous protolith Formation/crystallization age of igneous protolith Peak of high-grade M_2 metamorphism and partial anatexis/formation of partial melt veins Peak of high-grade M_2 metamorphism and partial anatexis/formation of partial melt veins Formation/crystallization age of igneous protolith
	Laurent *et al.* (2011)	Bulai Gneiss Suite (granodiorite) Bulai Gneiss Suite (intrusive basic dyke)	2599 ± 11 - 2592 ± 9 2589 ± 12	U-Pb; zircon (LA-ICP-MS) U-Pb; zircon (LA-ICP-MS)	Formation/crystallization age Formation/crystallization age
	Barton & Key (1983)	Discordant granitic orthogneiss veins and diffuse zones within Zanzibar Gneiss / near Zanzibar (Botswana)	2554 ± 33	Rb-Sr; isochron	Formation/crystallization age of igneous protolith or metamorphic overprint of Zanzibar Gneiss?
	Holzer *et al.* (1998)	Metapelite / ~18 km northwest of Messina (RSA)	2521 ± 4 2518 ± 35	Pb-Pb; sillimanite Pb-Pb; garnet	Age of low-P/high-T metamorphism
PALAEOPROTEROZOIC (~2.2-1.6 Ga)	Walraven *et al.* (1987)	Alldays Gneiss / Limpopo Central Zone (RSA)	2221 +21/-20	U-Pb; zircon	No interpretation given; Partial thermal resetting age/event (this study)
	Hickman & Wakefield (1975)	Granitoid gneisses / Phikwe Complex (Botswana)	~2100	Rb-Sr; errorchron	Age of shearing (D_2) under retrograde amphibolite- to greenschist-facies grade metamorphism (M_2)
	Barton *et al.* (2003)	Quartzfeldspathic gneiss in Unit 4 of Venetia Klippe / Venetia kimberlite pipe cluster (RSA) Interlayered quartzfeldspathic gneisses, para- and ortho-amphibolites, quartzites & meta-carbonates (marble & limestone) of Venetia Klippe / Venetia kimberlite pipe cluster (RSA) Ortho-amphibolite in Unit 1 of Venetia Klippe / Venetia kimberlite pipe cluster (RSA)	2448 ± 53 2078 ± 26 - 1882 ± 28 ~2040 ~2020 1950-1850, 1830; 1750-40; ~1660-1650 2290 ± 38, 1974 ± 42	U-Pb; zircon U-Pb; zircon Ar-Ar, hornblende Ar-Ar, muscovite Ar-Ar; biotite U-Pb; zircon	Formation/crystallisation age; Partial thermal resetting age/event (this study) High-grade metamorphism at ~2000 Ma (with associated hydrothermal activity ~100 Ma before & after; this study) Age of D_1 & M_1 (crystallised in axial planes of E-W trending folds) Age of D_2 & M_1 (crystallised in axial planes of N-S trending folds) Episodic exhumation of Central Zone after peak metamorphism at ~2040 Ma; Various hydrothermal overprinting/resetting events (this study) Hydrothermal overprinting/resetting events (this study)
	Zeh & Gerdes (2014)	Amphibolite-facies overprint at Venetia	~2040	U-Pb; zircon (LA-ICP-MS)	Age of amphibolite-facies metamorphism
	Millonig *et al.* (2010)	Mahalapye Granite	2035 ± 9	U-Pb; zircon (LA-ICP-MS)	Formation/crystallization age
	Mapeo *et al.* (2000)	Mahalapye Granite / Mahalapye Complex (Botswana)	2023 ± 7	U-Pb; zircon	Formation/crystallization age
	McCourt & Armstrong (1998)	Mahalapye Granite	2023 ± 11	U-Pb; zircon (SHRIMP)	Formation/crystallization age
	Zeh *et al.* (2010)	Leucosome (Sand River Gneiss Suite)	2021 ± 6	U-Pb; zircon (LA-ICP-MS)	Formation/crystallization age
	Zeh *et al.* (2007)	Mokgware Granite	2019 ± 8	U-Pb; zircon (LA-ICP-MS)	Formation/crystallization age

APPENDIX 21-C: Summary of selected geochronological data pertinent to the Limpopo Central Zone Terrane.

Period	Reference	Lithology / Locality	Age (Ma)	Method	Interpretation by author(s)
PALAEOPROTEROZOIC (~2.2-1.6 Ga)	Walraven *et al.* (1987)	Pelitic gneisses of Beit Bridge Complex / Causeway Locality near Messina (RSA) Undeformed late metamorphic granitic melt patches within Beit Bridge Complex and Sand River Granitoid Suite and post-tectonic granites / Causeway Locality near Messina (RSA) Crosscutting granitoid (Sand River Gneiss Suite) Melt patches (in Sand River Gneiss Suite)	2026.5 ± 6.3 2005.6 ± 4.4 2004.5 ± 3 (mean) 2007.0 ± 6 (mean)	U-Pb; zircon U-Pb; zircon Evaporation and Vapour Digestion Evaporation and Vapour Digestion	Age of peak of granulite-facies metamorphism Crustal in-situ anatexis resulting from rehydration of granulitic assemblage due to rapid uplift and near-isothermal decompression Formation/crystallization age Formation/crystallization age
	Van Breemen & Dodson (1972)	Migmatites / Mahalapye Complex (Botswana) Granitoid gneisses / Phikwe Complex (Botswana) Granitoids / (Magogaphate area) Phikwe Complex (Botswana)	2010 ± 50 1970 ± 50 2010 ± 50 2000 ± 50 1970 ± 50	Rb-Sr; biotite Rb-Sr; whole-rock Rb-Sr; biotite Rb-Sr; biotite Rb-Sr; biotite	Formation/crystallization age Formation/crystallization age Age of anorogenic exhumation of Phikwe Complex Age of anorogenic exhumation of Phikwe Complex Age of anorogenic exhumation of Phikwe Complex
	Van Breemen & Hawkesworth (1980)	Sheared granulite / Triangle Shear Zone (Zimbabwe)	1980 ± 14, 1970 ± 14	Sm-Nd; garnet	Age of granulite-facies grade metamorphism
	Kamber *et al.* (1995a)	North Marginal Transition Zone (Zimbabwe)	1971 ± 17, 1958 ± 13 ~2001-1933	PbSL; titanite Ar-Ar; hornblende	Age of retrograde metamorphism in Triangle Shear Zone Age of retrograde metamorphism in Triangle Shear Zone
	Kamber *et al.* (1995b)	Sheared granulite / Triangle Shear Zone (Zimbabwe)	1978 ± 31 2040 ± 80	Sm-Nd; grt-px-ilm-ap Pb-Pb; grt-feldspar	Age of shearing under granulite-facies conditions Age of shearing under granulite-facies conditions
	Chavagnac *et al.* (1997)	Leucosome from migmatite of Lose gneiss / (Lose quarry) Mahalapye Complex (Botswana)	2023 ± 7 2002 ± 10	Sm-Nd: garnet U-Pb; monazite	Formation/crystallization age Formation/crystallization age
	Layer *et al.* (1996)	Trondhjemitic gneiss (2658 ± 2 Ma) / eastern part of Central Zone Terrane (RSA) Gneisses / central part of Central Zone Terrane (RSA) Gneiss / western extremity of Central Zone Terrane (RSA)	2024 ± 6 ~1990-1953 1931 ± 6	Ar-Ar, hornblende Ar-Ar, hornblende, biotite Ar-Ar, biotite	Age of peak of granulite-facies metamorphism Ages of crustal cooling after anatexis at ~2006 Ma Age of crustal cooling after anatexis at ~2006 Ma
	Holzer *et al.* (1999)	Leucosome from migmatite of Lose gneiss / (Lose quarry) Mahalapye Complex (Botswana) Granulite-facies calcsilicate gneiss / Koedesrand area adjacent to Palala Shear Zone (RSA) Granulite-facies quartzo-feldspathic gneiss / Koedesrand area adjacent to Palala Shear Zone (RSA) Swejane granite / Phikwe Complex (Botswana) Garnetiferous amphibolite in wall-rock contact zone of Selebi ore body / Phikwe Complex (Botswana)	1998 ± 4 2017 ± 6 1999 ± 27 2517 ± 33 2001 ± 6 1997 ± 7 2076 ± 55	U-Pb; apatite PbSL; titanite U-Pb; rutile U-Pb; zircon PbSL; titanite U-Pb; apatite PbSL; garnet	Formation/crystallization age Age of granulite-facies grade metamorphism Formation/crystallization age Formation/crystallization age Resetting event = metamorphism and deformation Resetting event = metamorphism and deformation Maximum age of D_2 deformation of wall-rock & ore body
	Schaller *et al.* (1999)	Granulite-facies calcsilicate gneiss within Palala shear zone / Koedoesrand Window (RSA) Synkinematic biotite in greenschist-facies metapelitic mylonite within Palala shear zone / Koedoesrand Window (RSA)	2020 ± 8 1971 ± 26	PbSL; titanite Rb-Sr; biotite	Age of granulite-facies grade metamorphism Age of retrograde greenschist-facies grade metamorphism
	Belluso *et al.* (2000)	Amphibolite-granulite-facies retrogressed charnoenderbite within northern part of Palala shear zone / Koedoesrand Window (RSA) Amphibolite-granulite-facies recrystallised gabbro adjacent toPalala shear zone / Koedoesrand Window (RSA)	~2020 ~2020-2010	Ar-Ar, hornblende Ar-Ar, hornblende	Age of granulite-facies grade metamorphism Age of granulite-facies grade metamorphism
	Kröner *et al.* (1999)	Anatectic granite intrusive into porphyroblastic (Alldays-type) granite gneiss / Worcester farm (RSA) Porphyroblastic granite gneiss (Alldays Gneiss) / south of Alldays at type locality (RSA) Porphyroblastic granite augen-/flaser-gneiss / Worcester farm (RSA)	2022.1 ± 0.4 2032 ± 22 2014 ± 14	U-Pb; zircon (SHRIMP) U-Pb; zircon (SHRIMP) U-Pb; zircon (SHRIMP)	Formation/crystallization age Peak of granulite-facies metamorphism and local in-situ melting Peak of granulite-facies metamorphism and local in-situ melting
	Barton *et al.* (2003)	Undeformed pegmatite intrusive into rocks of Venetia Klippe / Venetia kimberlite pipe cluster (RSA)	~2000	Ar-Ar, muscovite	Formation/crystallization age (post D_1 - D_2 & M_1)
	Dorland (2004)	Youngest detrital zircon in Manganese Member of Selika Formation (base of Palapye Group) / Borehole near Gootau in Tswapong Hills (Botswana) Youngest detrital zircon in quartzite of Tswapong Formation (middle Palapye Group) / Tshweneng Hills (Botswana)	1906 ± 9 1945 ± 19	U-Pb; zircon U-Pb; zircon	Maximum age of deposition/sedimentation Maximum age of deposition/sedimentation
	Barton (1979)	Unaltered tholeiitic (Sand River) dykes associated with Cu mineralisation / ~10 km east of Messina (RSA)	1899 ± 104, 1876 ± 68	Rb-Sr; whole-rock isochron	Formation/crystallisation age
	Barton *et al.* (1983b)	Hydrothermally altered & deformed mafic dyke of assumed Archaean age in supracrustal gneisses / Campbell Mine (Messina Copper Mines Ltd.), Northern Province (RSA)	1857 ± 31	Rb-Sr; whole-rock, isochron	Age of hydrothermal alteration with associated copper mineralisation
	Barton *et al.* (1979b)	Altered Singelele Gneiss / near Messina copper deposits, Northern Province (RSA)	1788 +72/-76	Pb-Pb; whole-rock	Age of hydrothermal alteration with associated copper mineralisation
	Jacobsen *et al.* (1975)	Hydrothermally altered mafic dykes / Messina area, Northern Province (RSA)	~1800	K-Ar; whole-rock	Formation/crystallisation age; time of hydrothermal alteration with associated copper mineralisation (Barton & Pretorius, 1997)
	Barton *et al.* (2003)	Quartzfeldspathic gneiss in Unit 4 of Venetia Klippe / Venetia kimberlite pipe cluster (RSA)	1634 ± 22, 1602 ± 30	U-Pb; zircon	Age of partial hydrothermal alteration (this study)
	Mapeo *et al.* (2000)	Tuff from top of Palapye Group (*i.e.* Lotsane/Shoshong Formation) / Botswana	1604 ± 33	U-Pb; zircon	Formation/emplacement age; either partial thermal resetting age/event or stratigraphic unit younger than Waterberg Group (this study)

APPENDIX 22

CORRELATION OF PALAEOPROTEROZOIC (~2.6-1.45 Ga) STRATIGRAPHIC UNITS AND TECTONIC EVENTS WITHIN THE KAAPVAAL, REHOBOTH, ZIMBABWE, PILBARA, YILGARN, SINGHBHUM, BASTAR AND DHARWAR CRATONS AND LIMPOPO CENTRAL ZONE TERRANE

APPENDIX 22: Correlation of Palaeoproterozoic (~2.6-1.45 Ga) stratigraphic units and tectonic events within the Kaapvaal, Rehoboth, Zimbabwe Pilbara, Yilgarn, Singhbhum, Bastar and Dharwar cratons and Limpopo Central Zone Terrane.

AGE (Ma)	SOUTH AFRICA	NAMIBIA	BOTSWANA	ZIMBABWE	WESTERN AUSTRALIA	INDIA	TECTONIC SETTING
~2590 - 2430	Ghaap & Chuniespoort Groups	–	Taupone Group	Kariba, Chipisa, Chiroti & Chitumbi gneisses	Hamersley Group	Dhanjori Formation & Sakoli Group	Stable continental platform with marine transgression
Mtshingwe-Kalahari-Gascoyne Orogenic Cycle (Cycle = ~ 2470 - 2350 Ma; Mtshingwe Orogeny = ~ 2470 - 2430 Ma; Kalahari-Gascoyne Orogeny = ~2430 - 2350 Ma) = Formation of proto-Kalahari Craton							
~2350 - 2220	Lower Postmasburg Group *(Asbestos Hills Formation – Ongeluk Formation)* Lower Pretoria Group *(Rooihoogte Formation – Hekpoort Formation)*	–	Lower Segwagwa Group *(Ditlhojana, Lephala, Tsokwane & Tlaameng Formations)*	–	Turee Creek Group	Dhalbhum & Chaibasa Formations	Peripheral foreland basin ahead of E- to SE-migrating fold-and-thrust belt (Lower Postmasburg, Lower Segwagwa and Turee Creek Groups) Intra-cratonic rift basin (Lower Pretoria Group, Dhalbhum & Chaibasa F.)
Ubendian (Magondi & Okwa) Orogenic Cycle (Cycle = ~ 2200 - 1930 Ma; Magondi Orogeny = ~ 2150 - 1970 Ma & Okwa Orogeny = ~1970 - 1860 Ma) = Formation of Ubendia Supercontinent							
Early (Ubendian) orogenic phase (~ 2150 - 2055 Ma)							
~2220 - 2050	Upper Postmasburg Group *(Hotazel Formations to top)*	–			Yerrida Group, Lower Wyloo Group		Intracratonic rift basin (Upper Postmasburg, Upper Segwagwa, Upper Pretoria, Kolhan & Lower Wyloo Groups); Epicratonic rift basin (Deweras & Yerrida Groups) Epicratonic retroarc back-arc basin (Lower Aravalli Supergroup)
~2220 - 2100	Upper Pretoria Group *(Dwaalheuwel Formation to top)*		Upper Segwagwa Group *(Tsatsu Formation – Gatespane & Mogapinyana Formations; Ditlhojana Volcanic Formation – Sengoma Quartzite Formation)*	Deweras Group (+ Malaputese Formation of Dete-Kamativi Inlier)		Kolhan Group & Lower Aravalli Supergroup	
~2100 - 2050	Rooiberg Group		Okwa Group Otse Group & Upper Woodlands Formation	Lomagundi & Piriwiri Groups (+ Inyantue, Tshontanda & Kamativi Formations of Dete-Kamativi Inlier)		Middle Aravalli Supergroup	Epi-/intracratonic magmatic arc (Okwa Group & Middle Aravalli Supergroup) Intracratonic rift basin (Upper Woodlands Formation, Otse & Rooiberg Groups) Epi-/intracratonic retroarc back-arc basin (Lomagundi & Piriwiri Groups, Middle Aravalli Supergroup)
Main (Ubendian) orogenic phase (~2055 - 1970 Ma) & Okwa orogenic phase (~1970 - 1860 Ma)							
~2050 - 1930	Blouberg Formation Lower Waterberg Group *(Nylstroom & lower Matlabas Subgroups)* Elim Group *(Lucknow & Mapedi Formations) & Lower Olitantshoek Group (Neylan Formation)* Lower Vaalkoppies Group *(Dagbreek F.)*		Lower Waterberg Group	–	Bryah Group	Upper Aravalli Supergroup	Intracratonic pull-apart rift basin (Blouberg Formation, Lower Waterberg Group, Lower Olifantshoek & Vaalkoppies Groups) Thermal subsidence basin(s) above BIC & MFC (Lower Waterberg G.) Intracratonic back-arc basin (Bryah Group, Upper Aravalli Supergroup)
~2050 - 1860		Metamorphic Suite			Upper Wyloo Group		Intracratonic back-arc basin (Upper Wyloo Group)
~2050 - 1830	Orange River Group	Orange River & Grünau/Onseepkan Groups					Oceanic magmatic arc / back-arc basin (Orange River & Grünau/Onseepkan Groups & Metamorphic Suite)
Kheis, Richtersveld & Capricorn Orogenic Cycle (Cycle = ~ 2050 - 1730 Ma; Orogeny = ~ 1830 - 1730 Ma) = Formation of Atlantica (Columbia) Supercontinent							
~1930 - 1860	Upper Waterberg Group *(Upper Matlabas & Kransberg Subgroups)*		Upper Waterberg Group	–		–	Intracratonic pull-apart rift basin (Upper Waterberg Group)
~1930 - 1830	Middle Olifantshoek Supergroup *(Hartley Formation)* Upper Vaalkoppies Group (Sultanaoord F.) Brulpan Group *(Uitdraai/Prynnsberg & Groblershoop F.)*		Lower Palapye Group *(Selika & Moeng Formations)* Roodeberg Formation (= equivalent to lower Palapye Group in South Africa)		Padburry Group		Intracratonic pull-apart rift basin (Lower Palapye Group, Middle Olifantshoek Supergroup) Intracratonic back-arc basin (Padbury Group) Intracratonic peripheral foreland basin (Upper Olifantshoek, Vaalkoppies & Brulpan Groups)
~1860 - 1730		Khoabendus Group, Okapuka & Elim Formations					Epicratonic back-arc, later peripheral foreland basin (Khoabendus Group & Okapuka Formation) Intracratonic retroarc foreland basin (Elim Formation)
~1830 - 1730	Lower Soutpansberg Group (Tshifhefhe, Sibasa & Funduzi Formations) Upper Olifantshoek Supergroup *(Matsap & Brulsand Formations = Volop G.)*	Rehoboth Sequence	Middle Palapye Group *(Tswapong Formation)*		Earaheedy Group, Capricorn Formation, Mount Barren Group and related units		Intracratonic pull-apart rift basin (Lower Soutpansberg Group) Intracratonic foreland basin (Upper Olifantshoek Supergroup) Intracratonic retroarc foreland basin (Rehoboth Sequence, Earaheedy G.); Intracratonic peripheral foreland basin (Capricorn Formation, Mount Barren G.)
Post-Kheis Orogeny Extension / Continental Fragmentation of Atlantica (Columbia) Supercontinent (~ 1730 – 1400 Ma)							
~1730 - 1400	Upper Soutpansberg Group (Wylliespoort, Ngwanedsi & Nzhelele Formations) Wilgenhoutsdrift Group	–	Upper Palapye Group (Lotsane/Shoshong Formation)	Sijarira & Makuti Groups	Bangemall, Mt. Minnie & Bresnahan Groups, Capricorn & Mt. James Formations	–	Thermal subsidence of pull-apart rift basins (Upper Soutpansberg & Palapye Groups), followed by renewed rifting within and around cratons during break-up of supercontinent Atlantica

APPENDIX 23

SUMMARY OF PALAEOPROTEROZOIC (SYN-TRANSVAAL SUPERGROUP; ~2.49-2.41 Ga) FORMATION AND RESETTING AGES REPORTED FROM THE KAAPVAAL AND ZIMBABWE CRATONS AND LIMPOPO CENTRAL ZONE TERRANE

APPENDIX 23: Summary of Palaeoproterozoic (syn-Transvaal Supergroup; ~2.49-2.41 Ga) formation and resetting ages reported from the Kaapvaal and Zimbabwe cratons and Limpopo Central Zone Terrane.

Area	Reference	Lithology / Locality	Age (Ma)	Method	Interpretation by author(s)
KAAPVAAL CRATON	Barton *et al.* (2003)	Quartzfeldspathic gneiss in Unit 4 of Venetia Klippe / Venetia kimberlite pipe cluster)	2448 ± 53	U-Pb; zircon	Formation/crystallisation age; Partial thermal resetting age/event (this study)
	Vearncombe *et al.* (1987)	Rooiwater Complex / Murchison Greenstone Belt (RSA)	2544 +29/-31 2490 ± 35	Pb-Pb; whole-rock Rb-Sr; whole-rock	Resetting event = hydrothermal alteration Resetting event = hydrothermal alteration
	Key & Wright (1982)	Gaborone Granite Complex / (Botswana)	2428 ± 55, 2394 ± 26	Rb-Sr; whole-rock	Partial thermal resetting ages/events
	Poujol *et al.* (1998, 1999)	Authigenic pyrite from altered Kimberley Reef / Evander Goldfield (RSA)	2380 ± 25, 2373 ± 18, ~2487, ~2448	Pb-Pb; pyrite	Formation/crystallisation age of pyrite
	Barton *et al.* (1999)	Leucosome from migmatite / Johannesburg Dome (RSA) Tonalite / Johannesburg Dome (RSA)	2430 ± 50 2385 ± 127 2321 ± 23	Rb-Sr; whole-rock Rb-Sr; whole-rock Rb-Sr; biotite	Partial thermal resetting age/event Partial thermal resetting age/event Partial thermal resetting age/event
	Armstrong *et al.* (1986)	Township Quartz Porphyry (Makwassie Formation) / Klerksdorp (SA) Mafic lavas (Klipriviersberg Group) / Central Rand Goldfield (SA)	2350 +160/-180 2430 ± 50	Pb-Pb; whole-rock Pb-Pb; whole-rock	Partial thermal resetting age/event Partial thermal resetting age/event
	Barton *et al.* (1983)	Palmietfontein Granite / Southern Marginal Zone (SA)	2456 ± 78	Rb-Sr; whole-rock	Formation/crystallisation age
	Armstrong (unpubl. data)	Tuff bed at top of Kuruman Iron Formation (Griqualand West Supergroup) /(SA)	2465 ± 7	U-Pb; zircon	Formation/crystallisation age
	Pickard (2003)	Felsic tuffaceous mudrocks at top of Riries Member (top of Kuruman Iron Formation (Griqualand West Supergroup)) / (RA)	2460 ± 5	U-Pb; zircon	Age of deposition
	Trendall *et al.* (1990)	Tuff bed in lower part of Griquatown Iron Formation (Griqualand West Supergroup) / (SA)	2432 ± 31	U-Pb; zircon	Formation/crystallisation age (= upper age limit for deposition of Chuniespoort / Ghaap Group)
	Holzer *et al.* (1999)	Shashe granite (Motlutse Complex) / Bobonong area, Limpopo Central Zone Terrane (Botswana)	2497 ± 19	U-Pb; zircon	Formation/crystallization age
LIMPOPO CENTRAL ZONE	Barton *et al.* (2003)	Quartzfeldspathic gneiss in Unit 4 of Venetia Klippe / Venetia kimberlite pipe cluster (RSA)	2448 ± 53	U-Pb; zircon	Formation/crystallisation age; Partial thermal resetting age/event (this study)
ZIMBABWE CRATON	Darbyshire *et al.* (1996)	Scheelites from gold-tungsten veins crosscutting S1 / (Lily-Whitewaters area) Midlands G.B. Scheelites from gold-tungsten veins crosscutting S1 / (Rhodesdale terrane) Midlands G.B.	2413 ± 71 2444 ± 102	Sm-Nd; scheelite Sm-Nd; scheelite	Age of hydrothermal gold mineralisation Age of hydrothermal gold mineralisation
	Frei & Pettke (1996)	Shear zone-hosted gold-sulfide-tourmaline hydrothermal veins / Kimberley mine (Harare-Bindura-Shamva Greenstone Belt)	~2415-2285	Ar-Ar; biotite	Formation/crystallization age
	Pitfield & Campbell (1993)	Hatchland porphyry / Midlands Greenstone Belt	2457 ± 65	Rb-Sr; whole-rock	Formation/crystallization age
	Berger *et al.* (1993)	Post-tectonic granite intrusive into Northern Marginal Thrust Zone	2428 ± 7	U-Pb; zircon	Formation/crystallization age
	Tomschi *et al.* (1989)	Galena in hydrothermal veins in Jumbo/Mazowe pluton / Harare-Bindura-Shamva Greenstone Belt	2410 ± 20	Pb-Pb; galena	Formation/crystallization age
	Oberthür *et al.* (2000)	Scheelite in gold-pyrite-quartz-carbonate veins / (Mazowe Mine) Harare-Bindura-Shamva Greenstone Belt	2430 ± 460 2410 ± 200	Rb-Sr; scheelite Sm-Nd; scheelite	Resetting event = hydrothermal alteration; age of hydrothermal gold mineralisation (this study)
	McCourt *et al.* (2001)	Hurungwe granite (intrusive into Piriwiri Group) / Magondi Orogenic Belt	2742 ± 12, 2454 ± 12, 2198 ± 5	U-Pb; zircon (cores)	Inherited zircons = ages of basement units
	Jahn & Condie (1976)	Upper Bulawayan Group / Harare-Bindura-Shamva Greenstone Belt Upper Bulawayan Group / Bulawayo Greenstone Belt	2472 ± 156 2383 ± 119	Rb-Sr; whole-rock Rb-Sr; w.-r. & min.	Resetting event = hydrothermal alteration (Cahen *et al.*, 1984) Resetting event = hydrothermal alteration (Cahen *et al.*, 1984)
	Bolhar *et al.* (2002)	Limestone of Cheshire Formation (Ngezi Group) / Belingwe Greenstone Belt	2543 ± 70	Pb-Pb; whole-rock	1. Late-stage diagenesis, or 2. Resetting event = hydrothermal alteration, or 3. Tectonic activity along Mtshingwe Fault
	Hawkesworth *et al.* (1975)	Upper Bulawayan Group / Bulawayo Greenstone Belt Mixed Lower and Upper Bulawayan Group / Belingwe Greenstone Belt Mafic volcanics / Bulawayo area Mafic volcanics / Kwekwe area Lower Bulawayan Group (pre-Maliyama Formation) / Midlands Greenstone Belt Maliyami Formation (Upper Bulawayan Group) / Midlands Greenstone Belt	2532 ± 70 2507 ± 110 2485 ± 90 2480 ± 140 2452 ± 84 2403 ± 42 2397 ± 91	Rb-Sr; whole-rock Rb-Sr; whole-rock Rb-Sr; whole-rock Rb-Sr; whole-rock Rb-Sr; whole-rock Rb-Sr; w.-r. & min. Rb-Sr; whole-rock	Resetting event = hydrothermal alteration (Cahen *et al.*, 1984) Resetting event = hydrothermal alteration (Cahen *et al.*, 1984) Resetting event = hydrothermal alteration Resetting event = hydrothermal alteration Resetting event = hydrothermal alteration (Cahen *et al.*, 1984) Resetting event = hydrothermal alteration (Cahen *et al.*, 1984) Resetting event = hydrothermal alteration (Cahen *et al.*, 1984)
	Taylor *et al.* (1991)	Mafic volcanics / Kwekwe area	2380 +309/-394	Pb-Pb;	Resetting event = hydrothermal alteration
	Van Breemen & Dodson (1972)	Volcanics / Tati Greenstone Belt	2523 ± 33	Rb-Sr; whole-rock	Resetting event = hydrothermal alteration (Cahen *et al.*, 1984)
	Hamilton (1977) recalculated by Cahen *et al.* (1984) recalculated by Mukasa *et al.* (1998)	Picrite and gabbro of Hartley and Wedza complexes / Great Dyke	2514 ± 16, 2461 ± 16 2452 ± 14 2455 ± 16	Rb-Sr; whole-rock Rb-Sr; whole-rock Rb-Sr; whole-rock	Resetting event = hydrothermal alteration (this study) Resetting event = hydrothermal alteration (this study) Resetting event = hydrothermal alteration (Mukasa *et al.* 1998)
	Davies *et al.* (1970)	Picrite and gabbro of Hartley, Selukwe and Wedza complexes / Great Dyke	2478 ± 87	Rb-Sr; whole-rock	Resetting event = hydrothermal alteration (this study)
	Hahn *et al.* (1991)	West and Umvimeela dykes / gabbroic satellites of Great Dyke	2490 ± 120	Rb-Sr; whole-rock	Resetting event = hydrothermal alteration (this study)
	Allsopp (1965) recalculated by Mukasa *et al.* (1998)	Picrite of Hartley and Wedza complexes / Great Dyke	2505 ± 50 2478 ± 100 2476 ± 30	K-Ar; biotite K-Ar; pyroxene K-Ar; pyroxene	Resetting event = hydrothermal alteration (this study) Resetting event = hydrothermal alteration (this study) Resetting event = hydrothermal alteration (Mukasa *et al.* 1998)
	Mukasa *et al.* (1998)	Darwendale Subchamber / Great Dyke	2467 ± 85	Rb-Sr; w-r & min.	Resetting event = hydrothermal alteration
	Bagai *et al.* (2002)	G2 Sebina granitic gneiss/migmatite / Vumba granite-greenstone terrain G5 granitoid (Domboshaba granite) / Vumba granite-greenstone terrain	2489 ± 9, 2478 ± 46, 2466 ± 8, 2464 ± 9, 2464 ± 5, 2339 ± 4, 2318 ± 6, 2305 ± 4, 2303 ± 38 2455 ± 16	U-Pb; zircon U-Pb; zircon	Formation/crystallization age of igneous precursor; Resetting event = hydroth. alteration (this study) Formation/crystallization age; Resetting event = hydrothermal alteration (this study)
	Loney (1969) recalculated by Master (1991)	Kariba paragneisses (part of Hurungwe paragneisses) / Hurungwe area	2420 ± 100, 2287 ± 92 2368 ± 92	Rb-Sr; whole-rock	Age of metamorphism Age of metamorphism = minimum age of deposition (Master, 1991)
	Loney (1969) recalculated by Master (1991)	Chipisa paragneisses (part of Hurungwe paragneisses) / Hurungwe area	2500 ± 100, 2360 ± 90 2443 ± 90	Rb-Sr; whole-rock	Age of metamorphism Age of metamorphism = minimum age of deposition (Master, 1991)
	Loney (1969)	Pelitic gneisses (correlatives to Piriwiri Group? (= correlatives to Kariba, Chipisa, Chitumbi, Chiroti paragneisses; this study)) / eastern end of Lake Kariba	2465 ± 54	Rb-Sr; whole-rock	Age of deposition; age of metamorphism = minimum age of deposition (this study)
	Vail & Snelling (1971)	Pyroxene-gneiss / Nyamanji (northern Zimbabwe Craton)	2406 ± 170	Rb-Sr; whole-rock	Resetting event = hydrothermal alteration
	Hawkesworth *et al.* (1979)	Chibi batholith / southeast of Belingwe Greenstone Belt near Mukwakwe	2400 ± 170	Rb-Sr; whole-rock	Resetting event = hydrothermal alteration (this study)
	Wingate (2000)	Darwendale Subchamber / Great Dyke and Umvimeela and East dykes Darwendale Subchamber / Great Dyke	2351 ± 20 2466 ± 22 - 2327 ± 11	U-Pb; baddeleyite U-Pb; zircon	Resetting event = hydrothermal alteration Resetting event = hydrothermal alteration

APPENDIX 24

SUMMARY OF PALAEO- TO MESOPROTEROZOIC (POST-TRANSVAAL SUPERGROUP; ~2.15-1.0 Ga) DEFORMATION EVENTS REPORTED FROM THE AREA OF THE WITWATERSRAND BASIN AND BUSHVELD COMPLEX (*i.e.,* CENTRAL KAAPVAAL CRATON) AND THEIR CORRELATION WITH FAR FIELD STRESS RELATED TO THE MAGONDI AND OKWA OROGENIES, BUSHVELD COMPLEX EMPLACEMENT, AND VREDEFORT METEORITE IMPACT, AS WELL AS KHEIS, KIBARAN AND LOMANIAN (NAMAQUA-NATAL) OROGENIES

APPENDIX 24: Summary of Palaeo- to Mesoproterozoic (post-Transvaal Supergroup; ~2.15-1.0 Ga) deformation events reported from the area of the Witwatersrand Basin and Bushveld Complex (*i.e.,* central Kaapvaal Craton) and their correlation with far field stress related to the Magondi and Okwa orogenies, Bushveld Complex emplacement, and Vredefort meteorite impact, as well as Kheis, Kibaran and Lomanian (Namaqua-Natal) orogenies.

Area	Author(s) [Study Area]	Early phase of Magondi Orogeny (~2.15-2.055 Ga) *[SE-directed far field compression]*	Bushveld Complex Emplacement (~2.056-2.055 Ga) *[radially BC-outward compression]*	Main & late phase of Magondi Orogeny (~2.055-2.02 Ga & ~2.02-1.97 Ga) Okwa Orogeny (~1.93-1.86 Ga) *[SE-directed far field compression]*	Vredefort Impact (~2.02 Ga) *[Crater formation: radially outward compression]* *[Crater extensional collapse: radially inward extension]* *[Central uplift collapse: radially outward compression]* *[Isostatic compensation; radially outward compression]*	Kheis Orogeny (~1.83-1.73 Ga) *[E-directed far field compression]*	Kibaran Orogeny (~1.35-1.25 Ga) *[N-directed far field compression]* Lomanian Orogeny (~1.2-1.0 Ga) *[NW-directed far field compression]*
EVANDER GOLDFIELD	Tweedie (1981, 1986)		Northerly tilting (up to 12°) of entire basin (related to Bushveld Complex crustal loading, this study)				Development of NE/SW-striking, SE-dipping reverse & thrust faults of at least post-Ventersdorp-age (related to Lomanian Orogeny, this study)
SOUTH RAND GOLDFIELD	Spencer (1992)				NW/SE-trending folds with an associated NW/SE-striking, SW-dipping axial planar cleavage (related to post-impact isostatic compensational mantle upwelling and crustal uplift, this study)		
	Friese (2008a) [Burnstone Prospect]		Emplacement of a major Bushveld-age sill with break-through along an extensionally reactivated NNW/SSE-striking Pongola rift fault				Development of N-S striking, extensional fault zones developed in response to Kibaran Orogeny
EAST RAND GOLDFIELD	Cluver (1957), Antrobus & Whiteside (1964), De Jager (1964), Papenfus (1964), McCarthy *et al.* (1986)		Development of large- & small-scale NW/SE-trending, open-overturned, periclinal folds with axial planar cleavage in Black Reef Quartzite Formation (related to radial Bushveld load stress, this study)		Development of NW/SE-trending folds (related to post-impact isostatic compensational mantle upwelling and crustal uplift, this study)		Development of E/W-striking, subvertical dextral strike-slip faults parallel to E/W-striking Platberg Group-age sinistral strike-slip faults (*e.g.*, Vogels Tear Fault) displacing post-Transvaal dykes (related to Lomanian Orogeny, this study)
	McCarthy *et al.* (1986)						Development of NE/SW-trending, large-scale, open folds (related to Lomanian Orogeny, this study)
	Pitts (1990), Pitts & Roering (1992)			Development of steep, NE/SW- and ESE/WNW-striking dextral strike-slip faults	Development of E/W-striking, shallow S-dipping normal faults & normal oblique-slip movements towards S along pre-existing NE/SW-striking faults (related to syn-impact extensional collapse of Vredefort transient crater, this study) NE-directed bedding-parallel thrust movements in Central Rand Group (related to post-impact isostatic compensational mantle upwelling and crustal uplift, this study)		Development of NW/SE-striking strike-slip faults; NW-directed bedding-subparallel thrust movements and tilting of steep NW/SE-trending mid-Ventersdorp fold axes; development of steep, E/W-striking dextral strike-slip faults & reactivation of pre-existing E/W-striking, shallow S-dipping normal faults to dextral strike-slip faults displacing Bushveld- and Pilanesberg-age dykes & acting as oblique ramps during the NW-thrust faulting (related to Lomanian Orogeny, this study)
CENTRAL RAND GOLDFIELD	Pretorius (1964a,1976,1981)			Development of NE/SW-trending folds in the Witwatersrand Supergroup			Development of NE/SW-trending folds in the Witwatersrand Supergroup (related to Lomanian Orogeny, this study)
	McCarthy *et al.* (1986)						NW- to NNW-directed, bedding-parallel thrust movements (calculated from the data of McCarthy *et al.* (1986) using the cleavage vergence method of Bell (1981); this study) in the vicinity of the South Hills and Linksfield (~2km S & N of Rietfontein Fault) within Witwatersrand & Ventersdorp supergroups strata (related to Lomanian Orogeny, this study)
	Roering & Smit (1987)						N- to NW-directed, ductile, bedding-parallel thrust movements in Central Rand Group quartzites (related to Lomanian O., this study)
	Grohmann (1988)	Rise of Johannesburg Dome in post-Transvaal to pre-Bushveld time causing N-S crustal shortening & formation of a zone of steep S-dipping reverse faults along northern margin of Witwatersrand Basin through reactivation of syn-depositional basin edge faults	Emplacement of Bushveld-age dykes along extensionally reactivated pre-existing NW/SE-striking faults	Dextral strike-slip reactivation of E/W-striking Rietfontein Fault and adjacent parallel-striking faults			Emplacement of NNW/SSE-trending Pilanesberg-age dykes along pre-existing faults, two phases of Pilanesberg intrusion (an early mafic and later syenitic phase); the irregular course of syenite dykes & apparent scarcity of Pilanesberg intrusions in the eastern half of the Central Rand Goldfield indicates that this area remained under compression during Pilanesberg-time, hence was not amenable to dyke-intrusion, whereas in the western half of the goldfield, the partial relaxation of Pilanesberg-age compression allowed emplacement of Pilanesberg dykes (related to Lomanian Orogeny, this study)
	Abraham (2005), Khangale (2005), Hlangwane & Hein (2006), Amuntenya (2007)				N-verging thrusts interpreted as splay shears to Rietfontein Fault Zone (related to post-impact isostatic compensational mantle upwelling and crustal uplift, this study)		

APPENDIX 24 (continued)

Area	Author(s) [Study Area]	Early phase of Magondi Orogeny (~2.15-2.055 Ga) *[SE-directed far field compression]*	Bushveld Complex Emplacement (~2.056-2.055 Ga) *[radially BC-outward compression]*	Main & late phase of Magondi Orogeny (~2.055-2.02 Ga & ~2.02-1.97 Ga) Okwa Orogeny (~1.93-1.86 Ga) *[SE-directed far field compression]*	Vredefort Impact (~2.02 Ga) *[Crater formation: radially outward compression]* *[Crater extensional collapse: radially inward extension]* *[Central uplift collapse: radially outward compression]* *[Isostatic compensation; radially outward compression]*	Kheis Orogeny (~1.83-1.73 Ga) *[E-directed far field compression]*	Kibaran Orogeny (~1.35-1.25 Ga) *[N-directed far field compression]* Lomanian Orogeny (~1.2-1.0 Ga) *[NW-directed far field compression]*
JOHANNESBURG DOME	Roering (1984) [Swartkops]				Development of an imbricate system of NNE-directed thrusts & nappes (with mylonite, pseudotachylite & breccia), NNE-verging isoclinal folds & a shallow (30°) SSW-dipping cleavage in Witwatersrand & Ventersdorp Supergroup strata of pre-Transvaal age (related to post-impact isostatic compensational mantle upwelling and crustal uplift, this study)		
	McCarthy *et al.* (1986) [Johannesburg Dome]				Upfolding (rise) of Johannesburg & Devon domes within core of a regional anticline developed in post-Vredefort impact time as a result of concentric folding around Vredefort Dome (related to post-impact isostatic compensational mantle upwelling and crustal uplift, this study)		
	Roering (1986) [NW margin of Johannesburg Dome]				Development of ductile (mylonite-bearing), up to 1 km wide, E/W-striking, S-dipping, N-directed shear (thrust) zones (*e.g.,* Jukskei River shear zone) of post-Transvaal age in basement granites with thrust-interleaved quartzites (possibly correlatives to Witwatersrand SG), which are post-dated by a set of NE/SW-striking sinistral strike-slip shear zones (related to post-impact isostatic compensational mantle upwelling and crustal uplift, this study)		
	Roering *et al.* (1987) [NE- & E-edge of Johannesburg Dome]		WSW- to W-directed thrusting of Chuniespoort Group over Pretoria Group and onto NE- and E-edge of Johannesburg Dome (related to radial Bushveld load stress, this study)				
	Hilliard (1994), Hilliard & McCourt (1995) [Northcliff Promontary]			ENE/WSW-striking, subvertical, brittle-ductile, dextral strike-slip shear zones in West Rand Group strata (~2 km dextral strike-slip displacement)	NNE-directed bedding-parallel thrusting along the contact between granitoid-greenstone basement and overlying West Rand Group and in the shale bands of West Rand Group under brittle-ductile conditions in post-Platberg Group to pre-Black Reef Formation time (related to post-impact isostatic compensational mantle upwelling and crustal uplift, this study)		Brittle, sinistral strike-slip reactivation of earlier NNW/SSE-striking, ductile, dextral strike-slip shear zones (reactivation of Pongola rift faults during Lomanian Orogeny, this study)
	Courtnage (1995) [N of Johannesburg Dome]		WSW-directed thrusting (duplexing) in Transvaal Supergroup (D2) (related to radial Bushveld load stress, this study)	Development of large-scale, open, upright, E-W-trending, W-plunging, S-verging folds and associated, E/W-striking steep N-dipping shear zones in Chuniespoort Group (D3)	Development of N-verging, ductile, bedding-parallel thrust zones with internal small-scale, N-verging, tight-isoclinal recumbent folds & S-C fabrics & meso-scale periclinal, open-close folds with associated E/W-striking, S-dipping axial planar cleavage in Chuniespoort Group strata (D1) related to partial collapse of central Vredefort Dome uplift due to overcompensation of rebound for uplift (related to post-impact isostatic compensational mantle upwelling and crustal uplift, this study)	Development of small-scale, E-verging folds within bedding-sub parallel shear zones in Transvaal Supergroup strata (D4)	Development of N/S-striking, sinistral and dextral strike-slip faults (up to several hundreds of metres displacement), displacing D1-D4 folds and shear zones and a NW/SE-striking syenite dyke of Pilanesberg-age (D5) (formation of faults during Kibaran Orogeny, strike-slip reactivation during Lomanian Orogeny, this study)
	Gibson *et al.* (1999) [N of Johannesburg Dome]				N-verging, bedding-parallel shear (thrust) zones and associated folds, cleavage and a strong N-trending lineation in Black Reef Quartzite Formation and Chuniespoort Group strata related to partial collapse of central Vredefort Dome uplift due to overcompensation of rebound for uplift (related to post-impact isostatic compensational mantle upwelling and crustal uplift, this study)		
	Jamison *et al.* (2004) [Cradle of Humankind]		Development of bedding-parallel thrusts with associated sheath folds in response to Bushveld Complex crustal loading		Development of WNW/ESE-striking, NNE-verging multiple thrust stacks separated by thin (5-10cm) phyllitic/slaty breccia- & chert-bearing and thick (~2m) mylonitic slate-bearing bedding-parallel thrusts (related to post-impact isostatic compensational mantle upwelling and crustal uplift, this study)	Development of WNW/ESE-striking sinistral strike-slip shear zones in Chuniespoort Group strata	
	Alexandre *et al.* (2006) [NW & W of Johannesburg Dome]	W-verging recumbent F2 fold with sub-horizontal S2 cleavage parallel to, and directly above, a sub-horizontal, gently undulating WSW-directed thrust plane in phyllites of Pretoria Group at Syferbult dated ~2.15 Ga	Development of SW-verging thrusts and NW/SE-trending, SW-verging recumbent, disharmonic F2 folds with NW/SE-striking axial planar crenulation S2 cleavage in hornfelses of Pretoria Group near Meerhof (D2) dated at 2042.1 ± 2.9 Ma		Development of E/W- trending, N-verging monoclinal F1 folds with shallow S-dipping, axial planar S1 cleavage (D1) (related to post-impact isostatic compensational mantle upwelling and crustal uplift, this study)	E-verging, shallow dipping thrusts & N/S-trending, recumbent, disharmonic F3 folds with a N/S-striking, subvertical axial planar S3 cleavage overprinting hornfelses of Pretoria Group near Meerhof (D3)	
	Ormond (2018) [Swartkops]			WSW/ENE-trending folds with associated subvertical axial planar cleavage under lower greenschist facies conditions in lower Transvaal Supergroup dated at 2072-2044 Ma (D4)	Development of NNE-verging, open, decametre-scale folds with associated moderately to shallow SSW-dipping axial planar cleavage under lower greenschist facies conditions in lower Transvaal Supergroup strata dated at 2026-2016 Ma (D3) (related to post-impact isostatic compensational mantle upwelling and crustal uplift, this study)		

APPENDIX 24 (continued)

Area	Author(s) [Study Area]	Early phase of Magondi Orogeny (~2.15-2.055 Ga) *[SE-directed far field compression]*	Bushveld Complex Emplacement (~2.056-2.055 Ga) *[radially BC-outward compression]*	Main & late phase of Magondi Orogeny (~2.055-2.02 Ga & ~2.02-1.97 Ga) Okwa Orogeny (~1.93-1.86 Ga) *[SE-directed far field compression]*	Vredefort Impact (~2.02 Ga) *[Crater formation: radially outward compression]* *[Crater extensional collapse: radially inward extension]* *[Central uplift collapse: radially outward compression]* *[Isostatic compensation; radially outward compression]*	Kheis Orogeny (~1.83-1.73 Ga) *[E-directed far field compression]*	Kibaran Orogeny (~1.35-1.25 Ga) *[N-directed far field compression]* Lomanian Orogeny (~1.2-1.0 Ga) *[NW-directed far field compression]*
WEST RAND GOLDFIELD	Toens & Griffiths (1964) [West Rand Goldfield]			Development of NW/SE-striking dextral strike-slip faults and a conjugate set of NE/SW-striking sinistral strike-slip faults displacing Transvaal Supergroup strata	Development of E/W-trending folds in Transvaal Supergroup strata & of a reverse fault closely associated with Doornkop Fault (= compressive reactivation of E/W-striking, S-dipping, extensional Vredefort transient crater faults related to post-impact isostatic compensational mantle upwelling and crustal uplift, this study)		
	Roering (1968) [West Rand Goldfield]				Development of large-scale, WNW/ESE-striking reverse faults post-dating West Rand Syncline (related to post-impact isostatic compensational mantle upwelling and crustal uplift, this study)		
	McCarthy *et al.* (1986) [West Rand Goldfield]				NW/SE-trending folds in Transvaal Supergroup strata forming an interference pattern with NE/SW-trending post-Transvaal folds (related to post-impact isostatic compensational mantle upwelling and crustal uplift, this study)		NE/SW-trending folds in Transvaal Supergroup strata forming an interference pattern with NW/SE-trending post-Transvaal folds (related to Lomanian Orogeny, this study)
	Killick *et al.* (1988) [Westonaria Gold Mine]						NNW/NW-directed thrust reactivation (mylonite) of Platberg Group-age, bedding-parallel Western Areas Fault Zone at contact between Witwatersrand & Ventersdorp Supergroups (related to Lomanian Orogeny, this study)
	Parsons & Killick (1990) [Westonaria Gold Mine]				Development of E/W-striking, S-dipping, flat thrust faults, E/W-trending, large-scale open folds (= hangingwall ramps developed above thrust ramps), and E/W-striking, S-dipping cleavage in dolomites of Chuniespoort Group (related to post-impact isostatic compensational mantle upwelling and crustal uplift, this study)		NW-directed oblique-reverse reactivation of older (post-Chuniespoort Group) E/W-striking, southerly dipping, flat thrust faults, development of NW-directed thrusts and a SE-dipping cleavage (related to Lomanian Orogeny, this study)
	Swartz (1989), Swartz *et al.* (1991), Swartz & Killick (1991) [Western Areas & Cooke Section Gold Mines]	Development of NNW/NW-SSE/SE-striking normal faults (quartz cataclasite and quartz mylonite)		Significant dextral strike-slip reactivation along E/W-striking Platberg-age faults (quartz-cataclasite, fracture-type faults), which formed due to a compressive stress field with o_1 oriented NNW/NW-SSE/SE	Extensional and compressional ENE/WSW-striking pseudotachylite-ultracataclasite veins along flat faults (slab-duplex geometry) (related to syn-impact formation and modification stages of Vredefort transient crater, this study) N-directed, bedding-parallel thrusting (mylonite) (related to post-impact isostatic compensational mantle upwelling and crustal uplift, this study)		NW-directed, bedding-parallel thrusting (mylonite) and development of open, NE/SW-folds due to ramping on thrust faults (related to Lomanian Orogeny, this study)
	Swartz (1991) [Lindum Reefs Goldmine]				E/W trending cross-folding (large open folds, wavelength min. 200 m & parasitic E/W-trending folds) of (older?) N-S folds, and E/W-striking, N-verging cleavage in Black Reef Quartzite Formation both indicating N-directed thrusting (related to post-impact isostatic compensational mantle upwelling and crustal uplift, this study)	Development of N/S-trending open, large-scale (wavelength >300 m) folds with meso-scale parasitic folds & N/S-striking, E-verging thrusts effecting Black Reef Quartzite Formation	
	Killick (1992) [West Rand Goldfield]			Development of NE/SW-striking, shallow NW-dipping, SE-directed thrusts (cataclasite, protomylonite) in Transvaal Supergroup; dextral strike-slip reactivation of Rietfontein Fault and development of strike-slip related en echelon folds in Black Reef Quartzite Formation	Development of low-angle, E/W-striking, S-dipping extensional faults (*e.g.,* Doornkop Fault) with cataclasite & pseudotachylitic veins (related to syn-impact modification stage of Vredefort transient crater, this study) Northward-directed thrusting and development of E/W-trending folds, compressive reactivation of E/W-striking, S-dipping extensional Vredefort impact crater faults (*e.g.,* Doornkop Fault) (related to post-impact isostatic compensational mantle upwelling and crustal uplift, this study)		Dominantly dextral strike-slip reactivation of E/W- (*e.g.,* Doornkop Fault) and WNW/ESE-striking faults(*e.g.,* Rietfontein Fault), minor sinistral strike-slip reactivation of NE/SW-striking faults; NNW/NW-directed thrust reactivation (mylonite) of bedding-parallel Western Areas Fault Zone at contact between Witwatersrand & Ventersdorp Supergroups (related to Lomanian Orogeny, this study)
	Killick & Roering (1994) [Randfontein Estates Gold Mine, Cooke Section]				NNE-directed bedding-parallel thrusting in post-Klipriviersberg Group to pre-Transvaal Supergroup time (related to post-impact isostatic compensational mantle upwelling and crustal uplift, this study)		NW-directed bedding-parallel thrusting in post-Klipriviersberg Group to pre-Transvaal Supergroup time (related to Lomanian Orogeny, this study)

APPENDIX 24 (continued)

Area	Author(s) [Study Area]	Early phase of Magondi Orogeny (~2.15-2.055 Ga) *[SE-directed far field compression]*	Bushveld Complex Emplacement (~2.056-2.055 Ga) *[radially BC-outward compression]*	Main & late phase of Magondi Orogeny (~2.055-2.02 Ga & ~2.02-1.97 Ga) Okwa Orogeny (~1.93-1.86 Ga) *[SE-directed far field compression]*	Vredefort Impact (~2.02 Ga) *[Crater formation: radially outward compression]* *[Crater extensional collapse: radially inward extension]* *[Central uplift collapse: radially outward compression]* *[Isostatic compensation; radially outward compression]*	Kheis Orogeny (~1.83-1.73 Ga) *[E-directed far field compression]*	Kibaran Orogeny (~1.35-1.25 Ga) *[N-directed far field compression]* Lomanian Orogeny (~1.2-1.0 Ga) *[NW-directed far field compression]*
CARLETONVILLE GOLDFIELD	De Kock (1964)			Minor movements on West Rand Fault (no major vertical displacement of Black Reef; could indicate rather strike-slip, this study)	Development of the extensional, mylonite- & breccia-bearing Master Bedding Plane Fault (with fragments of Transvaal Supergroup strata) within shales of Jeppestown Subgroup in post-Transvaal Supergroup time (related to syn-impact modification stage of Vredefort transient crater, this study)		
	Fletcher & Gay (1971)				Development of the extensional, mylonite- & breccia-bearing Master Bedding Plane Fault (with fragments of Transvaal Supergroup strata) within shales of Jeppestown Subgroup in post-Transvaal Supergroup time (related to syn-impact modification stage of Vredefort transient crater, this study)		
	Adam (1990) [Tau Tona Gold Mine]						Post-Bushveld dextral strike-slip reactivation of major ENE/WSW-striking "Big Boy" fault system by up to 170m (related to Lomanian O., this study)
	Vermaakt & Roering (1991), Vermaakt (1994),Vermaakt & Chunnett (1994), Vermaakt (1995) [East Driefontein Mine]	Post-Transvaal reactivational normal movements (~200m) with associated drag-folding along N/S-striking, W-dipping Bank Fault		Sinistral strike-slip reactivation of N/S-striking Bank Fault and NE/SW-striking faults with development of associated drag-fold in Pretoria Group strata	Sinistral strike-slip reactivation of Bank Fault and development of the extensional bedding-(sub)parallel Master Bedding Fault (with pseudotachylite formation) using Bank Fault as lateral ramp (related to syn-impact modification stage of Vredefort transient crater, this study) Dextral oblique-slip reactivation (~1.5 km) of N/S-striking Bank Fault, sinistral strike-slip reactivation of NE/SW- and E/W-striking faults and compressional reactivation of Master Bedding Fault and other bedding-(sub)parallel extensional faults to N-verging thrusts (related to post-impact isostatic compensational mantle upwelling and crustal uplift, this study)		
	Berlenbach (1993) [Kloof Gold Mine]				Development of NE-verging thrusts in Witwatersrand and Ventersdorp supergroups strata under semi-brittle conditions (cataclasite, breccia and pseudotachylite formation) (related to post-impact isostatic compensational mantle upwelling and crustal uplift, this study)		Development of NW-verging thrusts and compressional reactivation (inversion) of listric Platberg Group normal faults in Witwatersrand & Ventersdorp supergroups in pre-Transvaal time under brittle-ductile conditions (foliation formation) (related to Lomanian Orogeny, this study)
	Hall (1993), Lowman (1995) [East Driefontein Gold Mine]				Bedding-(sub)parallel thrusting (*e.g.,* Skelm Fault and others) towards NNE effecting Carbon Leader and VCR reefs (related to post-impact isostatic compensational mantle upwelling and crustal uplift, this study)		
	Jolley *et al.* (1999, 2004) [Elandsrand, Mponeng & Deelkraal gold mines]			Development of a series of stacked NE/SW-striking, SE-vergent thrusts (displacement: 1-10 m, locally several tens of metres) rising from Booysens Shale horizon & merging with base of Klipriviersberg Group duplicating VCR in at least post-Klipriviersberg Group time	Development of a series of stacked ENE/WSW-striking, NNW-vergent thrusts in at least post-Klipriviersberg Group time (related to post-impact isostatic compensational mantle upwelling and crustal uplift, this study)		Development of a series of stacked NE/SW-striking, NW-vergent thrusts(displacements <10 m) in at least post-Klipriviersberg Group time (related to Lomanian Orogeny, this study)
	Friese (2011c) [Deelkraal South Project]				Development of at least 4 prominent, post-Transvaal, ENE/WSW-striking, subvertical faults as part of Vredefort transient crater formation		<u>Lomanian Orogeny</u>: Dextral strike-slip reactivation of ENE/WSW-striking transient crater fault system as indicated by offset of ~1.3 Ga old Oberholzer alkaline dyke
	Terracin *et al.* (2016) [Potchefstroom Gap Area]				Extensional reactivation of the Platberg Group-age, NE/SW-striking, SE-dipping, bedding-parallel Potchefstroom Master Fault, leading to the formation of a listric, extensional Potchefstroom sympathetic fault in post-Transvaal time (related to syn-impact modification stage of Vredefort transient crater, this study)		
KLERKSDORP GOLDFIELD	Brink (1982, 1986)				Development of bedding-parallel extensional faults crosscutting Ventersdorp-age dykes & faults owing to gravity sliding and subsidence during formation of Vredefort rim synclinorium & development of the Fakawi Fault (related to syn-impact modification stage of Vredefort transient crater, this study)		
	McCarthy *et al.* (1986)			Development of NE/SW-trending, small-scale, open folds within Transvaal Supergroup strata			
	Clendenin *et al.* (1990) [Oukop, NW margin of Witwatersrand Basin]					Post-Ventersdorp Supergroup positive inversion of late-CRG thrusts & Platberg Group extensional faults, development of E-verging thrust faults, displacing lower West Rand Group strata by >500 m to E	

APPENDIX 24 (continued)

Area	Author(s) [Study Area]	Early phase of Magondi Orogeny (~2.15-2.055 Ga) *[SE-directed far field compression]*	Bushveld Complex Emplacement (~2.056-2.055 Ga) *[radially BC-outward compression]*	Main & late phase of Magondi Orogeny (~2.055-2.02 Ga & ~2.02-1.97 Ga) Okwa Orogeny (~1.93-1.86 Ga) *[SE-directed far field compression]*	Vredefort Impact (~2.02 Ga) *[Crater formation: radially outward compression]* *[Crater extensional collapse: radially inward extension]* *[Central uplift collapse: radially outward compression]* *[Isostatic compensation; radially outward compression]*	Kheis Orogeny (~1.83-1.73 Ga) *[E-directed far field compression]*	Kibaran Orogeny (~1.35-1.25 Ga) *[N-directed far field compression]* Lomanian Orogeny (~1.2-1.0 Ga) *[NW-directed far field compression]*
FREESTATE GOLDFIELD	Buck & Rickus (1977), Minter *et al.* (1986)					Post-Ventersdorp Supergroup reverse-slip reactivation of N/S-striking, W-dipping, Platberg Group-age extensional De Bron fault	Post-Ventersdorp Supergroup reverse-slip reactivation of NE/SW-striking, SE-dipping Platberg Group-age extensional Homestead fault (related to Lomanian Orogeny, this study)
	De Wet & Hall (1994) [Oryx Gold Mine]						System of shallow-angle, NE/SW-striking, NW-verging bedding-(sub)parallel thrusts with 50-200 m up-throws of base of Eldorado Formation (subdividing mine lease area into a northern deeper and a southern shallower area) interpreted as being late-CRG of age (interpreted by Friese *et al.* (1995) to be at least post-Platberg Group in age as thrusts post-date the late-CRG Rheedersdam thrust zone & Platberg Group-age extensional faults) (related to Lomanian Orogeny, this study)
	Minter *et al.* (1986), Grant (1989), Rompel (1995) [President Brand & President Steyn gold mines]					N/S-striking, W-dipping, mylonitic reverse faults developed parallel- to subparallel on western down-thrown side of De Bron, Dagbreek, & Stuirmanspan-Arrarat faults	
	Stuart *et al.* (2000), Jolley *et al.* (2007) [Loraine & Target gold mines, Sun Project]						Development of syn-Klipriviersberg Group W-vergent backthrusts (*e.g.,* Zuurbron backthrust) in response to continuing late-CRG E-vergent Rheedersdam forethrusting together forming a passive roof duplex (related to Lomanian Orogeny, this study)
	Friese *et al.* (2003) [H.J. Joel & Harmony gold mines]	^{40}Ar-^{39}Ar ages of ~2095-2065 Ma for cataclasites & mylonites from Platberg Group-age faults documenting complete resetting of their isotope system during a (tectono-)thermal overprinting event (Magondi Orogeny)			^{40}Ar-^{39}Ar ages of ~2020 Ma for ultracataclastic-pseudotachylitic breccias cutting across Platberg Group-age cataclasites and mylonites developed along the De Bron fault and Merriespruit thrust zone, documenting thermal and deformational effects related to the Vredefort impact event	^{40}Ar-^{39}Ar ages of ~1830-1750 Ma for cataclasites & mylonites from Platberg Group-age faults documenting partial resetting of their isotope system during a low-temperature (tectono-)thermal overprinting event	<u>Kibaran Orogeny</u>: ^{40}Ar-^{39}Ar ages of ~1345-1200 Ma for cataclasites & mylonites from Platberg Group-age faults documenting partial resetting of their isotope system during a low-temperature (tectono-)thermal overprinting event
	Jolley *et al.* (2004,) [Tshepong & Matjhabeng gold mines]			Development of a second set of NNE/SSW-striking, ESE-vergent thrusts overprinting pyrophyllite-sulphide alteration associated with older generation of low-angle, NW/SE-striking, SW-verging (Platberg-age, this study) thrusts			
	Friese (2005) [Lindley Project]						<u>Lomanian Orogeny</u>: Several NE/SW-striking, shallow SE-dipping thrusts & reverse-slip reactivated, NE/SW-striking, steep SE-dipping, extensional Platberg Group-age faults interpreted from reflection seismic data
	Friese (2011b) [Jeanette Project]						<u>Lomanian Orogeny</u>: Several NE/SW-striking, shallow SE-dipping thrusts (*e.g.,* Damspruit Thrust) interpreted from reflection seismic data to transect and minor displace (30-50m net vertical upthrows towards NW) Central Rand Group & Klipriviersberg Group strata & Platberg-age fault system. A major thrust is interpreted to straddle the eastern boundary of the prospect area with an estimated net vertical upthrow of ~1km towards NW, which caused strata of Central Rand & Klipriviersberg groups to be removed by erosion in pre-Karoo Supergroup time, with West Rand Group strata subcropping directly beneath Karoo Supergroup E of thrust
	Friese (this study)			Semi-ductile (protomylonite) oblique reverse-slip reactivation towards SE along bedding planes and Platberg Group-age De Bron fault & Merriespruit thrust; development of large-scale, open, symmetric, NE/SW-trending De Bron Anticline & Virginia-Kroonstad Syncline across northern & central parts of goldfield	Formation of brittle ultracataclastic-pseudotachylitic breccias along Platberg Group-age De Bron fault & Merriespruit thrust zone in response to seismic compressional and/or extensional faulting and reverse and/or normal dip-slip reactivation related to syn-impact crater formation and extensional collapse stages of Vredefort transient crater, respectively	Semi-ductile (protomylonite) oblique reverse-slip reactivation towards E along bedding planes and Platberg Group-age De Bron fault & Merriespruit thrust zone	<u>Lomanian Orogeny</u>: Semi-ductile (protomylonite) oblique reverse-slip reactivation towards NW along bedding planes and Platberg Group-age De Bron fault & Merriespruit thrust zone

APPENDIX 24 (continued)

Area	Author(s) [Study Area]	Early phase of Magondi Orogeny (~2.15-2.055 Ga) *[SE-directed far field compression]*	Bushveld Complex Emplacement (~2.056-2.055 Ga) *[radially BC-outward compression]*	Main & late phase of Magondi Orogeny (~2.055-2.02 Ga & ~2.02-1.97 Ga) Okwa Orogeny (~1.93-1.86 Ga) *[SE-directed far field compression]*	Vredefort Impact (~2.02 Ga) *[Crater formation: radially outward compression]* *[Crater extensional collapse: radially inward extension]* *[Central uplift collapse: radially outward compression]* *[Isostatic compensation; radially outward compression]*	Kheis Orogeny (~1.83-1.73 Ga) *[E-directed far field compression]*	Kibaran Orogeny (~1.35-1.25 Ga) *[N-directed far field compression]* Lomanian Orogeny (~1.2-1.0 Ga) *[NW-directed far field compression]*
VREDEFORT IMPACT CRATER	Truter (1936) [~5km W of Potchefstroom]			Prominent, post-Bushveld to pre-Pilanesberg, SE-verging Potchefstroom thrust (with associated NNE/SSW-trending folds) displacing Chuniespoort Group on top of Pretoria Group strata			
	Van der Merwe (1986); Van der Merwe *et al.* (1988) [Potchefstroom area]				Development of the NE/SW-striking, SE-dipping Potchefstroom Master Fault as a normal fault under brittle conditions (breccia- & pseudotachylite-bearing) (D1) (related to syn-impact modification stage of Vredefort transient crater, this study) Development of a series of large-scale, NNE/SSW-trending, shallow SSW-plunging folds with subvertical axial planes E and W of Potchefstroom Fault in Transvaal Supergroup (D2) (related to post-impact isostatic compensational mantle upwelling and crustal uplift, this study)		Sinistral strike-slip reactivation of Potchefstroom Fault under brittle conditions (D3) (related to Lomanian Orogeny, this study)
	Simpson (1977, 1978), Lilly (1978), McCarthy *et al.* (1990c), Brink *et al.* (1997, 2000b), Wieland (2006), Wieland *et al.* (2005, 2006) [Potchefstroom synclinorium]				Development of doubly-plunging synclines & anticlines (with thrusts occupying their hinge zones) within a broad-scale open fold in Pretoria Group strata (Potchefstroom Synclinorium) concentric around & outward-verging from Vredefort Dome; low-angle normal faults (downthrow towards the Vredefort Dome) crosscut the folds; radial (sinistral & dextral strike-slip), oblique & tangential fault sets (with respect to centre of Vredefort crater) crosscutting the collar (all related to syn-impact modification stage of Vredefort transient crater, this study)		
	Friese *et al.* (1995) [W & E collar region]						Development of a system of NW-verging thrusts of post-Transvaal age around Vredefort Dome & in the Westerdam Dome and Rand Anticline areas; thrust displacements range between ~500 m (*e.g.,* Spitskop Thrust) and ~1500 m (*e.g.,* Enselspruit Thrust), indicating an apparent decrease in displacement magnitude towards NW (related to Lomanian Orogeny, this study)
	Tinker *et al.* (2002) [W & SW collar region]						Development of a NW-verging, low-angle thrust in post-Pretoria Group time (related to Lomanian Orogeny, this study)
	Molezzi (2017), Molezzi *et al.* (2019) [W, S & E collar region]			Development of gentle, open folds (*e.g.,* Vaal Dam Anticline) in post-Magaliesberg Formation and pre-Vredefort impact time	Development of a listric fault across the southeastern margin of the Vredefort Dome, constrained as late to post-central uplift formation (related to syn-impact modification stage of Vredefort transient crater, this study); Post-impact isostatic upwelling of upper mantle beneath Vredefort Dome by ~15 km		NW-verging thrusts and thrust-reactivated Platberg Group-age listric extensional faults developed in at least post-Ventersdorp time (related to Lomanian Orogeny, this study)
BUSHVELD COMPLEX	Du Plessis &Clendenin (1988) [S of Thabazimbi]						Reactivation of Bobbejaanswater fault system (= Thabazimbi-Murchison lineament) leading to the development of normal dip-slip and reverse-slip P-shears and potential normal faulting along Riedel shears (= transpression) (related to Lomanian Orogeny, this study)
	Alexandre *et al.* (2006) [Mazista, Delmas, SE of Pretoria]		Quarried slates at Mazista, near Delmas, and SE of Pretoria close to WSW-verging Centurion thrust complex				
	Hall (1918), Ehlers & Vorster (1998) [Malips area]		Mined amosite and crocidolite from second and third order folds within an anticlinorium of the Mohlapitse fold belt				
	Hall (undated), Du Toit (1954), Hammerbeck (1986), Harley & Charlesworth (1994) [Malip (Mphogodima) River - Penge – Pilgrim's Rest areas]		Dynamothermal metamorphic rocks comprising slates (± chiastolite-staurolite), sericitic/micaceous schists and cordierite-sillimanite-biotite-muscovite "gneisses" in pelitic units of Pretoria Group				

APPENDIX 24 (continued)

Area	Author(s) [Study Area]	Early phase of Magondi Orogeny (~2.15-2.055 Ga) *[SE-directed far field compression]*	Bushveld Complex Emplacement (~2.056-2.055 Ga) *[radially BC-outward compression]*	Main & late phase of Magondi Orogeny (~2.055-2.02 Ga & ~2.02-1.97 Ga) Okwa Orogeny (~1.93-1.86 Ga) *[SE-directed far field compression]*	Vredefort Impact (~2.02 Ga) *[Crater formation: radially outward compression]* *[Crater extensional collapse: radially inward extension]* *[Central uplift collapse: radially outward compression]* *[Isostatic compensation; radially outward compression]*	Kheis Orogeny (~1.83-1.73 Ga) *[E-directed far field compression]*	Kibaran Orogeny (~1.35-1.25 Ga) *[N-directed far field compression]* Lomanian Orogeny (~1.2-1.0 Ga) *[NW-directed far field compression]*
BUSHVELD COMPLEX	Killick & Morgan-Jones (1988), Killick & Scheepers (2005) [Witwatersberg Goldfield W of Magaliesberg]		Development of WNW/ESE-trending F1 folds with a shallow (30°) N-dipping, S-verging, penetrative axial planar S1 cleavage & WNW/ESE-striking, low-angle, N-dipping, S-directed, ductile thrusts (with Au-bearing quartz veins) in Pretoria Group strata (D1)		Development of WNW/ESE- trending, asymmetric, upright F2 folds (coaxial to earlier formed (Bushveld Complex-related) F1 folds) with a WNW/ESE-striking, SSW-dipping axial planar S2 (crenulation to pressure solution) cleavage & of WNW/SSE-striking, S-dipping, N-directed brittle-ductile thrusts (with Au-bearing quartz veins) in Pretoria Group strata (D2) (related to post-impact isostatic compensational mantle upwelling and crustal uplift, this study)		
	Martin (1990) [SW of Thabazimbi]						Normal dip-slip followed by sinistral strike-slip reactivation of Thabazimbi-Murchison Lineament & development of ENE/WSW- to E/W-striking, subvertical sinistral strike-slip faults & NNE/SSW-striking dextral Riedel faults displacing (up to a few 100m) NW/SE-striking Pilanesberg-age dykes (related to Lomanian Orogeny, this study)
	Swartz (1993) [Kruidfontein Prospect]						Pre-Pilanesberg cataclastic-ultracataclastic normal dip-slip faults intruded by Pilanesberg-age dykes. This extensional event also gave rise to the Rustenburg Fault and Brits Graben (related to Kibaran Orogeny, this study) Post-Pilanesberg carbonate-quartz filled cataclastic & fracture-type strike-/oblique-slip faults(related to Lomanian Orogeny, this study)
	Harley (1993) Harley & Charlesworth (1994, 1995) [Sabie-Pilgrim's Rest Goldfield]		Syn-Bushveld Complex development of E-directed bedding-parallel flexural-slip thrusts, out-of-sequence thrusts & back-thrusts with associated hydrothermal Au mineralisation along them in Transvaal Supergroup strata under initial ductile, later brittle conditions in response to BC crustal loading and thermal subsidence				
	Bumby *et al.* (1998) [Rustenburg Fault Zone]	Pre-Bushveld Complex development of NW/SE-trending F1 folds (D1) & ENE/ WSW-trending F2 folds (D2) forming a F1/F2 interference pattern, D2 culminated in dextral strike-slip (10.6 km) along Rustenburg Fault					
	Clarke *et al.* (2000) [Spruitfontein inlier]	Development of pre-Bushveld, mega- to mesoscopic, ENE/WSW-trending, ENE-plunging, upright-steeply dipping, gently, cuspate folds (F1) with an axial planar steeply inclined, penetrative cleavage & axial parallel boudins, pinch & swell structures & mineral elongation lineations in highly recrystallised quartzite of Spruitfontein inlier in Marginal Zone (D1)	Development of syn-RLS NNW/SSE-striking, anastomosing, bifurcating, ductile extensional joints & tension gashes (D1)				Development of a NNW/SSE-striking, subvertical, conjugate, hybrid, brittle extension fault & shear-joint system (D2) (related to Lomanian Orogeny, this study)
	Friese (2003b, 2009), Friese & Chunnett (2004) [Mogalakwena Mine]	Reactivation of Neoarchaean (~2.98- 2.96 Ga) NW/SW-striking Pongola impactogenal rift system resulting in the development of NW/SE-trending fault-bend (roll-over) folds (F1) and NW/SE- to WNW/ESE-striking, moderate- to steeply dipping extensional faults/fault zones (D1) in pre- to syn-RLS time	Syn-Bushveld Complex ENE-verging, layer-parallel flexural-slip thrusts developed along major litho-stratigraphic boundaries under ductile conditions in response to BC crustal loading and thermal subsidence (D2)	<u>Early phase of Magondi Orogeny (D3)</u>: Reactivation of a ~2.78-2.64 Ga old, E/W-striking sinistral strike-slip shear zone system resulting in the development of an ENE/WSW- to NE/SW-striking, subvertical, dextral strike-slip shear zone system (= lateral ramps) and associated NE-directed, layer/bedding-parallel thrusts (= oblique-frontal ramps) accompanied by the intrusion of LGS dykes along shears and thrusts, minor LGS dyke emplacement also along extensionally reactivated NW/SE-striking Pongola rift faults <u>Main phase of Magondi Orogeny (D4)</u>: Regional, shallow NW-dipping, SE-directed thrusting & ENE/WSW-trending, open, low-amplitude folding (F2) in Archaean basement, Transvaal SG & RLS in syn-Critical Zone time		Extensional reactivation of ENE/WSW- to NNE/SSW-striking, subvertical, dextral strike-slip shear zone system and emplacement of dolerite dykes (= feeders to Sibasa Group lavas) along shear zones (D5)	<u>Kibaran Orogeny (D6)</u>: Development of N-S striking, moderate W-dipping extensional "Kibaran" fault zones with typical undulating geometry and an imbricate fan of normal dip-slip duplexes in their hangingwall; calcite and alkaline quartz-feldspar formation along fault zones <u>Lomanian Orogeny (D7)</u>: Sinistral strike-slip reactivation of N/S-striking "Kibaran" fault zones leading to the formation of an imbricate fan of combined normal dip-slip and sinistral strike-slip duplexes in their hangingwall; calcite vein formation along fault zones

APPENDIX 24 (continued)

Area	Author(s) [Study Area]	Early phase of Magondi Orogeny (~2.15-2.055 Ga) *[SE-directed far field compression]*	Bushveld Complex Emplacement (~2.056-2.055 Ga) *[radially BC-outward compression]*	Main & late phase of Magondi Orogeny (~2.055-2.02 Ga & ~2.02-1.97 Ga) Okwa Orogeny (~1.93-1.86 Ga) *[SE-directed far field compression]*	Vredefort Impact (~2.02 Ga) *[Crater formation: radially outward compression]* *[Crater extensional collapse: radially inward extension]* *[Central uplift collapse: radially outward compression]* *[Isostatic compensation; radially outward compression]*	Kheis Orogeny (~1.83-1.73 Ga) *[E-directed far field compression]*	Kibaran Orogeny (~1.35-1.25 Ga) *[N-directed far field compression]* Lomanian Orogeny (~1.2-1.0 Ga) *[NW-directed far field compression]*
BUSHVELD COMPLEX	Mapeo *et al.* (2004)	Post-Transvaal to pre-Bushveld SE-vergent folding & thrusting along NW-edge of Gaborone Granite Complex (SE Botswana)					
	Nomade *et al.* (2004) [Impala Platinum Mine]			Wide-spread, pervasive, post-crystallisation, syn-cooling alteration and overprinting of UG2 Chromitite Layer by hydrothermal fluids circulating along low-angle thrusts leading to biotite formation dated at 2049-2037 Ma (weighted mean age: 2042.4 ± 3.2 Ma; ^{40}Ar-^{39}Ar, biotite)			
	Friese (2004b) [Amandelbult Platinum Mine]	Extensional reactivation of NW/SE-striking Pongola rift faults in Archaean basement controlling crustal emplacement of Rustenburg Layered Suite and is accompanied by the development of large-scale, NW/SE-trending, low-amplitude, open fault-bend (roll-over) folds (F1) and NW/SE-striking normal faults in the crest of F1 anticlines (*i.e.,* crestal collapse grabens) (D1)	Syn-Bushveld Complex NW-verging, layer-parallel flexural-slip thrusts developed along major litho-stratigraphic (competence contrast) boundaries under ductile conditions in response to Bushveld Complex crustal loading and thermal subsidence (D2)	Dextral and sinistral strike-slip (transpressional) reactivation of NW/SE-striking Pongola rift faults and NE/SW-striking Ventersdorp rift faults, respectively, leading to the formation of dextral and sinistral strike-slip shears and strike-slip related, SE- and SW-verging, low-angle compressional frontal and oblique ramps (thrusts) between them, respectively (D3)		Sinistral normal oblique-slip (transtensional) reactivation of NW/SE-striking Pongola rift faults leading to the formation of a linking array of WNW/ESE-striking, low-angle sinistral transtensional faults (D5)	<u>Kibaran Orogeny (D6)</u>: Dextral normal oblique-slip (transtensional) reactivation of NW/SE-striking Pongola rift faults leading to the formation of a linking array of N/S-striking, low-angle dextral transtensional faults; Formation of regional N/S-striking, moderate-steep dipping extensional (normal dip-slip) faults accompanied by the intrusion of alkaline dykes formed in response to E-W extension <u>Lomanian Orogeny (D7)</u>: Sinistral strike-slip reactivation of NW/SE-striking Pongola rift faults in Archaean basement leading to the formation of an array of linking NW/SE- to NNW/SSE-striking, subvertical sinistral strike-slip shear zones
	Friese (2005) [Blue Ridge Prospect]		Development of subvertical ENE/WSW-striking shear zones, interlinking NE/SW-striking shears and layer-parallel extensional (normal dip-slip) shearing in response to the dextral strike-slip reactivation of Steelpoort Fault & dextral transtensional stress field conditions				
	Friese (2007c) [NE sector of Eastern Limb]		Dextral transtensional reactivation of pre-BC, NE/SW-striking Wonderkop-Stofpoort & Steelpoort faults & formation of NE/SW-striking, dextral transtensional faults intruded by Main Zone & Upper Zone feeder dykes in syn-Critical Zone (post-UG2) time, all controlling facies & grade distribution in Merensky Reef	Dextral transpressional reactivation of NW/SE-striking Pongola rift faults in Archaean basement leading to the formation of a NW/SE-striking, subvertical, anastomosing, dextral transpressional fault zone system			<u>Kibaran Orogeny</u>: Development of N/S-striking extensional fault/fracture zones
	Perritt & Roberts (2007) [Helena, Horizon, Kroondal chrome mines]		Syn-Bushveld Complex outward-verging, layer-parallel flexural-slip thrusting developed along major litho-stratigraphic boundaries under ductile conditions in response to Bushveld Complex crustal loading and thermal subsidence				
	Friese (2008b) [Bushveld-wide PlatMine Collaborative Project]	Extensional reactivation of NW/SE-striking Pongola rift faults in Archaean basement controlling crustal emplacement of Rustenburg Layered Suite, accompanied by the development of large-scale, NW/SE-trending, low-amplitude, open fault-bend (roll-over) folds (F1) and NW/SE-striking normal faults in the crest of F1 anticlines (*i.e.,* crestal collapse grabens) (D1)	Syn-Bushveld Complex outward-verging, layer-parallel flexural-slip thrusting developed along major litho-stratigraphic (competence contrast) boundaries under ductile conditions in response to Bushveld Complex crustal loading and thermal subsidence; contact-metamorphism related syn-RLS basement doming with radially dome-outward thrusting (D2)	Dextral and sinistral strike-slip (transpressional) reactivation of NW/SE-striking Pongola and NE/SW-striking Ventersdorp rift faults, respectively, leading to the formation of dextral and sinistral strike-slip shears and strike-slip related, SE- and SW-verging, low-angle compressional frontal and oblique ramps between them, respectively (D3); Regional, open, gentle, ENE/WSW-trending folding (F2) of RLS (D4)		E-vergent folding and thrusting in SW-sector of Western Limb of Bushveld Complex (*e.g.,* at Brakspruit Section of Rustenburg Platinum Mines)	
	Friese (2012, 2014) [Platreef Project]	Extensional reactivation of NW/SE-striking Pongola rift faults in Archaean basement controlling emplacement of Rustenburg Layered Suite, accompanied by the development of large-scale, NW/SE-trending, low-amplitude, open fault-bend (roll-over) folds (F1) and NW/SE-striking normal faults in the crest of F1 anticlines (*i.e.,* crestal collapse grabens) (D1)	Development of ENE- to NE-directed layer-parallel flexural-slip thrusts in response to BC crustal loading/thermal subsidence, penecontemporaneously with the development of WSW- to SW-verging, low-angle thrusts (*e.g.,* Bikkuri thrust) and syn-kinematic intrusion of LGS dykes along them in response to the formation of a large-scale roll-over anticline above a NNW/SSE-striking, WSW-dipping "Pongola" rift fault (D2)	Development of NE- to NNE-trending, subvertical "Ventersdorp" dextral strike-slip shear zones (= lateral ramps) with associated NE-directed, layer/bedding-parallel thrust zones (= oblique-frontal ramps) by reactivation of Neoarchaean Ventersdorp sinistral strike-slip system (D3), followed by the formation of low-angle, SE-verging thrusts & regional, ENE/WSW-trending, subhorizontal, low-amplitude F2 folds (D4)		Development of WNW/ESE- to WSW/ENE-striking "Soutpansberg" extensional fracture zones and intrusion of associated dolerite dykes (= feeders to Sibasa Lavas) (D5)	<u>Kibaran Orogeny (D6)</u>: Development of N-S striking, moderately W-dipping extensional "Kibaran" fault zones, with typical undulating geometry and an imbricate fan of combined normal dip-slip and Lomanian-age sinistral strike-slip duplexes in their hangingwall <u>Lomanian Orogeny (D7)</u>: Sinistral strike-slip reactivation of Kibaran-age, N/S-striking, extensional fault zones

APPENDIX 25

SUMMARY OF PALAEO- TO MESOPROTEROZOIC (POST-TRANSVAAL SUPERGROUP; ~2.15-1.0 Ga) (A) FORMATION AND (B) RESETTING AGES REPORTED FROM THE KAAPVAAL CRATON

APPENDIX 25-A: Summary of Palaeo- to Mesoproterozoic (post-Transvaal Supergroup; ~2.1-1.0 Ga) formation ages reported from the Kaapvaal Craton.

Area	Reference	Lithology / Locality	Age (Ma)	Method	Interpretation by author(s)
WITWATERSRAND BASIN	Fumerton (1978)	Felsites & porphyritic felsite dykes / East Rand Goldfield	2127 ± 13, 2105 ± 26	Rb-Sr; whole-rock	Formation/crystallisation age
	Moser & Hart (1996), Moser (1997)	Schurwedraai & Baviaanskranz Alkali Granites / Vredefort Dome collar area	2078 ± 12	U-Pb; zircon	Formation/crystallisation age
	Graham *et al.* (2005)	Schurwedraai alkali granite	2052 ± 14	U-Pb; zircon	Formation/crystallisation age
	De Waal *et al.* (2006)	Lindeques Drift Complex / Vredefort Dome collar area	2054.8 ± 5.7	U-Pb; zircon	Formation/crystallisation age
	De Waal *et al.* (2006)	Roodekraal Complex / Vredefort Dome collar area	2053 ± 9.2	U-Pb; zircon	Formation/crystallisation age
	Coetzee & Kruger (1989)	Losberg Complex / Vredefort Dome collar area	2041 ± 41	Rb-Sr; whole-rock & minerals	Formation/crystallisation age
	McHalvie Clarke (1972)	Roodekraal Complex / Vredefort Dome collar area	post-Transvaal	geological interpretation	Formation/crystallisation age
	Allsopp *et al.* (1991)	Rietfontein Alkaline Granite / Vredefort Dome collar area	>2008 ± 10; 2004 ± 16;	^{40}Ar-^{39}Ar; hornblende	Formation/crystallisation age
	Nel & Jansen (1957), Frick (1975a, 1979)	Kaffirskraal Ultramafic Complex / south of Deneysville	post-Ventersdorp	geological interpretation	Formation/crystallisation age
	Jansen (1953)	Vereeniging Gabbroid / south of Deneysville	Probably Bushveld	geological interpretation	Formation/crystallisation age
	Cousins (1959)	Vogelstruisfontein Gabbroid / Central Rand Goldfield	Probably Bushveld	geological interpretation	Formation/crystallisation age
	McCarthy *et al.* (1990), Cawthorn *et al.* (1981), Grohman (1986), Jeffery (1975) and Antrobus & Whiteside (1964)	Epidiorite & norite dykes and sills / Carletonville and East, Central & West Rand goldfields	pre-/syn-Bushveld	geological interpretation	Formation/crystallisation age
	Reimold *et al.* (1990)	Pseudotachylite / Vredefort Dome	2010 ± 60	^{40}Ar-^{39}Ar; whole rock	Formation/crystallisation age
	Walraven *et al.* (1990)	Granophyre dykes / Vredefort Dome	2016 ± 24	^{40}Ar-^{39}Ar; whole rock	Formation/crystallisation age
	Allsopp *et al.* (1991)	Granophyre dykes / Vredefort Dome	2006 ± 9	^{40}Ar-^{39}Ar; whole rock	Formation/crystallisation age
	Compston & Nicolaysen (unpubl.)	Granophyre dykes / Vredefort Dome	2002 ± 52	U-Pb; zircon	Formation/crystallisation age
	Hart *et al.* (1981)	Central Intrusive Granite / centre of Vredefort Dome	1944 ± 92	Rb-Sr; whole-rock	Formation/crystallisation age
	Burger & Walraven (1980)	Dolerite / Ottosdal	1740 ± 13	^{40}Ar-^{39}Ar; whole-rock	Formation/crystallisation age
	Reimold *et al.* (1988)	High-Ti dioritic dyke / Vredefort Dome	1620 ± 120	Rb-Sr; whole-rock & minerals	Formation/crystallisation age
	Cousins (1959) Friese *et al.* (1995)	Gabbroid of Brandfort Complex	post-Ventersdorp Mesoproterozoic (~1450-1300)	geological interpretation geological interpretation	Formation/crystallisation age Formation/crystallisation age
	Verwoerd *et al.* (1989)	Carbonatite of Stukpan Complex	1354 ± 11	Rb-Sr; mica	Formation/crystallisation age
	Harmer (1993, 1999)	Carbonatite of Stukpan Complex	1345 ± 13	Rb-Sr; mica	Formation/crystallisation age
	Van Niekerk (1962) recalc. By Anhaeusser & Burger (1982)	Venterspost-Gemspost-Bank-Oberholzer dyke swarm / Venterspost Mine, Carletonville Goldfield	1330 ± 80 1302 ± 78	Rb-Sr; biotite	Formation/crystallisation age Formation/crystallisation age
	Antrobus *et al.* (1986), Verwoerd (1993)	Klerksdorp dyke swarm / Klerksdorp Goldfield	Pilanesberg-age	geol. Interpretation	Formation/crystallisation age
	Van Niekerk (1962)	Robynson Dyke	1310 ± 80	Rb-Sr; biotite	Formation/crystallisation age
	Schreiner & Van Niekerk (1958) recalc. by Anhaeusser & Burger (1982)	Robynson Dyke	1290 ± 180 1263 ± 176	Rb-Sr; biotite	Formation/crystallisation age Formation/crystallisation age
	McDougall (1963)	East Rand dyke swarm / East Rand Goldfield	1120 ± 45	K-Ar; feldspar	Formation/crystallisation age
	Pybus *et al.* (1994)	Gabbro of Anna's Rust Sheet / Vredefort Dome	1054 ± 13	Rb-Sr; ?	Formation/crystallisation age
	Reimold *et al.* (1995)	Gabbro of Anna's Rust Sheet / Vredefort Dome	1068 ± 7	Ar-Ar; ?	Formation/crystallisation age
	Reimold *et al.* (2000)	Gabbros of Anna's Rust Sheet and Vredefort Mafic Complex / Vredefort Dome and Majuba Gabbro / Majuba Colliery, Mpumalanga Province	1052 ± 11	Rb-Sr; biotite, plagioclase	Preferred formation/crystallisation age

APPENDIX 25-A (continued)

Area	Reference	Lithology / Locality	Age (Ma)	Method	Interpretation by author(s)
BUSHVELD IGNEOUS PROVINCE	Schweitzer (unpubl.)	Andesitic and rhyolitic lavas of Dullstroom Formation / Bushveld Complex	2089 ± 26	Pb-Pb, zircon	Formation/crystallisation age
	Walraven (1987a)	Klipkloof Granite (Lebowa Granite Suite) / Bushveld Complex	2065 ± 70	Rb-Sr; whole-rock	Formation/crystallisation age
	De Waal *et al.* (2002)	Marble Hall breccia associated with diorite / central Bushveld Complex	2062 ± 8	$^{40}Ar/^{39}Ar$; amphibole in breccia-fill	Formation/crystallisation age
	Harmer & Armstrong (2000)	Rooikop porphyry of Rashoop Granophyre Suite / Bushveld Complex	2061.8 ± 5.5	U-Pb; zircon	Formation/crystallisation age
	Walraven *et al.* (1990)	Rustenburg Layered Suite of Bushveld Complex / Bushveld Complex	2061 ± 27	Rb-Sr; whole-rock	Formation/crystallisation age
	Walraven (1997)	Rhyolite of Selons River Formation (Rooiberg Group) / Bushveld Complex Rooikop porphyry of Rashoop Granophyre Suite / Bushveld Complex	2061 ± 2 2060 ± 2	Pb-Pb; mean whole-rock age Pb-evaporation; zircon	Formation/crystallisation age Formation/crystallisation age
	Scoates *et al.* (2012)	Pyroxenite beneath UG2 (Lower Critical Zone) / Bushveld Complex	2060.5 ± 1.4 – 2059.8 ± 1.2	U-Pb; zircon	Formation/crystallisation age
	Walraven & Elsenbroek (1991), Walraven *et al.* (1992)	Schiel Alkaline Complex / Northern Province	2059 +35/-36	Pb-Pb; ?	Formation/crystallisation age
	Buick *et al.* (2001)	Newly grown titanite in a completely retrogressed calcsilicate xenoliths within Rustenburg Layered Suite of Bushveld Complex / Platreef Platinum Mine, northern Bushveld Complex	2058.9 ± 0.8	U-Pb; titanite	Age of complete retrogression due to hydroth. circulation related to cooling of RLS (= min. age of RLS emplacement)
	Wabo *et al.* (2016b)	Mafic B1-sills (initial parental feeder magmas to the Lower Zone-Lower Critical Zone of Bushveld Complex) intrusive into the Transvaal Supergroup / east of the Bushveld Complex	2058.4 ± 1.3; 2058.1 ± 6	U–Pb‘ baddeleyite	Formation/crystallisation age
	Olsson *et al.* (2010)	Marginal Zone (Rustenburg Layered Suite) / Bushveld Complex	2057.7 ± 1.6	U-Pb; baddeleyite	Formation/crystallisation age
	Bowring & Knoper (unpubl.)	Merensky Reef / Adit in Hackney area, eastern Bushveld Complex	2057 ± 0.3	U-Pb; zircon	Formation/crystallisation age
	Harmer & Armstrong (2000)	Rhyolite of Loskop Formation (Rooiberg Group) / Bushveld Complex Rhyolite of Kwaggasnek Formation Rooiberg Group) / Bushveld Complex	2057 ± 4 2057 ± 4	U-Pb; zircon U-Pb; zircon	Formation/crystallisation age Formation/crystallisation age
	Scoates *et al.* (2012)	Stavoren Granophyre of Rashoop Granophyre Suite / Bushveld Complex	2056 ± 1	U-Pb; zircon	Formation/crystallisation age
	Scoates *et al.* (2011)	Pyroxenite of Merensky Reef (Rustenburg Layered Suite) / Bushveld Complex	2056.1 ± 0.7, 2055.3 ± 0.6	U-Pb; zircon	Formation/crystallisation age
	De Waal & Armstrong (2000)	Marble Hall diorite / central Bushveld Complex	2055.6 ± 3.1	Pb-Pb; zircon	Formation/crystallisation age
	Zeh *et al.* (2015)	Marginal Zone / Bushveld Complex Critical Zone / Bushveld Complex	2055.91 ± 0.26 2054.89 ± 0.37	U-Pb; zircon U-Pb; zircon	Emplacement/crystallisation age Emplacement/crystallisation age
	Scoates & Friedman (2008)	Pegmatitic pyroxenite of Merensky Reef / Rustenburg Platinum Mine, western Bushveld Complex	2055 ± 3.9, 2054.4 ± 1.3	U-Pb; rutile & zircon	Formation/crystallisation age
	Friese (unpublished)	NE/SW-striking granite dykes of Lebowa Granite Suite cross-cutting Platreef / Mogalakwena Platinum Mine, northern Bushveld Complex NE-trending, remanent positive magnetic diabase dyke (= Upper Zone feeder dyke) / Modikwa Platinum Mine, eastern Bushveld Complex Pyroxenite (‘C’ facies) / Mogalakwena Platinum Mine, northern Bushveld Complex Pyroxenite (‘A’ facies) / Mogalakwena Platinum Mine, northern Bushveld Complex Gabbro-norite of Main Zone / / Mogalakwena Platinum Mine, northern Bushveld Complex	2066 ± 11, 2060 ± 10, 2060 ± 6, 2058 ± 10, 2057 ± 13, 2057 ± 5, 2054 ± 19 2057 ± 4 2059 ± 14 2056 ± 5, 2057 ± 5, 2054 ± 6 2056 ± 6	U-Pb; zircon	Formation/crystallisation age
	Yudovskaya *et al.* (2013)	Chromitite from Platreef / Mogalakwena Platinum Mine, Bushveld Complex Chromitite from Merensky Reef / Bushveld Complex	2056 ± 5 2051 ± 9	U-Pb; zircon U-Pb; zircon	Formation/crystallisation age Formation/crystallisation age
	Harmer & Armstrong (2000)	Pyroxenite of Merensky Reef (Rustenburg Layered Suite) / Bushveld Complex	2055 ± 2, 2054 ± 3	U-Pb; zircon	Formation/crystallisation age
	Hutchinson *et al.* (2004)	Granite dyke of Lebowa Granite Suite cross-cutting Platreef / northern Bushveld Complex	2054 ± 3	U-Pb; zircon	Formation/crystallisation age
	Scoates *et al.* (2012)	Lebowa granite of Lebowa Granite Suite / Bushveld Complex	2054.2 ± 0.8	U-Pb; zircon	Formation/crystallisation age
	Walraven & Hattingh (1993)	Nebo Granite (Lebowa Granite Suite) / Bushveld Complex	2054 ± 2	Pb-evaporation; zircon	Formation/crystallisation age
	Harmer & Armstrong (2000)	Steelpoort Park granite of Lebowa Granite Suite / Bushveld Complex Nebo granite of Lebowa Granite Suite / Bushveld Complex Makhutso granite of Lebowa Granite Suite / Bushveld Complex	2057.5 ± 4.2 2054.2 ± 2.8 2053.4 ± 3.9	U-Pb; zircon U-Pb; zircon U-Pb; zircon	Formation/crystallisation age Formation/crystallisation age Formation/crystallisation age
	Wabo *et al.* (2016a)	Uitkomst Complex / 70 km SE of Bushveld Complex, Mpumalanga Province	2054 ± 7	U–Pb; baddeleyite	Formation/crystallisation age
	Coertze *et al.* (1978)	Stavoren Granophyre (Rashoop Granophyre Suite) / Bushveld Complex	2053 ± 12	U-Pb; zircon	Formation/crystallisation age
	Dorland (2004)	Quartz porphyry lavas (Swaershoek Formation = base of Waterberg Group / Rhenosterpoort 402 farm, W of Nylstroom Quartz porphyry lavas (Rust de Winter Formation = base of Waterberg Group) / Rust de Winter 180 farm Youngest detrital zircon in Swaershoek Formation (= base of Waterberg Group) / Rhenosterpoort 402 farm, W of Nylstroom	2054 ± 8 2051 ± 8 2050 ± 7	U-Pb; zircon U-Pb; zircon U-Pb; zircon	Formation/crystallisation age (= maximum deposition age for Waterberg Group) Formation/crystallisation age (= maximum deposition age for Waterberg Group) Maximum age of deposition/sedimentation
	Walraven *et al.* (1982)	Nebo Granite (Lebowa Granite Suite) / Bushveld Complex	2052 ± 48	U-Pb; zircon	Formation/crystallisation age
	Hamilton (1977)	Nebo Granite / Bushveld Complex	2050 ± 12	Rb-Sr; whole-rock	Formation/crystallisation age
	Curl (2001)	B1 and B2 sills / eastern Bushveld Complex	2050 ± 4, 2052 ± 6	U-Pb; zircon	Formation/crystallisation age
	R. Armstrong, 1998 pers. comm. to N. Good	Cassiterite in Rooiberg Tin deposits / Bushveld Complex	2048 ± 8	U-Pb; monazite	Time of hydrothermal fluid flow and tin mineralisation
	Good (1999)	Monazite from contact between fluorite vein and leptite (= granitised Rooiberg Group sediments) / Buffalo Fluorspar Mine, near Naboomspruit, Bushveld Complex	2048.5 ± 1.7	U-Pb; monazite	Time of hydrothermal fluid flow and fluorite mineralisation
	Buick *et al.* (2011)	Pegmatites and veins in Nebo granite / Houtenbek 194 JR farm, central Bushveld Complex	2059 ± 4, 2046 ± 10	U-Pb; monazite	Formation/crystallisation age
	Walraven (1988)	Makhutso Granite (Lebowa Granite Suite) / Bushveld Complex	2046 ± 55 2049 +69/-72 2045 +122/-133	Rb-Sr; whole-rock Pb-Pb; whole-rock Pb-Pb; whole-rock	Formation/crystallisation age Formation/crystallisation age Formation/crystallisation age
	Schoenberg *et al.* (1999)	Poikilitic pyroxenites of Bastard Unit / Western Bushveld Complex	2043 ± 11	Re-Os; chromite & sulphides	Formation/crystallisation age
	Dorland (2004)	Entabeni Granite / Northern Province	2021 ± 5	U-Pb; zircon	Formation/crystallisation age (= maximum deposition age for unconformably overlying Soutpansberg Group)
	Schutte *et al.*(1960), Willemse(1969)	Koringkoppies Complex / Makoppa Dome	post-Transvaal	geological interpretation	Formation/crystallisation ages
	Tyler (1979)	Modipe Gabbro Complex / Makoppa Dome	post-Transvaal	geological interpretation	Formation/crystallisation age
	Brandl (unpubl.)	Palala Granite / Northern Province	~1972	U-Pb; zircon	Formation/crystallisation age

APPENDIX 25-A (continued)

Area	Reference	Lithology / Locality	Age (Ma)	Method	Interpretation by author(s)
BUSHVELD IGNEOUS PROVINCE	Barton *et al.* (1996)	Schiel Alkaline Complex / Northern Province	1853 ± 6	U-Pb; zircon	Formation/crystallisation age
	C.B. Smith (pers. comm., 1997)	Klipspringer (Rustland) kimberlite dykes / Potgietersrus area	~1881	Rb-Sr, mica	Formation/crystallisation age
	Lee (2016)	White foyaite (syenite) from southern edge of Pilanesberg Complex	1602 ± 38, 1583 ± 10	$^{40}Ar/^{39}Ar$; amphibole	Formation/crystallisation age
	Oosthuyzen & Burger (1964)	Leeuwfontein Complex / Pienaars River Complex	1420 ± 70	U-Pb; ?	Formation/crystallisation age
	Harmer (1985)	Leeuwfontein Complex / Pienaars River Complex Leeuwkraal Complex / Pienaars River Complex Rondawel Complex / Pienaars River Complex Franspoort, Buffelsdrift, Klipdrift, Haakdoornfontein complexes / Pienaars River Complex	1430 ± 50 1334 ± 26 1361 ± 142 1306 ± 11	Rb-Sr; whole-rock Rb-Sr; whole-rock Rb-Sr; whole-rock Rb-Sr; whole-rock	Formation/crystallisation age Formation/crystallisation age Formation/crystallisation age Formation/crystallisation age
	Harmer & Armstrong (unpubl.) in Hanson *et al*. (2006)	Phonolite of Leeuwkraal Complex / Pienaars River Complex Syenite of Haakdoornfontein Complex / Pienaars River Complex Syenite of Klipdrift Complex / Pienaars River Complex Syenite of Rondavel Complex / Pienaars River Complex Syenite of Leeuwfontein Complex / Pienaars River Complex	1395 ± 80 1385 ± 5 1385 ± 5 1381 ± 10 1374 ± 10	U-Pb; titanite U-Pb; zircon U-Pb; zircon U-Pb; zircon U-Pb; zircon	Formation/crystallisation age Formation/crystallisation age Formation/crystallisation age Formation/crystallisation age Formation/crystallisation age
	Brandt *et al.* (1996)	Roodeplaat Complex / Saltpan Crater (Pienaars River Complex)	1342 ± 11	Rb-Sr; ?	Formation/crystallisation age
	Harmer (1993, 1999)	Rietfontein nepheline syenites of Spitzkop Complex Ijolites of Spitzkopf Complex Ijolites & nepheline syenites of Spitzkop Complex	1326 ± 35 1357 ± 67 1341 ± 37	Rb-Sr; Rb-Sr; Rb-Sr; whole-rock (34-point isochron)	Formation/crystallisation age Formation/crystallisation age Formation/crystallisation age
	Harmer & Armstrong (unpubl.) in Hanson *et al*. (2006)	White nepheline syenite of Pilanesberg Complex	1397 ± 47	U-Pb; titanite	Formation/crystallisation age
	Van Niekerk (1962)	Pilanesberg Complex	1330 ± 80	Rb-Sr; stable Isotope dilution	Formation/crystallisation age
	Schreiner & Van Niekerk (1958)	Pilanesberg Complex	1290 ± 180	Rb-Sr; stable Isotope dilution	Formation/crystallisation age
	Harmer (1993, 1999)	Carbonatites of Nooitgedacht, Tweerivier, Bulhoek and Derdepoort complexes Carbonatite dykes of Kruidfontein Complex Green foyaite (syenite) of Pilanesberg Complex	1269 ± 171 1246 ± 26 1193 ± 98	Sm-Nd; ? Sm-Nd; ? Rb-Sr; regressed isochron	Formation/crystallisation age Formation/crystallisation age Formation/crystallisation age
	Olivo & Williams-Jones (1999)	Pilanesberg Complex	1260 ± 50	U-Pb; titanite	Formation/crystallisation age
	Retief (1963) in Olivo & William-Jones (1999)	Pilanesberg Complex	1250 ± 50	K-Ar; ?	Formation/crystallisation age
	Snelling (1963)	Foyaite (syenite) of Pilanesberg Complex	1250 ± 60	K-Ar; biotite	Formation/crystallisation age
	Emerman (1991)	NW-trending dyke swarm / NW-extension of Pilanesberg dyke swarm in SE Botswana	Pilanesberg-age	geological/geophysical interpretation	Formation/crystallisation age
	Van Niekerk (1962), Schreiner & Van Niekerk (1958) in Hanson *et al*. (2006)	Dolerite / Pilanesberg dyke swarm	1302 ± 80, 1263 ± 180	Rb-Sr; biotite	Formation/crystallisation age
	Lee (2016)	NW-trending red syenite dyke / Pilanesberg dyke swarm NW-trending grey syenite dyke / Pilanesberg dyke swarm	1268 ± 10 –1219 ± 6 1139 ± 18	$^{40}Ar/^{39}Ar$; feldspar $^{40}Ar/^{39}Ar$; amphibole	Formation/crystallisation age Formation/crystallisation age
	Van Niekerk (1962), Emerman (1991)	Pilanesberg dyke swarm	1290 ± 80	Rb-Sr; biotite	Formation/crystallisation age
	Cawthorn *et al*. (2012)	Olivine–magnetite–apatite-clinopyroxenite pipe intrusive into Bushveld Complex / central Bushveld Complex at the Elandskraal Volcano	1207 ± 200	Sm-Nd; apatite-clinopyroxene pairs (isochron)	Formation/crystallisation age
	Nelson *et al*. (1988), Harmer (1993)	Carbonatite of Goudini Complex	1190 ± 80	Sm-Nd; whole-rock (two-point isochron)	Formation/crystallisation age
	Kramers & Smith (1983)	Premier Kimberlite Group / near Pretoria	1202 ± 72	Pb-Pb; whole-rock & minerals (isochron)	Formation/crystallisation age
	Doppelhammer & Hargraves (1994)	Premier kimberlite field / near Pretoria	~1200	?	Formation/crystallisation age
	Burgess *et al*. (1989), Phillips *et al*. (1989)	Premier Kimberlite Group / near Pretoria	1198 ± 14	$^{40}Ar/^{39}Ar$; clinopyroxene	Formation/crystallisation age
	Jones (1987)	Premier Kimberlite Group / near Pretoria	1198 ± 32	Sm-Nd; garnet-clinopyroxene (isochron)	Formation/crystallisation age
	Richardson *et al*. (1993)	Premier Kimberlite Group / near Pretoria	1190 ± 20	Sm-Nd; garnet two-point isochron	Formation/crystallisation age
	Richardson (1986)	Premier Kimberlite Group / near Pretoria	1180 ± 30 1150 ± 60	Rb-Sr, whole-rock Sm-Nd; garnet-clinopyroxene (isochron)	Formation/crystallisation age
	Allsopp *et al*. (1989)	Premier Kimberlite Group / near Pretoria	1179 ± 36, 1180 ± 30, 1140 ± 16	Rb-Sr; clinopyroxene & phlogopite	Formation/crystallisation age
	Pearson *et al*. (1995)	Premier Kimberlite Group / near Pretoria	1150 ± 41	Sm-Nd; garnet-clinopyroxene-orthopyroxene internal (isochron)	Formation/crystallisation age
	De Kock *et al*. (2014)	WNW-trending dyke from Dibete swarm	1110 ± 4	U-Pb; baddeleyite	Formation/crystallisation age
	Allsopp *et al*. (1967)	Dolerite sill cross-cutting Premier Mine Kimberlite / Pretoria	~1100	Rb-Sr; biotite	Formation/crystallisation age (= min. age of kimberlite)
	Verwoerd (1967)	Carbonatite of Glenover Complex	1000 ± 200	Pb-Pb; monazite	Formation/crystallisation age

APPENDIX 25-A (continued)

Area	Reference	Lithology / Locality	Age (Ma)	Method	Interpretation by author(s)
KRAAIPAN SUBPROVINCE	Ramokate *et al.* (1996)	Granitic gneisses intrusive into porphyritic felsic volcanics / Okwa inlier within Kalahari desert; northwestern Kaapvaal Craton (Botswana)	2101 ± 4 – 2055 ± 1.3	U-Pb; zircon	Formation/crystallisation age
	Key *et al.* (1996)	Kukong felsites / Kanye Basin (Botswana)	2074 ± 4, 2058 ± 3	U-Pb; zircon	Formation/crystallisation age
	K. Kenyon/Anglo Gold (pers. comm., 1998)	Kukong felsites / Kanye Basin (Botswana)	~2054	U-Pb, zircon	Formation/crystallisation age
	Mapeo *et al.* (2006)	Foliated monzogranite / Okwa Basement Complex; northwestern Kaapvaal Craton (Botswana) Augen gneiss / Okwa Basement Complex; northwestern Kaapvaal Craton (Botswana) Meta-rhyolite / Okwa Basement Complex; northwestern Kaapvaal Craton (Botswana)	2057 ± 2 – 2056.3 ± 1.3 2055.3 ± 1.3 2055 ± 4 Ma	U-Pb, zircon	Formation/crystallisation age
	Key *et al.* (1996)	Moshaneng Complex (comprising gabbros, diorites, syenites, granite) / (Botswana)	2054 ± 2	U-Pb; zircon	Formation/crystallisation age
	Mapeo *et al.* (2004b)	Moshaneng Complex (comprising gabbros, diorites, syenites, granite) / (Botswana)	2054 ± 2 Ma	U-Pb; zircon, titanite	Formation/crystallisation age
	Mapeo & Wingate (2009)	Segwagwa-Masoke Complex (comprising granite, diorite, syenite) / (Botswana)	2054 ± 9 Ma		Formation/crystallisation age
	De Kock *et al.* (2016), Ravhura *et al.* (2016)	Molopo Farms Complex / (South Africa)	2052 ± 16 Ma	U-Pb; zircon, baddeleyite	Formation/crystallisation age
	Barton (in: Gould *et al.*, 1987)	Molopo Farms Complex / {Botswana}	~2050	Rb-Sr; minerals	Formation/crystallisation age
	Kruger (1989)	Molopo Farms Complex / {Botswana}	2044 ± 24	Rb-Sr; minerals	Formation/crystallisation age
	Walraven & Elsenbroek (1991)	Dolerite & diorite dykes intrusive into ~2.1-2.055 Ga old granitoids prior to D1 and M1 at ~1.8 Ga / Okwa inlier within Kalahari desert; northwestern Kaapvaal Craton (Botswana)	1971 ± 31	K-Ar; hornblende	Formation/crystallisation age
	Cornell *et al.* (1989)	Carbonatite of Keikamspoort Complex / Prieska area	~1930	Sm-Nd depleted mantle model age	Formation/crystallisation age
	Cornell *et al.* (1998)	Basalt of Hartley Formation / Kheis Belt	1928 ± 4	Pb-Pb; zircon	Formation/crystallisation age
	Maier *et al.* (2003)	Gabbro of Trompsburg Complex / Trompsburg	1915 ± 6	U-Pb, zircon	Formation/crystallisation age
	Clement *et al.* (1979)	Picrite dykes / Wesselton & De Beers diamond mines near Kimberley	1910 ± 60	Rb-Sr; whole-rock & mica	Formation/crystallisation age
	Armstrong (1987)	Basalt of Hartley Formation / Kheis Belt	1893 ± 48	Rb-Sr; whole-rock	Formation/crystallisation age
	Stowe (1990)	Granitic gneiss / Kheis Belt	~1800	U-Pb; zircon	Formation/crystallisation age or age of metamorphism/deformation
	Cornell *et al.* (1998)	Mamatlun Dolerite intrusive into basalts of Hartley Formation / Mamatlun (Botswana)	1750 ± 60	Rb-Sr; biotite	Formation/crystallisation age
	C.B. Smith (pers. comm., 1997)	Kuruman kimberlite province / Kuruman area	1649 ± 42 1626 ± 20 1643 ± 14	Rb-Sr; mica isochron U-Pb; perovskite Ar-Ar; mica, cpx	Formation/crystallisation age Formation/crystallisation age Formation/crystallisation age
	Shee *et al.* (1986)	Kuruman kimberlite province / Kuruman area	~1606, ~1635, ~1674	Rb-Sr; mica errorchron	Formation/crystallisation age
	Ramokate *et al.* (1996)	Tuffaceous siltstone of Takatswaane Formation (Upper Okwa Group = correlative to Kgwebe Formation of Ghanzi-Chobe Belt) / Okwa Inlier (Botswana)	1246 ± 4	U-Pb; zircon	Formation/crystallisation age (age of deposition)
	Onstott *et al.* (1986)	Eastern zone of Namaqua orogenic belt	1244 ± 30	Ar-Ar; ?	
	Gutzmer *et al.* (2000)	Koras Group / Namaqua orogenic belt, Northern Cape Province	~1170		Formation/crystallisation age
	Hanson *et al.* (2004)	Gabbronorite of mafic layered intrusion & volcanics of Xade Complex / (Botswana)	1109.0 ± 1.3	U-Pb; zircon	Formation/crystallisation age
	Pouliquen *et al.* (2008)	Gabbronorite of Tsetseng Complex / (Botswana)	~1100	geological interpretation	Formation/crystallisation age
	Barton J.M. Jr. (pers. comm., 1989)	Gabbro of Tshane Complex / Tshane (Botswana)	1021 ± 86	Rb-Sr; ?	Formation/crystallisation age
SWAZI SUBPROVINCE	Wu *et al.* (2011)	Phalaborwa Complex / Phalaborwa	2062 ± 2 Ma - 2060 ± 1 Ma	U-Pb; zircon, baddeleyite	Formation/crystallisation age
	Reischmann (1995)	Phalaborwa Complex / Phalaborwa	2060 ± 0.5	U-Pb; baddeleyite	Formation/crystallisation age
	Wabo *et al.* (2016a)	Uitkomst Complex / 70 km SE of Bushveld Complex, Mpumalanga Province	2054 ± 7 Ma	U–Pb; baddeleyite	Formation/crystallisation age
	Eriksson (1984)	Phalaborwa Complex / Phalaborwa	2047 +11/-8 2012 ± 19	U-Pb; uranothorite, baddeleyite Rb-Sr; whole-rock	Formation/crystallisation age Formation/crystallisation age
	De Ronde & Kamo (2000)	Mafic meso-tonalite dyke (unstrained) cutting Kaap Valley Tonalite Pluton/greenstone belt contact and F_4-folds / Barberton Greenstone Belt	2024 ± 10	U-Pb; zircon	Formation/crystallisation age and upper age limit of D_4
	Bristow *et al.* (1982)	Gabbro of Timbavati Complex / Mpumalanga Province	1454 ± 59	Rb-Sr; ?	Formation/crystallisation age
	Burger & Walraven (1979, 1980)	Gabbro of Timbavati Complex / Mpumalanga Province	1072 ± 4, 1123 ± 5	Ar-Ar; ?	Formation/crystallisation age
	Nicolaysen & Burger (1965)	Carbonatite of Bull's Run Complex / Natal orogenic belt	1140 ± 35, 1100 ± 40	U/Th/Pb	Formation/crystallisation age
	Eglington & Harmer (unpubl.)	Carbonatite of Bull's Run Complex / Natal orogenic belt	1138 ± 45	Rb-Sr; isochron	Formation/crystallisation age

APPENDIX 25-B: Summary of Palaeo- to Mesoproterozoic (post-Transvaal Supergroup; ~2.1-1.0 Ga) resetting ages reported from the Kaapvaal Craton.

Area	Reference	Lithology / Locality	Age (Ma)	Method	Interpretation by author(s)
WITWATERSRAND BASIN	Gibson *et al.* (2000)	Greenschist-amphibolite facies metasediments of Witwatersrand Supergroup and mafic meta-lava of Dominion Group / Vredefort Dome	2101 ± 5, 2068 ± 4, 2040 ± 4, 2056 ± 13 (2069 ± 4), 2072 ± 12 (2078 ± 6), 2039 ± 13 (2036 ± 4), 2061 ± 13 (2027 ± 14)	^{40}Ar-^{39}Ar; sericite, biotite & hornblende	M1 and M2 metamorphism accompanying the Bushveld magmatic and Vredefort Impact events at ~2.06 and 2.02 Ga, respectively
	Layer *et al.* (1988)	Witwatersrand Supergroup shales / West Rand Goldfield	1945 ± 40	K-Ar; illite	Hydrothermal resetting/low-grade metamorphic overprint event
	Zhao *et al.* (1995, 1999)	Conglomerates & quartzites (VCR), Klipriviersberg lava, Elsburg quartzites / Western Deep Levels G.M., Carletonville Goldfield	~2056 - 1830 ± 38 1994 ± 60, 1917 ± 66	K-Ar; sericite	Retrograde metamorphism & hydrothermal alteration subsequent to Bushveld/Vredefort events and related to Kheis Orogeny
	Friese (this study)	Platberg Group-age tectonites / H.J. Joel Gold Mine, Free State Goldfield Ultracataclastic-pseudotachylitic breccias & mylonites / Harmony Gold Mine, Free State Goldfield	2076 ± 5, 2088 ± 7, ~1750 2020 ± 52, 2019 ± 8, 2029 ± 156, 1829 ± 14, 1761 ± 22, 1699 ± 69	^{40}Ar-^{39}Ar; whole-rock ^{40}Ar-^{39}Ar; whole-rock	Partial thermal resetting ages/events Partial thermal resetting ages/events
	Feather (1981)	Witwatersrand Supergroup conglomerates	1770 ± 60	U-Pb; uraninite	Partial/complete thermal resetting age/event
	Burger & Walraven (1980)	Klipriviersberg Group lavas / Johannesburg	~1960	Rb-Sr; whole-rock	Partial thermal resetting age/event
	Walraven *et al.* (1990)	Zoetlief Group / Vryburg	1901 ± 82 1987 ± 122, 1990 ± 100	Rb-Sr; whole-rock Pb-Pb; whole-rock	Partial thermal resetting age/event Partial thermal resetting age/event
	Armstrong *et al.* (1991)	Klipriviersberg Group lavas / Central Rand Goldfield	2104 ± 31, 1915 ± 41, 1869 ± 61, 1764 ± 21	U-Pb; zircon	Partial thermal resetting ages/events
	Armstrong *et al.* (1991)	Township Quartz Porphyry (Makwassie Formation) / Klerksdorp	2152 ± 9, 2097 ± 11	U-Pb; zircon	Partial thermal resetting ages/events
	Armstrong *et al.* (1991)	Crown Lava (West Rand Group) / Klerksdorp	2052 ± 10	U-Pb; zircon	Partial thermal resetting age/event
	Nicolaysen *et al.* (1963)	Schurwedraai Alkali Granite / within northwestern collar of Vredefort Dome Granophyre dyke / Vredefort Dome	2016 ± 61 1931 ± 26	Rb-Sr; whole-rock Rb-Sr; whole-rock	Partial thermal resetting age/event (this study) Resetting age/event ?
	Allsopp *et al.* (1991)	Outer Granite Gneiss / northeastern sector of Vredefort Dome Outer Granite Gneiss / northwestern sector of Vredefort Dome Granophyre dyke / close to core-collar contact in northwestern sector of Vredefort Dome Rietfontein Alkali Granite / Vredefort Dome	2054 ± 11 1935 ± 8, 1847 ± 22 2006 ± 9 1905 ± 11	^{40}Ar-^{39}Ar; biotite ^{40}Ar-^{39}Ar; biotite ^{40}Ar-^{39}Ar; biotite, whole-rock ^{40}Ar-^{39}Ar; biotite,hornblende	Age of uplift of basement gneiss during formation of Vredefort Dome or thermal overprint during Bushveld magmatism Partial thermal resetting ages/events Age of dyke emplacement or total thermal resetting age/event Complete/partial thermal resetting age/event
	Allsopp (1961, 1964) recalc. by Layer *et al.* (1988)	Witkoppen Granite / Johannesburg Dome	2120 ± 20, 2075 ± 20 2031 ± 10	Rb-Sr; biotite	Partial thermal resetting age/event
	Rundle & Snelling (1977)	Various conglomerate reefs (Witwatersrand Supergroup & Black Reef) / Free State, Klerksdorp, Carletonville & East Rand goldfields	2040 ± 100	U-Pb; uraninite	Formation/crystallization age of galena and complete/partial thermal resetting age/event of uraninite in all reefs, with greater intensity in the northern part of the Witwatersrand Basin)
	Clay (1986)	Malmani dolomites (Chuniespoort G.) / Western Deep Levels G.M., Carletonville Goldfield	~1700	Pb-Pb; galena	Pb-Zn mineralisation age/event
	Barton *et al.* (1988)	Muscovite in shear-zones post-dating extension fractures / Carletonville Goldfield	~2050	Rb-Sr; muscovite	Compressional tectonics due to emplacement of Bushveld Complex
	Köppel & Saager (1974)	'B' Reef Zone / Harmony Gold Mine, Free State Goldfield	1945 ± 25	Pb-Pb; pyrite	Formation/crystallization age of pyrite; thermal resetting age/event
	De Waal *et al.* (1998)	"Spotted dyke" = albitite (dioritic) feeder dyke to Goedgenoeg & Rietgat formations (Platberg Group) / West Driefontein Mine, Carletonville Goldfield	1933 ± 54	Rb-Sr; albite, amphibole	Partial thermal resetting event caused by hydrothermal activity during prolonged metamorphism related to intrusion of Bushveld Complex
	Burger *et al.* (1962)	Galena from quartz/calcite veins cutting Witwatersrand reefs & uraninite from various Witwatersrand reefs and Dominion Reef / various localities within Witwatersrand Basin	2040 ± 60	Pb-Pb; galena & U-Pb; uraninite	Formation/crystallization age of galena and complete/partial thermal resetting age of uraninite in all reefs throughout Witwatersrand Basin
	Louw & Strelow (1954)	Uraninite concentrates and galena from various reefs from all goldfields / Witwatersrand Basin	~2100-2000 and ~1913-1861	Pb-Pb; uraninite Pb-Pb; galena	Formation/crystallization ages of galena and complete/partial thermal resetting ages of uraninite in all reefs throughout Witwatersrand Basin (this study)
	Poujol *et al.* (1998, 1999)	Detrital pyrite and zircon from altered H.W.2 quartzite and Kimberley Reef / Evander Goldfield	2020 ± 120 2088 ± 99	Pb-Pb; pyrite U-Pb; zircon	Resetting of detrital pyrite at Bushveld/Vredefort time Resetting of detrital zircon at Bushveld time
	Barton *et al.* (1999)	Granodiorite, granite and leucosome from migmatite / Johannesburg Dome	2087 ± 42, 2081 ± 42	Rb-Sr; biotite	Partial thermal resetting age/event
	Kositcin *et al.* (2001)	Vaal Reef (Johannesburg Subgroup) / Vaal Reef No. 8 Shaft, Klerksdorp Goldfield	~2382 - 2039	U-Pb; .xenotime	Post-diagenetic thermo-tectonic events
	Layer *et al.* (1989)	Silicified stromatolite of Rooihoogte Formation (base of Pretoria Group)	2068 ± 37; 2015 ± 14, 2009 ± 14	^{40}Ar-^{39}Ar; whole-rock	Age of hydrothermal silicification/overprinting

APPENDIX 25-B (continued)

Area	Reference	Lithology / Locality	Age (Ma)	Method	Interpretation by author(s)
WITWATERSRAND BASIN	Friese (this study)	Platberg Group-age tectonites / H.J. Joel Gold Mine, Free State Goldfield	~1345-1200	^{40}Ar-^{39}Ar; whole-rock	Partial thermal resetting ages/events
	Davies *et al.* (1970)	Trompsburg Complex / Tromsburg	1372 ± 142	Rb-Sr; ?	Formation/crystallisation age; Partial thermal resetting age/event (this study)
	Poujol *et al.* (2000)	Leuco-trondhjemite dyke intrusive into trondhjemitic basement gneiss / ~7km south of Amalia; Amalia granite-greenstone terrane	1252 ± 59	U-Pb; zircon	Thermal resetting age/event
	Hargraves (1987)	Lindequesdrift intrusion / Vredefort Dome	1248 ± 22	^{40}Ar-^{39}Ar; plagioclase	Thermal resetting age/event associated with igneous intrusions (*e.g.,* Pilanesberg dykes)
	Reimold *et al.* (1990)	Pseudotachylites from widely spaced localities / Vredefort Dome	1440 ± 80 1390 ± 80 1330 ± 40 1090 ± 100	^{40}Ar-^{39}Ar; whole rock	Formation or resetting ages?
	Allsopp *et al.* (1991)	Rietfontein alkali granite / Vredefort Dome	1162.6 ± 28.8, 1166.2 ± 9.7, 1441.2 ± 21.3, 1472.2 ± 10.7	^{40}Ar-^{39}Ar; hornblende, biotite, w.-r.	Several partial resetting plateaux ages (repeated partial overprinting activity)
		Granophyre dyke / Vredefort Dome (SA)	1206.4 ± 29.4, 1281.8 ± 18.4, 1316.9 ± 15.5, 1345.8 ± 11.7, 1415.5 ± 19.9, 1458.0 ± 8.1	^{40}Ar-^{39}Ar; biotite, whole-rock	Several partial resetting plateaux ages (repeated partial overprinting activity)
	Spray *et al.* (1995)	Coesite-/stishovite-bearing pseudotachylites/Broodkop farm, Vredefort Dome	1227 ± 17, 1337 ± 12, 1357 ± 12, 1401 ± 27, 1407 ±14, 1413 ± 22, 1437 ± 9	^{40}Ar-^{39}Ar; whole rock	Resetting ages of older pseudotachylites and formation ages of younger endogenic pseudotachylites
	Reimold *et al.* (1995)	"Epidiorites" from collar region / Vredefort Dome	~1400 - 900	^{40}Ar-^{39}Ar; plag., amph.	Partial thermal resetting ages/events
	Reimold *et al.* (1994)	Basal Reef / F.S.G. Goldmine, Free State Goldfield	1035 ± 50	Xe_s-Xe_n; uraninite	Partial thermal resetting age/event
	Armstrong *et al.* (1991)	Crown lava / Klerksdorp Goldfield	1066 ± 31	U-Pb; whole rock	Thermal overprinting age/event
		Syferfontein volcanics / Klerksdorp Goldfield	1201 ± 161	U-Pb; whole rock	Thermal overprinting age/event
	Trieloff *et al.* (1994)	Ventersdorp Contact Reef / Vaal Reef Goldmine, Klerksdorp Goldfield	~1380	^{40}Ar-^{39}Ar; whole rock	Low temperature thermal resetting age/event
	Reimold *et al.* (1994)	Ventersdorp Contact Reef / Kloof Goldmine, Carletonville Goldfield	1260 ± 20	Xe_s-Xe_n; uraninite	Partial thermal resetting age/event
	Trieloff *et al.* (1994)	Pseudotachylites from the Ventersdorp Contact Reef / Elandsrand Goldmine, Carletonville Goldfield	~1280	^{40}Ar-^{39}Ar; whole rock	Low temperature partial thermal resetting age/event
	Armstrong *et al.* (1991)	Klipriviersberg Group lavas / Central Rand Goldfield	1253 ± 34, 936 ± 154, 1001 ± 139	U-Pb; zircon	No interpretation given; Partial thermal resetting event/age (this study)
	Reimold *et al.* (1994)	Main Reef / Sub Nigel Goldmine, Central Rand Goldfield	1120 ± 50	Xe_s-Xe_n; uraninite	Partial thermal resetting age/event
	Robb *et al.* (1992)	Granites from western hinterland of Witwatersrand Basin	~1089	U-Pb; zircon	No interpretation given; Partial thermal resetting event/age (this study)
	Robb *et al.* (1992b)	Basement granites / east of the FS Goldfield near Kroonstadt	1280 ± 1	U-Pb; kerogen	No interpretation given; Partial thermal resetting event/age (this study)
BUSHVELD IGNEOUS PROVINCE	Nomade *et al.* (2004)	Biotite from UG2 chromitite layer / Impala Platinum Mine, Bushveld Complex	2049-2037 (weighted mean age: 2042.4 ± 3.2)	^{40}Ar-^{39}Ar, biotite	Wide-spread, pervasive, post-crystallisation, syn-cooling alteration & over-printing by hydroth. fluids circulating along low-angle thrusts leading to biotite formation
	Adlakha *et al.* (2011)	Biotite from UG2 chromitite layer (Critical Zone) / Bushveld Complex	2044 ± 23, 2023 ± 12	^{40}Ar-^{39}Ar, biotite	Formation/crystallisation age; thermal resetting age/event (this study)
	McCandless & Ruiz (1991)	Pyroxenite of Bastard Reef (Critical Zone) / Bushveld Complex	2043 ± 11	Re–Os; whole-rock	Formation/crystallisation age; thermal resetting age/event (this study)
	Schoenberg *et al.* (1999)	Poikilitic pyroxenites of the Bastard Unit / Western Bushveld Complex	2043 ± 11	Re–Os; whole-rock	Formation/crystallisation age; thermal resetting age/event (this study)
	Coggon *et al.* (2011)	Euhedral sperrylite crystal from hydroth. veins in breccia zones in BIFs of Chuniespoort Group close to Platreef / Tweefontein Hill, Northern BC	2042 ± 102	Pt–Os; sperrylite	Hydrothermal PGE mineralisation
		Heavy mineral concentrate from Merensky Reef / Rustenburg Platinum Mine	2024 ± 101	Pt–Os; cooperate	Merensky Reef formation/crystallisation age; thermal resetting age/event (this study)
		Heavy mineral concentrate from Merensky Reef / Rustenburg Platinum Mine	1995 ± 50	Pt–Os; mixed PGMs	Merensky Reef formation/crystallisation age; thermal resetting age/event (this study)
		All samples combined (isochron age)	2012 ± 47	Pt–Os; mixed PGMs	Combined Merensky Reef formation age; thermal resetting age/event (this study)

APPENDIX 25-B (continued)

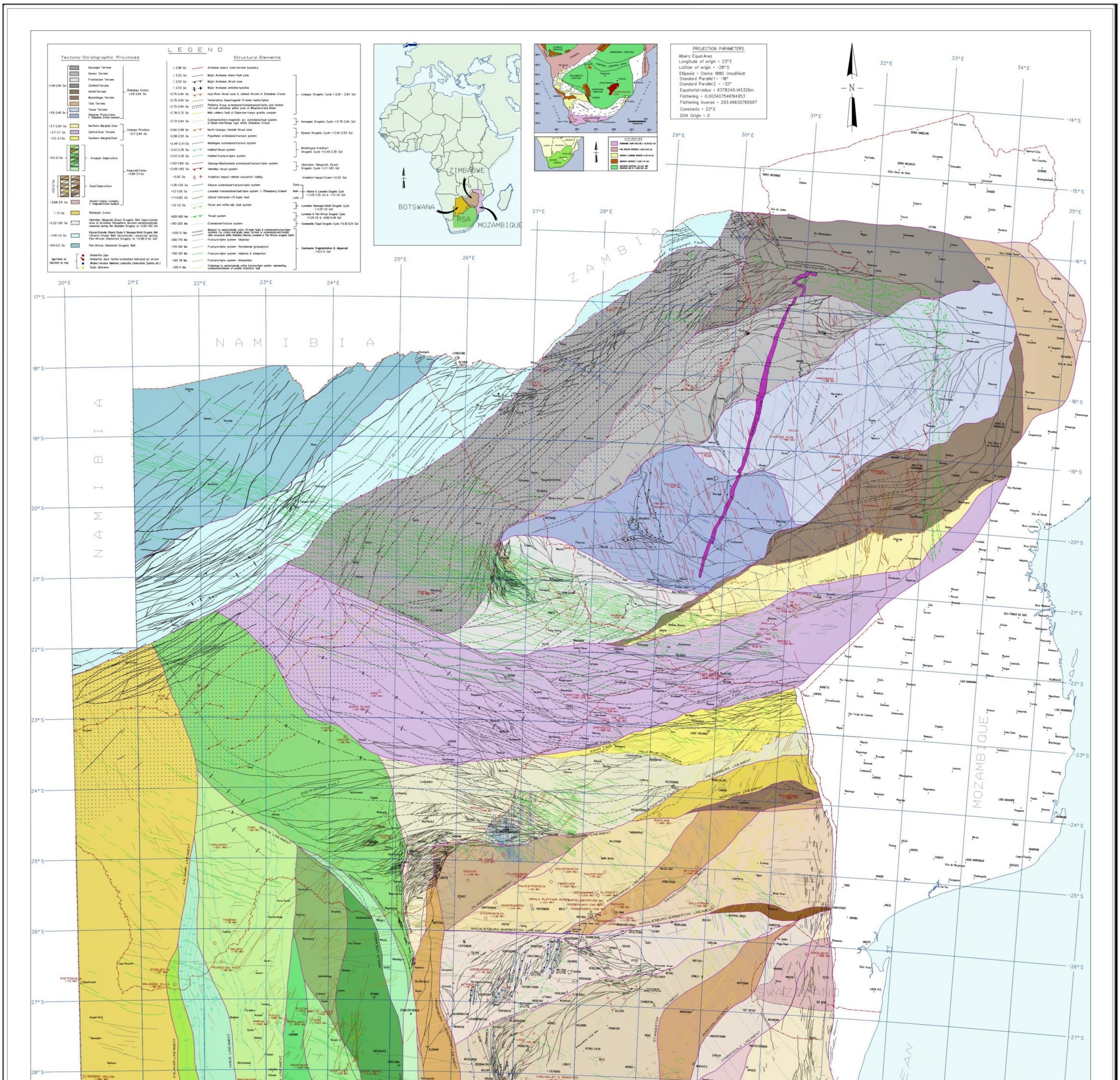
Area	Reference	Lithology / Locality	Age (Ma)	Method	Interpretation by author(s)
BUSHVELD IGNEOUS PROVINCE	Friese (unpublished)	NE/SW-striking granite dykes & quartz-feldspar veins of Lebowa Granite Suite cross-cutting Platreef / Mogalakwena Platinum Mine	2045 ± 5, 2034 ± 7, 2037 ± 7, 2033 ± 13, 2028 ± 10, 2001 ± 7, 1987 ± 31, 1986 ± 5, 1985 ± 6, 1985 ± 5, 1928 ± 5, 1927 ± 6, 1922 ± 11, 1871 ± 8, 1867 ± 6, 1857 ± 15, 1845 ± 4, 1829 ± 19, 1828 ± 9, 1818 ± 18, 1775 ± 13, 1761 ± 5, 1757 ± 19, 1698 ± 12, 1631 ± 7, 1578 ± 56, 1535 ± 42, 1361 ± 25, 1322 ± 25, 1279 ± 6, 524 ± 331, 551 ± 16	U-Pb; zircon	Partial thermal resetting age/event
		NE-trending, remanent positive magnetic diabase dyke (= Upper Zone feeder dyke) / Modikwa Platinum Mine, Eastern Bushveld Complex	2018 ± 4,	* ^{40}Ar-^{39}Ar; plagioclase (INT = integrated age. ISO = isochron age)	
		Pyroxenite ('C' facies) / Mogalakwena Platinum Mine	1913 ± 14, 1817 ± 21, *1427 ± 32 (ISO), *1107 ± 10 (ISO), *1043 ± 44 (ISO), *1033 ± 5 (ISO), 594 ± 103		
		Pyroxenite ('A' facies) / Mogalakwena Platinum Mine	*2043 ± 18 (INT), *2033 ± 6 (INT), *2019 ± 6 (INT), 2003 ± 17, 1995 ± 7, *1989 ± 12 (INT), 1968 ± 13, 1758 ± 18, 1706 ± 10, 1580 ± 14, 1405 ± 24, *1038 ± 13 (ISO), *1090 ± 15 (ISO), *1128 ± 12 (ISO), *1052 ± 9 (ISO)		
		Gabbro-norite of Main Zone / Mogalakwena Platinum Mine	1977 ± 6, 1847 ± 12		
	Reisberg *et al.* (2011)	Pyroxenite of Platreef / Mogalakwena Platinum Mine	2011 ± 51	Re–Os; whole-rock	Formation/crystallisation age; thermal resetting age/event (this study)
	Burger *et al.* (1967)	Nebo Granite	1955 +37/-36, 1915 ± 18	U-Pb; monazite, zircon	No interpretation given
	Davies *et al.* (1970)	Nebo Granite	1946 ± 45	Rb-Sr; whole-rock	No interpretation given
	Faurie (1977)	Nebo Granite	1920 ± 80	U-Pb; zircon	No interpretation given
	Coertze *et al.* (1978)	Ferrogabbro of Upper Zone Nebo Granite	~1750 1920 ± 40, 1948 +42/-39, 1939 ± 17	^{40}Ar-^{39}Ar; whole-rock U-Pb; zircon	Partial thermal resetting age/event Partial thermal resetting ages/events
	Hunter & Hamilton (1978)	Granite	1871 ± 102, 1745 ± 11	Rb-Sr; whole-rock	Partial thermal resetting ages/events
	Burger & Walraven (1980)	Stavoren Granophyre Bushveld Granite Makhutso Granite	1772 ± 45 1709 ± 40 1841 ± 45	U-Pb; whole-rock U-Pb; whole-rock U-Pb; whole-rock	Partial thermal resetting age/event Partial thermal resetting age/event No interpretation given
	Walraven (1981)	Klipkloof Granite	1790 ± 114	Rb-Sr; whole-rock	Partial thermal resetting age/event
	Walraven *et al.* (1982)	Granodiorite (Rustenburg Layered Suite) Klipkloof Granite Nebo Granite	1792 ± 170 1788 ± 112, 1721 ± 158, 1689 ± 15	Rb-Sr; whole-rock Rb-Sr; whole-rock U-Pb; zircon	Partial thermal resetting age/event Partial thermal resetting age/event Partial thermal resetting ages/events
	Walraven *et al.* (1983)	Nebo Granite	1833 ± 46, 1792 ± 45, 1738 ± 43, 1711 ± 43, 1955 ± 40	U-Pb; zircon	Partial thermal resetting ages/events
	Walraven *et al.* (1985)	Nebo Granite	1779 ± 102 1982 ± 63	Rb-Sr; whole-rock Rb-Sr; biotite	Partial thermal resetting age/event Partial thermal resetting age/event
	Walraven *et al.* (1987)	Nebo Granite Klipkloof Granite	1832 ± 41, 1825 ± 41, 1980 +48/-43, 1990 ± 9 1788 ± 112	U-Pb; zircon Rb-Sr; whole-rock	Partial thermal resetting ages/events Partial thermal resetting age/event
	Walraven (1987)	Stavoren Granophyre	1829 ± 98	Rb-Sr; whole-rock	Partial thermal resetting age/event
	Walraven *et al.* (1990)	Nebo Granite	1998 ± 45	Rb-Sr; whole-rock	Partial thermal resetting age/event
	Robb *et al.* (2000)	Quartz-polymetallic sulphide veins in Lebowa Granite / Spoedwel Mine	1957 ± 15	U-Pb; zircon	Time of hydrothermal activity and late-stage base-metal sulphide mineralisation
	Oosthuizen (1964)	Quartz porphyry lava of Rust de Winter Formation (Lower Waterberg Group) / Rust de Winter 180 farm	1790 ± 90	U-Pb; whole-rock	Formation/crystallization age; thermal resetting age/event (this study)
	Coertze *et al.* (1978)	Makhutso Granite (Lebowa Granite Suite)	1670 ± 70, 1645 +64/-59, 1637 ± 21	U-Pb; zircon	Partial thermal resetting ages/events
	Walraven *et al.* (1983)	Nebo Granite (Lebowa Granite Suite)	1657 ± 41	U-Pb; zircon	Partial thermal resetting ages/events
	Walraven (1982)	Klipkloof Granite (Lebowa Granite Suite)	1648 ± 218	Rb-Sr; whole-rock	No interpretation given
	Walraven *et al.* (1982)	Rhyolite (Rooiberg Group)	1644 ± 209	U-Pb; whole-rock	Partial thermal resetting age/event
	Walraven (1987)	Rhyolite and rhyodacite (Rooiberg Group)	1605 ± 28	Rb-Sr; whole-rock	Partial thermal resetting age/event
	Letts *et al.* (2004)	Dolerite dyke / Paschaaskraal area, Eastern Limb	1649± 10	Ar-Ar; plagioclase	Partial thermal resetting age/event
	Burger & Walraven (1977)	Upper Zone / western Bushveld Complex	1285 ± 44	^{40}Ar-^{39}Ar; whole rock	Metamorphic overprint event
	Coertze *et al.* (1978)	Ferrogabbro of Upper Zone / Bushveld Complex Klipkloof and Klipvoor granites / Bushveld Complex	1216 ± 44 1400 ± 190	^{40}Ar-^{39}Ar; whole rock U-Pb; zircon	Partial resetting age/geol. event Controversial age - no interpretation given
	Walraven & Hattingh (1993)	Pegmatite near the upper contact between Bushveld granites and over-lying roof rocks / near Zaaiplaats and Rooiberg, Bushveld Complex	~1200	Rb-Sr; K-feldspar	Post-crystallization strong isotopic disturbance
	McNaughton *et al.* (1993)	Bobbejaankop & Lease Granites (hosts to Zaaiplaats tin deposit) / Northern limb of Bushveld Complex	~1187-961	Pb-Pb; whole-rock & minerals	Partial thermal resetting event/age

APPENDIX 25-B (continued)

Area	Reference	Lithology / Locality	Age (Ma)	Method	Interpretation by author(s)
KRAAIPAN SUBPROVINCE	Mapeo *et al.* (2004)	Fine-grained and porphyritic granites of Moshaneng Complex / (SE Botswana)	2040.2 ± 6.3, 2015.8 ± 2.7, 2042.4 ± 3.3	U-Pb; zircon	Formation/crystallization age; thermal resetting age/event (this study)
	Harding & Snelling (1972)	Plantation Porphyry (Lobatse Volcanic Group) / Botswana Kanye Volcanic Formation / Botswana	1754 ± 247 1904 ± 292	Rb-Sr; whole-rock Rb-Sr; whole-rock	Partial thermal resetting age/event Partial thermal resetting age/event
	Harding *et al.* (1974)	Plantation Porphyry (Lobatse Volcanic Group) / Botswana	2154 ± 210	Rb-Sr; whole-rock	Formation/crystallization age
	Crampton (1974)	Felsic volcanics of Matsap Formation (Ventersdorp Supergroup) / Derdepoort	~2150	Rb-Sr; whole-rock	Formation/crystallization age
	Rundle (1984)	Gaborone Granite Complex / Botswana	2132 ± 164, 1768 ± 94	Rb-Sr; whole-rock	Partial thermal resetting ages/events
	Kruger *et al.* (1999)	Calcite and chlorite amygdales of highly altered Ventersdorp lavas / Roode Koppies and Katlani Zn-Pb MVT deposits near Douglas Molopo Farms Complex / (Botswana)	~2023 1999 ± 22	Rb-Sr; calcite, chlorite & whole-rock Rb-Sr; biotite	Age of hydrothermal fluid flow and Pb-Zn MVT mineralisation Thermal resetting age/overprinting event
	Duane *et al.* (1991), Kruger *et al.* (1999)	Galena from various Pb-Zn MVT deposits within Ghaap Group and Ventersdorp Supergroup / Pering, Zeerust, Douglas	~2050-2000	Pb-Pb; galena	Age of hydrothermal fluid flow and Pb-Zn MVT mineralisation
	Walraven *et al.* (1991)	Kareefontein Quartz Porphyry (Zoetlief Group)	1901 ± 83 1982 +169/-191	Rb-Sr; whole-rock Pb-Pb; whole-rock	Partial thermal resetting age/event Partial thermal resetting age/event
	Barton *et al.* (1995b)	Felsic volcanics (Witfonteinrand Formation) / Thabazimbi	~2000, ~1700	U-Pb; zircon	Partial thermal resetting ages/events
	Armstrong (1987)	Mafic lavas of Ongeluk Formation (Postmasburg Group) / Griqualand West Basin	2034 ± 139	Rb-Sr; whole-rock	Partial thermal resetting age/event
	Barton *et al.* (1986)	BIF from Marydale Group / Marydale Greenstone Belt	~2200	Pb-Pb; whole-rock	Partial resetting event = age of amphibolite metamorphism
	Cornell (1977)	Andesitic lavas of Marydale Group / Marydale Greenstone Belt	1899 ± 57	?	Formation age; Partial thermal resetting age/event (this study)
	Barton *et al.* (1994)	Banded-tuff horizon in Nauga Formation (upper Campbell Group) / Griqualand West Basin	1876 ± 12	U-Pb; zircon	Contaminant zircon grain introduced during sample preparation; Partial thermal resetting age/event (this study)
	Burger & Coertze (1974)	Groblershoop Schist Formation (Olifantshoek Sequence) / Kheis Province	~1780	Ar-Ar; whole-rock	Age of metamorphism
SWAZI SUBPROVINCE	De Waal *et al.* (2001)	Uitkomst Complex / 70 km SE of Bushveld Complex, Mpumalanga Province	2044 ± 8	Pb-Pb; zircon	Formation/crystallization age; thermal resetting age/event (this study)
	De Ronde *et al.* (1991)				Widespread thermal overprint of the Barberton greenstone belt related to large-scale tectono-thermal activity in the Kaapvaal Craton dated at ~2120-2025 Ma
	Layer *et al.* (1998)	NW-trending dykes / Barberton Greenstone Belt	1902 ± 6, 1876 ± 6	^{40}Ar-^{39}Ar; whole-rock	Formation/crystallisation age; thermal resetting event (this study)
PIETERSBURG TERRANE	Byron & Barton (1990)	Granitic dykes related to Turfloop batholith	~2176	Rb-Sr; whole-rock	Hydrothermal alteration phase
	Good (1999)	Mica from sheared schist/slate within Droogekloof Thrust / Zwartkloof Mica from Goedgedacht Au deposit / near Dwaalboom Mica from ancient Cu workings / Genadenthal	2061.28, 2064.34 2002.57, 1944.65 1890.08	Rb-Sr; mica model ages	Time of hydrothermal fluid flow /mineralisation and tectonic reactivation along Thabazimbi-Murchison Lineament
	Cheney *et al.* (1990)	Entabeni Granite / Northern Province	1974 ± 17	Rb-Sr; musc. & w.-r.	Formation/crystallisation age; partial thermal resetting age/event (this study))
	Barton *et al.* (1995a)	Entabeni Granite / Northern Province	1957 ± 3	U-Pb; zircon	Formation/crystallisation age; partial thermal resetting age/event (this study))
	Barton *et al.* (1980)	Turfloop Batholith	1939 ± 39, 1822 ± 36	Rb-Sr; whole-rock	Cooling below 300° as a result of regional uplift and erosion
	Burger & Coertze (1975)	Palala Granite	1770 ± 30	U-Pb; zircon	Formation/crystallization age
	Walraven *et al.* (1982)	Palala Granite	1769 ± 113, 1856 ± 54, 1908 ± 45	U-Pb; zircon	Formation/crystallization ages
	Barton (1979)	Hydrothermally altered basaltic lavas and sills (Sibasa Formation) of Soutpansberg Group / Northern Province	1756 ± 27, 1769 ± 34 1749 ± 104	Rb-Sr; whole-rock Rb-Sr; errorchron	Time of formation/crystallisation and coeval alteration of lavas & sills and copper-mineralisation
	Barton & Ryan (1977)	Hydrothermally altered basalt of Soutpansberg Group / Northern Province	1752 ± 100	Rb-Sr; whole-rock	Formation/crystallisation age; time of hydroth. alteration (this study)
	Barton & McCourt (1983)	Palala Granite	1725 ± 245	Rb-Sr; whole-rock	Partial thermal resetting age/deformation event
	Walraven *et al.* (1983)	Palala Granite	1708 ± 43	U-Pb; zircon	Partial thermal resetting age/deformation event
	Barton *et al.* (1995b)	Granodiorite of the Makoppa Dome (Archaean Basement Complex to the Hampton Formation (Buffelsfontein Group) / Thabazimbi	~1700	Rb-Sr; muscovite	Partial thermal resetting age/event
	Cheney *et al.* (1990)	Entabeni Granite	1617 ± 16	Rb-Sr; biotite	Partial thermal resetting age/event
	Anhaeusser & Poujol (2004)	Makoppa-type granodiorite-monzogranite / Makoppa Dome	1280 +160/-140	U-Pb; zircon	Formation/crystallisation age

APPENDIX 26

TECTONIC/STRUCTURAL AND TERRANE INTERPRETATION SUMMARY MAP FOR THE KAAPVAAL CRATON, LIMPOPO PROVINCE AND ZIMBABWE CRATON, COVERING THE COUNTRIES OF BOTSWANA, ZIMBABWE, SOUTH AFRICA, AND PARTS OF MOZAMBIQUE


LEGEND
Tectono-Stratigraphic Provinces
Hurungwe Terrane
Harare Terrane
Francistown Terrane
Zambesi Terrane
Umtali Terrane
Mozambique Terrane
Tete Terrane
Tokwe Terrane
Sebakwe Protocraton (= Zimbabwe Craton nucleus)
~3.46-2.64 Ga
~3.8-3.46 Ga
Zimbabwe Craton ~3.8-2.64 Ga
~3.7-2.64 Ga Northern Marginal Zone
~3.7-3.1 Ga Central Zone Terrane
~3.5-3.1 Ga Southern Marginal Zone
Limpopo Province ~3.7-2.64 Ga
~3.5-3.1 Ga Kraaipan Subprovince
Swazi Subprovince
~3.68-3.5 Ga Ancient Gneiss Complex (= Kaapvaal Craton nucleus)
Kaapvaal Craton ~3.68-3.1 Ga
> 3.1 Ga Rehoboth Craton
~2.22-1.83 Ga Ubendian (Magondi, Okwa) Orogenic Belt (approximate area of Archaean lithosphere tectono-metamorphically reworked during the Ubendian Orogeny at ~2.05-1.83 Ga)
~1.45-1.0 Ga Kibaran/Grenville (Ghanzi-Chobe & Namaqua-Natal) Orogenic Belt (Ghanzi-Chobe Belt tectonically reworked during Pan-African (Damaran) Orogeny at ~0.58-0.52 Ga)
~0.9-0.5 Ga Pan-African (Damaran) Orogenic Belt
Age/name as indicated on map
Kimberlite pipe
Kimberlite dyke (strike-orientation indicated by arrow)
Alkaline intrusion (Melnoite, Lamproite, Carbonatite, Syenite, etc.)
Sodic diatreme
Structural Elements
> 2.99 Ga Archaean suture zone/terrane boundary
> 2.53 Ga Major Archaean shear/fault zone
> 2.53 Ga Major Archaean thrust zone
> 2.53 Ga Major Archaean anticline/syncline
~2.75-2.64 Ga Hout River thrust zone & related thrusts in Zimbabwe Craton
~2.75-2.64 Ga Ventersdorp impactogenal rift basin faults/dykes
~2.75-2.64 Ga Platberg Group extensional/transtensional faults and related roll-over anticlines within area of Witwatersrand Basin
~2.78-2.72 Ga Main caldera fault of Gaborone-Kanye granite complex
Limpopo Orogenic Cycle (~2.81 - 2.64 Ga)
~2.72-2.64 Ga Continental intra-magmatic arc extensional fault system of Basin-and-Range type within Zimbabwe Craton
Hurungwe Orogenic Cycle (~2.75-2.64 Ga)
~2.64-2.58 Ga North Limpopo (Umtali) thrust zone
~2.58-2.53 Ga Popotheke extensional fracture system
Nyassa Orogenic Cycle (~2.64-2.53 Ga)
~2.46-2.41 Ga Mtshingwe extensional fracture system
~2.42-2.35 Ga Kalahari thrust system
~2.42-2.35 Ga Kalahari fracture/dyke system
Mtshingwe-Kalahari Orogenic Cycle (~2.46-2.35 Ga)
~1.93-1.83 Ga Sebanga-Mashonaland extensional fracture/dyke system
~2.05-1.83 Ga Ubendian thrust system
Ubendian (Magondi, Okwa) Orogenic Cycle (~2.1-1.83 Ga)
~2.02 Ga Vredefort impact related concentric folding
Vredefort Impact Event (~2.02 Ga)
~1.35-1.25 Ga Kibaran extensional fracture/dyke system
~1.2-1.05 Ga Lomanian transtensional fault/dyke system (= Pilanesberg Graben)
~1.1-0.82 Ga Gairezi (Umkondo) rift basin fault
Early / Main / Late
Kibaran & Lomanian Orogenic Cycle (~1.45-1.25 Ga & ~1.2-1.0 Ga)
~1.2-1.0 Ga Thrust and strike-slip fault system
Lomanian (Namaqua-Natal) Orogenic Cycle (~1.25-1.0 Ga)
~820-500 Ma Thrust system
Lomanian & Pan-African Orogenic Cyles (~1.25-1.0 & ~0.83-0.48 Ga)
~310-200 Ma Extensional fracture system
Gondwanide (Cape) Orogenic Cycle (~0.35-0.24 Ga)
~200-0 Ma Mesozoic to neotectonically active rift basin faults & extensional fracture/dyke systems (i.e. craton-marginally newly formed or extensional reactivated older structures within Ubendian, Kibaran, Lomanian & Pan-African orogenic belts)
~200-170 Ma Fracture/dyke system (dolerite)
~170-150 Ma Fracture/dyke system (hornblende-granophyre)
~150-120 Ma Fracture/dyke system (dolerite & kimberlite)
~120-78 Ma Fracture/dyke system (kimberlite)
~120-0 Ma Cretaceous to neotectonically active fracture/dyke system representing continental extension of oceanic transform fault
Gondwana fragmentation & dispersal (~0.2-0 Ga)
ZIMBABWE
BOTSWANA
RSA
MOZAMBIQUE
CONGO CRATON
ZIMBABWE CRATON
LIMPOPO CENTRAL ZONE
REHOBOTH CRATON
KAAPVAAL CRATON
ATLANTIC OCEAN
INDIAN OCEAN
EXPLANATION
PROJECTION PARAMETERS
Albers Equal Area
Longitude of origin = 23°E
Latitde of origin = -28°S
Ellipsoid = Clarke 1880 (modified)
Standard Parallel 1 = -18°
Standard Parallel 2 = -32°
Equatorial radius = 6378249.145326m
Flattening = 0.003407546194953
Flattening inverse = 293.46630765597
Constants = 23°E
DGN Origin = 0
N
NAMIBIA
ZAMBIA
MOZAMBIQUE
LESOTHO
SWAZILAND
INDIAN OCEAN
Zambesi Escarpment Fault
Great Dyke
Popotheke Fault
Mtshingwe Fault
HARARE LINEAMENT
North Limpopo Thrust Zone
Triangle Shear Zone
South Gwanda Shear Zone
Bosbokpoort Fault
Tshipise Fault
PALALA LINEAMENT
Palala Fault
Hout River Shear Zone
PIETERSBURG LINEAMENT
MURCHISON LINEAMENT
OFKALACO LINEAMENT
THABAZIMBI LINEAMENT
ZOETFONTEIN FAULT
KANG AMALIA LINEAMENT
KRAAIPAN LINEAMENT
KALAHARI LINEAMENT
KHEIS LINEAMENT
KURUMAN LINEAMENT
DE AAR LINEAMENT
KIMBERLEY LINEAMENT
AMALIA LINEAMENT
COLESBERG - MAFIKENG LINEAMENT
TROMPSBURG - GABORONE LINEAMENT
BLOEMFONTEIN LINEAMENT
PILANESBERG LINEAMENT
MAGALIESBURG-BARBERTON LINEAMENT
SUGARBUSH-INYOKA LINEAMENT
KWAGGASRANT LINEAMENT
SWAVELPOORT LINEAMENT
STANDERTON LINEAMENT
ASSEGAAI LINEAMENT
COMMONDALE LINEAMENT
NONDWENI LINEAMENT
BRANDFORT-TUGELA LINEAMENT
APPENDIX 26
SOUTH AFRICA, BOTSWANA, ZIMBABWE AND PARTS OF MOZAMBIQUE
TECTONO-STRUCTURAL AND TERRANE INTERPRETATION SUMMARY MAP FOR THE KAAPVAAL CRATON, LIMPOPO CENTRAL ZONE TERRANE AND ZIMBABWE CRATON
SCALE 1 : 2 000 000
GEOLOGY BY : AEW FRIESE
JANUARY 2020